

From Nuclei to Compact Stars

Contents

1. Topics	1289
2. Participants	1291
2.1. ICRA Net participants	1291
2.2. Past collaborators	1291
2.3. On going collaborations	1291
2.4. Ph.D. Students	1292
3. Brief description	1293
3.1. Nuclear and Atomic Astrophysics	1294
3.2. White Dwarf Physics and Astrophysics	1298
3.3. Neutron Star Physics and Astrophysics	1300
4. Publications (before 2010)	1303
4.1. Refereed Journals	1303
4.2. Conference Proceedings	1304
5. Publications (2010-2011)	1307
5.1. Refereed Journals	1307
5.2. Conference Proceedings	1314
6. Attended International Conferences	1319
7. APPENDICES	1321
A. Nuclear and Atomic Astrophysics	1323
A.1. On gravitationally and electro dynamically bound massive nu- clear density cores	1323
A.1.1. Introduction	1323
A.1.2. The relativistic Thomas-Fermi equation and the beta equi- librium condition	1325
A.1.3. The ultra-relativistic analytic solutions	1327
A.1.4. New results derived from the analytic solutions	1331
A.1.5. Estimates of gravitational effects in a Newtonian ap- proximation	1332
A.1.6. Possible applications to neutron stars	1333
A.1.7. Conclusions	1334

A.2. On the relativistic Thomas-Fermi treatment of compressed atoms and compressed nuclear matter cores of stellar dimensions . . .	1337
A.2.1. Introduction	1337
A.2.2. The Thomas-Fermi model for compressed atoms: the Feynman-Metropolis-Teller treatment	1339
A.2.3. The relativistic generalization of the Feynman-Metropolis-Teller treatment	1343
A.2.4. Comparison and contrast with approximate treatments	1348
A.2.5. Application to nuclear matter cores of stellar dimensions	1353
A.2.6. Compressional energy of nuclear matter cores of stellar dimensions	1359
A.2.7. Conclusions	1361
A.3. Electrodynamics for Nuclear Matter in Bulk	1370
A.4. On the Charge to Mass Ratio of Neutron Cores and Heavy Nuclei	1380
A.4.1. Introduction	1380
A.4.2. The theoretical model	1380
A.4.3. N_p - A relation	1382
A.4.4. Conclusions	1385
A.5. Supercritical fields on the surface of massive nuclear cores: neutral core vs. charged core	1388
A.5.1. Equilibrium of electron distribution in neutral cores.	1388
A.5.2. Equilibrium of electron distribution in super charged cores	1389
A.5.3. Ultra-relativistic solution	1390
A.6. The Extended Nuclear Matter Model with Smooth Transition Surface	1392
A.6.1. The Relativistic Thomas-Fermi Equation	1392
A.6.2. The Woods-Saxon-like Proton Distribution Function	1392
A.6.3. Results of the Numerical Integration.	1393
A.7. Electron-positron pairs production in a macroscopic charged core	1396
A.7.1. Introduction	1396
A.7.2. Classical description of electrons in potential of cores	1398
A.7.3. Semi-Classical description	1401
A.7.4. Production of electron-positron pair	1404
A.7.5. Summary and remarks	1407
A.8. On Magnetic Fields in Rotating Nuclear Matter Cores of Stellar Dimensions	1410
A.8.1. Introduction	1410
A.8.2. The Relativistic Thomas-Fermi equation	1411
A.8.3. The ultra-relativistic analytic solutions	1413
A.8.4. Rotating Nuclear Matter Cores of Stellar Dimensions in Classical Electrodynamics	1413
A.8.5. Conclusions	1416

B. White Dwarfs Physics and Astrophysics	1419
B.1. The relativistic Feynman-Metropolis-Teller theory for white dwarfs in general relativity	1419
B.1.1. Introduction	1419
B.1.2. The Equation of State	1423
B.1.3. General relativistic equations of equilibrium	1437
B.1.4. Mass and radius of general relativistic stable white dwarfs	1441
B.1.5. Conclusions	1448
B.2. On the maximum mass and minimum period of general rela- tivistically uniformly rotating white dwarfs	1450
B.3. SGRs and AXPs as rotation powered massive white dwarfs . .	1457
B.3.1. Introduction	1457
B.3.2. SGRs and AXPs within the white dwarf model	1458
B.3.3. SGRs and AXPs within the magnetar model	1461
B.3.4. Observations of massive fast rotating highly magnetized white dwarfs	1463
B.3.5. Rotational instability of white dwarfs	1465
B.3.6. Glitches and outbursts in SGRs and AXPs	1466
B.3.7. Magnetosphere emission from white dwarfs	1467
B.3.8. The connection with supernova remnants	1470
B.3.9. On the fiducial neutron star and white dwarf parame- ters in light of recent theoretical progress	1472
B.3.10. Conclusions and remarks	1473
C. Neutron Stars Physics and Astrophysics	1485
C.1. The self-consistent general relativistic solution for a system of degenerate neutrons, protons and electrons in β -equilibrium .	1485
C.1.1. Introduction	1485
C.1.2. The impossibility of a solution with local charge neu- trality	1487
C.1.3. The solution with global charge neutrality	1490
C.1.4. Numerical integration of the equilibrium equations . .	1490
C.1.5. Conclusions	1494
C.2. The Klein first integrals in an equilibrium system with electro- magnetic, weak, strong and gravitational interactions	1496
C.2.1. Introduction	1496
C.2.2. The Constitutive General Relativistic Equations	1497
C.2.3. The Thermodynamic Laws and the Field Equations in the Spherically Symmetric Case	1500
C.2.4. Constancy of the Klein potentials and β -equilibrium .	1503
C.2.5. Concluding Remarks	1505

C.3. On the constitutive equations of a self-gravitating system of neutrons, protons and electrons in β -equilibrium at finite temperatures	1507
C.3.1. Introduction	1507
C.3.2. Einstein-Maxwell-Thomas-Fermi equations in the degenerate case	1508
C.3.3. Newtonian limit	1511
C.3.4. Introducing strong interactions	1514
C.3.5. Finite temperature effects	1517
C.3.6. Concluding Remarks	1522
C.4. Neutron star equilibrium configurations within a fully relativistic theory with strong, weak, electromagnetic, and gravitational interactions	1527
C.4.1. Introduction	1527
C.4.2. The Constitutive Relativistic Equations	1528
C.4.3. Neutron star structure	1539
C.4.4. Observational constraints on the mass-radius relation	1541
C.4.5. Comparison with the traditional TOV treatment	1542
C.4.6. Concluding Remarks	1543
C.5. The Role of Thomas-Fermi approach in Neutron Star Matter	1559
C.5.1. Introduction	1559
C.5.2. Thomas-Fermi model	1561
C.5.3. White dwarfs and Neutron Stars as Thomas-Fermi systems	1562
C.5.4. The relativistic Thomas-Fermi equation	1563
C.5.5. The essential role of the non point-like nucleus	1563
C.5.6. Nuclear matter in bulk: $A \approx 300$ or $A \approx (m_{\text{Planck}}/m_n)^3$	1565
C.5.7. The energetically favorable configurations	1569
C.5.8. Conclusions	1571
C.6. A Self-consistent Approach to Neutron Stars	1572
C.6.1. Introduction	1572
C.6.2. The Equilibrium Equations	1573
C.6.3. Some Specific Solutions	1574
C.6.4. Conclusions	1575
C.7. On the electrostatic structure of neutron stars	1576
C.7.1. Introduction	1576
C.7.2. Structure Equations	1577
C.7.3. The Equation of State	1578
C.7.4. Numerical Integration	1581
C.8. A New Family of Neutron Star Models: Global Neutrality vs. Local Neutrality	1588
C.8.1. Introduction	1588
C.8.2. The equilibrium equations	1588
C.8.3. Discussion	1589

C.9. The Outer Crust of Neutron Stars	1591
C.9.1. The General Relativistic Model	1591
C.9.2. The mass and the thickness of the crust	1592
C.9.3. The Fireshell Model of GRBs	1593
C.9.4. The mass of the crust and M_B	1594
C.10. Cooling of young neutron stars in GRB associated to Supernova	1596
C.10.1. Introduction	1596
C.10.2. Cooling of Young, Hot Neutron Stars	1597
C.10.3. Late X-Ray Emission in GRBs associated to Supernovae: URCAs	1601
C.10.4. Neo-Neutron Star Luminosity and the URCAs	1602
C.10.5. Discussion and Conclusions	1604
 Bibliography	 1609

1. Topics

- Nuclear and Atomic Astrophysics.
- White Dwarfs Physics and Astrophysics.
- Neutron Stars Physics and Astrophysics.

2. Participants

2.1. ICRAANet participants

- D. Arnett (Steward Observatory, University of Arizona, USA)
- H. Kleinert (Free University of Berlin , Germany)
- V. Popov (ITEP, Moscow, Russia)
- M. Rotondo (ICRAANet, University of Rome, Italy)
- Jorge A. Rueda (ICRAANet, University of Rome, Italy)
- R. Ruffini (ICRAANet, University of Rome, Italy)
- G.'t Hooft (Institute for Theoretical Physic Universiteit Utrecht)
- S.-S. Xue (ICRAANet, University of Rome, Italy)

2.2. Past collaborators

- L. Stella (Rome Astronomical Observatory, Italy)
- W. Greiner (Institut für Theoretical Physics Johann Wolfgang Goethe-Universität, Frankfurt am Main)

2.3. On going collaborations

- M. Malheiro (Instituto Tecnológico de Aeronáutica, Brazil)
- R. Negreiros (Frankfurt Institute for Advanced Studies, Johann Wolfgang Goethe University, Germany)
- D. Pugliese (School of Mathematical Sciences, Queen Mary, University of London, United Kingdom)

2.4. Ph.D. Students

- R. Belvedere (ICRANet, University of Rome, Italy)
- K. Boshkayev (ICRANet, University of Rome, Italy)
- M. Haney (ICRANet, University of Rome, Italy)
- S. Martins de Carvalho (ICRANet, University of Rome, Italy)
- C. Argüelles (ICRANet, University of Rome, Italy)
- Y. Bin (ICRANet, University of Rome, Italy)
- J. Pereira (ICRANet, University of Rome, Italy)

3. Brief description

One of the most active field of research has been to analyze a general approach to compact stars e.g. white dwarfs and neutron stars, based on the Thomas-Fermi ultrarelativistic equations amply adopted in the study of superheavy nuclei. The aim is to have a unified approach for nuclei, for superheavy nuclei up to atomic numbers of the order of $A \sim 10^3$ – 10^6 , and for macroscopic objects $A \sim 10^{57}$ as white dwarfs and neutron stars which are composed partly or fully by nuclear matter.

In the earliest description of neutron stars in the works of Tolman (1939) and Oppenheimer and Volkoff (1939) only a gas of neutrons was considered and the equation of equilibrium (hereafter TOV equations) was written in the Schwarzschild metric. They considered the model of a degenerate gas of neutrons to hold from the center to the border, with the density monotonically decreasing away from the center.

In the intervening years, a more realistic model has been presented challenging the original considerations of Tolman (1939) and Oppenheimer and Volkoff (1939). The TOV equations considered the existence of neutrons all the way to the surface of the star. The presence of neutrons, protons and electrons in β -equilibrium were instead introduced by Harrison et al. (1965). Still more important, the neutron stars have been shown to be composed of two sharply different components: the core at nuclear and supra-nuclear densities consisting of degenerate neutrons, protons and electrons in β -equilibrium and a crust of white dwarf like material, namely a nuclei lattice in a background of degenerate electrons (see Harrison et al. (1965); Baym et al. (1971a) for details). Further works describing the nuclear interactions were later introduced. Clearly all these considerations departed profoundly from the TOV assumption of a neutron star made only of neutrons.

The matching between the core and the crust is still today an open issue in neutron star physics. In order to handle with this interesting problem, a step-by-step procedure is needed. In such a case, the neutron, proton, and electron fluid is confined within the core radius due to the compression exerted by the crust component of the neutron star.

In the case of white dwarfs, no fully consistent theory of the equilibrium of the electron-nuclei lattice system within general relativity exists. Such a theory needs the complete description of the electron-electron and electron-nucleus Coulomb interactions within a self-consistent relativistic framework.

The study of both white dwarfs and neutron stars requires the interplay between nuclear and atomic physics together with relativistic field theories

e.g. general relativity, quantum electrodynamics, quantum chromodynamics, as well as particle physics. The works done and currently being developed within our group can be divided into three topics:

1. Nuclear and Atomic Astrophysics
2. White Dwarfs Physics and Astrophysics
3. Neutron Stars Physics and Astrophysics

3.1. Nuclear and Atomic Astrophysics

By Nuclear and Atomic Astrophysics we mean the study of nuclear and atomic physics related to astrophysical systems as white dwarfs and neutron stars. The aim is to have a unified approach for nuclei, for superheavy nuclei up to atomic numbers of the order of 10^5 – 10^6 , and for what we have called “nuclear matter cores of stellar dimensions”, which are

- characterized by atomic number of the order of 10^{57} ;
- composed by a degenerate fluid of neutrons, protons and electrons in β -equilibrium;
- globally neutral configurations;
- expected to be kept at nuclear density by self gravity.

It is known that the Thomas-Fermi model has been extensively applied in atomic physics, also has been applied extensively in atomic physics in its relativistic form as well as in the study of atoms with heavy nuclei (see Gombás (1949) for instance). Similarly there have been considerations of relativistic Thomas-Fermi model for quark stars pointing out the existence of critical electric fields on their surfaces Alcock et al. (1986). Similar results have also been obtained in the transition at very high densities, from the normal nuclear matter phase in the core to the color-flavor-locked phase of quark matter in the inner core of hybrid stars Alford et al. (2001). However, no example exists to the application of the electromagnetic Thomas-Fermi model to white dwarfs and neutron stars.

The analysis of superheavy nuclei has historically represented a major field of research, developed by Prof. V. Popov and Prof. W. Greiner and their schools. This same problem was studied in the context of the relativistic Thomas-Fermi equation also by R. Ruffini and L. Stella, already in the '80s. The recent approach was started with the Ph.D. Thesis of M. Rotondo and has shown the possibility to extrapolate this treatment of superheavy nuclei to the case of nuclear matter cores of stellar dimensions (see App. A.3). The very unexpected result has been that also around these massive cores there is

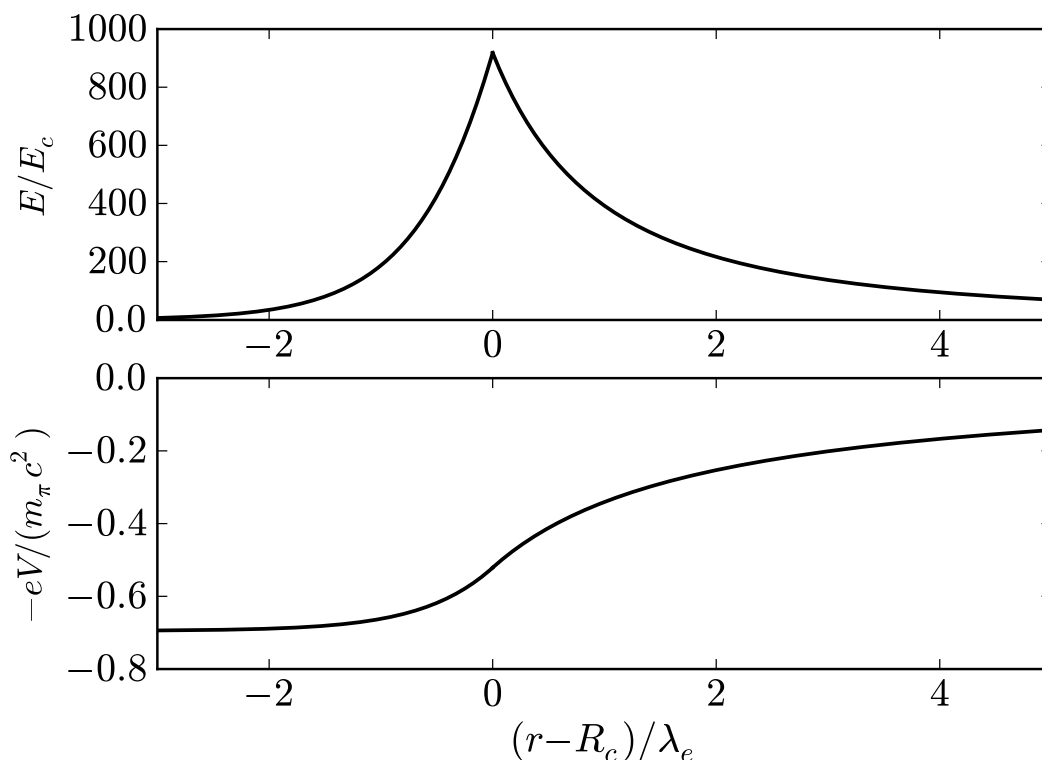


Figure 3.1.: Upper panel: electric field around the surface of a nuclear matter core of stellar dimensions in units of the critical field E_c . Lower panel: corresponding sharp increasing of the electron Coulomb potential $-eV$. Here R_c denotes the core radius and $\lambda_e = \hbar/(m_e c)$ is the electron Compton wavelength.

the distinct possibility of having an electromagnetic field close to the critical value

$$E_c = \frac{m_e^2 c^3}{e \hbar},$$

although localized in a very narrow shell of the order of the electron Compton wavelength (see Fig. 3.1).

The welcome result has been that all the analytic work developed by Prof. V. Popov and the Russian school can be applied using scaling laws satisfied by the relativistic Thomas-Fermi equation to the case of nuclear matter cores of stellar dimensions, if the β -equilibrium condition is properly taken into account (see App. A.1 and A.3). This has been the result obtained and published by Ruffini, Rotondo and Xue already in 2007. Since then, a large variety of problems has emerged, which have seen the direct participation at ICRANet of Prof. Greiner, Prof. Popov, and Prof. 't Hooft.

One of the crucial issues to be debated is the stability of such cores under the competing effects of self-gravity and Coulomb repulsion. In App. A.1

it has been demonstrated their stability against nuclear fission, as opposed to the case of heavy nuclei. In particular, on the basis of Newtonian gravitational energy considerations it has been found the existence of a possible new island of stability for mass numbers $A > A_R = 0.039 \left(\frac{N_p}{A}\right)^{1/2} \left(\frac{m_{\text{Planck}}}{m_n}\right)^3$, where N_p is the number of protons, A is the total number of baryons, m_n is the neutron mass and $m_{\text{Planck}} = (\hbar c/G)^{1/2}$ is the Planck mass. The equilibrium against Coulomb repulsion originates now from the combined effect of the screening of the relativistic electrons, of the surface tension due to strong interactions, and of the gravitational interaction of these massive cores.

By enforcing the condition of β -equilibrium, it has been also obtained a generalization to the relation between the mass number A and atomic number N_p which encompasses phenomenological expressions (see App. A.1 and A.4 for details).

All these considerations have been made for an isolated core with constant proton density whose boundary has been sharply defined by a step function. No external forces are exerted. Consequently, the Fermi energy of the electrons has been assumed to be equal to zero.

Different aspects concerning these macroscopic systems have been also considered. For instance, the analysis of the electron distribution around such cores in both the case of global charge neutrality and the case of not global charge neutrality has been presented (see e.g. App. A.5).

The assumption of a sharp proton density profile has been relaxed and, consequently, a smooth surface modeled by a Woods-Saxon-like proton distribution has been introduced (see App. A.6 for details). The presence of overcritical electric fields close to their surface has been confirmed also in this more general case.

The classical and semi-classical energy states of relativistic electrons bounded by a massive and charged core with the charge-mass-ratio Q/M and macroscopic radius R_c are discussed (see App. A.7). It is shown that the energies of semi-classical (bound) states can be much smaller than the negative electron mass-energy ($-mc^2$), and thus energy-level crossing to negative energy continuum occurs. It has been then advanced the possibility that in neutral cores with equal proton and electron number, the configuration of relativistic electrons in these semi-classical (bound) states should be stabilized by photon emission.

Another topic of current interest concerns the case of rotating nuclear matter cores of stellar dimensions. The induced magnetic field by electric field rotation has been recently obtained (see App. A.8). Such analysis has been done in the framework of classical electrodynamics under the assumption of uniform rigid rotation of the macroscopic nuclear cores in the non-compressed case. For a period of rotation ~ 10 ms, overcritical magnetic fields has been obtained near the surface of the configuration.

The existence of the scaling laws of the ultrarelativistic Thomas-Fermi equation (see App. A.1) has led to the very exciting possibility of having macroscopic configurations of nuclear matter in β -equilibrium exhibiting strong electric fields on their surfaces. In order to go one step further towards a more realistic description of macroscopic configurations as white-dwarfs and neutron stars, further improvements and extensions must be applied to the starting model.

It is therefore interesting, in order to approach both the complex problem of a neutron star core and its interface with the neutron star crust and the problem of the equilibrium of gas in a white dwarf taking into account all possible global electromagnetic interactions between the nucleus and the relativistic electrons, to extend the model to the compressed case in which the Fermi energy of electrons turns to be positive.

The analysis of globally neutral and compressed configurations composed by a nucleus made of relativistic degenerate neutrons and protons surrounded by relativistic degenerate electrons in β -equilibrium has been recently accomplished. This work has generalized the Feynman-Metropolis-Teller treatment of compressed atoms to relativistic regimes, and the concept of compressed nuclear matter cores of stellar dimensions has been introduced (see App. A.2 for details).

In the relativistic generalization of the Feynman-Metropolis-Teller approach, the equation to be integrated is the relativistic Thomas-Fermi equation. The integration of this equation does not admit any regular solution for a point-like nucleus and both the nuclear radius and the nuclear composition have necessarily to be taken into account. This introduces a fundamental difference from the non-relativistic Thomas-Fermi model where a point-like nucleus was adopted.

Due to the introduction of the concept of Wigner-Seitz cells, the study of degenerate compressed matter in white dwarfs can be addressed. This problem presents, still today, open issues of great interest such as the equilibrium of the electron gas and the associated nuclear component, taking into account the electromagnetic, the gravitational and the weak interactions formulated in a correct special and general relativistic framework.

A complete analysis of the properties of such configurations as a function of the compression can be duly done through the relativistic generalization of the Feynman-Metropolis-Teller approach (see App. A.2 for details). It is then possible to derive a consistent equation of state for compressed matter which generalizes both the uniform free-electron fluid approximation, adopted for instance by Chandrasekhar (1931b) in his famous treatment of white-dwarfs, and the well-known work of Salpeter (1961) which describes the electro-dynamical and relativistic effects by a sequence of approximations. Apart from taking into account all possible electromagnetic and special relativistic corrections to the equation of state of white-dwarf matter, the new equation of state, which incorporates the β -equilibrium condition, leads to a self-consistent cal-

ulation of the onset for inverse β -decay of a given nuclear composition as function of the Fermi energy of electrons or equivalently, as a function of the density of the system, which is very important for the analysis of the stability of white dwarfs against gravitational collapse (see App. B.1).

In neutron star cores, nuclear matter is under very extreme conditions of density and pressure. The importance of the strong interactions between nucleons at such extreme pressures it has been known for years (see e.g. Cameron (1970); Shapiro and Teukolsky (1983)). However, due to the absence of a complete theory of the strong interactions, and due to the impossibility of performing terrestrial experiments with similar extreme pressure-density conditions, the equation of state of nuclear matter at densities larger than the nuclear saturation density $\sim 2.7 \times 10^{14} \text{ g/cm}^3$, is still today unknown.

The construction of nuclear equations of state within a fully consistent formulation of the equations of equilibrium in general relativity both for white dwarfs and neutron stars (see below) is an active topic of research within our group. In the recent past, some Ph. D. Theses have been devoted to this topic e.g. the doctoral works of J. Rueda and D. Pugliese. Currently, such a topic is being covered by the Ph. D. works of R. Belvedere, K. Boshkayev, M. Haney, S. Martins de Carvalho, C. Arguëlles, Y. Bin and J. Pereira. We summarized these activities below.

3.2. White Dwarf Physics and Astrophysics

A branch of research which is currently under continuous evolution corresponds to the extension to the case of general relativity, all the previous theory about the Thomas-Fermi model and the relativistic Thomas-Fermi model, applied initially to the study of heavy nuclei, superheavy nuclei as well as to the theoretical hypothesis of nuclear matter cores of stellar dimensions. The aim is to construct a self-consistent theory of self-gravitating systems obeying relativistic quantum statistics, electromagnetic, weak and strong interactions in the framework of general relativity, from which it is possible to study the properties of compact objects e.g. white dwarfs and neutron stars.

The recent generalization of the Feynman-Metropolis-Teller treatment to relativistic regimes, which led to a new equation of state of white-dwarf matter (see App. A.2), has been recently used to construct equilibrium configurations of white-dwarfs in general relativity (see App. B.1).

The description of the inverse β -decay within the relativistic Feynman-Metropolis-Teller equation of state in conjunction with general relativity, leads to a self-consistent calculation of the critical mass of white-dwarfs (see App. B.1 for details). The numerical value of the mass, of the radius, and of the critical mass of white-dwarfs turn to be smaller with respect to the ones obtained with approximate equations of state (see e.g. Hamada and Salpeter (1961)). Therefore, the analysis of compressed atoms following the relativistic-

tic Feynman-Metropolis-Teller treatment has important consequences in the determination of the mass-radius relation of white dwarfs, leading to the possibility of a direct confrontation of these results with observations, in view of the current great interest for the cosmological implications of the type Ia supernovae.

The generalization of the above general relativistic theory of white dwarfs to the case of rotation is part of the thesis work of K. Boshkayev, see App. B.2 for details. The entire family of uniformly rotating stable white dwarfs has been already obtained by studying the mass-shedding, the inverse β -decay, as well as the axisymmetric instabilities. Both the maximum mass and the minimum(maximum) rotation period(frequency) have been obtained for selected nuclear compositions. This work is relevant for the theory of type Ia supernovae as well as for the recent proposal of describing the Soft-Gamma-Ray Repeaters (SGRs) and the Anomalous X-Ray Pulsars (AXPs) as rotation powered white dwarfs, see App. B.3.

SGRs and AXPs are a class of compact objects that show interesting observational properties: rotational periods in the range $P \sim (2-12)$ s, a narrow range with respect to the wide range of ordinary pulsars $P \sim (0.001-10)$ s; spin-down rates $\dot{P} \sim (10^{-13}-10^{-10})$, larger than ordinary pulsars $\dot{P} \sim 10^{-15}$; strong outburst of energies $\sim (10^{41}-10^{43})$ erg, and for the case of SGRs, giant flares of even large energies $\sim (10^{44}-10^{47})$ erg, not observed in ordinary pulsars.

The recent observation of SGR 0418+5729 with a rotational period of $P = 9.08$ s, an upper limit of the first time derivative of the rotational period $\dot{P} < 6.0 \times 10^{-15}$, and an X-ray luminosity of $L_X = 6.2 \times 10^{31}$ erg/s, promises to be an authentic Rosetta Stone, a powerful discriminant for alternative models of SGRs and AXPs. The loss of rotational energy of a neutron star with this spin-down rate \dot{P} cannot explain the X-ray luminosity of SGR 0418+5729, excluding the possibility of identifying this source as an ordinary spin-down powered pulsar. The inferred upper limit of the surface magnetic field of SGR 0418+5729 $B < 7.5 \times 10^{12}$ G, describing it as a neutron star within the magnetic braking scenario, is well below the critical field challenging the power mechanism based on magnetic field decay purported in the magnetar scenario.

We have shown that the observed upper limit on the spin-down rate of SGR 0418+5729 is, instead, perfectly in line with a model based on a massive fast rotating highly magnetized white dwarf of mass $M = 1.4M_\odot$, radius $R = 10^3$ km, and moment of inertia $I \approx 10^{49}$ g cm². We analyze the energetics of all SGRs and AXPs including their outburst activities and show that they can be well explained through the change of rotational energy of the white dwarf associated to the observed sudden changes of the rotational period, the glitches. All SGRs and AXPs can be interpreted as rotating white dwarfs that generate their energetics from the rotational energy and therefore there is no need to invoke the magnetic field decay of the magnetar model. Details

can be found in App. B.3.

3.3. Neutron Star Physics and Astrophysics

Concerning neutron stars, most of effort have been given to the construction of self-consistent solutions of the equations of equilibrium for neutron stars in general relativity taking into account the traditionally neglected electromagnetic interaction. In nearly all the scientific literature on neutron stars, a “local approach”, where the equation of state of neutron star matter is constructed ignoring global gravitational and Coulombian effects by assuming not only flat space but also local charge neutrality, has been traditionally used. The gravitational effects are then taken into account by embedding such an equation of state into the TOV equations of hydrostatic equilibrium.

We have introduced a new approach which thanks to the existence of scaling laws can apply to compressed atoms as well as to massive nuclear matter cores of stellar dimensions. This approach on the compressed atom has already given a new contribution in the study of white dwarfs. It represents the first self-consistent calculation taking into due account the electromagnetic contribution in a relativistic treatment of the Thomas-Fermi equation, within global formulation of the equilibrium of white dwarfs in general relativity.

The application of the above results to the case of neutron stars is much more complex and it has been approached stepwise. As a first step we have considered the application of this novel approach to the case of a system of neutrons, protons, and electrons in β -equilibrium at zero temperatures within general relativity (see App. C.1). The crucial role of the generalized Fermi energy of particles, for short Klein potentials, and their constancy on the entire equilibrium configuration has been outlined. Such a solution, although does not represent a realistic model for a neutron star, contains all the essential physics of the phenomenon of gravito-polarization in neutron star interiors: the existence of an electric potential and consequently an electric field over the entire configuration has been there evidenced.

We have there proved, for the case of this simplified example where strong interactions are neglected, that the traditional approach of describing the system imposing the condition of local charge neutrality and solving the corresponding TOV equations is conceptually inconsistent. We have then substitute the condition of local charge neutrality with the condition of global charge neutrality and derived the correct equations within the Einstein-Maxwell-Thomas-Fermi system. The boundary conditions are also different from a traditional Cauchy data with the values of the functions and first derivatives at the center into a boundary condition at the center and delicate eigenvalue problem at the boundary determining the condition of charge neutrality at the border (see App. C.1). The conceptual differences and the alternative

mathematical equations of the two approaches, the ones imposing local versus global charge neutrality, lead to the presence of additional electro-dynamical global structures. However, in this specific simple example, they do not give significant quantitative differences in the mass-radius relation for the equilibrium configurations. A very different situation occurs when strong interactions are also taken into account.

The next step has been to introduce self-consistently the strong interactions in the construction of the equilibrium configurations. We have indeed recently generalized the Einstein-Maxwell-Thomas-Fermi equations to the case of strong interactions, see App. C.2 for details. There the major aim has been to prove the constancy of the Klein potentials in the case in which the nuclear interactions are described by a Lagrangian including in addition to the gravitational, electromagnetic, and weak interactions, also the presence of σ , ω , and ρ virtual mesons that mediate the nuclear interactions.

We have also extended to finite temperatures the theoretical treatment of gravito-polarization for a system of neutrons, protons and electrons in β -equilibrium, taking into account strong interactions modeled through the exchange of σ , ω and ρ virtual mesons (see App. C.3 for details). The crucial role of the Klein potentials of particles is outlined as well as the condition of isothermality of Tolman. We have shown that, the gravito-polarization effect although energetically much weaker than the corresponding gravitational and thermal effects, do survive in the case of finite temperatures. Their role, when strong interactions are considered, is of fundamental astrophysical importance.

Many interesting aspects of the physics and astrophysics of neutron stars are the research topic of the Ph. D. thesis of R. Belvedere and were part of the Ph. D. thesis of D. Pugliese. The construction of realistic neutron star with core and crust satisfying global (but not local) charge neutrality has been already accomplished (see App. C.4). The solutions lead to a new structure of the star: a positively charged core at supranuclear densities surrounded by an electronic distribution of thickness $\sim \hbar/(m_e c) \sim 10^2 \hbar/(m_\pi c)$ of opposite charge, as well as a neutral crust at lower densities. Inside the core there is a Coulomb potential well of depth $\sim m_\pi c^2/e$. The constancy of the Klein potentials in the transition from the core to the crust, impose the presence of an overcritical electric field $\sim (m_\pi/m_e)^2 E_c$. For each central density, an entire family of core-crust interface boundaries can be constructed, each of them reaching the neutrality point at a different electron density at the edge of the crust. This leads consequently to crusts with masses and thickness smaller than the ones obtained from the traditional TOV treatment, resulting in a novel neutron star mass-radius relation.

Additional details from some other works we have published on this subject can be also found in Apps. C.5–C.9.

The entire formulation of the equilibrium equations of rotating neutron stars as well as their numerical integration are part of the K. Boshkayev's

Ph. D. thesis. M. Haney is studying the problem of the matching conditions between the core and the crust of neutron stars taking into account the novel electrodynamical structure described by the Einstein-Maxwell-Thomas-Fermi equations. This work implies also the generalization of the well-known Hartle & Thorne method for the construction of rotating stars, in order to allow the presence of the Coulomb potential and density discontinuities. As a by product, also the pulsational modes of these neutron star configurations with strong electric fields in the core-crust boundary can be duly analyzed.

S. Martins de Carvalho is working on the influence of the temperature on the properties of the core and the crust of these novel neutron star equilibrium configurations. The traditional study of neutron star cooling has been generally applied to quite old objects as the Crab Pulsar (957 years) or the Central Compact Object in Cassiopeia A (330 years) with an observed surface temperature $\sim 10^6$ K. However, recent observations of the late ($t = 10^8$ – 10^9 s) emission of Supernovae associated to GRBs (GRB-SN) show a distinctive emission in the X-ray regime consistent with temperatures $\sim 10^7$ – 10^8 K. Similar features have been also observed in two Type Ic Supernova SN 2002ap and SN 1994I not associated to GRBs. We have recently advanced the possibility that such a late X-ray emission observed in GRB-SN and in isolated SN is associated to a hot neutron star just formed in the Supernova event, what we have defined as a *neo-neutron star* (see App. C.10 for details). The traditional thermal processes taking place in the neutron star crust might be enhanced by the extreme high temperature conditions of neo-neutron star and therefore the study of the thermal behavior especially of the crust of neo-neutron stars deserve the appropriate attention.

4. Publications (before 2010)

4.1. Refereed Journals

1. R. Ruffini, M. Rotondo and S.-S. Xue, *Electrodynamics for Nuclear Matter in Bulk*, International Journal of Modern Physics D **16**, 1 (2007).

A general approach to analyze the electrodynamics of nuclear matter in bulk is presented using the relativistic Thomas-Fermi equation generalizing to the case of $N \simeq (m_{\text{Planck}}/m_n)^3$ nucleons of mass m_n the approach well tested in very heavy nuclei ($Z \simeq 10^6$). Particular attention is given to implement the condition of charge neutrality globally on the entire configuration, versus the one usually adopted on a microscopic scale. As the limit $N \simeq (m_{\text{Planck}}/m_n)^3$ is approached the penetration of electrons inside the core increases and a relatively small tail of electrons persists leading to a significant electron density outside the core. Within a region of 10^2 electron Compton wavelength near the core surface electric fields close to the critical value for pair creation by vacuum polarization effect develop. These results can have important consequences on the understanding of physical process in neutron stars structures as well as on the initial conditions leading to the process of gravitational collapse to a black hole.

2. R. Ruffini and L. Stella, *Some comments on the relativistic Thomas-Fermi model and the Vallarta-Rosen equation*, Physics Letters B **102**, 442 (1981).

Some basic differences between the screening of the nuclear charge due to a relativistic cloud of electrons in a neutral atom and the screening due to vacuum polarization effects induced by a superheavy ion are discussed.

3. J. Ferreira, R. Ruffini and L. Stella, *On the relativistic Thomas-Fermi model*, Physics Letters B **91**, 314 (1980).

The relativistic generalization of the Thomas-Fermi model of the atom is derived. It approaches the usual nonrelativistic equation in the limit $Z \ll Z_{\text{crit}}$, where Z is the total number of electrons of the atom and $Z_{\text{crit}} = (3\pi/4)^{1/2} \alpha^{-3/2}$ and α is the fine structure constant. The new equation leads to the breakdown of scaling laws and to the appearance of a critical charge, purely as a consequence of relativistic effects. These results are compared and contrasted with those corresponding to N self-gravitating degenerate relativistic fermions, which for $N \approx N_{\text{crit}} = (3\pi/4)^{1/2} (m/m_p)^3$ give rise to the concept of

a critical mass against gravitational collapse. Here m is the mass of the fermion and $m_p = (\hbar c/G)^{1/2}$ is the Planck mass.

4.2. Conference Proceedings

1. R. Ruffini, M. Rotondo and S.-S. Xue, *Neutral nuclear core vs super charged one*, Proceedings of the 11th Marcel Grossmann Meeting, Eds. R. Jantzen, H. Kleinert, R. Ruffini, World Scientific, Singapore (2008).

Based on the Thomas-Fermi approach, we describe and distinguish the electron distributions around extended nuclear cores: (i) in the case that cores are neutral for electrons bound by protons inside cores and proton and electron numbers are the same; (ii) in the case that super charged cores are bare, electrons (positrons) produced by vacuum polarization are bound by (fly into) cores (infinity).

2. B. Patricelli, M. Rotondo and R. Ruffini, *On the Charge to Mass Ratio of Neutron Cores and Heavy Nuclei*, AIP Conference Proceedings **966**, 143–146 (2008).

We determine theoretically the relation between the total number of protons N_p and the mass number A (the charge to mass ratio) of nuclei and neutron cores with the model recently proposed by Ruffini et al. (2007) and we compare it with other N_p versus A relations: the empirical one, related to the Periodic Table, and the semi-empirical relation, obtained by minimizing the Weizsäcker mass formula. We find that there is a very good agreement between all the relations for values of A typical of nuclei, with differences of the order of per cent. Our relation and the semi-empirical one are in agreement up to $A \approx 10^4$ for higher values, we find that the two relations differ. We interpret the different behavior of our theoretical relation as a result of the penetration of electrons (initially confined in an external shell) inside the core, that becomes more and more important by increasing A ; these effects are not taken into account in the semi-empirical mass-formula.

3. M. Rotondo, R. Ruffini and S.-S. Xue, *On the Electrodynamical properties of Nuclear matter in bulk*, AIP Conference Proceedings **966**, 147–152 (2008).

We analyze the properties of solutions of the relativistic Thomas-Fermi equation for globally neutral cores with radius of the order of $R \approx 10$ Km, at constant densities around the nuclear density. By using numerical techniques as well as well tested analytic procedures developed in the study of heavy ions, we confirm the existence of an electric field close to the critical value $E_c = m_e^2 c^3 / e \hbar$ in a shell $\Delta R \approx 10^4 \hbar / m_\pi c$ near the core surface. For a core of ≈ 10 Km the difference in binding energy reaches 10^{49} ergs. These results can be of interest for the understanding of very heavy nuclei as well as physics of

neutron stars, their formation processes and further gravitational collapse to a black hole.

4. B. Patricelli, M. Rotondo, J. A. Rueda H. and R. Ruffini, *The Electrodynamics of the Core and the Crust components in Neutron Stars*, AIP Conference Proceedings **1059**, 68–71 (2008).

We study the possibility of having a strong electric field (E) in Neutron Stars. We consider a system composed by a core of degenerate relativistic electrons, protons and neutrons, surrounded by an oppositely charged leptonic component and show that at the core surface it is possible to have values of E of the order of the critical value for electron-positron pair creation, depending on the mass density of the system. We also describe Neutron Stars in general relativity, considering a system composed by the core and an additional component: a crust of white dwarf - like material. We study the characteristics of the crust, in particular we calculate its mass M_{crust} . We propose that, when the mass density of the star increases, the core undergoes the process of gravitational collapse to a black hole, leaving the crust as a remnant; we compare M_{crust} with the mass of the baryonic remnant considered in the fireshell model of GRBs and find that their values are compatible.

5. R. Ruffini, *The Role of Thomas-Fermi approach in Neutron Star Matter*, Proceedings of the 9th International Conference "Path Integrals-New trends and perspectives", Eds. W. Janke and A. Pelster, World Scientific, Singapore (2008).

The role of the Thomas-Fermi approach in Neutron Star matter cores is presented and discussed with special attention to solutions globally neutral and not fulfilling the traditional condition of local charge neutrality. A new stable and energetically favorable configuration is found. This new solution can be of relevance in understanding unsolved issues of the gravitational collapse processes and their energetics.

6. R. Ruffini, M. Rotondo, S.-S. Xue, *The Thomas-Fermi Approach and Gamma-Ray Bursts*, AIP Conference Proceedings **1053**, 243-252 (2008).

The energy extraction process from a black hole which is considered at the basis of modeling Gamma-Ray Bursts appear to be mediated by an electron-positron plasma created in an overcritical electric field. The role of the Thomas-Fermi approach in Neutron Star matter cores is presented and discussed with special attention to solutions globally neutral and not fulfilling the traditional condition of local charge neutrality. A new stable configuration is found with a field well above the critical value, confined to a shell close to the surface with a thickness of a few electron Compton wavelength. This new solution can be of relevance in understanding unsolved issues of the gravitational collapse processes and their energetics leading to the formation of a Kerr-Newman black hole.

7. Jorge A. Rueda, B. Patricelli, M. Rotondo, R. Ruffini, and S. S. Xue, *The Extended Nuclear Matter Model with Smooth Transition Surface*, Proceedings of the Third Stueckelberg Workshop on Relativistic Field Theories, Pescara-Italy (2008).

The existence of electric fields close to their critical value $E_c = m_e^2 c^3 / (e\hbar)$ has been proved for massive cores of 10^7 up to 10^{57} nucleons using a proton distribution of constant density and a sharp step function at its boundary. We explore the modifications of this effect by considering a smoother density profile with a proton distribution fulfilling a Woods-Saxon dependence. The occurrence of a critical field has been confirmed. We discuss how the location of the maximum of the electric field as well as its magnitude is modified by the smoother distribution.

5. Publications (2010-2011)

5.1. Refereed Journals

1. R. Belvedere, D. Pugliese, Jorge A. Rueda, R. Ruffini, and S.-S. Xue, *Neutron star equilibrium configurations within a fully relativistic theory with strong, weak, electromagnetic, and gravitational interactions*, submitted to Nuclear Physics A.

We formulate the equations of equilibrium of neutron stars taking into account strong, weak, electromagnetic, and gravitational interactions within the framework of general relativity. The nuclear interactions are described by the exchange of the σ , ω , and ρ virtual mesons. The equilibrium conditions are given by our recently developed theoretical framework based on the Einstein-Maxwell-Thomas-Fermi equations along with the constancy of the general relativistic Fermi energies of particles, the “Klein potentials”, throughout the configuration. The equations are solved numerically in the case of zero temperatures and for selected parameterizations of the nuclear models. The solutions lead to a new structure of the star: a positively charged core at supranuclear densities surrounded by an electronic distribution of thickness $\sim \hbar/(m_e c) \sim 10^2 \hbar/(m_\pi c)$ of opposite charge, as well as a neutral crust at lower densities. Inside the core there is a Coulomb potential well of depth $\sim m_\pi c^2/e$. The constancy of the Klein potentials in the transition from the core to the crust, impose the presence of an overcritical electric field $\sim (m_\pi/m_e)^2 E_c$, the critical field being $E_c = m_e^2 c^3/(e\hbar)$. The electron chemical potential and the density decrease, in the boundary interface, until values $\mu_e^{\text{crust}} < \mu_e^{\text{core}}$ and $\rho_{\text{crust}} < \rho_{\text{core}}$. For each central density, an entire family of core-crust interface boundaries and, correspondingly, an entire family of crusts with different mass and thickness, exist. The configuration with $\rho_{\text{crust}} = \rho_{\text{drip}} \sim 4.3 \times 10^{11} \text{ g/cm}^3$ separates neutron stars with and without inner crust. We present here the novel neutron star mass-radius for the especial case $\rho_{\text{crust}} = \rho_{\text{drip}}$ and compare and contrast it with the one obtained from the traditional Tolman-Oppenheimer-Volkoff treatment.

2. M. Rotondo, Jorge A. Rueda, R. Ruffini, and S.-S. Xue, *On the constitutive equations of a self-gravitating system of neutrons, protons and electrons in β -equilibrium at finite temperatures*, submitted to Physical Review D.

The relativistic Thomas-Fermi equation has been the essential theoretical tool to generalize the Feynman-Metropolis-Teller treatment of compressed atoms,

crucial for a complete general relativistic description of white dwarfs. These equations appear to be equally important to the analysis of neutron stars where the treatment leads to a generalization of the classical work on gravito-polarization. Such a treatment becomes considerably more difficult than the Newtonian one and the general relativistic treatment for neutral fermions described by the Tolman-Oppenheimer-Volkoff (TOV) equations. It involves the electrodynamics and general relativistic effects describable by the Einstein-Maxwell system of equations coupled to the general relativistic Thomas-Fermi equations. We extend here to finite temperatures the theoretical treatment of gravito-polarization for a system of neutrons, protons and electrons in β -equilibrium, taking into account strong interactions modeled through the exchange of σ , ω and ρ virtual mesons. The crucial role of the Klein potentials of particles is outlined as well as the condition of isothermality of Tolman. The gravito-polarization effect, although energetically much weaker than the corresponding gravitational and thermal effects, do survive in the case of finite temperatures. Their role, when strong interactions are considered, is of fundamental astrophysical importance.

3. M. Malheiro, Jorge A. Rueda, and R. Ruffini, *SGRs and AXPs as rotation powered massive white dwarfs*, submitted to Publications of the Astronomical Society of Japan.

The recent observations of SGR 0418+5729 offer an authentic Rosetta Stone for deciphering the energy source of Soft Gamma Ray Repeaters (SGRs) and Anomalous X-ray Pulsars (AXPs). The main contention is to determine if SGRs and AXPs are strongly magnetized neutron stars originating their energy from the decay of overcritical magnetic fields in the magnetar model or if instead their energetics can be explained by using the rotational energy loss of a massive white dwarf. We show how a consistent model for SGRs and AXPs can be expressed in terms of canonical physics and astrophysics within rotation powered white dwarfs in total analogy with the case of pulsars originating their energy from the rotational energy of the neutron stars. The pioneering works of M. Morini et al. (1988) and of B. Paczynski (1990) on 1E 2259+586 are extended and further developed to describe the observed properties of SGRs and AXPs by assuming spin-down powered massive, fast rotating, and highly magnetized white dwarfs. We show that SGR 0418+5729 is well described by a spin-down powered white dwarf and, within such a model, we obtain the theoretical prediction for the lower limit of its spin-down rate, $\dot{P} \geq L_X P^3 / (4\pi^2 I) = 1.18 \times 10^{-16}$ where I is the moment of inertia of the white dwarf. We also analyze the energetics of SGRs and AXPs including their outburst activities and show that they can be well explained through the change of rotational energy of the white dwarf associated to the observed sudden changes of the rotational period, the glitches. All SGRs and AXPs can be interpreted as rotating white dwarfs that generate their energetics from the rotational energy and therefore there is no need to invoke the magnetic field

decay of the magnetar model. The important observational campaigns carried out by the X-ray Japanese satellite Suzaku on AE Aquarii as well as the corresponding theoretical work by Japanese groups and recent results of the Hubble Space Telescope, give crucial information for our theoretical model. Follow-on missions of Hubble Telescope and VLT are highly recommended.

4. K. Boshkayev, Jorge A. Rueda, and R. Ruffini, *On the maximum mass and minimum period of general relativistic uniformly rotating white dwarfs*, submitted to *Astrophysical Journal Letters*.

The properties of rotating white dwarfs are analyzed within the framework of general relativity. The Hartle's formalism is applied to construct self-consistently the internal and external solutions to the Einstein equations. Within this formalism the mass, the radius, the angular momentum, the eccentricity and quadrupole moment of rotating white dwarfs have been calculated as a function of both the central density and angular velocity of the star. The mass-shedding limit, the inverse β -decay as well as the axisymmetric instabilities are used to establish the minimum rotation period and the maximum mass of uniformly rotating white dwarfs. These results are relevant both for the theory of delayed type Ia supernovae explosions as well as for the white dwarf model of Soft Gamma-Ray Repeaters and Anomalous X-Ray Pulsars.

5. R. Negreiros, C. Bianco, Jorge A. Rueda, and Remo Ruffini, *Cooling of young neutron stars in GRB associated to SN*, *Astronomy & Astrophysics*, to appear.

The traditional study of neutron star cooling has been generally applied to quite old objects as the Crab Pulsar (957 years) or the Central Compact Object in Cassiopeia A (330 years) with an observed surface temperature $\sim 10^6$ K. However, recent observations of the late ($t = 10^8$ – 10^9 s) emission of Supernovae associated to GRBs (GRB-SN) show a distinctive emission in the X-ray regime consistent with temperatures $\sim 10^7$ – 10^8 K. Similar features have been also observed in two Type Ic Supernova SN 2002ap and SN 1994I not associated to GRBs. We advance the possibility that the late X-ray emission observed in GRB-SN and in isolated SN is associated to a hot neutron star just formed in the Supernova event, here defined as a neo-neutron star. We discuss the thermal evolution of neo-neutron stars in the age regime that spans from ~ 1 minute (just after the proto-neutron star phase) all the way up to ages < 10 – 100 yr. We examine critically the key factor governing the neo-neutron star cooling with special emphasis on the neutrino emission by introducing a phenomenological heating source as well as new boundary conditions in order to mimic the high temperature of the atmosphere for young neutron stars. We match the neo-neutron star luminosity to the observed late X-ray emission of the GRB-SN events: URCA-1 in GRB980425-SN1998bw, URCA-2 in GRB030329-SN2003dh, and URCA-3 in GRB031203-SN2003lw, and identify the major role played by

the neutrino emissivity in the thermal evolution of neo-neutron stars. By calibrating our additional heating source at early times to $\sim 10^{12}$ – 10^{15} erg/g/s, we find a striking agreement of the luminosity obtained from the cooling of a neo-neutron stars with the prolonged ($t = 10^8$ – 10^9 s) X-ray emission observed in GRB associated with Supernova. It is therefore appropriate a revision of the boundary conditions usually used in the thermal cooling theory of neutron stars, in order to match the proper conditions of the atmosphere at young ages. The traditional thermal processes taking place in the crust might be enhanced by the extreme high temperature conditions of neo-neutron star. Additional heating processes yet not studied within this context, e.g. e^+e^- pair creation by overcritical fields and nuclear fusion and fission energy release, might also take place under such conditions and deserve further analysis. The observation of GRB-SN has evidenced the possibility of witnessing the thermal evolution of neo-neutron stars. A new campaign of dedicated observations both of GRB-SN and of isolated Type Ic SN is recommended.

6. K. Boshkayev, Jorge A. Rueda, and R. Ruffini, *On the critical mass of uniformly rotating white dwarfs in general relativity*, International Journal of Modern Physics E, to appear.

The properties of uniformly rotating white dwarfs are analyzed within the framework of general relativity. Hartle's formalism is applied to construct self-consistently the internal and external solutions to the Einstein equations. The mass, the radius, the moment of inertia and quadrupole moment of rotating white dwarfs have been calculated as a function of both the central density and rotation period of the star. The maximum mass of rotating white dwarfs for stable configurations has been obtained.

7. Jorge A. Rueda, and R. Ruffini, *Towards a relativistic Thomas-Fermi theory of white dwarfs and neutron stars*, International Journal of Modern Physics E, to appear.

We summarize recent progress in the formulation of a theory for white dwarfs and neutron stars based on the general relativistic Thomas-Fermi equations of equilibrium.

8. R. Belvedere, Jorge A. Rueda, and R. Ruffini, *Mass, radius and moment of inertia of neutron stars*, International Journal of Modern Physics E, to appear.

We construct the ground-state equilibrium configurations of neutron star cores. The system of equilibrium equations, taking into account quantum statistics, electro-weak, and strong interactions, is formulated within the framework of general relativity both in the rotating and non-rotating spherically symmetric case. The core is assumed to be composed of interacting degenerate neutrons, protons and electrons in beta equilibrium. The strong interaction between nucleons is mediated by the sigma-omega-rho virtual mesons. The mass-radius

relation for neutron star cores is obtained for various parametrizations of the nuclear model. The equilibrium conditions are given by our recently developed theoretical framework based on the Einstein-Maxwell-Thomas-Fermi equations along with the constancy of the general relativistic Fermi energies of particles, the “Klein potentials”, throughout the configuration. These equations are here solved numerically in the case of zero temperatures and for selected parameterizations of the nuclear model. We present here the new neutron star mass-radius relation.

9. Jorge A. Rueda, R. Ruffini, and S.-S. Xue, *The Klein first integrals in an equilibrium system with electromagnetic, weak, strong and gravitational interactions*, Nuclear Physics A **872**, 286 (2011).

The isothermal Tolman condition and the constancy of the Klein potentials originally expressed for the sole gravitational interaction in a single fluid are here generalized to the case of a three quantum fermion fluid duly taking into account the strong, electromagnetic, weak and gravitational interactions. The set of constitutive equations including the Einstein-Maxwell-Thomas-Fermi equations as well as the ones corresponding to the strong interaction description are here presented in the most general relativistic isothermal case. This treatment represents an essential step to correctly formulate a self-consistent relativistic field theoretical approach of neutron stars.

10. M. Rotondo, Jorge A. Rueda, R. Ruffini, and S.-S. Xue, *The self-consistent general relativistic solution for a system of degenerate neutrons, protons and electrons in β -equilibrium*, Physics Letters B **701**, 667–671 (2011).

We present the self-consistent treatment of the simplest, nontrivial, self-gravitating system of degenerate neutrons, protons and electrons in β -equilibrium within relativistic quantum statistics and the Einstein-Maxwell equations. The impossibility of imposing the condition of local charge neutrality on such systems is proved, consequently overcoming the traditional Tolman-Oppenheimer-Volkoff treatment. We emphasize the crucial role of imposing the constancy of the generalized Fermi energies. A new approach based on the coupled system of the general relativistic Thomas-Fermi-Einstein-Maxwell equations is presented and solved. We obtain an explicit solution fulfilling global and not local charge neutrality by solving a sophisticated eigenvalue problem of the general relativistic Thomas-Fermi equation. The value of the Coulomb potential at the center of the configuration is $eV(0) \sim m_\pi c^2$ and the system is intrinsically stable against Coulomb repulsion in the proton component. This approach is necessary, but not sufficient, when strong interactions are introduced.

11. M. Rotondo, Jorge A. Rueda, R. Ruffini, and S.-S. Xue, *Relativistic Feynman-Metropolis-Teller theory for white dwarfs in general relativity*, Physical Review D **84**, 084007 (2011).

The recent formulation of the relativistic Thomas-Fermi model within the Feynman-Metropolis-Teller theory for compressed atoms is applied to the study of general relativistic white dwarf equilibrium configurations. The equation of state, which takes into account the β -equilibrium, the nuclear and the Coulomb interactions between the nuclei and the surrounding electrons, is obtained as a function of the compression by considering each atom constrained in a Wigner-Seitz cell. The contribution of quantum statistics, weak, nuclear, and electromagnetic interactions is obtained by the determination of the chemical potential of the Wigner-Seitz cell. The further contribution of the general relativistic equilibrium of white dwarf matter is expressed by the simple formula $\sqrt{g_{00}}\mu_{ws} = \text{constant}$, which links the chemical potential of the Wigner-Seitz cell μ_{ws} with the general relativistic gravitational potential g_{00} at each point of the configuration. The configuration outside each Wigner-Seitz cell is strictly neutral and therefore no global electric field is necessary to warranty the equilibrium of the white dwarf. These equations modify the ones used by Chandrasekhar by taking into due account the Coulomb interaction between the nuclei and the electrons as well as inverse β -decay. They also generalize the work of Salpeter by considering a unified self-consistent approach to the Coulomb interaction in each Wigner-Seitz cell. The consequences on the numerical value of the Chandrasekhar-Landau mass limit as well as on the mass-radius relation of ${}^4\text{He}$, ${}^{12}\text{C}$, ${}^{16}\text{O}$ and ${}^{56}\text{Fe}$ white dwarfs are presented. All these effects should be taken into account in processes requiring a precision knowledge of the white dwarf parameters.

12. M. Rotondo, Jorge A. Rueda, R. Ruffini, and S.-S. Xue, *Relativistic Thomas-Fermi treatment of compressed atoms and compressed nuclear matter cores of stellar dimensions*, Physical Review C **83**, 045805 (2011).

The Feynman, Metropolis and Teller treatment of compressed atoms is extended to the relativistic regimes. Each atomic configuration is confined by a Wigner-Seitz cell and is characterized by a positive electron Fermi energy. The non-relativistic treatment assumes a point-like nucleus and infinite values of the electron Fermi energy can be attained. In the relativistic treatment there exists a limiting configuration, reached when the Wigner-Seitz cell radius equals the radius of the nucleus, with a maximum value of the electron Fermi energy $(E_e^F)_{max}$, here expressed analytically in the ultra-relativistic approximation. The corrections given by the relativistic Thomas-Fermi-Dirac exchange term are also evaluated and shown to be generally small and negligible in the relativistic high density regime. The dependence of the relativistic electron Fermi energies by compression for selected nuclei are compared and contrasted to the non-relativistic ones and to the ones obtained in the uniform approximation. The relativistic Feynman, Metropolis, Teller approach here presented overcomes some difficulties in the Salpeter approximation generally adopted for compressed matter in physics and astrophysics. The treatment is then extrapolated to compressed nuclear matter cores of stellar dimensions

with $A \simeq (m_{\text{Planck}}/m_n)^3 \sim 10^{57}$ or $M_{\text{core}} \sim M_{\odot}$. A new family of equilibrium configurations exists for selected values of the electron Fermi energy varying in the range $0 < E_e^F \leq (E_e^F)_{\text{max}}$. Such configurations fulfill global but not local charge neutrality. They have electric fields on the core surface, increasing for decreasing values of the electron Fermi energy reaching values much larger than the critical value $E_c = m_e^2 c^3 / (e\hbar)$, for $E_e^F = 0$. We compare and contrast our results with the ones of Thomas-Fermi model in strange stars.

13. Jorge A. Rueda, M. Rotondo, R. Ruffini, and S.-S. Xue, *On Compressed Nuclear Matter: from Nuclei to Neutron Stars*, International Journal of Modern Physics D **20**, 1789–1796 (2011).

We address the description of neutron-proton-electron degenerate matter in beta equilibrium subjected to compression both in the case of confined nucleons into a nucleus as well as in the case of deconfined nucleons. We follow a step-by-step generalization of the classical Thomas-Fermi model to special and general relativistic regimes, which leads to a unified treatment of beta equilibrated neutron-proton-electron degenerate matter applicable from the case of nuclei all the way up to the case of white-dwarfs and neutron stars. New gravito-electrodynamical effects, missed in the traditional approach for the description of neutron star configurations, are found as a consequence of the new set of general relativistic equilibrium equations.

14. M. Rotondo, R. Ruffini, S.-S. Xue, and V. Popov, *On Gravitationally and Electrostatically Bound Nuclear Matter Cores of Stellar Dimensions*, International Journal of Modern Physics D **20**, 1995–2002 (2011).

In a unified treatment we extrapolate results for neutral atoms with heavy nuclei to nuclear matter cores of stellar dimensions with mass numbers $A \approx (m_{\text{Planck}}/m_n)^3 \sim 10^{57}$. We give explicit analytic solutions for the relativistic Thomas-Fermi equation of N_n neutrons, N_p protons and N_e electrons in beta equilibrium, fulfilling global charge neutrality, with $N_p = N_e$. We give explicit expressions for the physical parameters including the Coulomb and the surface energies and we study as well the stability of such configurations. Analogous to heavy nuclei these macroscopic cores exhibit an overcritical electric field near their surface.

15. R. Ruffini and S.-S. Xue, *Electron-positron pairs production in a macroscopic charged core*, Physics Letters B **696**, 416–421 (2011).

Classical and semi-classical energy states of relativistic electrons bounded by a massive and charged core with the charge-mass ratio Q/M and macroscopic radius R_c are discussed. We show that the energies of semi-classical (bound) states can be much smaller than the negative electron mass-energy ($-mc^2$), and energy-level crossing to negative energy continuum occurs. Electron-positron pair production takes place by quantum tunneling, if these bound states are not occupied. Electrons fill into these bound states and positrons go

to infinity. We explicitly calculate the rate of pair-production, and compare it with the rates of electron-positron production by the Sauter-Euler-Heisenberg-Schwinger in a constant electric field. In addition, the pair-production rate for the electro-gravitational balance ratio $Q/M = 10^{-19}$ is much larger than the pair-production rate due to the Hawking processes.

16. Jorge A. Rueda, M. Rotondo, R. Ruffini, and S.-S. Xue, *A self-consistent approach to neutron stars*, Journal of the Korean Physical Society **57**, 560 (2010).

We present a set of equilibrium equations for a self-gravitating system of degenerate neutrons, protons and electrons in beta equilibrium in the framework of relativistic quantum statistics and the Einstein-Maxwell equations. Special emphasis is given to the crucial role of the constancy of the generalized Fermi energy of particles, from which we formulate the general relativistic version of the Thomas-Fermi equation. We discuss briefly the consequences of this approach in the general case of neutron star configurations with a core and a crust.

5.2. Conference Proceedings

1. Jorge A. Rueda, M. Rotondo, R. Ruffini, and S.-S. Xue, *On the relativistic Feynman-Metropolis-Teller equation of state and general relativistic white-dwarfs*, Proceedings of Science, PoS(Texas2010), 269 (2011).

The recently formulation of the relativistic Thomas-Fermi model for compressed atoms is applied to the study of white-dwarf equilibrium configurations in the framework of general relativity. The equation of state is obtained as a function of the compression by considering each atom constrained in a Wigner-Seitz cell and it takes into account the β -equilibrium and the Coulomb interaction between the nuclei and the surrounding electrons. The consequences on the numerical value of the Chandrasekhar-Landau mass limit are presented as well as the modifications to the mass-radius relation for ${}^4\text{He}$ and ${}^{56}\text{Fe}$ white-dwarf equilibrium configurations.

2. D. Pugliese, Jorge A. Rueda, R. Ruffini, and S.-S. Xue, *A general relativistic Thomas-Fermi treatment of neutron star cores*, Proceedings of Science, PoS(Texas 2010), 271 (2011).

We formulate the set of selfconsistent groundstate equilibrium equations for neutron star cores taking into account quantum statistics, electroweak, and strong interactions, within the framework of general relativity. The strong interaction between nucleons is modeled through the sigma omegarho meson exchange in the context of the extended Walecka model, all duly expressed in general relativity. We found the generalization to the works of Klein (1949), of Kodama and Yamada (1972), and of Olson and Baylin (1975) by demonstrating

that the thermodynamic equilibrium condition of the constancy of the Fermi energy of each particlespecie can be properly generalized to include the contribution of all fields. The consequences of these new conditions of equilibrium on the structure of neutron stars are discussed.

3. R. Belvedere, *On the structure of the crust of neutron stars*, Proceedings of Science, PoS(Texas 2010), 270 (2011).

We calculate the mass and the thickness of neutron star crusts corresponding for different neutron star core mass-radius relations. The system of equilibrium equations, taking into account quantum statistics, electro-weak, and strong interactions, is formulated within the framework of general relativity in the non-rotating spherically symmetric case. The core is assumed to be composed of interacting degenerate neutrons, protons and electrons in beta equilibrium. The strong interaction between nucleons is modeled through sigma-omega-rho meson exchange in the context of the extended Walecka model.

4. K. Boshkayev, *On the Stability of Rotating Nuclear Matter Cores of Stellar Dimensions*, Proceedings of Science, PoS(Texas 2010), 275 (2011).

A globally neutral system of stellar dimensions consisting of degenerate neutrons, protons and electrons in beta equilibrium is considered using the ultra-relativistic solution of the Thomas- Fermi equation. Such a system at nuclear density having mass numbers $A \approx 10^{57}$ can exhibit a charge distribution different from zero. The analysis to investigate the magnetic field induced by the rotation of the system as a whole rigid body and its stability is presented in the framework of classical electrodynamics.

5. K. Boshkayev, Jorge A. Rueda, and R. Ruffini, *On the minimum rotational period of fast rotating white dwarfs*, Proceedings of Les Houches workshop "From Nuclei to White Dwarfs to Neutron Stars", Eds. A. Mezzacappa, World Scientific (2011).

The properties of rotating white dwarfs are calculated within the framework of general relativity. Hartle's formalism is applied to construct self-consistently the internal and the external solution to the Einstein equations. Within this formalism we calculate the mass, the radius, the moment of inertia, the eccentricity and quadrupole moment of rotating white dwarfs as a function both of the central density and the rotational period of the star. The minimum rotational period (maximum angular velocity) for stable configurations has been obtained as well as the contribution of rotation to the maximum mass of white dwarfs.

6. K. Boshkayev, M. Rotondo, and R. Ruffini, *On Nuclear Matter Cores and Their Applications*, Astronomical Society of the Pacific Conference Series, to appear.

We review a recent series of articles considering electromagnetic effects in self-gravitating systems of nuclear matter. The results find their explicit application within the theory of neutron stars.

7. D. Bini, K. Boshkayev, R. Ruffini, and I. Siutsou, *Equatorial and circular geodesics in the Hartle-Thorne space-time*, *Nuovo Cimento C*, to appear.

The Hartle-Thorne metric is an approximate solution of vacuum Einstein field equations that describes the exterior region of any slowly and rigidly rotating, stationary and axially symmetric body. The metric is given with accuracy up to the second order terms in the body's angular momentum, and first order in its quadrupole moment. We investigate equatorial and circular geodesics and give, with the same accuracy, analytic formulae for circular geodesics in the Hartle-Thorne metrics.

8. Jorge A. Rueda, M. Rotondo, R. Ruffini, and S.-S. Xue, *A New Family of Neutron Star Models: Global Neutrality vs. Local Neutrality*, *Proceedings of the Twelfth Marcel Grossmann Meeting on General Relativity*, Eds. Thibault Damour, Robert T Jantzen and Remo Ruffini, World Scientific, Singapore (2011).

We formulate the set of self-consistent ground-state equilibrium equations of a system of degenerate neutrons, protons and electrons in beta equilibrium taking into account quantum statistics and electro-weak interactions within the framework of general relativity. We point out the existence of globally neutral neutron star configurations in contrast with the traditional locally neutral ones. We discuss new gravito-electrodynamic effects present in such globally neutral neutron star equilibrium configurations.

9. D. Pugliese, Jorge A. Rueda, R. Ruffini, and S.-S. Xue, *A general relativistic Thomas Fermi treatment of neutron star cores II. Generalized Fermi energies and β -equilibrium*, *Proceedings of the 2nd Galileo-Xu Guangqi Meeting*, Ventimiglia-Italy (2010).

We formulate the set of self-consistent ground-state equilibrium equations of a system of degenerate neutrons, protons and electrons in beta equilibrium taking into account quantum statistics, electro-weak, and strong interactions, within the framework of general relativity. The strong interaction between nucleons is modeled through sigma-omega-rho meson exchange in the context of the extended Walecka model, all duly expressed in general relativity. We demonstrate that, as in the non-interacting case, the thermodynamic equilibrium condition given by the constancy of the Fermi energy of each particle-specie can be properly generalized to include the contribution of all fields.

10. K. Boshkayev, M. Rotondo, and R. Ruffini, *On Magnetic Fields in Rotating Nuclear Matter Cores of Stellar Dimensions*, *Proceedings of the 2nd Galileo-Xu Guangqi Meeting*, Ventimiglia-Italy (2010).

We consider a globally neutral system of a stellar dimension consisting of degenerate and mostly non-interacting N_n neutrons, N_p protons and N_e electrons in beta equilibrium. Such a system at nuclear density having mass numbers $A \approx 10^{57}$ can exhibit a charge distribution different from zero. We present the analysis in the framework of classical electrodynamics to investigate the magnetic field induced by this charge distribution when the system is allowed to rotate as a whole rigid body with constant angular velocity around the axis of symmetry.

11. R. Mohammadi, Jorge A. Rueda, R. Ruffini, and S.-S. Xue, *The solution of the Thomas-Fermi equation in the presence of strong magnetic fields*, Contribution to the Proceedings of the 2nd Galileo-Xu Guangqi Meeting, Ventimiglia-Italy (2010).

We study the influence of strong constant magnetic fields on a globally but not locally neutral compressed system of degenerate neutrons, protons and electrons in beta equilibrium. The ultrarelativistic Thomas-Fermi equation for such a compressed magnetized system is obtained and solved analytic closed form. We analyze the effects of the magnetic field on the properties of the configuration such as the Coulomb potential, the electric field, and the proton fraction.

12. Jorge A. Rueda, R. Ruffini, and S.-S. Xue, *On the electrostatic structure of neutron stars*, AIP Conference Proceedings **1205**, 143–147 (2010).

We consider neutron stars composed by, (1) a core of degenerate neutrons, protons, and electrons above nuclear density; (2) an inner crust of nuclei in a gas of neutrons and electrons; and (3) an outer crust of nuclei in a gas of electrons. We use for the strong interaction model for the baryonic matter in the core an equation of state based on the phenomenological Weizsacker mass formula, and to determine the properties of the inner and the outer crust below nuclear saturation density we adopt the well-known equation of state of Baym-Bethe-Pethick. The integration of the Einstein-Maxwell equations is carried out under the constraints of β -equilibrium and global charge neutrality. We obtain baryon densities that sharply go to zero at nuclear density and electron densities matching smoothly the electron component of the crust. We show that a family of equilibrium configurations exists fulfilling overall neutrality and characterized by a non-trivial electrodynamical structure at the interface between the core and the crust. We find that the electric field is overcritical and that the thickness of the transition surface-shell separating core and crust is of the order of the electron Compton wavelength.

6. Attended International Conferences

1. 3rd Galileo-Xu Guangqi Meeting, October 11–15, 2011 Beijing (China).
2. IRAP Ph.D. Erasmus Mundus Workshop “Gamma Ray Bursts, their progenitors and the role of thermal emission”, October 2–7, 2011 Les Houches (France).
3. 12th Italian-Korean Symposium on Relativistic Astrophysics, July 4–8, 2011 Pescara (Italy).
4. 2nd International Symposium on Strong Electromagnetic Fields and Neutron Stars, May 5–7, 2011 Varadero (Cuba).
5. 1st Caribbean Symposium on Nuclear and Astroparticle Physics, May 1–4, 2011 La Habana (Cuba).
6. IRAP Ph.D. Erasmus Mundus Workshop “From Nuclei to White Dwarfs and Neutron Stars”, April 3–8, 2011 Les Houches (France).
7. IRAP Ph.D. Erasmus Mundus Workshop “Recent News from the MeV, GeV and TeV Gamma-Ray Domains”, March 21–26, 2011 Pescara (Italy).
8. 25th Texas Symposium on Relativistic Astrophysics, December 6–10, 2010 Heidelberg (Germany).
9. 2nd Galileo-Xu Guangqi Meeting, July 12–18, 2010 Ventimiglia (Italy).
10. 11th Italian-Korean Symposium on Relativistic Astrophysics, November 2–4, 2009 Seoul (Korea).
11. 1st Galileo-Xu Guangqi Meeting, October 26–30, 2009 Shanghai (China).
12. 12th Marcel Grossmann Meeting On General Relativity, July 12–18, 2009 Paris (France).
13. 6th Italian-Sino Workshop on Relativistic Astrophysics, June 29–July 1, 2009 Pescara (Italy).
14. 1st Sobral Meeting, May 26–29, 2009 Fortaleza (Brazil).

6. Attended International Conferences

15. Probing stellar populations out to the distant universe, September 7–19, 2008 Cefalù (Italy).
16. 13th Brazilian School of Cosmology and Gravitation, July 20–August 2, 2008 Rio de Janeiro (Brazil).
17. 3rd Stueckelberg Workshop, July 8–18, 2008 Pescara (Italy).
18. 5th Italian-Sino Workshop, May 28–June 1, 2008 Taipei (Taiwan).
19. APS April meeting, April 12–15, 2008 Saint Louis (USA).
20. Path Integrals - New Trends and Perspectives, September 23–28, 2007 Dresden (Germany).
21. APS April meeting, April 14–17, 2007 Jacksonville (USA).
22. 11th Marcel Grossmann Meeting on General Relativity, July 23–29, 2006 Berlin (Germany).

7. APPENDICES

A. Nuclear and Atomic Astrophysics

A.1. On gravitationally and electrostatically bound massive nuclear density cores

A.1.1. Introduction

Models involving e^+e^- plasmas of total energy $\leq 10^{55}$ ergs originating from a vacuum polarization process during the formation of a black hole are being studied to explain a variety of ultra-relativistic astrophysics events (Ruffini et al., 2010b; Cherubini et al., 2009; Aksenov et al., 2007). The formation of such a Kerr-Newman black hole with overcritical electromagnetic fields can only occur during the process of gravitational collapse, e.g., of two coalescing neutron stars. Accordingly in this article we consider new electrostatic properties of massive nuclear density cores which have been neglected in the astrophysics literature. This issue has been overlooked in the traditional description of neutron stars by considering only neutrons (Oppenheimer and Volkoff, 1939) or by imposing *ab initio* local charge neutrality, i.e., local identity of the densities of protons and electrons $n_p = n_e$, thus bypassing the description of any possible electrostatic effect (Harrison et al., 1965; Baym et al., 1971a).

The model we consider here generalizes the relativistic Thomas-Fermi treatment for neutral atoms with heavy nuclei (Pieper and Greiner, 1969; Müller et al., 1972; Greenberg and Greiner, 1982; Popov, 1971b; Zeldovich and Popov, 1972; Migdal et al., 1976). The study of neutral atoms with nuclei of mass number $A \sim 10^2$ – 10^6 is a classic problem of theoretical physics (Zeldovich and Popov, 1972; Ruffini et al., 2010b). Special attention has been given to a possible vacuum polarization process and the creation of e^+e^- pairs (Pieper and Greiner, 1969; Zeldovich and Popov, 1972; Ruffini et al., 2010b) as well as to the study of nuclear stability against Coulomb repulsion (Greenberg and Greiner, 1982). The existence of electric fields larger than the critical value $E_c = m_e^2 c^3 / (e\hbar)$ near their surfaces (Popov, 1971b) has also been shown. We have generalized these models by enforcing the beta equilibrium conditions (Ruffini et al., 2007c).

We have then extrapolated those results by numerical integration to the case of massive nuclear density cores of mass $\approx 1M_\odot$ and radius $R_c \approx 10$ km

(Ruffini et al., 2007c). Such a massive nuclear density core is a globally neutral system of N_n neutrons, N_p protons and N_e electrons in beta equilibrium at nuclear density having mass numbers $A \sim (m_{\text{Planck}}/m_n)^3$ where m_n (m_e) is the neutron (electron) mass and $m_{\text{Planck}} = (\hbar c/G)^{1/2}$ (Ruffini et al., 2007c). As in the nuclear model (Migdal et al., 1976), the proton distribution is here assumed to be constant up to the core radius R_c . We have obtained configurations with global charge neutrality $N_p = N_e$ but $n_p \neq n_e$, in contrast with the local condition $n_p = n_e$ traditionally assumed in astrophysics. As a result electric fields of critical value are confirmed to exist, near the surface, also in the case of massive nuclear density cores in analogy to the case of heavy nuclei.

Recently a new dimensionless form of the relativistic Thomas-Fermi treatment for a nuclear density core has been obtained which reveals the existence of new scaling laws for this model.

In this article we present a unified treatment extending from heavy nuclei to massive nuclear density cores by using an explicit analytic solitonic solution of the new dimensionless form of the relativistic Thomas-Fermi equation. We confirm the existence of and give an analytic expression for the overcritical electric field near the surface of massive nuclear density cores already obtained in (Ruffini et al., 2007c) by numerical integration. Furthermore there are a variety of new results made possible by the new analytic formulation. First we give an explicit expression for the Coulomb energy of such cores, demonstrating their stability against nuclear fission, as opposed to the case of heavy nuclei. Secondly on the basis of Newtonian gravitational energy considerations we propose the existence of a possible new island of stability for mass numbers $A > A_R = 0.039 \left(\frac{N_p}{A}\right)^{1/2} \left(\frac{m_{\text{Planck}}}{m_n}\right)^3$. The equilibrium against Coulomb repulsion originates now from the combined effect of the screening of the relativistic electrons, of the surface tension due to strong interactions and of the gravitational interaction of the massive dense cores. By enforcing the condition of beta equilibrium, we also obtain a generalized relation between the mass number A and atomic number N_p which encompasses previous phenomenological expressions.

All the above solutions have been obtained assuming the electron Fermi energy to be equal to zero. The necessity and the methodology of extending these results to the case of compressed atoms along the lines of the Feynman-Metropolis-Teller treatment (Feynman et al., 1949), corresponding to positive values of the Fermi energy of electrons, are outlined here. We also motivate the clear necessity and the general methodology of justifying the above results using a self-consistent general relativistic treatment of the system. These ideas will be pursued in detail elsewhere.

A.1.2. The relativistic Thomas-Fermi equation and the beta equilibrium condition

It has been known since the classic work of Fermi (Fermi, 1950) that the phenomenological drop model of the nucleus gives excellent results for a variety of properties including the isobaric behavior and nuclear fission. In addition to the masses of the baryonic components and the asymmetry energy and pairing term, the mass formula contains terms estimating the surface tension energy of the nucleus (Fermi, 1950)

$$\varepsilon_s = 17.5 \cdot A^{2/3} \text{ MeV}, \quad (\text{A.1.1})$$

and the Coulomb energy (Fermi, 1950)

$$\varepsilon_c = \frac{3\alpha N_p^2}{5R_c}, \quad (\text{A.1.2})$$

where $R_c = r_0 A^{1/3}$, $r_0 = 1.5 \cdot 10^{-13}$ cm and the numerical factors are derived by fitting the observational data. From the extremization of the mass formula the following relation between A and N_p is obtained (Fermi, 1950)

$$N_p \simeq \left[\frac{2}{A} + \frac{3}{200} \frac{1}{A^{1/3}} \right]^{-1}, \quad (\text{A.1.3})$$

which in the limit of small A gives

$$N_p \simeq \frac{A}{2}. \quad (\text{A.1.4})$$

The analysis of the stability of the nucleus against finite deformation leads to a stability condition against fission given by the equality of the surface energy term to the Coulomb energy. This leads to the condition (Fermi, 1950)

$$\frac{N_p^2}{A} < 45. \quad (\text{A.1.5})$$

A novel situation occurs when super-heavy nuclei ($A > \tilde{A} \sim 10^4$) are examined (Ferreirinho et al., 1980; Ruffini et al., 2007c). The distribution of electrons penetrates inside the nucleus: a much smaller effective net charge of the nucleus occurs due to the screening of relativistic electrons (Migdal et al., 1976; Ferreira et al., 1980). In Ruffini and Stella (1981) a definition of an effective nuclear charge due to the penetration of the electrons was presented. A treatment based on the relativistic Thomas-Fermi model has been developed in order to describe the penetration of the electrons and their effective screening of the positive nuclear charge. In particular, by assuming

$N_p \simeq A/2$, Pieper and Greiner (1969); Müller et al. (1972); Greenberg and Greiner (1982) and Popov (1971b); Zeldovich and Popov (1972); Migdal et al. (1976) in a series of papers were able to solve the non-linear Thomas-Fermi equation. It was demonstrated in Migdal et al. (1976) that the effective positive nuclear charge is confined to a small layer of thickness $\sim \hbar/\sqrt{\alpha}m_\pi c$ where m_π is the pion mass and as usual $\alpha = e^2/\hbar c$. Correspondingly electric fields of strength much larger than the critical value E_c for vacuum polarization at the surface of the core are created. However, the creation of electron-positron pairs due to the vacuum polarization process does not occur because of the Pauli blocking by the degenerate electrons Ruffini et al. (2010b).

Here we generalize the work of Pieper and Greiner (1969); Müller et al. (1972); Greenberg and Greiner (1982) and Popov (1971b); Zeldovich and Popov (1972); Migdal et al. (1976). We have relaxed the condition $N_p \simeq A/2$ adopted by Popov and Greiner as well as the condition $N_p \simeq [2/A + 3/200A^{1/3}]^{-1}$ adopted by Ferreira et al. (1980). Instead we explicitly impose the beta decay equilibrium between neutrons, protons and electrons. We then extrapolate such model to the case $A \approx (m_{\text{Planck}}/m_n)^3 \sim 10^{57}$. A supercritical field still exists in a shell of thickness $\sim \hbar/\sqrt{\alpha}m_\pi c$ at the core surface, and a charged lepton-baryonic core is surrounded by an oppositely charged leptonic component. Such massive nuclear density cores, including the leptonic component, are globally neutral.

As usual we assume that the protons are distributed at constant density n_p within a radius

$$R_c = \Delta \frac{\hbar}{m_\pi c} N_p^{1/3}, \quad (\text{A.1.6})$$

where Δ is a parameter such that $\Delta \approx 1$ ($\Delta < 1$) corresponds to nuclear (supranuclear) densities when applied to ordinary nuclei. The overall Coulomb potential satisfies the Poisson equation

$$\nabla^2 V(r) = -4\pi e [n_p(r) - n_e(r)], \quad (\text{A.1.7})$$

with the boundary conditions $V(\infty) = 0$ (due to the global charge neutrality of the system) and finiteness of $V(0)$. The density $n_e(r)$ of the electrons of charge $-e$ is determined by the Fermi energy condition on their Fermi momentum P_e^F ; we assume here

$$E_e^F = [(P_e^F c)^2 + m_e^2 c^4]^{1/2} - m_e c^2 - eV(r) = 0, \quad (\text{A.1.8})$$

which leads to

$$n_e(r) = \frac{(P_e^F)^3}{3\pi^2 \hbar^3} = \frac{1}{3\pi^2 \hbar^3 c^3} \left[e^2 V^2(r) + 2m_e c^2 eV(r) \right]^{3/2}. \quad (\text{A.1.9})$$

By introducing $x = r/[\hbar/m_\pi c]$, $x_c = R_c/[\hbar/m_\pi c]$ and $\chi/r = eV(r)/c\hbar$, the relativistic Thomas-Fermi equation takes the form

$$\frac{1}{3x} \frac{d^2\chi(x)}{dx^2} = -\frac{\alpha}{\Delta^3} \theta(x_c - x) + \frac{4\alpha}{9\pi} \left[\frac{\chi^2(x)}{x^2} + 2 \frac{m_e \chi}{m_\pi x} \right]^{3/2}, \quad (\text{A.1.10})$$

where $\chi(0) = 0, \chi(\infty) = 0$. The neutron density $n_n(r)$ is determined by the Fermi energy condition on their Fermi momentum P_n^F imposed by beta decay equilibrium

$$\begin{aligned} E_n^F &= [(P_n^F c)^2 + m_n^2 c^4]^{1/2} - m_n c^2 \\ &= [(P_p^F c)^2 + m_p^2 c^4]^{1/2} - m_p c^2 + eV(r), \end{aligned} \quad (\text{A.1.11})$$

which in turn is related to the proton and electron densities by Eqs. (A.1.7), (A.1.9) and (A.1.10). These equations have been integrated numerically (see Ruffini et al. (2007c)).

A.1.3. The ultra-relativistic analytic solutions

In the ultrarelativistic limit, the relativistic Thomas-Fermi equation admits an analytic solution. Introducing the new function ϕ defined by $\phi = \frac{4^{1/3}}{(9\pi)^{1/3}} \Delta \frac{\chi}{x}$ and the new variables $\hat{x} = (12/\pi)^{1/6} \sqrt{\alpha} \Delta^{-1} x$, $\xi = \hat{x} - \hat{x}_c$, where $\hat{x}_c = (12/\pi)^{1/6} \sqrt{\alpha} \Delta^{-1} x_c$, then Eq. (A.1.10) becomes

$$\frac{d^2\hat{\phi}(\xi)}{d\xi^2} = -\theta(-\xi) + \hat{\phi}(\xi)^3, \quad (\text{A.1.12})$$

where $\hat{\phi}(\xi) = \phi(\xi + \hat{x}_c)$. The boundary conditions on $\hat{\phi}$ are: $\hat{\phi}(\xi) \rightarrow 1$ as $\xi \rightarrow -\hat{x}_c \ll 0$ (at the massive nuclear density core center) and $\hat{\phi}(\xi) \rightarrow 0$ as $\xi \rightarrow \infty$. The function $\hat{\phi}$ and its first derivative $\hat{\phi}'$ must be continuous at the surface $\xi = 0$ of the massive nuclear density core. Equation (A.1.12) admits an exact solution

$$\hat{\phi}(\xi) = \begin{cases} 1 - 3 \left[1 + 2^{-1/2} \sinh(a - \sqrt{3}\xi) \right]^{-1}, & \xi < 0, \\ \frac{\sqrt{2}}{(\xi + b)}, & \xi > 0, \end{cases} \quad (\text{A.1.13})$$

where the integration constants a and b have the values $a = \text{arcsinh}(11\sqrt{2}) \approx 3.439$, $b = (4/3)\sqrt{2} \approx 1.886$. Next we evaluate the Coulomb potential energy

function

$$eV(\xi) = \left(\frac{9\pi}{4}\right)^{1/3} \frac{1}{\Delta} m_\pi c^2 \hat{\phi}(\xi), \quad (\text{A.1.14})$$

and by differentiation, the electric field

$$E(\xi) = - \left(\frac{3^5 \pi}{4}\right)^{1/6} \frac{\sqrt{\alpha} m_\pi^2 c^3}{\Delta^2 e \hbar} \hat{\phi}'(\xi). \quad (\text{A.1.15})$$

Details are given in Figs. A.1 and A.2.

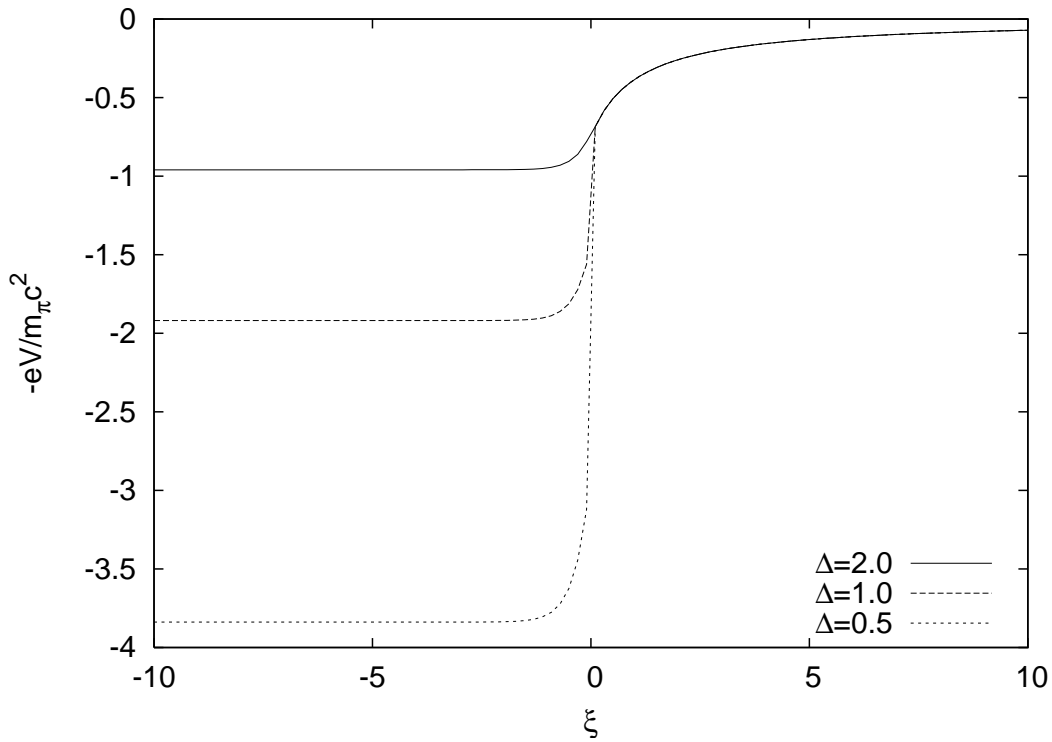


Figure A.1.: The electron Coulomb potential energy $-eV$, in units of pion mass m_π is plotted as a function of the radial coordinate $\xi = \hat{x} - \hat{x}_c$, for selected values of the density parameter Δ .

We now estimate three crucial quantities:

1) the Coulomb potential at the center of the configuration,

$$eV(0) \approx \left(\frac{9\pi}{4}\right)^{1/3} \frac{1}{\Delta} m_\pi c^2, \quad (\text{A.1.16})$$

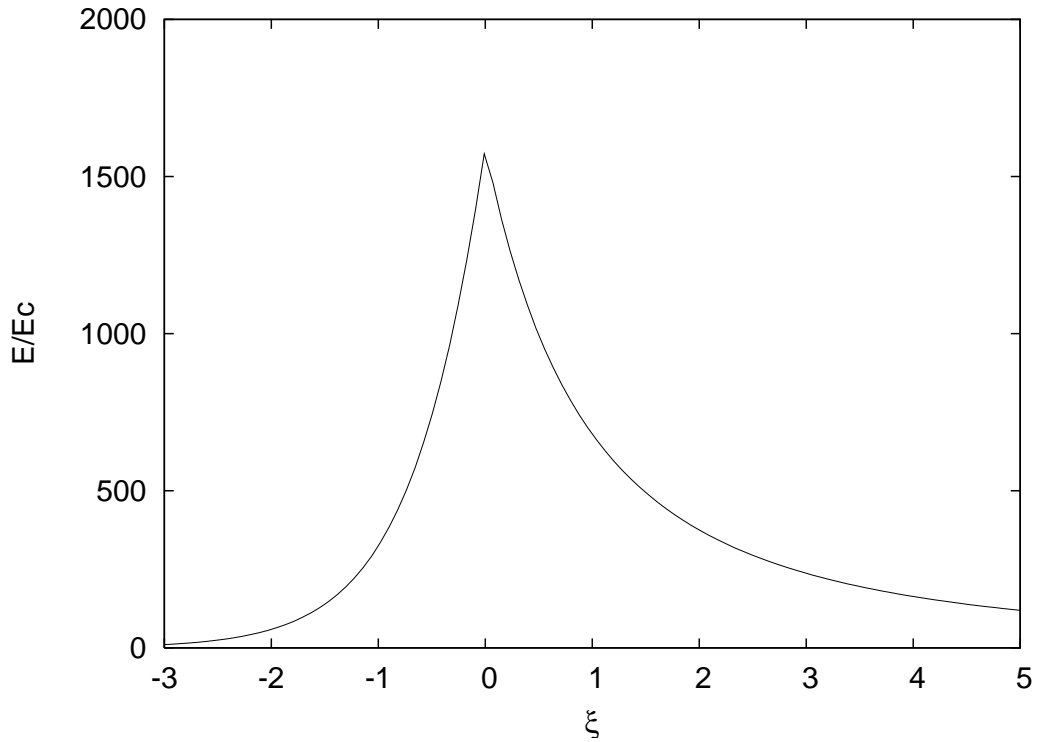


Figure A.2.: The electric field is plotted in units of the critical field E_c as a function of the radial coordinate ξ for $\Delta=2$, showing a sharp peak at the core radius.

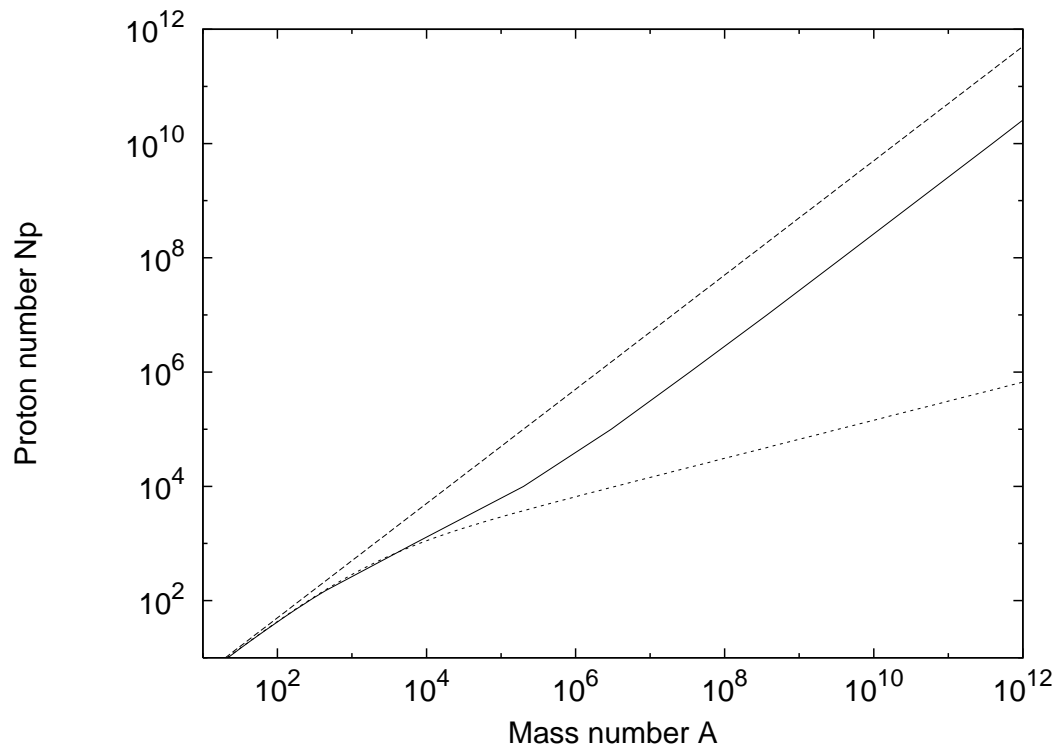


Figure A.3.: The A - N_p relation at nuclear density (solid line) obtained from first principles compared with the phenomenological expressions given by $N_p \simeq A/2$ (dashed line) and Eq. (A.1.3) (dotted line). The asymptotic value, for $A \rightarrow (m_{\text{Planck}}/m_n)^3$, is $N_p \approx 0.0046A$.

2) the electric field at the surface of the core

$$E_{\max} \approx 0.95\sqrt{\alpha}\frac{1}{\Delta^2}\frac{m_\pi^2 c^3}{e\hbar} = 0.95\frac{\sqrt{\alpha}}{\Delta^2}\left(\frac{m_\pi}{m_e}\right)^2 E_c. \quad (\text{A.1.17})$$

3) the Coulomb electrostatic energy of the core

$$\mathcal{E}_{\text{em}} = \int \frac{E^2}{8\pi} d^3r \approx 0.15\frac{3\hbar c(3\pi)^{1/2}}{4\Delta\sqrt{\alpha}}A^{2/3}\frac{m_\pi c}{\hbar}\left(\frac{N_p}{A}\right)^{2/3}. \quad (\text{A.1.18})$$

These three quantities are functions only of the pion mass m_π , the density parameter Δ and of the fine structure constant α . Their formulas apply over the entire range from superheavy nuclei with $N_p \sim 10^3$ all the way up to massive cores with $N_p \approx (m_{\text{Planck}}/m_n)^3$.

A.1.4. New results derived from the analytic solutions

Starting from the analytic solutions of the previous section we obtain the following new results.

a) Using the solution (A.1.13), we have obtained a new generalized relation between A and N_p for any value of A . In the limit of small A this result agrees well with the phenomenological relations given by Eqs. (A.1.3) and (A.1.4), as is clearly shown in Fig. A.3. It appears that the explicit evaluation of the beta equilibrium, in contrast with the previously adopted Eqs.(3,4), leads to an effect comparable in magnitude and qualitatively similar to the asymmetry energy in the phenomenological liquid drop model.

b) The charge-to-mass ratio of the effective charge Q at the core surface to the core mass M is given by

$$\frac{Q}{\sqrt{GM}} \approx \frac{E_{\max}R_c^2}{\sqrt{G}m_n A} \approx \frac{m_{\text{Planck}}}{m_n}\left(\frac{1}{N_p}\right)^{1/3}\frac{N_p}{A}. \quad (\text{A.1.19})$$

For superheavy nuclei with $N_p \approx 10^3$, the charge-to-mass ratio for the nucleus is

$$\frac{Q}{\sqrt{GM}} > \frac{1}{20}\frac{m_{\text{Planck}}}{m_n} \sim 10^{18}. \quad (\text{A.1.20})$$

Gravitation obviously plays no role in the stabilization of these nuclei.

Instead for massive nuclear density cores where $N_p \approx (m_{\text{Planck}}/m_n)^3$, the ratio Q/\sqrt{GM} given by Eq. (A.1.19) is simply

$$\frac{Q}{\sqrt{GM}} \approx \frac{N_p}{A}, \quad (\text{A.1.21})$$

which is approximately 0.0046 (see Fig. A.3). It is well-known that the charge-to-mass ratio (A.1.21) smaller than 1 evidences the equilibrium of self-gravitating mass-charge system both in Newtonian gravity and general relativity (see, e.g., Chandrasekhar (1992)).

c) For a massive core at nuclear density the criterion of stability against fission ($\mathcal{E}_{em} < 2\mathcal{E}_s$) is satisfied. In order to see this we use Eqs. (A.1.1) and (A.1.18)

$$\frac{\mathcal{E}_{em}}{2\mathcal{E}_s} \approx 0.15 \frac{3}{8} \sqrt{\frac{3\pi}{\alpha}} \frac{1}{\Delta} \left(\frac{N_p}{A} \right)^{2/3} \frac{m_\pi c^2}{17.5 \text{ MeV}} \sim 0.1 < 1. \quad (\text{A.1.22})$$

A.1.5. Estimates of gravitational effects in a Newtonian approximation

In order to investigate the possible effects of gravitation on these massive neutron density cores we proceed to some qualitative and quantitative estimates based on the Newtonian approximation.

a) The *maximum* Coulomb energy per proton is given by Eq. (A.1.16) where the potential is evaluated at the center of the core. The Newtonian gravitational potential energy per proton (of mass m_p) in the field of a massive nuclear density core with $A \approx (m_{\text{Planck}}/m_n)^3$ is given by

$$\mathcal{E}_g = -G \frac{M m_p}{R_c} = -\frac{1}{\Delta} \frac{m_{\text{Planck}}}{m_n} \frac{m_\pi c^2}{N_p^{1/3}} \simeq -\frac{m_\pi c^2}{\Delta} \left(\frac{A}{N_p} \right)^{1/3}. \quad (\text{A.1.23})$$

Since $A/N_p \sim 0.0046$ (see Fig. A.3) for any value of Δ , the gravitational energy is larger in magnitude than and opposite in sign to the Coulomb potential energy per proton of Eq. (A.1.16) so the system should be gravitationally stable.

b) There is yet a more accurate derivation of the gravitational stability based on the analytic solution of the Thomas-Fermi equation Eq. (A.1.12). The Coulomb energy \mathcal{E}_{em} given by (A.1.18) is mainly distributed within a thin shell of width $\delta R_c \approx \hbar \Delta / (\sqrt{\alpha} m_\pi c)$ and proton number $\delta N_p = n_p 4\pi R_c^2 \delta R_c$ at the surface. To ensure the stability of the system, the attractive gravitational energy of the thin proton shell

$$\mathcal{E}_{gr} \approx -3 \frac{G}{\Delta} \frac{A^{4/3}}{\sqrt{\alpha}} \left(\frac{N_p}{A} \right)^{1/3} m_n^2 \frac{m_\pi c}{\hbar} \quad (\text{A.1.24})$$

must be larger than the repulsive Coulomb energy (A.1.18). For small A , the gravitational energy is always negligible. However, since the gravitational energy increases proportionally to $A^{4/3}$ while the Coulomb energy only increases proportionally to $A^{2/3}$, the two must eventually cross, which occurs at

$$A_R = 0.039 \left(\frac{N_p}{A} \right)^{1/2} \left(\frac{m_{\text{Planck}}}{m_n} \right)^3. \quad (\text{A.1.25})$$

This establishes a *lower* limit for the mass number A_R necessary for the existence of an island of stability for massive nuclear density cores. The *upper* limit of the island of stability will be determined by general relativistic effects.

c) Having established the role of gravity in stabilizing the Coulomb interaction of the massive nuclear density core, we outline the importance of the strong interactions in determining its surface. We find for the neutron pressure at the surface:

$$P_n = \frac{9}{40} \left(\frac{3}{2\pi} \right)^{1/3} \left(\frac{m_\pi}{m_n} \right) \frac{m_\pi c^2}{(\hbar/m_\pi c)^3} \left(\frac{A}{N_p} \right)^{5/3} \frac{1}{\Delta^5}, \quad (\text{A.1.26})$$

and for the surface tension, as extrapolated from nuclear scattering experiments,

$$P_s = - \left(\frac{0.13}{4\pi} \right) \frac{m_\pi c^2}{(\hbar/m_\pi c)^3} \left(\frac{A}{N_p} \right)^{2/3} \frac{1}{\Delta^2}. \quad (\text{A.1.27})$$

We then obtain

$$\frac{|P_s|}{P_n} = 0.39 \cdot \Delta^3 \left(\frac{N_p}{A} \right) = 0.24 \cdot \frac{\rho_{\text{nucl}}}{\rho_{\text{surf}}}, \quad (\text{A.1.28})$$

where $\rho_{\text{nucl}} = 3m_n A / 4\pi R_c^3$. The relative importance of the nuclear pressure and nuclear tension is a very sensitive function of the density ρ_{surf} at the surface.

It is important to emphasize a major difference between nuclei and the massive nuclear density cores treated in this article: the gravitational binding energy in these massive nuclear density cores is instead $\varepsilon_{\text{gr}} \approx GM_\odot m_n / R_c \approx 0.1 m_n c^2 \approx 93.8 \text{ MeV}$. In other words it is much bigger than the nuclear energy in ordinary nuclei $\varepsilon_{\text{nuclear}} \approx \hbar^2 / m_n r_0^2 \approx 28.8 \text{ MeV}$.

A.1.6. Possible applications to neutron stars

All the above considerations have been made for an isolated massive core at constant density whose boundary has been sharply defined by a step func-

tion. No external forces are exerted. Consequently due to the global charge neutrality, the Fermi energy of the electrons has been assumed to be equal to zero. In the earliest description of neutron stars in the work of Oppenheimer and Volkoff (1939) only a gas of neutrons was considered and the equation of equilibrium was written in the Schwarzschild metric. They considered the model of a degenerate gas of neutrons to hold from the center to the border, with the density monotonically decreasing away from the center.

In the intervening years a more realistic model has been presented challenging the original considerations of Tolman (1939); Oppenheimer and Volkoff (1939). Their TOV equations considered the existence of neutrons all the way to the surface of the star. The presence of neutrons, protons and electrons in beta equilibrium were instead introduced in Harrison et al. (1965). Still more important the neutron stars have been shown to be composed of two sharply different components: the core at nuclear and/or supra-nuclear density consisting of neutrons, protons and electrons and a crust of white dwarf like material, namely of degenerate electrons in a nuclei lattice (Harrison et al., 1965; Baym et al., 1971a). The pressure and the density of the core are mainly due to the baryons while the pressure of the crust is mainly due to the electrons with the density due to the nuclei and possibly with some free neutrons due to neutron drip (see e.g. Baym et al. (1971a)). Further works describing the nuclear interactions were later introduced (see e.g. Haensel et al. (2007)). Clearly all these considerations departed profoundly from the TOV approximation. The matching between the core component and the crust is the major unsolved problem. To this issue this article introduces some preliminary results in a simplified model which has the advantage to present explicit analytic solutions.

In all the above treatments in order to close the system of equations the condition of local charge neutrality $n_e = n_p$ was adopted without a proof. The considerations of massive neutron density cores presented in this article offer an alternative to the local charge neutrality condition $n_e = n_p$. In a specific example which can be solved also analytically such condition is substituted by the Thomas-Fermi relativistic equations implying $n_e \neq n_p$ and an overall charge neutral system ($N_e = N_p$). The condition of global charge neutrality as opposed to the local one, leads to the existence of overcritical electric fields at the core surface which may be relevant in the description of neutron stars.

A.1.7. Conclusions

We have first generalized the treatment of heavy nuclei by enforcing the condition of beta equilibrium in the relativistic Thomas-Fermi equation, avoiding the imposition of $N_p \simeq A/2$ between N_p and A traditionally assumed in the literature. In doing so we have obtained (see Fig. A.3) an $A - N_p$ relation which extends the ones adopted in the literature. Using the existence

of scaling laws for the system of equations considered, we extend the results obtained for heavy nuclei to the case of massive nuclear density cores. The novelty in this article is to show how both the considerations of heavy nuclei and of systems of macroscopic astrophysical dimensions can take advantage from a rigorous and analytic solution of the Thomas-Fermi relativistic equations and the beta equilibrium conditions. This task is achieved by obtaining explicit analytic solutions fulfilling precise boundary conditions and using the scaling laws introduced in this article.

Indeed the Thomas-Fermi treatment has been considered also in the context of quark stars with a charge and a density distribution analogous to the one of massive nuclear density cores we consider in this article Itoh (1970); Witten (1984); Alcock et al. (1986); Kettner et al. (1995); Usov (1998). There are however a variety of differences both in the boundary conditions adopted and in the solution obtained. In the present article we show that we can indeed obtain overcritical electric fields at nuclear density on macroscopic scales of $R_c \approx 10$ Km and $M \approx 1M_\odot$ for existing field theories involving only neutrons, protons and electrons and their fundamental interactions and no quarks present. We obtain explicit analytic solutions of the relativistic Thomas-Fermi equations, self-consistently solved with the condition of beta equilibrium. Such analytic solutions allow to give explicit expressions for the Coulomb energy, surface energy and Newtonian gravitational energy of such massive nuclear density cores.

These cores are stable against fission (see Eq. (A.1.22)), the surface tension determines the sharpness of their boundary (see Eq. (A.1.28)) and the gravitational interaction, at Newtonian level, balances the Coulomb repulsion for mass numbers larger than the critical value given by Eq. (A.1.25).

As a by-product of these results, we also conclude that the arguments often quoted concerning limits on the electric fields of an astrophysical system based on a free test particle (the dust approximation) considering only the gravitational and electric interactions

$$(E_{\max})_{\text{dust}} \approx \frac{m_e m_n c^3}{e \hbar} \frac{m_n}{m_{\text{Planck}}}, \quad (\text{A.1.29})$$

$$\left(\frac{Q}{\sqrt{GM}} \right)_{\text{dust}} \approx \sqrt{G} \frac{m_e}{e} = \frac{1}{\sqrt{\alpha}} \frac{m_e}{m_{\text{Planck}}}, \quad (\text{A.1.30})$$

appear to be inapplicable for $A \sim (m_{\text{Planck}}/m_n)^3$. Here nuclear densities are reached and the roles of *all* fundamental interactions, including weak and strong interactions in addition to the electromagnetic and gravitational ones and including as well quantum statistics, have to be taken into account through the relativistic Thomas-Fermi model. Eqs. (A.1.29) and (A.1.30) are

replaced by Eqs. (A.1.17) and (A.1.21),

$$E_{\max} \approx \frac{0.95\sqrt{\alpha} m_{\text{Planck}}}{\Delta^2 m_e} \left(\frac{m_\pi}{m_n}\right)^2 (E_{\max})_{\text{dust}}, \quad (\text{A.1.31})$$

$$\frac{Q}{\sqrt{GM}} \approx \frac{N_p}{A} \sqrt{\alpha} \frac{m_{\text{Planck}}}{m_e} \left(\frac{Q}{\sqrt{GM}}\right)_{\text{dust}}. \quad (\text{A.1.32})$$

A.2. On the relativistic Thomas-Fermi treatment of compressed atoms and compressed nuclear matter cores of stellar dimensions

A.2.1. Introduction

In a classic article Baym et al. (1971a) presented the problem of matching, in a neutron star, a liquid core, composed of N_n neutrons, N_p protons and N_e electrons, to the crust taking into account the electro-dynamical and surface tension effects. After discussing the different aspects of the problem they concluded: *The details of this picture requires further elaboration; this is a situation for which the Thomas-Fermi method is useful.* This statement, in first instance, may appear surprising: the Thomas-Fermi model has been extensively applied in atomic physics (see e.g. Gombás (1949); March (1957); Lundqvist and March (1983)), also has been applied extensively in atomic physics in its relativistic form (see e.g. Ferreira et al. (1980); Ruffini and Stella (1981)) as well as in the study of atoms with heavy nuclei in the classic works of Migdal et al. (1976, 1977). Similarly there have been considerations of relativistic Thomas-Fermi model for quark stars pointing out the existence of critical electric fields on their surfaces (see e.g. Alcock et al. (1986); Usov (1998)). Similar results have also been obtained by Alford et al. (2001) in the transition at very high densities, from the normal nuclear matter phase in the core to the color-flavor-locked phase of quark matter in the inner core of hybrid stars. No example exists of the application of the electromagnetic Thomas-Fermi model for neutron stars. This problem can indeed be approached with merit by studying the simplified but rigorous concept of a nuclear matter core of stellar dimensions which fulfills the relativistic Thomas-Fermi equation as discussed by Ruffini et al. (2007c), by Rotondo et al. (2011e) and by Popov (2010). As we will see this work leads to the prediction of the existence of a critical electric field at the interface between the core and the crust of a neutron star.

In Ruffini et al. (2007c) and Rotondo et al. (2011e) it is described a degenerate system of N_n neutrons, N_p protons and N_e electrons constrained to a constant density distribution for the protons and it is solved the corresponding relativistic Thomas-Fermi equation and derived for the neutrons the distribution following the implementation of the beta equilibrium condition. This generalizes e.g. the works of Migdal et al. (1976, 1977); Popov (1971b,a) and Pieper and Greiner (1969); Greenberg and Greiner (1982) by eliminating the constraint $N_p \approx A/2$, clearly not valid for heavy nuclei, and enforcing self-consistently in a new relativistic Thomas-Fermi equation the condition of beta equilibrium. Using then the existence of scaling laws we have extended in Rotondo et al. (2011e) the results from heavy nuclei to the case of nuclear matter cores of stellar dimensions. In both these treatments we had assumed

the Fermi energy of the electrons $E_e^F = 0$. The aim of this article is to proceed with this dual approach and to consider first the case of compressed atoms and then, using the existence of scaling laws, the compressed nuclear matter cores of stellar dimensions with a positive value of their electron Fermi energies.

It is well known that Salpeter has been among the first to study the behavior of matter under extremely high pressures by considering a Wigner-Seitz cell of radius R_{WS} (Salpeter, 1961). Salpeter assumed as a starting point the nucleus point-like and a uniform distribution of electrons within a Wigner-Seitz cell, and then considered corrections to the above model due to the inhomogeneity of electron distribution. The first correction corresponds to the inclusion of the lattice energy $E_C = -(9N_p^2\alpha)/(10R_{WS})$, which results from the point-like nucleus-electron Coulomb interaction and, from the electron-electron Coulomb interaction inside the cell of radius R_{WS} . The second correction is given by a series-expansion of the electron Fermi energy about the average electron density n_e of the uniform approximation. The electron density is then assumed equals to $n_e[1 + \epsilon(r)]$ with $\epsilon(r)$ considered as infinitesimal. The Coulomb potential energy is assumed to be the one of the point-like nucleus with the uniform distribution of electrons of density n_e thus the correction given by $\epsilon(r)$ is neglected on the Coulomb potential. The electron distribution is then calculated at first-order by expanding the relativistic electron kinetic energy about its value given by the uniform approximation considering as infinitesimal the ratio eV/E_e^F between the Coulomb potential energy eV and the electron Fermi energy $E_e^F = \sqrt{[cP_e^F(r)]^2 + m_e^2c^4} - m_e c^2 - eV$. The inclusion of each additional Coulomb correction results in a decreasing of the pressure of the cell P_S by comparison to the uniform one.

It is quite difficult to assess the self-consistency of all the recalled different approximations adopted by Salpeter. In order to validate and also to see the possible limits of the Salpeter approach, we consider the relativistic generalization of the Feynman, Metropolis, Teller treatment (Feynman et al., 1949) which takes automatically and globally into account all electromagnetic and special relativistic contributions. We show explicitly how this new treatment leads in the case of atoms to electron distributions markedly different from the ones often adopted in the literature of constant electron density distributions. At the same time it allows to overcome some of the difficulties in current treatments.

Similarly the point-like description of the nucleus often adopted in literature is confirmed to be unacceptable in the framework of a relativistic treatment.

In Sec. A.2.2 we first recall the non-relativistic treatment of the compressed atom by Feynman, Metropolis and Teller. In Sec. A.2.3 we generalize that treatment to the relativistic regime by integrating the relativistic Thomas-Fermi equation, imposing also the condition of beta equilibrium. In Sec. A.2.4

we first compare the new treatment with the one corresponding to a uniform electron distribution often used in the literature and to the Salpeter treatment. We also compare and contrast the results of the relativistic and the non-relativistic treatment.

In Sec. A.2.5, using the same scaling laws adopted by Ruffini et al. (2007c) and Rotondo et al. (2011e) we turn to the case of nuclear matter cores of stellar dimensions with mass numbers $A \approx (m_{\text{Planck}}/m_n)^3 \sim 10^{57}$ or $M_{\text{core}} \sim M_{\odot}$ where m_n is the neutron mass and $m_{\text{Planck}} = (\hbar c/G)^{1/2}$ is the Planck mass. Such a configuration presents global but not local charge neutrality. Analytic solutions for the ultra-relativistic limit are obtained. In particular we find:

1) explicit analytic expressions for the electrostatic field and the Coulomb potential energy,

2) an entire range of possible Fermi energies for the electrons between zero and a maximum value $(E_e^F)_{\text{max}}$, reached when $R_{WS} = R_c$, which can be expressed analytically,

3) the explicit analytic expression of the ratio between the proton number N_p and the mass number A when $R_{WS} = R_c$.

We turn then in Sec. A.2.6 to the study of the compressional energy of the nuclear matter cores of stellar dimensions for selected values of the electron Fermi energy. We show that the solution with $E_e^F = 0$ presents the largest value of the electro-dynamical structure.

We finally summarize the conclusions in Sec. A.2.7.

A.2.2. The Thomas-Fermi model for compressed atoms: the Feynman-Metropolis-Teller treatment

The classical Thomas-Fermi model

The Thomas-Fermi model assumes that the electrons of an atom constitute a fully degenerate gas of fermions confined in a spherical region by the Coulomb potential of a point-like nucleus of charge $+eN_p$. Feynman, Metropolis and Teller have shown that this model can be used to derive the equation of state of matter at high pressures by considering a Thomas-Fermi model confined in a Wigner-Seitz cell of radius R_{WS} (Feynman et al., 1949).

We recall that the condition of equilibrium of the electrons in an atom, in the non-relativistic limit, is expressed by

$$\frac{(P_e^F)^2}{2m_e} - eV = E_e^F, \quad (\text{A.2.1})$$

where m_e is the electron mass, V is the electrostatic potential and E_e^F is their constant Fermi energy.

The electrostatic potential fulfills, for $r > 0$, the Poisson equation

$$\nabla^2 V = 4\pi e n_e, \quad (\text{A.2.2})$$

where the electron number density n_e is related to the Fermi momentum P_e^F by

$$n_e = \frac{(P_e^F)^3}{3\pi^2 \hbar^3}. \quad (\text{A.2.3})$$

For neutral atoms and ions n_e vanishes at the boundary so the electron Fermi energy is, respectively, zero or negative. In the case of compressed atoms n_e does not vanish at the boundary while the Coulomb potential energy eV does. Consequently E_e^F is positive.

Defining

$$eV(r) + E_e^F = e^2 N_p \frac{\phi(r)}{r}, \quad (\text{A.2.4})$$

and introducing the new dimensionless radial coordinate η as

$$r = b\eta \quad \text{with} \quad b = \frac{(3\pi)^{2/3}}{2^{7/3}} \frac{1}{N_p^{1/3}} \frac{\hbar^2}{m_e e^2} = \frac{\sigma}{N_p^{1/3}} r_{Bohr}, \quad (\text{A.2.5})$$

where $\sigma = (3\pi)^{2/3}/2^{7/3} \approx 0.88$, $r_{Bohr} = \hbar^2/(m_e e^2)$ is the Bohr radius, we obtain the following expression for the electron number density

$$n_e(\eta) = \frac{N_p}{4\pi b^3} \left(\frac{\phi(\eta)}{\eta} \right)^{3/2}, \quad (\text{A.2.6})$$

and then Eq. (A.2.2) can be written in the form

$$\frac{d^2 \phi(\eta)}{d\eta^2} = \frac{\phi(\eta)^{3/2}}{\eta^{1/2}}, \quad (\text{A.2.7})$$

which is the classic Thomas-Fermi equation. A first boundary condition for this equation follows from the point-like structure of the nucleus

$$\phi(0) = 1. \quad (\text{A.2.8})$$

A second boundary condition comes from the conservation of the number of electrons $N_e = \int_0^{R_{WS}} 4\pi n_e(r) r^2 dr$

$$1 - \frac{N_e}{N_p} = \phi(\eta_0) - \eta_0 \phi'(\eta_0), \quad (\text{A.2.9})$$

where $\eta_0 = R_{WS}/b$ defines the radius R_{WS} of the Wigner-Seitz cell. In the case

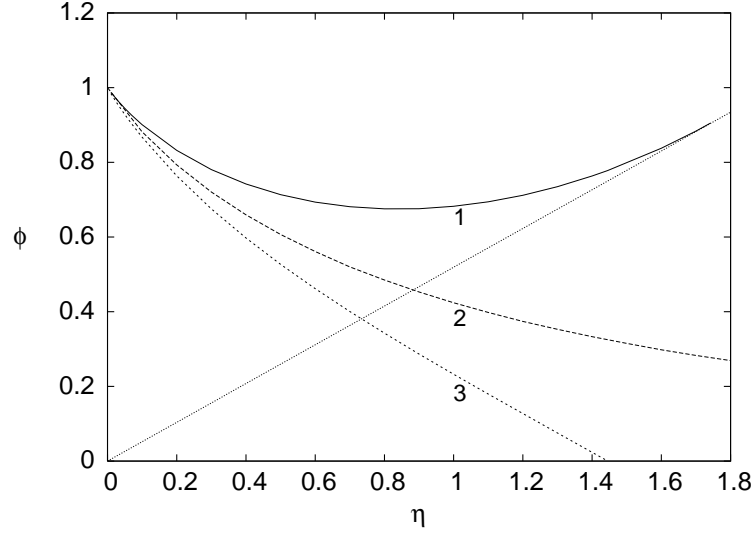


Figure A.4.: Physically relevant solutions of the Thomas-Fermi Equation (A.2.7) with the boundary conditions (A.2.8) and (A.2.9). The curve 1 refers to a neutral compressed atom. The curve 2 refers to a neutral free atom. The curve 3 refers to a positive ion. The dotted straight line is the tangent to the curve 1 at the point $(\eta_0, \phi(\eta_0))$ corresponding to overall charge neutrality (see Eq. (A.2.9)).

of compressed atoms $N_e = N_p$ so the Coulomb potential energy eV vanishes at the boundary R_{WS} . As a result, using Eqs. (A.2.1) and (A.2.3), the Fermi energy of electrons satisfies the universal relation

$$\frac{\sigma r_{Bohr}}{e^2} \frac{E_e^F}{N_p^{4/3}} = \frac{\phi(\eta_0)}{\eta_0}, \quad (\text{A.2.10})$$

while the Wigner-Seitz cell radius R_{WS} satisfies the universal relation

$$\frac{R_{WS}}{\sigma r_{Bohr} N_p^{-1/3}} = \eta_0. \quad (\text{A.2.11})$$

Therefore in the classic treatment η_0 can approach zero and consequently the range of the possible values of the Fermi energy extends from zero to infinity.

The results are summarized in Figs. A.4 and A.5.

The Thomas-Fermi-Dirac model

Dirac has introduced modifications to the original Thomas-Fermi theory to include effects of the exchange interaction (Dirac, 1930). In this case the con-

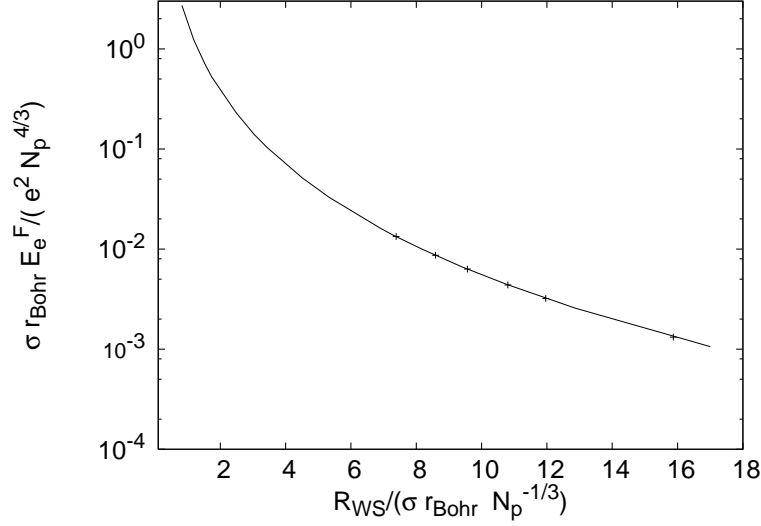


Figure A.5.: The electron Fermi energy E_e^F , in units of $e^2 N_p^{4/3} / (\sigma r_{Bohr})$ is plotted as a function of the Wigner-Seitz cell radius R_{WS} , in units of $\sigma r_{Bohr} N_p^{-1/3}$ (see Eqs. (A.2.10), (A.2.11)). Points refer to the numerical integrations of the Thomas-Fermi equation (A.2.7) performed originally by Feynman, Metropolis and Teller in Feynman et al. (1949).

dition of equilibrium of the electrons in the atom is generalized as follows

$$\frac{(P_e^F)^2}{2m_e} - eV - \frac{e^2}{\pi\hbar} P_e^F = E_e^F. \quad (\text{A.2.12})$$

The electron number density is now connected to the Coulomb potential energy by

$$n_e = \frac{1}{3\pi^5} \frac{1}{r_{Bohr}^3} \left[1 + \sqrt{1 + 2\pi^2 \frac{r_{Bohr}}{e^2} (eV + E_e^F)} \right]^3. \quad (\text{A.2.13})$$

Defining

$$\frac{1}{2\pi^2} \frac{e^2}{r_{Bohr}} + eV(r) + E_e^F = e^2 N_p \frac{\chi(r)}{r}, \quad (\text{A.2.14})$$

the Eq. (A.2.2) can be written in dimensionless form as

$$\frac{d^2\phi(\eta)}{d\eta^2} = \eta \left[d + \left(\frac{\phi(\eta)}{\eta} \right)^{1/2} \right]^3, \quad (\text{A.2.15})$$

where $d = (3/(32\pi^2))^{1/3}(1/N_p)^{2/3}$. The boundary condition for Eq. (A.2.15) are $\phi(0) = 1$ and $\eta_0\phi'(\eta_0) = \phi(\eta_0)$.

A.2.3. The relativistic generalization of the Feynman-Metropolis-Teller treatment

The relativistic Thomas-Fermi model for atoms

In the relativistic generalization of the Thomas-Fermi equation the point-like approximation of the nucleus must be abandoned (Ferreirinho et al., 1980; Ruffini and Stella, 1981) since the relativistic equilibrium condition

$$E_e^F = \sqrt{(P_e^F c)^2 + m_e^2 c^4} - m_e c^2 - eV(r), \quad (\text{A.2.16})$$

which generalizes the Eq. (A.2.1), would lead to a non-integrable expression for the electron density near the origin. Consequently we adopt an extended nucleus. Traditionally the radius of an extended nucleus is given by the phenomenological relation $R_c = r_0 A^{1/3}$ where A is the number of nucleons and $r_0 = 1.2 \times 10^{-13}$ cm. Further it is possible to show from the extremization of the semi-empirical Weizsacker mass-formula that the relation between A and N_p is given by (see e.g. Segré (1977) and Ferreirinho et al. (1980))

$$N_p \approx \left[\frac{2}{A} + \frac{2a_C}{a_A} \frac{1}{A^{1/3}} \right]^{-1} \approx \left[\frac{2}{A} + \frac{3}{200} \frac{1}{A^{1/3}} \right]^{-1}, \quad (\text{A.2.17})$$

where $a_C \approx 0.71$ MeV, $a_A \approx 93.15$ MeV are the Coulomb and the asymmetry coefficients respectively. In the limit of small A Eq. (A.2.17) gives

$$N_p \approx \frac{A}{2}. \quad (\text{A.2.18})$$

In Rotondo et al. (2011e) we have relaxed the condition $N_p \approx A/2$ adopted e.g. in Migdal et al. (1977) as well as the condition $N_p \approx [2/A + 3/(200A^{1/3})]^{-1}$ adopted e.g. in Ferreirinho et al. (1980); Ruffini and Stella (1981) by imposing explicitly the beta decay equilibrium between neutron, protons and electrons.

In particular, following the previous treatments (see e.g. Rotondo et al. (2011e)), we have assumed a constant distribution of protons confined in a

radius R_c defined by

$$R_c = \Delta \frac{\hbar}{m_\pi c} N_p^{1/3}, \quad (\text{A.2.19})$$

where m_π is the pion mass and Δ is a parameter such that $\Delta \approx 1$ ($\Delta < 1$) corresponds to nuclear (supranuclear) densities when applied to ordinary nuclei. Consequently, the proton density can be written as

$$n_p(r) = \frac{N_p}{\frac{4}{3}\pi R_c^3} \theta(R_c - r) = \frac{3}{4\pi} \frac{m_\pi^3 c^3}{\hbar^3} \frac{1}{\Delta^3} \theta(R_c - r), \quad (\text{A.2.20})$$

where $\theta(x)$ is the Heaviside function which by definition is given by

$$\theta(x) = \begin{cases} 0, & x < 0, \\ 1, & x > 0. \end{cases} \quad (\text{A.2.21})$$

The electron density is given by

$$n_e(r) = \frac{(P_e^F)^3}{3\pi^2 \hbar^3} = \frac{1}{3\pi^2 \hbar^3 c^3} \left[e^2 V^2(r) + 2m_e c^2 e V(r) \right]^{3/2}, \quad (\text{A.2.22})$$

where V is the Coulomb potential.

The overall Coulomb potential satisfies the Poisson equation

$$\nabla^2 V(r) = -4\pi e [n_p(r) - n_e(r)], \quad (\text{A.2.23})$$

with the boundary conditions $V(\infty) = 0$ (due to global charge neutrality) and finiteness of $V(0)$.

Using Eqs. (A.2.4), (A.2.5) and replacing the particle densities (A.2.20) and (A.2.22) into the Poisson equation (A.2.23) we obtain the relativistic Thomas-Fermi equation

$$\frac{d^2 \phi(\eta)}{d\eta^2} = -\frac{3\eta}{\eta_c^3} \theta(\eta_c - \eta) + \frac{\phi^{3/2}}{\eta^{1/2}} \left[1 + \left(\frac{N_p}{N_p^{crit}} \right)^{4/3} \frac{\phi}{\eta} \right]^{3/2}, \quad (\text{A.2.24})$$

where $\phi(0) = 0$, $\phi(\infty) = 0$ and $\eta_c = R_c/b$. The critical number of protons N_p^{crit} is defined by

$$N_p^{crit} = \sqrt{\frac{3\pi}{4}} \alpha^{-3/2}, \quad (\text{A.2.25})$$

where, as usual, $\alpha = e^2/(\hbar c)$.

It is interesting that by introducing the new dimensionless variable

$$x = \frac{r}{\lambda_\pi} = \frac{b}{\lambda_\pi} \eta, \quad (\text{A.2.26})$$

and the function

$$\chi = \alpha N_p \phi, \quad (\text{A.2.27})$$

where $\lambda_\pi = \hbar/(m_\pi c)$, Eq. (A.2.24) assumes a canonical form, the master relativistic Thomas-Fermi equation (see Ruffini (2008b))

$$\frac{1}{3x} \frac{d^2 \chi(x)}{dx^2} = -\frac{\alpha}{\Delta^3} \theta(x_c - x) + \frac{4\alpha}{9\pi} \left[\frac{\chi^2(x)}{x^2} + 2 \frac{m_e \chi}{m_\pi x} \right]^{3/2}, \quad (\text{A.2.28})$$

where $x_c = R_c/\lambda_\pi$ with the boundary conditions $\chi(0) = 0$, $\chi(\infty) = 0$. The neutron density $n_n(r)$, related to the neutron Fermi momentum $P_n^F = (3\pi^2 \hbar^3 n_n)^{1/3}$, is determined, as in the previous case Rotondo et al. (2011e), by imposing the condition of beta equilibrium

$$\begin{aligned} E_n^F &= \sqrt{(P_n^F c)^2 + m_n^2 c^4} - m_n c^2 \\ &= \sqrt{(P_p^F c)^2 + m_p^2 c^4} - m_p c^2 + eV(r), \end{aligned} \quad (\text{A.2.29})$$

which in turn is related to the proton density n_p and the electron density by Eqs. (A.2.22), (A.2.23). Integrating numerically these equations we have obtained a new generalized relation between A and N_p for any value of A . In the limit of small A this result agrees with the phenomenological relations given by Eqs. (A.2.17, A.2.18), as is clearly shown in Fig. (A.6).

The relativistic Thomas-Fermi model for compressed atoms

We turn now to the case of compressed atoms in which the electron Fermi energy is positive. The relativistic generalization of the equilibrium condition (A.2.1) now reads

$$E_e^F = \sqrt{(P_e^F c)^2 + m_e^2 c^4} - m_e c^2 - eV(r) > 0. \quad (\text{A.2.30})$$

Adopting an extended-nucleus with a radius given by Eq. (A.2.19) and a proton density given by Eq. (A.2.20) the Poisson equation (A.2.23), with the fol-

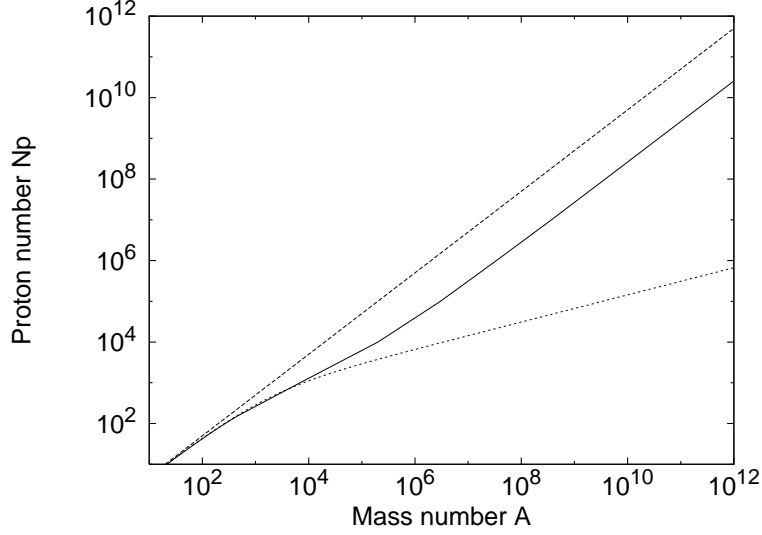


Figure A.6.: The A - N_p relation at nuclear density (solid line) obtained from first principles compared with the phenomenological expressions given by $N_p \approx A/2$ (dashed line) and Eq. (A.2.17) (dotted line). The asymptotic value, for $A \rightarrow (m_{\text{Planck}}/m_n)^3$, is $N_p \approx 0.0046A$.

lowing electron density

$$n_e(r) = \frac{(P_e^F)^3}{3\pi^2\hbar^3} = \frac{1}{3\pi^2\hbar^3 c^3} \left[e^2 \hat{V}^2(r) + 2m_e c^2 e \hat{V}(r) \right]^{3/2}, \quad (\text{A.2.31})$$

gives again the master relativistic Thomas-Fermi equation (A.2.28) where $\chi/r = e\hat{V}(r)/(c\hbar)$ and $e\hat{V} = eV + E_e^F$.

In this case Eq. (A.2.28) has to be integrated with the boundary conditions $\chi(0) = 0$, $\chi(x_{WS}) = x_{WS}\chi'(x_{WS})$, $x_{WS} = R_{WS}/\lambda_\pi$. Using Eqs. (A.2.4), (A.2.26) and (A.2.27) we obtain the electron Fermi energy in the form

$$E_e^F = m_\pi c^2 \frac{\chi(x_{WS})}{x_{WS}}. \quad (\text{A.2.32})$$

The neutron density $n_n(r)$, related to the neutron Fermi momentum $P_n^F = (3\pi^2\hbar^3 n_n)^{1/3}$, is determined by imposing the condition of beta equilibrium

$$\begin{aligned} E_n^F &= \sqrt{(P_n^F c)^2 + m_n^2 c^4} - m_n c^2 \\ &= \sqrt{(P_p^F c)^2 + m_p^2 c^4} - m_p c^2 + eV(r) + E_e^F. \end{aligned} \quad (\text{A.2.33})$$

Using this approach, it is then possible to determine the beta equilibrium nuclide as a function of the density of the system. Infact, electrons and pro-

tons can be converted to neutrons in inverse beta decay $p + e^- \rightarrow n + \nu_e$ if the condition $E_n^F < \sqrt{(P_p^F c)^2 + m_p^2 c^4} - m_p c^2 + eV(r) + E_e^F$ holds. The condition of equilibrium (A.2.33) is crucial, for example, in the construction of a self-consistent equation of state of high energy density matter present in white dwarfs and neutron star crusts. In the case of zero electron Fermi energy the generalized $A - N_p$ relation of Fig. (A.6) is obtained.

The relativistic Thomas-Fermi-Dirac model for compressed atoms

We now take into account the exchange corrections to the relativistic Thomas-Fermi equation (A.2.28). In this case we have (see Migdal et al. (1977) for instance)

$$E_e^F = \sqrt{(cP_e^F)^2 + m_e^2 c^4} - m_e c^2 - eV - \frac{\alpha}{\pi} c P_e^F = \text{constant}. \quad (\text{A.2.34})$$

Introducing the function $\chi(r)$ as before

$$E_e^F + eV = e\hat{V} = \hbar c \frac{\chi}{r}, \quad (\text{A.2.35})$$

we obtain the electron number density

$$n_e = \frac{1}{3\pi^2 \hbar^3 c^3} \left\{ \gamma (m_e c^2 + e\hat{V}) + [(e\hat{V})^2 + 2m_e c^2 e\hat{V}]^{1/2} \right. \\ \left. \times \left[\frac{(1 + \gamma^2)(m_e c^2 + e\hat{V})^2 - m_e^2 c^4}{(m_e c^2 + e\hat{V})^2 - m_e^2 c^4} \right]^{1/2} \right\}^3, \quad (\text{A.2.36})$$

where $\gamma = (\alpha/\pi)/(1 - \alpha^2/\pi^2)$.

If we take the approximation $1 + \gamma^2 \approx 1$ the above equation becomes

$$n_e = \frac{1}{3\pi^2 \hbar^3 c^3} \left\{ \gamma (m_e c^2 + e\hat{V}) + [(e\hat{V})^2 + 2m_e c^2 e\hat{V}]^{1/2} \right\}^3. \quad (\text{A.2.37})$$

The second term on the right-hand-side of Eq. (A.2.37) has the same form of the electron density given by the relativistic Thomas-Fermi approach without the exchange correction (A.2.31) and therefore the first term shows the explicit contribution of the exchange term to the electron density.

Using the full expression of the electron density given by Eq. (A.2.36) we

obtain the relativistic Thomas-Fermi-Dirac equation

$$\begin{aligned} \frac{1}{3x} \frac{d^2\chi(x)}{dx^2} = & -\frac{\alpha}{\Delta^3} \theta(x_c - x) + \frac{4\alpha}{9\pi} \left\{ \gamma \left(\frac{m_e}{m_\pi} + \frac{\chi}{x} \right) + \left[\left(\frac{\chi}{x} \right)^2 + 2 \frac{m_e}{m_\pi} \frac{\chi}{x} \right]^{1/2} \right. \\ & \times \left. \left[\frac{(1 + \gamma^2)(m_e/m_\pi + \chi/x)^2 - (m_e/m_\pi)^2}{(m_e/m_\pi + \chi/x)^2 - (m_e/m_\pi)^2} \right]^{1/2} \right\}^3, \end{aligned} \quad (\text{A.2.38})$$

which by applying the approximation $1 + \gamma^2 \approx 1$ becomes

$$\frac{1}{3x} \frac{d^2\chi(x)}{dx^2} = -\frac{\alpha}{\Delta^3} \theta(x_c - x) + \frac{4\alpha}{9\pi} \left\{ \gamma \left(\frac{m_e}{m_\pi} + \frac{\chi}{x} \right) + \left[\left(\frac{\chi}{x} \right)^2 + 2 \frac{m_e}{m_\pi} \frac{\chi}{x} \right]^{1/2} \right\}^3. \quad (\text{A.2.39})$$

The boundary conditions for Eq. (A.2.38) are $\chi(0) = 0$ and $\chi(x_{WS}) = x_{WS}\chi'(x_{WS})$. The neutron density can be obtained as before by using the beta equilibrium condition (A.2.33) with the electron Fermi energy given by Eq. (A.2.34).

In Fig. A.7 we show the results of the numerical integration of the relativistic Thomas-Fermi equation (A.2.28) and of the relativistic Thomas-Fermi-Dirac equation (A.2.38) for helium, carbon and iron. In particular, we show the electron Fermi energy multiplied by $N_p^{-4/3}$ as a function of the ratio R_{WS}/R_c between the Wigner-Seitz cell radius R_{WS} and the nucleus radius R_c given by Eq. (A.2.19).

The effects of the exchange term are appreciable only in the low density (low compression) region, i.e. when $R_{WS} \gg R_c$ (see Fig. A.7). We can then conclude in total generality that the correction given by the Thomas-Fermi-Dirac exchange term is, small in the non-relativistic low compression (low density) regime, and negligible in the relativistic high compression (high density) regime.

A.2.4. Comparison and contrast with approximate treatments

There exists in the literature a variety of semi-qualitative approximations adopted in order to describe the electron component of a compressed atom (see e.g. Bürvenich et al. (2007) for applications of the uniform approximation and e.g. Chabrier and Potekhin (1998); Potekhin et al. (2009); Douchin and Haensel (2001); Haensel and Zdunik (1990a,b), for applications of the Salpeter approximate treatment).

We shall see how the relativistic treatment of the Thomas-Fermi equation affects the current analysis of compressed atoms in the literature by introducing qualitative and quantitative differences which deserve attention.

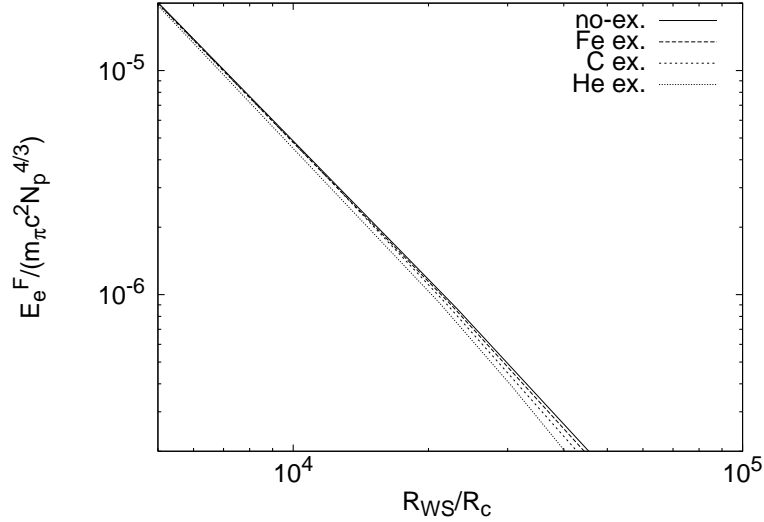


Figure A.7.: The electron Fermi energy in units of $m_{\pi}c^2N_p^{4/3}$ is plotted for helium, carbon and iron, as a function of the ratio R_{WS}/R_c in the relativistic Feynman-Metropolis-Teller (FMT) treatment with and without the exchange effects. Here R_{WS} denotes the Wigner-Seitz cell radius and R_c is the nucleus radius as given by Eq. (A.2.19). It is clear that the exchange terms are appreciable only in the low density region and are negligible as $R_{WS} \rightarrow R_c$.

Relativistic FMT treatment vs. relativistic uniform approximation

One of the most used approximations in the treatment of the electron distribution in compressed atoms is the one in which, for a given nuclear charge $+eN_p$, the Wigner-Seitz cell radius R_{WS} is defined by

$$N_p = \frac{4\pi}{3}R_{WS}^3n_e, \quad (\text{A.2.40})$$

where $n_e = (P_e^F)^3/(3\pi^2\hbar^3)$. The Eq. (A.2.40) ensures the global neutrality of the Wigner-Seitz cell of radius R_{WS} assuming a uniform distribution of electrons inside the cell.

We shall first compare the Feynman-Metropolis-Teller treatment, previously introduced, with the uniform approximation for the electron distribution. In view of the results of the preceding section, hereafter we shall consider the non-relativistic and the relativistic formulation of the Feynman-Metropolis-Teller treatment with no Thomas-Fermi-Dirac exchange correction.

In Fig. A.8 we have plotted the electron number density obtained from Eq. (A.2.31) where the Coulomb potential is related to the function χ , which is obtained from numerical integration of the relativistic Thomas-Fermi equa-

tion (A.2.28) for different compressions for helium and iron. We have normalized the electron density to the average electron number density $n_0 = 3N_e/(4\pi R_{WS}^3) = 3N_p/(4\pi R_{WS}^3)$ as given by Eq. (A.2.40).

We can see in Fig. A.8 how our treatment, based on the numerical integration of the relativistic Thomas-Fermi equation (A.2.28) and imposing the condition of beta equilibrium (A.2.33), leads to electron density distributions markedly different from the constant electron density approximation.

From Eqs. (A.2.30), (A.2.40) and taking into account the global neutrality condition of the Wigner-Seitz cell $eV(R_{WS}) = 0$, the electron Fermi energy in the uniform approximation can be written as

$$E_e^F \simeq \left[-\frac{m_e}{m_\pi} + \sqrt{\left(\frac{m_e}{m_\pi}\right)^2 + \left(\frac{9\pi}{4}\right)^{2/3} \frac{N_p^{2/3}}{x_{WS}^2}} \right] m_\pi c^2. \quad (\text{A.2.41})$$

We show in Fig. A.9 the electron Fermi energy as a function of the average electron density $n_0 = 3N_e/(4\pi R_{WS}^3) = 3N_p/(4\pi R_{WS}^3)$ in units of the nuclear density $n_{nuc} = 3A/(4\pi\Delta^3 N_p \lambda_\pi^3)$. For selected compositions we show the results for the relativistic Feynman-Metropolis-Teller treatment, based on the numerical integration of the relativistic Thomas-Fermi equation (A.2.28), and for the relativistic uniform approximation.

As clearly shown in Fig. A.8 and summarized in Fig. A.9 the relativistic treatment leads to results strongly dependent at low compression from the nuclear composition. The corresponding value of the electron Fermi energy derived from a uniform approximation overevaluates the true electron Fermi energy (see Fig. A.9). In the limit of high compression the relativistic curves asymptotically approach the uniform one (see also Fig. A.8).

The uniform approximation becomes exact in the limit when the electron Fermi energy acquires its maximum value as given by

$$(E_e^F)_{max} \simeq \left[-\frac{m_e}{m_\pi} + \sqrt{\left(\frac{m_e}{m_\pi}\right)^2 + \left(\frac{3\pi^2}{2}\right)^{2/3} \left(\frac{N_p}{A}\right)^{2/3}} \right] m_\pi c^2, \quad (\text{A.2.42})$$

which is attained when R_{WS} coincides with the nuclear radius R_c . Here, the maximum electron Fermi energy (A.2.42) is obtained by replacing in Eq. (A.2.41) the value of the normalized Wigner-Seitz cell radius $x_{WS} = x_c = R_c/\lambda_\pi \approx [(3/2)\pi]^{1/3} A^{1/3}$.

Relativistic FMT treatment vs. Salpeter approximate treatment

Corrections to the uniform distribution were also studied by Salpeter (1961) and his approximations are largely applied in physics (see e.g. Chabrier and Potekhin (1998); Potekhin et al. (2009)) and astrophysics (see e.g. Douchin

and Haensel (2001); Haensel and Zdunik (1990a,b)).

Keeping the point-like nucleus assumption, Salpeter (1961) studied the corrections to the above models due to the inhomogeneity of the electron distribution inside the Wigner-Seitz cell. He expressed an analytic formula for the total energy of a Wigner-Seitz cell based on Coulomb corrections to the uniform distribution of electrons. The first correction corresponds to the inclusion of the lattice energy $E_C = -(9N_p^2\alpha)/(10R_{WS})$, which results from the point-like nucleus-electron Coulomb interaction and, from the electron-electron Coulomb interaction inside the cell of radius R_{WS} . The second correction is given by a series-expansion of the electron Fermi energy about the average electron density n_e given by Eq. (A.2.40) the uniform approximation $n_e = 3N_p/(4\pi R_{WS}^3)$. The electron density is then assumed equals to $n_e[1 + \epsilon(r)]$ with $\epsilon(r)$ considered as infinitesimal. The Coulomb potential energy is assumed to be the one of the point-like nucleus with the uniform distribution of electrons of density n_e , thus the correction given by $\epsilon(r)$ is neglected on the Coulomb potential. The electron distribution is then calculated at first-order by expanding the relativistic electron kinetic energy

$$\begin{aligned}\epsilon_k &= \sqrt{[cP_e^F(r)]^2 + m_e^2c^4} - m_e c^2 \\ &= \sqrt{(3\pi^2 n_e)^{2/3}[1 + \epsilon(r)]^{2/3} + m_e^2c^4} - m_e c^2,\end{aligned}\quad (\text{A.2.43})$$

about its value given by the uniform approximation

$$\epsilon_k^{\text{unif}} = \sqrt{(3\pi^2 n_e)^{2/3} + m_e^2c^4} - m_e c^2,\quad (\text{A.2.44})$$

considering as infinitesimal the ratio eV/E_e^F between the Coulomb potential energy eV and the electron Fermi energy $E_e^F = \sqrt{[cP_e^F(r)]^2 + m_e^2c^4} - m_e c^2 - eV$.

The effect of the Dirac electron-exchange correction (Dirac, 1930) on the equation of state was also considered by Salpeter (1961). However, adopting the general approach of Migdal et al. (1977), these effects are negligible in the relativistic regime (see Subsec. A.2.3).

The inclusion of each additional Coulomb correction results in a decreasing of the pressure of the cell P_S . However, despite to be very interesting in identifying piecewise contributions to the total pressure, the validity of the Salpeter approach needs a verification by a more general treatment. For instance, the failure of the Salpeter formulas can be seen at densities of the order of $\sim 10^2 - 10^3 \text{ g cm}^{-3}$ for nuclei with large N_p , as in the case of iron, where the pressure becomes negative (see Table (A.1)). Therefore, the problem of solving the relativistic Thomas-Fermi equation within the Feynman, Metropolis, Teller approach becomes a necessity, since this approach gives all the possible Coulomb and relativistic contributions automatically and correctly.

Table A.1.: Pressure for iron as a function of the density ρ in the uniform approximation (P), in the Salpeter approximation (P_S) and in the relativistic Feynman-Metropolis-Teller approach (P_{FMTrel}). Here $x_S = P_{e,S}^F/(m_e c)$, $x_{FMTrel} = P_e^F/(m_e c)$ are respectively the normalized Salpeter Fermi momentum and the relativistic Feynmann-Metropolis-Teller Fermi momentum.

ρ (g/cm ³)	x_S	x_{FMTrel}	P (bar)	P_S (bar)	P_{FMTrel} (bar)
2.63×10^2	0.05	0.0400	2.9907×10^{10}	-1.8800×10^8	9.9100×10^9
2.10×10^3	0.10	0.0857	9.5458×10^{11}	4.4590×10^{11}	5.4840×10^{11}
1.68×10^4	0.20	0.1893	3.0227×10^{13}	2.2090×10^{13}	2.2971×10^{13}
5.66×10^4	0.30	0.2888	2.2568×10^{14}	1.8456×10^{14}	1.8710×10^{14}
1.35×10^5	0.40	0.3887	9.2964×10^{14}	8.0010×10^{14}	8.0790×10^{14}
2.63×10^5	0.50	0.4876	2.7598×10^{15}	2.4400×10^{15}	2.4400×10^{15}
4.53×10^5	0.60	0.5921	6.6536×10^{15}	6.0040×10^{15}	6.0678×10^{15}
7.19×10^5	0.70	0.6820	1.3890×10^{16}	1.2693×10^{16}	1.2810×10^{16}
1.08×10^6	0.80	0.7888	2.6097×10^{16}	2.4060×10^{16}	2.4442×10^{16}
2.10×10^6	1.00	0.9853	7.3639×10^{16}	6.8647×10^{16}	6.8786×10^{16}
3.63×10^6	1.20	1.1833	1.6902×10^{17}	1.5900×10^{17}	1.5900×10^{17}
5.77×10^6	1.40	1.3827	3.3708×10^{17}	3.1844×10^{17}	3.1898×10^{17}
8.62×10^6	1.6	1.5810	6.0754×10^{17}	5.7588×10^{17}	5.7620×10^{17}
1.23×10^7	1.80	1.7790	1.0148×10^{18}	9.6522×10^{17}	9.6592×10^{17}
1.68×10^7	2.0	1.9770	1.5981×10^{18}	1.5213×10^{18}	1.5182×10^{18}
3.27×10^7	2.50	2.4670	4.1247×10^{18}	3.9375×10^{18}	3.9101×10^{18}
5.66×10^7	3.00	2.965	8.8468×10^{18}	8.4593×10^{18}	8.4262×10^{18}
1.35×10^8	4.00	3.956	2.9013×10^{19}	2.7829×10^{19}	2.7764×10^{19}
2.63×10^8	5.00	4.939	7.2160×10^{19}	6.9166×10^{19}	6.9062×10^{19}
8.85×10^8	7.50	7.423	3.7254×10^{20}	3.5700×10^{20}	3.5700×10^{20}

Relativistic FMT treatment vs. non-relativistic FMT treatment

We now compare and contrast the Fermi energy, given by Eq. (A.2.32), of a compressed atom in the non-relativistic and the relativistic limit (see Fig. A.10).

There are major differences:

1) The electron Fermi energy in the relativistic treatment is strongly dependent on the nuclear composition, while the non-relativistic treatment presents a universal behavior in the units of Fig. A.10. In the limit of low densities the relativistic curves approach the universal non-relativistic curve. In the non-relativistic treatment the ratio $E_e^F / (m_\pi c^2 N_p^{4/3})$ does not depend on the number of protons N_p if the Wigner-Seitz cell radius R_{WS} is multiplied by $N_p^{1/3}$ (see Eqs. (A.2.10), (A.2.11)). This universality is lost in the relativistic treatment since there is no way to eliminate the dependence of the electron Fermi energy on the nuclear composition (see Eq. (A.2.28)).

2) The relativistic treatment leads to values of the electron Fermi energy consistently smaller than the ones of the non-relativistic treatment.

3) While in the non-relativistic treatment the electron Fermi energy can reach, by compression, infinite values as $R_{WS} \rightarrow 0$, in the relativistic treatment it reaches a perfectly finite value given by Eq. (A.2.42) attained when R_{WS} coincides with the nuclear radius R_c .

It is clear then, from above considerations, the relativistic treatment of the Thomas-Fermi equation introduces significant differences from the current approximations in the literature: a) the uniform electron distribution (Bürvenich et al., 2007), b) the approximate perturbative solutions departing from the uniform distribution (Salpeter, 1961) and c) the non-relativistic treatment (Feynman et al., 1949). We have recently applied these results of the relativistic Feynman, Metropolis, Teller treatment of a compressed atom to the study of white dwarfs and their consequences on the determination of their masses, radii and critical mass (Rotondo et al., 2011b).

A.2.5. Application to nuclear matter cores of stellar dimensions

We turn now to nuclear matter cores of stellar dimensions of $A \simeq (m_{\text{Planck}}/m_n)^3 \sim 10^{57}$ or $M_{\text{core}} \sim M_\odot$.

Following the treatment presented in Rotondo et al. (2011e), we use the existence of scaling laws and proceed to the ultra-relativistic limit of Eqs. (A.2.20), (A.2.28), (A.2.31), (A.2.33). For positive values of the electron Fermi energy E_e^F , we introduce the new function $\phi = 4^{1/3}(9\pi)^{-1/3}\chi\Delta/x$ and the new variable $\hat{x} = kx$ where $k = (12/\pi)^{1/6}\sqrt{\alpha}\Delta^{-1}$, as well as the variable $\xi = \hat{x} - \hat{x}_c$ in order to describe better the region around the core radius.

Eq. (A.2.28) becomes

$$\frac{d^2\hat{\phi}(\xi)}{d\xi^2} = -\theta(-\xi) + \hat{\phi}(\xi)^3, \quad (\text{A.2.45})$$

where $\hat{\phi}(\xi) = \phi(\xi + \hat{x}_c)$ and the curvature term $2\hat{\phi}'(\xi)/(\xi + \hat{x}_c)$ has been neglected.

The Coulomb potential energy is given by

$$eV(\xi) = \left(\frac{9\pi}{4}\right)^{1/3} \frac{1}{\Delta} m_\pi c^2 \hat{\phi}(\xi) - E_e^F, \quad (\text{A.2.46})$$

corresponding to the electric field

$$E(\xi) = - \left(\frac{3^5\pi}{4}\right)^{1/6} \frac{\sqrt{\alpha} m_\pi^2 c^3}{\Delta^2 e\hbar} \hat{\phi}'(\xi), \quad (\text{A.2.47})$$

and the electron number-density

$$n_e(\xi) = \frac{1}{3\pi^2\hbar^3 c^3} \left(\frac{9\pi}{4}\right) \frac{1}{\Delta^3} (m_\pi c^2)^3 \hat{\phi}^3(\xi). \quad (\text{A.2.48})$$

In the core center we must have $n_e = n_p$. From Eqs. (A.2.20) and (A.2.48) we then have that, for $\xi = -\hat{x}_c$, $\hat{\phi}(-\hat{x}_c) = 1$.

In order to consider a compressed nuclear density core of stellar dimensions, we then introduce a Wigner-Seitz cell determining the outer boundary of the electron distribution which, in the new radial coordinate ξ is characterized by ξ^{WS} . In view of the global charge neutrality of the system the electric field goes to zero at $\xi = \xi^{WS}$. This implies, from Eq. (A.2.47), $\hat{\phi}'(\xi^{WS}) = 0$.

We now turn to the determination of the Fermi energy of the electrons in this compressed core. The function $\hat{\phi}$ and its first derivative $\hat{\phi}'$ must be continuous at the surface $\xi = 0$ of the nuclear density core.

This boundary-value problem can be solved analytically and indeed Eq. (A.2.45) has the first integral,

$$2[\hat{\phi}'(\xi)]^2 = \begin{cases} \hat{\phi}^4(\xi) - 4\hat{\phi}(\xi) + 3, & \xi < 0, \\ \hat{\phi}^4(\xi) - \hat{\phi}^4(\xi^{WS}), & \xi > 0, \end{cases} \quad (\text{A.2.49})$$

with boundary conditions at $\xi = 0$:

$$\begin{aligned} \hat{\phi}(0) &= \frac{\hat{\phi}^4(\xi^{WS}) + 3}{4}, \\ \hat{\phi}'(0) &= -\sqrt{\frac{\hat{\phi}^4(0) - \hat{\phi}^4(\xi^{WS})}{2}}. \end{aligned} \quad (\text{A.2.50})$$

Having fulfilled the continuity condition we integrate Eq. (A.2.49) obtaining for $\xi \leq 0$

$$\hat{\phi}(\xi) = 1 - 3 \left[1 + 2^{-1/2} \sinh(a - \sqrt{3}\xi) \right]^{-1}, \quad (\text{A.2.51})$$

where the integration constant a has the value

$$\sinh(a) = \sqrt{2} \left(\frac{11 + \hat{\phi}^4(\xi^{WS})}{1 - \hat{\phi}^4(\xi^{WS})} \right). \quad (\text{A.2.52})$$

In the interval $0 \leq \xi \leq \xi^{WS}$, the field $\hat{\phi}(\xi)$ is implicitly given by

$$F \left(\arccos \frac{\hat{\phi}(\xi^{WS})}{\hat{\phi}(\xi)}, \frac{1}{\sqrt{2}} \right) = \hat{\phi}(\xi^{WS})(\xi - \xi^{WS}), \quad (\text{A.2.53})$$

where $F(\varphi, k)$ is the elliptic function of the first kind, and $F(0, k) \equiv 0$. For $F(\varphi, k) = u$, the inverse function $\varphi = F^{-1}(u, k) = \text{am}(u, k)$ is the well known Jacobi amplitude. In terms of it, we can express the solution (A.2.53) for $\xi > 0$ as,

$$\hat{\phi}(\xi) = \hat{\phi}(\xi^{WS}) \left\{ \cos \left[\text{am} \left(\hat{\phi}(\xi^{WS})(\xi - \xi^{WS}), \frac{1}{\sqrt{2}} \right) \right] \right\}^{-1}. \quad (\text{A.2.54})$$

In the present case of $E_e^F > 0$ the ultra-relativistic approximation is indeed always valid up to $\xi = \xi^{WS}$ for high compression factors, i.e. for $R_{WS} \simeq R_c$. In the case $E_e^F = 0$, $\xi^{WS} \rightarrow \infty$, there is a breakdown of the ultra-relativistic approximation when $\xi \rightarrow \xi^{WS}$.

Details are given in Figs. A.11, A.12, A.13.

We can now estimate two crucial quantities of the solutions: the Coulomb potential at the center of the configuration and the electric field at the surface of the core

$$eV(0) \simeq \left(\frac{9\pi}{4} \right)^{1/3} \frac{1}{\Delta} m_\pi c^2 - E_e^F, \quad (\text{A.2.55})$$

$$E_{\max} \simeq 2.4 \frac{\sqrt{\alpha}}{\Delta^2} \left(\frac{m_\pi}{m_e} \right)^2 E_c |\hat{\phi}'(0)|, \quad (\text{A.2.56})$$

where $E_c = m_e^2 c^3 / (e\hbar)$ is the critical electric field for vacuum polarization. These functions depend on the value $\hat{\phi}(\xi^{WS})$ via Eqs. (A.2.49)–(A.2.53). At the boundary $\xi = \xi^{WS}$, due to the global charge neutrality, both the electric field $E(\xi^{WS})$ and the Coulomb potential $eV(\xi^{WS})$ vanish. From Eq. (A.2.46),

we determine the value of $\hat{\phi}(\xi)$ at $\xi = \xi^{WS}$

$$\hat{\phi}(\xi^{WS}) = \Delta \left(\frac{4}{9\pi} \right)^{1/3} \frac{E_e^F}{m_\pi c^2}, \quad (\text{A.2.57})$$

as a function of the electron Fermi energies E_e^F . From the above Eq. (A.2.57), one can see that there exists a solution, characterized by the value of electron Fermi energy

$$\frac{(E_e^F)_{max}}{m_\pi c^2} = \frac{1}{\Delta} \left(\frac{9\pi}{4} \right)^{1/3}, \quad (\text{A.2.58})$$

such that $\hat{\phi}(\xi^{WS}) = 1$. From Eq. (A.2.53) and $\xi = 0$, we also have

$$\xi^{WS}(\hat{\phi}(\xi^{WS})) = \left\{ \frac{1}{\hat{\phi}(0)} F \left[\arccos \left(4 - \frac{3}{\hat{\phi}(0)} \right), \frac{1}{\sqrt{2}} \right] \right\}. \quad (\text{A.2.59})$$

For $\hat{\phi}(\xi^{WS}) = 1$, from Eq. (A.2.50) follows $\hat{\phi}(0) = 1$ hence Eq. (A.2.59) becomes

$$\xi^{WS}(\hat{\phi}(0)) = F \left[0, \frac{1}{\sqrt{2}} \right]. \quad (\text{A.2.60})$$

It is well known that if the inverse Jacobi amplitude $F[0, 1/\sqrt{2}]$ is zero, then

$$\xi^{WS}(\hat{\phi}(\xi^{WS}) = \hat{\phi}(0) = 1) = 0. \quad (\text{A.2.61})$$

Indeed from $\hat{\phi}(\xi^{WS}) = 1$ follows $\hat{\phi}(0) = 1$ and $\xi^{WS} = 0$. When $\xi^{WS} = 0$ from Eq. (A.2.50) follows $\hat{\phi}'(0) = 0$ and, using Eq. (A.2.56), $E_{max} = 0$. In other words for the value of E_e^F fulfilling Eq. (A.2.57) no electric field exists on the boundary of the core and from Eq. (A.2.48) and Eqs. (A.2.19, A.2.20) it follows that indeed this is the solution fulfilling both global $N_e = N_p$ and local $n_e = n_p$ charge neutrality. In this special case, starting from Eq. (A.2.33) and $A = N_p + N_n$, we obtain

$$(E_e^F)_{max}^{3/2} = \frac{\frac{9\pi}{4}(\hbar c)^3 \frac{A}{R_c^3} - (E_e^F)_{max}^3}{2^{3/2} \left[\left(\frac{9\pi}{4}(\hbar c)^3 \frac{A}{R_c^3} - (E_e^F)_{max}^3 \right)^{2/3} + m_n^2 c^4 \right]^{3/4}}. \quad (\text{A.2.62})$$

In the ultra-relativistic approximation $(E_e^F)_{max}^3 / \frac{9\pi}{4}(\hbar c)^3 \frac{A}{R_c^3} \ll 1$ so Eq. (A.2.62)

can be approximated to

$$(E_e^F)_{max} = 2^{1/3} \frac{m_n}{m_\pi} \gamma \left[-1 + \sqrt{1 + \frac{\beta}{2\gamma^3}} \right]^{2/3} m_\pi c^2, \quad (\text{A.2.63})$$

where

$$\beta = \frac{9\pi}{4} \left(\frac{\hbar}{m_n c} \right)^3 \frac{A}{R_c^3}, \quad \gamma = \sqrt{1 + \beta^{2/3}}. \quad (\text{A.2.64})$$

The corresponding limiting value to the N_p/A ratio is obtained as follows

$$\frac{N_p}{A} = \frac{2\gamma^3}{\beta} \left[-1 + \sqrt{1 + \frac{\beta}{2\gamma^3}} \right]^2. \quad (\text{A.2.65})$$

Inserting Eqs. (A.2.63), (A.2.64) in Eq. (A.2.65) one obtains the ultra-relativistic limit of Eq. (A.2.42), since the electron Fermi energy, in view of the scaling laws introduced in Rotondo et al. (2011e), is independent of the value of A and depends only on the density of the core.

The N_p -independence in the limiting case of maximum electron Fermi energy attained when $R_{WS} = R_c$, in which the ultra-relativistic treatment approaches the uniform one, and the N_p -dependence for smaller compressions $R_{WS} > R_c$ can be understood as follows. Let see the solution to the ultra-relativistic equation (A.2.45) for small $\xi > 0$. Analogously to the Feynman-Metropolis-Teller approach to the non-relativistic Thomas-Fermi equation, we solve the ultra-relativistic equation (A.2.45) for small ξ . Expanding $\hat{\phi}(\xi)$ about $\xi = 0$ in a semi convergent power series,

$$\frac{\hat{\phi}(\xi)}{\hat{\phi}(0)} = 1 + \sum_{n=2}^{\infty} a_n \xi^{n/2} \quad (\text{A.2.66})$$

and substituting it into the ultra-relativistic equation (A.2.45), we have

$$\sum_{k=3}^{\infty} a_k \frac{k(k-2)}{4} \xi^{(k-4)/2} = \phi^2(0) \exp \left[3 \ln \left(1 + \sum_{n=2}^{\infty} a_n \xi^{n/2} \right) \right]. \quad (\text{A.2.67})$$

This leads to a recursive determination of the coefficients:

$$\begin{aligned} a_3 &= 0, a_4 = \phi^2(0)/2, a_5 = 0, a_6 = \phi^2(0)a_2/2, a_7 = 0, \\ a_8 &= \phi^2(0)(1 - a_2^2)/8, \dots, \end{aligned} \quad (\text{A.2.68})$$

with $a_2 = \hat{\phi}'(0)/\hat{\phi}(0)$ determined by the initial slope, namely, the boundary

condition $\hat{\phi}'(0)$ and $\hat{\phi}(0)$ in Eq. (A.2.50):

$$\hat{\phi}(0) = \frac{\hat{\phi}^4(\xi^{WS}) + 3}{4}, \quad \hat{\phi}'(0) = -\sqrt{\frac{\hat{\phi}^4(0) - \hat{\phi}^4(\xi^{WS})}{2}} \quad (\text{A.2.69})$$

Thus the series solution (A.2.66) is uniquely determined by the boundary value $\hat{\phi}(\xi^{WS})$ at the Wigner-Seitz cell radius.

Now we consider the solution up to the leading orders

$$\begin{aligned} \hat{\phi}(\xi) &= \hat{\phi}(0) + \hat{\phi}'(0)\xi + \frac{1}{2}\hat{\phi}''(0)\xi^2 + \frac{1}{2}\hat{\phi}'''(0)a_2\xi^3 \\ &+ \frac{1}{8}\hat{\phi}^{(4)}(0)(1 - a_2^2)\xi^4 + \dots \end{aligned} \quad (\text{A.2.70})$$

Using Eq. (A.2.70), the electron Fermi energy (A.2.57) becomes

$$\begin{aligned} E_e^F &= (E_e^F)_{max} \left[1 + a_2\xi^{WS} + \frac{1}{2}\hat{\phi}''(0)(\xi^{WS})^2 + \frac{1}{2}\hat{\phi}''(0)a_2(\xi^{WS})^3 \right. \\ &\left. + \frac{1}{8}\hat{\phi}^{(4)}(0)(1 - a_2^2)(\xi^{WS})^4 + \dots \right] \hat{\phi}(0), \end{aligned} \quad (\text{A.2.71})$$

where $(E_e^F)_{max} = (9\pi/4)^{1/3}\Delta^{-1}$ is the maximum Fermi energy which is attained when the Wigner-Seitz cell radius equals the nucleus radius R_c (see Eq. A.2.58). For $\hat{\phi}(\xi^{WS}) < 1$, we approximately have $\hat{\phi}(0) = 3/4$, $\hat{\phi}'(0) = -(3/4)^2/\sqrt{2}$ and the initial slope $a_2 = \hat{\phi}'(0)/\hat{\phi}(0) = -(3/4)/\sqrt{2}$. Therefore Eq. (A.2.71) becomes

$$\begin{aligned} E_e^F &\approx (E_e^F)_{max} \left[1 - \frac{3}{4\sqrt{2}}\xi^{WS} + \frac{1}{2}\left(\frac{3}{4}\right)^2(\xi^{WS})^2 - \frac{1}{2^{3/2}}\left(\frac{3}{4}\right)^3(\xi^{WS})^3 \right. \\ &\left. + \frac{1}{8}\left(\frac{3}{4}\right)^2\left(\frac{41}{32}\right)(\xi^{WS})^4 + \dots \right]. \end{aligned} \quad (\text{A.2.72})$$

By the definition of the coordinate ξ , we know all terms except the first term in the square bracket depend on the values of N_p . In the limit of maximum compression when the electron Fermi energy acquires its maximum value, namely when $\xi^{WS} = 0$, the electron Fermi energy (A.2.72) is the same as the one obtained from the uniform approximation which is independent of N_p . For smaller compressions, namely for $\xi^{WS} > 0$ the electron Fermi energy deviates from the one given by the uniform approximation becoming N_p -dependent.

In Fig. A.14 we plot the Fermi energy of electrons, in units of the pion rest energy, as a function of the dimensionless parameter ξ^{WS} and, as $\xi^{WS} \rightarrow 0$, the limiting value given by Eq. (A.2.63) is clearly displayed.

In Alcock et al. (1986), in order to study the electro-dynamical properties of strange stars, the ultra-relativistic Thomas-Fermi equation was numerically solved in the case of bare strange stars as well as in the case of strange stars with a crust (see e.g. curves (a) and (b) in Fig. 6 of Alcock et al. (1986)). In Fig. 6 of Alcock et al. (1986) was plotted what they called the Coulomb potential energy, which we will denote as V_{Alcock} . The potential V_{Alcock} was plotted for different values of the electron Fermi momentum at the edge of the crust. Actually, such potential V_{Alcock} is not the Coulomb potential eV but it coincides with our function $e\hat{V} = eV + E_e^F$. Namely, the potential V_{Alcock} corresponds to the Coulomb potential shifted by the the Fermi energy of the electrons. We then have from Eq. (A.2.46)

$$e\hat{V}(\xi) = \left(\frac{9\pi}{4}\right)^{1/3} \frac{1}{\Delta} m_\pi c^2 \hat{\phi}(\xi) = V_{\text{Alcock}}. \quad (\text{A.2.73})$$

This explains why in Alcock et al. (1986), for different values of the Fermi momentum at the crust the depth of the potential V_{Alcock} remains unchanged. Instead, the correct behavior of the Coulomb potential is quite different and, indeed, its depth decreases with increasing of compression as can be seen in Fig. A.11.

A.2.6. Compressional energy of nuclear matter cores of stellar dimensions

We turn now to the compressional energy of these family of compressed nuclear matter cores of stellar dimensions each characterized by a different Fermi energy of the electrons. The kinematic energy-spectra of complete degenerate electrons, protons and neutrons are

$$\epsilon^i(p) = \sqrt{(pc)^2 + m_i^2 c^4}, \quad p \leq P_i^F, \quad i = e, p, n. \quad (\text{A.2.74})$$

So the compressional energy of the system is given by

$$\mathcal{E} = \mathcal{E}_B + \mathcal{E}_e + \mathcal{E}_{\text{em}}, \quad \mathcal{E}_B = \mathcal{E}_p + \mathcal{E}_n, \quad (\text{A.2.75})$$

$$\mathcal{E}_i = 2 \int_i \frac{d^3 r d^3 p}{(2\pi\hbar)^3} \epsilon^i(p), \quad i = e, p, n, \quad \mathcal{E}_{\text{em}} = \int \frac{E^2}{8\pi} d^3 r. \quad (\text{A.2.76})$$

Using the analytic solution (A.2.54) we calculate the energy difference between two systems, I and II ,

$$\Delta\mathcal{E} = \mathcal{E}(E_e^F(II)) - \mathcal{E}(E_e^F(I)), \quad (\text{A.2.77})$$

with $E_e^F(II) > E_e^F(I) \geq 0$, at fixed A and R_c .

We first consider the infinitesimal variation of the total energy $\delta\mathcal{E}_{\text{tot}}$ with

respect to the infinitesimal variation of the electron Fermi energy δE_e^F

$$\delta \mathcal{E} = \left[\frac{\partial \mathcal{E}}{\partial N_p} \right]_{VWS} \left[\frac{\partial N_p}{\partial E_e^F} \right] \delta E_e^F + \left[\frac{\partial \mathcal{E}}{\partial VWS} \right]_{N_p} \left[\frac{\partial VWS}{\partial E_e^F} \right] \delta E_e^F. \quad (\text{A.2.78})$$

For the first term of this relation we have

$$\left[\frac{\partial \mathcal{E}}{\partial N_p} \right]_{VWS} = \left[\frac{\partial \mathcal{E}_p}{\partial N_p} + \frac{\partial \mathcal{E}_n}{\partial N_p} + \frac{\partial \mathcal{E}_e}{\partial N_p} + \frac{\partial \mathcal{E}_{em}}{\partial N_p} \right]_{VWS} \simeq \left[E_p^F - E_n^F + E_e^F + \frac{\partial \mathcal{E}_{em}}{\partial N_p} \right]_{VWS}, \quad (\text{A.2.79})$$

where the general definition of chemical potential $\partial \epsilon_i / \partial n_i = \partial \mathcal{E}_i / \partial N_i$ is used ($i = e, p, n$) neglecting the mass defect $m_n - m_p - m_e$. Further using the condition of the beta-equilibrium (A.2.33) we have

$$\left[\frac{\partial \mathcal{E}}{\partial N_p} \right]_{VWS} = \left[\frac{\partial \mathcal{E}_{em}}{\partial N_p} \right]_{VWS}. \quad (\text{A.2.80})$$

For the second term of the Eq. (A.2.78) we have

$$\left[\frac{\partial \mathcal{E}}{\partial VWS} \right]_{N_p} = \left[\frac{\partial \mathcal{E}_p}{\partial VWS} + \frac{\partial \mathcal{E}_n}{\partial VWS} + \frac{\partial \mathcal{E}_e}{\partial VWS} + \frac{\partial \mathcal{E}_{em}}{\partial VWS} \right]_{N_p} = \left[\frac{\partial \mathcal{E}_e}{\partial VWS} \right]_{N_p} + \left[\frac{\partial \mathcal{E}_{em}}{\partial VWS} \right]_{N_p}, \quad (\text{A.2.81})$$

since in the process of increasing the electron Fermi energy namely, by decreasing the radius of the Wigner-Seitz cell, the system by definition maintains the same number of baryons A and the same core radius R_c .

Now $\delta \mathcal{E}$ reads

$$\delta \mathcal{E} = \left\{ \left[\frac{\partial \mathcal{E}_e}{\partial VWS} \right]_{N_p} \frac{\partial VWS}{\partial E_e^F} + \left[\frac{\partial \mathcal{E}_{em}}{\partial VWS} \right]_{N_p} \frac{\partial VWS}{\partial E_e^F} + \left[\frac{\partial \mathcal{E}_{em}}{\partial N_p} \right]_{VWS} \frac{\partial N_p}{\partial E_e^F} \right\} \delta E_e^F, \quad (\text{A.2.82})$$

so only the electromagnetic energy and the electron energy give non-null contributions.

From this equation it follows that

$$\Delta \mathcal{E} = \Delta \mathcal{E}_{em} + \Delta \mathcal{E}_e, \quad (\text{A.2.83})$$

where $\Delta \mathcal{E}_{em} = \mathcal{E}_{em}(E_e^F(II)) - \mathcal{E}_{em}(E_e^F(I))$ and $\Delta \mathcal{E}_e = \mathcal{E}_e(E_e^F(II)) - \mathcal{E}_e(E_e^F(I))$.

In the particular case in which $E_e^F(II) = (E_e^F)_{max}$ and $E_e^F(I) = 0$ we obtain

$$\Delta \mathcal{E} \simeq 0.75 \frac{3^{5/3}}{2} \left(\frac{\pi}{4} \right)^{1/3} \frac{1}{\Delta \sqrt{\alpha}} \left(\frac{\pi}{12} \right)^{1/6} N_p^{2/3} m_\pi c^2, \quad (\text{A.2.84})$$

which is positive.

The compressional energy of a nuclear matter core of stellar dimensions increases with its electron Fermi energy as expected.

A.2.7. Conclusions

The results presented in this article are in the realm of theoretical physics of nuclear physics and of atomic physics and give special attention to relativistic effects. They generalize to the relativistic regimes classical results obtained by Feynman, Metropolis and Teller (Feynman et al., 1949) and, by the introduction of scaling laws, they generalize the classical results obtained by Migdal et al. (1976, 1977); Rotondo et al. (2011e) in heavy nuclei to massive cores of $\sim M_{\odot}$. As such they find their justification. They acquire also special meaning in astrophysics: the considerations contained in Secs. I–IV lead to a consistent treatment of white dwarfs and the ones in Secs. V and VI lead to a deeper understanding of neutron star physics.

We have generalized to the relativistic regime the classic work of Feynman, Metropolis and Teller by solving the relativistic Thomas-Fermi equation in a Wigner-Seitz cell corresponding to a compressed atom. The integration of this equation does not admit regular solutions for a point-like nucleus and both the nuclear radius and the nuclear composition have necessarily to be taken into account (Ferreirinho et al., 1980; Ruffini and Stella, 1981). This introduces a fundamental difference from the non-relativistic Thomas-Fermi model where a point-like nucleus is traditionally adopted.

As in previous works by Ferreira et al. (1980), Ruffini and Stella (1981) and Rotondo et al. (2011e), the protons in the nuclei have been assumed to be at constant density, the electron distribution has been derived by the relativistic Thomas-Fermi equation and the neutron component by the beta equilibrium between neutrons, protons and electrons.

We have examined, for completeness, the relativistic generalization of the Thomas-Fermi-Dirac equation by taking into due account the exchange terms (Dirac, 1930), adopting the general approach of Migdal et al. (1977), and shown that these effects, generally small, can be neglected in the relativistic treatment.

There are marked differences between the relativistic and the non-relativistic treatments.

The first is that the existence of a finite size nucleus introduces a limit to the compressibility: the dimension of the Wigner-Seitz cell can never be smaller than the nuclear size. Consequently the electron Fermi energy which in the non-relativistic approach can reach arbitrarily large values, reaches in the present case a perfectly finite value: an expression for this finite value of the electron Fermi energy has been given in analytic form. There are in the literature many papers adopting a relativistic treatment for the electrons, with a point-like approximation for the nucleus, which are clearly inconsistent (see e.g. Chabrier and Potekhin (1998) and Potekhin et al. (2009)).

The second is the clear difference of the electron distribution as a function of the radius and of the nuclear composition as contrasted to the uniform approximation (see Fig. A.8 of Sec. A.2.4), often adopted in the literature (see

e.g. Bürvenich et al. (2007)). Therefore the validity of inferences based on a uniform approximation should be duly verified both in the relativistic and in the non-relativistic regime.

The third is that the relativistic Feynman-Metropolis-Teller treatment allows to treat precisely the electro-dynamical interaction within a compressed atom with all the relativistic corrections. This allows to validate and in some cases overcome the difficulties of treatments describing the electro-dynamical effect by a sequence of successive approximations. This is the case of validation of the Salpeter approach at high densities and the overcome of negative pressures at low densities. The new treatment evidences a softening of the dependence of the electron Fermi energy on the compression factor, as well as a gradual decrease of the exchange terms in proceeding from the non-relativistic to the fully relativistic regimes. It is then possible to derive, as shown in Table A.1 of Sec. A.2.4, a consistent equation of state for compressed matter.

The equation of state obtained in Table A.1 of Sec. A.2.4 has been recently applied to the study of the general relativistic white-dwarf equilibrium configurations by Rotondo et al. (2011b). The contribution of quantum statistics, weak and electromagnetic interactions here considered have been further generalized there by considering the contribution of the general relativistic equilibrium of white dwarf matter. This is expressed by the simple formula $\sqrt{g_{00}}\mu_{ws} = \text{constant}$, which links the chemical potential of the Wigner-Seitz cell μ_{ws} with the general relativistic gravitational potential g_{00} at each point of the configuration. The configuration outside each Wigner-Seitz cell is strictly neutral and therefore no global electric field is necessary to warranty the equilibrium of the white dwarf. These equations modify the ones used by Chandrasekhar by taking into due account the Coulomb interaction between the nuclei and the electrons as well as inverse beta decay. They also generalize the work of Salpeter by considering a unified self-consistent approach to the Coulomb interaction in each Wigner-Seitz cell. The consequences on the numerical value of the Chandrasekhar-Landau mass limit have been then presented as well as on the mass-radius relation of white dwarfs (Rotondo et al., 2011b). This leads to the possibility of a direct confrontation of these results with observations, in view of the current great interest for the cosmological implications of the type Ia supernovae (Phillips, 1993; Riess et al., 1998; Perlmutter et al., 1999; Riess et al., 2004) and in the case of low mass white dwarf companion of the Pulsar PSRJ1141-6545 (Kramer, 2010) as well as the role of white dwarfs in novae.

In Secs. V and VI we have then extrapolated these results to the case of nuclear matter cores of stellar dimensions for $A \approx (m_{\text{Planck}}/m_n)^3 \sim 10^{57}$ or $M_{\text{core}} \sim M_{\odot}$. The aim here is to explore the possibility of obtaining for these systems a self-consistent solution presenting global and not local charge neutrality. The results generalize the considerations presented in the previous article by Rotondo et al. (2011e) corresponding to a nuclear matter core of stel-

lar dimensions with null Fermi energy of the electrons. The ultra-relativistic approximation allows to obtain analytic expressions for the fields in the case of positive electron Fermi energies. An entire family of configurations exist with values of the Fermi energy of the electrons ranging from zero to a maximum value $(E_e^F)_{max}$ which is reached when the Wigner-Seitz cell coincides with the core radius. The configuration with $E_e^F = (E_e^F)_{max}$ corresponds to the configuration with $N_p = N_e$ and $n_p = n_e$: for this limiting value of the Fermi energy the system fulfills both the global and the local charge neutrality and, correspondingly, no electro-dynamical structure is present in the core. The other configurations present generally overcritical electric fields close to their surface. The configuration with $E_e^F = 0$ has the maximum value of the electric field at the core surface, well above the critical value E_c (see Fig. A.11, Fig. A.12 and Fig. A.13 of Section A.2.5). All these cores with overcritical electric fields are stable against the vacuum polarization process due to the Pauli blocking by the degenerate electrons (see e.g. Ruffini et al. (2010b)). We have also compared and contrasted our treatment of the relativistic Thomas-Fermi solutions to the corresponding one addressed in the framework of strange stars by Alcock et al. (1986), pointing out in these treatments some inconsistency in the definition of the Coulomb potential. We have finally compared the compressional energy of configurations with selected values of the electron Fermi energy.

The above problem is theoretically well defined, represents a necessary step in order to approach the more complex problem of a neutron star core and its interface with the neutron star crust.

Neutron stars are composed of two sharply different components: the liquid core at nuclear and/or supra-nuclear density consisting of neutrons, protons and electrons and a crust of degenerate electrons in a lattice of nuclei (see e.g. Baym et al. (1971a)) and Harrison et al. (1965)) and possibly of free neutrons due to neutron drip when this process occurs (see e.g. Baym et al. (1971a)). Consequently, the boundary conditions for the electrons at the surface of the neutron star core will have generally a positive value of the electron Fermi energy in order to take into account the compressional effects of the neutron star crust on the core. The case of zero electron Fermi energy corresponds to the limiting case of absence of the crust.

In a set of interesting papers Glendenning (1992); Glendenning and Pei (1995); Christiansen and Glendenning (1997); Glendenning and Schaffner-Bielich (1999); Christiansen et al. (2000); Glendenning (2001) have relaxed the local charge neutrality condition for the description of the mixed phases in hybrid stars. In such configurations the global charge neutrality condition, as opposed to the local one, is applied to the limited regions where mixed phases occur while in the pure phases the local charge neutrality condition still holds. We have generalized Glendenning's considerations by looking to a violation of the local charge neutrality condition on the entire configuration, still keeping its overall charge neutrality. This effect cannot occur locally, and

requires a global description of the equilibrium configuration. To exemplified this novel approach we have considered in Rotondo et al. (2011d) the simplest, nontrivial, self-gravitating system of degenerate neutrons, protons and electrons in beta equilibrium in the framework of relativistic quantum statistics and the Einstein-Maxwell equations. The impossibility of imposing the condition of local charge neutrality on such systems is proved in complete generality. The crucial role of the constancy of the generalized electron Fermi energy is emphasized and consequently the coupled system of the general relativistic Thomas-Fermi equations and the Einstein-Maxwell equations is solved. We then give an explicit solution corresponding to a violation of the local charge neutrality condition on the entire star, still fulfilling the global charge neutrality when electromagnetic, weak and general relativistic effects are taken into account.

The results presented in the second part of this article on nuclear matter cores of stellar dimensions evidence the possibility of having the existence of critical electromagnetic fields at the core surface.

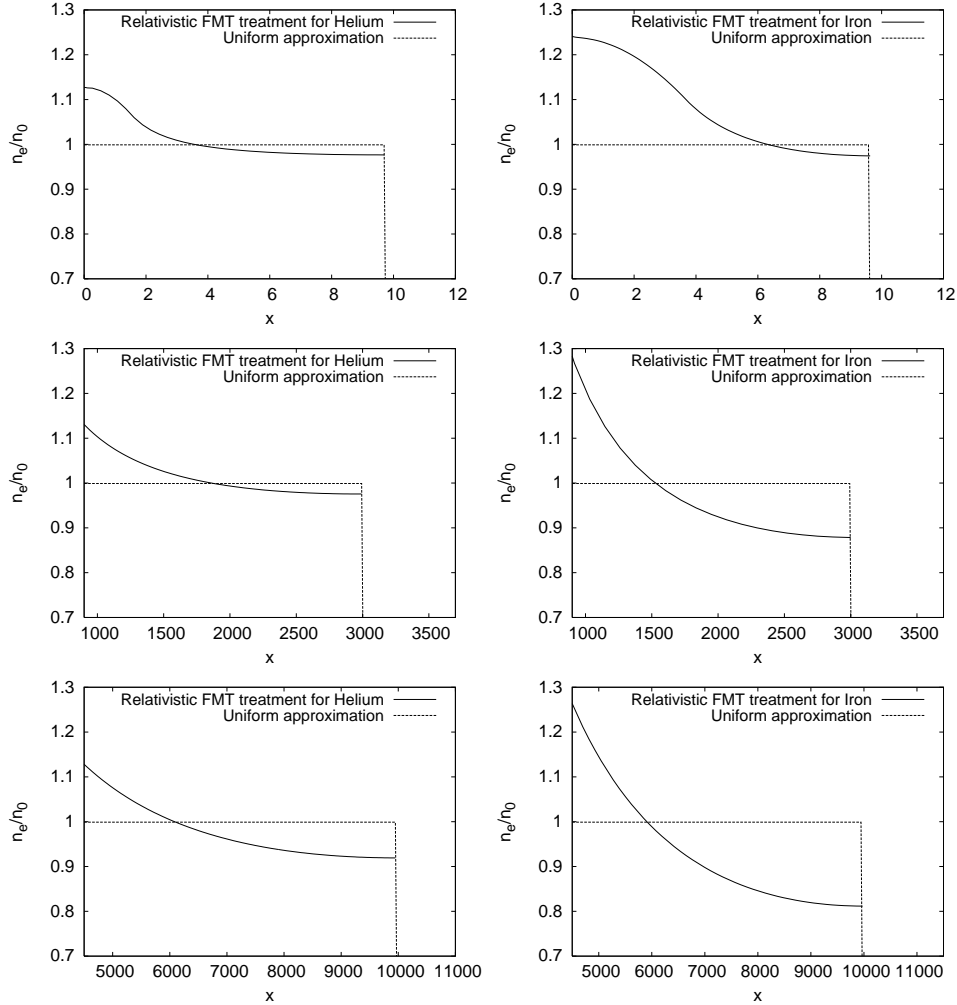


Figure A.8.: The electron number density n_e in units of the average electron number density $n_0 = 3N_e/(4\pi R_{WS}^3)$ is plotted as a function of the dimensionless radial coordinate $x = r/\lambda_\pi$ for the selected compressions $x_{WS} = 9.7$ (upper panels), $x_{WS} = 3 \times 10^3$ (middle panels) and $x_{WS} = 10^4$ (bottom panels), in both the relativistic Feynman, Metropolis, Teller approach and the uniform approximation respectively for helium (panels on the left) and iron (panels on the right).

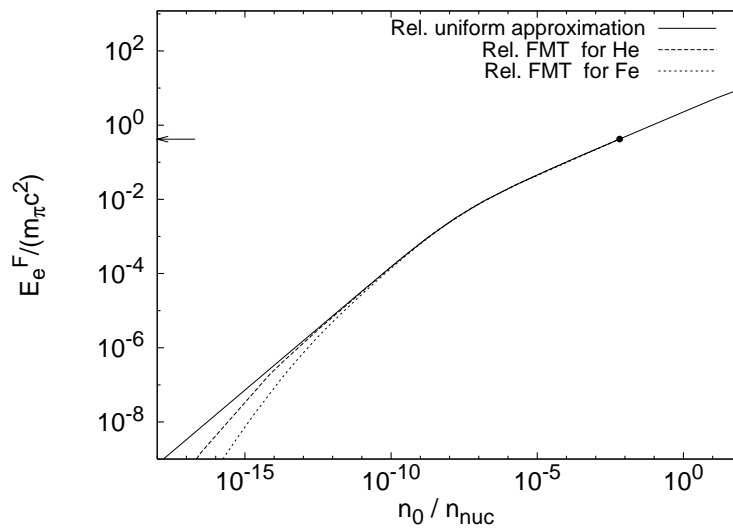


Figure A.9.: The electron Fermi energy E_e^F in units of the pion rest energy is plotted as a function of the average electron density $n_0 = 3N_e / (4\pi R_{WS}^3)$ in units of the nuclear density $n_{nuc} = 3A / (4\pi \Delta^3 N_p \lambda_\pi^3)$ for a uniform approximation (solid line), compared and contrasted to the ones obtained considering the relativistic Feynman, Metropolis, Teller approach. The arrow and the dot indicate the value of the maximum electron Fermi energy as given by Eq. (A.2.42), consistent with the finite size of the nucleus.

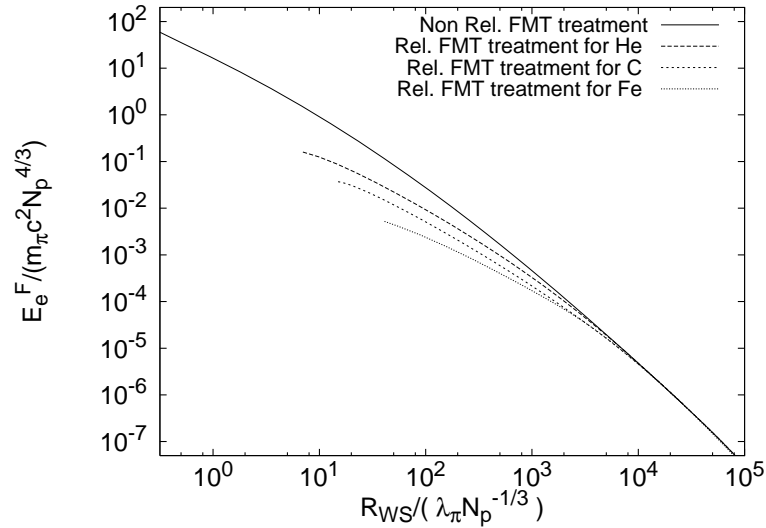


Figure A.10.: The electron Fermi energies in units of $m_{\pi}c^2N_p^{4/3}$ for helium, carbon and iron are plotted as a function of the ratio $R_{WS}/(\lambda_{\pi}N_p^{-1/3})$ respectively in the non-relativistic and in the relativistic Feynman-Metropolis-Teller (FMT) treatment. The dimensionless quantities have been chosen in order to obtain an universal curve in the non relativistic treatment following Eqs. (A.2.10) and (A.2.11). The relativistic treatment leads to results of the electron Fermi energy dependent on the nuclear composition and systematically smaller than the non-relativistic ones. The electron Fermi energy can attain arbitrary large values, in the non relativistic treatment, as the point-like nucleus is approached.

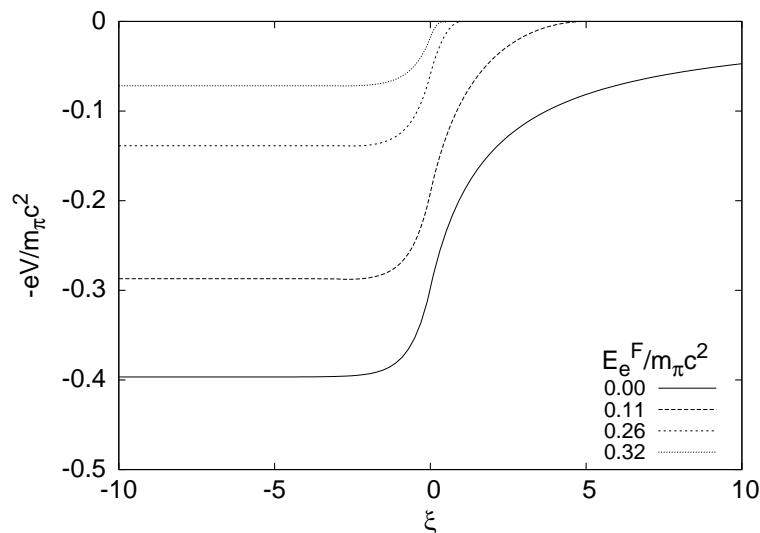


Figure A.11.: The electron Coulomb potential energies in units of the pion rest energy in a nuclear matter core of stellar dimensions with $A \simeq 10^{57}$ or $M_{core} \sim M_{\odot}$ and $R_c \approx 10^6$ cm, are plotted as a function of the dimensionless variable ξ , for different values of the electron Fermi energy also in units of the pion rest energy. The solid line corresponds to the case of null electron Fermi energy. By increasing the value of the electron Fermi energy the electron Coulomb potential energy depth is reduced.

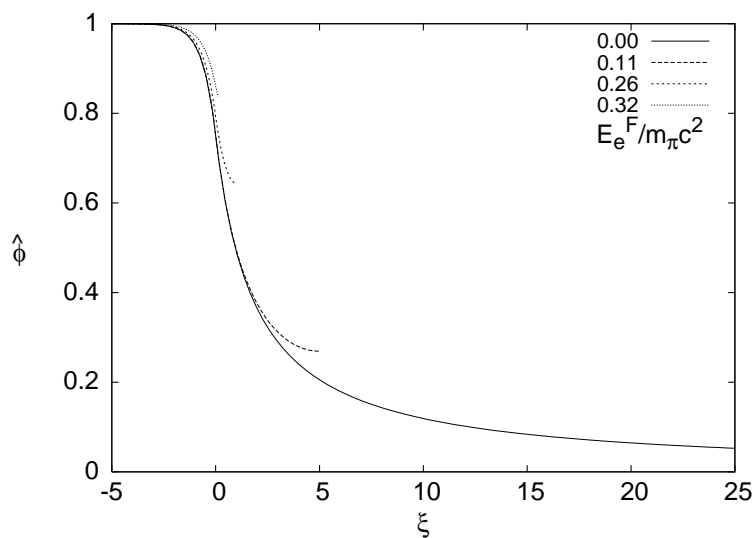


Figure A.12.: Solutions of the ultra-relativistic Thomas-Fermi equation (A.2.45) for different values of the Wigner-Seitz cell radius R_{WS} and correspondingly of the electron Fermi energy in units of the pion rest energy as in Fig. A.11, near the core surface. The solid line corresponds to the case of null electron Fermi energy.

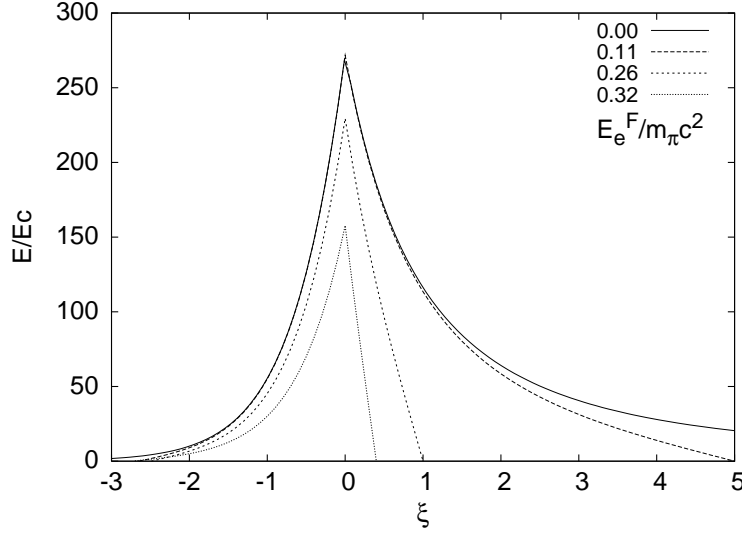


Figure A.13.: The electric field in units of the critical field for vacuum polarization $E_c = m_e^2 c^3 / (e\hbar)$ is plotted as a function of the coordinate ξ , for different values of the electron Fermi energy in units of the pion rest energy. The solid line corresponds to the case of null electron Fermi energy. To an increase of the value of the electron Fermi energy it is found a reduction of the peak of the electric field.

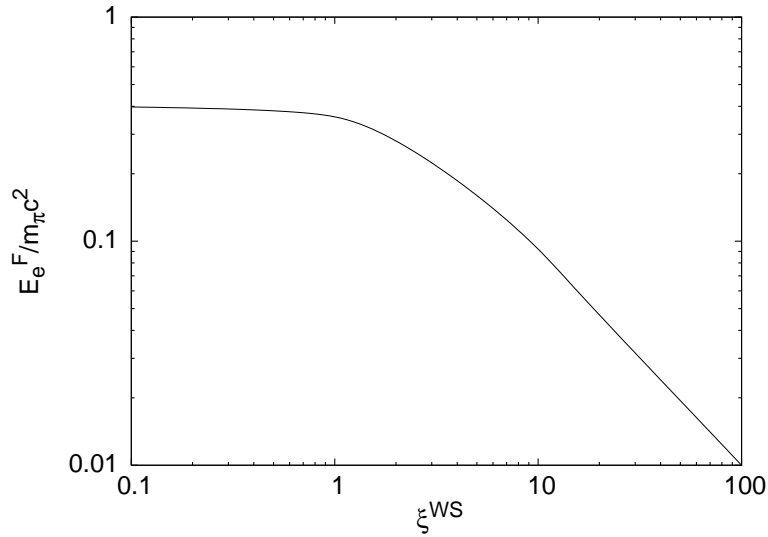


Figure A.14.: The Fermi energy of electrons in units of the pion rest energy is plotted for different Wigner-Seitz cell dimensions (i.e for different compressions) ξ^{WS} in the ultra-relativistic approximation. In the limit $\xi^{WS} \rightarrow 0$ the electron Fermi energy approaches asymptotically the value $(E_e^F)_{max}$ given by Eq. (A.2.63).

A.3. Electrodynamics for Nuclear Matter in Bulk

It is well known that the Thomas-Fermi equation is the exact theory for atoms, molecules and solids as $Z \rightarrow \infty$ (Lieb and Simon, 1973). We show in this letter that the relativistic Thomas-Fermi theory developed for the study of atoms for heavy nuclei with $Z \simeq 10^6$ Pieper and Greiner (1969); Greenberg and Greiner (1982); Müller et al. (1972); Popov (1971b); Zeldovich and Popov (1972); Ferreira et al. (1980); Ruffini and Stella (1981); Müller and Rafelski (1975); Migdal et al. (1976) gives important basic new information on the study of nuclear matter in bulk in the limit of $N \simeq (m_{\text{Planck}}/m_n)^3$ nucleons of mass m_n and on its electrodynamic properties. The analysis of nuclear matter bulk in neutron stars composed of degenerate gas of neutrons, protons and electrons, has traditionally been approached by implementing microscopically the charge neutrality condition by requiring the electron density $n_e(x)$ to coincide with the proton density $n_p(x)$,

$$n_e(x) = n_p(x). \quad (\text{A.3.1})$$

It is clear however that especially when conditions close to the gravitational collapse occur, there is an ultra-relativistic component of degenerate electrons whose confinement requires the existence of very strong electromagnetic fields, in order to guarantee the overall charge neutrality of the neutron star. Under these conditions equation (A.3.1) will be necessarily violated. We are going to show in this letter that they will develop electric fields close to the critical value E_c introduced by Sauter (1931), Heisenberg and Euler (1936), and by Schwinger (1951, 1954a,b)

$$E_c = \frac{m^2 c^3}{e \hbar}. \quad (\text{A.3.2})$$

Special attention for the existence of critical electric fields and the possible condition for electron-positron (e^+e^-) pair creation out of the vacuum in the case of heavy bare nuclei, with the atomic number $Z \geq 173$, has been given by Popov (1971b); Zeldovich and Popov (1972); Greenberg and Greiner (1982); Müller et al. (1972). They analyzed the specific pair creation process of an electron-positron pair around both a point-like and extended bare nucleus by direct integration of Dirac equation. These considerations have been extrapolated to much heavier nuclei $Z \gg 1600$, implying the creation of a large number of e^+e^- pairs, by using a statistical approach based on the relativistic Thomas-Fermi equation by Müller and Rafelski (1975); Migdal et al. (1976). Using substantially the same statistical approach based on the relativistic Thomas-Fermi equation, Ferreira et al. (1980); Ruffini and Stella (1981) have analyzed the electron densities around an extended nucleus in a neutral atom all the way up to $Z \simeq 6000$. They have shown the effect

of penetration of the electron orbitals well inside the nucleus, leading to a screening of the nuclei positive charge and to the concept of an “effective” nuclear charge distribution. All the above works assumed for the radius of the extended nucleus the semi-empirical formulae (Segré, 1977),

$$R_c \approx r_0 A^{1/3}, \quad r_0 = 1.2 \cdot 10^{-13} \text{cm}, \quad (\text{A.3.3})$$

where the mass number $A = N_n + N_p$, N_n and N_p are the neutron and proton numbers. The approximate relation between A and the atomic number $Z = N_p$,

$$Z \simeq \frac{A}{2}, \quad (\text{A.3.4})$$

was adopted in Müller and Rafelski (1975); Migdal et al. (1976), or the empirical formulae

$$Z \simeq \left[\frac{2}{A} + \frac{3}{200} \frac{1}{A^{1/3}} \right]^{-1}, \quad (\text{A.3.5})$$

was adopted in Ferreira et al. (1980); Ruffini and Stella (1981).

The aim of this letter is to outline an alternative approach of the description of nuclear matter in bulk: it generalizes, to the case of $N \simeq (m_{\text{Planck}}/m_n)^3$ nucleons, the above treatments, already developed and tested for the study of heavy nuclei. This more general approach differs in many aspects from the ones in the current literature and recovers, in the limiting case of A smaller than 10^6 , the above treatments. We shall look for a solution implementing the condition of overall charge neutrality of the star as given by

$$N_e = N_p, \quad (\text{A.3.6})$$

which significantly modifies Eq. (A.3.1), since now $N_e(N_p)$ is the total number of electrons (protons) of the equilibrium configuration. Here we present only a simplified prototype of this approach. We outline the essential relative role of the four fundamental interactions present in the neutron star physics: the gravitational, weak, strong and electromagnetic interactions. In addition, we also implement the fundamental role of Fermi-Dirac statistics and the phase space blocking due to the Pauli principle in the degenerate configuration. The new results essentially depend from the coordinated action of the five above theoretical components and cannot be obtained if any one of them is neglected. Let us first recall the role of gravity. In the case of neutron stars, unlike in the case of nuclei where its effects can be neglected, gravitation has the fundamental role of defining the basic parameters of the equilibrium configuration. As pointed out by Gamow (1931), at a Newtonian level and by Oppenheimer and Volkoff (1939) in general relativity, configurations of equilibrium exist at approximately one solar mass and at an average

density around the nuclear density. This result is obtainable considering only the gravitational interaction of a system of Fermi degenerate self-gravitating neutrons, neglecting all other particles and interactions. It can be formulated within a Thomas-Fermi self-gravitating model (see e.g. Ruffini and Bonazzola (1969)). In the present case of our simplified prototype model directed at evidencing new electrodynamic properties, the role of gravity is simply taken into account by considering, in line with the generalization of the above results, a mass-radius relation for the baryonic core

$$R^{NS} = R_c \approx \frac{\hbar}{m_\pi c} \frac{m_{\text{Planck}}}{m_n}. \quad (\text{A.3.7})$$

This formula generalizes the one given by Eq. (A.3.3) extending its validity to $N \approx (m_{\text{Planck}}/m_n)^3$, leading to a baryonic core radius $R_c \approx 10\text{km}$. We also recall that a more detailed analysis of nuclear matter in bulk in neutron stars (see e.g. Bethe et al. (1970) and Cameron (1970)) shows that at mass densities larger than the "melting" density of

$$\rho_c = 4.34 \cdot 10^{13} \text{g/cm}^3, \quad (\text{A.3.8})$$

all nuclei disappear. In the description of nuclear matter in bulk we have to consider then the three Fermi degenerate gas of neutrons, protons and electrons. In turn this naturally leads to consider the role of strong and weak interactions among the nucleons. In the nucleus, the role of the strong and weak interaction, with a short range of one Fermi, is to bind the nucleons, with a binding energy of 8 MeV, in order to balance the Coulomb repulsion of the protons. In the neutron star case we have seen that the neutrons confinement is due to gravity. We still assume that an essential role of the strong interactions is to balance the effective Coulomb repulsion due to the protons, partly screened by the electrons distribution inside the neutron star core. We shall verify, for self-consistency, the validity of this assumption on the final equilibrium solution we are going to obtain. We now turn to the essential weak interaction role in establishing the relative balance between neutrons, protons and electrons via the direct and inverse β -decay

$$p + e \longrightarrow n + \nu_e, \quad (\text{A.3.9})$$

$$n \longrightarrow p + e + \bar{\nu}_e. \quad (\text{A.3.10})$$

Since neutrinos escape from the star and the Fermi energy of the electrons is null, as we will show below, the only non-vanishing terms in the equilibrium condition given by the weak interactions are:

$$\sqrt{(P_n^F c)^2 + M_n^2 c^4} - M_n c^2 = \sqrt{(P_p^F c)^2 + M_p^2 c^4} - M_p c^2 + eV_{\text{coul}}^p, \quad (\text{A.3.11})$$

where P_n^F and P_p^F are respectively, the neutron and proton Fermi momenta, and V_{coul}^p is the Coulomb potential of protons. At this point, having fixed all these physical constraints, the main task is to find the electrons distributions fulfilling in addition to the Dirac-Fermi statistics also the Maxwell equations for the electrostatic. The condition of equilibrium of the Fermi degenerate electrons implies the null value of the Fermi energy:

$$\sqrt{(P_e^F c)^2 + m^2 c^4} - mc^2 + eV_{\text{coul}}(r) = 0, \quad (\text{A.3.12})$$

where P_e^F is the electron Fermi momentum and $V_{\text{coul}}(r)$ the Coulomb potential. In line with the procedure already followed for the heavy atoms Ferreira et al. (1980); Ruffini and Stella (1981) we here adopt the relativistic Thomas-Fermi Equation:

$$\frac{1}{x} \frac{d^2 \chi(x)}{dx^2} = -4\pi\alpha \left\{ \theta(x - x_c) - \frac{1}{3\pi^2} \left[\left(\frac{\chi(x)}{x} + \beta \right)^2 - \beta^2 \right]^{3/2} \right\}, \quad (\text{A.3.13})$$

where $\alpha = e^2/(\hbar c)$, $\theta(x - x_c)$ represents the normalized proton density distribution, the variables x and χ are related to the radial coordinate and the electron Coulomb potential V_{coul} by

$$x = \frac{r}{R_c} \left(\frac{3N_p}{4\pi} \right)^{1/3}; \quad eV_{\text{coul}}(r) \equiv \frac{\chi(r)}{r}, \quad (\text{A.3.14})$$

and the constants $x_c(r = R_c)$ and β are respectively

$$x_c \equiv \left(\frac{3N_p}{4\pi} \right)^{1/3}; \quad \beta \equiv \frac{mcR_c}{\hbar} \left(\frac{4\pi}{3N_p} \right)^{1/3}. \quad (\text{A.3.15})$$

The solution has the boundary conditions

$$\chi(0) = 0; \quad \chi(\infty) = 0, \quad (\text{A.3.16})$$

with the continuity of the function χ and its first derivative χ' at the boundary of the core R_c . The crucial point is the determination of the eigenvalue of the first derivative at the center

$$\chi'(0) = \text{const.}, \quad (\text{A.3.17})$$

which has to be determined by fulfilling the above boundary conditions (A.3.16) and constraints given by Eq. (A.3.11) and Eq. (A.3.6). The difficulty of the integration of the Thomas-Fermi Equations is certainly one of the most celebrated chapters in theoretical physics and mathematical physics, still chal-

lenging a proof of the existence and uniqueness of the solution and strenuously avoiding the occurrence of exact analytic solutions. We recall after the original papers of Thomas (1927) and Fermi (1927), the works of Sommerfeld (1932), all the way to the many hundredth papers reviewed in the classical articles of Lieb and Simon (1973), Lieb (1981) and Spruch (1991). The situation here is more difficult since we are working on the special relativistic generalization of the Thomas-Fermi Equation. Also in this case, therefore, we have to proceed by numerical integration. The difficulty of this numerical task is further enhanced by a consistency check in order to fulfill all different constraints. It is so that we start the computations by assuming a total number of protons and a value of the core radius R_c . We integrate the Thomas-Fermi Equation and we determine the number of neutrons from the Eq. (A.3.11). We iterate the procedure until a value of A is reached consistent with our choice of the core radius. The paramount difficulty of the problem is the numerical determination of the eigenvalue in Eq. (A.3.17) which already for $A \approx 10^4$ had presented remarkable numerical difficulties Ferreirinho et al. (1980). In the present context we have been faced for a few months by an apparently unsurmountable numerical task: the determination of the eigenvalue seemed to necessitate a significant number of decimals in the first derivative (A.3.17) comparable to the number of the electrons in the problem! The solution is given in Fig. (A.15) and Fig. (A.16).

A relevant quantity for exploring the physical significance of the solution is given by the number of electrons within a given radius r :

$$N_e(r) = \int_0^r 4\pi(r')^2 n_e(r') dr'. \quad (\text{A.3.18})$$

This allows to determine, for selected values of the A parameter, the distribution of the electrons within and outside the core and follow the progressive penetration of the electrons in the core at increasing values of A [see Fig. (A.17)]. We can then evaluate, generalizing the results in Ferreirinho et al. (1980); Ruffini and Stella (1981) , the net charge inside the core

$$N_{\text{net}} = N_p - N_e(R_c) < N_p, \quad (\text{A.3.19})$$

and consequently determine the electric field at the core surface, as well as within and outside the core [see Fig. (A.18)] and evaluate as well the Fermi degenerate electron distribution outside the core [see Fig. (A.19)]. It is interesting to explore the solution of the problem under the same conditions and constraints imposed by the fundamental interactions and the quantum statistics and imposing instead of Eq. (A.3.1) the corresponding Eq. (A.3.6). Indeed a solution exist and is much simpler

$$n_n(x) = n_p(x) = n_e(x) = 0, \quad \chi = 0. \quad (\text{A.3.20})$$

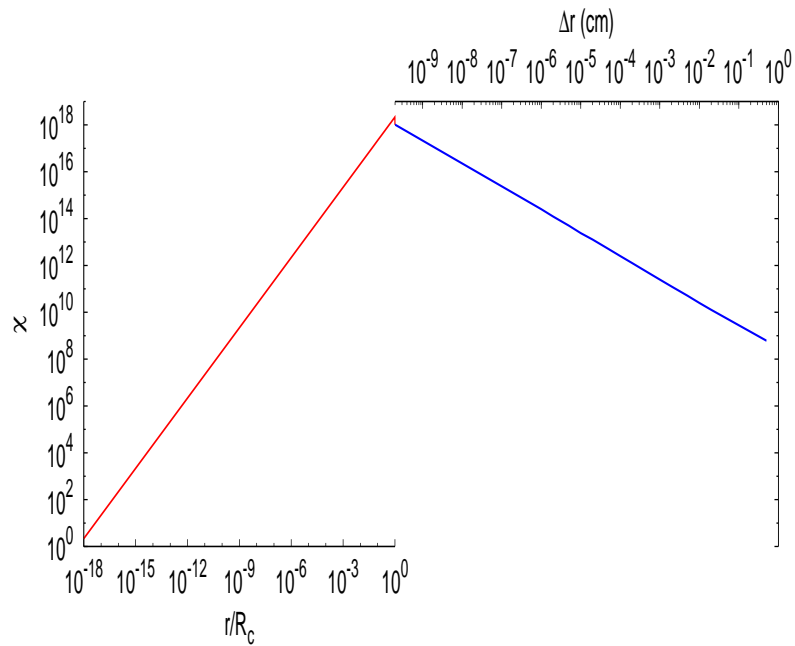


Figure A.15.: The solution χ of the relativistic Thomas-Fermi Equation for $A = 10^{57}$ and core radius $R_c = 10\text{km}$, is plotted as a function of radial coordinate. The left red line corresponds to the internal solution and it is plotted as a function of radial coordinate in unit of R_c in logarithmic scale. The right blue line corresponds to the solution external to the core and it is plotted as function of the distance Δr from the surface in the logarithmic scale in centimeter.

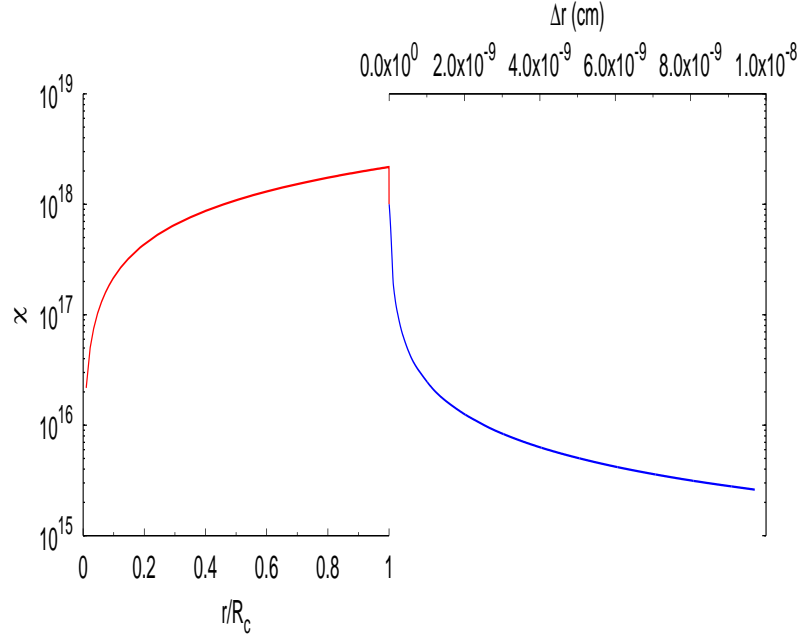


Figure A.16.: The same as Fig. (A.15): enlargement around the core radius R_c showing explicitly the continuity of function χ and its derivative χ' from the internal to the external solution.

Before concluding as we announce we like to check on the theoretical consistency of the solution. We obtain an overall neutral configuration for the nuclear matter in bulk, with a positively charged baryonic core with

$$N_{\text{net}} = 0.92 \left(\frac{m}{m_\pi} \right)^2 \left(\frac{e}{m_n \sqrt{G}} \right)^2 \left(\frac{1}{\alpha} \right)^2, \quad (\text{A.3.21})$$

and an electric field on the baryonic core surface (see Fig. (A.18))

$$\frac{E}{E_c} = 0.92. \quad (\text{A.3.22})$$

The corresponding Coulomb repulsive energy per nucleon is given by

$$U_{\text{coul}}^{\text{max}} = \frac{1}{2\alpha} \left(\frac{m}{m_\pi} \right)^3 mc^2 \approx 1.78 \cdot 10^{-6} (\text{MeV}), \quad (\text{A.3.23})$$

well below the nucleon binding energy per nucleon. It is also important to verify that this charge core is gravitationally stable. We have in fact

$$\frac{Q}{\sqrt{GM}} = \alpha^{-1/2} \left(\frac{m}{m_\pi} \right)^2 \approx 1.56 \cdot 10^{-4}. \quad (\text{A.3.24})$$

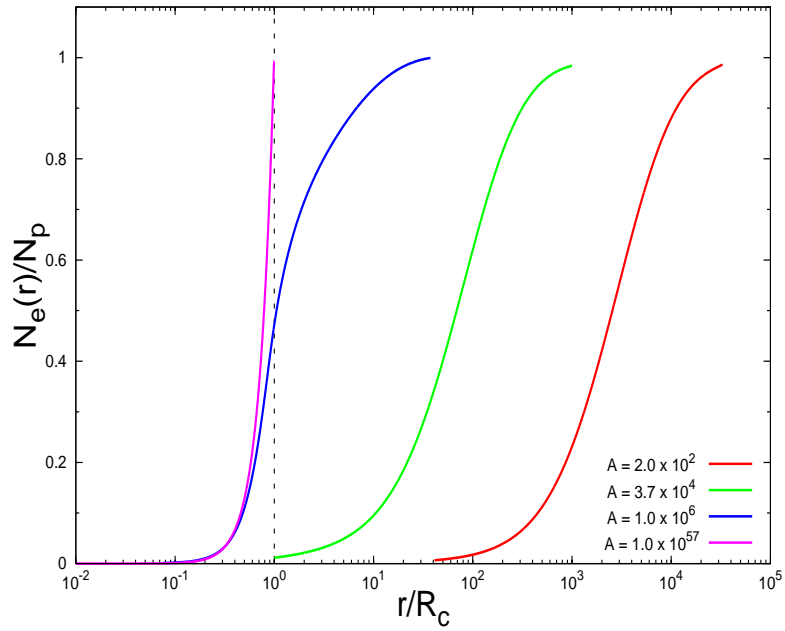


Figure A.17.: The electron number (A.3.18) in the unit of the total proton number N_p , for selected values of A , is given as function of radial distance in the unit of the core radius R_c , again in logarithmic scale. It is clear how by increasing the value of A the penetration of electrons inside the core increases. The detail shown in Fig. (A.18) and Fig. (A.19) demonstrates how for $N \simeq (m_{\text{Planck}}/m_n)^3$ a relatively small tail of electron outside the core exists and generates on the baryonic core surface an electric field close to the critical value. A significant electron density outside the core is found.

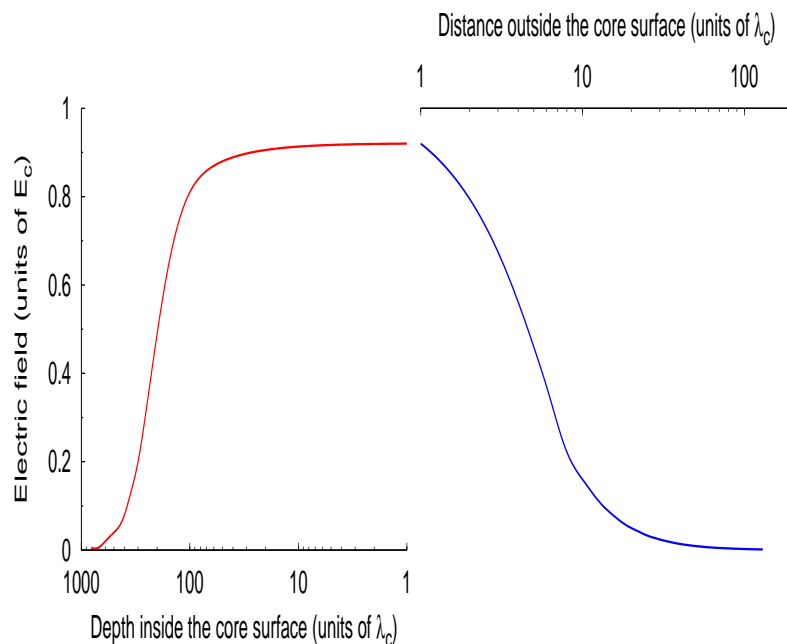


Figure A.18.: The electric field in the unit of the critical field E_c is plotted around the core radius R_c . The left (right) diagram in the red (blue) refers the region just inside (outside) the core radius plotted logarithmically. By increasing the density of the star the field approaches the critical field.

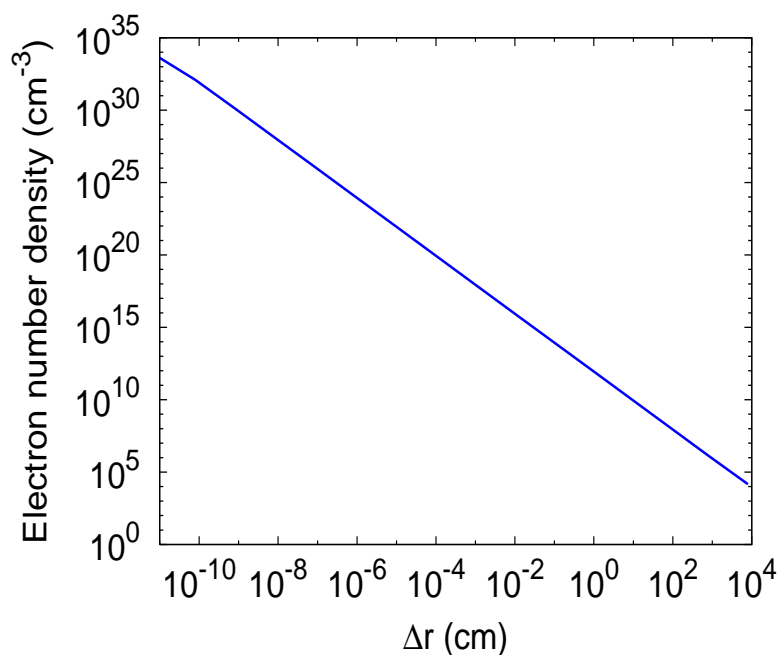


Figure A.19.: The density of electrons for $A = 10^{57}$ in the region outside the core; both scale are logarithmically.

The electric field of the baryonic core is screened to infinity by an electron distribution given in Fig. (A.19). As usual any new solution of Thomas-Fermi systems has relevance and finds its justification in the theoretical physics and mathematical physics domain. We expect that as in the other solutions previously obtained in the literature of the relativistic Thomas-Fermi equations also this one we present in this letter will find important applications in physics and astrophysics. There are a variety of new effects that such a generalized approach naturally leads to: (1) the mass-radius relation of neutron star may be affected; (2) the electrodynamic aspects of neutron stars and pulsars will be different; (3) we expect also important consequence in the initial conditions in the physics of gravitational collapse of the baryonic core as soon as the critical mass for gravitational collapse to a black hole is reached. The consequent collapse to a black hole will have very different energetics properties.

A.4. On the Charge to Mass Ratio of Neutron Cores and Heavy Nuclei

A.4.1. Introduction

It is well known that stable nuclei are located, in the N_n - N_p plane (where N_n and N_p are the total number of neutrons and protons respectively), in a region that, for small values of N_p , is almost a line well described by the relation $N_n = N_p$.

In the past, several efforts have been made to explain theoretically this property, for example with the liquid drop model of atoms, that is based on two properties common to all nuclei: their mass densities and their binding energies for nucleons are almost independent from the mass number $A = N_n + N_p$ (Segré, 1977). This model takes into account the strong nuclear force and the Coulombian repulsion between protons and explains different properties of nuclei, for example the relation between N_p and A (the charge to mass ratio).

In this work we derive theoretically the charge to mass ratio of nuclei and extend it to neutron cores (characterized by higher values of A) with the model of Ruffini et al. (2007c). We consider systems composed of degenerate neutrons, protons and electrons and we use the relativistic Thomas-Fermi equation and the equation of β -equilibrium to determine the number density and the total number of these particles, from which we obtain the relation between N_p and A .

A.4.2. The theoretical model

Following the work of Ruffini et al. (2007c), we describe nuclei and neutron cores as spherically symmetric systems composed of degenerate protons, electrons and neutrons and impose the condition of global charge neutrality. We assume that the proton's number density $n_p(r)$ is constant inside the core ($r \leq R_C$) and vanishes outside the core ($r > R_C$):

$$n_p(r) = \left(\frac{3N_p}{4\pi R_C^3} \right) \theta(R_C - r), \quad (\text{A.4.1})$$

where N_p is the total number of protons and R_C is the core-radius, parametrized as:

$$R_C = \Delta \frac{\hbar}{m_\pi c} N_p^{1/3}. \quad (\text{A.4.2})$$

We choose Δ in order to have $\rho \sim \rho_N$, where ρ and ρ_N are the mass density of the system and the nuclear density respectively ($\rho_N = 2.314 \cdot 10^{14} \text{ g cm}^{-3}$).

The electron number density $n_e(r)$ is given by:

$$n_e(r) = \frac{1}{3\pi^2\hbar^3} \left[p_e^F(r) \right]^3, \quad (\text{A.4.3})$$

where $p_e^F(r)$ is the electron Fermi momentum. It can be calculated from the condition of equilibrium of Fermi degenerate electrons, that implies the null value of their Fermi energy $\epsilon_e^F(r)$:

$$\epsilon_e^F(r) = \sqrt{[p_e^F(r)c]^2 + m_e^2c^4} - m_e c^2 + V_c(r) = 0, \quad (\text{A.4.4})$$

where $V_c(r)$ is the Coulomb potential energy of electrons.

From this condition we obtain:

$$p_e^F(r) = \frac{1}{c} \sqrt{V_c^2(r) - 2m_e c^2 V_c(r)}, \quad (\text{A.4.5})$$

hence the electron number density is:

$$n_e(r) = \frac{1}{3\pi^2\hbar^3 c^3} \left[V_c^2(r) - 2m_e c^2 V_c(r) \right]^{3/2}. \quad (\text{A.4.6})$$

The Coulomb potential energy of electrons, necessary to derive $n_e(r)$, can be determined as follows. Based on the Gauss law, $V_c(r)$ obeys the following Poisson equation:

$$\nabla^2 V_c(r) = -4\pi e^2 [n_e(r) - n_p(r)], \quad (\text{A.4.7})$$

with the boundary conditions $V_c(\infty) = 0$, $V_c(0) = \text{finite}$. Introducing the dimensionless function $\chi(r)$, defined by the relation:

$$V_c(r) = -\hbar c \frac{\chi(r)}{r}, \quad (\text{A.4.8})$$

and the new variable $x = rb^{-1} = r \left(\frac{\hbar}{m\pi c} \right)^{-1}$, from Eq. (A.4.7) we obtain the relativistic Thomas-Fermi equation:

$$\frac{1}{3x} \frac{d^2 \chi(x)}{dx^2} = -\alpha \left\{ \frac{1}{\Delta^3} \theta(x_c - x) - \frac{4}{9\pi} \left[\frac{\chi^2(x)}{x^2} + 2 \frac{m_e}{m\pi} \frac{\chi(x)}{x} \right]^{3/2} \right\}. \quad (\text{A.4.9})$$

The boundary conditions for the function $\chi(x)$ are:

$$\chi(0) = 0, \quad \chi(\infty) = 0, \quad (\text{A.4.10})$$

as well as the continuity of $\chi(x)$ and its first derivative $\chi'(x)$ at the boundary

of the core.

The number density of neutrons $n_n(r)$ is:

$$n_n(r) = \frac{1}{3\pi^2\hbar^3} \left[p_n^F(r) \right]^3, \quad (\text{A.4.11})$$

where $p_n^F(r)$ is the neutron Fermi momentum. It can be calculated with the condition of equilibrium between the processes

$$e^- + p \rightarrow n + \nu_e; \quad (\text{A.4.12})$$

$$n \rightarrow p + e^- + \bar{\nu}_e, \quad (\text{A.4.13})$$

Assuming that neutrinos escape from the core as soon as they are produced, this condition (condition of β -equilibrium) is

$$\epsilon_e^F(r) + \epsilon_p^F(r) = \epsilon_n^F(r). \quad (\text{A.4.14})$$

Eq. (A.4.14) can be explicitly written as:

$$\sqrt{[p_p^F(r)c]^2 + m_p^2c^4} - m_pc^2 - V_c(r) = \sqrt{[p_n^F(r)c]^2 + m_n^2c^4} - m_nc^2. \quad (\text{A.4.15})$$

A.4.3. N_p - A relation

Using the previous equations, we derive $n_e(r)$, $n_n(r)$ and $n_p(r)$ and, by integrating these, we obtain the N_e , N_n and N_p . We also derive a theoretical relation between N_p and A and we compare it with the data of the Periodic Table and with the semi-empirical relation:

$$N_p = \left(\frac{A}{2} \right) \cdot \frac{1}{1 + \left(\frac{3}{400} \right) \cdot A^{2/3}} \quad (\text{A.4.16})$$

that, in the limit of low A , gives the well known relation $N_p = A/2$ (Segré, 1977).

Eq. (A.4.16) can be obtained by minimizing the semi-empirical mass formula, that was first formulated by Weizsäcker in 1935 and is based on empirical measurements and on theory (the liquid drop model of atoms).

The liquid drop model approximates the nucleus as a sphere composed of protons and neutrons (and not electrons) and takes into account the Coulombian repulsion between protons and the strong nuclear force. Another important characteristic of this model is that it is based on the property that the mass densities of nuclei are approximately the same, independently from A . In fact, from scattering experiments it was found the following expression for the nuclear radius R_N :

$$R_N = r_0A^{1/3}, \quad (\text{A.4.17})$$

with $r_0 = 1.2$ fm. Using eq. (A.4.17) the nuclear density can be write as follows:

$$\rho_N = \frac{Am_N}{V} = \frac{3Am_N}{4\pi r_0^3 A} = \frac{3m_N}{4\pi r_0^3}, \quad (\text{A.4.18})$$

where m_N is the nucleon mass. From eq. (A.4.18) it is clear that nuclear density is independent from A , so it is constant for all nuclei.

The property of constant density for all nuclei is a common point with our model: in fact, we choose Δ in order to have the same mass density for every value of A ; in particular we consider the case $\rho \sim \rho_N$, as previously said.

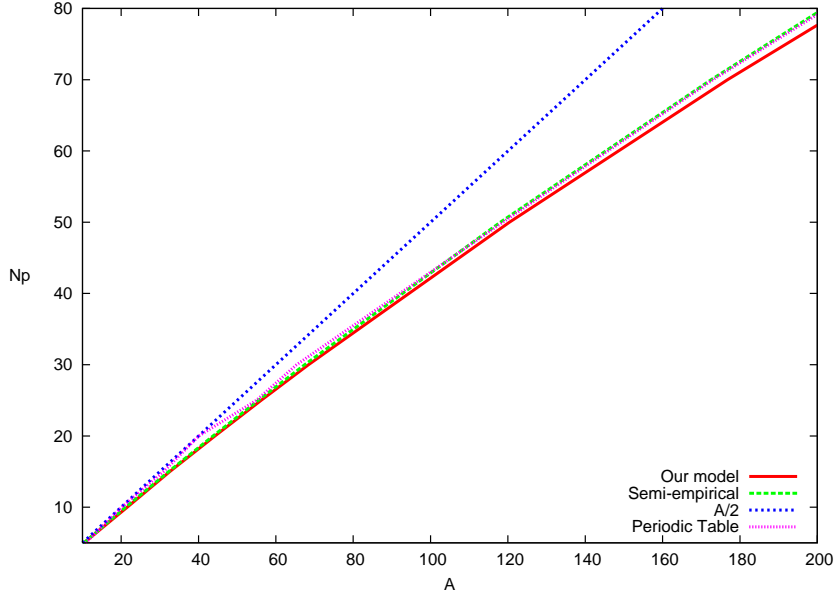


Figure A.20.: The $N_p - A$ relation obtained with our model and with the semi-empirical mass formula, the $N_p = A/2$ relation and the data of the Periodic Table; relations are plotted for values of A from 0 to 200.

In table (A.2) are listed some values of A obtained with our model and the semi-empirical mass formula, as well as the data of the Periodic Table; in fig. (A.20) and (A.21) it is shown the comparison between the various $N_p - A$ relations.

It is clear that there is a good agreement between all the relations for values of A typical of nuclei, with differences of the order of per cent. Our relation and the semi-empirical one are in agreement up to $A \sim 10^4$; for higher values, we find that the two relations differ. We interpret these differences as due to the effects of penetration of electrons inside the core [see fig. (A.22)]: in our model we consider a system composed of degenerate protons, neutrons and electrons. For the smallest values of A , all the electrons are in a shell outside the core; by increasing A , they progressively penetrate into the core (Ruffini et al., 2007c). These effects, which need the relativistic approach introduced in Ruffini et al. (2007c), are not taken into account in the semi-empirical mass

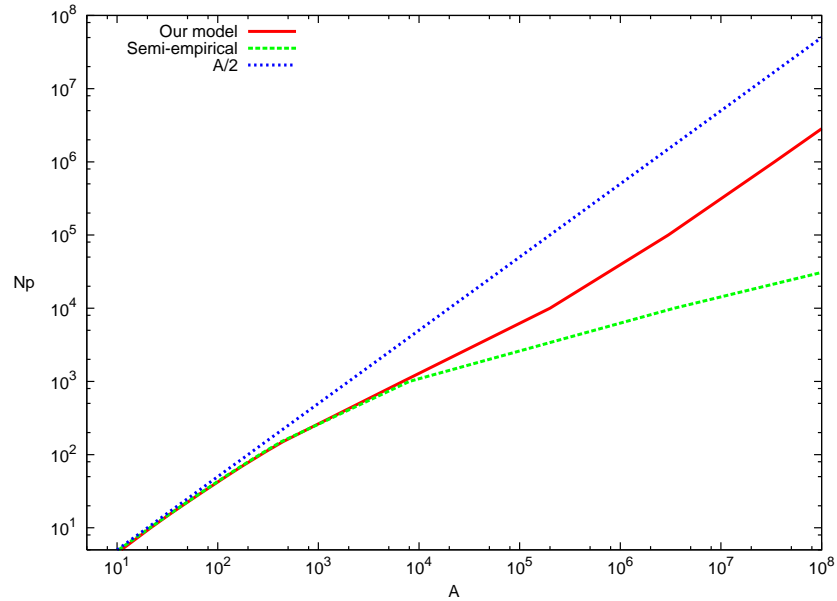


Figure A.21.: The $N_p - A$ relation obtained with our model and with the semi-empirical mass formula and the $N_p = A/2$ relation; relations are plotted for values of A from 0 to 10^8 . It is clear how the semi-empirical relation and the one obtained with our model are in good agreement up to values of A of the order of 10^4 ; for greater values of A the two relation differ because our model takes into account the penetration of electrons inside the core, which is not considered in the semi-empirical mass formula.

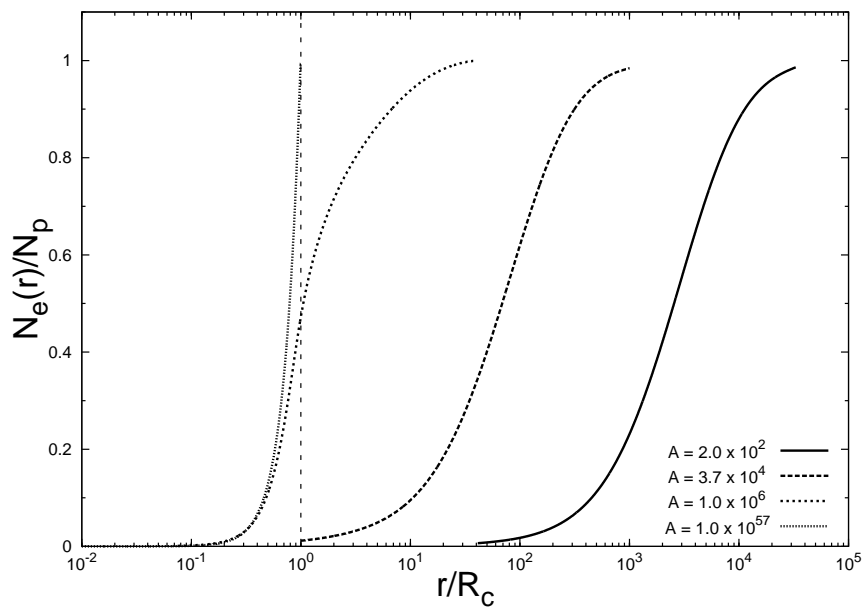


Figure A.22.: The electron number in units of the total proton number N_p as function of the radial distance in units of the core radius R_C , for different values of A . It is clear that, by increasing the value of A , the penetration of electrons inside the core increases. Figure from Ruffini et al. (2007c).

formula.

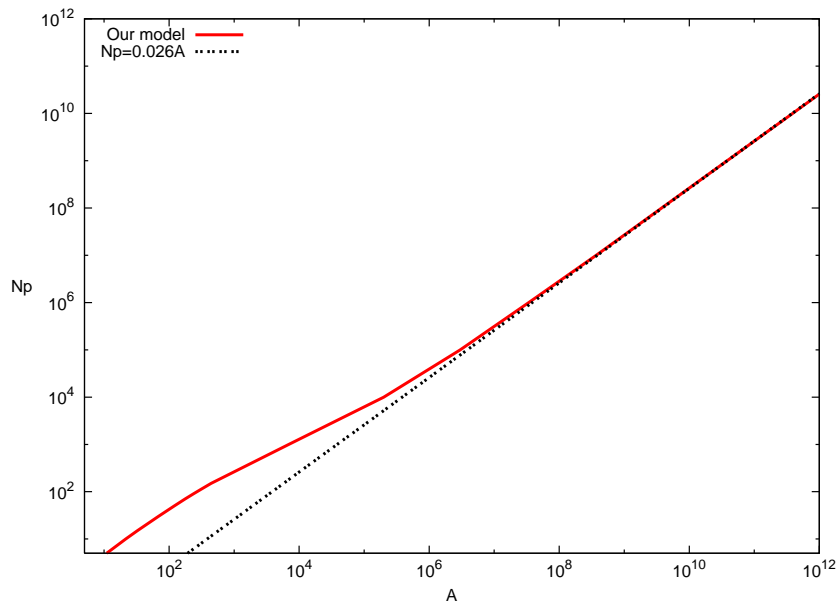


Figure A.23.: The $N_p - A$ relation obtained with our model and the asymptotic limit $N_p = 0.026A$

We also note that the charge to mass ratio become constant for A greater than 10^7 ; in particular, it is well approximated by the relation $N_p = 0.026A$ [see fig. (A.23)].

A.4.4. Conclusions

In this work we have derived theoretically a relation between the total number of protons N_p and the mass number A for nuclei and neutron cores with the model recently proposed by Ruffini et al. (2007c)).

We have considered spherically symmetric systems composed of degenerate electrons, protons and neutrons having global charge neutrality and the same mass densities ($\rho \sim \rho_N$). By integrating the relativistic Thomas-Fermi equation and using the equation of β -equilibrium, we have determined the total number of protons, electrons and neutrons in the system and hence a theoretical relation between N_p and A .

We have compared this relation with the empirical data of the Periodic Table and with the semi-empirical relation, obtained by minimizing the Weizsäcker mass formula by considering systems with the same mass densities. We have shown that there's a good agreement between all the relations for values of A typical of nuclei, with differences of the order of per cent. Our relation and the semi-empirical one are in agreement up to $A \sim 10^4$; for higher values, we find that the two relations differ. We interpret the different behaviour of our

N_p	A_M	A_{PT}	A_{SE}
5	10.40	10.811	10.36
10	21.59	20.183	21.15
15	32.58	30.9738	32.28
20	44.24	40.08	43.72
25	56.17	54.938	55.45
30	68.43	65.37	67.46
50	120.40	118.69	118.05
70	176.78	173.04	172.54
90	237.41	232.038	230.79
110	302.18	271	292.75
150	443.98		427.73
200	644.03		617.56
250	869.32		831.63
300	1119.71		1071.08
350	1395.12		1337.23
450	2019.48		1955.57
500	2367.77		2310.96
550	2739.60		2699.45
600	3134.28		3122.83
10^3	$6.9 \cdot 10^3$		$8 \cdot 10^3$
10^4	$2.0 \cdot 10^5$		$3.45 \cdot 10^6$
10^5	$3.0 \cdot 10^6$		$3.38 \cdot 10^9$
10^6	$3.4 \cdot 10^7$		$3.37 \cdot 10^{12}$
10^7	$3.7 \cdot 10^8$		$3.37 \cdot 10^{15}$
10^{10}	$3.9 \cdot 10^{11}$		$3.37 \cdot 10^{24}$

Table A.2.: Different values of N_p (column 1) and corresponding values of A from our model (A_M , column 2), the Periodic Table (A_{PT} , column 3) and the semi-empirical mass formula (A_{SE} , column 4).

theoretical relation as a result of the penetration of electrons (initially confined in an external shell) inside the core [see fig.(A.22)], that becomes more and more important by increasing A ; these effects, which need the relativistic approach introduced in Ruffini et al. (2007c), are not taken into account in the semi-empirical mass-formula.

A.5. Supercritical fields on the surface of massive nuclear cores: neutral core vs. charged core

A.5.1. Equilibrium of electron distribution in neutral cores.

In Ruffini et al. (2007c); Ferreira et al. (1980); Ruffini and Stella (1981), the Thomas-Fermi approach was used to study the electrostatic equilibrium of electron distributions $n_e(r)$ around extended nuclear cores, where total proton and electron numbers are the same $N_p = N_e$. Proton's density $n_p(r)$ is constant inside core $r \leq R_c$ and vanishes outside the core $r > R_c$,

$$n_p(r) = n_p \theta(R_c - r), \quad (\text{A.5.1})$$

where R_c is the core radius and n_p proton density. Degenerate electron density,

$$n_e(r) = \frac{1}{3\pi^2 \hbar^3} (P_e^F)^3, \quad (\text{A.5.2})$$

where electron Fermi momentum P_e^F , Fermi-energy $\mathcal{E}_e(P_e^F)$ and Coulomb potential energy $V_{\text{coul}}(r)$ are related by,

$$\mathcal{E}_e(P_e^F) = [(P_e^F c)^2 + m_e^2 c^4]^{1/2} - m_e c^2 - V_{\text{coul}}(r). \quad (\text{A.5.3})$$

The electrostatic equilibrium of electron distributions is determined by

$$\mathcal{E}_e(P_e^F) = 0, \quad (\text{A.5.4})$$

which means the balance of electron's kinetic and potential energies in Eq. (A.5.3) and degenerate electrons occupy energy-levels up to $+m_e c^2$. Eqs. (A.5.2), (A.5.3), and (A.5.4) give the relationships:

$$P_e^F = \frac{1}{c} \left[V_{\text{coul}}^2(r) + 2m_e c^2 V_{\text{coul}}(r) \right]^{1/2}; \quad (\text{A.5.5})$$

$$n_e(r) = \frac{1}{3\pi^2 (c\hbar)^3} \left[V_{\text{coul}}^2(r) + 2m_e c^2 V_{\text{coul}}(r) \right]^{3/2}. \quad (\text{A.5.6})$$

The Gauss law leads the following Poisson equation and boundary conditions,

$$\Delta V_{\text{coul}}(r) = 4\pi\alpha [n_p(r) - n_e(r)]; \quad V_{\text{coul}}(\infty) = 0, \quad V_{\text{coul}}(0) = \text{finite} \quad (\text{A.5.7})$$

These equations describe a Thomas-Fermi model for neutral nuclear cores, and have numerically solved together with the empirical formula (Ferreira et al., 1980; Ruffini and Stella, 1981) and β -equilibrium equation (Ruffini

et al., 2007c) for the proton number N_p and mass number $A = N_p + N_n$, where N_n is the neutron number.

A.5.2. Equilibrium of electron distribution in super charged cores

In Müller and Rafelski (1975); Migdal et al. (1976), assuming that super charged cores of proton density (A.5.1) are bare, electrons (positrons) produced by vacuum polarization fall (fly) into cores (infinity), one studied the equilibrium of electron distribution when vacuum polarization process stop. When the proton density is about nuclear density, super charged core creates a negative Coulomb potential well $-V_{\text{coul}}(r)$, whose depth is much more profound than $-m_e c^2$ (see Fig. [A.24]), production of electron-positron pairs take places, and electrons bound by the core and screen down its charge. Since the phase space of negative energy-levels $\epsilon(p)$

$$\epsilon(p) = [(pc)^2 + m_e^2 c^4]^{1/2} - V_{\text{coul}}(r), \quad (\text{A.5.8})$$

below $-m_e c^2$ for accommodating electrons is limited, vacuum polarization process completely stops when electrons fully occupy all negative energy-levels up to $-m_e c^2$, even electric field is still critical. Therefore an equilibrium of degenerate electron distribution is expected when the following condition is satisfied,

$$\epsilon(p) = [(pc)^2 + m_e^2 c^4]^{1/2} - V_{\text{coul}}(r) = -m_e c^2, \quad p = P_e^F, \quad (\text{A.5.9})$$

and Fermi-energy

$$\mathcal{E}_e(P_e^F) = \epsilon(P_e^F) - m_e c^2 = -2m_e c^2, \quad (\text{A.5.10})$$

which is rather different from Eq. (A.5.4). This equilibrium condition (A.5.10) leads to electron's Fermi-momentum and number-density (A.5.2),

$$P_e^F = \frac{1}{c} \left[V_{\text{coul}}^2(r) - 2m_e c^2 V_{\text{coul}}(r) \right]^{1/2}; \quad (\text{A.5.11})$$

$$n_e(r) = \frac{1}{3\pi^2 (c\hbar)^3} \left[V_{\text{coul}}^2(r) - 2m_e c^2 V_{\text{coul}}(r) \right]^{3/2}. \quad (\text{A.5.12})$$

which have a different sign contracting to Eqs. (A.5.5,A.5.6). Eq. (A.5.7) remains the same. However, contracting to the neutrality condition $N_e = N_p$ and $n_e(r)|_{r \rightarrow \infty} \rightarrow 0$ in the case of neutral cores, the total number of electrons is given by

$$N_e^{\text{ion}} = \int_0^{r_0} 4\pi r^2 dr n_e(r) < N_p, \quad (\text{A.5.13})$$

where r_0 is the finite radius at which electron distribution $n_e(r)$ (A.5.12) vanishes: $n_e(r_0) = 0$, i.e., $V_{\text{coul}}(r_0) = 2m_e c^2$, and $n_e(r) \equiv 0$ for the range $r > r_0$. $N^{\text{ion}} < N_p$ indicates that such configuration is not neutral. These equations describe a Thomas-Fermi model for super charged cores, and have numerically (Müller and Rafelski, 1975) and analytically (Migdal et al., 1976) solved with assumption $N_p = A/2$.

A.5.3. Ultra-relativistic solution

In the analytical approach (Migdal et al., 1976), the ultra-relativistic approximation is adopted for $V_{\text{coul}}(r) \gg 2m_e c^2$, the term $2m_e c^2 V_{\text{coul}}(r)$ in Eqs. (A.5.5), (A.5.6), (A.5.11), and (A.5.12) is neglected. It turns out that approximated Thomas-Fermi equations are the same for both cases of neutral and charged cores, and solution $V_{\text{coul}}(r) = \hbar c (3\pi^2 n_p)^{1/3} \phi(x)$,

$$\phi(x) = \begin{cases} 1 - 3 \left[1 + 2^{-1/2} \sinh(3.44 - \sqrt{3}x) \right]^{-1}, & \text{for } x < 0, \\ \frac{\sqrt{2}}{(x+1.89)}, & \text{for } x > 0, \end{cases}, \quad (\text{A.5.14})$$

where $x = 2(\pi/3)^{1/6} \alpha^{1/2} n_p^{1/3} (r - R_c) \sim 0.1(r - R_c)/\lambda_\pi$ and the pion Compton length $\lambda_\pi = \hbar/(m_\pi c)$. At the core center $r = 0$ ($x \rightarrow -\infty$), $V_{\text{coul}}(0) = \hbar c (3\pi^2 n_p)^{1/3} \sim m_\pi c^2$. On the surface of the core $r = R_c$, namely $x = 0$, and $V_{\text{coul}}(R_c) = (3/4)V_{\text{coul}}(0) \gg m_e c^2$, indicating that the ultra-relativistic approximation is applicable for $r \lesssim R_c$. This approximation breaks down at $r \gtrsim r_0$. Clearly, it is impossible to determine the value r_0 out of ultra-relativistically approximated equation, and full Thomas-Fermi equation (A.5.7) with source terms Eq. (A.5.6) for the neutral case, and Eq. (A.5.12) for the charged case have to be solved.

For $r < r_0$ where $V_{\text{coul}}(r) > 2m_e c^2$, we treat the term $2m_e c^2 V_{\text{coul}}(r)$ in Eqs. (A.5.6, A.5.12) as a small correction term, and find the following inequality is always true

$$n_e^{\text{neutral}}(r) > n_e^{\text{charged}}(r), \quad r < r_0, \quad (\text{A.5.15})$$

where $n_e^{\text{neutral}}(r)$ and $n_e^{\text{charged}}(r)$ stand for electron densities of neutral and super charged cores. For the range $r > r_0$, $n_e^{\text{charged}}(r) \equiv 0$ in the case of super charged core, while $n_e^{\text{neutral}}(r) \rightarrow 0$ in the case of neutral core, which should be calculated in non-relativistic approximation: the term $V_{\text{coul}}^2(r)$ in Eq. (A.5.6) is neglected.

In conclusion, the physical scenarios and Thomas-Fermi equations of neutral and super charged cores are slightly different. When the proton density n_p of cores is about nuclear density, ultra-relativistic approximation applies for the Coulomb potential energy $V_{\text{coul}}(r) \gg m_e c^2$ in $0 < r < r_0$ and $r_0 > R_c$, and approximate equations and solutions for electron distributions

A.5. Supercritical fields on the surface of massive nuclear cores: neutral core vs. charged core

inside and around cores are the same. As relativistic regime $r \sim r_0$ and non-relativistic regime $r > r_0$ (only applied to neutral case) are approached, solutions in two cases are somewhat different, and need direct integrations.

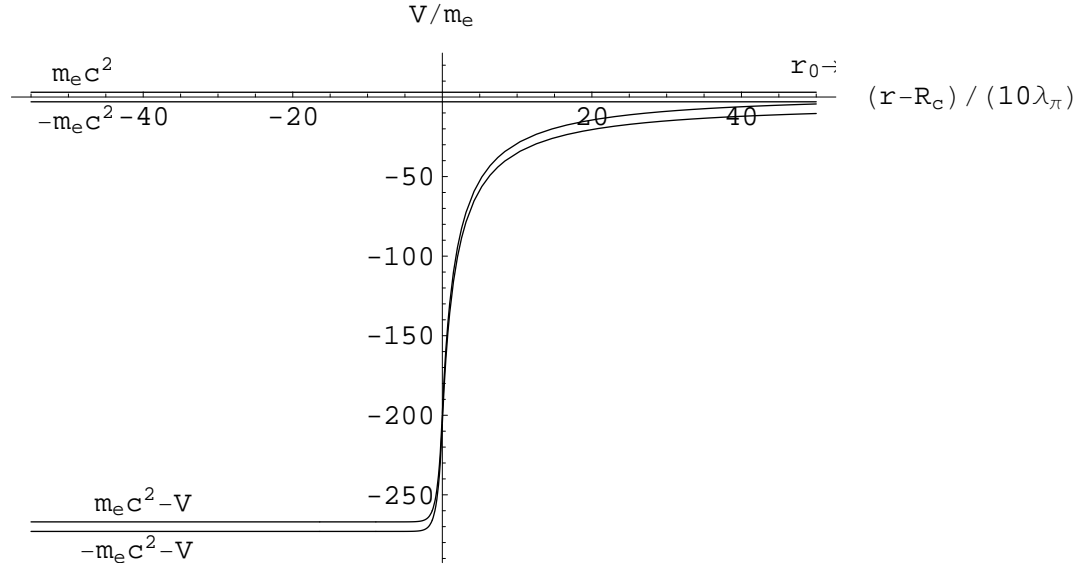


Figure A.24.: Potential energy-gap $\pm m_e c^2 - V_{\text{coul}}(r)$ and electron mass-gap $\pm m_e c^2$ in the unit of $m_e c^2$ are plotted as a function of $(r - R_c)/(10\lambda_\pi)$. The potential depth inside core ($r < R_c$) is about pion mass $m_\pi c^2 \gg m_e c^2$ and potential energy-gap and electron mass-gap are indicated. The radius r_0 where electron distribution $n_e(r_0)$ vanishes in super charged core case is indicated as r_0- , since it is out of plotting range.

A.6. The Extended Nuclear Matter Model with Smooth Transition Surface

A.6.1. The Relativistic Thomas-Fermi Equation

Let us to introduce the proton distribution function $f_p(x)$ by mean of $n_p(x) = n_p^c f_p(x)$, where n_p^c is the central number density of protons. We use the dimensionless unit $x = (r - b)/a$, with $a^{-1} = \sqrt{4\pi\alpha\lambda_e n_p^c}$, λ_e is the electron Compton wavelength, b the length where initial conditions are given ($x = 0$) and α is the fine structure constant.

Using the Poisson's equation and the equilibrium condition for the gas of electrons

$$E_F^e = m_e c^2 \sqrt{1 + x_e^2} - m_e c^2 - eV = 0, \quad (\text{A.6.1})$$

where e is the fundamental charge, x_e the normalized electron Fermi momentum and V the electrostatic potential, we obtain the relativistic Thomas-Fermi equation

$$\zeta_e''(x) + \left(\frac{2}{x + b/a} \right) \zeta_e'(x) - \frac{[\zeta_e^2(x) - 1]^{3/2}}{\mu} + f_p(x) = 0, \quad (\text{A.6.2})$$

where $\mu = 3\pi^2 \lambda_e^3 n_p^c$ and we have introduced the normalized electron chemical potential in absence of any field $\zeta_e = \sqrt{1 + x_e^2}$. For a given distribution function $f_p(x)$ and a central number density of protons n_p^c , the above equation can be integrated numerically with the boundary conditions

$$\zeta_e(0) = \sqrt{1 + [\mu \delta f_p(0)]^{2/3}}, \quad \zeta_e'(0) < 0, \quad (\text{A.6.3})$$

where $\delta \equiv n_e(0)/n_p(0)$.

A.6.2. The Woods-Saxon-like Proton Distribution Function

We simulate a monotonically decreasing proton distribution function fulfilling a Woods-Saxon dependence

$$f_p(x) = \frac{\gamma}{\gamma + e^{\beta x}}, \quad (\text{A.6.4})$$

where $\gamma > 0$ and $\beta > 0$. In Fig. A.25 we show the proton distribution function for a particular set of parameters.

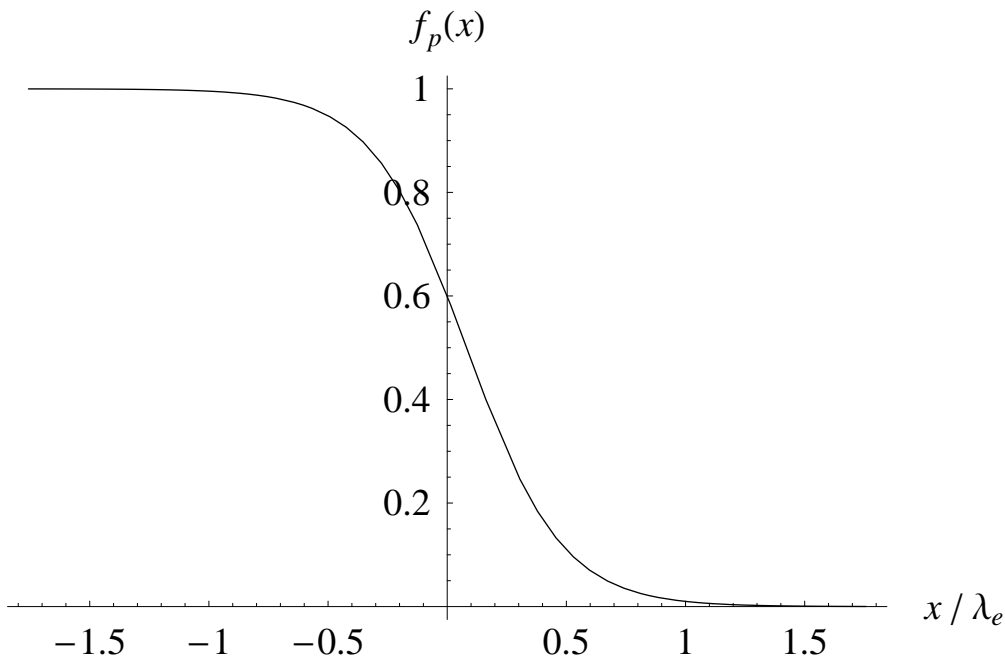


Figure A.25.: Proton distribution function for $\gamma = 1.5$, $\beta \approx 0.0585749$.

A.6.3. Results of the Numerical Integration.

We have integrated numerically the Eq. (A.6.2) for several sets of parameters and initial conditions. As an example, we show the results for the proton distribution function shown in Fig. A.25, with $n_p^c = 1.38 \times 10^{36} (\text{cm}^{-3})$. This system was integrated with $N_e = N_p = 10^{54}$, mass number $A = 1.61 \times 10^{56}$ and $\delta \approx 0.967$.

We summarize the principal features of our model in Figs. A.26 and A.27, where we have plotted the electric field in units of the critical field $E_c = \frac{m_e^2 c^3}{e \hbar}$, (m_e and e are the electron mass and charge), and the normalized charge separation function

$$\Delta(x) = \frac{n_p(x) - n_e(x)}{n_p(0)}. \quad (\text{A.6.5})$$

We see that the electric field is overcritical but smaller respect to the case of a sharp step proton distribution used in Ruffini et al. (2007c); Migdal et al. (1976). We have performed several numerical integrations expanding the transition surface and confirm the existence of overcritical fields but it is worth to mention that it could be subcritical expanding the width of the transition surface several orders of magnitude in electron Compton wavelength units.

We also see a displacement of the location of the maximum of intensity. This effect is due to the displacement of the point where $n_e = n_p$. After this point, the charge density becomes negative producing an effect of screening

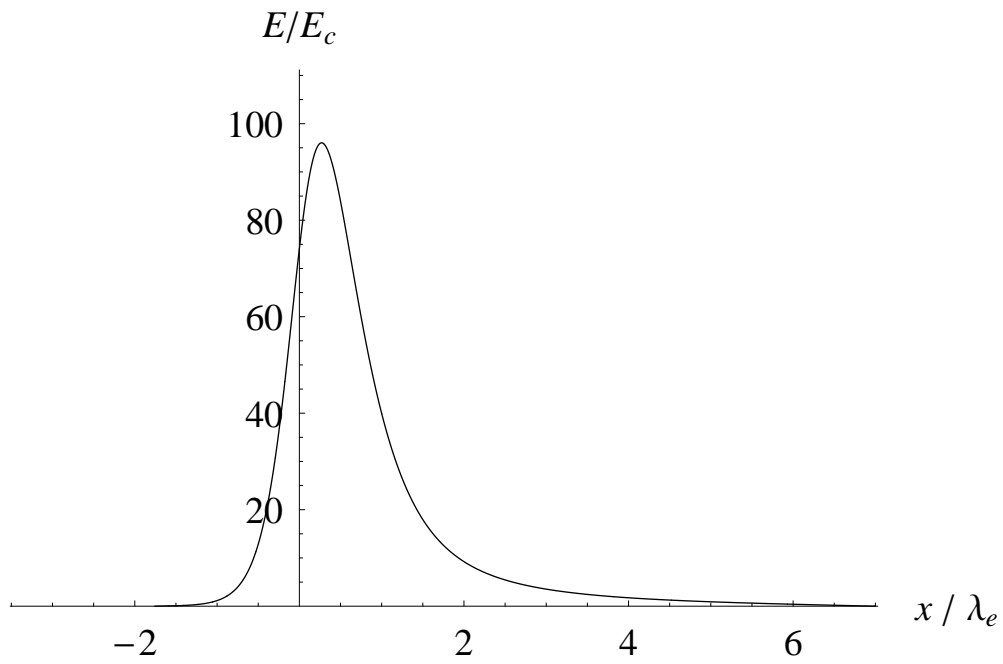


Figure A.26.: Electric field in units of the critical field E_c .

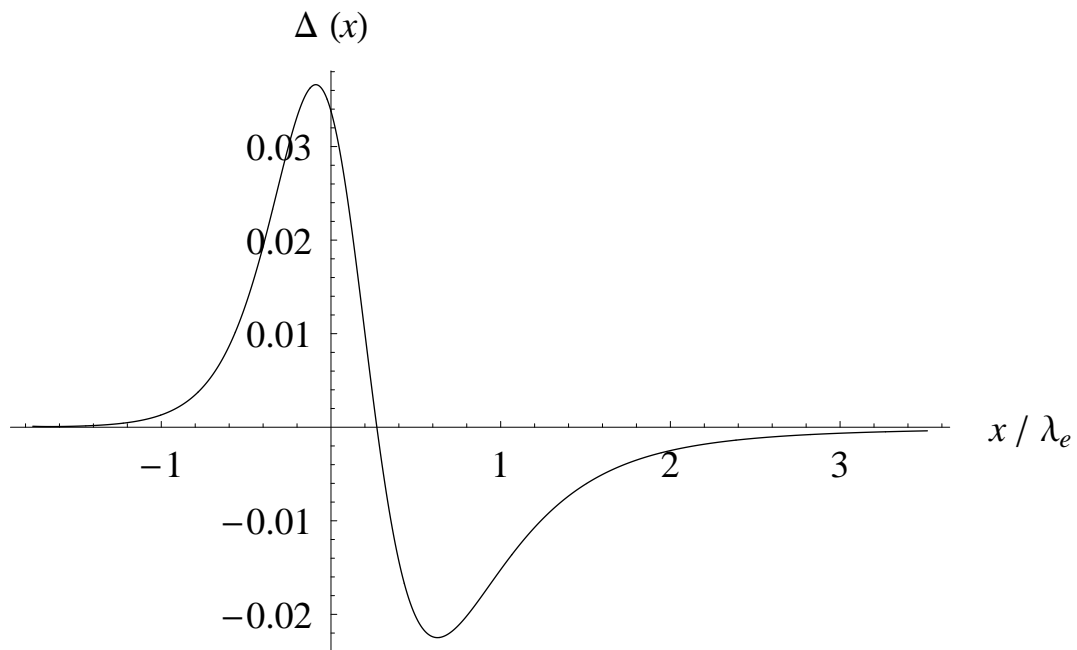


Figure A.27.: Charge separation function.

of the charged core up to global charged neutrality is achieved.

A.7. Electron-positron pairs production in a macroscopic charged core

A.7.1. Introduction

Very soon after the Dirac equation for a relativistic electron was discovered (Dirac, 1928a,b, 1958), Gordon (1928) (for all $Z < 137$) and Darwin (1928) (for $Z = 1$) found its solution in the point-like Coulomb potential $V(r) = -Z\alpha/r$, they obtained the well-known Sommerfeld's formula for energy-spectrum,

$$\varepsilon(n, j) = mc^2 \left[1 + \left(\frac{Z\alpha}{n - |K| + (K^2 - Z^2\alpha^2)^{1/2}} \right)^2 \right]^{-1/2}, \quad (\text{A.7.1})$$

where the fine-structure constant $\alpha = e^2/\hbar c$, the principle quantum number $n = 1, 2, 3, \dots$ and

$$K = \begin{cases} -(j + 1/2) = -(l + 1), & \text{if } j = l + \frac{1}{2}, \quad l \geq 0 \\ (j + 1/2) = l, & \text{if } j = l - \frac{1}{2}, \quad l \geq 1 \end{cases} \quad (\text{A.7.2})$$

$l = 0, 1, 2, \dots$ is the orbital angular momentum corresponding to the upper component of Dirac bi-spinor, j is the total angular momentum. The integer values n and j label bound states whose energies are $\varepsilon(n, j) \in (0, mc^2)$. For the example, in the case of the lowest energy states, one has

$$\varepsilon(1S_{\frac{1}{2}}) = mc^2 \sqrt{1 - (Z\alpha)^2}, \quad (\text{A.7.3})$$

$$\varepsilon(2S_{\frac{1}{2}}) = \varepsilon(2P_{\frac{1}{2}}) = mc^2 \sqrt{\frac{1 + \sqrt{1 - (Z\alpha)^2}}{2}}, \quad (\text{A.7.4})$$

$$\varepsilon(2P_{\frac{3}{2}}) = mc^2 \sqrt{1 - \frac{1}{4}(Z\alpha)^2}. \quad (\text{A.7.5})$$

For all states of the discrete spectrum, the binding energy $mc^2 - \varepsilon(n, j)$ increases as the nuclear charge Z increases. No regular solution with $n = 1, l = 0, j = 1/2$ and $K = -1$ (the $1S_{1/2}$ ground state) is found for $Z > 137$, this was first noticed by Gordon in his pioneer paper (Gordon, 1928). This is the problem so-called "Z = 137 catastrophe".

The problem was solved (Case, 1950; Werner and Wheeler, 1958; Popov, 1970, 1971b,a) by considering the fact that the nucleus is not point-like and has an extended charge distribution, and the potential $V(r)$ is not divergent when $r \rightarrow 0$. The $Z = 137$ catastrophe disappears and the energy-levels $\varepsilon(n, j)$ of the bound states $1S, 2P$ and $2S, \dots$ smoothly continue to drop toward the negative energy continuum ($E_- < -mc^2$), as Z increases to values larger than 137. The critical values Z_{cr} for $\varepsilon(n, j) = -mc^2$ were found

(Werner and Wheeler, 1958; Popov, 1970, 1971b,a; Rafelski et al., 1978; Kleinert et al., 2008): $Z_{cr} \simeq 173$ is a critical value at which the lowest energy-level of the bound state $1S_{1/2}$ encounters the negative energy continuum, while other bound states $2P_{1/2}, 2S_{3/2}, \dots$ encounter the negative energy continuum at $Z_{cr} > 173$, thus energy-level-crossings and productions of electron and positron pair takes place, provided these bound states are unoccupied. We refer the readers to Popov (1970, 1971b,a); Rafelski et al. (1978); Kleinert et al. (2008) for mathematical and numerical details.

The energetics of this phenomenon can be understood as follow. The energy-level of the bound state $1S_{1/2}$ can be estimated as follow,

$$\mathcal{E}(1S_{1/2}) = mc^2 - \frac{Ze^2}{\bar{r}} < -mc^2, \quad (\text{A.7.6})$$

where \bar{r} is the average radius of the $1S_{1/2}$ state's orbit, and the binding energy of this state $Ze^2/\bar{r} > 2mc^2$. If this bound state is unoccupied, the bare nucleus gains a binding energy Ze^2/\bar{r} larger than $2mc^2$, and becomes unstable against the production of an electron-positron pair. Assuming this pair-production occur around the radius \bar{r} , we have energies of electron (ϵ_-) and positron (ϵ_+):

$$\epsilon_- = \sqrt{(c|\mathbf{p}_-|)^2 + m^2c^4} - \frac{Ze^2}{\bar{r}}; \quad \epsilon_+ = \sqrt{(c|\mathbf{p}_+|)^2 + m^2c^4} + \frac{Ze^2}{\bar{r}}, \quad (\text{A.7.7})$$

where \mathbf{p}_\pm are electron and positron momenta, and $\mathbf{p}_- = -\mathbf{p}_+$. The total energy required for a pair production is,

$$\epsilon_{-+} = \epsilon_- + \epsilon_+ = 2\sqrt{(c|\mathbf{p}_-|)^2 + m^2c^4}, \quad (\text{A.7.8})$$

which is independent of the potential $V(\bar{r})$. The potential energies $\pm eV(\bar{r})$ of electron and positron cancel each other and do not contribute to the total energy (A.7.8) required for pair production. This energy (A.7.8) is acquired from the binding energy ($Ze^2/\bar{r} > 2mc^2$) by the electron filling into the bound state $1S_{1/2}$. A part of the binding energy becomes the kinetic energy of positron that goes out. This is analogous to the familiar case that a proton ($Z = 1$) catches an electron into the ground state $1S_{1/2}$, and a photon is emitted with the energy not less than 13.6 eV.

In this article, we study classical and semi-classical states of electrons, electron-positron pair production in an electric potential of macroscopic cores with charge $Q = Z|e|$, mass M and macroscopic radius R_c .

A.7.2. Classical description of electrons in potential of cores

Effective potentials for particle's radial motion

Setting the origin of spherical coordinates (r, θ, ϕ) at the center of such cores, we write the vectorial potential $A_\mu = (\mathbf{A}, A_0)$, where $\mathbf{A} = 0$ and A_0 is the Coulomb potential. The motion of a relativistic electron with mass m and charge e is described by its radial momentum p_r , total angular momenta p_ϕ and the Hamiltonian,

$$H_\pm = \pm mc^2 \sqrt{1 + \left(\frac{p_r}{mc}\right)^2 + \left(\frac{p_\phi}{mcr}\right)^2} - V(r), \quad (\text{A.7.9})$$

where the potential energy $V(r) = eA_0$, and \pm corresponds for positive and negative energies. The states corresponding to negative energy solutions are fully occupied. The total angular momentum p_ϕ is conserved, for the potential $V(r)$ is spherically symmetric. For a given angular momentum $p_\phi = mv_\perp r$, where v_\perp is the transverse velocity, the effective potential energy for electron's radial motion is

$$E_\pm(r) = \pm mc^2 \sqrt{1 + \left(\frac{p_\phi}{mcr}\right)^2} - V(r). \quad (\text{A.7.10})$$

Outside the core ($r \geq R_c$), the Coulomb potential energy $V(r)$ is given by

$$V_{\text{out}}(r) = \frac{Ze^2}{r}, \quad (\text{A.7.11})$$

where \pm indicates positive and negative effective energies. Inside the core ($r \leq R_c$), the Coulomb potential energy is given by

$$V_{\text{in}}(r) = \frac{Ze^2}{2R_c} \left[3 - \left(\frac{r}{R_c}\right)^2 \right], \quad (\text{A.7.12})$$

where we postulate the charged core has a uniform charge distribution with constant charge density $\rho = Ze/V_c$, and the core volume $V_c = 4\pi R_c^3/3$. Coulomb potential energies outside the core (A.7.11) and inside the core (A.7.12) is continuous at $r = R_c$. The electric field on the surface of the core,

$$E_s = \frac{Q}{R_c^2} = \frac{\lambda_e}{R_c} E_c, \quad \beta \equiv \frac{Ze^2}{mc^2 R_c} \quad (\text{A.7.13})$$

where the electron Compton wavelength $\lambda_e = \hbar/(mc)$, the critical electric field $E_c = m^2 c^3 / (e\hbar)$ and the parameter β is the electric potential-energy on the surface of the core in unit of the electron mass-energy.

Stable classical orbits (states) outside the core.

Given different values of total angular momenta p_ϕ , the stable circulating orbits R_L (states) are determined by the minimum of the effective potential $E_+(r)$ (A.7.10) (see Fig. A.28), at which $dE_+(r)/dr = 0$. We obtain stable orbits locate at the radii R_L ,

$$R_L = \left(\frac{p_\phi^2}{Ze^2 m} \right) \sqrt{1 - \left(\frac{Ze^2}{cp_\phi} \right)^2}, \quad R_L \geq R_c, \quad (\text{A.7.14})$$

for different p_ϕ -values. Substituting Eq. (A.7.14) into Eq. (A.7.10), we find the energy of electron at each stable orbit,

$$\varepsilon \equiv \min(E_+) = mc^2 \sqrt{1 - \left(\frac{Ze^2}{cp_\phi} \right)^2}. \quad (\text{A.7.15})$$

For the condition $R_L \gtrsim R_c$, we have

$$\left(\frac{Ze^2}{cp_\phi} \right)^2 \lesssim \frac{1}{2} [\beta(4 + \beta^2)^{1/2} - \beta^2], \quad (\text{A.7.16})$$

where the semi-equality holds for the last stable orbits outside the core $R_L \rightarrow R_c + 0^+$. In the point-like case $R_c \rightarrow 0$, the last stable orbits are

$$cp_\phi \rightarrow Ze^2 + 0^+, \quad R_L \rightarrow 0^+, \quad \varepsilon \rightarrow 0^+. \quad (\text{A.7.17})$$

Eq. (A.7.15) shows that only positive or null energy solutions (states) to exists in the case of a point-like charge, which is the same as the energy-spectrum Eqs. (A.7.3,A.7.4,A.7.5) in quantum mechanic scenario. While for $p_\phi \gg 1$, radii of stable orbits $R_L \gg 1$ and energies $\varepsilon \rightarrow mc^2 + 0^-$, classical electrons in these orbits are critically bound for their banding energy goes to zero. We conclude that the energies (A.7.15) of stable orbits outside the core must be smaller than mc^2 , but larger than zero, $\varepsilon > 0$. Therefore, no energy-level crossing with the negative energy spectrum occurs.

Stable classical orbits inside the core.

We turn to the stable orbits of electrons inside the core. Analogously, using Eqs. (A.7.10,A.7.12) and $dE_+(r)/dr = 0$, we obtain the stable orbit radius $R_L \leq 1$ in the unit of R_c , obeying the following equation,

$$\beta^2(R_L^8 + \kappa^2 R_L^6) = \kappa^4; \quad \kappa = \frac{p_\phi}{mcR_c}. \quad (\text{A.7.18})$$

and corresponding to the minimal energy (binding energy) of these states

$$\varepsilon = \frac{Ze^2}{R_c} \left[\left(\frac{cp_\phi}{Ze^2} \right)^2 \frac{1}{R_L^4} - \frac{1}{2}(3 - R_L^2) \right]. \quad (\text{A.7.19})$$

There are 8 solutions to this polynomial equation (A.7.18), only one is physical solution R_L that has to be real, positive and smaller than one. As example, the numerical solution to Eq. (A.7.18) is $R_L = 0.793701$ for $\beta = 4.4 \cdot 10^{16}$ and $\kappa = 2.2 \cdot 10^{16}$. In following, we respectively adopt non-relativistic and ultra-relativistic approximations to obtain analytical solutions.

First considering the non-relativistic case for those stable orbit states whose the kinetic energy term characterized by angular momentum term p_ϕ , see Eq. (A.7.10), is much smaller than the rest mass term mc^2 , we obtain the following approximate equation,

$$\beta^2 R_L^8 \simeq \kappa^4, \quad (\text{A.7.20})$$

and the solutions for stable orbit radii are,

$$R_L \simeq \frac{\kappa^{1/2}}{\beta^{1/4}} = \left(\frac{cp_\phi}{Ze^2} \right)^{1/2} \beta^{1/4} < 1, \quad (\text{A.7.21})$$

and energies,

$$\varepsilon \simeq \left(1 - \frac{3}{2}\beta + \frac{1}{2}\kappa\beta^{1/2} \right) mc^2. \quad (\text{A.7.22})$$

The consistent conditions for this solution are $\beta^{1/2} > \kappa$ for $R_L < 1$, and $\beta \ll 1$ for non-relativistic limit $v_\perp \ll c$. As a result, the binding energies (A.7.22) of these states are $mc^2 > \varepsilon > 0$, are never less than zero. These in fact correspond to the stable states which have large radii closing to the radius R_c of cores and $v_\perp \ll c$.

Second considering the ultra-relativistic case for those stable orbit states whose the kinetic energy term characterized by angular momentum term p_ϕ , see Eq. (A.7.10), is much larger than the rest mass term mc^2 , we obtain the following approximate equation,

$$\beta^2 R_L^6 \simeq \kappa^2, \quad (\text{A.7.23})$$

and the solutions for stable orbit radii are,

$$R_L \simeq \left(\frac{\kappa}{\beta} \right)^{1/3} = \left(\frac{p_\phi c}{Ze^2} \right)^{1/3} < 1, \quad (\text{A.7.24})$$

which gives $R_L \simeq 0.7937007$ for the same values of parameters β and κ in above. The consistent condition for this solution is $\beta > \kappa \gg 1$ for $R_L < 1$.

The energy levels of these ultra-relativistic states are,

$$\varepsilon \simeq \frac{3}{2}\beta \left[\left(\frac{p_\phi c}{Ze^2} \right)^{2/3} - 1 \right] mc^2, \quad (\text{A.7.25})$$

and $mc^2 > \varepsilon > -1.5\beta mc^2$. The particular solutions $\varepsilon = 0$ and $\varepsilon \simeq -mc^2$ are respectively given by

$$\left(\frac{p_\phi c}{Ze^2} \right) \simeq 1; \quad \left(\frac{p_\phi c}{Ze^2} \right) \simeq \left(1 - \frac{2}{3\beta} \right)^{3/2}. \quad (\text{A.7.26})$$

These in fact correspond to the stable states which have small radii closing to the center of cores and $v_\perp \lesssim c$.

To have the energy-level crossing to the negative energy continuum, we are interested in the values $\beta > \kappa \gg 1$ for which the energy-levels (A.7.25) of stable orbit states are equal to or less than $-mc^2$,

$$\varepsilon \simeq \frac{3}{2}\beta \left[\left(\frac{p_\phi c}{Ze^2} \right)^{2/3} - 1 \right] mc^2 \leq -mc^2. \quad (\text{A.7.27})$$

As example, with $\beta = 10$ and $\kappa = 2$, $R_L \simeq 0.585$, $\varepsilon_{\min} \simeq -9.87mc^2$. The lowest energy-level of electron state is $p_\phi/(Ze^2) = \kappa/\beta \rightarrow 0$ with the binding energy,

$$\varepsilon_{\min} = -\frac{3}{2}\beta mc^2, \quad (\text{A.7.28})$$

locating at $R_L \simeq (p_\phi c/Ze^2)^{1/3} \rightarrow 0$, the bottom of the potential energy $V_{\text{in}}(0)$ (A.7.12).

A.7.3. Semi-Classical description

Bohr-Sommerfeld quantization

In order to have further understanding, we consider the semi-classical scenario. Introducing the Planck constant $\hbar = h/(2\pi)$, we adopt the semi-classical Bohr-Sommerfeld quantization rule

$$\int p_\phi d\phi \simeq h\left(l + \frac{1}{2}\right), \quad \Rightarrow \quad p_\phi(l) \simeq \hbar\left(l + \frac{1}{2}\right), \quad l = 0, 1, 2, 3, \dots, \quad (\text{A.7.29})$$

which are discrete values selected from continuous total angular momentum p_ϕ in the classical scenario. The variation of total angular momentum $\Delta p_\phi = \pm\hbar$ in th unit of the Planck constant \hbar . Substitution

$$\left(\frac{p_\phi c}{Ze^2} \right) \Rightarrow \left(\frac{2l + 1}{2Z\alpha} \right), \quad (\text{A.7.30})$$

where the fine-structure constant $\alpha = e^2/(\hbar c)$, must be performed in classical solutions that we obtained in section (A.7.2).

1. The radii and energies of stable states outside the core (A.7.14) and (A.7.15) become:

$$R_L = \lambda \left(\frac{2l+1}{Z\alpha} \right) \sqrt{1 - \left(\frac{2Z\alpha}{2l+1} \right)^2}, \quad (\text{A.7.31})$$

$$\varepsilon = mc^2 \sqrt{1 - \left(\frac{2Z\alpha}{2l+1} \right)^2}, \quad (\text{A.7.32})$$

where λ is the electron Compton length.

2. The radii and energies of non-relativistic stable states inside the core (A.7.21) and (A.7.22) become:

$$R_L \simeq \left(\frac{2l+1}{2Z\alpha} \right)^{1/2} \beta^{1/4}, \quad (\text{A.7.33})$$

$$\varepsilon \simeq \left(1 - \frac{3}{2}\beta + \frac{\lambda(2l+1)}{4R_c} \beta^{1/2} \right) mc^2. \quad (\text{A.7.34})$$

3. The radii and energies of ultra-relativistic stable states inside the core (A.7.24) and (A.7.25) become:

$$R_L \simeq \left(\frac{2l+1}{2Z\alpha} \right)^{1/3}, \quad (\text{A.7.35})$$

$$\varepsilon \simeq \frac{3}{2}\beta \left[\left(\frac{2l+1}{2Z\alpha} \right)^{2/3} - 1 \right] mc^2. \quad (\text{A.7.36})$$

Note that radii R_L in the second and third cases are in unit of R_c .

Stability of semi-classical states

When these semi-classical states are not occupied as required by the Pauli Principle, the transition from one state to another with different discrete values of total angular momentum l (l_1, l_2 and $\Delta l = l_2 - l_1 = \pm 1$) undergoes by emission or absorption of a spin-1 (\hbar) photon. Following the energy and angular-momentum conservations, photon emitted or absorbed in the transition have angular momenta $p_\phi(l_2) - p_\phi(l_1) = \hbar(l_2 - l_1) = \pm\hbar$ and energy $\varepsilon(l_2) - \varepsilon(l_1)$. In this transition of stable states, the variation of radius is $\Delta R_L = R_L(l_2) - R_L(l_1)$.

We first consider the stability of semi-classical states against such transition in the case of point-like charge, i.e., Eqs. (A.7.31,A.7.32) with $l = 0, 1, 2, \dots$. As

required by the Heisenberg indeterminacy principle $\Delta\phi\Delta p_\phi \simeq 4\pi p_\phi(l) \gtrsim h$, the absolute ground state for minimal energy and angular momentum is given by the $l = 0$ state, $p_\phi \sim \hbar/2$, $R_L \sim \lambda(Z\alpha)^{-1} \sqrt{1 - (2Z\alpha)^2} > 0$ and $\mathcal{E} \sim mc^2 \sqrt{1 - (2Z\alpha)^2} > 0$, which corresponds to the last stable orbit (A.7.17) in the classical scenario. Thus the stability of all semi-classical states $l > 0$ is guaranteed by the Pauli principle. This is only case for $Z\alpha \leq 1/2$. While for $Z\alpha > 1/2$, there is not an absolute ground state in the semi-classical scenario. This can be understood by examining how the lowest energy states are selected by the quantization rule in the semi-classical scenario out of the last stable orbits (A.7.17) in the classical scenario. For the case of $Z\alpha \leq 1/2$, equating p_ϕ in Eq. (A.7.17) to $p_\phi = \hbar(l + 1/2)$ (A.7.29), we find the selected state $l = 0$ is only possible solution so that the ground state $l = 0$ in the semi-classical scenario corresponds to the last stable orbits (A.7.17) in the classical scenario. While for the case of $Z\alpha > 1/2$, equating p_ϕ in Eq. (A.7.17) to $p_\phi = \hbar(l + 1/2)$ (A.7.29), we find the selected semi-classical state

$$\tilde{l} = \frac{Z\alpha - 1}{2} > 0, \quad (\text{A.7.37})$$

in the semi-classical scenario corresponds to the last stable orbits (A.7.17) in the classical scenario. This state $l = \tilde{l} > 0$ is not protected by the Heisenberg indeterminacy principle from quantum-mechanically decaying in \hbar -steps to the states with lower angular momenta and energies (correspondingly smaller radius R_L (A.7.31)) via photon emissions. This clearly shows that the “Z = 137-catastrophe” corresponds to $R_L \rightarrow 0$, falling to the center of the Coulomb potential and all semi-classical states (l) are unstable.

Then we consider the stability of semi-classical states against such transition in the case of charged cores $R_c \neq 0$. Substituting p_ϕ in Eq. (A.7.29) into Eq. (A.7.16), we obtain the selected semi-classical state \tilde{l} corresponding to the last stable orbit outside the core,

$$\tilde{l} = \sqrt{2} \left(\frac{R_c}{\lambda} \right) \left[\left(\frac{4R_c}{Z\alpha\lambda} + 1 \right)^{1/2} - 1 \right]^{-1/2} \approx (Z\alpha)^{1/4} \left(\frac{R_c}{\lambda} \right)^{3/4} > 0. \quad (\text{A.7.38})$$

Analogously to Eq. (A.7.37), the same argument concludes the instability of this semi-classical state, which must quantum-mechanically decay to states with angular momentum $l < \tilde{l}$ inside the core, provided these semi-classical states are not occupied. This conclusion is independent of $Z\alpha$ -value.

We go on to examine the stability of semi-classical states inside the core. In the non-relativistic case ($1 \gg \beta > \kappa^2$), the last classical stable orbits locate at $R_L \rightarrow 0$ and $p_\phi \rightarrow 0$ given by Eqs. (A.7.21,A.7.22), corresponding to the lowest semi-classical state (A.7.33,A.7.34) with $l = 0$ and energy $mc^2 > \mathcal{E} > 0$. In the ultra-relativistic case ($\beta > \kappa \gg 1$), the last classical stable orbits locate

at $R_L \rightarrow 0$ and $p_\phi \rightarrow 0$ given by Eqs. (A.7.24,A.7.25), corresponding to the lowest semi-classical state (A.7.35,A.7.36) with $l = 0$ and minimal energy,

$$\mathcal{E} \simeq \frac{3}{2}\beta \left[\left(\frac{1}{2Z\alpha} \right)^{2/3} - 1 \right] mc^2 \approx -\frac{3}{2}\beta mc^2. \quad (\text{A.7.39})$$

This concludes that the $l = 0$ semi-classical state inside the core is an absolute ground state in both non- and ultra-relativistic cases. The Pauli principle assure that all semi-classical states $l > 0$ are stable, provided all these states accommodate electrons. The electrons can be either present inside the neutral core or produced from the vacuum polarization, later will be discussed in details.

We are particular interested in the ultra-relativistic case $\beta > \kappa \gg 1$, i.e., $Z\alpha \gg 1$, the energy-levels of semi-classical states can be profound than $-mc^2$ ($\mathcal{E} < -mc^2$), energy-level crossings and pair-productions occur if these states are unoccupied, as discussed in introductory section. It is even more important to mention that neutral cores like neutron stars of proton number $Z \sim 10^{52}$, the Thomas-Fermi approach has to be adopted to find the configuration of electrons in these semi-classical states, which has the depth of energy-levels $\mathcal{E} \sim -m_\pi c^2$ to accommodate electrons and a supercritical electric field ($E > E_c$) on the surface of the core (Ruffini et al., 2007c).

A.7.4. Production of electron-positron pair

When the energy-levels of semi-classical (bound) states $\mathcal{E} \leq -mc^2$ (A.7.27), energy-level crossings between these energy-levels (A.7.25) and negative energy continuum (A.7.10) for $p_r = 0$, as shown in Fig. A.29. The energy-level-crossing indicates that \mathcal{E} (A.7.25) and E_- (A.7.10) are equal,

$$\mathcal{E} = E_-, \quad (\text{A.7.40})$$

where angular momenta p_ϕ in \mathcal{E} (A.7.36) and E_- (A.7.10) are the same for angular-momentum conservation. The production of electron-positron pairs must takes place, provided these semi-classical (bound) states are unoccupied. The phenomenon of pair production can be understood as a quantum-mechanical tunneling process of relativistic electrons. The energy-levels \mathcal{E} of semi-classical (bound) states are given by Eq. (A.7.36) or (A.7.27). The probability amplitude for this process can be evaluated by a semi-classical calculation using WKB method (Kleinert et al., 2008):

$$W_{\text{WKB}}(|\mathbf{p}_\perp|) \equiv \exp \left\{ -\frac{2}{\hbar} \int_{R_b}^{R_n} p_r dr \right\}, \quad (\text{A.7.41})$$

where $|\mathbf{p}_\perp| = p_\phi/r$ is transverse momenta and the radial momentum,

$$p_r(r) = \sqrt{(c|\mathbf{p}_\perp|)^2 + m^2c^4 - [\mathcal{E} + V(r)]^2}. \quad (\text{A.7.42})$$

The energy potential $V(r)$ is either given by $V_{\text{out}}(r)$ (A.7.11) for $r > R_c$, or $V_{\text{in}}(r)$ (A.7.12) for $r < R_c$. The limits of integration (A.7.41): $R_b = R_L < R_c$ (A.7.24) or (A.7.35) indicating the location of the classical orbit (classical turning point) of semi-classical (bound) state; while another classical turning point R_n is determined by setting $p_r(r) = 0$ in Eq. (A.7.42). There are two cases: $R_n < R_c$ and $R_n > R_c$, depending on β and κ values.

To obtain a maximal WKB-probability amplitude (A.7.41) of pair production, we only consider the case that the charge core is bare and

- the lowest energy-levels of semi-classical (bound) states: $p_\phi/(Ze^2) = \kappa/\beta \rightarrow 0$, the location of classical orbit(A.7.24) $R_L = R_b \rightarrow 0$ and energy (A.7.25) $\mathcal{E} \rightarrow \mathcal{E}_{\text{min}} = -3\beta mc^2/2$ (A.7.28);
- another classical turning point $R_n \leq R_c$, since the probability is exponentially suppressed by a large tunneling length $\Delta = R_n - R_b$.

In this case ($R_n \leq R_c$), Eq. (A.7.42) becomes

$$p_r = \sqrt{(c|\mathbf{p}_\perp|)^2 + m^2c^4} \sqrt{1 - \frac{\beta^2 m^2 c^4}{4[(c|\mathbf{p}_\perp|)^2 + m^2c^4]} \left(\frac{r}{R_c}\right)^4}, \quad (\text{A.7.43})$$

and $p_r = 0$ leads to

$$\frac{R_n}{R_c} = \left(\frac{2}{\beta mc^2}\right)^{1/2} [(c|\mathbf{p}_\perp|)^2 + m^2c^4]^{1/4}. \quad (\text{A.7.44})$$

Using Eqs. (A.7.41,A.7.43,A.7.44), we have

$$\begin{aligned} W_{\text{WKB}}(|\mathbf{p}_\perp|) &= \exp \left\{ -\frac{2^{3/2}[(c|\mathbf{p}_\perp|)^2 + m^2c^4]^{3/4} R_c}{c\hbar(mc^2\beta)^{1/2}} \int_0^1 \sqrt{1-x^4} dx \right\} \\ &= \exp \left\{ -0.87 \frac{2^{3/2}[(c|\mathbf{p}_\perp|)^2 + m^2c^4]^{3/4} R_c}{c\hbar(mc^2\beta)^{1/2}} \right\}. \end{aligned} \quad (\text{A.7.45})$$

Dividing this probability amplitude by the tunneling length $\Delta \simeq R_n$ and time interval $\Delta t \simeq 2\hbar\pi/(2mc^2)$ in which the quantum tunneling occurs, and integrating over two spin states and the transverse phase-space $2 \int d\mathbf{r}_\perp d\mathbf{p}_\perp / (2\pi\hbar)^2$, we approximately obtain the rate of pair-production per the unit of time and

volume,

$$\Gamma_{\text{NS}} \equiv \frac{d^4 N}{dt d^3 x} \simeq \frac{1.15}{6\pi^2} \left(\frac{Z\alpha}{\tau R_c^3} \right) \exp \left\{ -\frac{2.46}{(Z\alpha)^{1/2}} \left(\frac{R_c}{\lambda} \right)^{3/2} \right\}, \quad (\text{A.7.46})$$

$$= \frac{1.15}{6\pi^2} \left(\frac{\beta}{\tau \lambda R_c^2} \right) \exp \left\{ -\frac{2.46 R_c}{\beta^{1/2} \lambda} \right\}, \quad (\text{A.7.47})$$

$$= \frac{1.15}{6\pi^2} \left(\frac{1}{\tau \lambda^2 R_c} \right) \left(\frac{E_s}{E_c} \right) \exp \left\{ -2.46 \left(\frac{R_c}{\lambda} \right)^{1/2} \left(\frac{E_c}{E_s} \right)^{1/2} \right\}, \quad (\text{A.7.48})$$

where $E_s = Ze/R_c^2$ being the electric field on the surface of the core and the Compton time $\tau = \hbar/mc^2$.

To have the size of this pair-production rate, we compare it with the Sauter-Euler-Heisenberg-Schwinger rate of pair-production in a constant field E (Heisenberg and Euler, 1936; Sauter, 1931; Schwinger, 1951, 1954a,b),

$$\Gamma_S \equiv \frac{d^4 N}{dt d^3 x} \simeq \frac{1}{4\pi^3 \tau \lambda^3} \left(\frac{E}{E_c} \right)^2 \exp \left\{ -\pi \frac{E_c}{E} \right\}. \quad (\text{A.7.49})$$

When the parameter $\beta \simeq (R_c/\lambda)^2$, Eq. (A.7.47) becomes

$$\Gamma_{\text{NS}} \equiv \frac{d^4 N}{dt d^3 x} \simeq \frac{1.15}{6\pi^2} \left(\frac{1}{\tau \lambda^3} \right) \exp \{-2.46\} = 1.66 \cdot 10^{-3}/(\tau \lambda^3), \quad (\text{A.7.50})$$

which is close to the Sauter-Euler-Heisenberg-Schwinger rate (A.7.49) $\Gamma_S \simeq 3.5 \cdot 10^{-4}/(\tau \lambda^3)$ at $E \simeq E_c$. Taking a neutron star with core mass $M = M_\odot$ and radius $R_c = 10\text{km}$, we have $R_c/\lambda = 2.59 \cdot 10^{16}$ and $\beta = 3.86 \cdot 10^{-17} Z\alpha$, leading to $Z \simeq 2.4 \cdot 10^{51}$ and the electric field on the core surface $E_s/E_c = Z\alpha(\lambda/R_c)^2 \simeq 2.6 \cdot 10^{16}$. In this case, the charge-mass ratio $Q/(G^{1/2}M) = 2 \cdot 10^{-6}|e|/(G^{1/2}m_p) = 2.2 \cdot 10^{12}$, where where G is the Newton constant and proton's charge-mass ratio $|e|/(G^{1/2}m_p) = 1.1 \cdot 10^{18}$.

Let us consider another case that the electric field on the core surface E_s (A.7.13) is about the critical field ($E_s \simeq E_c$). In this case, $Z = \alpha^{-1}(R_c/\lambda)^2 \simeq 9.2 \cdot 10^{34}$, $\beta = Z\alpha\lambda/R_c = R_c/\lambda \simeq 2.59 \cdot 10^{16}$, and the rate (A.7.47) becomes

$$\Gamma_{\text{NS}} \equiv \frac{d^4 N}{dt d^3 x} \simeq \frac{1.15}{6\pi^2} \left(\frac{1}{\tau \lambda^3} \right) \left(\frac{\lambda}{R_c} \right) \exp \left\{ -2.46 \left(\frac{R_c}{\lambda} \right) \right\}, \quad (\text{A.7.51})$$

which is exponentially smaller than Eq. (A.7.50) for $R_c \gg \lambda$. In this case, the charge-mass ratio $Q/(G^{1/2}M) = 8.46 \cdot 10^{-5}$.

A.7.5. Summary and remarks

In this letter, analogously to the study in atomic physics with large atomic number Z , we study the classical and semi-classical (bound) states of electrons in the electric potential of a massive and charged core, which has a uniform charge distribution and macroscopic radius. We have found negative energy states of electrons inside the core, whose energies can be smaller than $-mc^2$, and the appearance of energy-level crossing to the negative energy spectrum. As results, quantum tunneling takes place, leading to electron-positron pairs production, electrons then occupy these semi-classical (bound) states and positrons are repelled to infinity. Assuming that massive charged cores are bare and non of these semi-classical (bound) states are occupied, we analytically obtain the maximal rate of electron-positron pair production in terms of core's radius, charge and mass, and we compare it with the Sauter-Euler-Heisenberg-Schwinger rate of pair-production in a constant field.

Any electron occupations of these semi-classical (bound) states must screen core's charge and the massive core is no longer bare. The electric potential inside the core is changed. For the core consists of a large number of electrons, the Thomas-Fermi approach has to be adopted. We recently study (Ruffini et al., 2007c) the electron distribution inside and outside the massive core, i.e., the distribution of electrons occupying stable states of the massive core, and find the electric field on the surface of the massive core is overcritical.

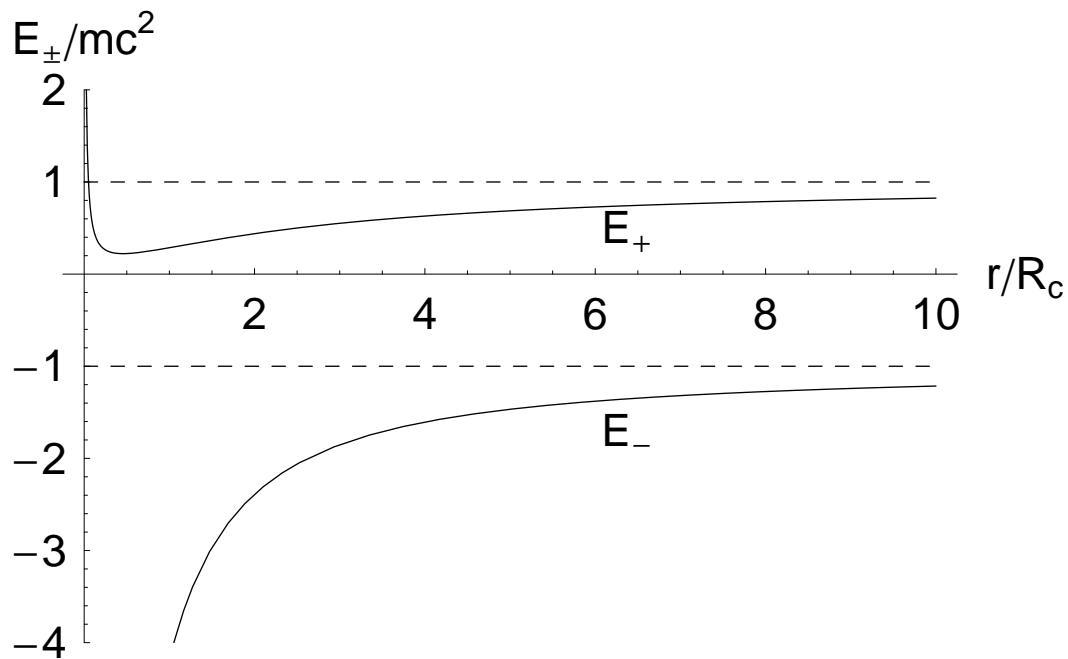


Figure A.28.: In the case of point-like charge distribution, we plot the positive and negative effective potential energies E_{\pm} (A.7.10), $p_{\phi}/(mcR_c) = 2$ and $Ze^2 = 1.95mc^2R_c$, to illustrate the radial location R_L (A.7.14) of stable orbits where E_+ has a minimum (A.7.15). All stable orbits are described by $cp_{\phi} > Ze^2$. The last stable orbits are given by $cp_{\phi} \rightarrow Ze^2 + 0^+$, whose radial location $R_L \rightarrow 0$ and energy $\mathcal{E} \rightarrow 0^+$. There is no any stable orbit with energy $\mathcal{E} < 0$ and the energy-level crossing with the negative energy spectrum E_- is impossible.

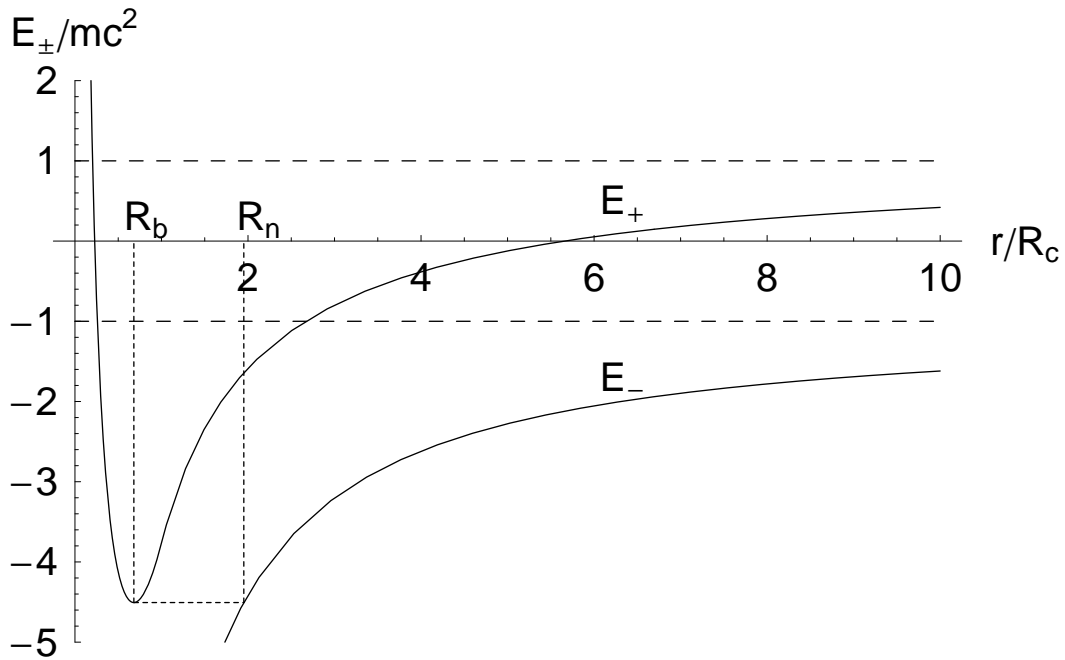


Figure A.29.: For the core $\kappa = 2$ and $\beta = 6$, we plot the positive and negative effective potentials E_{\pm} (A.7.10), in order to illustrate the radial location (A.7.24) $R_L < R_c$ of stable orbit, where E_+ 's minimum (A.7.25) $\mathcal{E} < mc^2$ is. All stable orbits inside the core are described by $\beta > \kappa > 1$. The last stable orbit is given by $\kappa/\beta \rightarrow 0$, whose radial location $R_L \rightarrow 0$ and energy $\mathcal{E} \rightarrow \mathcal{E}_{\min}$ (A.7.28). We indicate that the energy-level crossing between bound state (stable orbit) energy at $R_L = R_b$ and negative energy spectrum E_- (A.7.25) at the turning point R_n .

A.8. On Magnetic Fields in Rotating Nuclear Matter Cores of Stellar Dimensions

A.8.1. Introduction

Neutron stars are mainly detected as pulsars, whose regular pulsations in the radio, X-ray, and optical bands are produced by constant, ordered magnetic fields that are the strongest known in the Universe. However the origin of the magnetic field in the neutron stars is not fully understood, so far. Nevertheless in the literature one may find various hypotheses explaining the formation of the magnetic field (Ginzburg, 1964; Woltjer, 1964; Ruderman, 1972, 1995; Reisenegger, 2001, 2007; Reisenegger et al., 2007). The simplest hypothesis to explain the presence of the strong fields observed in neutron stars is the conservation of the magnetic flux already present in the progenitor stars during the gravitational collapse. This idea is based on the assumption that all stars at all stages of their evolution have some magnetic field, due to electronic currents circulating in their interiors. Thus this argument led to the prediction of the fields $B \approx 10^{12}$ G in neutron stars a few years before the discovery of pulsars (Ginzburg, 1964; Woltjer, 1964). However, there is no detailed physical picture of such a flux conserving collapse. Thompson and Duncan (1993) put forward the hypothesis that newborn neutron stars are likely to combine vigorous convection and differential rotation making a dynamo process operate in them. They predicted fields up to $10^{15} - 10^{16}$ G in neutron stars with few millisecond initial periods, and suggested that such fields could explain much of the phenomenology associated with Soft Gamma Repeaters and Anomalous X-ray Pulsars (Thompson and Duncan, 1995, 1996).

Probably, these processes are not mutually exclusive. A strong field might be present in the collapsing star, but later be deformed and perhaps amplified by some combination of convection, differential rotation, and magnetic instabilities (Tayler, 1973; Spruit, 2002). The relative importance of these ingredients depends on the initial field strength and rotation rate of the star. For both mechanisms, the field and its supporting currents are not likely to be confined to the solid crust of the star, but distributed in most of the stellar interior, which is mostly a fluid mixture of neutrons, protons, electrons, and other, more exotic particles.

Unlike aforementioned hypotheses which are based on the assumptions that all stars are magnetized or charged with some net charge different from zero, we explore the system recently considered by Ruffini et al. (2007c). According to that work the system consisting of degenerate neutrons, protons and electrons in beta equilibrium is globally neutral and expected to be kept at nuclear density by self gravity. In what follows these systems are termed as Nuclear Matter Cores of Stellar Dimensions. Despite the global neutrality the charge distribution turned out to be different from zero inside and out-

side (near the surface) the star. The magnitude of the net charge inside and outside the core is equal, but the sign is opposite. Such an effect takes place as a consequence of the beta equilibrium, the penetration of electrons into the core, hence the screening of the core charge and global charge neutrality. As a result of this effect, one may show the presence of an electric field close to the critical value $E_c = m_e^2 c^3 / e \hbar$ near the surface of the massive cores, although localized in a very narrow shell. Thus in this case the magnetic field of the neutron star may be generated only if it spins like pulsars, even though the progenitor star has not been magnetized or electrically charged.

A.8.2. The Relativistic Thomas-Fermi equation

The Thomas-Fermi equation is the exact theory for atoms, molecules and solids as $Z \rightarrow \infty$ (Lieb and Simon, 1973). The relativistic Thomas-Fermi theory developed for the study of atoms for heavy nuclei with $Z = 10^6$ (Ferreirinho et al., 1980; Ruffini and Stella, 1981) gives important basic new information on the study of nuclear matter in bulk in the limit of $A = (m_{Planck}/m_n)^3$ nucleons of mass m_n and on its electrodynamic properties. The analysis of nuclear matter bulk in neutron stars composed of degenerate gas of neutrons, protons and electrons, has traditionally been approached by implementing microscopically the charge neutrality condition by requiring the electron density $n_e(r)$ to coincide with the proton density $n_p(r)$,

$$n_e(r) = n_p(r). \tag{A.8.1}$$

It is clear however that especially when conditions close to the gravitational collapse occur, there is an ultra-relativistic component of degenerate electrons whose confinement requires the existence of very strong electromagnetic fields, in order to guarantee the overall charge neutrality of the neutron star. Under these conditions equation (A.8.1) will be necessarily violated.

Using substantially a statistical approach based on the relativistic Thomas-Fermi equation, Ferreira et al. (1980); Ruffini and Stella (1981) have analyzed the electron densities around an extended nucleus in a neutral atom all the way up to $Z = 6000$. They have shown the effect of penetration of the electron orbital well inside the nucleus, leading to a screening of the nuclei positive charge and to the concept of an “effective” nuclear charge distribution.

In the work of Ruffini et al. (2007c) and Rotondo et al. (2011e) the relativistic Thomas-Fermi equation has been used to extrapolate the treatment of super heavy nuclei to the case of nuclear matter cores of stellar dimensions. These cores represent the inner part of neutron stars and are characterized by an atomic number of order of $A = (m_{Planck}/m_n)^3 \approx 10^{57}$, composed of degenerate N_n neutrons, N_p protons and N_e electrons in beta equilibrium and expected to be kept at nuclear density by self gravity. It has been shown that

near the surface of the massive cores it is possible to have an electric field close to the critical value E_c , although localized in a very narrow shell of the order of the λ_e electron Compton wavelength. Now let us review the main assumptions and results of those works.

According to Ruffini et al. (2007c) and Rotondo et al. (2011e) the protons are distributed at constant density n_p within a radius

$$R_c = \Delta \frac{\hbar}{m_\pi c} N_p^{1/3}, \quad (\text{A.8.2})$$

where Δ is a parameter such that $\Delta \approx 1$ ($\Delta < 1$) corresponds to nuclear (supranuclear) densities when applied to ordinary nuclei. The overall Coulomb potential satisfies the Poisson equation

$$\nabla^2 V(r) = -4\pi e [n_p(r) - n_e(r)], \quad (\text{A.8.3})$$

with the boundary conditions $V(\infty) = 0$ (due to the global charge neutrality of the system) and finiteness of $V(0)$. The density $n_e(r)$ of the electrons of charge $-e$ is determined by the Fermi energy condition on their Fermi momentum P_e^F ; we assume here

$$E_e^F = [(P_e^F c)^2 + m_e^2 c^4]^{1/2} - m_e c^2 - eV(r) = 0, \quad (\text{A.8.4})$$

which leads to

$$n_e(r) = \frac{(P_e^F)^3}{3\pi^2 \hbar^3} = \frac{1}{3\pi^2 \hbar^3 c^3} [e^2 V^2(r) + 2m_e c^2 eV(r)]^{3/2}. \quad (\text{A.8.5})$$

Introducing the dimensionless quantities $x = r/[\hbar/m_\pi c]$, $x_c = R_c/[\hbar/m_\pi c]$ and $\chi/r = eV(r)/c\hbar$, the relativistic Thomas-Fermi equation takes the form

$$\frac{1}{3x} \frac{d^2 \chi(x)}{dx^2} = -\frac{\alpha}{\Delta^3} H(x_c - x) + \frac{4\alpha}{9\pi} \left[\frac{\chi^2(x)}{x^2} + 2 \frac{m_e}{m_\pi} \frac{\chi}{x} \right]^{3/2}, \quad (\text{A.8.6})$$

where $\alpha = e^2/(\hbar c)$ is the fine structure constant, $H(x_c - x)$ is the Heaviside step function and the boundary conditions for $\chi(x)$ are $\chi(0) = 0, \chi(\infty) = 0$. The neutron density $n_n(r)$ is determined by the Fermi energy condition on their Fermi momentum P_n^F imposed by beta decay equilibrium

$$E_n^F = [(P_n^F c)^2 + m_n^2 c^4]^{1/2} - m_n c^2 = [(P_p^F c)^2 + m_p^2 c^4]^{1/2} - m_p c^2 + eV, \quad (\text{A.8.7})$$

which in turn is related to the proton and electron densities by Eqs. (A.8.3), (A.8.5) and (A.8.6).

A.8.3. The ultra-relativistic analytic solutions

In the ultrarelativistic limit with the planar approximation the relativistic Thomas-Fermi equation admits an analytic solution. Introducing the new function ϕ defined by $\phi = 4^{1/3}(9\pi)^{-1/3}\Delta\chi/x$ and the new variables $\hat{x} = (12/\pi)^{1/6}\sqrt{\alpha}\Delta^{-1}x$, $\xi = \hat{x} - \hat{x}_c$, where $\hat{x}_c = (12/\pi)^{1/6}\sqrt{\alpha}\Delta^{-1}x_c$, Eq. (A.8.6) becomes

$$\frac{d^2\hat{\phi}(\xi)}{d\xi^2} = -H(-\xi) + \hat{\phi}(\xi)^3, \quad (\text{A.8.8})$$

where $\hat{\phi}(\xi) = \phi(\xi + \hat{x}_c)$. The boundary conditions on $\hat{\phi}$ are: $\hat{\phi}(\xi) \rightarrow 1$ as $\xi \rightarrow -\hat{x}_c \ll 0$ (at the nuclear matter core center) and $\hat{\phi}(\xi) \rightarrow 0$ as $\xi \rightarrow \infty$. The function $\hat{\phi}$ and its first derivative $\hat{\phi}'$ must be continuous at the surface $\xi = 0$ of the nuclear matter core of stellar dimensions. Hence equation (A.8.8) admits an exact solution

$$\hat{\phi}(\xi) = \begin{cases} 1 - 3 \left[1 + 2^{-1/2} \sinh(a - \sqrt{3}\xi) \right]^{-1}, & \xi < 0, \\ \frac{\sqrt{2}}{(\xi + b)}, & \xi > 0, \end{cases} \quad (\text{A.8.9})$$

where the integration constants a and b have the values $a = \text{arccosh}(9\sqrt{3}) \approx 3.439$, $b = (4/3)\sqrt{2} \approx 1.886$. Next we evaluate the Coulomb potential function

$$V(\xi) = \left(\frac{9\pi}{4} \right)^{1/3} \frac{m_\pi c^2}{\Delta e} \hat{\phi}(\xi), \quad (\text{A.8.10})$$

and by differentiation, the electric field

$$E(\xi) = - \left(\frac{3^5 \pi}{4} \right)^{1/6} \frac{\sqrt{\alpha} m_\pi^2 c^3}{\Delta^2 e \hbar} \hat{\phi}'(\xi). \quad (\text{A.8.11})$$

Details are given in Figs. A.30 and A.31.

A.8.4. Rotating Nuclear Matter Cores of Stellar Dimensions in Classical Electrodynamics

In section A.8.2 and A.8.3 we have seen that in the massive nuclear density cores the electric charge distribution is different from zero, although it is globally neutral. In this section we investigate the case when this charge distribution is allowed to rotate with the constant angular velocity Ω around the axis of symmetry. Thus the magnetic field of the resultant current density is calculated in terms of the charge distribution.

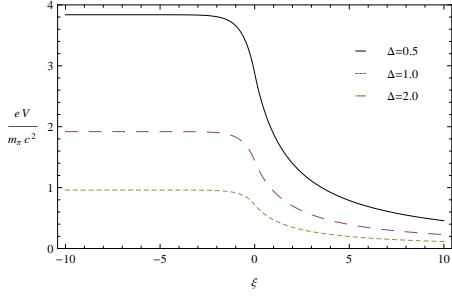


Figure A.30.: The electron Coulomb potential energy eV , in units of pion mass m_π is plotted as a function of the radial coordinate $\xi = \hat{x} - \hat{x}_c$, for selected values of the density parameter Δ .

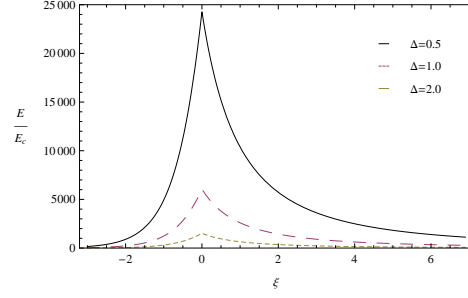


Figure A.31.: The electric field is plotted in units of the critical field E_c as a function of the radial coordinate ξ , showing a sharp peak at the core radius, for selected values of Δ .

Consider a charge distribution moving in a such way that at every point in space the charge density and the current density remain constant. In this case the magnetic field is defined by

$$\mathbf{B}(\mathbf{r}) = \nabla \times \mathbf{A}(\mathbf{r}), \quad \mathbf{A}(\mathbf{r}) = (\boldsymbol{\Omega}/c^2) \times \mathbf{F}(\mathbf{r}), \quad \mathbf{F}(\mathbf{r}) = \frac{1}{4\pi} \int \frac{\mathbf{r}'\rho(\mathbf{r}')d^3\mathbf{r}'}{|\mathbf{r}-\mathbf{r}'|}, \quad (\text{A.8.12})$$

where \mathbf{A} is the vector potential of the magnetic field, $\mathbf{F}(\mathbf{r})$ is the "superpotential" in general form. In the case of spherical symmetry, $\mathbf{F}(\mathbf{r})$ may be taken as radial (see Marsh (1982)). Writing $\mathbf{F}(\mathbf{r}) = \mathbf{e}_r F(r)$, where \mathbf{e}_r is the unit radial vector, one has

$$F(r) = \frac{1}{r^2} \int_0^r r'^2 \frac{d}{dr'} [r'V(r')] dr'. \quad (\text{A.8.13})$$

This expression allows to calculate the magnetic field due to rotation of any spherically symmetric distribution of charge in terms of its electrostatic Coulomb potential. Note that in fact due to rotation the shape of the neutron star must deviate from spherical symmetry. Since we are interested in the estimation of the order of the magnetic field the distortions to the shape of the star can be neglected for simplicity. Thus the magnetic field is defined by

$$\mathbf{B}(\mathbf{r}) = B_r \mathbf{e}_r + B_\theta \mathbf{e}_\theta, \quad B_r = \frac{2\Omega F}{c^2 r} \cos \theta, \quad B_\theta = -\frac{2\Omega}{c^2} \left[\frac{F}{r} + \frac{r}{2} \frac{d}{dr} \left(\frac{F}{r} \right) \right] \sin \theta, \quad (\text{A.8.14})$$

where B_r is the radial component and B_θ is the angular component of the magnetic field, θ is the angle between r and z axis, and \mathbf{e}_θ is the unit vector along θ . Consequently the expression for the magnitude (the absolute value)

of the magnetic field can be written as

$$B(r, \theta) = \frac{\Omega r}{c^2} \sqrt{\left(\frac{2F}{r^2}\right)^2 + \left\{ \frac{4F}{r^2} \frac{d}{dr} \left(\frac{F}{r}\right) + \left[\frac{d}{dr} \left(\frac{F}{r}\right) \right]^2 \right\} \sin^2 \theta}. \quad (\text{A.8.15})$$

Using the relation between r and ξ

$$r = R_c + \left(\frac{\pi}{12}\right)^{1/6} \frac{\Delta}{\sqrt{\alpha}} \frac{\hbar}{m_{\pi} c} \xi, \quad (\text{A.8.16})$$

one may estimate the value of the magnetic field. In Figs. A.32, A.33, A.34 and A.35 details are given.

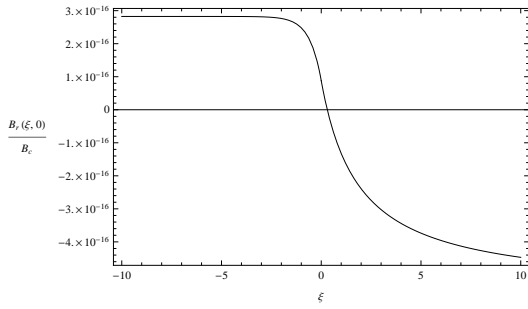


Figure A.32.: The radial component of the magnetic field is plotted as a function of the radial coordinate ξ in units of the critical field $B_c = m_c^2 c^3 / e \hbar \approx 4.5 \times 10^{13}$ G. Here the period is taken to be $P = 10$ ms, $\theta = 0$, $\Delta = 1$ and the radius of the core $R_c = 10$ km. Note that B_r is considered at the poles of star, where it has maximum value. Outside the star B_r has very small negative value and it tends to zero. Because of visualization difficulties it is not seen in the figure.

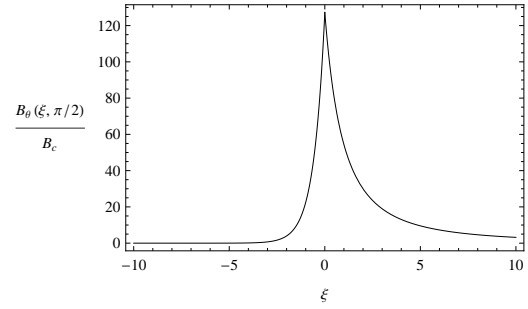


Figure A.33.: The angular component of the magnetic field is plotted in units of the B_c . Here $P = 10$ ms, $\theta = \pi/2$, $\Delta = 1$ and $R_c = 10$ km. Note that B_θ is considered at the equator, where it has maximum value. Inside the star it has very small constant negative value. Outside the star first it becomes negative (the value is very small) then it tends to zero. Because of scale problems this behavior is not seen from the figure.

Examining the Fig. A.32 one can see very small value of B_r which almost does not make a significant contribution to the magnitude of the field, except for the poles of the star. On the contrary, B_θ Fig. A.33 has values exceeding the critical magnetic field near the surface of the core although localized in a narrow region between positively and negatively charged shells as expected. Outside the core the magnetic field becomes negative. The magnitude of the

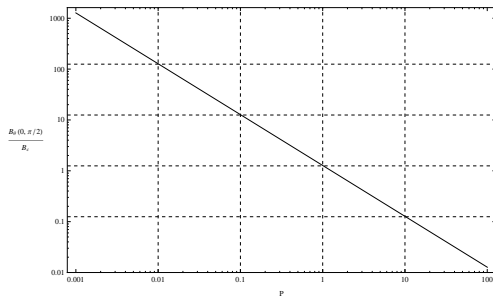


Figure A.34.: The magnitude of the magnetic field is plotted as a function of the period of the star P in the units of the critical field B_c at the surface of the core $R_c = 10 \text{ km}$ on the equator in the logarithmic scale.

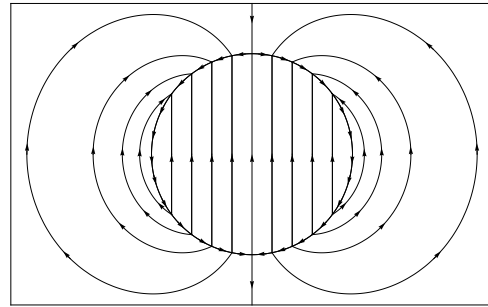


Figure A.35.: The magnetic lines of forces. Outside the star the magnetic field looks like a dipole field. Extra lines along the surface of the star indicate overcritical value of the field between positively and negatively charged shells.

field has very small and eventually vanishing values. This effect can not be seen from the figures, because of visualization difficulties.

In Fig. A.34 the magnitude of the magnetic field is presented as a function of the rotational period P on the surface of the core at the equator. Practically it demonstrates the upper limit of possible values of the magnetic field in the range between 1 ms and 100 s . Fig. A.35 represents magnetic lines of force inside, outside and on the surface of the star. It turned out that the lines of force of the overcritical magnetic field are oppressed between two shells along the surface of the core.

A.8.5. Conclusions

In this paper we have investigated the behavior of the magnetic field induced due to rotation on the basis of the research works considered in Ruffini et al. (2007c) and Rotondo et al. (2011e) using the technique developed by Marsh (1982).

For this purpose considering a rotating neutron star with the period of 10 ms we have obtained the magnetic field of order of the critical field near the surface of the star and analyzed the magnetic lines of forces.

According to our results the magnetic fields of the neutron stars could be generated due to the rotation of the star as a whole rigid body. We believe that the generation of the magnetic field due to the rotation is the reason for the formation of the constant magnetic fields at the initial moments of neutron stars birth.

The problem of investigating the magnetic field in general relativity for a self-gravitating system of degenerate fermions in beta equilibrium is beyond

the scope of the present work. We expect to investigate this problem in the nearest future.

B. White Dwarfs Physics and Astrophysics

B.1. The relativistic Feynman-Metropolis-Teller theory for white dwarfs in general relativity

B.1.1. Introduction

The necessity of introducing the Fermi-Dirac statistics in order to overcome some conceptual difficulties in explaining the existence of white dwarfs leading to the concept of degenerate stars was first advanced by (Fowler, 1926) in a classic paper. Following that work, Stoner (1929) introduced the effect of special relativity into the Fowler considerations and he discovered the critical mass of white dwarfs

$$M_{\text{crit}}^{\text{Stoner}} = \frac{15}{16} \sqrt{5\pi} \frac{M_{\text{Pl}}^3}{\mu^2 m_n^2} \approx 3.72 \frac{M_{\text{Pl}}^3}{\mu^2 m_n^2}, \quad (\text{B.1.1})$$

where $M_{\text{Pl}} = \sqrt{\hbar c / G} \approx 10^{-5}$ g is the Planck mass, m_n is the neutron mass, and $\mu = A/Z \approx 2$ is the average molecular weight of matter which shows explicitly the dependence of the critical mass on the chemical composition of the star.

Following the Stoner's work, Chandrasekhar (1931b) pointed out the relevance of describing white dwarfs by using an approach, initiated by Milne (1930), of using the mathematical method of the solutions of the Lane-Emden polytropic equations (Emden, 1907). The same idea of using the Lane-Emden equations taking into account the special relativistic effects to the equilibrium of stellar matter for a degenerate system of fermions, came independently to Landau (1932). Both the Chandrasekhar and Landau treatments were explicit in pointing out the existence of the critical mass

$$M_{\text{crit}}^{\text{Ch-L}} = 2.015 \frac{\sqrt{3\pi}}{2} \frac{M_{\text{Pl}}^3}{\mu^2 m_n^2} \approx 3.09 \frac{M_{\text{Pl}}^3}{\mu^2 m_n^2}, \quad (\text{B.1.2})$$

where the first numerical factor on the right hand side of Eq. (B.1.2) comes from the boundary condition $-(r^2 du/dr)_{r=R} = 2.015$ (see last entry of Table 7 on Pag. 80 in Emden (1907)) of the $n = 3$ Lane-Emden polytropic equation.

Namely for $M > M_{\text{crit}}^{\text{Ch-L}}$, no equilibrium configuration should exist.

Some of the basic assumptions adopted by Chandrasekhar and Landau in their idealized approach e.g. the treatment of the electron as a free-gas without taking into due account the electromagnetic interactions, as well as the stability of the distribution of the nuclei against the gravitational interaction led to some criticisms by Eddington (1935). It was unfortunate that the absence of interest of E. Fermi on the final evolution of stars did not allow Fermi himself to intervene in these well-posed theoretical problems (Boccaletti and Ruffini, 2010). Indeed, we are showing in this article how the solution of the conceptual problems of the white dwarf models, left open for years, can be duly addressed by considering the relativistic Thomas-Fermi model of the compressed atom (see Subsec. B.1.2 and Sec. B.1.4).

The original work on white dwarfs was motivated by astrophysics and found in astrophysics strong observational support. The issue of the equilibrium of the electron gas and the associated component of nuclei, taking into account the electromagnetic, the gravitational and the weak interactions is a theoretical physics problem, not yet formulated in a correct special and general relativistic context.

One of the earliest alternative approaches to the Chandrasekhar-Landau work was proposed by Salpeter (1961). He followed an idea originally proposed by Frenkel (1928): to adopt in the study of white dwarfs the concept of a Wigner-Seitz cell. Salpeter introduced to the lattice model of a point-like nucleus surrounded by a uniform cloud of electrons, corrections due to the non-uniformity of the electron distribution (see Subsec. B.1.2 for details). In this way Salpeter (1961) obtained an analytic formula for the total energy in a Wigner-Seitz cell and derived the corresponding equation of state of matter composed by such cells, pointing out explicitly the relevance of the Coulomb interaction.

The consequences of the Coulomb interactions in the determination of the mass and radius of white dwarfs, was studied in a subsequent paper by Hamada and Salpeter (1961) by using the equation of state constructed in Salpeter (1961). They found that the critical mass of white dwarfs depends in a nontrivial way on the specific nuclear composition: the critical mass of Chandrasekhar-Landau which depends only on the mass to charge ratio of nuclei A/Z , now depends also on the proton number Z .

This fact can be seen from the approximate expression for the critical mass of white dwarfs obtained by Hamada and Salpeter (1961) in the ultrarelativistic limit for the electrons

$$M_{\text{crit}}^{\text{H\&S}} = 2.015 \frac{\sqrt{3\pi}}{2} \frac{1}{\mu_{\text{eff}}^2} \frac{M_{\text{Pl}}^3}{m_n^2}, \quad (\text{B.1.3})$$

where

$$\mu_{\text{eff}} = \mu \left(\frac{P_S}{P_{\text{Ch}}} \right)^{-3/4}, \quad (\text{B.1.4})$$

being P_S the pressure of the Wigner-Seitz cell obtained by Salpeter (1961) (see Subsec. B.1.2) and P_{Ch} is the pressure of a free-electron fluid used by Chandrasekhar (see Subsec. B.1.2). The ratio P_S/P_{Ch} is a function of the number of protons Z (see Eq. (20) in Salpeter (1961)) and it satisfies $P_S/P_{\text{Ch}} < 1$. Consequently, the effective molecular weight satisfies $\mu_{\text{eff}} > \mu$ and the critical mass of white dwarfs turns to be smaller than the original one obtained by Chandrasekhar-Landau (see Eq. (B.1.2)).

In the mean time, the problem of the equilibrium gas in a white dwarf taking into account possible global electromagnetic interactions between the nucleus and the electrons was addressed by Olson and Bailyn (1975, 1976). They well summarized the status of the problem: Traditional models for the white dwarf are non-relativistic and electrically neutral. Although an electric field is needed to support the pressureless nuclei against gravitational collapse, the star is treated essentially in terms of only one charge component, where charge neutrality is assumed. Their solution to the problem invokes the breakdown of the local charge neutrality and the presence of an overall electric field as a consequence of treating also the nuclei inside the white dwarf as a fluid. They treated the white dwarf matter through a two-fluid model not enforcing local charge neutrality. The closure equation for the Einstein-Maxwell system of equations was there obtained from a minimization procedure of the mass-energy of the configuration. This work was the first pointing out the relevance of the Einstein-Maxwell equations in the description of an astrophysical system by requiring global and non local charge neutrality. As we will show here, this interesting approach does not apply to the case of white dwarfs. It represents, however, a new development in the study of neutron stars (see e.g. Rotondo et al. (2011d))

An alternative approach to the Salpeter treatment of a compressed atom was reconsidered in gur (2000) by applying for the first time to white dwarfs a relativistic Thomas-Fermi treatment of the compressed atom introducing a finite size nucleus within a phenomenological description (see also Bertone and Ruffini (2000)).

Recently, the study of a compressed atom has been revisited in Rotondo et al. (2011c) by extending the global approach of Feynman et al. (1949) taking into account weak interactions. This treatment takes also into account all the Coulomb contributions duly expressed relativistically without the need of any piecewise description. The relativistic Thomas-Fermi model has been solved by imposing in addition to the electromagnetic interaction also the weak equilibrium between neutrons, protons and electrons self-consistently. This presents some conceptual differences with respect to previous approaches and can be used in order both to validate and to establish their limitations.

In this article we apply the considerations presented in Rotondo et al. (2011c) of a compressed atom in a Wigner-Seitz cell to the description of non-rotating white dwarfs in general relativity. This approach improves all previous treatments in the following aspects:

1. In order to warranty self-consistency with a relativistic treatment of the electrons, the point-like assumption of the nucleus is abandoned introducing a finite sized nucleus (Rotondo et al., 2011c). We assume for the mass as well as for charge to mass ratio of the nucleus their experimental values instead of using phenomenological descriptions based on the semi-empirical mass-formula of Weizsacker (see e.g. gur (2000); Bertone and Ruffini (2000)).
2. The electron-electron and electron-nucleus Coulomb interaction energy is calculated without any approximation by solving numerically the relativistic Thomas-Fermi equation for selected energy-densities of the system and for each given nuclear composition.
3. The energy-density of the system is calculated taking into account the contributions of the nuclei, of the Coulomb interactions as well as of the relativistic electrons; the latter being neglected in all previous treatments. This particular contribution turns to be very important at high-densities and in particular for light nuclear compositions e.g. ${}^4\text{He}$ and ${}^{12}\text{C}$.
4. The β -equilibrium between neutrons, protons, and electrons is also taken into account leading to a self-consistent calculation of the threshold density for triggering the inverse β -decay of a given nucleus.
5. The structure of the white dwarf configurations is obtained by integrating the general relativity equations of equilibrium.
6. Due to 4) and 5) we are able to determine if the instability point leading to a maximum stable mass of the non-rotating white dwarf is induced by the inverse β -decay instability of the composing nuclei or by general relativistic effects.

Paradoxically, after all this procedure which takes into account many additional theoretical features generalizing the Chandrasekhar-Landau and the Hamada and Salpeter works, a most simple equation is found to be fulfilled by the equilibrium configuration in a spherically symmetric metric. Assuming the metric

$$ds^2 = e^{\nu(r)}c^2dt^2 - e^{\lambda(r)}dr^2 - r^2d\theta^2 - r^2\sin^2\theta d\varphi^2, \quad (\text{B.1.5})$$

we demonstrate how the entire system of equations describing the equilibrium of white dwarfs, taking into account the weak, the electromagnetic and

the gravitational interactions as well as quantum statistics all expressed consistently in a general relativistic approach, is simply given by

$$\sqrt{g_{00}}\mu_{\text{ws}} = e^{\nu(r)/2}\mu_{\text{ws}}(r) = \text{constant}, \quad (\text{B.1.6})$$

which links the chemical potential of the Wigner-Seitz cell μ_{ws} , duly solved by considering the relativistic Feynman-Metropolis-Teller model following Rotondo et al. (2011c), to the general relativistic gravitational potential at each point of the configuration. The overall system outside each Wigner-Seitz cell is strictly neutral and no global electric field exists, contrary to the results reported in Olson and Bailyn (1976). The same procedure will apply as well to the case of neutron star crusts.

The article is organized as follows. In Sec. B.1.2 we summarize the most common approaches used for the description of white dwarfs and neutron star crusts: the uniform approximation for the electron fluid (see e.g. Chandrasekhar (1931b)); the often called lattice model assuming a point-like nucleus surrounded by a uniform electron cloud (see e.g. Baym et al. (1971b)); the generalization of the lattice model due to Salpeter (1961); the Feynman, Metropolis and Teller approach (Feynman et al., 1949) based on the non-relativistic Thomas-Fermi model of compressed atoms and, the relativistic generalization of the Feynman-Metropolis-Teller treatment recently formulated in Rotondo et al. (2011c).

In Sec. B.1.3 we formulate the general relativistic equations of equilibrium of the system and show how, from the self-consistent definition of chemical potential of the Wigner-Seitz cell and the Einstein equations, comes the equilibrium condition given by Eq. (B.1.6). In addition, we obtain the Newtonian and the first-order post-Newtonian equations of equilibrium.

Finally, we show in Sec. B.1.4 the new results of the numerical integration of the general relativistic equations of equilibrium and discuss the corrections to the Stoner critical mass $M_{\text{crit}}^{\text{Stoner}}$, to the Chandrasekhar-Landau mass limit $M_{\text{crit}}^{\text{Ch-L}}$, as well as to the one of Hamada and Salpeter $M_{\text{crit}}^{\text{H\&S}}$, obtained when all interactions are fully taken into account through the relativistic Feynman-Metropolis-Teller equation of state (Rotondo et al., 2011c).

B.1.2. The Equation of State

There exists a large variety of approaches to model the equation of state of white dwarf matter, each one characterized by a different way of treating or neglecting the Coulomb interaction inside each Wigner-Seitz cell, which we will briefly review here. Particular attention is given to the calculation of the self-consistent chemical potential of the Wigner-Seitz cell μ_{ws} , which plays a very important role in the conservation law (B.1.6) that we will derive in Sec. B.1.3.

The uniform approximation

In the uniform approximation used by Chandrasekhar (1931b), the electron distribution as well as the nucleons are assumed to be locally constant and therefore the condition of local charge neutrality

$$n_e = \frac{Z}{A_r} n_N, \quad (\text{B.1.7})$$

where A_r is the average atomic weight of the nucleus, is applied. Here n_N denotes the nucleon number density and Z is the number of protons of the nucleus. The electrons are considered as a fully degenerate free-gas and then described by Fermi-Dirac statistics. Thus, their number density n_e is related to the electron Fermi-momentum P_e^F by

$$n_e = \frac{(P_e^F)^3}{3\pi^2\hbar^3}, \quad (\text{B.1.8})$$

and the total electron energy-density and electron pressure are given by

$$\begin{aligned} \mathcal{E}_e &= \frac{2}{(2\pi\hbar)^3} \int_0^{P_e^F} \sqrt{c^2p^2 + m_e^2c^4} 4\pi p^2 dp \\ &= \frac{m_e^4c^5}{8\pi^2\hbar^3} [x_e \sqrt{1+x_e^2}(1+2x_e^2) - \text{arcsinh}(x_e)], \quad (\text{B.1.9}) \\ P_e &= \frac{1}{3} \frac{2}{(2\pi\hbar)^3} \int_0^{P_e^F} \frac{c^2p^2}{\sqrt{c^2p^2 + m_e^2c^4}} 4\pi p^2 dp \\ &= \frac{m_e^4c^5}{8\pi^2\hbar^3} [x_e \sqrt{1+x_e^2}(2x_e^2/3 - 1) \\ &\quad + \text{arcsinh}(x_e)], \quad (\text{B.1.10}) \end{aligned}$$

where we have introduced the dimensionless Fermi momentum $x_e = P_e^F / (m_e c)$ with m_e the electron rest-mass.

The kinetic energy of nucleons is neglected and therefore the pressure is assumed to be only due to electrons. Thus the equation of state can be written as

$$\mathcal{E}_{\text{unif}} = \mathcal{E}_N + \mathcal{E}_e \approx \frac{A_r}{Z} M_u c^2 n_e + \mathcal{E}_e, \quad (\text{B.1.11})$$

$$P_{\text{unif}} \approx P_e, \quad (\text{B.1.12})$$

where $M_u = 1.6604 \times 10^{-24}$ g is the unified atomic mass and \mathcal{E}_e and P_e are given by Eqs. (B.1.9)–(B.1.10).

Within this approximation, the total self-consistent chemical potential is

given by

$$\mu_{\text{unif}} = A_r M_u c^2 + Z \mu_e, \quad (\text{B.1.13})$$

where

$$\mu_e = \frac{\mathcal{E}_e + P_e}{n_e} = \sqrt{c^2 (P_e^F)^2 + m_e^2 c^4}, \quad (\text{B.1.14})$$

is the electron free-chemical potential.

As a consequence of this effective approach which does not take into any account the Coulomb interaction, it is obtained an effective one-component electron-nucleon fluid approach where the kinetic pressure is given by electrons of mass m_e and their gravitational contribution is given by an effective mass $(A_r/Z)M_u$ attached to each electron (see e.g. Landau and Lifshitz (1980)). This is even more evident when the electron contribution to the energy-density in Eq. (B.1.11) is neglected and therefore the energy-density is attributed only to the nuclei. Within this approach followed by Chandrasekhar (1931b), the equation of state reduces to

$$\mathcal{E}_{\text{Ch}} = \frac{A_r}{Z} M_u c^2 n_e, \quad (\text{B.1.15})$$

$$P_{\text{Ch}} = P_{\text{unif}} = P_e. \quad (\text{B.1.16})$$

The lattice model

The first correction to the above uniform model, corresponds to abandon the assumption of the electron-nucleon fluid through the so-called “lattice” model which introduces the concept of Wigner-Seitz cell: each cell contains a point-like nucleus of charge $+Ze$ with A nucleons surrounded by a uniformly distributed cloud of Z fully-degenerate electrons. The global neutrality of the cell is guaranteed by the condition

$$Z = V_{\text{ws}} n_e = \frac{n_e}{n_{\text{ws}}}, \quad (\text{B.1.17})$$

where $n_{\text{ws}} = 1/V_{\text{ws}}$ is the Wigner-Seitz cell density and $V_{\text{ws}} = 4\pi R_{\text{ws}}^3/3$ is the cell volume.

The total energy of the Wigner-Seitz cell is modified by the inclusion of the Coulomb energy, i.e

$$E_L = \mathcal{E}_{\text{unif}} V_{\text{ws}} + E_C, \quad (\text{B.1.18})$$

being

$$E_C = E_{e-N} + E_{e-e} = -\frac{9}{10} \frac{Z^2 e^2}{R_{\text{ws}}}, \quad (\text{B.1.19})$$

where $\mathcal{E}_{\text{unif}}$ is given by Eq. (B.1.11) and E_{e-N} and E_{e-e} are the electron-nucleus

and the electron-electron Coulomb energies

$$\begin{aligned} E_{e-N} &= - \int_0^{R_{ws}} 4\pi r^2 \left(\frac{Ze}{r} \right) en_e dr \\ &= - \frac{3}{2} \frac{Z^2 e^2}{R_{ws}}, \end{aligned} \quad (\text{B.1.20})$$

$$E_{e-e} = \frac{3}{5} \frac{Z^2 e^2}{R_{ws}}. \quad (\text{B.1.21})$$

The self-consistent pressure of the Wigner-Seitz cell is then given by

$$P_L = - \frac{\partial E_L}{\partial V_{ws}} = P_{unif} + \frac{1}{3} \frac{E_C}{V_{ws}}, \quad (\text{B.1.22})$$

where P_{unif} is given by Eq. (B.1.12). It is worth to recall that the point-like assumption of the nucleus is incompatible with a relativistic treatment of the degenerate electron fluid (see Ferreira et al. (1980); Ruffini and Stella (1981) for details). Such an inconsistency has been traditionally ignored by applying, within a point-like nucleus model, the relativistic formulas (B.1.9) and (B.1.10) and their corresponding ultrarelativistic limits (see e.g. Salpeter (1961)).

The Wigner-Seitz cell chemical potential is in this case

$$\mu_L = E_L + P_L V_{ws} = \mu_{unif} + \frac{4}{3} E_C. \quad (\text{B.1.23})$$

By comparing Eqs. (B.1.12) and (B.1.22) we can see that the inclusion of the Coulomb interaction results in a decreasing of the pressure of the cell due to the negative lattice energy E_C . The same conclusion is achieved for the chemical potential from Eqs. (B.1.13) and (B.1.23).

Salpeter approach

A further development to the lattice model came from Salpeter (1961) whom studied the corrections due to the non-uniformity of the electron distribution inside a Wigner-Seitz cell.

Following the Chandrasekhar (1931b) approximation, Salpeter also neglects the electron contribution to the energy-density. Thus, the first term in the Salpeter formula for the energy of the cell comes from the nuclei energy (B.1.15). The second contribution is given by the Coulomb energy of the lattice model (B.1.19). The third contribution is obtained as follows: the electron density is assumed as $n_e[1 + \epsilon(r)]$, where $n_e = 3Z/(4\pi R_{ws}^3)$ is the average electron density as given by Eq. (B.1.17), and $\epsilon(r)$ is considered infinitesimal. The Coulomb potential energy is assumed to be the one of the point-like nucleus surrounded by a uniform distribution of electrons, so the correction

given by $\epsilon(r)$ on the Coulomb potential is neglected. The electron distribution is then calculated at first-order by expanding the relativistic electron kinetic energy

$$\begin{aligned}\epsilon_k &= \sqrt{[cP_e^F(r)]^2 + m_e^2c^4} - m_e c^2 \\ &= \sqrt{\hbar^2 c^2 (3\pi^2 n_e)^{2/3} [1 + \epsilon(r)]^{2/3} + m_e^2 c^4} \\ &\quad - m_e c^2,\end{aligned}\tag{B.1.24}$$

about its value in the uniform approximation

$$\epsilon_k^{\text{unif}} = \sqrt{\hbar^2 c^2 (3\pi^2 n_e)^{2/3} + m_e^2 c^4} - m_e c^2,\tag{B.1.25}$$

considering as infinitesimal the ratio eV/E_e^F between the Coulomb potential energy eV and the electron Fermi energy

$$E_e^F = \sqrt{[cP_e^F(r)]^2 + m_e^2 c^4} - m_e c^2 - eV.\tag{B.1.26}$$

The influence of the Dirac electron-exchange correction (Dirac, 1930) on the equation of state was also considered by Salpeter (1961). However, adopting the general approach of Migdal et al. (1977), it has been shown that these effects are negligible in the relativistic regime (Rotondo et al., 2011c). We will then consider here only the major correction of the Salpeter treatment.

The total energy of the Wigner-Seitz cell is then given by (see Salpeter (1961) for details)

$$E_S = E_{\text{Ch}} + E_C + E_S^{TF},\tag{B.1.27}$$

being

$$E_S^{TF} = -\frac{162}{175} \left(\frac{4}{9\pi}\right)^{2/3} \alpha^2 Z^{7/3} \mu_e,\tag{B.1.28}$$

where $E_{\text{Ch}} = \mathcal{E}_{\text{Ch}} V_{\text{ws}}$, E_C is given by Eq. (B.1.19), μ_e is given by Eq. (B.1.14), and $\alpha = e^2/(\hbar c)$ is the fine structure constant.

Correspondingly, the self-consistent pressure of the Wigner-Seitz cell is

$$P_S = P_L + P_{TF}^S,\tag{B.1.29}$$

where

$$P_{TF}^S = \frac{1}{3} \left(\frac{P_e^F}{\mu_e}\right)^2 \frac{E_S^{TF}}{V_{\text{ws}}}.\tag{B.1.30}$$

The Wigner-Seitz cell chemical potential can be then written as

$$\mu_S = \mu_L + E_{TF}^S \left[1 + \frac{1}{3} \left(\frac{P_e^F}{\mu_e} \right)^2 \right]. \quad (\text{B.1.31})$$

From Eqs. (B.1.29) and (B.1.31), we see that the inclusion of each additional Coulomb correction results in a further decreasing of the pressure and of the chemical potential of the cell. The Salpeter approach is very interesting in identifying piecewise Coulomb contribution to the total energy, to the total pressure and, to the Wigner-Seitz chemical potential. However, it does not have the full consistency of the global solutions obtained with the Feynman-Metropolis-Teller approach (Feynman et al., 1949) and its generalization to relativistic regimes (Rotondo et al., 2011c) which we will discuss in detail below.

The Feynman-Metropolis-Teller treatment

Feynman et al. (1949) showed how to derive the equation of state of matter at high pressures by considering a Thomas-Fermi model confined in a Wigner-Seitz cell of radius R_{ws} .

The Thomas-Fermi equilibrium condition for degenerate non-relativistic electrons in the cell is expressed by

$$E_e^F = \frac{(P_e^F)^2}{2m_e} - eV = \text{constant} > 0, \quad (\text{B.1.32})$$

where V denotes the Coulomb potential and E_e^F denotes the Fermi energy of electrons, which is positive for configurations subjected to external pressure, namely, for compressed cells.

Defining the function $\phi(r)$ by $eV(r) + E_e^F = e^2 Z \phi(r) / r$, and introducing the dimensionless radial coordinate η by $r = b\eta$, where $b = (3\pi)^{2/3} (\lambda_e / \alpha) 2^{-7/3} Z^{-1/3}$, being $\lambda_e = \hbar / (m_e c)$ the electron Compton wavelength; the Poisson equation from which the Coulomb potential V is calculated self-consistently becomes

$$\frac{d^2 \phi(\eta)}{d\eta^2} = \frac{\phi(\eta)^{3/2}}{\eta^{1/2}}. \quad (\text{B.1.33})$$

The boundary conditions for Eq. (B.1.33) follow from the point-like structure of the nucleus $\phi(0) = 1$ and, from the global neutrality of the Wigner-Seitz cell $\phi(\eta_0) = \eta_0 d\phi/d\eta|_{\eta=\eta_0}$, where η_0 defines the dimensionless radius of the Wigner-Seitz cell by $\eta_0 = R_{ws}/b$.

For each value of the compression, e.g. η_0 , it corresponds a value of the electron Fermi energy E_e^F and a different solution of Eq. (B.1.33), which determines the self-consistent Coulomb potential energy eV as well as the self-

consistent electron distribution inside the cell through

$$n_e(\eta) = \frac{Z}{4\pi b^3} \left[\frac{\phi(\eta)}{\eta} \right]^{3/2}. \quad (\text{B.1.34})$$

In the non-relativistic Thomas-Fermi model, the total energy of the Wigner-Seitz cell is given by (see Slater and Krutter (1935); Feynman et al. (1949) for details)

$$E_{\text{ws}} = E_N + E_k^{(e)} + E_C, \quad (\text{B.1.35})$$

being

$$E_N = M_N(Z, A)c^2, \quad (\text{B.1.36})$$

$$\begin{aligned} E_k^{(e)} &= \int_0^{R_{\text{ws}}} 4\pi r^2 \mathcal{E}_e[n_e(r)] dr \\ &= \frac{3Z^2 e^2}{7} \frac{1}{b} \left[\frac{4}{5} \eta_0^{1/2} \phi^{5/2}(\eta_0) - \phi'(0) \right], \end{aligned} \quad (\text{B.1.37})$$

$$\begin{aligned} E_C &= E_{e-N} + E_{e-e} \\ &= -\frac{6Z^2 e^2}{7} \frac{1}{b} \left[\frac{1}{3} \eta_0^{1/2} \phi^{5/2}(\eta_0) - \phi'(0) \right], \end{aligned} \quad (\text{B.1.38})$$

where $M_N(Z, A)$ is the nucleus mass, $\mathcal{E}_e[n_e(r)]$ is given by Eq. (B.1.9) and E_{e-N} and E_{e-e} are the electron-nucleus Coulomb energy and the electron-electron Coulomb energy, which are given by

$$E_{e-N} = - \int_0^{R_{\text{ws}}} 4\pi r^2 \left(\frac{Ze}{r} \right) e n_e(r) dr, \quad (\text{B.1.39})$$

$$\begin{aligned} E_{e-e} &= \frac{1}{2} \int_0^{R_{\text{ws}}} 4\pi r^2 e n_e(\vec{r}) dr \\ &\times \int_0^{R_{\text{ws}}} 4\pi r'^2 \frac{e n_e(\vec{r}')}{|\vec{r} - \vec{r}'|} dr'. \end{aligned} \quad (\text{B.1.40})$$

From Eqs. (B.1.37) and (B.1.38) we recover the well-known relation between the total kinetic energy and the total Coulomb energy in the Thomas-Fermi model (Slater and Krutter, 1935; Feynman et al., 1949)

$$E_k^{(e)} = E_k^{\text{unif}}[n_e(R_{\text{ws}})] - \frac{1}{2} E_C, \quad (\text{B.1.41})$$

where $E_k^{\text{unif}}[n_e(R_{\text{ws}})]$ is the non-relativistic kinetic energy of a uniform electron distribution of density $n_e(R_{\text{ws}})$, i.e.

$$E_k^{\text{unif}}[n_e(R_{\text{ws}})] = \frac{3}{5} Z^* \mu_e(R_{\text{ws}}), \quad (\text{B.1.42})$$

with Z^* defined by

$$Z^* = V_{\text{ws}} n_e(R_{\text{ws}}), \quad (\text{B.1.43})$$

and $\mu_e(R_{\text{ws}}) = \hbar^2 [3\pi^2 n_e(R_{\text{ws}})]^{2/3} / (2m_e)$.

The self-consistent pressure of the Wigner-Seitz cell given by the non-relativistic Thomas-Fermi model is (see Slater and Krutter (1935); Feynman et al. (1949) for details)

$$P_{\text{TF}} = \frac{2}{3} \frac{E_k^{\text{unif}}[n_e(R_{\text{ws}})]}{V_{\text{ws}}}. \quad (\text{B.1.44})$$

The pressure of the Thomas-Fermi model (B.1.44) is equal to the pressure of a free-electron distribution of density $n_e(R_{\text{ws}})$. Being the electron density inside the cell a decreasing function of the distance from the nucleus, the electron density at the cell boundary, $n_e(R_{\text{ws}})$, is smaller than the average electron distribution $3Z/(4\pi R_{\text{ws}}^3)$. Then, the pressure given by (B.1.44) is smaller than the one given by the non-relativistic version of Eq. (B.1.10) of the uniform model of Subsec. B.1.2. Such a smaller pressure, although faintfully given by the expression of a free-electron gas, contains in a self-consistent fashion all the Coulomb effects inside the Wigner-Seitz cell.

The chemical potential of the Wigner-Seitz cell of the non-relativistic Thomas-Fermi model can be then written as

$$\mu_{\text{TF}} = M_N(Z, A)c^2 + Z^* \mu_e(R_{\text{ws}}) + \frac{1}{2}E_C, \quad (\text{B.1.45})$$

where we have used Eqs. (B.1.41)–(B.1.43).

Integrating by parts the total number of electrons

$$Z = \int_0^{R_{\text{ws}}} 4\pi r^2 n_e(r) dr = Z^* + I(R_{\text{ws}}), \quad (\text{B.1.46})$$

where

$$I(R_{\text{ws}}) = \int_0^{R_{\text{ws}}} \frac{4\pi}{3} r^3 \frac{\partial n_e(r)}{\partial r} dr, \quad (\text{B.1.47})$$

we can rewrite finally the following semi-analytical expression of the chemical potential (B.1.45) of the cell

$$\begin{aligned} \mu_{\text{TF}} = & M_N(Z, A)c^2 + Z\mu_e^{\text{unif}} \left[1 + \frac{I(R_{\text{ws}})}{Z} \right]^{2/3} \\ & + \mu_e^{\text{unif}} I(R_{\text{ws}}) \left[1 + \frac{I(R_{\text{ws}})}{Z} \right]^{2/3} + \frac{1}{2}E_C, \end{aligned} \quad (\text{B.1.48})$$

where μ_e^{unif} is the electron free-chemical potential (B.1.14) calculated with the average electron density, namely, the electron chemical potential of the uniform approximation. The function $I(R_{\text{ws}})$ depends explicitly on the gradient

of the electron density, i.e. on the non-uniformity of the electron distribution.

In the limit of absence of Coulomb interaction both the last term and the function $I(R_{\text{ws}})$ in Eq. (B.1.48) vanish and therefore in this limit μ_{TF} reduces to

$$\mu_{\text{TF}} \rightarrow \mu_{\text{unif}}, \quad (\text{B.1.49})$$

where μ_{unif} is the chemical potential in the uniform approximation given by Eq. (B.1.13).

The relativistic Feynman-Metropolis-Teller treatment

We recall now how the above classic Feynman, Metropolis, and Teller treatment of compressed atoms has been recently generalized to relativistic regimes (see Rotondo et al. (2011c) for details). One of the main differences in the relativistic generalization of the Thomas-Fermi equation is that, the point-like approximation of the nucleus, must be abandoned since the relativistic equilibrium condition of compressed atoms

$$E_e^F = \sqrt{c^2(P_e^F)^2 + m_e^2 c^4} - m_e c^2 - eV(r) = \text{constant} > 0, \quad (\text{B.1.50})$$

would lead to a non-integrable expression for the electron density near the origin (see e.g. Ferreira et al. (1980); Ruffini and Stella (1981)).

It is then assumed a constant distribution of protons confined in a radius R_c defined by

$$R_c = \Delta \lambda_\pi Z^{1/3}, \quad (\text{B.1.51})$$

where $\lambda_\pi = \hbar/(m_\pi c)$ is the pion Compton wavelength. If the system is at nuclear density $\Delta \approx (r_0/\lambda_\pi)(A/Z)^{1/3}$ with $r_0 \approx 1.2$ fm. Thus, in the case of ordinary nuclei (i.e., for $A/Z \approx 2$) we have $\Delta \approx 1$. Consequently, the proton density can be written as

$$n_p(r) = \frac{Z}{\frac{4}{3}\pi R_c^3} \theta(r - R_c) = \frac{3}{4\pi} \left(\frac{1}{\Delta \lambda_\pi} \right)^3 \theta(r - R_c), \quad (\text{B.1.52})$$

where $\theta(r - R_c)$ denotes the Heaviside function centered at R_c . The electron density can be written as

$$n_e(r) = \frac{(P_e^F)^3}{3\pi^2 \hbar^3} = \frac{1}{3\pi^2 \hbar^3 c^3} \left[\hat{V}^2(r) + 2m_e c^2 \hat{V}(r) \right]^{3/2}, \quad (\text{B.1.53})$$

where $\hat{V} = eV + E_e^F$ and we have used Eq. (B.1.50).

The overall Coulomb potential satisfies the Poisson equation

$$\nabla^2 V(r) = -4\pi e [n_p(r) - n_e(r)], \quad (\text{B.1.54})$$

with the boundary conditions $dV/dr|_{r=R_{\text{ws}}} = 0$ and $V(R_{\text{ws}}) = 0$ due to the global charge neutrality of the cell.

By introducing the dimensionless quantities $x = r/\lambda_\pi$, $x_c = R_c/\lambda_\pi$, $\chi/r = \hat{V}(r)/(\hbar c)$ and replacing the particle densities (B.1.52) and (B.1.53) into the Poisson equation (B.1.54), it is obtained the relativistic Thomas-Fermi equation (Ruffini, 2008b)

$$\begin{aligned} \frac{1}{3x} \frac{d^2\chi(x)}{dx^2} &= -\frac{\alpha}{\Delta^3} \theta(x_c - x) \\ &+ \frac{4\alpha}{9\pi} \left[\frac{\chi^2(x)}{x^2} + 2\frac{m_e}{m_\pi} \frac{\chi(x)}{x} \right]^{3/2}, \end{aligned} \quad (\text{B.1.55})$$

which must be integrated subjected to the boundary conditions $\chi(0) = 0$, $\chi(x_{\text{ws}}) \geq 0$ and $d\chi/dx|_{x=x_{\text{ws}}} = \chi(x_{\text{ws}})/x_{\text{ws}}$, where $x_{\text{ws}} = R_{\text{ws}}/\lambda_\pi$.

The neutron density $n_n(r)$, related to the neutron Fermi momentum $P_n^F = (3\pi^2\hbar^3 n_n)^{1/3}$, is determined by imposing the condition of beta equilibrium

$$\begin{aligned} E_n^F &= \sqrt{c^2(P_n^F)^2 + m_n^2c^4} - m_nc^2 = \sqrt{c^2(P_p^F)^2 + m_p^2c^4} \\ &- m_pc^2 + eV(r) + E_e^F, \end{aligned} \quad (\text{B.1.56})$$

subjected to the baryon number conservation equation

$$A = \int_0^{R_c} 4\pi r^2 [n_p(r) + n_n(r)] dr. \quad (\text{B.1.57})$$

In Fig. B.1 we see how the relativistic generalization of the Feynman-Metropolis-Teller treatment leads to electron density distributions markedly different from the constant electron density approximation. The electron distribution is far from being uniform as a result of the solution of Eq. (B.1.55), which takes into account the electromagnetic interaction between electrons and between the electrons and the finite sized nucleus. Additional details are given in Rotondo et al. (2011c).

Rotondo et al. (2011e) have shown how the solution of the relativistic Thomas-Fermi equation (B.1.55) together with the self-consistent implementation of the β -equilibrium condition (B.1.56) leads, in the case of zero electron Fermi energy ($E_e^F = 0$), to a theoretical prediction of the β -equilibrium line, namely a theoretical Z - A relation. Within this model the mass to charge ratio A/Z of nuclei is overestimated, e.g. in the case of ${}^4\text{He}$ the overestimate is $\sim 3.8\%$, for ${}^{12}\text{C} \sim 7.9\%$, for ${}^{16}\text{O} \sim 9.52\%$, and for ${}^{56}\text{Fe} \sim 13.2\%$. These discrepancies are corrected when the model of the nucleus considered above is improved by explicitly including the effects of strong interactions. This model, however, illustrates how a self-consistent calculation of compressed nuclear matter can be done including electromagnetic, weak, strong as well as special relativistic

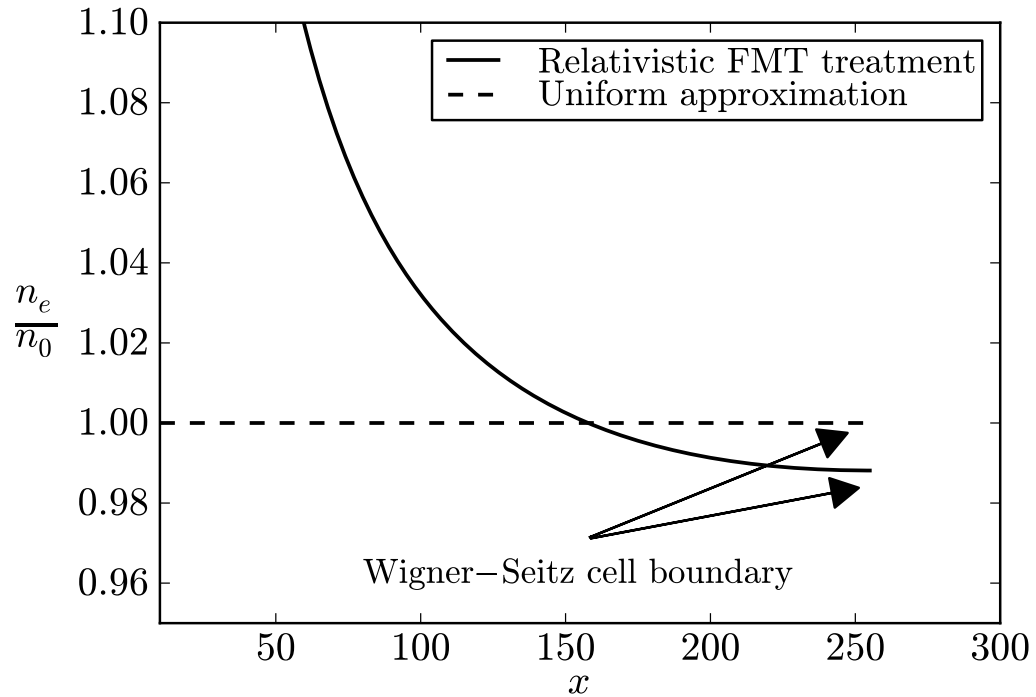


Figure B.1.: The electron number density n_e in units of the average electron number density $n_0 = 3Z/(4\pi R_{\text{ws}}^3)$ inside a Wigner-Seitz cell of ^{12}C . The dimensionless radial coordinate is $x = r/\lambda_\pi$ and Wigner-Seitz cell radius is $x_{\text{ws}} \approx 255$ corresponding to a density of $\sim 10^8 \text{ g/cm}^3$. The solid curve corresponds to the relativistic Feynman-Metropolis-Teller treatment and the dashed curve to the uniform approximation. The electron distribution for different levels of compression as well as for different nuclear compositions can be found in Rotondo et al. (2011c).

tic effects without any approximation. This approach promises to be useful when theoretical predictions are essential, for example in the description of nuclear matter at very high densities, e.g. nuclei close and beyond the neutron drip line.

The densities in white dwarf interiors are not highly enough to require such theoretical predictions. Therefore, in order to ensure the accuracy of our results we use for (Z, A) , needed to solve the relativistic Thomas-Fermi equation (B.1.55), as well as for the nucleus mass $M_N(Z, A)$, their known experimental values. In this way we take into account all the effects of the nuclear interaction.

Thus, the total energy of the Wigner-Seitz cell in the present case can be written as

$$E_{\text{FMT}}^{\text{rel}} = E_N + E_k^{(e)} + E_C, \quad (\text{B.1.58})$$

being

$$E_N = M_N(Z, A)c^2, \quad (\text{B.1.59})$$

$$E_k^{(e)} = \int_0^{R_{\text{ws}}} 4\pi r^2 (\mathcal{E}_e - m_e n_e) dr, \quad (\text{B.1.60})$$

$$E_C = \frac{1}{2} \int_{R_c}^{R_{\text{ws}}} 4\pi r^2 e [n_p(r) - n_e(r)] V(r) dr, \quad (\text{B.1.61})$$

where $M_N(Z, A) = A_r M_u$ is the experimental nucleus mass, e.g. for ${}^4\text{He}$, ${}^{12}\text{C}$, ${}^{16}\text{O}$ and ${}^{56}\text{Fe}$ we have $A_r = 4.003, 12.01, 16.00$ and 55.84 respectively. In Eq. (B.1.61) the integral is evaluated only outside the nucleus (i.e. for $r > R_c$) in order to avoid a double counting with the Coulomb energy of the nucleus already taken into account in the nucleus mass (B.1.59). In order to avoid another double counting we subtract to the electron energy-density \mathcal{E}_e in Eq. (B.1.60) the rest-energy density $m_e c^2 n_e$ which is also taken into account in the nucleus mass (B.1.59).

The total pressure of the Wigner-Seitz cell is given by

$$P_{\text{FMT}}^{\text{rel}} = P_e[n_e(R_{\text{ws}})], \quad (\text{B.1.62})$$

where $P_e[n_e(R_{\text{ws}})]$ is the relativistic pressure (B.1.10) computed with the value of the electron density at the boundary of the cell.

The electron density at the boundary R_{ws} in the relativistic Feynman-Metropolis-Teller treatment is smaller with respect to the one given by the uniform density approximation (see Fig. B.1). Thus, the relativistic pressure (B.1.62) gives systematically smaller values with respect to the uniform approximation pressure (B.1.10) as well as with respect to the Salpeter pressure (B.1.29).

In Fig. B.2 we show the ratio between the relativistic Feynman-Metropolis-Teller pressure $P_{\text{FMT}}^{\text{rel}}$ (B.1.62) and the Chandrasekhar pressure P_{Ch} (B.1.10) and the Salpeter pressure P_{S} (B.1.29) in the case of ${}^{12}\text{C}$. It can be seen how $P_{\text{FMT}}^{\text{rel}}$ is smaller than P_{Ch} for all densities as a consequence of the Coulomb interaction. With respect to the Salpeter case, we have that the ratio $P_{\text{FMT}}^{\text{rel}}/P_{\text{S}}$ approaches unity from below at large densities as one should expect.

However, at low densities $\lesssim 10^4\text{--}10^5 \text{ g/cm}^3$, the ratio becomes larger than unity due to the defect of the Salpeter treatment which, in the low density non-relativistic regime, leads to a drastic decrease of the pressure and even to negative pressures at densities $\lesssim 10^2 \text{ g/cm}^3$ or higher for heavier nuclear compositions e.g. ${}^{56}\text{Fe}$ (see Salpeter (1961); Rotondo et al. (2011c) and Table B.1). This is in contrast with the relativistic Feynman-Metropolis-Teller treatment which matches smoothly the classic Feynman-Metropolis-Teller equation of state in that regime (see Rotondo et al. (2011c) for details).

No analytic expression of the Wigner-Seitz cell chemical potential can be

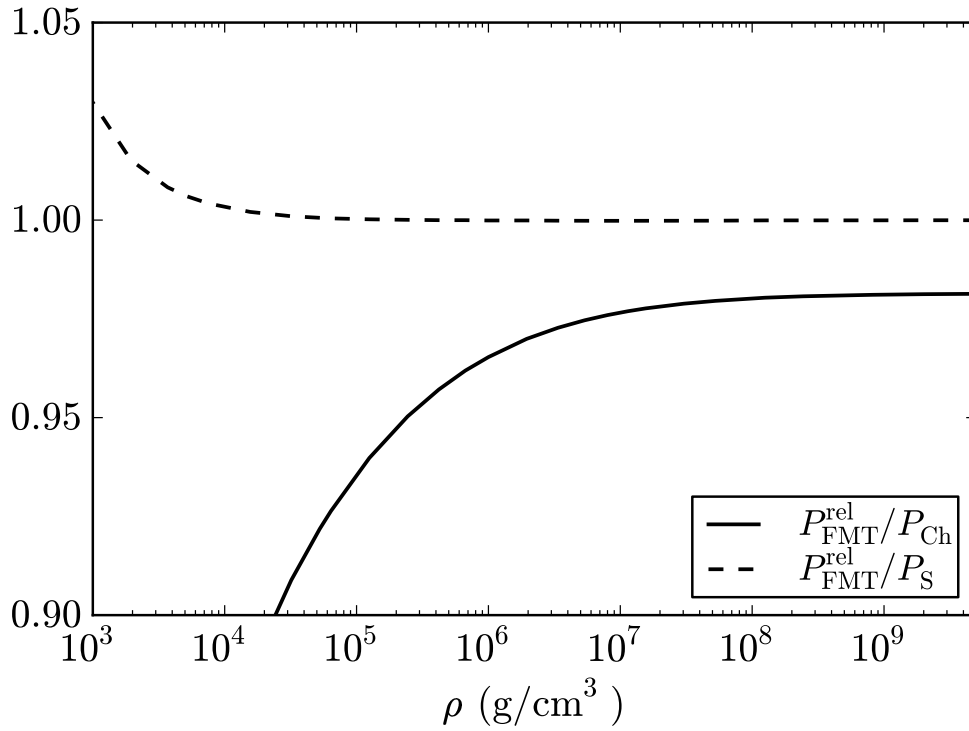


Figure B.2.: Ratio of the pressures in the different treatments as a function of the density for ^{12}C white dwarfs (see Table B.1). The solid curve corresponds to the ratio between the relativistic Feynman-Metropolis-Teller pressure $P_{\text{FMT}}^{\text{rel}}$ given by Eq. (B.1.62) and the Chandrasekhar pressure P_{Ch} given by Eq. (B.1.10). The dashed curve corresponds to the ratio between the relativistic Feynman-Metropolis-Teller pressure $P_{\text{FMT}}^{\text{rel}}$ given by Eq. (B.1.62) and the Salpeter pressure P_{S} given by Eq. (B.1.29).

ρ	P_{Ch}	P_{S}	$P_{\text{FMT}}^{\text{rel}}$
10	1.46731×10^{14}	-1.35282×10^{13}	4.54920×10^{14}
40	1.47872×10^{15}	4.60243×10^{14}	7.09818×10^{14}
70	3.75748×10^{15}	1.60860×10^{15}	2.05197×10^{15}
10^2	6.80802×10^{15}	3.34940×10^{15}	3.90006×10^{15}
10^3	3.15435×10^{17}	2.40646×10^{17}	2.44206×10^{17}
10^4	1.45213×10^{19}	1.28976×10^{19}	1.28965×10^{19}
10^5	6.50010×10^{20}	6.14494×10^{20}	6.13369×10^{20}
10^6	2.62761×10^{22}	2.54932×10^{22}	2.54431×10^{22}
10^7	8.46101×10^{23}	8.28899×10^{23}	8.27285×10^{23}
10^8	2.15111×10^{25}	2.11375×10^{25}	2.10896×10^{25}
10^9	4.86236×10^{26}	4.78170×10^{26}	4.76613×10^{26}
10^{10}	1.05977×10^{28}	1.04239×10^{28}	1.03668×10^{28}

Table B.1.: Equation of state for ^{12}C within the different treatments. The pressure in the uniform approximation for $\mu = 2$ is P_{Ch} , the Salpeter pressure is P_{S} and the relativistic Feynman-Metropolis-Teller pressure is $P_{\text{FMT}}^{\text{rel}}$. The units for the density are g/cm^3 and for the pressure dyn/cm^2 .

given in this case, so we only write its general expression

$$\mu_{\text{FMT}}^{\text{rel}} = E_{\text{FMT}}^{\text{rel}} + P_{\text{FMT}}^{\text{rel}} V_{\text{ws}}, \quad (\text{B.1.63})$$

where $E_{\text{FMT}}^{\text{rel}}$ and $P_{\text{FMT}}^{\text{rel}}$ are given by Eqs. (B.1.58) and (B.1.62) respectively. The above equation, contrary to the non-relativistic formula (B.1.45), in no way can be simplified in terms of its uniform counterparts. However, it is easy to check that, in the limit of no Coulomb interaction $n_e(R_{\text{ws}}) \rightarrow 3Z/(4\pi R_{\text{ws}}^3)$, $E_C \rightarrow 0$, and $E_k \rightarrow \mathcal{E}_{\text{Ch}} V_{\text{ws}}$ and, neglecting the nuclear binding and the proton-neutron mass difference, we finally obtain

$$\mu_{\text{FMT}}^{\text{rel}} \rightarrow \mu_{\text{unif}}, \quad (\text{B.1.64})$$

as it should be expected.

Now we summarize how the equation of state of compressed nuclear matter can be computed in the Salpeter case and in the relativistic Feynman-Metropolis-Teller case, parameterized by the total density of the system:

(i) For a given radius R_{ws} of the Wigner-Seitz cell the relativistic Thomas-Fermi equation (B.1.55) is integrated numerically and the density of the configuration is computed as $\rho = E_{\text{FMT}}^{\text{rel}}/(c^2 V_{\text{ws}})$ where $E_{\text{FMT}}^{\text{rel}}$ is the energy of the cell given by Eq. (B.1.58).

(ii) For that value of the density, the radius of the Wigner-Seitz cell in the

Salpeter treatment is

$$R_{\text{ws}} = \left(\frac{3A_r M_u}{4\pi\rho} \right)^{1/3}, \quad (\text{B.1.65})$$

where Eq. (B.1.15) has been used. On the contrary, in the relativistic Feynman-Metropolis-Teller treatment no analytic expression relating Wigner-Seitz cell radius and density can be written.

(iii) From this Wigner-Seitz cell radius, or equivalently using the value of the density, the electron density in the Salpeter model is computed from the assumption of uniform electron distribution and the charge neutrality condition, i.e. Eq. (B.1.15). In the relativistic Feynman-Metropolis-Teller treatment, the electron number density at the boundary of the Wigner-Seitz cell is, following Eq. (B.1.53), given by

$$n_e^{\text{relFMT}} = \frac{1}{3\pi^2 \lambda_\pi^3} \left[\frac{\chi^2(x_{\text{ws}})}{x_{\text{ws}}^2} + 2 \frac{m_e}{m_\pi} \frac{\chi(x_{\text{ws}})}{x_{\text{ws}}} \right]^{3/2}, \quad (\text{B.1.66})$$

where the function $\chi(x)$ is the solution of the relativistic Thomas-Fermi equation (B.1.55).

(iv) Finally, with the knowledge of the electron density at R_{ws} , the pressure can be calculated. In the Salpeter approach it is given by Eq. (B.1.29) while in the relativistic Feynman-Metropolis-Teller case it is given by Eq. (B.1.62).

B.1.3. General relativistic equations of equilibrium

Outside each Wigner-Seitz cell the system is electrically neutral, thus no overall electric field exists. Therefore, the above equation of state can be used to calculate the structure of the star through the Einstein equations. Introducing the spherically symmetric metric (B.1.5), the Einstein equations can be written in the Tolman-Oppenheimer-Volkoff form Tolman (1939); Oppenheimer and Volkoff (1939)

$$\frac{dv(r)}{dr} = \frac{2G}{c^2} \frac{4\pi r^3 P(r)/c^2 + M(r)}{r^2 \left[1 - \frac{2GM(r)}{c^2 r} \right]}, \quad (\text{B.1.67})$$

$$\frac{dM(r)}{dr} = 4\pi r^2 \frac{\mathcal{E}(r)}{c^2}, \quad (\text{B.1.68})$$

$$\frac{dP(r)}{dr} = -\frac{1}{2} \frac{dv(r)}{dr} [\mathcal{E}(r) + P(r)], \quad (\text{B.1.69})$$

where we have introduced the mass enclosed at the distance r through $e^{\lambda(r)} = 1 - 2GM(r)/(c^2 r)$, $\mathcal{E}(r)$ is the energy-density and $P(r)$ is the total pressure.

We turn now to demonstrate how, from Eq. (B.1.69), it follows the general relativistic equation of equilibrium (B.1.6), for the self-consistent Wigner-

Seitz chemical potential μ_{ws} . The first law of thermodynamics for a zero temperature fluid of N particles, total energy E , total volume V , total pressure $P = -\partial E/\partial V$, and chemical potential $\mu = \partial E/\partial N$ reads

$$dE = -PdV + \mu dN, \quad (\text{B.1.70})$$

where the differentials denote arbitrary but simultaneous changes in the variables. Since for a system whose surface energy can be neglected with respect to volume energy, the total energy per particle E/N depends only on the particle density $n = N/V$, we can assume E/N as an homogeneous function of first-order in the variables N and V and hence, it follows the well-known thermodynamic relation

$$E = -PV + \mu N. \quad (\text{B.1.71})$$

In the case of the Wigner-Seitz cells, Eq. (B.1.71) reads

$$E_{\text{ws}} = -P_{\text{ws}} V_{\text{ws}} + \mu_{\text{ws}} N_{\text{ws}}, \quad (\text{B.1.72})$$

where we have introduced the fact that the Wigner-Seitz cells are the building blocks of the configuration and therefore we must put in Eq. (B.1.71) $N_{\text{ws}} = 1$. Through the entire article we have used Eq. (B.1.72) to obtain from the knowns energy and pressure, the Wigner-Seitz cell chemical potential (see e.g. Eqs. (B.1.13) and (B.1.23)). From Eqs. (B.1.70) and (B.1.71) we obtain the so-called Gibbs-Duhem relation

$$dP = nd\mu. \quad (\text{B.1.73})$$

In a white dwarf the pressure P and the chemical potential μ are decreasing functions of the distance from the origin. Thus, the differentials in the above equations can be assumed as the gradients of the variables which, in the present spherically symmetric case, become just derivatives with respect to the radial coordinate r . From Eq. (B.1.73) it follows the relation

$$\frac{dP_{\text{ws}}}{dr} = n_{\text{ws}} \frac{d\mu_{\text{ws}}}{dr}. \quad (\text{B.1.74})$$

From Eqs. (B.1.69), (B.1.72) and (B.1.74) we obtain

$$n_{\text{ws}}(r) \frac{d\mu_{\text{ws}}(r)}{dr} = -\frac{1}{2} \frac{dv(r)}{dr} n_{\text{ws}}(r) \mu_{\text{ws}}(r), \quad (\text{B.1.75})$$

which can be straightforwardly integrated to obtain the first integral

$$e^{v(r)/2} \mu_{\text{ws}}(r) = \text{constant}. \quad (\text{B.1.76})$$

The above equilibrium condition is general and it also applies for non-zero temperature configurations (see e.g. Klein (1949)). In such a case, it can be

shown that in addition to the equilibrium condition (B.1.76) the temperature of the system satisfies the Tolman isothermality condition $e^{\nu(r)/2}T(r) = \text{constant}$ Tolman (1930); Tolman and Ehrenfest (1930).

The weak-field non-relativistic limit

In the weak-field limit we have $e^{\nu/2} \approx 1 + \Phi$, where the Newtonian gravitational potential has been defined by $\Phi(r) = \nu(r)/2$. In the non-relativistic mechanics limit $c \rightarrow \infty$, the chemical potential $\mu_{\text{ws}} \rightarrow \tilde{\mu}_{\text{ws}} + M_{\text{ws}}c^2$, where $\tilde{\mu}_{\text{ws}}$ denotes the non-relativistic free-chemical potential of the Wigner-Seitz cell and M_{ws} is the rest-mass of the Wigner-Seitz cell, namely, the rest-mass of the nucleus plus the rest-mass of the electrons. Applying these considerations to Eq. (B.1.76) we obtain

$$e^{\nu/2}\mu_{\text{ws}} \approx M_{\text{ws}}c^2 + \tilde{\mu}_{\text{ws}} + M_{\text{ws}}\Phi = \text{constant}. \quad (\text{B.1.77})$$

Absorbing the Wigner-Seitz rest-mass energy $M_{\text{ws}}c^2$ in the constant on the right-hand-side we obtain

$$\tilde{\mu}_{\text{ws}} + M_{\text{ws}}\Phi = \text{constant}. \quad (\text{B.1.78})$$

In the weak-field non-relativistic limit, the Einstein equations (B.1.67)–(B.1.69) reduce to

$$\frac{d\Phi(r)}{dr} = \frac{GM(r)}{r^2}, \quad (\text{B.1.79})$$

$$\frac{dM(r)}{dr} = 4\pi r^2 \rho(r), \quad (\text{B.1.80})$$

$$\frac{dP(r)}{dr} = -\frac{GM(r)}{r^2} \rho(r), \quad (\text{B.1.81})$$

where $\rho(r)$ denotes the rest-mass density. The Eqs. (B.1.79)–(B.1.80) can be combined to obtain the gravitational Poisson equation

$$\frac{d^2\Phi(r)}{dr^2} + \frac{2}{r} \frac{d\Phi(r)}{dr} = 4\pi G\rho(r). \quad (\text{B.1.82})$$

In the uniform approximation (see Subsec. B.1.2), the equilibrium condition given by Eq. (B.1.78) reads

$$\tilde{\mu}_e + \frac{A_r}{Z} M_u \Phi = \text{constant}, \quad (\text{B.1.83})$$

where we have neglected the electron rest-mass with respect to the nucleus rest-mass and we have divided the equation by the total number of electrons Z . This equilibrium equation is the classical condition of thermodynamic

equilibrium assumed for non-relativistic white dwarf models (see e.g. Landau and Lifshitz (1980) for details).

Introducing the above equilibrium condition (B.1.83) into Eq. (B.1.82), and using the relation between the non-relativistic electron chemical potential and the particle density $n_e = (2m_e)^{3/2} \tilde{\mu}_e^{3/2} / (3\pi^2 \hbar^3)$, we obtain

$$\frac{d^2 \tilde{\mu}_e(r)}{dr^2} + \frac{2}{r} \frac{d\tilde{\mu}_e(r)}{dr} = - \frac{2^{7/3} m_e^{3/2} (A_r/Z)^2 m_N^2 G}{3\pi \hbar^3} \tilde{\mu}_e^{3/2}(r), \quad (\text{B.1.84})$$

which is the correct equation governing the equilibrium of white dwarfs within Newtonian gravitational theory (Landau and Lifshitz, 1980). It is remarkable that the equation of equilibrium (B.1.84), obtained from the correct application of the Newtonian limit, does not coincide with the equation given by Chandrasekhar (1931b,a, 1935, 1939), which, as correctly pointed out by Eddington (1935), is a mixture of both relativistic and non-relativistic approaches. Indeed, the consistent relativistic equations should be Eq. (B.1.76). Therefore a dual relativistic and non-relativistic equation of state was used by Chandrasekhar. The pressure on the left-hand-side of Eq. (B.1.81) is taken to be given by relativistic electrons while, the term on the right-hand-side of Eq. (B.1.80) and (B.1.81) (or the source of Eq. (B.1.82)), is taken to be the rest-mass density of the system instead of the total relativistic energy-density. Such a procedure is equivalent to take the chemical potential in Eq. (B.1.78) as a relativistic quantity. As we have seen, this is inconsistent with the weak-field non-relativistic limit of the general relativistic equations.

The Post-Newtonian limit

Indeed, if one were to treat the problem of white dwarfs approximately without going to the sophistications of general relativity, but including the effects of relativistic mechanics, one should use at least the equations in the post-Newtonian limit. The first-order post-Newtonian expansion of the Einstein equations (B.1.67)–(B.1.69) in powers of P/\mathcal{E} and $GM/(c^2 r)$ leads to the equilibrium equations (Ciufolini and Ruffini, 1983)

$$\frac{d\Phi(r)}{dr} = - \frac{1}{\mathcal{E}(r)} \left[1 - \frac{P(r)}{\mathcal{E}(r)} \right] \frac{dP(r)}{dr}, \quad (\text{B.1.85})$$

$$\frac{dM(r)}{dr} = 4\pi r^2 \frac{\mathcal{E}(r)}{c^2}, \quad (\text{B.1.86})$$

$$\begin{aligned} \frac{dP(r)}{dr} = & - \frac{GM(r)}{r^2} \frac{\mathcal{E}(r)}{c^2} \left[1 + \frac{P(r)}{\mathcal{E}(r)} + \frac{4\pi r^3 P(r)}{M(r)c^2} \right. \\ & \left. + \frac{2GM(r)}{c^2 r} \right], \end{aligned} \quad (\text{B.1.87})$$

where Eq. (B.1.87) is the post-Newtonian version of the Tolman-Oppenheimer-Volkoff equation (B.1.69).

Replacing Eq. (B.1.74) into Eq. (B.1.85) we obtain

$$\left[1 - \frac{P(r)}{\mathcal{E}(r)}\right] \frac{d\mu_{\text{ws}}(r)}{dr} + \frac{\mathcal{E}(r)/c^2}{n_{\text{ws}}(r)} \frac{d\Phi(r)}{dr} = 0. \quad (\text{B.1.88})$$

It is convenient to split the energy-density as $\mathcal{E} = c^2\rho + U$, where $\rho = M_{\text{ws}}n_{\text{ws}}$ is the rest-energy density and U the internal energy-density. Thus, Eq. (B.1.88) becomes

$$\begin{aligned} \frac{d\mu_{\text{ws}}(r)}{dr} + M_{\text{ws}} \frac{d\Phi(r)}{dr} - \frac{P(r)}{\mathcal{E}(r)} \frac{d\mu_{\text{ws}}(r)}{dr} \\ + \frac{U/c^2}{n_{\text{ws}}(r)} \frac{d\Phi(r)}{dr} = 0, \end{aligned} \quad (\text{B.1.89})$$

which is the differential post-Newtonian version of the equilibrium equation (B.1.76) and where the post-Newtonian corrections of equilibrium can be clearly seen. Applying the non-relativistic limit $c \rightarrow \infty$ to Eq. (B.1.89): $P/\mathcal{E} \rightarrow 0$, $U/c^2 \rightarrow 0$, and $\mu_{\text{ws}} \rightarrow M_{\text{ws}}c^2 + \tilde{\mu}_{\text{ws}}$, we recover the Newtonian equation of equilibrium (B.1.78).

B.1.4. Mass and radius of general relativistic stable white dwarfs

Inverse β -decay instability

It is known that white dwarfs may become unstable against the inverse β -decay process $(Z, A) \rightarrow (Z - 1, A)$ through the capture of energetic electrons (see e.g. Hund (1936); Landau (1938); Zel'Dovich (1958); Harrison et al. (1958)). In order to trigger such a process, the electron Fermi energy must be larger than the mass difference between the initial nucleus (Z, A) and the final nucleus $(Z - 1, A)$. We denote this threshold energy as ϵ_Z^β . Usually it is satisfied $\epsilon_{Z-1}^\beta < \epsilon_Z^\beta$ and therefore the initial nucleus undergoes two successive decays, i.e. $(Z, A) \rightarrow (Z - 1, A) \rightarrow (Z - 2, A)$ (see e.g. Salpeter (1961); Shapiro and Teukolsky (1983)). Some of the possible decay channels in white dwarfs with the corresponding known experimental threshold energies ϵ_Z^β are listed in Table B.2. The electrons in the white dwarf may eventually reach the threshold energy to trigger a given decay at some critical density ρ_{crit}^β . Configurations with $\rho > \rho_{\text{crit}}^\beta$ become unstable (see Harrison et al. (1958); Salpeter (1961) for details).

Within the uniform approximation, e.g. in the case of the Salpeter equation of state Salpeter (1961), the critical density for the onset of inverse β -decay is

Decay	ϵ_Z^β	$\rho_{\text{crit}}^{\beta,\text{relFMT}}$	$\rho_{\text{crit}}^{\beta,\text{unif}}$
${}^4\text{He} \rightarrow {}^3\text{H} + n \rightarrow 4n$	20.596	1.39×10^{11}	1.37×10^{11}
${}^{12}\text{C} \rightarrow {}^{12}\text{B} \rightarrow {}^{12}\text{Be}$	13.370	3.97×10^{10}	3.88×10^{10}
${}^{16}\text{O} \rightarrow {}^{16}\text{N} \rightarrow {}^{16}\text{C}$	10.419	1.94×10^{10}	1.89×10^{10}
${}^{56}\text{Fe} \rightarrow {}^{56}\text{Mn} \rightarrow {}^{56}\text{Cr}$	3.695	1.18×10^9	1.14×10^9

Table B.2.: Onset of inverse beta decay instability for ${}^4\text{He}$, ${}^{12}\text{C}$, ${}^{16}\text{O}$ and ${}^{56}\text{Fe}$. The experimental inverse β -decay energies ϵ_Z^β are given in MeV and they have been taken from Table 1 of Audi et al. (2003). The corresponding critical density for the uniform electron density model, $\rho_{\text{crit}}^{\beta,\text{unif}}$ given by Eq. (B.1.90), is given in g/cm^3 as well as the critical density $\rho_{\text{crit}}^{\beta,\text{relFMT}}$ for the relativistic Feynman-Metropolis-Teller case. The numerical values of ϵ_Z^β are taken from Audi et al. (2003), see also Shapiro and Teukolsky (1983)

given by

$$\rho_{\text{crit}}^{\beta,\text{unif}} = \frac{A_r}{Z} \frac{M_u}{3\pi^2 \hbar^3 c^3} [(\epsilon_Z^\beta)^2 + 2m_e c^2 \epsilon_Z^\beta]^{3/2}, \quad (\text{B.1.90})$$

where Eq. (B.1.15) has been used.

Because the computation of the electron Fermi energy within the relativistic Feynman-Metropolis-Teller approach Rotondo et al. (2011c) involves the numerical integration of the relativistic Thomas-Fermi equation (B.1.55), no analytic expression for ρ_{crit}^β can be found in this case. The critical density $\rho_{\text{crit}}^{\beta,\text{relFMT}}$ is then obtained numerically by looking for the density at which the electron Fermi energy (B.1.50) equals ϵ_Z^β .

In Table B.2 we show, correspondingly to each threshold energy ϵ_Z^β , the critical density both in the Salpeter case $\rho_{\text{crit}}^{\beta,\text{unif}}$ given by Eq. (B.1.90) and in the relativistic Feynman-Metropolis-Teller case $\rho_{\text{crit}}^{\beta,\text{relFMT}}$. It can be seen that $\rho_{\text{crit}}^{\beta,\text{relFMT}} > \rho_{\text{crit}}^{\beta,\text{unif}}$ as one should expect from the fact that, for a given density, the electron density at the Wigner-Seitz cell boundary satisfies $n_e^{\text{relFMT}} < n_e^{\text{unif}}$. This means that, in order to reach a given energy, the electrons within the relativistic Feynman-Metropolis-Teller approach must be subjected to a larger density with respect to the one given by the approximated Salpeter analytic formula (B.1.90).

General relativistic instability

The concept of the critical mass has played a major role in the theory of stellar evolution. For Newtonian white dwarfs the critical mass is reached asymptotically at infinite central densities of the object. One of the most important

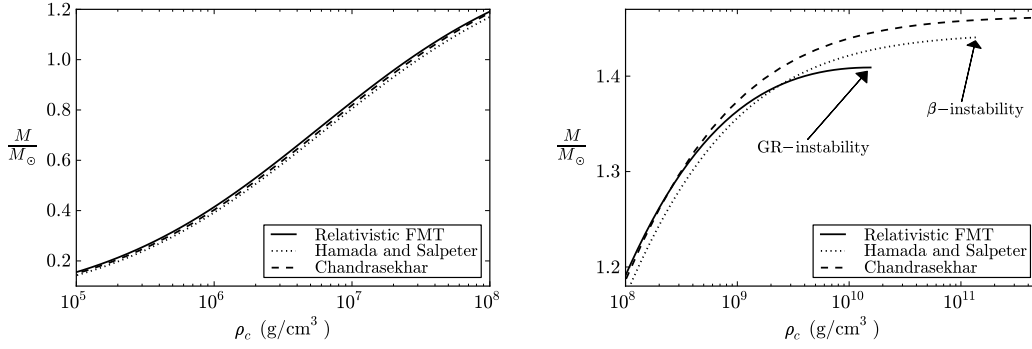


Figure B.3.: Mass in solar masses as a function of the central density in the range (left panel) 10^5 – 10^8 g/cm^3 and in the range (right panel) 10^8 – 5×10^{11} g/cm^3 for ${}^4\text{He}$ white dwarfs. The solid curve corresponds to the present work, the dotted curves are the Newtonian configurations of Hamada and Salpeter and the dashed curve are the Newtonian configurations of Chandrasekhar.

general relativistic effects is to shift this critical point to some finite density $\rho_{\text{crit}}^{\text{GR}}$.

This general relativistic effect is an additional source of instability with respect to the already discussed instability due to the onset of inverse β -decay which, contrary to the present general relativistic one, applies also in the Newtonian case by shifting the maximum mass of Newtonian white dwarfs to finite densities (see e.g. Harrison et al. (1958)).

Numerical results

In Figs. B.3–B.10 we have plotted the mass-central density relation and the mass-radius relation of general relativistic ${}^4\text{He}$, ${}^{12}\text{C}$, ${}^{16}\text{O}$ and ${}^{56}\text{Fe}$ white dwarfs. In particular, we show the results for the Newtonian white dwarfs of Hamada and Salpeter (1961), for the Newtonian white dwarfs of Chandrasekhar (1931b) and the general relativistic configurations obtained in this work based on the relativistic Feynman-Metropolis-Teller equation of state (Rotondo et al., 2011c).

Since our approach takes into account self-consistently both β -decay equilibrium and general relativity, we can determine if the critical mass is reached due either to inverse β -decay instability or to the general relativistic instability.

A comparison of the numerical value of the critical mass as given by Stoner (1929), Eq. (B.1.1), by Chandrasekhar (1931b) and Landau (1932), Eq. (B.1.2), by Hamada and Salpeter (1961) and, by the treatment presented here can be found in Table B.3.

From the numerical integrations we have obtained:

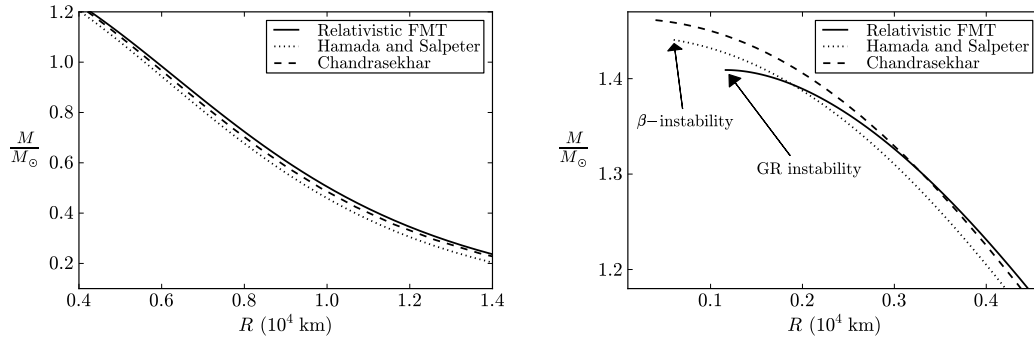


Figure B.4.: Mass in solar masses as a function of the radius in units of 10^4 km for ${}^4\text{He}$ white dwarfs. The left and right panels show the configurations for the same range of central densities of the corresponding panels of Fig. B.3. The solid curve corresponds to the present work, the dotted curves are the Newtonian configurations of Hamada and Salpeter and the dashed curve are the Newtonian configurations of Chandrasekhar.

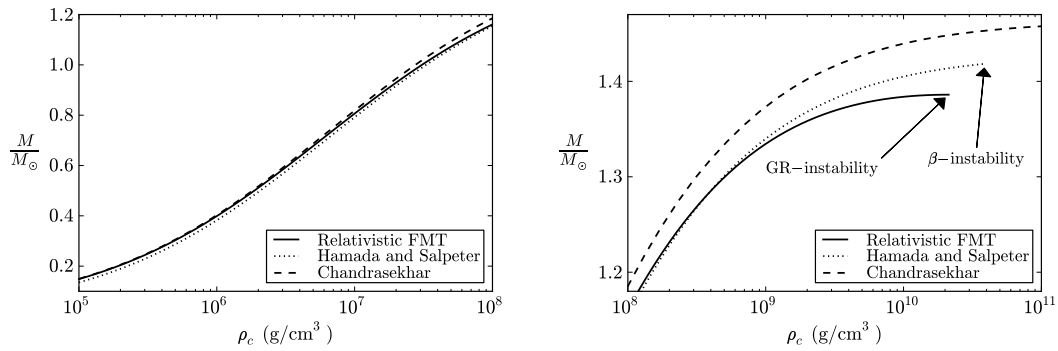


Figure B.5.: Mass in solar masses as a function of the central density in the range (left panel) 10^5 – 10^8 g/cm^3 and in the range (right panel) 10^8 – 10^{11} g/cm^3 for ${}^{12}\text{C}$ white dwarfs. The solid curve corresponds to the present work, the dotted curves are the Newtonian configurations of Hamada and Salpeter and the dashed curve are the Newtonian configurations of Chandrasekhar.

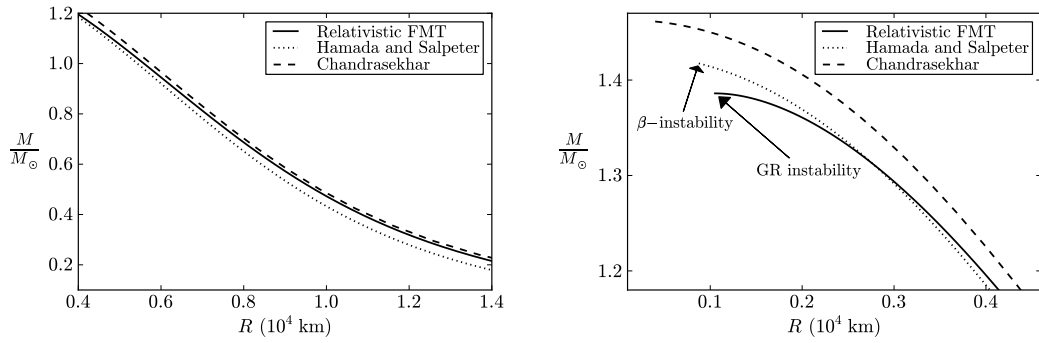


Figure B.6.: Mass in solar masses as a function of the radius in units of 10^4 km for ^{12}C white dwarfs. The left and right panels show the configurations for the same range of central densities of the corresponding panels of Fig. B.5. The solid curve corresponds to the present work, the dotted curves are the Newtonian configurations of Hamada and Salpeter and the dashed curve are the Newtonian configurations of Chandrasekhar.

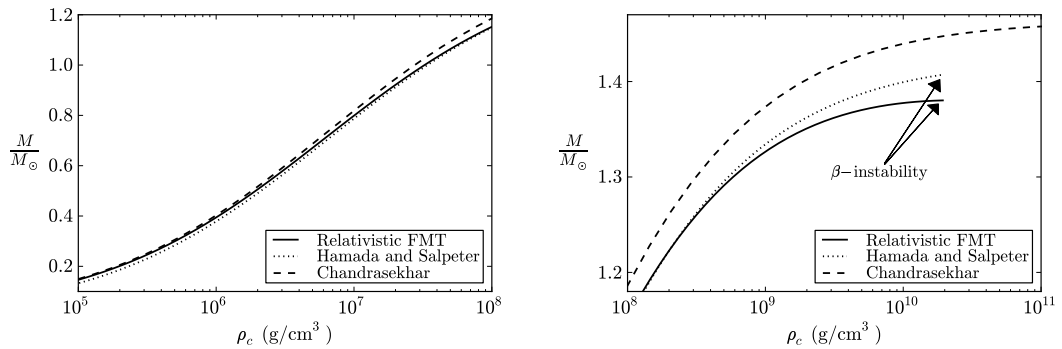


Figure B.7.: Mass in solar masses as a function of the central density in the range (left panel) 10^5 – 10^8 g/cm^3 and in the range (right panel) 10^8 – 10^{11} g/cm^3 for ^{16}O white dwarfs. The solid curve corresponds to the present work, the dotted curves are the Newtonian configurations of Hamada and Salpeter and the dashed curve are the Newtonian configurations of Chandrasekhar.

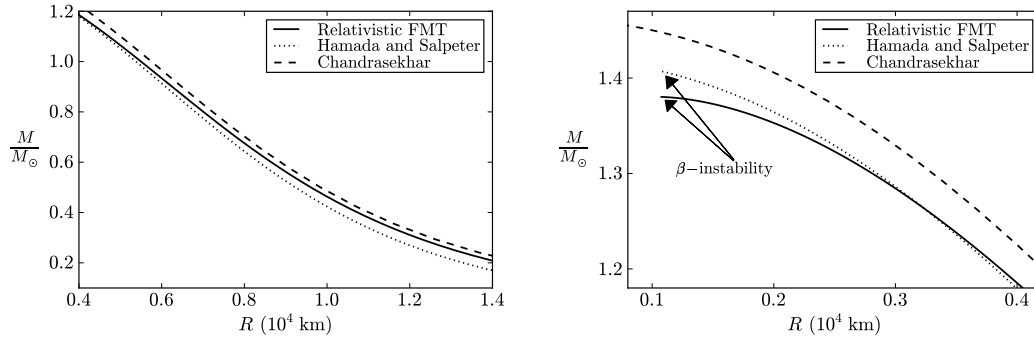


Figure B.8.: Mass in solar masses as a function of the radius in units of 10^4 km for ^{16}O white dwarfs. The left and right panels show the configurations for the same range of central densities of the corresponding panels of Fig. B.7. The solid curve corresponds to the present work, the dotted curves are the Newtonian configurations of Hamada and Salpeter and the dashed curve are the Newtonian configurations of Chandrasekhar.

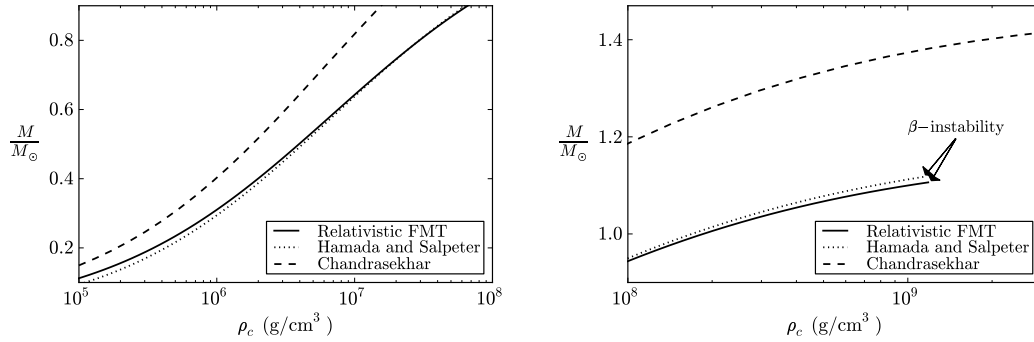


Figure B.9.: Mass in solar masses as a function of the central density in the range (left panel) 10^5 – 10^8 g/cm^3 and in the range (right panel) 10^8 – 3×10^9 g/cm^3 for ^{56}Fe white dwarfs. The solid curve corresponds to the present work, the dotted curves are the Newtonian configurations of Hamada and Salpeter and the dashed curve are the Newtonian configurations of Chandrasekhar.

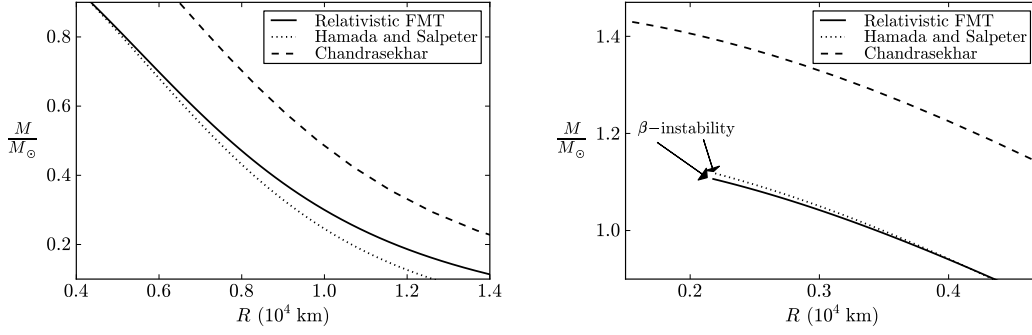


Figure B.10.: Mass in solar masses as a function of the radius in units of 10^4 km for ^{56}Fe white dwarfs. The left and right panels show the configurations for the same range of central densities of the corresponding panels of Fig. B.9. The solid curve corresponds to the present work, the dotted curves are the Newtonian configurations of Hamada and Salpeter and the dashed curve are the Newtonian configurations of Chandrasekhar.

1. ^4He and ^{12}C white dwarfs satisfy $\rho_{\text{crit}}^{\text{GR}} < \rho_{\text{crit}}^{\beta}$ (see Figs. B.3–B.6 and Tables B.2 and B.3), so they are unstable with respect to general relativistic effects. The critical density of ^{12}C white dwarfs is $\sim 2.12 \times 10^{10} \text{ g/cm}^3$, to be compared with the value $2.65 \times 10^{10} \text{ g/cm}^3$ obtained from calculations based on general relativistic corrections to the theory of polytropes (see e.g. Shapiro and Teukolsky (1983)).
2. White dwarfs composed of heavier material than ^{12}C , e.g. ^{16}O and ^{56}Fe are unstable due to inverse β -decay of the nuclei (see Figs. B.7–B.10 and Tables B.2 and B.3). It is worth to notice that the correct evaluation of general relativistic effects and of the combined contribution of the electrons to the energy-density of the system introduce, for ^{12}C white dwarfs, a critical mass not due to the inverse beta decay. When the contribution of the electrons to the energy-density is neglected (e.g. Chandrasekhar (1931b) and Hamada and Salpeter (1961), see Eq. (B.1.15)) the critical density for Carbon white dwarfs is determined by inverse beta decay irrespective of the effects of general relativity.
3. It can be seen from Figs. B.3–B.10 that the drastic decrease of the Salpeter pressure at low densities (see Salpeter (1961); Rotondo et al. (2011c) and Table B.1 for details) produces an underestimate of the mass and the radius of low density (low mass) white dwarfs.
4. The Coulomb effects are much more pronounced in the case of white dwarfs with heavy nuclear compositions e.g. ^{56}Fe (see Figs. B.9 and B.10).

	$\rho_{\text{crit}}^{\text{H\&S}}$	$M_{\text{crit}}^{\text{H\&S}} / M_{\odot}$	$\rho_{\text{crit}}^{\text{FM\&Trel}}$	$M_{\text{crit}}^{\text{FM\&Trel}} / M_{\odot}$
${}^4\text{He}$	1.37×10^{11}	1.44064	1.56×10^{10}	1.40906
${}^{12}\text{C}$	3.88×10^{10}	1.41745	2.12×10^{10}	1.38603
${}^{16}\text{O}$	1.89×10^{10}	1.40696	1.94×10^{10}	1.38024
${}^{56}\text{Fe}$	1.14×10^9	1.11765	1.18×10^9	1.10618

Table B.3.: Critical density and corresponding critical mass for the onset of gravitational collapse of the Newtonian ${}^4\text{He}$, ${}^{12}\text{C}$, ${}^{16}\text{O}$ and ${}^{56}\text{Fe}$ white dwarfs of Hamada and Salpeter (1961), based on the Salpeter equation of state (Salpeter, 1961), and of the corresponding general relativistic configurations obtained in this work based on the relativistic Feynman-Metropolis-Teller equation of state (Rotondo et al., 2011c). Densities are in g/cm^3 and masses in solar masses. For the sake of comparison, the critical mass of Stoner (B.1.1) and of the one of Chandrasekhar-Landau (B.1.2) are $M_{\text{crit}}^{\text{Stoner}} \sim 1.72M_{\odot}$ and $M_{\text{crit}}^{\text{Ch-L}} \sim 1.45M_{\odot}$, for the average molecular weight $\mu = A_r/Z = 2$.

B.1.5. Conclusions

We have addressed the theoretical physics aspects of the white dwarf configurations of equilibrium, quite apart from the astrophysical application.

The recently accomplished description of a compressed atom within the global approach of the relativistic Feynman, Metropolis and Teller (Rotondo et al., 2011c) has been here solved within the Wigner-Seitz cell and applied to the construction of white dwarfs in the framework of general relativity. From a theoretical physics point of view, this is the first unified approach of white dwarfs taking into account consistently the gravitational, the weak, the strong and the electromagnetic interactions, and it answers open theoretical physics issues in this matter. No analytic formula for the critical mass of white dwarfs can be derived and, on the contrary, the critical mass can be obtained only through the numerical integration of the general relativistic equations of equilibrium together with the relativistic Feynman-Metropolis-Teller equation of state.

The value of the critical mass and the radius of white dwarfs in our treatment and in the Hamada and Salpeter (1961) treatment becomes a function of the composition of the star. Specific examples have been given in the case of white dwarfs composed of ${}^4\text{He}$, ${}^{12}\text{C}$, ${}^{16}\text{O}$ and ${}^{56}\text{Fe}$. The results of Chandrasekhar, of Hamada and Salpeter and ours have been compared and contrasted (see Table B.3 and Figs. B.3–B.10).

The critical mass is a decreasing function of Z and Coulomb effects are more important for heavy nuclear compositions. The validity of the Salpeter approximate formulas increases also with Z , namely for heavy nuclear compositions the numerical values of the masses as well as of the radii of white dwarfs obtained using the Salpeter equation of state are closer to the ones ob-

tained from the full numerical integration of the general relativistic treatment presented here.

Turning now to astrophysics, the critical mass of white dwarfs is today acquiring a renewed interest in view of its central role in the explanation of the supernova phenomena (Phillips, 1993; Riess et al., 1998; Perlmutter et al., 1999; Riess et al., 2004). The central role of the critical mass of white dwarfs as related to supernova was presented by Hoyle and Fowler (1960) explaining the difference between type I and type II Supernova. This field has developed in the intervening years to a topic of high precision research in astrophysics and, very likely, both the relativistic and the Coulomb effects outlined in this article will become topic of active confrontation between theory and observation. For instance, the underestimate of the mass and the radius of low density white dwarfs within the Hamada and Salpeter (1961) treatment (see Figs. B.3–B.10) leads to the possibility of a direct confrontation with observations in the case of low mass white dwarfs e.g. the companion of the Pulsar J1141-6545 (Kramer, 2010).

We have finally obtained a general formula in Eq. (B.1.76) as a “first integral” of the general relativistic equations of equilibrium. This formula relates the chemical potential of the Wigner-Seitz cells, duly obtained from the relativistic Feynman-Metropolis-Teller model (Rotondo et al., 2011c) taking into account weak, nuclear and electromagnetic interactions, to the general relativistic gravitational potential at each point of the configuration. Besides its esthetic value, this is an important tool to examine the radial dependence of the white dwarf properties and it can be also applied to the crust of a neutron star as it approaches to the physical important regime of neutron star cores.

The formalism we have introduced allows in principle to evaluate subtle effects of a nuclear density distribution as a function of the radius and of the Fermi energy of the electrons and of the varying depth of the general relativistic gravitational potential. The theoretical base presented in this article establishes also the correct framework for the formulation of the more general case when finite temperatures and magnetic fields are present. This treatment naturally opens the way to a more precise description of the crust of neutron stars, which will certainly become an active topic of research in view of the recent results by Goriely et al. (2011a,b) on the importance of the Coulomb effects in the r-process nucleosynthesis of the crust material during its post-ejection evolution in the process of gravitational collapse and/or in the merging of neutron star binaries.

B.2. On the maximum mass and minimum period of general relativistic uniformly rotating white dwarfs

Equilibrium configurations of non-rotating ${}^4\text{He}$, ${}^{12}\text{C}$, ${}^{16}\text{O}$ and ${}^{56}\text{Fe}$ white dwarfs (WDs) within general relativity have been recently constructed (Rotondo et al., 2011b). The white dwarf matter has been there described by the relativistic generalization of the Feynman-Metropolis-Teller (RFMT) equation of state (EoS) obtained by Rotondo et al. (2011c). A new mass-radius relation that generalizes both the Chandrasekhar (1931b) and the Hamada and Salpeter (1961) works has been there obtained, leading to a smaller maximum mass and a larger minimum radius with respect to previous calculations. In addition, it has been there shown how both general relativity and inverse β -decay are relevant for the instability of non-rotating WDs upon their composition (see Rotondo et al. (2011b) and Table B.4, for details).

Comp.	ρ_{crit} (g/cm ³)	Instability	$M_{\text{max}}^{J=0}/M_{\odot}$
${}^4\text{He}$	1.56×10^{10}	GR	1.40906
${}^{12}\text{C}$	2.12×10^{10}	GR	1.38603
${}^{16}\text{O}$	1.94×10^{10}	inv. β -decay	1.38024
${}^{56}\text{Fe}$	1.18×10^9	inv. β -decay	1.10618

Table B.4.: Critical density and corresponding critical mass for the onset of gravitational collapse of the general relativistic non-rotating ${}^4\text{He}$, ${}^{12}\text{C}$, ${}^{16}\text{O}$ and ${}^{56}\text{Fe}$ WDs obtained in Rotondo et al. (2011b), based on the RFMT EoS Rotondo et al. (2011c). We indicate in the third column if the critical density is due either to inverse β -decay or to general relativistic effects, see Rotondo et al. (2011b) for details.

We here extend the previous results of Rotondo et al. (2011b) to the case of general relativistic uniformly rotating WDs within Hartle’s formalism. It describes the structure of rotating objects approximately up to second order terms in the angular velocity of the star Ω : in this “slow” approximation regime the solution of the Einstein equations in the exterior can be written in analytic closed form in terms of the mass, angular momentum and quadrupole moment of the star Hartle (1967a); Hartle and Thorne (1968a). The corresponding interior solution that matches with the exterior one can be then constructed by solving numerically a system of ordinary differential equations, see Hartle (1967a); Hartle and Thorne (1968a) for details.

We focus here mainly on two astrophysically important quantities: the maximum stable mass and the minimum rotation period of the WD. Rotating WDs have more stringent and complex stability criteria with respect to the non-rotating case. Besides the inverse β -decay instability, two additional lim-

Decay	ϵ_Z^β (MeV)	ρ_{crit}^β (g/cm ³)
${}^4\text{He} \rightarrow {}^3\text{H} + n \rightarrow 4n$	20.596	1.39×10^{11}
${}^{12}\text{C} \rightarrow {}^{12}\text{B} \rightarrow {}^{12}\text{Be}$	13.370	3.97×10^{10}
${}^{16}\text{O} \rightarrow {}^{16}\text{N} \rightarrow {}^{16}\text{C}$	10.419	1.94×10^{10}
${}^{56}\text{Fe} \rightarrow {}^{56}\text{Mn} \rightarrow {}^{56}\text{Cr}$	3.695	1.18×10^9

Table B.5.: Onset of inverse beta decay instability for ${}^4\text{He}$, ${}^{12}\text{C}$, ${}^{16}\text{O}$ and ${}^{56}\text{Fe}$. The experimental inverse β -decay energies ϵ_Z^β have been taken from Table 1 of Audi et al. (2003); see also Shapiro and Teukolsky (1983). The corresponding critical density ρ_{crit}^β is obtained from the RFMT EoS Rotondo et al. (2011c)

its on the stability of rotating WDs are due to mass-shedding at the equator and axisymmetric (secular) instability.

Inverse β -decay– White dwarfs may become unstable against the inverse β -decay process $(Z, A) \rightarrow (Z - 1, A)$ through the capture of energetic electrons. In order to trigger such a process, the electron Fermi energy must be larger than the mass difference between the initial nucleus (Z, A) and the final nucleus $(Z - 1, A)$. We denote this threshold energy as ϵ_Z^β . Usually it is satisfied $\epsilon_{Z-1}^\beta < \epsilon_Z^\beta$ and therefore the initial nucleus undergoes two successive decays, i.e. $(Z, A) \rightarrow (Z - 1, A) \rightarrow (Z - 2, A)$ (see e.g. Salpeter (1961); Shapiro and Teukolsky (1983)). Some of the possible decay channels in WDs with the corresponding known experimental threshold energies ϵ_Z^β are listed in Table B.5. The electrons in the white dwarf may eventually reach the threshold energy to trigger a given decay at some critical density ρ_{crit}^β . Configurations with $\rho > \rho_{\text{crit}}^\beta$ become unstable (see Harrison et al. (1958); Salpeter (1961) for details). In Table B.5 correspondingly to each threshold energy ϵ_Z^β , the critical density given by the RFMT EoS ρ_{crit}^β is shown; see Rotondo et al. (2011b) for details.

Mass-shedding limit–If the velocity of a particle on the surface of the star exceeds the velocity of a free-particle, the star should start to loose its mass becoming thus unstable (Stergioulas, 2003). A procedure to obtain the maximum possible angular velocity of the star before reaching this limit was developed in Friedman et al. (1986). However, in practice, it is less complicated to compute the mass-shedding angular velocity of a star Ω_{ms} , from the orbital angular velocity Ω_{orb} of a co-rotating test particle in the external field at the equatorial plane. For the Hartle-Thorne external solution Hartle and Thorne (1968a), the orbital angular velocity Ω_{orb} for corotating particles is given by

(see e.g. Torok et al., 2008; Bini et al., 2011)

$$\Omega_{orb}(r) = \frac{u^\phi}{u^t} = \frac{-g_{t\phi,r} + \sqrt{(g_{t\phi,r})^2 - g_{tt,r}g_{\phi\phi,r}}}{g_{\phi\phi,r}} \quad (\text{B.2.1})$$

where u^ϕ and u^t are the angular and time components of the four-velocity, and $g_{\alpha\beta,r}$, (so that $\alpha, \beta = t, \phi$), are the derivatives of the metric tensor components with respect to r , one obtains

$$\Omega_{orb}(r) = \Omega_0(r) \left[1 - F_1(r) \frac{J}{M^2} + F_2(r) \frac{J^2}{M^4} + F_3(r) \frac{Q}{M^3} \right] \quad (\text{B.2.2})$$

where

$$\begin{aligned} \Omega_0 &= \frac{M^{1/2}}{r^{3/2}}, & F_1 &= \frac{M^{3/2}}{r^{3/2}} \\ F_2 &= (48M^7 - 80M^6r + 4M^5r^2 - 18M^4r^3 + 40M^3r^4 \\ &+ 10M^2r^5 + 15Mr^6 - 15r^7) / [16M^2r^4(r - 2M)] + F \\ F_3 &= \frac{6M^4 - 8M^3r - 2M^2r^2 - 3Mr^3 + 3r^4}{16M^2r(r - 2M)/5} - F \\ F &= \frac{15(r^3 - 2M^3)}{32M^3} \ln \frac{r}{r - 2M} \end{aligned}$$

The parameters M , J and Q , related to the total mass, the angular momentum and the quadrupole moment, respectively, are obtained for a given EoS, from the matching procedure between the internal and external solutions. The total mass is defined by $M = M^{J \neq 0} = M^{J=0} + \delta M$, where $M^{J=0}$ is the mass of a static white dwarf with the same central density as $M^{J \neq 0}$, and δM is the contribution to the mass due to rotation. The value of Ω_{ms} can be computed by gradually increasing the value of Ω until it reaches Ω_{orb} . Clearly, the matching is carried out at the surface of the rotating star, therefore in the above formula we set $r = R_{eq}$.

Axisymmetric instability—A turning-point method has been used in Friedman et al. (1988) to obtain a simple criterion governing the secular stability of uniformly rotating relativistic stars to axisymmetric perturbations. This criterion has been used for uniformly rotating neutron stars and here we use it for uniformly rotating WDs. The main idea is that along a sequence of rotating stars with fixed angular momentum and increasing central density, the configuration with maximum mass establishes the onset of axisymmetric instability. Mathematically, this limit can be expressed by Friedman et al. (1988)

$$\left(\frac{\partial M(\rho_c, J)}{\partial \rho_c} \right)_J = 0, \quad (\text{B.2.3})$$

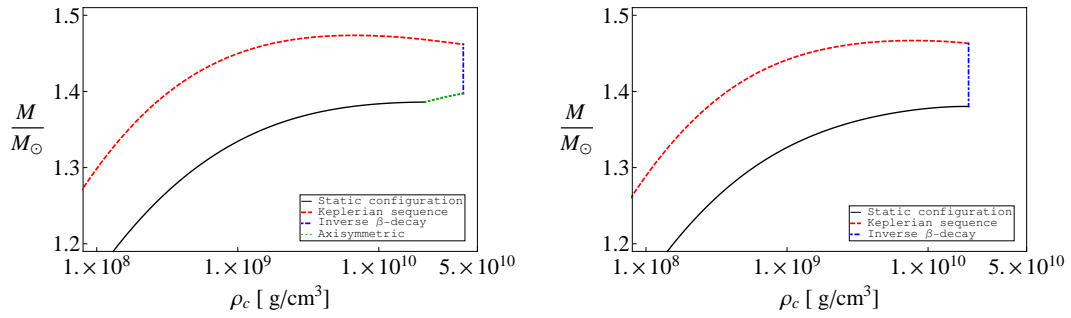


Figure B.11.: Mass in solar masses versus the central density for ^{12}C (left panel) and for ^{16}O (right panel) WDs. The solid curve corresponds to the static mass, the dashed curve corresponds to the Keplerian sequence, dashed-dotted to inverse β - instability boundary, and the dotted curve to the axisymmetric instability.

which separates regions of stable and unstable stars. In the particular case $J = 0$, the above limit reduces to the well-known concept of maximum mass of static stars.

Maximum mass—In Figs. B.11–B.12 we show the mass-central density relation and the mass-radius relation of general relativistic rotating ^{12}C and ^{16}O WDs. We explicitly show the above three limits on stability and, correspondingly, in Fig. B.13 we have plotted the allowed region of stability.

We have found that the maximum mass of rotating WDs belongs to the Keplerian sequence and it can be expressed as

$$M_{max}^{J \neq 0} = k M_{max}^{J=0}, \quad (\text{B.2.4})$$

where $M_{max}^{J=0}$ is the maximum stable mass of non-rotating WDs and k is the numerical factor depending upon nuclear composition; see Table B.6 and Figs. B.11 and B.12 for details. It is worth to mention that this maximum mass is not determined by a critical density as in the non-rotating case, see e.g. Rotondo et al. (2011b) and Table B.4. In the case of rotating WDs, the density is limited either by the critical density for inverse β -decay (see Table B.5) or by the critical density at which the limit given by Eq. (B.2.3) is reached. However, the angular momentum J along the Keplerian sequence is not constant and thus Eq. (B.2.3) does not limit, in principle, such a sequence. We have additionally verified that none of the rotating WDs belonging to the mass-shedding sequence is the maximum of some $J = \text{constant}$ sequence, and therefore they are indeed axisymmetrically stable. We then extend the Keplerian sequence in Fig. B.11 all the way up to the values $\rho_{\text{crit}}^{\beta}$ of Table B.5.

Using the weak-field approximation, Roxburgh and Durney (1966) computed the maximum mass $1.4825M_{\odot}$ for the mass-shedding WD sequence, as well as the critical polar radius 363 km for rotating instability; both of

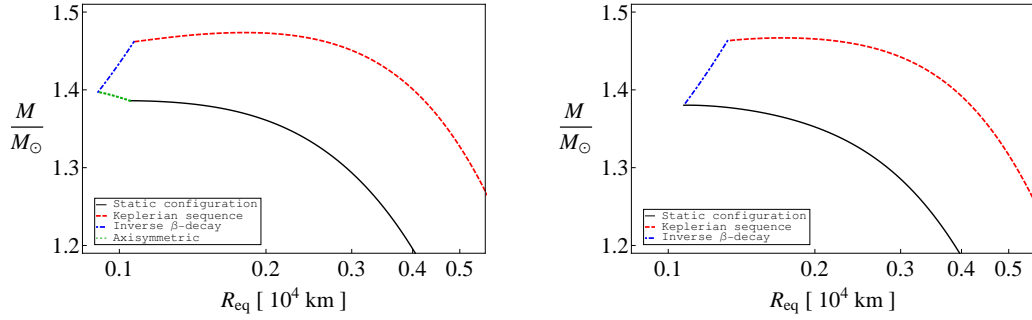


Figure B.12.: Mass in solar masses versus the equatorial radius in units of 10^4 km for ^{12}C (left panel) and for ^{16}O (right panel) WDs. The left and right panels show the configurations for the same range of central densities of the corresponding panels of Fig. B.11. The solid curve corresponds to the static mass, the dashed curve corresponds to the Keplerian sequence, dashed-dotted to inverse β -instability boundary, and the dotted curve to the axisymmetric instability.

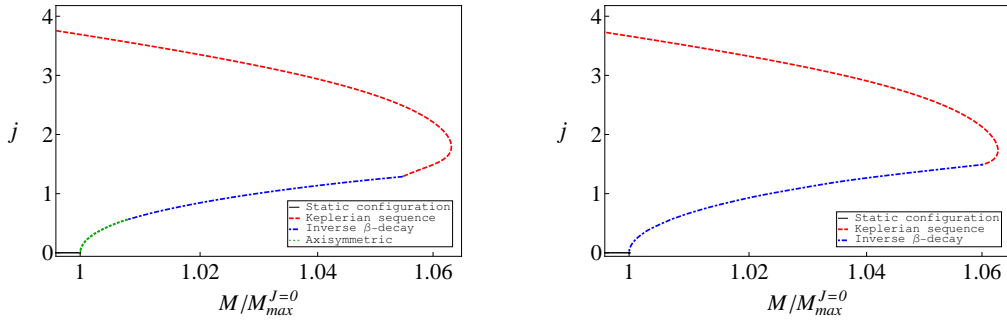


Figure B.13.: Dimensionless angular momentum $j \equiv cJ/(GM^2)$ versus the mass of rotating WDs, normalized to the maximum non-rotating mass. The left panel corresponds to ^{12}C WDs and the right panel to ^{16}O WDs.

B.2. On the maximum mass and minimum period of general relativistic uniformly rotating white dwarfs

Composition	σ	k	P_{min}	$M_{max}^{J=0}$	$R_{min}^{J=0}$	$R_p^{P_{min}}$
${}^4\text{He}$	0.26952	1.0646	0.284	1.40906	1163	564
${}^{12}\text{C}$	0.54692	1.0632	0.501	1.38603	1051	817
${}^{16}\text{O}$	0.72343	1.0626	0.687	1.38024	1076	1005
${}^{56}\text{Fe}$	0.71685	1.0864	2.195	1.10618	2180	2000

Table B.6.: The minimum period P_{min} of general relativistic ${}^4\text{He}$, ${}^{12}\text{C}$, ${}^{16}\text{O}$ and ${}^{56}\text{Fe}$ WDs. P_{min} is given in seconds, the maximum mass of non-rotating WDs $M_{max}^{J=0}$ obtained in Rotondo et al. (2011b) is given in solar masses and the corresponding minimum radius $R_{min}^{J=0}$ is in km. The polar radius of the configuration with P_{min} , $R_p^{P_{min}}$, is also given in km. It is worth to recall that the configuration with P_{min} is obtained for a WD rotating at mass-shedding limit and with central density given by the critical density for inverse β -decay (see Table B.5 and Fig. B.11).

them assuming an average molecular weight $\mu = 2$ for the EoS employed by Chandrasekhar in his classic work Chandrasekhar (1931b). This values must be compared with the ones obtained here and summarized in Table B.6. The Roxburgh critical radius is rather small with respect to our critical polar radii. It is clear that such a small radius would lead to a configuration with central density over the limit established by inverse β -decay: the average density obtained for the Roxburgh's critical configuration is $\sim 1.46 \times 10^{10}$ g/cm³, very close to $\rho_{crit}^\beta = 3.97 \times 10^{10}$ g/cm³ for ${}^{12}\text{C}$ WDs and even closer to $\rho_{crit}^\beta = 1.94 \times 10^{10}$ g/cm³ for ${}^{16}\text{O}$ WDs (see Table B.5).

Minimum period– We have found that the minimum rotation period P_{min} of WDs is obtained for a configuration rotating at Keplerian angular velocity at the critical inverse β -decay density; i.e. is the configuration lying at the crossing point between the mass-shedding and the inverse β -decay boundaries; see e.g. Figs. B.11 and B.13. The corresponding values of P_{min} for ${}^4\text{He}$, ${}^{12}\text{C}$, ${}^{16}\text{O}$ and ${}^{56}\text{Fe}$ WDs are shown in Table B.6. The value of P_{min} lies between 0.28 and 2.2 seconds and it can be expressed by the simple formula

$$P_{min} = \sigma \left(\frac{M_\odot}{M_{max}^{J=0}} \right)^{\frac{1}{2}} \left(\frac{R_{min}^{J=0}}{10^3 \text{km}} \right)^{\frac{3}{2}} \text{ sec}, \quad (\text{B.2.5})$$

where σ is a numerical factor depending on the nuclear composition (details are given in Table B.6).

Traditionally, the rotating stability of WDs has been studied assuming the EoS employed by Chandrasekhar in his classic work Chandrasekhar (1931b), based on the uniform approximation for the electron component without taking into account the microscopic screening caused by the Coulomb interaction. In addition, the process of inverse β -decay of the composing nuclei can-

not be properly studied within such an EoS, see e.g. Rotondo et al. (2011c,b) for details. Since the classic work of Ostriker and Bodenheimer (1968) on the stability of rotating WDs (see e.g. also Durisen (1975)), it has been believed that only very massive differentially rotating WDs could be axisymmetrically unstable. Indeed, we have shown in this letter that uniformly rotating WDs can be also axisymmetrically unstable, see Figs. B.11 and B.13.

Fig. B.13 is of particular astrophysical relevance. Configurations lying in the shaded region are stable against the mass-shedding, inverse β -decay and axisymmetric instabilities. WDs with masses smaller than the maximum non-rotating mass (the Chandrasekhar mass), i.e. $M^{J \neq 0} < M_{max}^{J=0}$ can rotate from the static limit all the way up to the mass-shedding limit. However, configurations with $M^{J \neq 0} > M_{max}^{J=0}$, hereafter super-Chandrasekhar WDs, must have an angular momentum larger than some value $J > 0$. Thus, super-Chandrasekhar WDs are stabilized by rotation and there is some minimum angular velocity, depending on their mass and composition, below which they undergo gravitational collapse. In this respect it is worth to stress that we have found that super-Chandrasekhar ^{12}C WDs present axisymmetric, inverse β -decay as well as mass-shedding instabilities. For heavier nuclear compositions e.g. ^{16}O WDs, the axisymmetric instability does not occur.

The results of the present work are relevant both for the theory of type Ia supernovae in the context of delayed explosions as well as for the white dwarf model of Soft Gamma-Ray Repeaters and Anomalous X-Ray Pulsars.

B.3. SGRs and AXPs as rotation powered massive white dwarfs

B.3.1. Introduction

Soft Gamma Ray Repeaters (SGRs) and Anomalous X-ray Pulsars (AXPs) are a class of compact objects that show interesting observational properties (see e.g. Mereghetti, 2008): rotational periods in the range $P \sim (2-12)$ s, a narrow range with respect to the wide range of ordinary pulsars $P \sim (0.001-10)$ s; spin-down rates $\dot{P} \sim (10^{-13}-10^{-10})$, larger than ordinary pulsars $\dot{P} \sim 10^{-15}$; strong outburst of energies $\sim (10^{41}-10^{43})$ erg, and for the case of SGRs, giant flares of even large energies $\sim (10^{44}-10^{47})$ erg, not observed in ordinary pulsars.

The recent observation of SGR 0418+5729 with a rotational period of $P = 9.08$ s, an upper limit of the first time derivative of the rotational period $\dot{P} < 6.0 \times 10^{-15}$ (Rea et al., 2010), and an X-ray luminosity of $L_X = 6.2 \times 10^{31}$ erg/s promises to be an authentic Rosetta Stone, a powerful discriminant for alternative models of SGRs and AXPs.

If described as a neutron star of $M = 1.4M_\odot$, $R = 10$ km and a moment of inertia $I \approx 10^{45}$ g cm², which we adopt hereafter as fiducial parameters, the loss of rotational energy of the neutron star

$$\dot{E}_{\text{rot}}^{\text{NS}} = -4\pi^2 I \frac{\dot{P}}{P^3} = -3.95 \times 10^{46} \frac{\dot{P}}{P^3} \text{ erg/s}, \quad (\text{B.3.1})$$

associated to its spin-down rate \dot{P} , cannot explain the X-ray luminosity of SGR 0418+5729, i.e. $\dot{E}_{\text{rot}}^{\text{NS}} < L_X$, excluding the possibility of identifying this source as an ordinary spin-down powered pulsar.

The magnetar model of SGRs and AXPs, based on a neutron star of fiducial parameters, needs a magnetic field larger than the critical field for vacuum polarization $B_c = m_e^2 c^3 / (e\hbar) = 4.4 \times 10^{13}$ G in order to explain the observed X-ray luminosity in terms of the release of magnetic energy (see Duncan and Thompson, 1992; Thompson and Duncan, 1995, for details). However, the inferred upper limit of the surface magnetic field of SGR 0418+5729 $B < 7.5 \times 10^{12}$ G describing it as a neutron star (see Rea et al., 2010, for details), is well below the critical field challenging the power mechanism based on magnetic field decay purported in the magnetar scenario.

We show that the observed upper limit on the spin-down rate of SGR 0418+5729 is, instead, perfectly in line with a model based on a massive fast rotating highly magnetized white dwarf (see e.g. Paczynski, 1990) of mass $M = 1.4M_\odot$, radius $R = 10^3$ km, and moment of inertia $I \approx 10^{49}$ g cm², which we adopt hereafter as fiducial white dwarf parameters. Such a configuration leads for SGR 0418+5729 to a magnetic field $B < 7.5 \times 10^8$ G. The X-ray luminosity can then be expressed as originating from the loss of rota-

tional energy of the white dwarf leading to a theoretical prediction for the first time derivative of the rotational period

$$\frac{L_X P^3}{4\pi^2 I} \leq \dot{P}_{\text{SGR0418+5729}} < 6.0 \times 10^{-15}, \quad (\text{B.3.2})$$

where the lower limit is established by assuming that the observed X-ray luminosity of SGR 0418+5729 coincides with the rotational energy loss of the white dwarf. For this specific source, the lower limit of \dot{P} given by Eq. (B.3.2) is $\dot{P}_{\text{SGR0418+5729}} \geq 1.18 \times 10^{-16}$. This prediction is left to be verified by the dedicated scientific missions.

The assumption of massive fast rotating highly magnetized white dwarfs appears to be very appropriate since their observation has been solidly confirmed in the last years thanks to observational campaigns carried out by the X-ray Japanese satellite Suzaku (see e.g. Terada et al., 2008c; Terada, 2008; Terada et al., 2008d,b,a). The magnetic fields observed in white dwarfs are larger than 10^6 G all the way up to 10^9 G (see e.g. Angel et al., 1981; Ferrario et al., 1997; Nalezyty and Madej, 2004; Ferrario and Wickramasinghe, 2005; Terada et al., 2008c; Külebi et al., 2009). These observed massive fast rotating highly magnetized white dwarfs share common properties with SGRs/AXPs. The specific comparison between SGR 0418+5729 and the white dwarf AE Aquarii (Terada et al., 2008c) is given in Sec. B.3.4.

The aim of this article is to investigate the implications of the above considerations to all observed SGRs and AXPs. The article is organized as follows. In Sec. B.3.2 we summarize the main features of a model for SGRs and AXPs based on rotation powered white dwarfs while, in Sec. B.3.3, we recall the magnetar model. In Sec. B.3.4 we present the observations of massive fast rotating highly magnetized white dwarfs. The constraints on the rotation rate imposed by the rotational instabilities of fast rotating white dwarfs are discussed in Sec. B.3.5 and in Sec. B.3.6 we analyze the glitch-outburst connection in SGRs and AXPs. The magnetospheric emission from the white dwarf is discussed in Sec. B.3.7 and the possible connection between SGRs and AXPs with supernova remnants is presented in Sec. B.3.8. In Sec. B.3.9 we address the problem of fiducial parameters of both white dwarfs and neutron stars and, in Sec. B.3.10, we summarize conclusions and remarks.

B.3.2. SGRs and AXPs within the white dwarf model

We first recall the pioneering works of Morini et al. (1988) and Paczynski (1990) on 1E 2259+586. This source is pulsating in the X-rays with a period $P = 6.98$ s (Fahlman and Gregory, 1981), a spin-down rate of $\dot{P} = 4.8 \times 10^{-13}$ (Davies et al., 1990) and X-ray luminosity $L_X = 1.8 \times 10^{34}$ erg/s (Gregory and Fahlman, 1980; Hughes et al., 1981; Morini et al., 1988). Specially relevant in the case of 1E 2259+586 is also its position within the supernova remnant

G109.1-1.0 with age estimated $t - t_0 = (12-17)$ kyr (Gregory and Fahlman, 1980; Hughes et al., 1981).

Paczynski developed for 1E 2259+586 a model based on a massive fast rotating highly magnetized white dwarf. The upper limit on the magnetic field (see e.g. Ferrari and Ruffini, 1969) obtained by requesting that the rotational energy loss due to the dipole field be smaller than the electromagnetic emission of the dipole, is given by

$$B = \left(\frac{3c^3}{8\pi^2} \frac{I}{R^6} P\dot{P} \right)^{1/2}, \quad (\text{B.3.3})$$

where P and \dot{P} are observed properties and the moment of inertia I and the radius R of the object are model dependent properties. For the aforementioned fiducial parameters of a fast rotating magnetized white dwarf, Eq. (B.3.3) becomes

$$B = 3.2 \times 10^{15} (P\dot{P})^{1/2} \text{ G}. \quad (\text{B.3.4})$$

The loss of rotational energy within this model is given by

$$\dot{E}_{\text{rot}}^{\text{WD}} = -4\pi^2 I \frac{\dot{P}}{P^3} = -3.95 \times 10^{50} \frac{\dot{P}}{P^3} \text{ erg/s}, \quad (\text{B.3.5})$$

which amply justifies the steady X-ray emission of 1E 2259+586 (see Table B.9).

A further development for the source 1E 2259+586, came from Usov (1994), who introduced the possibility in a white dwarf close to the critical mass limit, to observe sudden changes in the period of rotation, namely glitches.

When the rotation of the white dwarf slows down, centrifugal forces of the core decrease and gravity pulls it to a less oblate shape thereby stressing it. The release of such stresses leads to a sudden decrease of moment of inertia and correspondingly, by conservation of angular momentum

$$J = I\Omega = (I + \Delta I)(\Omega + \Delta\Omega) = \text{constant}, \quad (\text{B.3.6})$$

to a shortening of the rotational period

$$\frac{\Delta I}{I} = \frac{\Delta P}{P} = -\frac{\Delta\Omega}{\Omega}, \quad (\text{B.3.7})$$

leading to a gain of rotational energy in the spin-up process of the glitch

$$\Delta E_{\text{rot}}^{\text{WD}} = -\frac{2\pi^2 I}{P^2} \frac{\Delta P}{P} = -1.98 \times 10^{50} \frac{\Delta P}{P^3} \text{ erg}, \quad (\text{B.3.8})$$

which is then released in the burst activity on the time scales from months to years (see e.g. Fig. B.14).

For the evolution of the period close to a glitch we follow the parameterization by Manchester and Taylor (1977). The angular velocity $\Omega = 2\pi/P$, since the glitch time $t = t_g$, until the complete or partial recovery, can be described as

$$\Omega = \Omega_0(t) + \Delta\Omega[1 - Q(1 - e^{-(t-t_g)/\tau_d})], \quad (\text{B.3.9})$$

where $\Omega_0(t) = \Omega_0 + \dot{\Omega}(t - t_g)$ is the normal evolution of the frequency in absence of glitch, being Ω_0 the frequency prior to the glitch, $\Delta\Omega = -2\pi\Delta P/P^2$ is the initial frequency jump, which can be decomposed in the persistent and decayed parts, $\Delta\Omega_p$ and $\Delta\Omega_d$ respectively, τ_d is the timescale of the exponential decay of the frequency after the glitch and $Q = \Delta\Omega_d/\Delta\Omega = 1 - \Delta\Omega_p/\Delta\Omega$ is the recovery fraction or “healing parameter”. For full recovery we have $Q = 1$, $\Omega(t \gg \tau_d) = \Omega_0$, and for zero recovery $Q = 0$, $\Omega(t \gg \tau_d) = \Omega_0(t) + \Delta\Omega$. For simplicity we assume in the following and especially below in Sec. B.3.6, complete recovery $Q = 1$.

This mechanism in white dwarfs is similar, although simpler, than the one used to explain e.g. glitches in ordinary pulsars (see e.g. Baym and Pines, 1971; Shapiro and Teukolsky, 1983). The essential difference is that neutron stars are composed by a superfluid core and a solid crust, being the latter the place where starquakes can originate leading to glitches. A two-component description is then needed, see e.g. Shapiro and Teukolsky (1983). In the present case of a massive rotating white dwarf, such a two-component structure does not exist and the white dwarf behaves as a single solid system. What is important to stress is that the rotational energy released for $Q \geq 1$ is largely sufficient for the explanation of the bursting phenomena, see Sec. B.3.6 for details.

The crystallization temperature of a white dwarf composed of nuclei (Z, A) and mean density $\bar{\rho}$ is given by (see e.g. Shapiro and Teukolsky, 1983; Usov, 1994)

$$T_{\text{cry}} \simeq 2.28 \times 10^5 \frac{Z^2}{A^{1/3}} \left(\frac{\bar{\rho}}{10^6 \text{g/cm}^3} \right)^{1/3} \text{ K}. \quad (\text{B.3.10})$$

Thus, assuming an internal white dwarf temperature $\sim 10^7$ K we find that the mean density for the crystallization of the white dwarf should be $\sim 2.2 \times 10^7 \text{ g/cm}^3$ for ^{12}C , $\sim 5.2 \times 10^6 \text{ g/cm}^3$ for ^{16}O and $\sim 1.25 \times 10^6 \text{ g/cm}^3$ for ^{56}Fe . Very massive white dwarfs as the ones we are considering here have mean densities $\sim 10^9 \text{ g/cm}^3$ and therefore a considerable fraction of their size should be in principle solid at these high temperatures (see also Althaus et al., 2005, 2007). It is worth to mention that, the phase separation of the constituents of CO white dwarfs, theoretically expected to occur in the crystallization process (see Garcia-Berro et al., 1988, for details), has been recently observationally confirmed solving the puzzle of the age discrepancy of the open cluster NGC 6791 (García-Berro et al., 2010a).

Under these physical conditions, starquakes leading to glitches in the white

dwarf may occur with a recurrence time (see e.g. Baym and Pines, 1971; Usov, 1994)

$$\delta t_q = \frac{2D^2 |\Delta P|/P}{B |\dot{E}_{\text{rot}}|}, \quad (\text{B.3.11})$$

where \dot{E}_{rot} is the loss of rotational energy (B.3.5), $D = (3/25) GM_c^2/R_c$, $B = 0.33 (4\pi/3) R_c^3 e^2 Z^2 [\bar{\rho}_c / (Am_p)]^{4/3}$, M_c , R_c and $\bar{\rho}_c$ are the mass, the radius and the mean density of the solid core, and m_p is the proton mass.

For the specific case of 1E 2259+586, Usov predicted the possible existence of changes of period $\Delta P/P \approx -(1-3) \times 10^{-6}$ with a recurrence time between cracks $\delta t_q \approx 7 \times 10^6 |\Delta P|/P \text{ yr} \approx$ a few times (1–10) yr. It is impressive that in 2002 indeed changes of the order of $\Delta P/P \approx -4 \times 10^{-6}$ were observed in 1E 2259+586 (Kaspi et al., 2003; Woods et al., 2004) (see Fig. B.14 for details).

Our aim in the following is to show that this model can be also applied to the other SGRs and AXPs. Their entire energetics is explained by the rotational energy loss of fast rotating magnetized white dwarfs: 1) the X-ray luminosity is well below the rotational energy loss of the white dwarf (see Fig. B.15); 2) in all cases the large magnetic field is well below the critical field for vacuum polarization (see Fig. B.16 and Table B.9); 3) the energetics of all the bursts can be simply related to the change of rotational energy implied by the observed change of rotational period (see Fig. B.17, Sec. B.3.5 and Table B.8).

B.3.3. SGRs and AXPs within the magnetar model

Let us turn to the alternative model commonly addressed as “magnetar” (see e.g. Duncan and Thompson, 1992; Thompson and Duncan, 1995) based on an ultramagnetized neutron star of $M = 1.4M_\odot$ and $R = 10 \text{ km}$ and then $I \approx 10^{45} \text{ g cm}^2$ as the source of SGRs and AXPs. The limit of the magnetic field obtained from Eq. (B.3.3) becomes

$$B = 3.2 \times 10^{19} (P\dot{P})^{1/2} \text{ G}, \quad (\text{B.3.12})$$

which is four orders of magnitude larger than the surface magnetic field within the fast rotating magnetized white dwarf model (see Fig. B.18).

There are innumerable papers dedicated to this model and for a review covering more than 250 references on the subject see Mereghetti (2008). The crucial point is that in this model there is no role of the rotational energy of the source: the X-ray luminosity is much bigger than the loss of rotational energy of the neutron star (see Fig. B.19).

Paradoxically, although the bursts appear to be correlated to the presence of glitches in the rotational period, the corresponding increase of change of

rotational energy of the neutron star

$$\Delta E_{\text{rot}}^{\text{NS}} = -\frac{2\pi^2 I \Delta P}{P^2} \frac{\Delta P}{P} = -1.98 \times 10^{46} \frac{\Delta P}{P^3} \text{ erg}, \quad (\text{B.3.13})$$

cannot explain the burst energetic $\sim (10^{44}\text{--}10^{47})$ erg. This is a clear major difference between the two models based respectively on neutron stars and white dwarfs (see Figs. B.17 and B.20 for details).

In magnetars, the value of the rotational period and its first time derivative are only used to establish an upper limit to the magnetic field of the neutron star. In view of the smallness of the moment of inertia of a neutron star with respect to the moment of inertia of a white dwarf, the magnetic field reaches in many cases outstandingly large values $B \gg B_c \sim 4.4 \times 10^{13}$ G, from here the name magnetars (see Fig. B.18). The attempt has been proposed by Duncan and Thompson (1992) and Thompson and Duncan (1995) to assume a new energy source in physics and astrophysics: the magnetic energy in bulk. The role of thermonuclear energy has been well established by physics experiments on the ground as well as in astrophysics in the explanation of the energetics, life time, and build-up process of the nuclear elements in main sequence stars (see e.g. Bethe, 1968, and references therein); equally well established has been the role of rotational energy in pulsars (see e.g. Hewish, 1974; Bell and Hewish, 1967, and references therein); similarly well established has been the role of gravitational energy in accretion process into neutron stars and black holes and binary X-ray sources (see e.g. Giacconi, 2002; Giacconi and Ruffini, 1978 Reprinted 2010, and references therein). In the magnetars instead, it is introduced an alternative primary energy source not yet tested neither in the laboratory (the case of magnetic monopoles) nor in astrophysics: a primary energy source due to overcritical magnetic fields.

The mostly qualitative considerations in the magnetar model can be summarized, see e.g. Ng et al. (2010): in the twisted magnetosphere model of magnetars (Thompson et al., 2002), the observed X-ray luminosity of a magnetar is determined both by its surface temperature and by magnetospheric currents, the latter due to the twisted dipolar field structure. The surface temperature in turn is determined by the energy output from within the star due to magnetic field decay, as well as on the nature of the atmosphere and the stellar magnetic field strength. This surface thermal emission is resonantly scattered by the current particles, thus resulting in an overall spectrum similar to a Comptonized blackbody (e.g. Lyutikov and Gavriil, 2006; Rea et al., 2008; Zane et al., 2009). In addition, the surface heating by return currents is believed to contribute substantially to L_X , at least at the same level as the thermal component induced from the interior field decay (Thompson et al., 2002). Magnetar outbursts in this picture occur with sudden increases in twist angle, consistent with the generic hardening of magnetar spectra during outbursts (e.g. Kaspi et al., 2003; Woods et al., 2004; Israel et al., 2007).

It is worth to recall that magnetic field configurations corresponding to a dipole twisted field have been routinely adopted in rotating neutron stars (see e.g. Cohen et al., 1973). Magnetic field annihilation and reconnection have been analogously adopted in solar physics (see e.g. Parker, 1957; Sweet, 1958) and also magnetic instabilities have been routinely studied in Tokamak (see e.g. Coppi et al., 1976). These effects certainly occur in magnetized white dwarfs. What is important to stress here is that in none of these systems the magnetic field has been assumed to be the primary energy source of the phenomena, unlike in magnetars.

It is appropriate to recall just a few of the difficulties of the magnetar model in fitting observations, in addition to the main one of SGR 0418+5729 addressed in this article. In particular, e.g.: (1) as recalled by S. Mereghetti 2008, “up to now, attempts to estimate the magnetic field strength through the measurement of cyclotron resonance features, as successfully done for accreting pulsars, have been inconclusive”; (2) the prediction of the high-energy gamma ray emission expected in the magnetars has been found to be inconsistent with the recent observation of the Fermi satellite (see e.g. Tong et al., 2010, 2011); (3) finally, it has been shown to be not viable the attempt to relate magnetars to the energy of the supernova remnants (see e.g. Allen and Horvath, 2004; Ferrario and Wickramasinghe, 2006; Vink and Kuiper, 2006; Vink, 2008) or to the formation of black holes (see e.g. Kasen and Bildsten (2010); Woosley (2010), see however e.g. Patnaude et al. (2009)) and of Gamma Ray Bursts (see e.g. Levan et al. (2006); Castro-Tirado et al. (2008); Stefanescu et al. (2008); Bernardini et al. (2009), see however e.g. Goldstein et al. (2011); Rea et al. (2011)).

In Table B.9 we compare and contrast the parameters of selected SGRs and AXPs sources in the magnetar model and in the fast rotating highly magnetized white dwarf model: the larger radius of a white dwarf with respect to the radius of a neutron star of the same mass $M = 1.4M_{\odot}$, leads to the two models differing on the scale of mass density, moment of inertia, and rotational energy which imply a different scale for the surface magnetic fields, leading to a very different physical interpretation of the observations of SGRs and AXPs.

B.3.4. Observations of massive fast rotating highly magnetized white dwarfs

Some general considerations are appropriate. The white dwarf model appeals to standard and well tested aspects of physics and astrophysics. The observation of fast rotating white dwarfs with magnetic fields larger than 10^6 G all the way up to 10^9 G has been in the mean time solidly confirmed by observations (see e.g. Angel et al., 1981; Ferrario et al., 1997; Należyty and Madej, 2004; Ferrario and Wickramasinghe, 2005; Terada et al., 2008c). For a

recent and extensive analysis of the magnetic field structure of highly magnetized white dwarfs see Külebi et al. (2009) and for a catalog of them see Külebi et al. (2010a) and also Kepler et al. (2010).

A specific example is the highly magnetized white dwarf AE Aquarii. The rotational period of this fast rotating magnetized white dwarf obtained from the sinusoidal pulsed flux in soft X-rays < 4 keV (see e.g. Eracleous et al., 1991; Choi and Dotani, 2006) has been established to be $P = 33$ s and it is spinning down at a rate $\dot{P} = 5.64 \times 10^{-14}$. The mass of the white dwarf is $\sim M_{\odot}$ (de Jager et al., 1994) and the observed temperature is $kT \sim 0.5$ keV. In addition to the soft X-ray component, hard X-ray pulsations were observed with the Japanese satellite Suzaku in October–November 2005 and October 2006. The luminosity of AE Aquarii $\sim 10^{31}$ erg/s accounts for the 0.09% of the spin-down energy of the white dwarf (see Terada et al., 2008c, for details) and the inferred magnetic field of the source is $B \sim 10^8$ G (Ikhsanov and Beskrovnaya, 2008).

This white dwarf is one of the most powerful particle accelerators: there is at least one event of detected TeV emission from this source during its optical flaring activity monitored between 1988 and 1992 (see e.g. Meintjes et al., 1992, 1993; de Jager et al., 1994; Ikhsanov and Biermann, 2006; Ikhsanov and Beskrovnaya, 2008; Kashiyama et al., 2011). In addition, it shows burst activity in X-rays (Terada et al., 2008c). Although AE Aquarii is a binary system with orbital period ~ 9.88 hr (see de Jager et al., 1994, e.g.), very likely the power due to accretion of matter is inhibited by the fast rotation of the white dwarf (e.g. Itoh et al., 2006; Terada et al., 2008c).

Many of the observed physical properties of this white dwarf are very similar to the recently discovered SGR 0418+5729, as we explicitly show in Table B.7.

Although very fast, AE Aquarii is not the fastest white dwarf observed. The rotational period obtained from the pulsed X-ray emission of RXJ 0648.0-4418, the white dwarf in the binary system HD49798/RXJ 0648.0-4418, is $P = 13.2$ s (Israel et al., 1997). This white dwarf is one of the most massive white dwarfs with $M = 1.28 \pm 0.05 M_{\odot}$ (see Mereghetti et al., 2009, for details). Other very massive and highly magnetized white dwarfs are: REJ 0317-853 with $M \sim 1.35 M_{\odot}$ and $B \sim (1.7\text{--}6.6) \times 10^8$ G (see e.g. Barstow et al., 1995; Külebi et al., 2010b); PG 1658+441 with $M \sim 1.31 M_{\odot}$ and $B \sim 2.3 \times 10^6$ G (see e.g. Liebert et al., 1983; Schmidt et al., 1992); and PG 1031+234 with the highest magnetic field $\sim 10^9$ G (see e.g. Schmidt et al., 1986; Külebi et al., 2009). It is interesting to note that the most highly magnetized white dwarfs are massive as well as isolated (see e.g. Należyty and Madej, 2004, for details).

	SGR 0418+5729	AE Aquarii
P (s)	9.08	33.08
\dot{P} (10^{-14})	< 0.6	5.64
Age (Myr)	24	9.4
L_X (erg/s)	6.2×10^{31}	$\sim 10^{31}$
kT (keV)	0.67	0.5
B (G)	$< 7.45 \times 10^8$	$\sim 10^8$
Pulsed Fraction	0.3	$\sim 0.2-0.3$

Table B.7.: Comparison of the observational properties of SGR 0418+5729 and the white dwarf AE Aquarii. For SGR 0418+5729 P , \dot{P} , and L_X have been taken from Rea et al. (2010). The characteristic age is given by $\text{Age} = P/(2\dot{P})$ and the surface magnetic field B is given by Eq. (B.3.4). The pulsed fraction of SGR 0418+5729 is taken from Esposito et al. (2010) and the one of the white dwarf AE Aquarii from Eracleous et al. (1991) and Choi and Dotani (2006).

B.3.5. Rotational instability of white dwarfs

In order to be stable against secular instability of the MacClaurin versus the Jacobi ellipsoid (Ferrari and Ruffini, 1969), the minimal period of a white dwarf with the parameters discussed here is $P_{\text{crit}} \sim 0.94$ s. For $P \lesssim P_{\text{crit}}$ we would expect very significant emission of gravitational waves due to the transition from the triaxial Jacobi ellipsoids to the axially symmetric MacClaurin ellipsoids. This is well in agreement and explains the observed long periods of SGRs and AXPs $\gtrsim 2$ s (see Fig. B.21). In the specific case of the source 1E 2259+586, assuming that the supernova remnant G109.1-1.0 and 1E 2259+586 are coeval, we obtain the initial rotational period of the white dwarf in the range $0.94 \text{ s} < P_0 < 6.8 \text{ s}$ where, the lower limit, is given by the bifurcation point between MacClaurin spheroids and Jacobi ellipsoids (see e.g. Ferrari and Ruffini, 1969) and, the upper limit, is obtained for a constant value of \dot{P} . Describing today 1E 2259+586 by a MacClaurin spheroid, we obtain the ratio between the rotational energy and the gravitational energy $E_{\text{rot}}/|E_{\text{grav}}| \sim 0.011$ (see Fig. B.21), well below the secular instability ~ 0.14 and the dynamical instability ~ 0.25 (see Chandrasekhar, 1969; Shapiro and Teukolsky, 1983, for details).

The above considerations add interest in the recent theoretical analysis of white dwarfs taking into account nuclear, weak and electromagnetic interactions within a general relativistic treatment (Rotondo et al., 2011b). A specially relevant result has been recently obtained (Boshkayev et al., 2011) by analyzing a white dwarf endowed with mass, angular momentum, and quadrupole moment within the Hartle-Thorne formalism (Hartle, 1967b; Har-

tle and Thorne, 1968b). The rotating white dwarfs have been studied for the new equation of state given by Rotondo et al. (2011c) used for the construction of the non-rotating configurations by Rotondo et al. (2011b). The critical rotational periods for the onset of the axisymmetric, the mass-shedding and the inverse β -decay instabilities have been studied in detail. The exact value of the critical period of a white dwarf depends upon the central density of the configuration; rotationally stable white dwarfs exist for rotational periods $P > P_{\min}^{\text{WD}} \sim 0.3$ s. The shortest values for configurations supported by rotation with critical masses larger than the classical Chandrasekhar limit for non-rotating white dwarfs all the way up to $M_{\max} \sim 1.5M_{\odot}$ (see Boshkayev et al., 2011, for details).

Consequently, also the fastest sources e.g. 1E 1547.0-5408 with $P = 2.07$ s, SGR 1627-41 with $P = 2.59$ s, and PSR J 1622-4950 with $P = 4.33$ s, can be safely described as massive fast rotating white dwarfs as shown in Fig. B.15.

B.3.6. Glitches and outbursts in SGRs and AXPs

The energetic of the observed bursts within the white dwarf model of SGRs and AXPs can be fully explained by the observed change of period $\Delta P < 0$ (glitches). In the case of the famous event of 5th March 1979 in the SGR 0526-66 ($P = 8.05$ s), a fractional change of period of the white dwarf $\Delta P/P \sim -10^{-4}$ (see Fig. B.17) would be sufficient to explain the energetics $\sim 3.6 \times 10^{44}$ erg (Mereghetti, 2008). Unfortunately, such a change of period could not be observed at the time (see e.g. Mazets et al., 1979), lacking the observations of the source prior to the event. Instead, in the case of the flares of 1E 2259+586 on June 2002 ($P = 6.98$ s) and of 1E 1048.1-5937 ($P = 6.45$ s) on March 2007, observational data are available. For 1E 2259+586, using the observed fractional change of period $\Delta P/P \sim -4 \times 10^{-6}$ (Woods et al., 2004) (see also Fig. B.14), we obtain within the white dwarf model a change of rotational energy $|\Delta E_{\text{rot}}^{\text{WD}}| \sim 1.7 \times 10^{43}$ erg, to be compared with the measured energy released during the event $\sim 3 \times 10^{41}$ erg. For the glitch on the 26th March 2007 in 1E 1048.1-5937 with observed $\Delta P/P \sim -1.63 \times 10^{-5}$, we obtain $|\Delta E_{\text{rot}}^{\text{WD}}| \sim 7.73 \times 10^{43}$ erg which is strikingly in agreement (and safely superior) with the observed energy released in the event 4.3×10^{42} erg (see e.g. Dib et al., 2009). In the case of super giant flares, there is no clear observational evidence of their association to glitches. However, changes in the moment of inertia of the white dwarf originating fractional changes of period of order $\Delta P/P \sim -(10^{-5} - 10^{-3})$ (see Fig. B.17) could explain their large energetics ranging from 10^{44} erg all the way up to 10^{47} erg (see e.g. Mereghetti, 2008). For the giant flare of SGR 1806-20 on 27th December 2004 (see e.g. Borkowski et al., 2004; Hurley et al., 2005) with observed energy $\sim 10^{46}$ erg there is a gap of timing data of the source between October 2004 and March 2005 (see Mereghetti et al., 2005; Tiengo et al., 2005). The observed rotational period of

	SGR 0526-66	1E 2259+586	1E 1048.1-5937	SGR 1806-20
Date	March 1979	June 2002	March 2007	December 2004
Observed Energy (erg)	3.6×10^{44}	3×10^{41}	4.2×10^{42}	$\sim 10^{46}$
$ \Delta P /P$	1.2×10^{-4} (predicted)	4.24×10^{-6} (observed)	1.63×10^{-5} (observed)	3×10^{-3} (predicted)
Predicted Energy (erg)	3.6×10^{44}	1.7×10^{43}	7.7×10^{43}	$\sim 10^{46}$

Table B.8.: Glitches and Outbursts of some SGRs and AXPs within the white dwarf model. The predicted values of $|\Delta P|/P$ are calculated with Eq. (B.3.8) assuming $|\Delta E_{\text{rot}}^{\text{WD}}|$ equals the observed energy of the burst event. The predicted values of the energy released in the burst event is calculated with Eq. (B.3.8) using the observed fractional change of rotational period $|\Delta P|/P$.

SGR 1806-20 after March 2005 is not consistent with the expected rotational period obtained from the spin-down rate $\dot{P} = 5.5 \times 10^{-10}$; instead, this is consistent with $\dot{P} = 1.8 \times 10^{-10}$. The change of rotational period has been attributed to “global reconfigurations of the neutron star magnetosphere” (see e.g. Tiengo et al., 2005). Within the white dwarf model, such a burst activity is consistent with a glitch with fractional change of period $\sim -3 \times 10^{-3}$. All the above discussion is summarized in Table B.8 and Figs. B.14 and B.17.

In all the above cases the gain of rotational energy in the glitch is much larger than the energy observed in the flaring activities following the glitches. This means that there is ample room to explain these glitch-outburst events in a large range of recovery fractions Q . It appears to be appropriate to systematically monitor the Q factors for all the glitches in SGRs and AXPs.

It is interesting that PSR J1846-0258, $P = 0.3$ s, experienced in June 2006 a radiative event with estimated isotropic energy $\sim (3.8\text{--}4.8) \times 10^{41}$ erg (Kumar and Safi-Harb, 2008). Assuming that such an event was triggered by a glitch in the neutron star one obtains an associated fractional change of period $\Delta P/P \sim -(1.73\text{--}2.2) \times 10^{-6}$, as given by Eq. (B.3.13). Indeed, as shown by Kuiper and Hermsen (2009), the outburst emission was accompanied by a large glitch $\Delta P/P \sim -(2.0\text{--}4.4) \times 10^{-6}$ in perfect agreement with the theoretical prediction given by the loss of rotational power after the spin-up of the neutron star without advocate any magnetar phenomena. This fact reinforces the idea that PSR J1846-0258 is not a magnetar but an ordinary rotationally powered neutron star, also in line with the recent suggestions by Kuiper and Hermsen (2009) and Rea et al. (2010).

B.3.7. Magnetosphere emission from white dwarfs

We return now to the structure of the magnetosphere of the white dwarf model for SGRs and AXPs. In order to have an agreement between the observed X-ray luminosity and the X-ray spectral distribution, it is necessary that only a part of the surface of the white dwarf has to be X-ray emitter.

We can define the dimensionless filling factor

$$\mathcal{R} = \frac{L_X}{4\pi R^2 \sigma T^4}, \quad (\text{B.3.14})$$

where σ is the Stefan-Boltzmann constant and T the temperature of the source. This factor gives an estimate of the effective area of X-ray emission and consequently information about the structure of the magnetic field from the surface of the object. It is interesting that this factor for the white dwarf is in the range 10^{-6} – 10^{-5} (see Table B.9), quite similar to the one of the Sun $\mathcal{R}_\odot = L_\odot^X / (4\pi R_\odot^2 \sigma T_\odot^4) \approx (7.03 \times 10^{-8} - 1.2 \times 10^{-6})$ in the minimum $L_\odot^X = 2.7 \times 10^{26}$ erg/s and in the maximum $L_\odot^X = 4.7 \times 10^{27}$ erg/s of solar activity respectively (see e.g. Peres et al., 2000; Judge et al., 2003). This should be expected by the general argument of the conservation of flux in the transition from a highly magnetized main sequence star to a white dwarf. The magnetic field of the order of $\sim 10^9$ G on the surface of these white dwarfs must clearly have a filamentary structure in the range $\mathcal{R} \sim 10^{-6}$ – 10^{-5} .

In the specific case of SGR 0418+572 such an \mathcal{R} factor is $\sim 10^{-9}$, which is of the same order as the one of the white dwarf AE Aquarii, as can be seen from Table B.7 by comparing the values of L_X and KT , which are the quantities involved in Eq. (B.3.14).

At times the presence of an \mathcal{R} factor has been interpreted as originating from a spot-like radial emission of the radiation from the surface of the white dwarf. If one were to assume that the radiation occurs radially beamed and occurring just from the surface either of the neutron star or the white dwarf, a spot radiation would lead to a pulsed fraction of the emission flux determined by $\sqrt{1/n \sum_{i=1}^n (y_i - \bar{y})^2} / \bar{y} \sim 1$, where n is the number of phase bins per cycle, y_i is the number of counts in the i th phase bin and \bar{y} is the mean number of counts in the cycle (see e.g. Esposito et al., 2010, for details about this definition). This problem, which seems to be in contradiction with the observations of pulsed fractions < 1 in SGRs and AXPs (see e.g. Esposito et al., 2010), would be equally severe both for neutron stars and white dwarfs (see e.g. Table B.7).

It is appropriate to recall that all the SGRs and AXPs within a rotating white dwarf model have magnetic fields in the range $10^8 \text{ G} \lesssim B \lesssim 10^{11} \text{ G}$ (see Table B.9). It is quite natural to assume that the X-ray emission be linked to the presence of the magnetic field. It is worth to note that the modeling of the physics and the geometrical structure of the magnetic field and of the magnetospheres is a most active field of current research. As shown by Romani and Watters (2010), the morphology of the pulses as well as of the light curves strongly depend on many model parameters, e.g. special and general relativistic effects, the viewing angle, the magnetic moment-spin axis angle, the spin axis-line of sight angle, the specific location of the emission zone, and the adopted magnetospheric model including possible corrections

due to deviations from a pure dipolar structure.

From the broad sinusoidal pulsed flux of SGRs/AXPs (see e.g. Mereghetti, 2008), we know that the pulsed fraction is less than one and that the luminosity differs remarkably from a spiky one. We find then natural to assume that the emission comes from an area covering the white dwarf surface with a very marked filamentary structure. Similar considerations for neutron stars magnetospheres have been purported e.g. by Michel and Dessler (1981); Michel (1983) giving evidence of magnetospheric activity from the pole all the way up to the equator; see also the most interesting case of the pair production activities in the magnetosphere of a rotating white dwarf considered for the transient radio source GCRT J1745–3009 by Zhang and Gil (2005). Moreover, such structures are regularly observed in the Sun and in the Earth Aurora. Explicit sinusoidal pulsed flux in soft X-rays (< 4 keV) have been observed in AE Aquarii (see e.g. Eracleous et al., 1991; Choi and Dotani, 2006); and see also Fig. 6 in Mereghetti et al. (2011) for similar sinusoidal pulsed emission of the white dwarf RXJ 0648.0-4418 with rotational period $P = 13.2$ s. For all the above sources, a filamentary structure of the magnetic field is clearly expected.

We do not discuss here the issue of the spectral features within the white dwarf model. The aim of this article is just to point out that all these problems can be address with merit starting from the rotational energy of a rotating white dwarf rather than the magnetic energy of a magnetar. The spectrum of the persistent emission of SGRs and AXPs for energies < 10 keV is well fitted either by the superposition of a blackbody and a high energy tail or by a single blackbody or a double blackbody (see e.g. Mereghetti, 2008). Such a spectral feature is clearly already evidenced for rotating white dwarfs; following the work of Terada et al. (2008c): in addition to the thermal modulation in the softer X-ray band, spiky pulsations like the ones of pulsars have been observed by the Suzaku satellite in the hard X-ray band of over 4 keV in the white dwarf AE Aquarii. The X-ray spectrum requires an additional hard X-ray component on the well-known thermal emissions with temperatures of 0.5 and 2.9 keV. Combined with results from timing analyses, spectral shapes and flux, it was there concluded that the hard X-ray pulsations should have a non-thermal origin, for example, possible Synchrotron emission with sub MeV electrons. The claim of the first discovery of a white dwarf equivalent to a neutron star pulsar was there made. In view of the possible evidence of very high energy emission in the TeV region observed during the optical flares of AE Aquarii (see e.g. de Jager et al., 1994; Ikhsanov and Biermann, 2006; Ikhsanov and Beskrovnyaya, 2008; Terada et al., 2008c,d; Kashiyama et al., 2011, and references therein), it would be important to have observations by INTEGRAL and Fermi of rotating magnetized white dwarf in the 20-200 keV band in order to establish further analogies between fast rotating highly magnetized white dwarfs and magnetar candidates.

More specifically, for the source SGR 0418+5729 and its interpretation as

a white dwarf, a crucial result has been recently obtained by Durant et al. (2011). We first recall the observed range of temperatures of massive isolated white dwarfs $1.14 \times 10^4 \text{ K} \leq T \leq 5.52 \times 10^4 \text{ K}$; see Table 1 in (Ferrario et al., 2005). From the broad band Hubble Space Telescope imaging of the field of SGR 0418+5729, the upper limits of the black body surface temperature, $T < 3.14 \times 10^4 \text{ K}$ and $T < 1.18 \times 10^4 \text{ K}$ in the F110W and F606W filters, can be established for a radius $R = 10^8 \text{ cm}$. In this respect is also worth to recall the optical observations of AXP 4U0142+61 of Hulleman et al. (2000). The photometric results of the field of 4U0142+61 at the 60-inch telescope on Palomar Mountain are in agreement with a $1.3M_{\odot}$ white dwarf with a surface temperature $\sim 4 \times 10^5 \text{ K}$ (see Hulleman et al., 2000, for details). These results are therefore fully consistent with the SGR/AXP white dwarf model, and follow-on missions of Hubble and VLT are strongly recommended.

B.3.8. The connection with supernova remnants

We would like to address the special issue of the supernova remnants energetics and their association with SGRs and AXPs. A firm association between SGRs/AXPs and supernovae have been purported by Gaensler et al. (2001) in the cases 1E 1841–045 (SNR G27.4+0.0, Kes 73), AX J1845.0–0258 (SNR G29.6+0.1), and 1E 2259+586 (SNR G109.1–1.0, CTB 109). See also Gelfand and Gaensler (2007) for the possible association 1E 1547.0-5408 (SNR G327.24-0.13). What is of interest for us here is the special issue of the energetics of the supernova remnant and the present of an SGR or an AXP.

Paczynski, in the case of AXP 1E 2259+586, attempted to explain the supernova remnant by assuming a merger of a binary system of ordinary white dwarf of mass $\sim (0.7-1)M_{\odot}$ based on models by Iben and Tutukov (1984) and Paczynski (1985) leading both to the formation of a fast rotating white dwarf and to the supernova remnant. Recent simulations of white dwarf-white dwarf mergers (see e.g. Pakmor et al., 2010) point that mergers of $(0.8-0.9M_{\odot})$ produce supernova events generally not very efficient energetically, well below the observed explosion energy $\sim 7.4 \times 10^{50} \text{ erg}$ of the supernova remnant G109.1-1.0 associated to 1E 2259+586 (see e.g. Sasaki et al., 2004).

In the intervening years much more has been understood on the process of gravitational collapse and on the composition of the material surrounding neutron stars and black holes both from pulsar observations and Gamma Ray Bursts. Fascinating evidence for the presence of planets around pulsars in supernova remnants has been established (see e.g. Konacki et al., 1999; Hansen, 2002; Konacki and Wolszczan, 2003). Similarly, the presence of many body process of gravitational collapse has been evidenced for Gamma Ray Bursts (see e.g. Ruffini, 2009).

In view of the above, we advance the possible scenario in which the SGRs/AXPs and the supernova remnant originate from a very close binary system com-

posed of a white dwarf and a companion late evolved star, close to the process of gravitational collapse. The collapse of the companion star, either to a neutron star or to a black hole, leads to mass loss which can unbind the original binary system. Three possible cases can occur (see e.g. Ruffini, 1973): 1) if the loss of mass in the supernova explosion is $M_{\text{loss}} < M/2$, being M the total mass of the binary, the system holds bound; 2) if $M_{\text{loss}} \sim M/2$ then the system becomes unbound and the white dwarf is expelled at nearly orbital motion velocity; and 3) if $M_{\text{loss}} \gg M/2$ the white dwarf is kicked out with very high runaway velocities. Only in the first case the object will lie at the center of the supernova remnant. For a review on the evolution of binary systems see Stairs (2004) and for a detailed treatment of the problem of runaway velocities from supernova explosions see Tauris and Bailes (1996); Tauris and Takens (1998). The white dwarf in this picture does not participate either to the gravitational collapse nor to the formation of the supernova remnant: it can have a period and a life time determine essentially by the prior evolution of the binary system. This explains the disagreement between the age of the supernova remnant and the characteristic age of the SGR/AXP when inferred by a neutron star model. In the case of large kick velocities the runaway white dwarf can collide with the surrounding material in the supernova remnant and very likely also with planets. Such collisions may well originate changes in the moment of inertia of the white dwarf, consequently in its rotational period, leading to glitches and burst activity.

In the above context it is appropriate to recall the pioneering work of Katz (1996) on explaining the super-Eddington luminosities in the flaring episodes of SGRs and AXPs as originating in accretion process of planetary fragments, in particular, the important role of magnetic confinement of an e^+e^- pair plasma. The model explains the observed self-absorbed thermal spectrum of flares and their nearly independence on their luminosity. Katz (1996) has shown that the infall of planetary fragments may lead to a continuous injection of energy to the magnetosphere which leads to magnetic confinement of the source if the magnetic field satisfies

$$B > \sqrt{\frac{2L}{cR^2}} = 2.6 \times 10^7 \sqrt{\frac{L_{41}}{R_8^2}} \text{ G}, \quad (\text{B.3.15})$$

where L_{41} is the luminosity in units of 10^{41} erg/s and R_8 is the radius of the source in units of 10^8 cm.

In the case when the radiation is not being continuously resupplied, but it is initially contained within the volume $\sim 4\pi R^3/3$, the minimum magnetic field for confinement is given by

$$B > \sqrt{\frac{6L\tau}{R^3}} = 2.45 \times 10^8 \sqrt{\frac{L_{41}\tau_{0.1}}{R_8^3}} \text{ G}, \quad (\text{B.3.16})$$

where $\tau_{0.1}$ is the time τ during which the source is radiating at a luminosity L , in units of 0.1 s. The fiducial values for L and for τ has been chosen here to be typical of the bursting activity of SGRs/AXPs (see e.g. Mereghetti, 2008). The above two bounds for the magnetic field are indeed in line with the surface magnetic fields obtained in this paper; see Fig. B.16 for details. Thus, the super-Eddington luminosities observed in the outbursts can be well explained within the white dwarf model and there is no need of introducing the huge magnetic fields of the magnetar model (Paczynski, 1992; Thompson and Duncan, 1995).

B.3.9. On the fiducial neutron star and white dwarf parameters in light of recent theoretical progress

Before concluding, we would like to introduce a word of caution on the fiducial values adopted both for the neutron star and the white dwarf in the above Sections. In the intervening years much more have been learned on the equation of state and on a more complex description of the structure parameters of both white dwarfs and neutron stars.

The equations of equilibrium of neutron stars, traditionally based on the Tolman-Oppenheimer-Volkoff equations, have been superseded by an alternative formulation based on the general relativistic Thomas-Fermi conditions of equilibrium within the Einstein-Maxwell equations Rueda et al. (2011). Correspondingly, the above values of $\sqrt{I/R^6}$ in Eq. (B.3.3) estimated in the fiducial parameters, leading to Eq. (B.3.12), can acquire in fact values in the range $0.44 \lesssim \sqrt{I/R^6} / \sqrt{I_f/R_f^6} \lesssim 0.56$, where the subscript ‘f’ stands for fiducial parameter. This range corresponds to the range of masses $0.5 \lesssim M/M_\odot \lesssim 2.6$ (Belvedere et al., 2011). Correspondingly, the magnetic field is in the range $0.44 \lesssim B/B_f^{\text{NS}} \lesssim 0.56$, where B_f^{NS} is given by Eq. (B.3.12).

Similar considerations apply for the white dwarf case. General relativistic white dwarfs taking into account nuclear, weak and electromagnetic interactions have been recently constructed (Rotondo et al., 2011b) following the new equation of state for compressed nuclear matter given by Rotondo et al. (2011c). The case of rotating white dwarfs in general relativity has been studied by Boshkayev et al. (2011). It has been found that white dwarfs can be as fast as $P_{\text{min}}^{\text{WD}} \sim 0.3$ s and as massive as $M_{\text{max}} \sim 1.5M_\odot$; see Sec. B.3.5 for details. For example, a white dwarf of $M = 1.44M_\odot$ rotating with period $P = 3.2$ s, will have an equatorial radius $R_{\text{eq}} \sim 3604$ km, polar radius $R_p \sim 2664$ km, and moment of inertia $I \sim 2.9 \times 10^{49}$ g cm². In this case we will have $\sqrt{I/R^6} / \sqrt{I_f/R_f^6} \sim 0.01$ and therefore $B/B_f^{\text{WD}} \sim 0.01$ where B_f^{WD} is given by Eq. (B.3.4).

This issue is particularly relevant to the study of the four sources in Fig. B.19. These sources can be definitely explained within a unified framework of ro-

tating white dwarfs with all the other SGRs and AXPs. In view of the parameters recently obtained they may be also interpreted as regular neutron stars with a barely critical magnetic field. For these sources an option remain open for their interpretation as white dwarfs or neutron stars. A more refined analysis will clarify the correctness of the two possible interpretations both, in any case, alternative to the magnetar model.

B.3.10. Conclusions and remarks

The recent observations of the source SGR 0418+5729 cast a firm separatrix in comparing and contrasting the two models for SGRs and AXPs based respectively on an ultramagnetized neutron star and on a white dwarf. The limit on the magnetic field derived in the case of a neutron star $B = 7.5 \times 10^{12}$ G makes it not viable as an explanation based on the magnetar model both from a global energetic point of view and from the undercritical value of the magnetic field. In the white dwarf model, the picture is fully consistent. It is interesting that the rotational energy loss appears to approach the value of the observed X-ray luminosity with time (see Fig. B.22) as the magnetospheric activity settles down.

The description of SGR 0418+5729 as a white dwarf predicts the lower limit of the spin-down rate \dot{P} given by Eq. (B.3.2), the surface magnetic field field is, accordingly to Eq. (B.3.4), constrained by $1.05 \times 10^8 \text{ G} < B_{\text{SGR0418+5729}} < 7.47 \times 10^8 \text{ G}$ (see Fig. B.16). The campaign of observations launched by the Fermi and Agile satellites will address soon this issue and settle in the near future this theoretical prediction.

The characteristic changes of period $\Delta P/P \sim -(10^{-7}-10^{-3})$ and the relating bursting activity $\sim (10^{41}-10^{46})$ erg in SGRs and AXPs can be well explained in term of the rotational energy released after the glitch of the white dwarf. It is also appropriate to recall that fractional changes, on scales $|\Delta P|/P \lesssim 10^{-6}$ are also observed in pulsars and routinely expressed in terms of the release of rotational energy of the neutron star, without appealing to any magnetars phenomena; e.g. the glitch/outburst activity experienced in June 2006 by PSR J1846-0258 (see Sec. B.3.7) and the most recent event observed in the prototypical Crab pulsar B0531+21 in the Crab nebula (see e.g. Tavani, 2011; Fermi-LAT Collaboration, 2010).

The observation of massive fast rotating highly magnetized white dwarfs by dedicated missions as the one leadered by the X-ray Japanese satellite Suzaku (see e.g. Terada et al., 2008c) has led to the confirmation of the existence of white dwarfs sharing common properties with neutron star pulsars, hence their name white dwarf pulsars. The theoretical interpretation of the high-energy emission from white dwarf pulsars will certainly help to the understanding of the SGR and AXP phenomena (see e.g. Kashiyama et al., 2011).

We have given evidence that all SGRs and AXPs can be interpreted as rotating white dwarfs providing that the rotational period satisfies $P > P_{\min}^{\text{WD}} \sim 0.3$ s. The white dwarf generate their energetics from the rotational energy and therefore there is no need to invoke the magnetic field decay of the magnetar model.

Concerning the rotational period of SGRs and AXPs, it becomes interesting to confront our general relativistic results on uniformly rotating white dwarfs (Boshkayev et al., 2011) with the interesting work of Ostriker and Bodenheimer (1968) on differentially rotating Newtonian white dwarfs.

Regarding magnetized white dwarfs, the coupling between rotation and Rayleigh-Taylor instabilities arising from chemical separation upon crystallization may have an important role in the building of the magnetic field of the white dwarf Garcia-Berro et al. (2011).

We are grateful to the referee for a clear formulation of a number of fundamental issues which we have addressed and solved. We also thank for the careful reading of the manuscript and the many positive suggestions. We also thank for interesting discussions on this subject to E. García-Berro, Jorge Horvath, Jeremiah Ostriker, José Pacheco, Yukikatsu Terada and Vladimir Usov, as well as to all the participants of the IRAP Erasmus Mundus Ph. D. School “From Nuclei to White Dwarfs to Neutron Stars” held at Les Houches, France, April 2011. Manuel Malheiro acknowledges the hospitality and support of ICRANet, and the Brazilian agency FAPESP (fellowship BPE 2010/0558-1 in the thematic project 2007/03633-3) for the financial support.

	SGR 1806-20	SGR 0526-66	SGR 1900+14	SGR 0418+5729
P (s)	7.56	8.05	5.17	9.08
\dot{P} (10^{-11})	54.9	6.5	7.78	$< 6.0 \times 10^{-4}$
Age (kyr)	2.22	1.97	1.05	24.0×10^3
L_X (10^{35} erg/s)	1.50	2.1	1.8	6.2×10^{-4}
kT (keV)	0.65	0.53	0.43	0.67
$\dot{E}_{\text{rot}}^{\text{WD}}$ (10^{37} erg/s)	50.24	4.92	22.24	3.2×10^{-4}
B_{WD} (10^9 G)	206.10	73.18	64.16	0.75
\mathcal{R}_{WD} (10^{-5})	0.65	2.06	4.07	2.4×10^{-4}
$\dot{E}_{\text{rot}}^{\text{NS}}$ (10^{35} erg/s)	0.502	0.05	0.22	3.2×10^{-6}
B_{NS} (10^{14} G)	20.61	7.32	6.42	0.075
\mathcal{R}_{NS}	0.065	0.21	0.41	2.4×10^{-5}
	1E 1547-54	1E 1048-59	1E 1841-045	1E 2259+586
P (s)	2.07	6.45	11.78	6.98
\dot{P} (10^{-11})	2.32	2.70	4.15	0.048
Age (kyr)	1.42	3.79	4.50	228.74
L_X (10^{35} erg/s)	0.031	0.054	2.2	0.19
kT (keV)	0.43	0.62	0.38	0.41
$\dot{E}_{\text{rot}}^{\text{WD}}$ (10^{37} erg/s)	103.29	3.97	1.01	0.056
B_{WD} (10^9 G)	22.17	42.22	70.71	5.88
\mathcal{R}_{WD} (10^{-5})	0.07	0.028	8.16	0.49
$\dot{E}_{\text{rot}}^{\text{NS}}$ (10^{35} erg/s)	1.03	0.040	0.010	5.62×10^{-4}
B_{NS} (10^{14} G)	2.22	4.22	7.07	0.59
\mathcal{R}_{NS}	0.007	0.0028	0.82	0.049

Table B.9.: SGRs and AXPs as white dwarfs and neutron stars. The rotational period P , the spin-down rate \dot{P} , the X-ray luminosity L_X and the temperature T have been taken from the McGill online catalog at www.physics.mcgill.ca/~pulsar/magnetar/main.html. The characteristic age is given by $\text{Age} = P/(2\dot{P})$, the loss of rotational energy \dot{E}_{rot} is given by Eqs. (B.3.5) and Eq. (B.3.1) and the surface magnetic field is given by Eqs. (B.3.4) and (B.3.12) for white dwarfs and neutron stars respectively. The filling factor \mathcal{R} is given by Eq. (B.3.14).

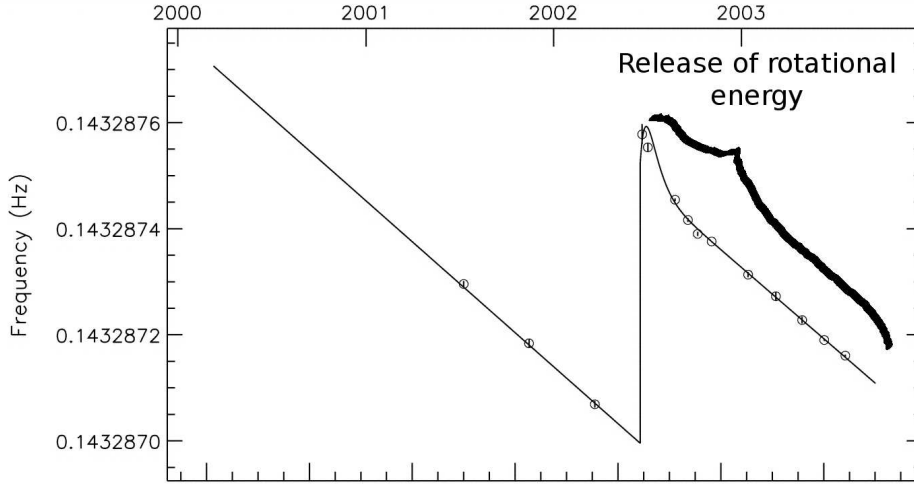


Figure B.14.: Timing analysis of the glitch of 1E 2259+586 on June 2002 (taken from Woods et al., 2004). The vertical axis shows the evolution of the spin frequency and the horizontal axis the date time. The observed fractional change of period is $\Delta P/P = -\Delta\Omega/\Omega \sim -4 \times 10^{-6}$ and the observed energy released during the event is $\sim 3 \times 10^{41}$ erg (Woods et al., 2004). Within the white dwarf model from such a $\Delta P/P$ we obtain $\Delta E_{\text{rot}}^{\text{WD}} \sim 1.7 \times 10^{43}$ erg as given by Eq. (B.3.8). We have modified the original figure (Woods et al., 2004) by indicating explicitly where the rotational energy is released after the spin-up, recovering its initial period prior to the glitch by the emission of a sequence of bursts on time scales from months to years (see e.g. Mereghetti, 2008).

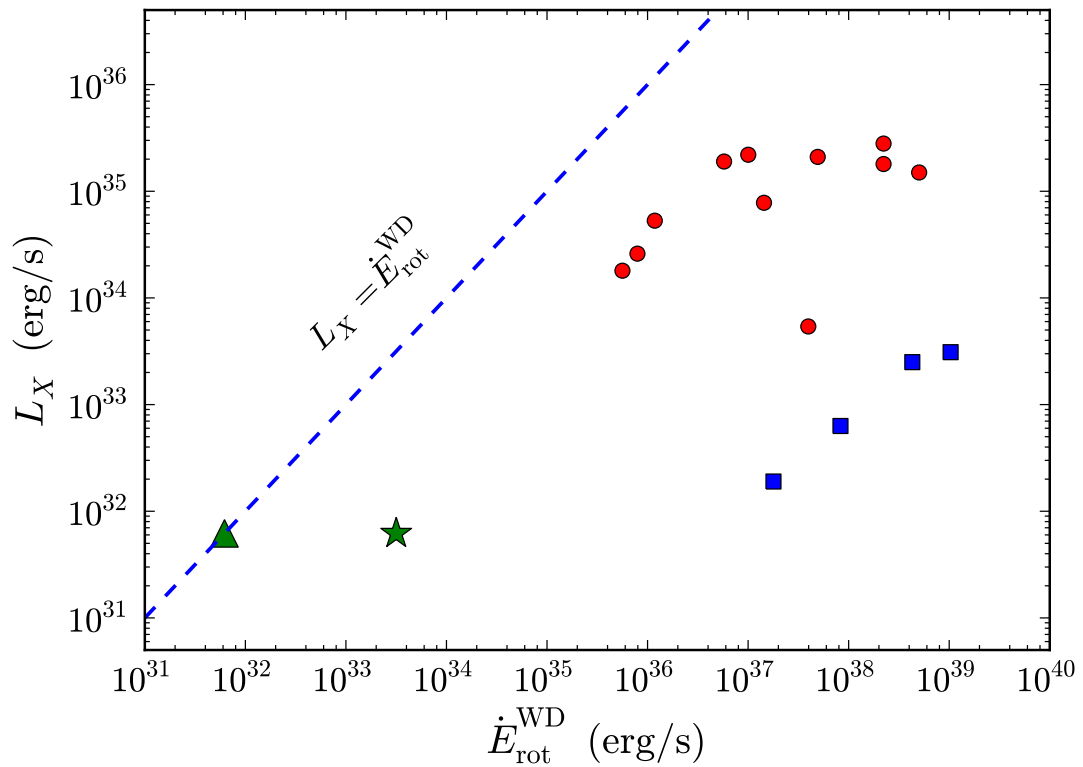


Figure B.15.: X-ray luminosity L_X versus the loss of rotational energy \dot{E}_{rot} describing SGRs and AXPs by rotation powered white dwarfs. The green star and the green triangle correspond to SGR 0418+5729 using respectively the upper and the lower limit of \dot{P} given by Eq. (B.3.2). The blue squares are the only four sources that satisfy $L_X < \dot{E}_{\text{rot}}$ when described as neutron stars (see Fig. B.19 for details).

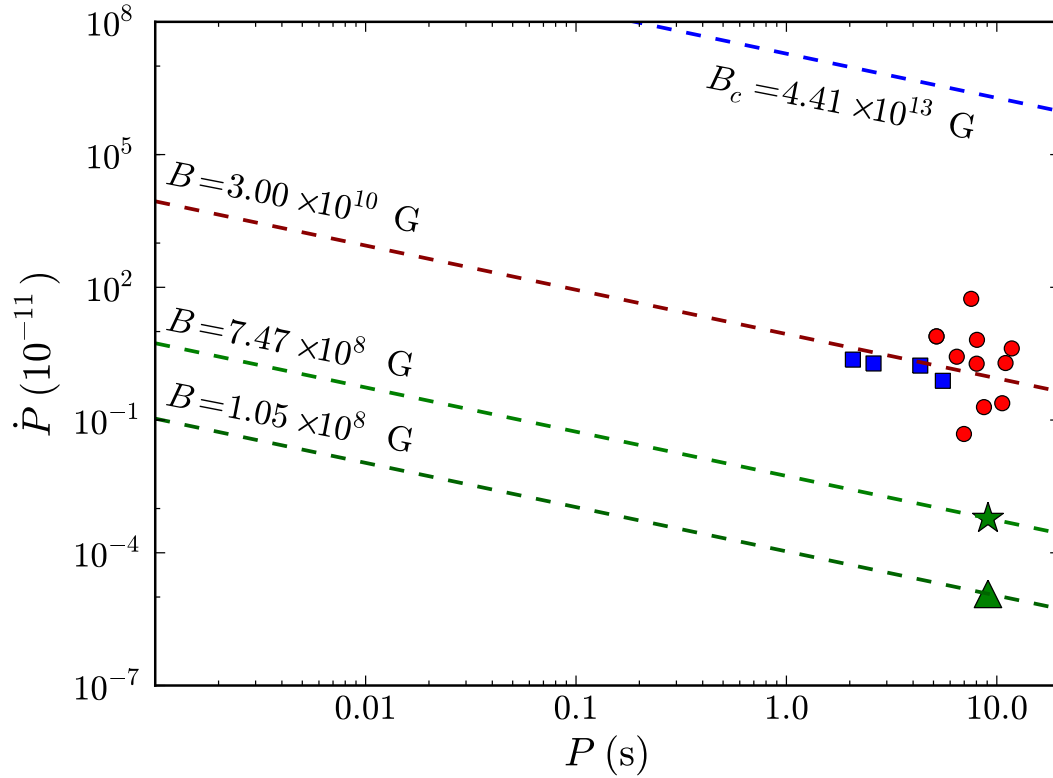


Figure B.16.: \dot{P} - P diagram for all known SGRs and AXPs. The curves of constant magnetic field for white dwarfs given by Eq. (B.3.4) are shown. The blue dashed line corresponds to the critical magnetic field $B_c = m_e^2 c^3 / (e \hbar)$. The green star and the green triangle correspond to SGR 0418+5729 using respectively the upper and the lower limit of \dot{P} given by Eq. (B.3.2). The blue squares are the only four sources that satisfy $L_X < \dot{E}_{\text{rot}}$ when described as rotation powered neutron stars (see Fig. B.19 for details).

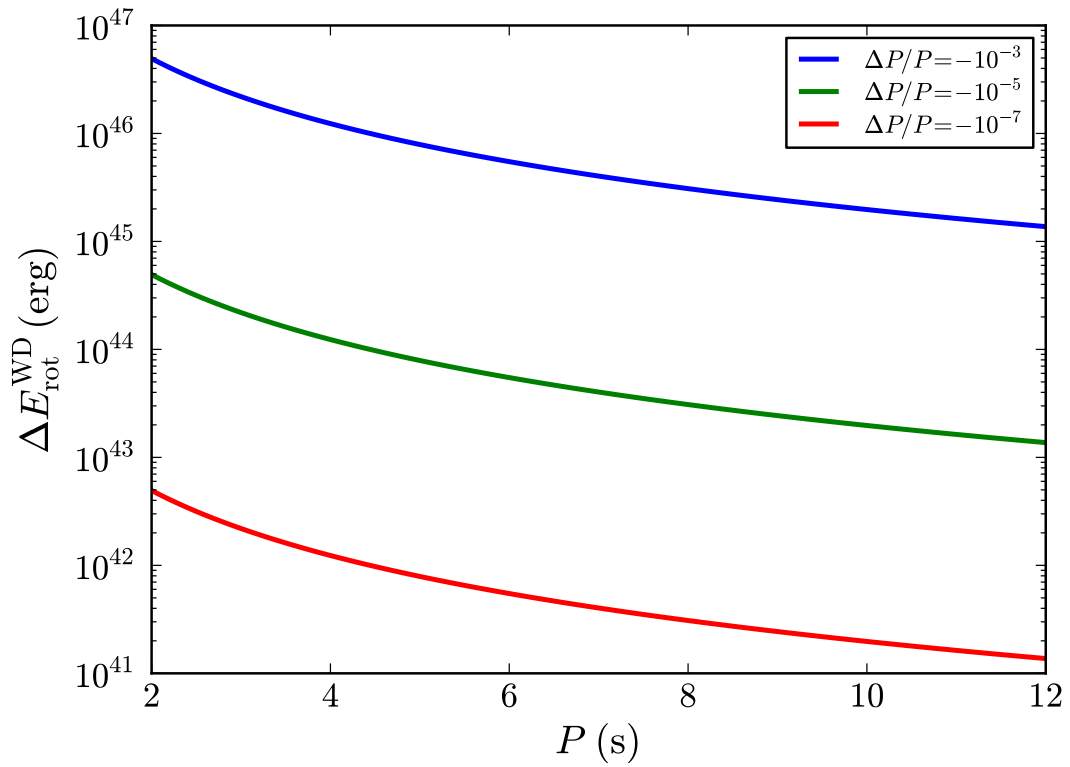


Figure B.17.: Change in the rotational energy of the white dwarf $\Delta E_{\text{rot}}^{\text{WD}}$ given by Eq. (B.3.8) as a function of the rotational period P in seconds for selected fractional changes of period $\Delta P/P$.

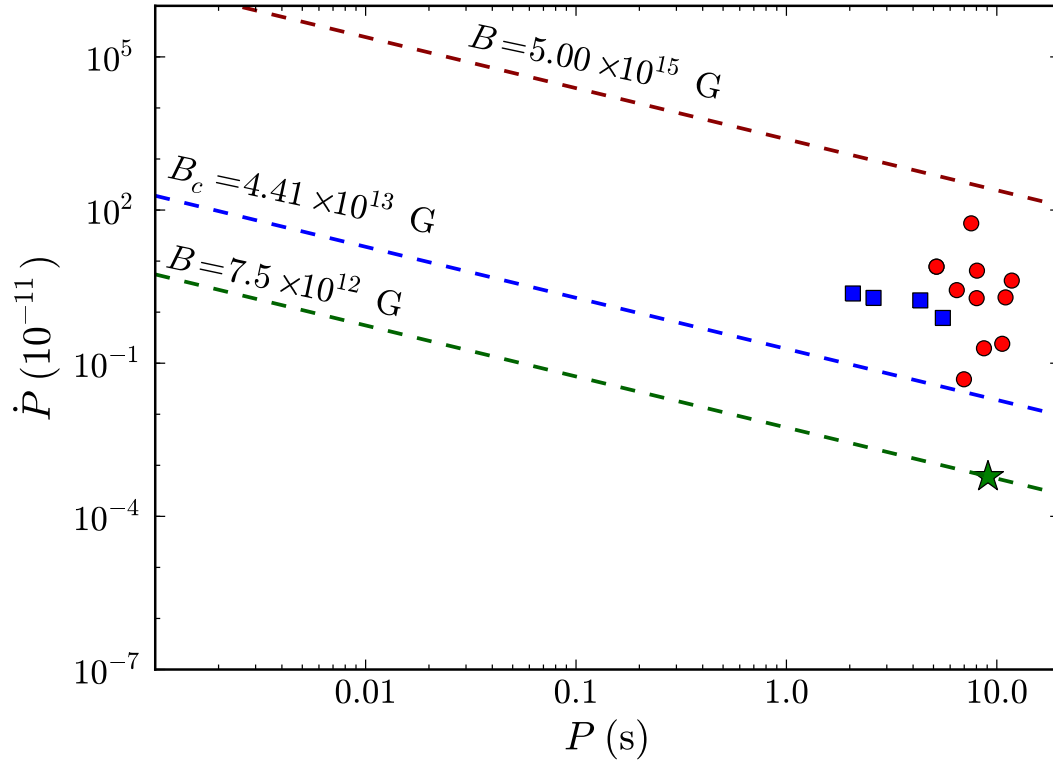


Figure B.18.: \dot{P} - P diagram for all known SGRs and AXPs. The curves of constant magnetic field for neutron stars given by Eq. (B.3.12) are shown. The blue dashed line corresponds to the critical magnetic field $B_c = m_e^2 c^3 / (e\hbar)$. The green star corresponds to SGR 0418+5729 using the upper limit of \dot{P} given by Eq. (B.3.2). The blue squares are the only four sources that satisfy $L_X < \dot{E}_{\text{rot}}$ when described as rotation powered neutron stars (see Fig. B.19 for details).

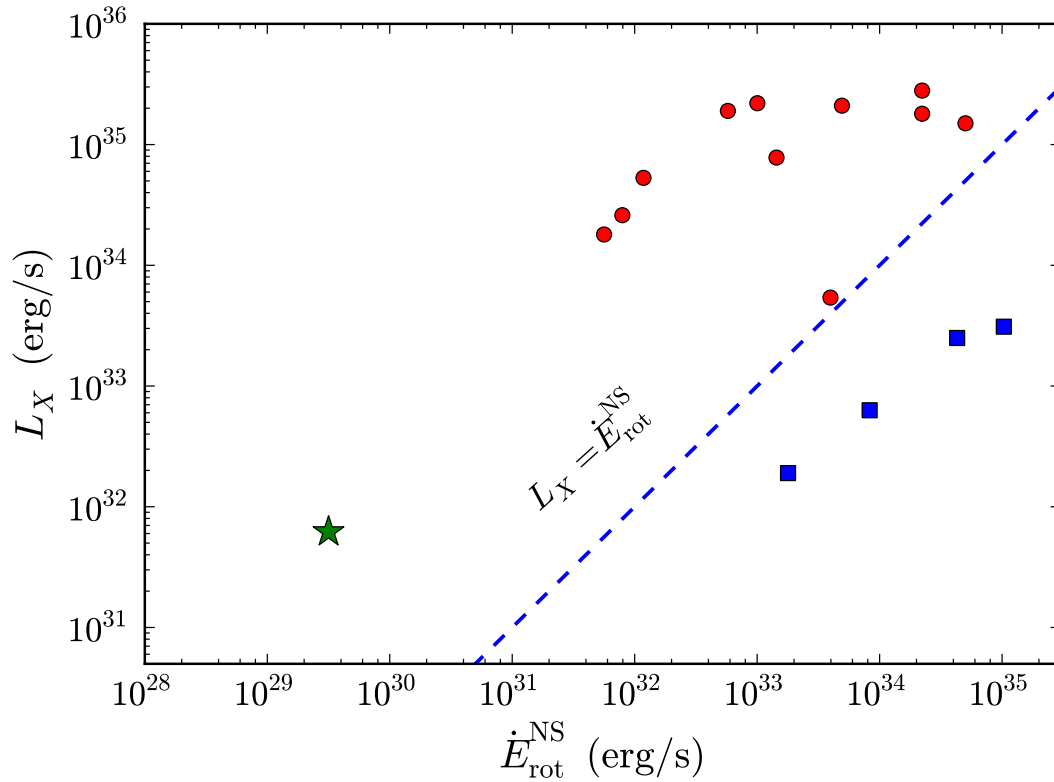


Figure B.19.: X-ray luminosity L_X versus the loss of rotational energy \dot{E}_{rot} describing SGRs and AXPs as neutron stars. The green star corresponds to SGR 0418+5729 using the upper limit of \dot{P} given by Eq. (B.3.2). The blue squares are the only four sources with $L_X < \dot{E}_{\text{rot}}$: 1E 1547.0-5408 with $P = 2.07$ s and $\dot{P} = 2.3 \times 10^{-11}$; SGR 1627-41 with $P = 2.59$ s and $\dot{P} = 1.9 \times 10^{-11}$; PSR J 1622-4950 with $P = 4.33$ s and $\dot{P} = 1.7 \times 10^{-11}$; and XTE J1810-197 with $P = 5.54$ s and $\dot{P} = 7.7 \times 10^{-12}$.

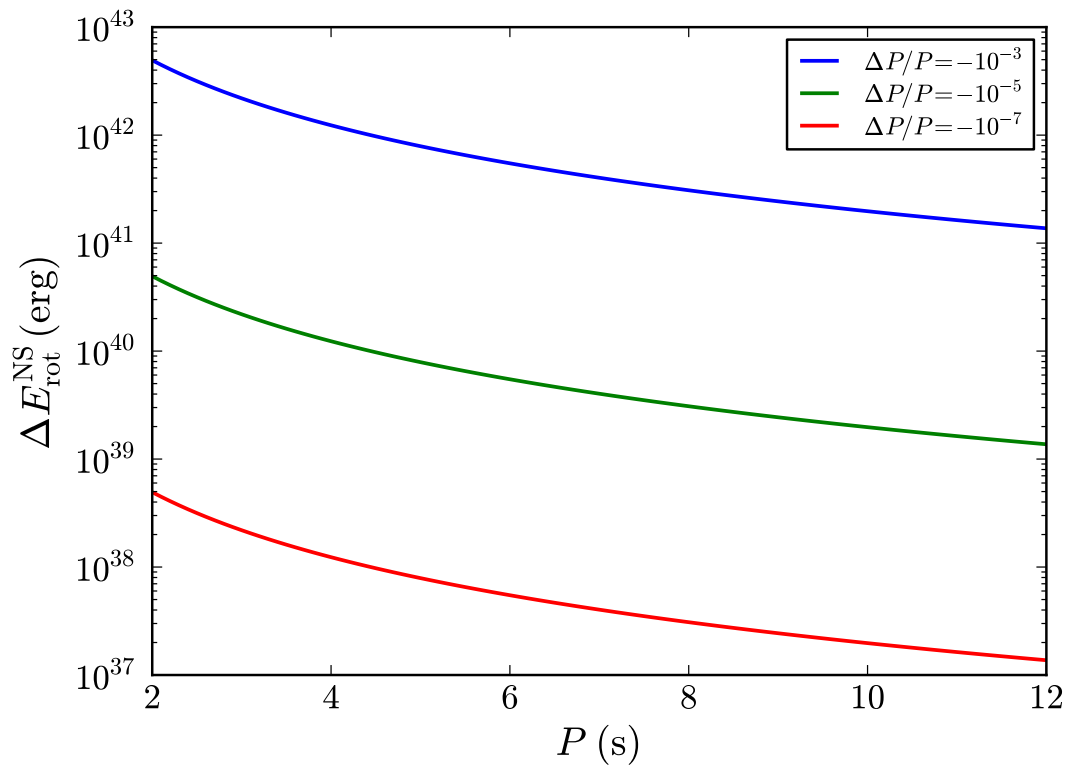


Figure B.20.: Change in the rotational energy of the neutron star $\Delta E_{\text{rot}}^{\text{NS}}$ given by Eq. (B.3.13) as a function of the rotational period P in seconds for selected fractional changes of period $\Delta P/P$.

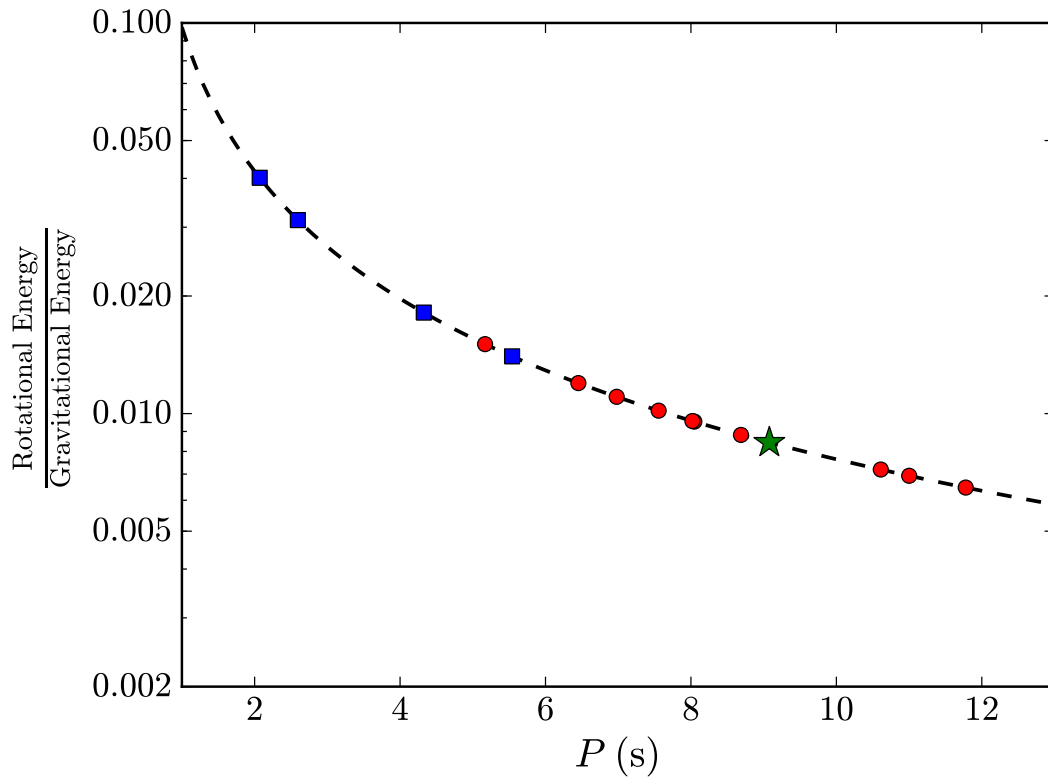


Figure B.21.: Ratio between the rotational energy and the gravitational energy of a MacClaurin spheroid of $M = 1.4M_{\odot}$ and $R = 10^3$ km as a function of its rotational period P . The rotational period between 2 and 12 s appears to be very appropriate for fast rotating white dwarfs. Fast rotating neutron stars present much shorter period in the millisecond region. We show on the curve the position of all known SGRs and AXPs. The green star corresponds to SGR 0418+5729. The blue squares are the only four sources that satisfy $L_X < \dot{E}_{\text{rot}}$ when described as rotation powered neutron stars (see Fig. B.19 for details).

C. Neutron Stars Physics and Astrophysics

C.1. The self-consistent general relativistic solution for a system of degenerate neutrons, protons and electrons in β -equilibrium

C.1.1. Introduction

The insurgence of critical electric fields in the process of gravitational collapse leading to vacuum polarization process (Ruffini et al., 2010b) has convinced us of the necessity of critically reexamining the gravitational and electro-dynamical properties in neutron stars. In this light we have recently generalized the Feynman, Metropolis and Teller treatment of compressed atoms to the relativistic regimes (Rotondo et al., 2011c). We have so enforced, self-consistently in a relativistic Thomas-Fermi equation, the condition of β -equilibrium extending the works of Popov (1971b), Zeldovich and Popov (1972), Migdal et al. (1976, 1977), Ferreira et al. (1980) and Ruffini and Stella (1981) for heavy nuclei. Thanks to the existence of scaling laws (see Rotondo et al. (2011c) and Ruffini (2008c)) this treatment has been extrapolated to compressed nuclear matter cores of stellar dimensions with mass numbers $A \simeq (m_{\text{Planck}}/m_n)^3 \sim 10^{57}$ or $M_{\text{core}} \sim M_{\odot}$. Such configurations fulfill global but not local charge neutrality. They have electric fields on the core surface, increasing for decreasing values of the electron Fermi energy E_e^F reaching values much larger than the critical value $E_c = m_e^2 c^3 / (e\hbar)$, for $E_e^F = 0$. The assumption of constant distribution of protons at nuclear densities simulates, in such a treatment, the confinement due to the strong interactions in the case of nuclei and heavy nuclei and due to both the gravitational field and the strong interactions in the case of nuclear matter cores of stellar sizes.

In this article we introduce explicitly the effects of gravitation by considering a general relativistic system of degenerate fermions composed of neutrons, protons and electrons in β -equilibrium: this is the simplest nontrivial system in which new electro-dynamical and general relativistic properties of the equilibrium configuration can be clearly and rigorously illustrated. We first prove that the condition of local charge neutrality can never be implemented since it violates necessary conditions of equilibrium at the micro-

physical scale. We then prove the existence of a solution with global, but not local, charge neutrality by taking into account essential gravito-electrodynamical effects. First we recall the constancy of the general relativistic Fermi energy of each specie pioneered by Klein (1949). We subsequently introduce the general relativistic Thomas-Fermi equations for the three fermion species fulfilling relativistic quantum statistics, governed by the Einstein-Maxwell equations. The solution of this system of equations presents a formidable mathematical challenge in theoretical physics. The traditional difficulties encountered in proving the existence and unicity of the solution of the Thomas-Fermi equation are here enhanced by the necessity of solving the general relativistic Thomas-Fermi equation coupled with the Einstein-Maxwell system of equations. We present the general solution for the equilibrium configuration, from the center of the star all the way to the border, giving the details of the gravitational field, of the electro-dynamical field as well as of the conserved quantities.

We illustrate such a solution by selecting a central density $\rho(0) = 3.94\rho_{\text{nuc}}$, where $\rho_{\text{nuc}} \simeq 2.7 \times 10^{14} \text{ g cm}^{-3}$ is the nuclear density. We point out the existence near the boundary of the core in the equilibrium configuration of three different radii, in decreasing order: R_e corresponding to the vanishing of the Fermi momentum of the electron component; $P_e^F = 0$, R_p corresponding to the vanishing of the Fermi momentum of the proton component; $P_p^F = 0$ and R_n corresponding to the radius at which the Fermi momentum of neutrons vanishes: $P_n^F = 0$. We then give explicit expressions for the proton versus electron density ratio and the proton versus neutron density ratio for any value of the radial coordinate as well as for the electric potential at the center of the configuration. A novel situation occurs: the description of the pressure and density is not anylonger a local one. Their determination needs prior knowledge of the global electro-dynamical and gravitational potentials on the entire system as well as of the radii R_n , R_p and R_e . This is a necessary outcome of the self-consistent solution of the eigenfunction within general relativistic Thomas-Fermi equation in the Einstein-Maxwell background. As expected from the considerations in Rotondo et al. (2011c), the electric potential at the center of the configuration fulfills $eV(0) \simeq m_\pi c^2$ and the gravitational potential $1 - e^{v(0)/2} \simeq m_\pi/m_p$. The implementation of the constancy of the general relativistic Fermi energy of each particle species and the consequent system of equations illustrated here is the simplest possible example admitting a rigorous nontrivial solution. It will necessarily apply in the case of additional particle species and of the inclusion of nuclear interactions: in this cases however it is not sufficient and the contribution of nuclear fields must be taken into due account.

C.1.2. The impossibility of a solution with local charge neutrality

We consider the equilibrium configurations of a degenerate gas of neutrons, protons and electrons with total matter energy density and total matter pressure

$$\varepsilon = \sum_{i=n,p,e} \frac{2}{(2\pi\hbar)^3} \int_0^{P_i^F} \epsilon_i(p) 4\pi p^2 dp, \quad (\text{C.1.1})$$

$$P = \sum_{i=n,p,e} \frac{1}{3} \frac{2}{(2\pi\hbar)^3} \int_0^{P_i^F} \frac{p^2}{\epsilon_i(p)} 4\pi p^2 dp, \quad (\text{C.1.2})$$

where $\epsilon_i(p) = \sqrt{c^2 p^2 + m_i^2 c^4}$ is the relativistic single particle energy. In addition, we require the condition of β -equilibrium between neutrons, protons and electrons

$$\mu_n = \mu_p + \mu_e, \quad (\text{C.1.3})$$

where P_i^F denotes the Fermi momentum and $\mu_i = \partial \mathcal{E} / \partial n_i = \sqrt{c^2 (P_i^F)^2 + m_i^2 c^4}$ is the free-chemical potential of particle-species with number density $n_i = (P_i^F)^3 / (3\pi^2 \hbar^3)$. We now introduce the extension to general relativity of the Thomas-Fermi equilibrium condition on the generalized Fermi energy E_e^F of the electron component

$$E_e^F = e^{\nu/2} \mu_e - m_e c^2 - eV = \text{constant}, \quad (\text{C.1.4})$$

where e is the fundamental charge, V is the Coulomb potential of the configuration and we have introduced the metric

$$ds^2 = e^{\nu(r)} c^2 dt^2 - e^{\lambda(r)} dr^2 - r^2 d\theta^2 - r^2 \sin^2 \theta d\varphi^2, \quad (\text{C.1.5})$$

for a spherically symmetric non-rotating neutron star. The metric function λ is related to the mass $M(r)$ and the electric field $E(r) = -e^{-(\nu+\lambda)/2} V'$ (a prime stands for radial derivative) through

$$e^{-\lambda} = 1 - \frac{2GM(r)}{c^2 r} + \frac{G}{c^4} r^2 E^2(r). \quad (\text{C.1.6})$$

Thus the equations for the neutron star equilibrium configuration consist of the following Einstein-Maxwell equations and general relativistic Thomas-

Fermi equation

$$M' = 4\pi r^2 \frac{\mathcal{E}}{c^2} - \frac{4\pi r^3}{c^2} e^{-\nu/2} \hat{V}' (n_p - n_e), \quad (\text{C.1.7})$$

$$\nu' = \frac{2G}{c^2} \frac{4\pi r^3 P/c^2 + M - r^3 E^2/c^2}{r^2 \left(1 - \frac{2GM}{c^2 r} + \frac{Gr^2 E^2}{c^4}\right)}, \quad (\text{C.1.8})$$

$$P' + \frac{\nu'}{2} (\mathcal{E} + P) = -(P^{\text{em}})' - \frac{4P^{\text{em}}}{r}, \quad (\text{C.1.9})$$

$$\hat{V}'' + \frac{2}{r} \hat{V}' \left[1 - \frac{r(\nu' + \lambda')}{4}\right] = -4\pi\alpha\hbar c e^{\nu/2} e^\lambda \left\{ n_p - \frac{e^{-3\nu/2}}{3\pi^2} [\hat{V}^2 + 2m_e c^2 \hat{V} - m_e^2 c^4 (e^\nu - 1)]^{3/2} \right\}, \quad (\text{C.1.10})$$

where α denotes the fine structure constant, $\hat{V} = E_e^F + eV$, $P^{\text{em}} = -E^2/(8\pi)$ and we have used Eq. (C.1.4) to obtain Eq. (C.1.10).

It can be demonstrated that the assumption of the equilibrium condition (C.1.4) together with the β -equilibrium condition (C.1.3) and the hydrostatic equilibrium (C.1.9) is enough to guarantee the constancy of the generalized Fermi energy

$$E_i^F = e^{\nu/2} \mu_i - m_i c^2 + q_i V, \quad i = n, p, e, \quad (\text{C.1.11})$$

for all particle species separately. Here q_i denotes the particle unit charge of the i -species. Indeed, as shown by Olson and Bailyn (1975, 1978), when the fermion nature of the constituents and their degeneracy is taken into account, in the configuration of minimum energy the generalized Fermi energies E_i^F defined by (C.1.11) must be constant over the entire configuration. These minimum energy conditions generalize the equilibrium conditions of Klein (1949) and of Kodama and Yamada (1972) to the case of degenerate multi-component fluids with particle species with non-zero unit charge.

If one were to assume, as often done in literature, the local charge neutrality condition $n_e(r) = n_p(r)$ instead of assuming the equilibrium condition (C.1.4), this would lead to $V = 0$ identically (since there will be no electric fields generated by the neutral matter distribution) implying via Eqs. (C.1.3) and (C.1.9)

$$\begin{aligned} E_e^F + E_p^F &= e^{\nu/2} (\mu_e + \mu_p) - (m_e + m_p) c^2 = E_n^F \\ &+ (m_n - m_e - m_p) c^2 = \text{constant}. \end{aligned} \quad (\text{C.1.12})$$

Thus the neutron Fermi energy would be constant throughout the configuration as well as the sum of the proton and electron Fermi energies but not

the individual Fermi energies of each component. In Fig. C.1 we show the results of the Einstein equations for a selected value of the central density of a system of degenerate neutrons, protons, and electrons in β -equilibrium under the constraint of local charge neutrality. In particular, we have plotted the Fermi energy of the particle species in units of the pion rest-energy. It can be seen that indeed the Fermi energies of the protons and electrons are not constant throughout the configuration which would lead to microscopic instability. This proves the impossibility of having a self-consistent configuration fulfilling the condition of local charge neutrality for our system. This result is complementary to the conclusion of Eq. (4.6) of Olson and Bailyn (1975) who found that, at zero temperature, only a dust solution with zero particle kinetic energy can satisfy the condition of local charge neutrality and such a configuration is clearly unacceptable for an equilibrium state of a self-gravitating system.

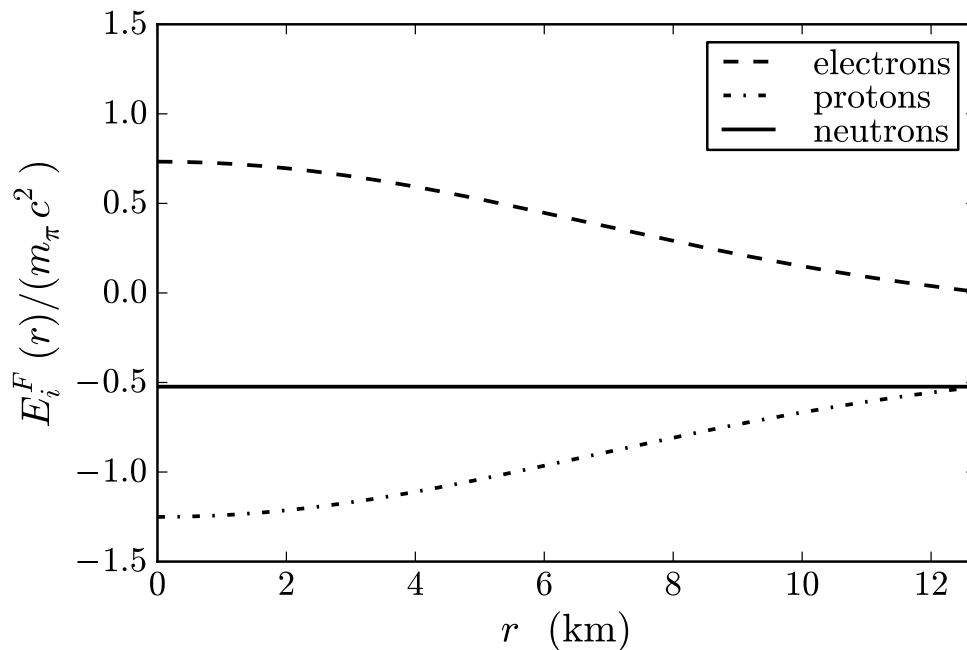


Figure C.1.: Fermi energies for neutrons, protons and electrons in units of the pion rest-energy for a locally neutral configuration with central density $\rho(0) = 3.94\rho_{\text{nuc}}$, where $\rho_{\text{nuc}} = 2.7 \times 10^{14} \text{ g cm}^{-3}$ denotes the nuclear density.

C.1.3. The solution with global charge neutrality

We turn now to describe the equilibrium configurations fulfilling only global charge neutrality. We solve self-consistently Eqs. (C.1.7) and (C.1.8) for the metric, Eq. (C.1.9) for the hydrostatic equilibrium of the three degenerate fermions and, in addition, we impose Eq. (C.1.3) for the β -equilibrium. The crucial equation relating the proton and the electron distributions is then given by the general relativistic Thomas-Fermi equation (C.1.10). The boundary conditions are: for Eq. (C.1.7) the regularity at the origin: $M(0) = 0$, for Eq. (C.1.9) a given value of the central density, and for Eq. (C.1.10) the regularity at the origin $n_e(0) = n_p(0)$, and a second condition at infinity which results in an eigenvalue problem determined by imposing the global charge neutrality conditions

$$\hat{V}(R_e) = E_e^F, \quad \hat{V}'(R_e) = 0, \quad (\text{C.1.13})$$

at the radius R_e of the electron distribution defined by

$$P_e^F(R_e) = 0, \quad (\text{C.1.14})$$

from which follows

$$\begin{aligned} E_e^F &= m_e c^2 e^{\nu(R_e)/2} - m_e c^2 \\ &= m_e c^2 \sqrt{1 - \frac{2GM(R_e)}{c^2 R_e}} - m_e c^2. \end{aligned} \quad (\text{C.1.15})$$

Then the eigenvalue problem consists in determining the gravitational potential and the Coulomb potential at the center of the configuration that satisfy the conditions (C.1.13)–(C.1.15) at the boundary.

C.1.4. Numerical integration of the equilibrium equations

The solution for the particle densities, the gravitational potential, the Coulomb potential and the electric field are shown in Fig. (C.2) for a configuration with central density $\rho(0) = 3.94\rho_{\text{nuc}}$. In order to compare our results with those obtained in the case of nuclear matter cores of stellar dimensions Rotondo et al. (2011c) as well as to analyze the gravito-electrodynamical stability of the configuration we have plotted the electric potential in units of the pion rest-energy and the gravitational potential in units of the pion-to-proton mass ratio. One particular interesting new feature is the approach to the boundary of the configuration: three different radii are present corresponding to distinct radii at which the individual particle Fermi pressure vanishes. The radius R_e for the electron component corresponding to $P_e^F(R_e) = 0$, the radius R_p for the proton component corresponding to $P_p^F(R_p) = 0$ and the radius R_n for

the neutron component corresponding to $P_n^F(R_n) = 0$.

The smallest radius R_n is due to the threshold energy for β -decay which occurs at a density $\sim 10^7 \text{ g cm}^{-3}$. The radius R_p is larger than R_n because the proton mass is slightly smaller than the neutron mass. Instead, $R_e > R_p$ due to a combined effect of the difference between the proton and electron masses and the implementation of the global charge neutrality condition through the Thomas-Fermi equilibrium conditions.

For the configuration of Fig. C.2 we found $R_n \simeq 12.735 \text{ km}$, $R_p \simeq 12.863 \text{ km}$ and $R_e \simeq R_p + 10^3 \lambda_e$ where $\lambda_e = \hbar / (m_e c)$ denotes the electron Compton wavelength. We find that the electron component follows closely the proton component up to the radius R_p and neutralizes the configuration at R_e without having a net charge, contrary to the results e.g in Olson and Bailyn (1978).

It can be seen from Fig. C.2 that the negative proton gravitational potential energy is indeed always larger than the positive proton electric potential energy. Therefore the configuration is stable against Coulomb repulsion. This confirms the results in the simplified case analyzed by Rotondo et al. (2011c).

From Eq. (C.1.11) and the relation between Fermi momentum and the particle density $P_i^F = (3\pi^2 \hbar^3 n_i)^{1/3}$, we obtain the proton-to-electron and proton-to-neutron ratio for any value of the radial coordinate

$$\frac{n_p(r)}{n_e(r)} = \left[\frac{f^2(r) \mu_e^2(r) - m_p^2 c^4}{\mu_e^2(r) - m_e^2 c^4} \right]^{3/2}, \quad (\text{C.1.16})$$

$$\frac{n_p(r)}{n_n(r)} = \left[\frac{g^2(r) \mu_n^2(r) - m_p^2 c^4}{\mu_n^2(r) - m_n^2 c^4} \right]^{3/2}, \quad (\text{C.1.17})$$

where $f(r) = (E_p^F + m_p c^2 - eV) / (E_e^F + m_e c^2 + eV)$, $g(r) = (E_p^F + m_p c^2 - eV) / (E_n^F + m_n c^2)$ and the constant values of the generalized Fermi energies are given by

$$E_n^F = m_n c^2 e^{\nu(R_n)/2} - m_n c^2, \quad (\text{C.1.18})$$

$$E_p^F = m_p c^2 e^{\nu(R_p)/2} - m_p c^2 + eV(R_p), \quad (\text{C.1.19})$$

$$E_e^F = m_e c^2 e^{\nu(R_e)/2} - m_e c^2. \quad (\text{C.1.20})$$

A novel situation occurs: the determination of the quantities given in Eqs. (C.1.16) and (C.1.18) necessarily require the prior knowledge of the global electro-dynamical and gravitational potential from the center of the configuration all the way out to the boundary defined by the radii R_e , R_p and R_n . This necessity is an outcome of the solution for the eigenfunction of the general relativistic Thomas-Fermi equation (C.1.10).

From the regularity condition at the center of the star $n_e(0) = n_p(0)$ to-

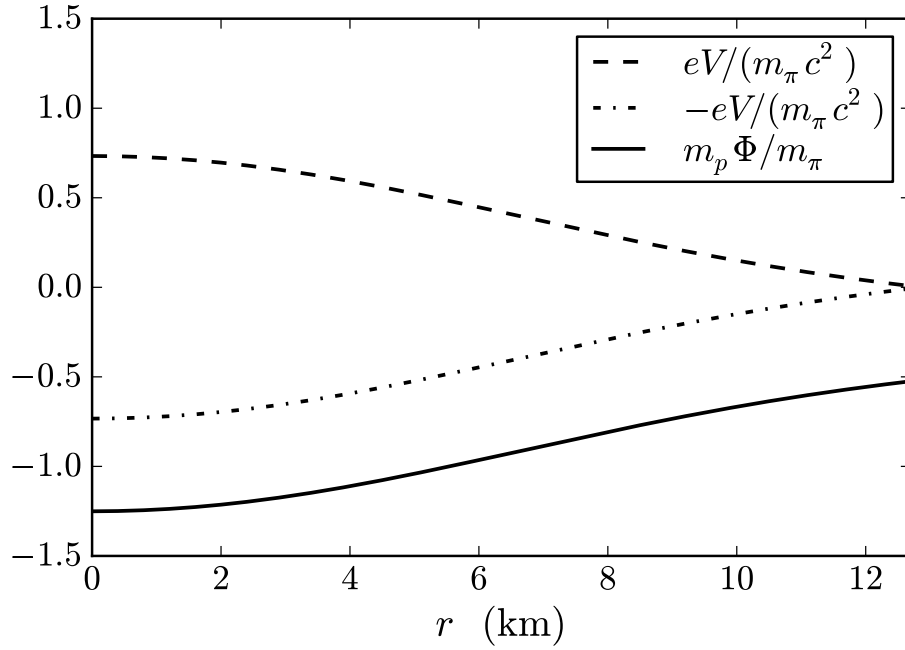
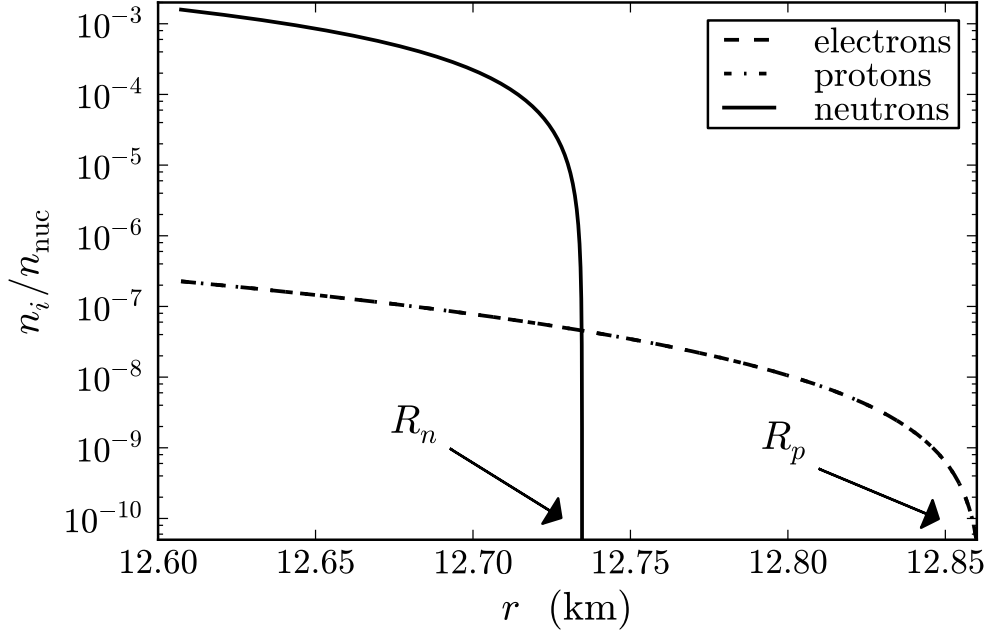


Figure C.2.: Top panel: particle number density of neutrons, protons, and electrons approaching the boundary of the configuration in units of the nuclear density $n_{\text{nuc}} \simeq 1.6 \times 10^{38} \text{ cm}^{-3}$. Bottom panel: proton and electron Coulomb potentials in units of the pion rest-energy $eV/(m_{\pi}c^2)$ and $-eV/(m_{\pi}c^2)$ respectively and the proton gravitational potential in units of the pion mass $m_p \Phi/m_{\pi}$ where $\Phi = (e^{v/2} - 1)$.

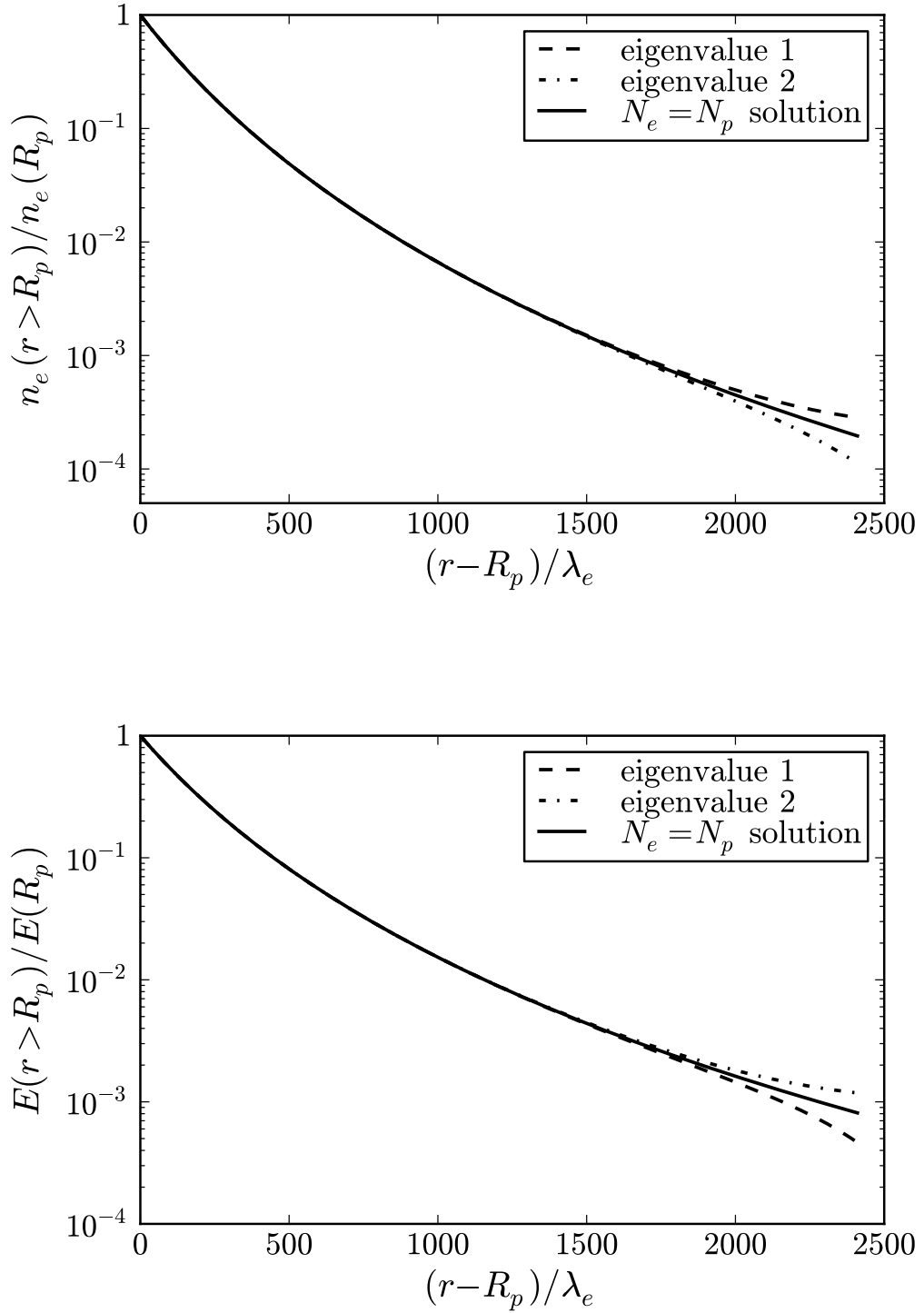


Figure C.3.: Top panel: electron number density for $r \geq R_p$ normalized to its value at $r = R_p$. Bottom panel: electric field for $r \geq R_p$ normalized to its value at $r = R_p$. We have shown also the behavior of the solution of the general relativistic Thomas-Fermi equation (C.1.10) for two different eigenvalues close to the one which gives the globally neutral configuration.

gether with Eq. (C.1.16) we obtain the Coulomb potential at the center of the configuration

$$eV(0) = \frac{(m_p - m_e)c^2}{2} \left[1 + \frac{E_p^F - E_e^F}{(m_p - m_e)c^2} - \frac{(m_p + m_e)c^2}{E_n^F + m_n c^2} e^{\nu(0)} \right], \quad (\text{C.1.21})$$

which after some algebraic manipulation and defining the central density in units of the nuclear density $\eta = \rho(0)/\rho_{\text{nuc}}$ can be estimated as

$$\begin{aligned} eV(0) &\simeq \frac{1}{2} \left[m_p c^2 e^{\nu(R_p)/2} - m_e c^2 e^{\nu(R_e)/2} - \frac{m_n c^2 e^{\nu(R_n)/2}}{1 + [P_n^F(0)/(m_n c)]^2} \right] \\ &\simeq \frac{1}{2} \left[\frac{(3\pi^2 \eta / 2)^{2/3} m_p}{(3\pi^2 \eta / 2)^{2/3} m_\pi + m_n^2 / m_\pi} \right] m_\pi c^2, \end{aligned} \quad (\text{C.1.22})$$

where we have approximated the gravitational potential at the boundary as $e^{\nu(R_e)/2} \simeq e^{\nu(R_p)/2} \simeq e^{\nu(R_n)/2} \simeq 1$. Then for configurations with central densities larger than the nuclear density we necessarily have $eV(0) \gtrsim 0.35 m_\pi c^2$. In particular, for the configuration we have exemplified with $\eta = 3.94$ in Fig. C.2, from the above expression (C.1.22) we obtain $eV(0) \simeq 0.85 m_\pi c^2$. This value of the central potential agrees with the one obtained in the simplified case of nuclear matter cores with constant proton density (Rotondo et al., 2011c).

C.1.5. Conclusions

We have proved in the first part of this letter that the treatment generally used for the description of neutron stars adopting the condition of local charge neutrality, is not consistent with the Einstein-Maxwell equations and microphysical conditions of equilibrium consistent with quantum statistics (see Fig. C.1). We have shown how to construct a self-consistent solution for a general relativistic system of degenerate neutrons, protons and electrons in β -equilibrium fulfilling global but not local charge neutrality.

Although the mass-radius relation in the simple example considered here in our new treatment, differs slightly from the one of the traditional approaches, the differences in the electrodynamic structure are clearly very large. As is well-known these effects can lead to important astrophysical conse-

quences on the physics of the gravitational collapse of a neutron star to a black hole Ruffini et al. (2010b).

Having established in the simplest possible example the new set of Einstein-Maxwell and general relativistic Thomas-Fermi equations, we now proceed to extend this approach when strong interactions are present Rueda et al. (2011). The contribution of the strong fields to the energy-momentum tensor, to the four-vector current and consequently to the Einstein-Maxwell equations have to be taken into account. Clearly in this more general case, the conditions introduced in this letter have to be still fulfilled: the r -independence of the generalized Fermi energy of electrons and the fulfillment of the general relativistic Thomas-Fermi equation Rueda et al. (2011). In addition, the generalized Fermi energy of protons and neutrons will depend on the nuclear interaction fields. The fluid of neutrons, protons and electrons in this more general case does not extend all the way to the neutron star surface but is confined to the neutron star core endowed with overcritical electric fields, in precise analogy with the case of the compressed nuclear matter core of stellar dimension described in Rotondo et al. (2011c).

C.2. The Klein first integrals in an equilibrium system with electromagnetic, weak, strong and gravitational interactions

C.2.1. Introduction

The unsolved problems of supernovae theories as well as the necessity of processes leading to electrodynamical phenomena during the gravitational collapse to a black hole (Ruffini et al., 2010b) lead to the necessity of critically reexamining the current treatment of neutron stars. In a series of articles (see Rotondo et al. (2011c,d)), we have recently developed the first steps towards a new consistent treatment for the description of neutron stars, well beyond the traditional Tolman-Oppenheimer-Volkoff equations.

First we have generalized the treatment of compressed atoms of Feynman, Metropolis and Teller to the relativistic regimes (see Rotondo et al. (2011c) for details). There, it has been enforced self-consistently in a relativistic Thomas-Fermi equation, the condition of β -equilibrium extending the works of Popov (1971b), Zeldovich and Popov (1972), Migdal et al. (1976, 1977), Ferreira et al. (1980) and Ruffini and Stella (1981) for heavy nuclei. Then, through the using of scaling laws, following Ruffini (2008c); Popov (2010), this treatment was extrapolated to compressed nuclear matter cores at nuclear and supranuclear densities. Such cores have stellar dimensions and mass numbers $A \simeq (m_{\text{Planck}}/m_n)^3 \sim 10^{57}$ or $M_{\text{core}} \sim M_{\odot}$. In addition, they fulfill global but not local charge neutrality having electric fields on the core surface, increasing for decreasing values of the electron Fermi energy E_e^F reaching values much larger than the critical value $E_c = m_e^2 c^3 / (e\hbar)$, for $E_e^F = 0$. The assumption of constant distribution of protons at nuclear densities simulates, in such a treatment, the confinement due to the strong interactions in the case of nuclei and heavy nuclei and due to both the gravitational field and strong interactions in the case of nuclear matter cores of stellar sizes at nuclear and supranuclear densities.

In a subsequent work Rotondo et al. (2011d), we have generalized the above approach explicitly including the effects of the gravitational field by considering the most simplified nontrivial but rigorous treatment of a general relativistic system of neutrons, protons and electrons in β -equilibrium. It has been there proved that the traditional treatment for the description of neutron stars adopting the condition of local charge neutrality is not consistent with the Einstein-Maxwell equations and with microphysical conditions of equilibrium within quantum statistics. The role of the constancy of the general relativistic Fermi energy of each particle species pioneered by Klein (1949) has been there emphasized and, the full system of equilibrium equations consisting of the Einstein-Maxwell and general relativistic Thomas-Fermi equations has been formulated. The corresponding solution of such a system of

equations has been there given in the simplest possible example of a configuration of neutrons, protons and electrons in β -equilibrium with electromagnetic, weak and gravitational interactions. New electrodynamic and general relativistic properties of the equilibrium configurations have been there illustrated.

The aim of this article is to make an essential new step: we further proceed to the description of a system of neutrons, protons and electrons fulfilling strong, electromagnetic, weak and gravitational interactions. The essential role of the Klein first integrals is evidenced and their theoretical formulation is presented in the Einstein-Maxwell background. For the sake of generality the treatment is performed in the most general case in which finite temperature effects are also taking into account. We adopt throughout the article natural units $\hbar = c = 1$.

C.2.2. The Constitutive General Relativistic Equations

The densities in the core of a neutron star exceed the nuclear density $\rho_{\text{nuc}} \sim 2.7 \times 10^{14} \text{ g/cm}^3$ and may reach densities of order $\sim 10^{17} \text{ g/cm}^3$ at the verge of the gravitational collapse of the neutron star to a black hole. There is therefore the need of a consistent relativistic theory for the description of the interactions between the matter constituents. In particular, approaches for the nuclear interaction between nucleons based on phenomenological potentials and non-relativistic many-body theory become inapplicable (see Bowers et al. (1973b,a)).

A self-consistent relativistic and well-tested model for the nuclear interactions is the Walecka model (see Duerr (1956); Walecka (1974) for details). This model share common features with the model adopted by Bowers et al. in (Bowers et al., 1973b,a); in both of them the nucleons interact through a Yukawa coupling and the flat spacetime has been considered to construct the equation of state of nuclear matter. The technique of constructing the equation of state assuming flat spacetime has been generally used since, as pointed out in Bowers et al. (1973b,a), as long as $\rho < 10^{14} \text{ g/cm}^3$ the gravitational contributions to interactions between particles are negligible. However, when we turn to neutron star configurations at nuclear and supranuclear densities, it has been shown in Rotondo et al. (2011d) how the solution of the Einstein-Maxwell system of equations is mandatory.

In the often called extended version of the Walecka model, the strong interaction between nucleons is described by the exchange of three virtual mesons: σ is an isoscalar meson field providing the attractive long-range part of the nuclear force; ω is a massive vector field that models the repulsive short range and; ρ is the massive isovector field that takes account surface as well as isospin effects of nuclei (see also Boguta and Bodmer (1977); Ring (1996)).

The total Lagrangian density of the system is given by

$$\mathcal{L} = \mathcal{L}_g + \mathcal{L}_f + \mathcal{L}_\sigma + \mathcal{L}_\omega + \mathcal{L}_\rho + \mathcal{L}_\gamma + \mathcal{L}_{\text{int}}, \quad (\text{C.2.1})$$

where the Lagrangian densities for the free-fields are

$$\mathcal{L}_g = -\frac{R}{16\pi G}, \quad (\text{C.2.2})$$

$$\mathcal{L}_\gamma = -\frac{1}{4}F_{\mu\nu}F^{\mu\nu}, \quad (\text{C.2.3})$$

$$\mathcal{L}_\sigma = \frac{1}{2}\nabla_\mu\sigma\nabla^\mu\sigma - U(\sigma), \quad (\text{C.2.4})$$

$$\mathcal{L}_\omega = -\frac{1}{4}\Omega_{\mu\nu}\Omega^{\mu\nu} + \frac{1}{2}m_\omega^2\omega_\mu\omega^\mu, \quad (\text{C.2.5})$$

$$\mathcal{L}_\rho = -\frac{1}{4}\mathcal{R}_{\mu\nu}\mathcal{R}^{\mu\nu} + \frac{1}{2}m_\rho^2\rho_\mu\rho^\mu, \quad (\text{C.2.6})$$

where $\Omega_{\mu\nu} \equiv \partial_\mu\omega_\nu - \partial_\nu\omega_\mu$, $\mathcal{R}_{\mu\nu} \equiv \partial_\mu\rho_\nu - \partial_\nu\rho_\mu$, $F_{\mu\nu} \equiv \partial_\mu A_\nu - \partial_\nu A_\mu$ are the field strength tensors for the ω^μ , ρ and A^μ fields respectively, ∇_μ stands for covariant derivative and R is the Ricci scalar. We adopt the Lorenz gauge for the fields A_μ , ω_μ , and ρ_μ . The self-interaction scalar field potential $U(\sigma)$ is a quartic-order polynom for a renormalizable theory (see e.g. Lee and Wick (1974)). The specific functional form of $U(\sigma)$ is not relevant for the scope of this article, thus we will not adopt any particular form of it hereafter.

The Lagrangian density for the three fermion species is

$$\mathcal{L}_f = \sum_{i=e,N} \bar{\psi}_i (i\gamma^\mu D_\mu - m_i) \psi_i, \quad (\text{C.2.7})$$

where ψ_N is the nucleon isospin doublet, ψ_e is the electronic singlet, m_i states for the mass of each particle-specie and $D_\mu = \partial_\mu + \Gamma_\mu$, being Γ_μ the Dirac spin connections that satisfy the commutation relation

$$[\gamma_\mu, \Gamma_\nu] = \partial_\nu\gamma_\mu - \Gamma_{\mu\nu}^\alpha\gamma_\alpha, \quad (\text{C.2.8})$$

where $\Gamma_{\mu\nu}^\alpha$ denotes the Christoffel symbols.

The interacting part of the Lagrangian density is, in the minimal coupling assumption, given by

$$\mathcal{L}_{\text{int}} = -g_\sigma\sigma\bar{\psi}_N\psi_N - g_\omega\omega_\mu J_\omega^\mu - g_\rho\rho_\mu J_\rho^\mu + eA_\mu J_{\gamma,e}^\mu - eA_\mu J_{\gamma,N}^\mu, \quad (\text{C.2.9})$$

where the conserved currents are

$$J_\omega^\mu = \bar{\psi}_N \gamma^\mu \psi_N, \quad (\text{C.2.10})$$

$$J_\rho^\mu = \bar{\psi}_N \tau_3 \gamma^\mu \psi_N, \quad (\text{C.2.11})$$

$$J_{\gamma,e}^\mu = \bar{\psi}_e \gamma^\mu \psi_e, \quad (\text{C.2.12})$$

$$J_{\gamma,N}^\mu = \bar{\psi}_N \left(\frac{1 + \tau_3}{2} \right) \gamma^\mu \psi_N. \quad (\text{C.2.13})$$

The coupling constants of the σ , ω and ρ -fields are g_σ , g_ω and g_ρ , and e is the fundamental electric charge. The Dirac matrices γ^μ and the isospin Pauli matrices satisfy the Dirac algebra in curved spacetime (see e.g. Lee and Pang (1987))

$$\{\gamma^\mu, \gamma^\nu\} = 2g^{\mu\nu}, \quad (\text{C.2.14})$$

$$\{\gamma_\mu, \gamma_\nu\} = 2g_{\mu\nu}, \quad (\text{C.2.15})$$

$$\{\gamma^\mu, \gamma_\nu\} = 2\delta_\nu^\mu, \quad (\text{C.2.16})$$

$$[\tau_i, \tau_j] = 2i\epsilon_{ijk}\tau^k. \quad (\text{C.2.17})$$

The Einstein-Maxwell-Dirac system of equations is then given by

$$G_{\mu\nu} + 8\pi GT_{\mu\nu} = 0, \quad (\text{C.2.18})$$

$$\nabla_\mu F^{\mu\nu} - eJ_{ch}^\nu = 0, \quad (\text{C.2.19})$$

$$\nabla_\mu \Omega^{\mu\nu} + m_\omega^2 \omega^\nu - g_\omega J_\omega^\nu = 0, \quad (\text{C.2.20})$$

$$\nabla_\mu \mathcal{R}^{\mu\nu} + m_\rho^2 \rho^\nu - g_\rho J_\rho^\nu = 0, \quad (\text{C.2.21})$$

$$\nabla_\mu \nabla^\mu \sigma + \partial_\sigma U(\sigma) + g_s n_s = 0, \quad (\text{C.2.22})$$

$$[\gamma_\mu (iD^\mu - V_N^\mu) - \tilde{m}_N] \psi_N = 0, \quad (\text{C.2.23})$$

$$[\gamma_\mu (iD^\mu + eA^\mu) - m_e] \psi_e = 0, \quad (\text{C.2.24})$$

where the scalar density $n_s = \bar{\psi}_N \psi_N$, the nucleon effective mass $\tilde{m}_N \equiv m_N + g_\sigma \sigma$, and

$$V_N^\mu \equiv g_\omega \omega^\mu + g_\rho \tau \rho^\mu + e \left(\frac{1 + \tau_3}{2} \right) A^\mu, \quad (\text{C.2.25})$$

is the effective four potential of nucleons. The energy-momentum tensor of free-fields and free-fermions $T^{\mu\nu}$ of the system (C.2.3)–(C.2.6) is

$$T^{\mu\nu} = T_f^{\mu\nu} + T_\gamma^{\mu\nu} + T_\sigma^{\mu\nu} + T_\omega^{\mu\nu} + T_\rho^{\mu\nu}, \quad (\text{C.2.26})$$

where

$$T_\gamma^{\mu\nu} = -F_\alpha^\mu F^{\alpha\nu} - \frac{1}{4}g^{\mu\nu}F_{\alpha\beta}F^{\alpha\beta}, \quad (\text{C.2.27})$$

$$T_\sigma^{\mu\nu} = \nabla^\mu \nabla^\nu \sigma - g^{\mu\nu} \left[\frac{1}{2} \nabla_\sigma \sigma \nabla^\sigma \sigma - U(\sigma) \right], \quad (\text{C.2.28})$$

$$T_\omega^{\mu\nu} = -\Omega_\alpha^\mu \Omega^{\alpha\nu} - \frac{1}{4}g^{\mu\nu} \Omega_{\alpha\beta} \Omega^{\alpha\beta} + m_\omega^2 \left(\omega^\mu \omega^\nu - \frac{1}{2}g^{\mu\nu} \omega_\alpha \omega^\alpha \right) \quad (\text{C.2.29})$$

$$T_\rho^{\mu\nu} = -\mathcal{R}_\alpha^\mu \mathcal{R}^{\alpha\nu} - \frac{1}{4}g^{\mu\nu} \mathcal{R}_{\alpha\beta} \mathcal{R}^{\alpha\beta} + m_\rho^2 \left(\mathcal{R}^\mu \mathcal{R}^\nu - \frac{1}{2}g^{\mu\nu} \mathcal{R}_\alpha \omega^\alpha \right), \quad (\text{C.2.30})$$

are the contribution due to free-fields and $T_f^{\mu\nu}$ is the contribution of free-fermions which we discuss below.

C.2.3. The Thermodynamic Laws and the Field Equations in the Spherically Symmetric Case

We first introduce the non-rotating spherically symmetric spacetime metric

$$ds^2 = e^{\nu(r)} dt^2 - e^{\lambda(r)} dr^2 - r^2 d\theta^2 - r^2 \sin^2 \theta d\varphi^2, \quad (\text{C.2.31})$$

where the $\nu(r)$ and $\lambda(r)$ are only functions of the radial coordinate r .

For very large number of fermions, we can adopt the mean-field approximation in which fermion-field operators are replaced by their expectation values (see e.g. Walecka (1974) for details).

We write the nucleon doublet and the electronic spinor as $\psi_i = \psi_i(k)e^{-ik_\mu x^\mu}$ in the phase-space. Suppose that neutrons, protons and electrons, and the corresponding antiparticles, are in thermodynamic equilibrium with a finite temperature T . The occupation fermion-number operators of the “ k ”-state, $N_i(k) = \psi_i^\dagger(k)\psi_i(k)$ with $i = e, p, n$, are replaced by their Fermi-distributions

$$f_i^\pm(k) = \langle \psi_i^\pm(k)^\dagger \psi_i^\pm(k) \rangle = \left[\exp \left(\frac{\epsilon_i(k) \mp \mu_i}{k_B T} \right) + 1 \right]^{-1}, \quad (\text{C.2.32})$$

where k_B is the Boltzmann constant, μ_i and $\epsilon_i(k) = \sqrt{k^2 + \tilde{m}_i^2}$ denote the single-particle chemical potential and energy-spectrum (we recall that for electrons $\tilde{m}_e = m_e$). The sign ‘+’ correspond to particles and ‘-’ to antiparticles. We do not consider “real” bosons to be present in the system; the only distribution functions involved in the computation are due to fermions and antifermions and therefore phenomena as Bose-Einstein condensation does not occur within this theory (see e.g. Bowers et al. (1973b) for details).

It is worth to recall that all the thermodynamic quantities, e.g. $k, \epsilon, T \dots$, are written here in the local frame which is related to the coordinate frame by the

Lorentz “boost”

$$\Lambda_\alpha^{(a)} = (u_\alpha, \chi_\alpha, \Theta_\alpha, \Phi_\alpha), \quad (\text{C.2.33})$$

where $u_\alpha = e^{v/2}\delta_\alpha^0$, $\chi_\alpha = e^{\lambda/2}\delta_\alpha^1$, $\Theta_\alpha = r\delta_\alpha^2$, and $\Phi_\alpha = r\sin\theta\delta_\alpha^3$, being δ_β^α the usual Kronecker delta symbol.

The number-density n_i of the i -specie, taking into account the antiparticle contribution is, within the mean-field approximation, given by

$$n_i = \frac{2}{(2\pi)^3} \int d^3k [f_i^+(k) - f_i^-(k)]. \quad (\text{C.2.34})$$

The contribution of free-fermions and antifermions to the energy-momentum tensor can be then written in the perfect fluid form (see e.g. Ruffini and Bonazzola (1969))

$$T_f^{\mu\nu} = (\mathcal{E} + \mathcal{P})u^\mu u^\nu - \mathcal{P}g^{\mu\nu}, \quad (\text{C.2.35})$$

where u^μ is the four-velocity of the fluid which satisfies $u^\mu u_\mu = 1$, and the energy-density \mathcal{E} and the pressure \mathcal{P} are given by

$$\mathcal{E} = \sum_{i=n,p,e} \mathcal{E}_i, \quad \mathcal{P} = \sum_{i=n,p,e} \mathcal{P}_i, \quad (\text{C.2.36})$$

being \mathcal{E}_i and \mathcal{P}_i the single fermion-antifermion fluid contributions

$$\mathcal{E}_i = \frac{2}{(2\pi)^3} \int d^3k \epsilon_i(k) [f_i^+(k) + f_i^-(k)], \quad (\text{C.2.37})$$

$$\mathcal{P}_i = \frac{1}{3} \frac{2}{(2\pi)^3} \int d^3k \frac{k^2}{\epsilon_i(k)} [f_i^+(k) + f_i^-(k)]. \quad (\text{C.2.38})$$

The equation of state (C.2.36)–(C.2.38) satisfies the thermodynamic law

$$\mathcal{E} + \mathcal{P} - T\mathcal{S} = \sum_{i=n,p,e} n_i \mu_i, \quad (\text{C.2.39})$$

where $\mathcal{S} = S/V$ is the entropy per unit volume (entropy density) and $\mu_i = \partial\mathcal{E}/\partial n_i$ is the free-chemical potential of the i -specie. At zero-temperature $T = 0$, $\mu_i = \sqrt{(K_i^F)^2 + \tilde{m}_i^2}$ and $n_i = (K_i^F)^3/(3\pi^2)$, where K_i^F denotes the Fermi momentum of the i -specie.

The scalar density n_s , within the mean-field approximation, is given by the following expectation value

$$n_s = \langle \bar{\psi}_N \psi_N \rangle = \frac{2}{(2\pi)^3} \sum_{i=n,p} \int d^3k \frac{\tilde{m}_N}{\epsilon_i(k)} [f_i^+(k) + f_i^-(k)]. \quad (\text{C.2.40})$$

In the static case, only the temporal components of the covariant currents survive, i.e. $\langle \bar{\psi}(x) \gamma^i \psi(x) \rangle = 0$. Thus, by taking the expectation values of

Eqs. (C.2.10)–(C.2.13), we obtain the non-vanishing components of the currents

$$J_0^{ch} = n_{ch}u_0 = (n_p - n_e)u_0, \quad (\text{C.2.41})$$

$$J_0^\omega = n_b u_0 = (n_n + n_p)u_0, \quad (\text{C.2.42})$$

$$J_0^\rho = n_3 u_0 = (n_p - n_n)u_0, \quad (\text{C.2.43})$$

where n_b , n_p , n_n and n_e are the baryon, proton, neutron and electron number densities which are functions only of the spatial coordinates, and $u_0 = \sqrt{g_{00}} = e^{v/2}$.

Making a variation of Eq. (C.2.39) and using Eqs. (C.2.36)–(C.2.38) and (C.2.40), we obtain the generalized Gibbs-Duhem relation

$$d\mathcal{P} = \sum_{i=n,p,e} n_i d\mu_i - g_\sigma n_s d\sigma + \mathcal{S} dT, \quad (\text{C.2.44})$$

which can be rewritten as

$$d\mathcal{P} = \sum_{i=n,p,e} n_i d\mu_i - g_\sigma n_s d\sigma + \left(\mathcal{E} + \mathcal{P} - \sum_{i=n,p,e} n_i \mu_i \right) \frac{dT}{T}, \quad (\text{C.2.45})$$

where we have used Eq. (C.2.39) to eliminate \mathcal{S} , and we have used the relation between the scalar density and the fluid energy-density $n_s = \partial\mathcal{E}/\partial\tilde{m}_N$, which follows from Eqs. (C.2.36)–(C.2.38) and (C.2.40).

Therefore, the Einstein-Maxwell equations (C.2.18)–(C.2.22), within the mean-field approximation, become

$$e^{-\lambda(r)} \left(\frac{1}{r^2} - \frac{1}{r} \frac{d\lambda}{dr} \right) - \frac{1}{r^2} = -8\pi G T_0^0, \quad (\text{C.2.46})$$

$$e^{-\lambda(r)} \left(\frac{1}{r^2} + \frac{1}{r} \frac{dv}{dr} \right) - \frac{1}{r^2} = -8\pi G T_1^1, \quad (\text{C.2.47})$$

$$e^{-\lambda(r)} \left[\frac{1}{2} \left(\frac{dv}{dr} - \frac{d\lambda}{dr} \right) \left(\frac{1}{r} + \frac{1}{2} \frac{dv}{dr} \right) + \frac{1}{2} \frac{d^2 v}{dr^2} \right] = -8\pi G T_3^3, \quad (\text{C.2.48})$$

$$\frac{d^2 V}{dr^2} + \frac{dV}{dr} \left[\frac{2}{r} - \frac{1}{2} \left(\frac{dv}{dr} + \frac{d\lambda}{dr} \right) \right] = -e^\lambda e J_{ch}^0, \quad (\text{C.2.49})$$

$$\frac{d^2 \sigma}{dr^2} + \frac{d\sigma}{dr} \left[\frac{2}{r} - \frac{1}{2} \left(\frac{dv}{dr} + \frac{d\lambda}{dr} \right) \right] = e^\lambda [\partial_\sigma U(\sigma) + g_s n_s], \quad (\text{C.2.50})$$

$$\frac{d^2 \omega}{dr^2} + \frac{d\omega}{dr} \left[\frac{2}{r} - \frac{1}{2} \left(\frac{dv}{dr} + \frac{d\lambda}{dr} \right) \right] = -e^\lambda [g_\omega J_\omega^0 - m_\omega^2 \omega], \quad (\text{C.2.51})$$

$$\frac{d^2 \rho}{dr^2} + \frac{d\rho}{dr} \left[\frac{2}{r} - \frac{1}{2} \left(\frac{dv}{dr} + \frac{d\lambda}{dr} \right) \right] = -e^\lambda [g_\rho J_\rho^0 - m_\rho^2 \rho], \quad (\text{C.2.52})$$

where we have introduced the notation $\omega_0 = \omega$, $\rho_0 = \rho$, and $A_0 = V$. The metric function λ is related to the mass $M(r)$ and the electric field $E(r) = -e^{-(\nu+\lambda)/2}V'$ through

$$e^{-\lambda(r)} = 1 - \frac{2GM(r)}{r} + Gr^2E^2(r) = 1 - \frac{2GM(r)}{r} + \frac{GQ^2(r)}{r^2}, \quad (\text{C.2.53})$$

where we have introduced also the conserved charge $Q(r) = r^2E(r)$.

An important equation, although not independent of the Einstein-Maxwell equations (C.2.46)–(C.2.52), is given the energy-momentum conservation law

$$\nabla_\mu T^{\mu\nu} = -g_\omega J_\mu^\omega \Omega^{\mu\nu} - g_\rho J_\mu^\rho \mathcal{R}^{\mu\nu} + eJ_\mu^{ch} F^{\mu\nu}, \quad (\text{C.2.54})$$

from which we have

$$\frac{d\mathcal{P}}{dr} = -\frac{(\mathcal{E} + \mathcal{P})}{2} \frac{d\nu}{dr} - g_\sigma n_s \frac{d\sigma}{dr} - g_\omega J_\omega^0 \frac{d\omega}{dr} - g_\rho J_\rho^0 \frac{d\rho}{dr} - eJ_{ch}^0 \frac{dV}{dr}, \quad (\text{C.2.55})$$

where we have used the energy-momentum tensor $T^{\mu\nu}$ given by Eq. (C.2.26).

C.2.4. Constancy of the Klein potentials and β -equilibrium

Introducing the nucleon doublet and the electronic spinor in the wave-form $\psi_i = \psi_i(k)e^{-ik_\mu x^\mu}$ in phase-space, the Dirac equations (C.2.24) become

$$(\gamma_\mu \mathcal{K}_i^\mu - \tilde{m}_i)\psi_i(k) = 0, \quad (\text{C.2.56})$$

where

$$\mathcal{K}_i^\mu \equiv k^\mu - V_i^\mu, \quad V_e^\mu = -eA^\mu. \quad (\text{C.2.57})$$

In the mean-field approximation, making the quadrature of Dirac operators in Eq. (C.2.56) and averaging over all states “ k ”, we obtain the generalized chemical potentials or, for short Klein potentials for electrons E_e , neutrons E_n and protons E_p

$$E_e = \sqrt{g_{00}}\mu_e - eV = e^{v/2}\mu_e - eV, \quad (\text{C.2.58})$$

$$E_p = \sqrt{g_{00}}\mu_p + g_\omega\omega + g_\rho\rho + eV = e^{v/2}\mu_p + g_\omega\omega + g_\rho\rho + eV \quad (\text{C.2.59})$$

$$E_n = \sqrt{g_{00}}\mu_n + g_\omega\omega - g_\rho\rho = e^{v/2}\mu_n + g_\omega\omega - g_\rho\rho, \quad (\text{C.2.60})$$

where we have used Eqs. (C.2.14)–(C.2.17) and Eqs. (C.2.32), (C.2.34), (C.2.36)–(C.2.38). In the zero-temperature case, they are generalized Fermi energies for electrons $E_e = E_e^F$, neutrons $E_n = E_n^F$ and protons $E_p = E_p^F$.

Using the equations of motion for the fields ρ , ω and σ , and using the generalized Gibbs-Duhem relation (C.2.45), the energy-momentum conservation

equation (C.2.55) can be rewritten as

$$e^{\nu/2} \sum_{i=n,p,e} n_i \left(d\mu_i - \frac{dT}{T} \mu_i \right) + (\mathcal{E} + \mathcal{P}) e^{\nu/2} \left(\frac{dT}{T} + \frac{1}{2} d\nu \right) + g_\omega n_b d\omega + g_\rho n_3 d\rho + e n_{ch} dV = 0. \quad (\text{C.2.61})$$

The isothermal Tolman condition (Tolman, 1930) (see also Klein (1949)) demands the constancy of the gravitationally red-shifted temperature

$$\frac{dT}{T} + \frac{1}{2} d\nu = 0, \quad \text{or} \quad e^{\nu/2} T = \text{constant}. \quad (\text{C.2.62})$$

Such a condition can be used into Eq. (C.2.61) to obtain

$$\sum_{i=n,p,e} n_i d(e^{\nu/2} \mu_i) + g_\omega n_b d\omega + g_\rho n_3 d\rho + e n_{ch} dV = 0. \quad (\text{C.2.63})$$

Moreover, using the expressions (C.2.58)–(C.2.59) of the generalized chemical potentials, Eq. (C.2.63) can be rewritten as

$$\sum_{i=n,p,e} n_i dE_i = 0, \quad (\text{C.2.64})$$

which leads for independent and non-zero particle number densities $n_i \neq 0$ to the constancy of the Klein potentials (C.2.58)–(C.2.60) for each particle-species, i.e.

$$E_e = e^{\nu/2} \mu_e - eV = \text{constant}, \quad (\text{C.2.65})$$

$$E_p = e^{\nu/2} \mu_p + \mathcal{V}_p = \text{constant}, \quad (\text{C.2.66})$$

$$E_n = e^{\nu/2} \mu_n + \mathcal{V}_n = \text{constant}, \quad (\text{C.2.67})$$

where

$$\mathcal{V}_p = g_\omega \omega + g_\rho \rho + eV, \quad (\text{C.2.68})$$

$$\mathcal{V}_n = g_\omega \omega - g_\rho \rho. \quad (\text{C.2.69})$$

In the case of nuclear matter in β -equilibrium (assuming not trapped neutrinos), the values of the constant Klein potentials (C.2.65)–(C.2.67) are linked by the condition

$$E_n = E_p + E_e, \quad (\text{C.2.70})$$

which can be rewritten explicitly in terms of the chemical potentials as

$$\mu_n = \mu_p + \mu_e + 2g_\rho \rho e^{-\nu/2}. \quad (\text{C.2.71})$$

C.2.5. Concluding Remarks

We have presented the self-consistent equations of equilibrium at finite temperatures for a system of neutrons, protons and electrons in β -equilibrium within the framework of general relativity including quantum statistics, electro-weak, and strong interactions. In the mean-field approximation, we obtained the generalized particle chemical potentials from the Dirac equations for nucleons and electrons.

From the Einstein-Maxwell equations, the thermodynamic laws and energy-momentum conservation, we obtain the constancy of the Klein potential of each particle-specie and of the gravitationally red-shifted temperature throughout the configuration, i.e. the first Klein integrals and the Tolman isothermal condition respectively. In the non-interacting degenerate case, following a minimization energy procedure, it was demonstrated that the thermodynamic equilibrium condition of constancy of the generalized particle Fermi energy of all particle species holds (see Olson and Baily (1975)). Such a procedure can be straightforwardly applied to the present case, being the final result given by the equilibrium conditions (C.2.65) and (C.2.66).

The precise values of such constants are linked, in the case of nuclear matter in β -equilibrium, by Eq. (C.2.70), and their full determination needs the inclusion of additional constraints to the system, e.g. global charge neutrality (see e.g. Rotondo et al. (2011d)).

The correct implementation of such generalized Thomas-Fermi equilibrium conditions needs the self-consistent solution of the global problem of equilibrium of the configuration following from the solution of the Einstein-Maxwell equations (C.2.46), (C.2.47), (C.2.49)–(C.2.53), the general relativistic thermodynamic equilibrium conditions (C.2.62), (C.2.65) and (C.2.66), together with the constraints, e.g. β -equilibrium and global charge neutrality.

Thus, the full system of Einstein-Maxwell-Thomas-Fermi equations can be

rewritten in the form

$$e^{-\lambda(r)} \left(\frac{1}{r^2} - \frac{1}{r} \frac{d\lambda}{dr} \right) - \frac{1}{r^2} = -8\pi GT_0^0, \quad (\text{C.2.72})$$

$$e^{-\lambda(r)} \left(\frac{1}{r^2} + \frac{1}{r} \frac{dv}{dr} \right) - \frac{1}{r^2} = -8\pi GT_1^1, \quad (\text{C.2.73})$$

$$V'' + \frac{2}{r} V' \left[1 - \frac{r(v' + \lambda')}{4} \right] = -4\pi e e^{v/2} e^\lambda (n_p - n_e), \quad (\text{C.2.74})$$

$$\frac{d^2\sigma}{dr^2} + \frac{d\sigma}{dr} \left[\frac{2}{r} - \frac{1}{2} \left(\frac{dv}{dr} + \frac{d\lambda}{dr} \right) \right] = e^\lambda [\partial_\sigma U(\sigma) + g_s n_s], \quad (\text{C.2.75})$$

$$\frac{d^2\omega}{dr^2} + \frac{d\omega}{dr} \left[\frac{2}{r} - \frac{1}{2} \left(\frac{dv}{dr} + \frac{d\lambda}{dr} \right) \right] = -e^\lambda [g_\omega J_\omega^0 - m_\omega^2 \omega], \quad (\text{C.2.76})$$

$$\frac{d^2\rho}{dr^2} + \frac{d\rho}{dr} \left[\frac{2}{r} - \frac{1}{2} \left(\frac{dv}{dr} + \frac{d\lambda}{dr} \right) \right] = -e^\lambda [g_\rho J_\rho^0 - m_\rho^2 \rho], \quad (\text{C.2.77})$$

$$E_e = e^{v/2} \mu_e - eV = \text{constant}, \quad (\text{C.2.78})$$

$$E_p = e^{v/2} \mu_p + \mathcal{V}_p = \text{constant}, \quad (\text{C.2.79})$$

$$E_n = e^{v/2} \mu_n + \mathcal{V}_n = \text{constant}, \quad (\text{C.2.80})$$

$$e^{v/2} T = \text{constant}, \quad (\text{C.2.81})$$

where the constants E_n , E_p and E_e are linked by Eq. (C.2.70) and $\mathcal{V}_{p,n}$ is given by Eq. (C.2.68). In particular, in the degenerate case $T = 0$, Eq. (C.2.74) becomes

$$\hat{V}'' + \frac{2}{r} \hat{V}' \left[1 - \frac{r(v' + \lambda')}{4} \right] = -4\pi\alpha e^{v/2} e^\lambda \left\{ n_p - \frac{e^{-3v/2}}{3\pi^2} [\hat{V}^2 + 2m_e \hat{V} - m_e^2 (e^v - 1)]^{3/2} \right\}, \quad (\text{C.2.82})$$

where $\hat{V} \equiv eV + E_e$ and we have used Eq. (C.2.78) into Eq. (C.2.74). This equation is the general relativistic extension of the relativistic Thomas-Fermi equation recently introduced in Rotondo et al. (2011c) for the study of compressed atoms. In addition, Eq. (C.2.82) has been recently used to obtain the globally neutral configurations in the simpler case of degenerate neutrons, protons and electrons in β -equilibrium (Rotondo et al., 2011d).

C.3. On the constitutive equations of a self-gravitating system of neutrons, protons and electrons in β -equilibrium at finite temperatures

C.3.1. Introduction

We have recently introduced a new approach which thanks to the existence of scaling laws can apply to compressed atoms as well as to massive nuclear matter cores of stellar dimensions (Rotondo et al., 2011c). This approach concerning the compressed atom has already given a new contribution in the study of white dwarfs. It represents the first self-consistent calculation taking into due account the electromagnetic contribution in a relativistic treatment of the Thomas-Fermi equation, within global formulation of the equilibrium of white dwarfs in general relativity (Rotondo et al., 2011b).

The application of the above results (Rotondo et al., 2011c,b) to the case of neutron stars is much more complex and it has been approached stepwise. As a first step we have considered the application of this novel approach to the case of a system of neutrons, protons, and electrons in β -equilibrium at zero temperatures within general relativity (Rotondo et al., 2011d). These results are shortly recalled in Sec. C.3.2. The essential role of the generalized Fermi energy of particles (the Klein potentials) and their constancy on the entire equilibrium configuration has been outlined. The existence of an electric potential over the entire configuration has been evidenced.

We have there proved, for the case of this simplified example where strong interactions are neglected, that the traditional approach of describing the system imposing the condition of local charge neutrality and solving the corresponding TOV equations (see e.g. Shapiro and Teukolsky (1983)) is conceptually inconsistent. We have then substitute the condition of local charge neutrality with the condition of global charge neutrality and derived the correct system of equations within the Einstein-Maxwell-Thomas-Fermi system. The boundary conditions are also different from a traditional Cauchy data with the values of the functions and first derivatives at the center into a boundary condition at the center and delicate eigenvalue problem at the boundary determining the condition of charge neutrality at the border; see Sec. C.3.2. The conceptual differences and the alternative mathematical equations of the two approaches, the ones imposing local versus global charge neutrality, lead to the presence of additional electro-dynamical global structures. However, in the specific simple example considered in Rotondo et al. (2011d), they do not give significant quantitative differences in the mass-radius relation for the equilibrium configurations. A very different situation occurs when strong interactions are also taken into account.

Interestingly, these results should have been expected on the ground of some classical works dating back to Rosseland (1924) about the gravito-polarization in self-gravitating ideal Boltzmann electron-ion plasma. We indeed show that our general relativistic equations for the case of global charge neutrality in the Newtonian regime reproduce the Rosseland result. The work of Rosseland has attracted in time additional attention and has been generalized to the case of multicomponent systems; see e.g. Iosilevskiy (2009) and also in the case of general relativity the important results (Klein, 1949; Kodama and Yamada, 1972; Olson and Bailyn, 1975).

In order to transfer these results in the treatment of realistic neutron stars, the introduction of strong interactions is clearly necessary. We have recently generalized our treatment to the case of strong interactions in Rueda et al. (2011). There the major aim has been to prove the constancy of the Klein potentials in the case in which the nuclear interactions are described by a Lagrangian including in addition to the gravitational, electromagnetic, and weak interactions, also the presence of σ , ω , and ρ virtual mesons that mediate the nuclear interactions. These results are shortly summarized for completeness in Sec. C.3.3.

It is clear that neutron stars are not at zero temperatures but have temperatures which in the case of the Crab pulsar are $T \sim 10^6$ K, see e.g. Tennant et al. (2001); Weisskopf et al. (2004). It has been pointed out to us that the thermal energy expected in a neutron star is much larger than the Coulomb energy obtained e.g. in Rotondo et al. (2011d). Before proceeding further in this research we have to prove that these gravito-polarization effect do survive in the presence of a system at $T \neq 0$. In any way, the study of the equilibrium of a system of neutrons, protons, and electrons including all the interactions need to be generalized to the case of finite temperatures. This treatment is here presented in Sec. C.3.4. The constancy of the Klein potentials in this more general case is presented in Sec. C.3.5 where it is also explicitly shown how the thermal effects do not modify the existence of gravito-polarization. The generality of the formalism here introduced allows to approach as well the classical Boltzmann limit consistently.

we have finally outlined in the conclusions how this theoretical formulation is now sufficient to approach the problem of the possible existence of overcritical fields at the interface between the the core and the crust of the neutron star.

C.3.2. Einstein-Maxwell-Thomas-Fermi equations in the degenerate case

Following Rotondo et al. (2011d), we consider the equilibrium configurations of a degenerate gas of neutrons, protons and electrons with total matter en-

ergy density and total matter pressure

$$\mathcal{E} = \sum_{i=n,p,e} \frac{2}{(2\pi\hbar)^3} \int_0^{P_i^F} \epsilon_i(p) 4\pi p^2 dp, \quad (\text{C.3.1})$$

$$P = \sum_{i=n,p,e} \frac{1}{3} \frac{2}{(2\pi\hbar)^3} \int_0^{P_i^F} \frac{p^2}{\epsilon_i(p)} 4\pi p^2 dp, \quad (\text{C.3.2})$$

where $\epsilon_i(p) = \sqrt{c^2 p^2 + m_i^2 c^4}$ is the relativistic single particle energy and P_i^F denote the Fermi momentum, related to the particle number density n_i by $n_i = (P_i^F)^3 / (3\pi^2 \hbar^3)$.

Introducing the metric for a spherically symmetric non-rotating configuration

$$ds^2 = e^{\nu(r)} c^2 dt^2 - e^{\lambda(r)} dr^2 - r^2 d\theta^2 - r^2 \sin^2 \theta d\varphi^2, \quad (\text{C.3.3})$$

the full system of equations composed by the Einstein-Maxwell-Thomas-Fermi equations can be written as (see Rotondo et al. (2011d) for details)

$$M' = 4\pi r^2 \frac{\mathcal{E}}{c^2} - \frac{4\pi r^3}{c^2} e^{-\nu/2} \hat{V}' \left\{ n_p - \frac{e^{-3\nu/2}}{3\pi^2} [\hat{V}^2 + 2m_e c^2 \hat{V} - m_e^2 c^4 (e^\nu - 1)]^{3/2} \right\}, \quad (\text{C.3.4})$$

$$\nu' = \frac{2G}{c^2} \frac{4\pi r^3 P / c^2 + M - r^3 E^2 / c^2}{r^2 \left(1 - \frac{2GM}{c^2 r} + \frac{Gr^2 E^2}{c^4} \right)}, \quad (\text{C.3.5})$$

$$E_e^F = e^{\nu/2} \mu_e - m_e c^2 - eV = \text{constant}, \quad (\text{C.3.6})$$

$$E_p^F = e^{\nu/2} \mu_p - m_p c^2 + eV = \text{constant}, \quad (\text{C.3.7})$$

$$E_n^F = E_e^F + E_p^F - (m_n - m_e - m_p) c^2, \quad (\text{C.3.8})$$

$$\hat{V}'' + \frac{2}{r} \hat{V}' \left[1 - \frac{r(\nu' + \lambda')}{4} \right] = -4\pi \alpha \hbar c e^{\nu/2} e^\lambda \left\{ n_p - \frac{e^{-3\nu/2}}{3\pi^2} [\hat{V}^2 + 2m_e c^2 \hat{V} - m_e^2 c^4 (e^\nu - 1)]^{3/2} \right\}, \quad (\text{C.3.9})$$

where a prime stands for radial derivative, Eqs. (C.3.6)–(C.3.7) are the extension to general relativity of the Thomas-Fermi equilibrium condition on the generalized Fermi energies of electrons and protons, Eq. (C.3.8) is the condition of β -equilibrium between neutrons, protons, and electrons. We recall that from Eqs. (C.3.6)–(C.3.8) it follows also the constancy of the generalized neutron Fermi energy. The Eq. (C.3.9) is the general relativistic extension of the relativistic Thomas-Fermi equation recently introduced in the rel-

ativistic Feynman-Metropolis-Teller treatment for the study of compressed atoms (Rotondo et al., 2011c). In the above equations e is the fundamental charge, α is the fine structure constant, V is the Coulomb potential, $\mu_i = \partial\mathcal{E}/\partial n_i = \sqrt{c^2(P_i^F)^2 + m_i^2 c^4}$ is the free-chemical potential of particle-species, $\lambda(r)$ is the metric function related to the mass $M(r)$ and the electric field $E(r) = -e^{-(\nu+\lambda)/2}V'$ through

$$e^{-\lambda} = 1 - \frac{2GM(r)}{c^2 r} + \frac{G}{c^4} r^2 E^2(r). \quad (\text{C.3.10})$$

and $\hat{V} = E_e^F + eV$.

As shown in Rotondo et al. (2011d), the condition of local charge neutrality $n_e(r) = n_p(r)$ often adopted in literature is not consistent with Eqs. (C.3.6) and (C.3.7), see Fig. 1 of Rotondo et al. (2011d) for details. Therefore, we consider equilibrium configurations fulfilling only global charge neutrality. We solve self-consistently Eq. (C.3.4) and (C.3.5) for the metric, Eqs. (C.3.6)–(C.3.8) for the equilibrium of the three degenerate fermion species and for the β -equilibrium. The crucial equation relating the proton and the electron distributions is then given by the general relativistic Thomas-Fermi equation (C.3.9). The boundary conditions are: for Eq. (C.3.4) the regularity at the origin: $M(0) = 0$, for Eqs. (C.3.6)–(C.3.8) a given value of the central density, and for Eq. (C.3.9) the regularity at the origin $n_e(0) = n_p(0)$, and a second condition at infinity which results in an eigenvalue problem determined by imposing the global charge neutrality conditions

$$\hat{V}(R_e) = E_e^F, \quad \hat{V}'(R_e) = 0, \quad (\text{C.3.11})$$

at the radius R_e of the electron distribution defined by

$$P_e^F(R_e) = 0, \quad (\text{C.3.12})$$

from which follows

$$\begin{aligned} E_e^F &= m_e c^2 e^{\nu(R_e)/2} - m_e c^2 \\ &= m_e c^2 \sqrt{1 - \frac{2GM(R_e)}{c^2 R_e}} - m_e c^2. \end{aligned} \quad (\text{C.3.13})$$

The eigenvalue problem consists in determining the gravitational potential and the Coulomb potential at the center of the configuration that satisfy the conditions (C.3.11)–(C.3.13) at the boundary. In Fig. 2 of Rotondo et al. (2011d) we have shown the solution for the density, the gravitational potential and electric potential for a configuration with central density $\rho(0) = 3.94\rho_{\text{nuc}}$, where $\rho_{\text{nuc}} \sim 2.7 \times 10^{14} \text{ g/cm}^3$.

A particular interesting new feature is the approach to the boundary of the

configuration where three different radii are present corresponding to distinct radii at which the individual particle Fermi pressures vanish. The radius R_e for the electron component corresponding to $P_e^F(R_e) = 0$, the radius R_p for the proton component corresponding to $P_p^F(R_p) = 0$ and the radius R_n for the neutron component corresponding to $P_n^F(R_n) = 0$. For a configuration with the aforementioned central density we found, for instance, $R_n \simeq 12.735$ km, $R_p \simeq 12.863$ km and $R_e \simeq R_p + 10^3 \lambda_e$ where $\lambda_e = \hbar/(m_e c)$ denotes the electron Compton wavelength (see Figs. 2 and 3 of Rotondo et al. (2011d), for details). The occurrence of the radius R_n is due to the threshold energy for inverse β -decay equilibrium between free neutrons, protons, and electrons, at around $\rho \sim 10^7$ (see e.g. Shapiro and Teukolsky (1983)). The electron component follows closely the proton component up to the radius R_p where the proton density drops to zero. The “proton skin”, $R_p - R_n \sim 0.1$ km, can be understood as being due to the difference between the proton and the neutron mass. The charge difference leads to gravitational and Coulomb forces acting on protons and only gravitational force on neutrons. The electron component then fully neutralizes the positive charge at R_e leading to a global configuration without net charge, contrary to the results presented e.g. in Olson and Bailyn (1978).

It can be seen from Fig. 2 in Rotondo et al. (2011d) that the depth of the Coulomb potential is of the order of $\lesssim m_\pi c^2$. In Fig. C.4 we have plotted the Coulomb potential and the corresponding electric field of the configuration studied here and in Rotondo et al. (2011d). A Coulomb potential $\sim m_\pi c^2/e$ decreasing in a typical macroscopic neutron star radius $R \sim \lambda_\pi(m_{\text{Planck}}/m_p)$ creates an electric field $\sim (m_p/m_{\text{Planck}})(m_\pi/m_e)^2 E_c \sim 10^{-14} E_c$, being $E_c = m_e^2 c^3/(e\hbar)$ the critical electric field for vacuum polarization.

C.3.3. Newtonian limit

Despite the fact that the strong gravitational field of neutron stars requires a general relativistic treatment, it is interesting to explore the Newtonian limit of all the above considerations. This can help to elucidate if the gravito-electromagnetic effects we have found are of general relativistic nature or to prove their validity in a Newtonian regime.

The Newtonian limit of the equilibrium equations can be obtained by the weak-field non-relativistic limit. We expand the gravitational potential at first-order $e^{v/2} \approx 1 + \Phi/c^2$, where Φ is the Newtonian gravitational potential. In the non-relativistic mechanics limit $c \rightarrow \infty$, the particle chemical potential becomes $\mu_i \rightarrow \tilde{\mu}_i + m_i c^2$, where $\tilde{\mu}_i = (P_i^F)^2/(2m_i)$ denotes the non-relativistic free-chemical potential. Applying these considerations, the electron and pro-

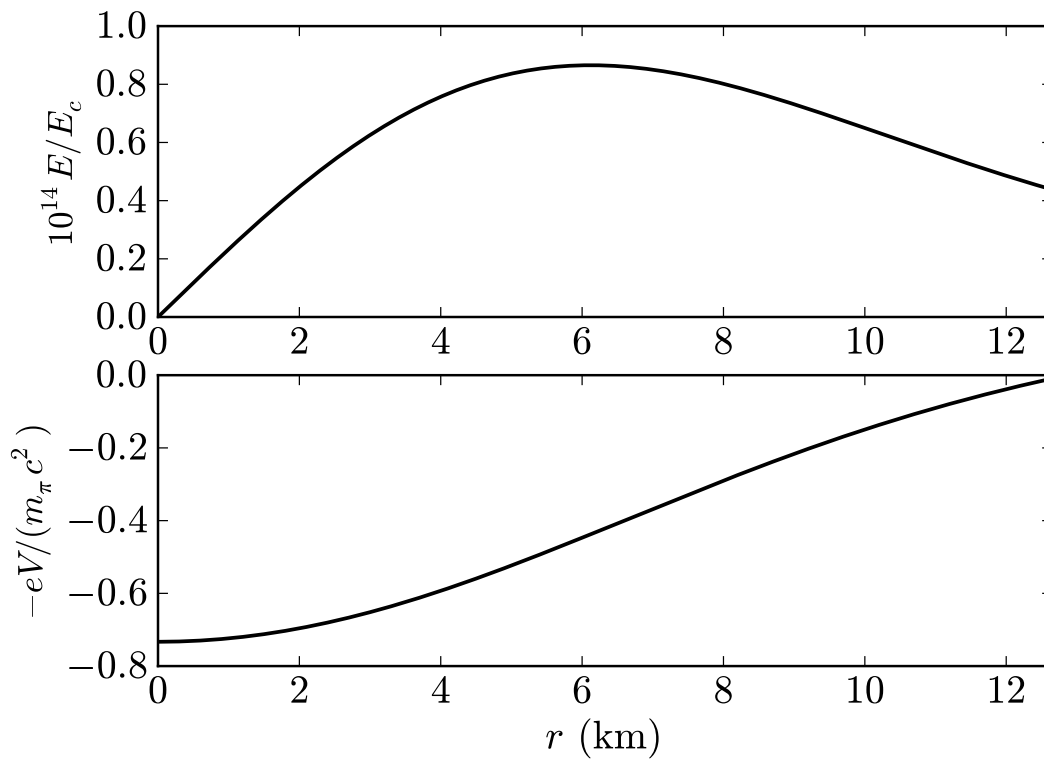


Figure C.4.: Electric field and electron Coulomb potential energy of the configuration of neutrons, protons, and electrons in β -equilibrium studied here and in Rotonondo et al. (2011d).

ton equilibrium law (C.3.6) becomes

$$E_p^{F,\text{Newt}} = \tilde{\mu}_p + m_p\Phi + eV = \text{constant}, \quad (\text{C.3.14})$$

$$E_e^{F,\text{Newt}} = \tilde{\mu}_e + m_e\Phi - eV = \text{constant}, \quad (\text{C.3.15})$$

which is the classical condition of thermodynamic equilibrium of a fluid of charged particles in presence of external gravitational and electrostatic fields.

The condition of β -equilibrium is, in this case, given by

$$E_n^{F,\text{Newt}} = E_p^{F,\text{Newt}} + E_e^{F,\text{Newt}}, \quad (\text{C.3.16})$$

which links the constants $E_p^{F,\text{Newt}}$ and $E_e^{F,\text{Newt}}$ to the constant neutron Fermi energy $E_n^{F,\text{Newt}}$.

From the constancy of the proton and electron Fermi energies it follows the relation

$$\tilde{\mu}_p - \tilde{\mu}_e + (m_p - m_e)\Phi + 2eV = \text{constant}, \quad (\text{C.3.17})$$

which in the case of an ideal electron-ion gas becomes the Rosseland relation of equilibrium (see Eq. 7 in Rosseland (1924)). It is interesting to obtain from the above equation an estimate of the Coulomb potential well inside the configuration. Evaluating Eq. (C.3.17) at the radius of the configuration where the particle free chemical potentials go to zero, we obtain an estimate of the ratio of the Coulomb potential energy and the gravitational energy close to the surface of the configuration

$$\frac{eV(R)}{\Phi(R)} \sim -\frac{m_p - m_e}{2}. \quad (\text{C.3.18})$$

Assuming that the system is at nuclear density, $\rho \sim m_p/\lambda_\pi^3$ where $\lambda_\pi = \hbar/(m_\pi c)$ is the pion Compton wavelength, the mass and the radius of the configuration are roughly given by $M \sim m_{\text{Planck}}^3/m_p^2$ and $R \sim \lambda_\pi(m_{\text{Planck}}/m_p)$ and therefore the gravitational potential will be $\Phi(R) = -GM/R \sim (m_\pi/m_p)c^2$. Consequently, the Coulomb potential energy close to the border is approximately $eV(R) \sim m_\pi c^2/2$. Assuming a constant charge density approximation, the Coulomb potential energy at the center of the configuration is 3/2 times its value at the surface, thus we obtain approximately

$$eV(0) \sim \frac{3}{4}m_\pi c^2, \quad (\text{C.3.19})$$

which is in full agreement with both with the numerical results and with the general relativistic formulas given by Eqs. (21) and (22) of Rotondo et al. (2011d). This numerical value is also in line with the Coulomb potential well obtained from the idealized treatment presented in Ruffini (2008c); Popov

(2010); Rotondo et al. (2011e,c).

In the weak-field non-relativistic limit, the Einstein-Maxwell equations (C.3.4)–(C.3.9) become

$$M' = 4\pi r^2 \rho(r), \quad (\text{C.3.20})$$

$$\Phi' = \frac{GM}{r^2}, \quad (\text{C.3.21})$$

$$P' = -\frac{GM}{r^2} \rho - \left[n_p - \frac{(2m_e)^{3/2}}{3\pi^2 \hbar^3} (\hat{V} - m_e \Phi)^{3/2} \right] \hat{V}', \quad (\text{C.3.22})$$

$$\hat{V}'' + \frac{2}{r} \hat{V}' = -4\pi e^2 \left[n_p - \frac{(2m_e)^{3/2}}{3\pi^2 \hbar^3} (\hat{V} - m_e \Phi)^{3/2} \right], \quad (\text{C.3.23})$$

where ρ in this case is the rest-mass density

$$\rho = \sum_{i=n,p,e} m_i n_i. \quad (\text{C.3.24})$$

The solution of Eqs. (C.3.14), (C.3.20)–(C.3.23) together with the β -equilibrium condition (C.3.16) leads to qualitatively similar electro-dynamical properties as the one obtained in the general relativistic case. In Fig. C.5 we show the electric field in the region $r < R_n$ ($R_n^{\text{Newt}} < R_n^{\text{GR}}$) both for the Newtonian as well as for the General Relativistic configuration for the given central density $\rho(0) = 3.94\rho_{\text{nuc}}$. From the quantitative point of view, the electric field of the Newtonian configuration is larger than the electric field of the general relativistic configuration.

C.3.4. Introducing strong interactions

It is clear now that if one considers a fluid of only neutrons, protons, and electrons in β -equilibrium neglecting the effects of the strong interactions and the presence of a crust, then the electromagnetic structure is the one shown in Figs. C.4 and C.5.

The effect of having different radii R_n , R_p , and R_e needs to be also studied in the more general case when strong interactions and the presence of the crust of the neutron star are included. The complete study of such a problem must to be necessarily done within a fully relativistic approach taking into account the strong, weak, electromagnetic, and gravitational interactions.

Indeed, in the mean time we have given an essential step forward in Rueda et al. (2011) by formulating such a treatment. The nuclear interactions have been there included through the Walecka model (see Duerr (1956); Walecka (1974) for details, and Bowers et al. (1973b,a) for a similar theory) in which nucleons interact by Yukawa-like couplings. The strong interaction between nucleons is thus described by the exchange of three virtual mesons: an isoscalar

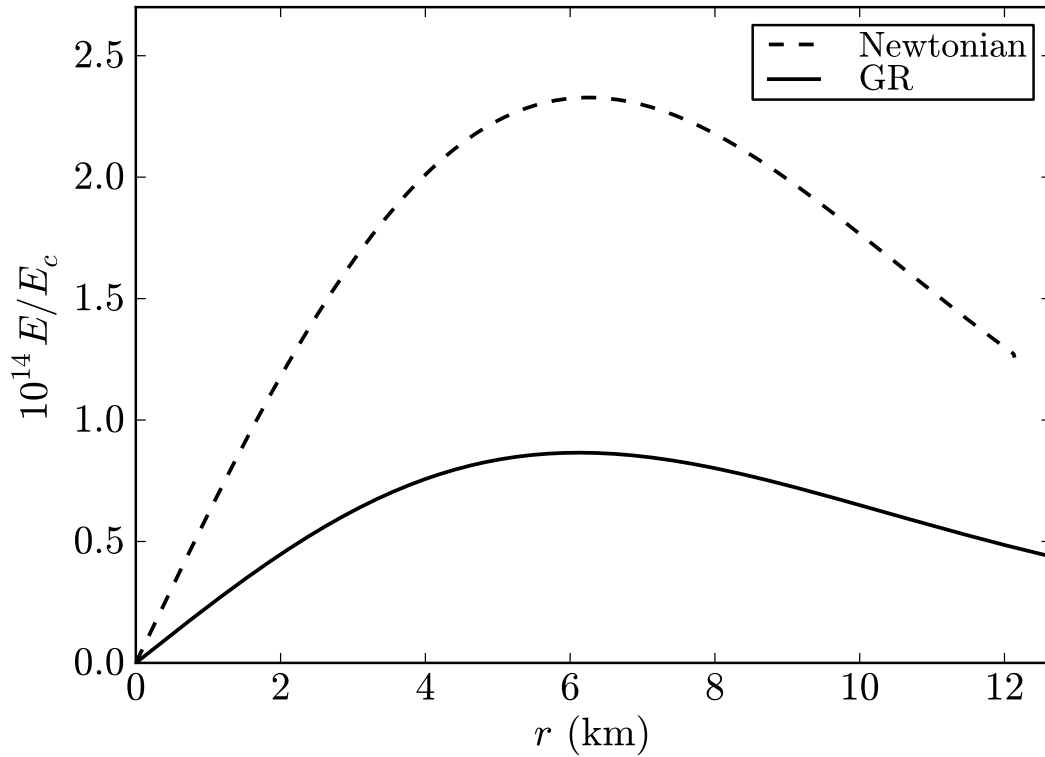


Figure C.5.: Electric field (multiplied by 10^{14}) in units of the critical field $E_c = m_e^2 c^3 / (e\hbar) \sim 10^{16}$ Volt/cm in the region $r < R_n$ both for the Newtonian and the General Relativistic configurations. The central density of both systems is $\rho(0) = 3.94\rho_{\text{nuc}}$ where $\rho_{\text{nuc}} = 2.7 \times 10^{14}$ g cm⁻³ is the nuclear density.

meson field σ providing the attractive long-range part of the nuclear force; the massive vector field ω_μ that models the repulsive short range and; the massive isovector field ρ_μ which takes account of the isospin effects of nuclei (see also Boguta and Bodmer (1977); Ring (1996)).

As shown in Rueda et al. (2011), the more general Einstein-Maxwell-Thomas-Fermi equations including strong interactions which generalizes Eqs. (C.3.65)–(C.3.71) can be written as (in units with $\hbar = c = 1$)

$$e^{-\lambda(r)} \left(\frac{1}{r^2} - \frac{\lambda'}{r} \right) - \frac{1}{r^2} = -8\pi G T_0^0, \quad (\text{C.3.25})$$

$$e^{-\lambda(r)} \left(\frac{1}{r^2} + \frac{\nu'}{r} \right) - \frac{1}{r^2} = -8\pi G T_1^1, \quad (\text{C.3.26})$$

$$\nabla^\mu \nabla_\mu V = -4\pi e^\lambda e J_0^{ch}, \quad (\text{C.3.27})$$

$$\nabla^\mu \nabla_\mu \sigma = e^\lambda [\partial_\sigma U(\sigma) + g_\sigma n_s], \quad (\text{C.3.28})$$

$$\nabla^\mu \nabla_\mu \omega = -e^\lambda (g_\omega J_\omega^0 - m_\omega^2 \omega), \quad (\text{C.3.29})$$

$$\nabla^\mu \nabla_\mu \rho = -e^\lambda (g_\rho J_\rho^0 - m_\rho^2 \rho), \quad (\text{C.3.30})$$

$$E_e = e^{\nu/2} \mu_e - eV = \text{constant}, \quad (\text{C.3.31})$$

$$E_p = e^{\nu/2} \mu_p + \mathcal{V}_p = \text{constant}, \quad (\text{C.3.32})$$

$$E_n = e^{\nu/2} \mu_n + \mathcal{V}_n = \text{constant}, \quad (\text{C.3.33})$$

$$e^{\nu/2} T = \text{constant}, \quad (\text{C.3.34})$$

where $\nabla^\mu \nabla_\mu = d^2/dr^2 + [2/r - (1/2)(\nu' + \lambda')]d/dr$, being ∇^μ the covariant derivative and

$$\mathcal{V}_p = g_\omega \omega + g_\rho \rho + eV, \quad (\text{C.3.35})$$

$$\mathcal{V}_n = g_\omega \omega - g_\rho \rho, \quad (\text{C.3.36})$$

are the effective potentials of nucleons, being $V \equiv A_0$, $\omega \equiv \omega_0$, $\rho \equiv \omega_0$ the time components of the electromagnetic and the meson potentials, and g_σ , g_ω , g_ρ denote the coupling constants between the nucleons and the massive mesons. The self-interaction scalar field potential $U(\sigma)$ can be in general a quartic-order polynom for a renormalizable theory (see e.g. Lee and Wick (1974)).

The scalar density is given by $n_s = \partial \mathcal{E} / \partial \tilde{m}_N$ where $\tilde{m}_N = m_N + g_\sigma \sigma$ is the effective nucleon mass. The only non-vanishing components of the currents are

$$J_0^{ch} = (n_p - n_e)u_0, \quad (\text{C.3.37})$$

$$J_0^\omega = (n_n + n_p)u_0, \quad (\text{C.3.38})$$

$$J_0^\rho = (n_p - n_n)u_0, \quad (\text{C.3.39})$$

C.3. On the constitutive equations of a self-gravitating system of neutrons, protons and electrons in β -equilibrium at finite temperatures

where $u_0 = \sqrt{g_{00}} = e^{v/2}$ is the covariant time component of the four-velocity of the fluid.

The function $\lambda(r)$ satisfies also in this case Eq. (C.3.10) and the energy-momentum tensor is

$$T^{\mu\nu} = T_f^{\mu\nu} + T_\gamma^{\mu\nu} + T_\sigma^{\mu\nu} + T_\omega^{\mu\nu} + T_\rho^{\mu\nu}, \quad (\text{C.3.40})$$

where

$$T_\gamma^{\mu\nu} = -\frac{1}{4\pi} \left(F_\alpha^\mu F^{\alpha\nu} + \frac{1}{4} g^{\mu\nu} F_{\alpha\beta} F^{\alpha\beta} \right), \quad (\text{C.3.41})$$

$$T_\sigma^{\mu\nu} = \nabla^\mu \nabla^\nu \sigma - g^{\mu\nu} \left[\frac{1}{2} \nabla_\sigma \sigma \nabla^\sigma \sigma - U(\sigma) \right], \quad (\text{C.3.42})$$

$$\begin{aligned} T_\omega^{\mu\nu} &= -\Omega_\alpha^\mu \Omega^{\alpha\nu} - \frac{1}{4} g^{\mu\nu} \Omega_{\alpha\beta} \Omega^{\alpha\beta} \\ &+ m_\omega^2 \left(\omega^\mu \omega^\nu - \frac{1}{2} g^{\mu\nu} \omega_\alpha \omega^\alpha \right), \end{aligned} \quad (\text{C.3.43})$$

$$\begin{aligned} T_\rho^{\mu\nu} &= -\mathcal{R}_\alpha^\mu \mathcal{R}^{\alpha\nu} - \frac{1}{4} g^{\mu\nu} \mathcal{R}_{\alpha\beta} \mathcal{R}^{\alpha\beta} \\ &+ m_\rho^2 \left(\mathcal{R}^\mu \mathcal{R}^\nu - \frac{1}{2} g^{\mu\nu} \mathcal{R}_\alpha \mathcal{R}^\alpha \right), \end{aligned} \quad (\text{C.3.44})$$

$$T_f^{\mu\nu} = (\mathcal{E} + P) u^\mu u^\nu - P g^{\mu\nu}, \quad (\text{C.3.45})$$

where $\Omega_{\mu\nu} \equiv \partial_\mu \omega_\nu - \partial_\nu \omega_\mu$, $\mathcal{R}_{\mu\nu} \equiv \partial_\mu \rho_\nu - \partial_\nu \rho_\mu$, $F_{\mu\nu} \equiv \partial_\mu A_\nu - \partial_\nu A_\mu$ are the field strength tensors for the ω^μ , ρ^μ and A^μ fields respectively.

The equilibrium conditions of the constancy of the Klein potentials of the particles throughout the configuration is expressed by Eqs. (C.3.31)–(C.3.33) and Eq. (C.3.34) is the Tolman isothermality condition analogous to Eq. (C.3.71).

There are additional contributions of the strong interaction to the nuclear symmetry energy given within this theory mainly by the ρ -meson. Such contributions change the proton skin structure $R_p > R_n$ shown in this article to a “neutron skin” effect $R_n > R_p$ in the core-crust boundary layer at nuclear density Belvedere et al. (2011), in close analogy to the neutron skin observed in neutron rich nuclei, see e.g. Tamii et al. (2011).

C.3.5. Finite temperature effects

The above results have been obtained within the zero temperature approximation. Temperatures of the order of $\sim 10^6$ K are expected to exist at the surface of old neutron stars (Tennant et al., 2001; Weisskopf et al., 2004), or temperatures of $10^8 - 10^9$ K could, in principle, exist in neutron star interiors. We are going to show that these thermal effects do not affect the considerations on gravito-polarization here introduced. For neutron stars, the Fermi

temperature

$$T_i^F = \frac{\mu_i - m_i c^2}{k}, \quad (\text{C.3.46})$$

where k is the Boltzmann constant, can be as large as $\sim 10^{12}$ K for electrons, $\sim 10^{11}$ K for protons and $\sim 10^{13}$ K for neutrons for typical central densities of neutron stars. This means that neutron stars interiors are, at a high degree of accuracy, degenerate systems. However, the total thermal energy of a neutron star $E_{\text{th}} \sim 10^{48} T_9^2$ erg (see e.g. Yakovlev and Pethick (2004)) where T_9 is the temperature in units of 10^9 K, is much larger than the Coulomb energy $E_C \sim (1/6)R^3 E^2 \sim 10^{16}$ erg, where E is the internal electric field here considered (see Figs. C.4 and C.5) and R is the radius of the configuration. It can be then of interest to ask the question if our electro-dynamical structure will still occur in presence of thermal effects.

In this more general case, the equation of state given by Eqs. (C.3.1) and (C.3.2), is replaced by

$$\mathcal{E} = \sum_{i=n,p,e} \frac{2}{(2\pi\hbar)^3} \int_0^\infty \tilde{\epsilon}_i(p) f_i(p) 4\pi p^2 dp, \quad (\text{C.3.47})$$

$$P = \sum_{i=n,p,e} \frac{1}{3} \frac{2}{(2\pi\hbar)^3} \int_0^\infty \frac{p^2 f_i(p)}{\tilde{\epsilon}_i(p) + m_i c^2} 4\pi p^2 dp, \quad (\text{C.3.48})$$

where

$$f_i(p) = \frac{1}{\exp[(\tilde{\epsilon}_i(p) - \tilde{\mu}_i)/(kT)] + 1}, \quad (\text{C.3.49})$$

is the Fermi-Dirac fermion distribution function which gives the particle number density n_i

$$n_i = \frac{2}{(2\pi\hbar)^3} \int_0^\infty f_i(p) 4\pi p^2 dp, \quad (\text{C.3.50})$$

where $\tilde{\epsilon}_i(p) = \epsilon_i(p) - m_i c^2 = \sqrt{c^2 p^2 + m_i^2 c^4} - m_i c^2$ and $\tilde{\mu}_i$ are the free single particle energy and the free particle chemical potential with the particle rest mass-energy $m_i c^2$ subtracted off.

Tolman isothermality and conserved Klein potentials

We turn now to demonstrate the constancy of the Klein potentials and the constancy of the gravitationally red-shifted temperature throughout the configuration.

The equation of state (C.3.47)–(C.3.48) satisfies the thermodynamic law

$$\mathcal{E} + P - Ts = \sum_{i=n,p,e} n_i \mu_i, \quad (\text{C.3.51})$$

C.3. *On the constitutive equations of a self-gravitating system of neutrons, protons and electrons in β -equilibrium at finite temperatures*

where $s = S/V$ is the entropy per unit volume and $\mu_i = \partial\mathcal{E}/\partial n_i$ is the free-chemical potential of the i -specie. At zero-temperature $T = 0$, $\mu_i = \sqrt{(cP_i^F)^2 + \tilde{m}_i^2 c^4}$ and $n_i = (P_i^F)^3 / (3\pi^2 \hbar^3)$, where P_i^F denotes the Fermi momentum of the i -specie.

From Eq. (C.3.51) follows the Gibbs-Duhem relation

$$dP = \sum_{i=n,p,e} n_i d\mu_i + s dT, \quad (\text{C.3.52})$$

which can be rewritten as

$$dP = \sum_{i=n,p,e} n_i d\mu_i + \left(\mathcal{E} + P - \sum_{i=n,p,e} n_i \mu_i \right) \frac{dT}{T}. \quad (\text{C.3.53})$$

Using the Gibbs-Duhem relation (C.3.53) the energy-momentum conservation equation (see Rotondo et al. (2011d) for details)

$$e^{\nu/2} dP + e^{\nu/2} \frac{d\nu}{2} (\mathcal{E} + P) + e dV (n_p - n_e) = 0, \quad (\text{C.3.54})$$

can be rewritten as

$$\begin{aligned} e^{\nu/2} \sum_{i=n,p,e} n_i \left(d\mu_i - \frac{dT}{T} \mu_i \right) + (\mathcal{E} + P) e^{\nu/2} \left(\frac{dT}{T} \right. \\ \left. + \frac{1}{2} d\nu \right) + e (n_p - n_e) dV = 0. \end{aligned} \quad (\text{C.3.55})$$

The Tolman isothermal condition (Tolman, 1930) (see also Klein (1949)) demands the constancy of the gravitationally red-shifted temperature

$$\frac{dT}{T} + \frac{1}{2} d\nu = 0, \quad \text{or} \quad T_\infty = e^{\nu/2} T = \text{constant}, \quad (\text{C.3.56})$$

which can be used into Eq. (C.3.55) to obtain

$$\sum_{i=n,p,e} n_i d(e^{\nu/2} \mu_i) + e (n_p - n_e) dV = 0. \quad (\text{C.3.57})$$

We now introduce the generalized chemical potentials, or Klein potentials, for electrons E_e , protons E_p and neutrons E_n

$$E_e = e^{\nu/2} \mu_e - m_e c^2 - eV, \quad (\text{C.3.58})$$

$$E_p = e^{\nu/2} \mu_p - m_p c^2 + eV, \quad (\text{C.3.59})$$

$$E_n = e^{\nu/2} \mu_n - m_n c^2, \quad (\text{C.3.60})$$

which in the zero temperature limit are the generalized Fermi energies for electrons $E_e = E_e^F$, neutrons $E_n = E_n^F$ and protons $E_p = E_p^F$ introduced in Sec. II (see Eq. (C.3.6)). Using Eqs. (C.3.58), (C.3.59) and (C.3.60), Eq. (C.3.57) becomes

$$\sum_{i=n,p,e} n_i dE_i = 0, \quad (\text{C.3.61})$$

which leads for independent and non-zero particle number densities $n_i \neq 0$ to the constancy of the Klein potentials (C.3.58)–(C.3.60) for each particle-species, i.e.

$$E_e = e^{v/2} \mu_e - m_e c^2 - eV = \text{constant}, \quad (\text{C.3.62})$$

$$E_p = e^{v/2} \mu_p - m_p c^2 + eV = \text{constant}, \quad (\text{C.3.63})$$

$$E_n = e^{v/2} \mu_n - m_n c^2 = \text{constant}. \quad (\text{C.3.64})$$

In the zero temperature limit the constancy of the Klein potential of each particle-specie becomes the constancy of the generalized Fermi energies introduced in Sec. C.3.2 (see Eqs. (C.3.6)–(C.3.8)). This is a crucial point because, as discussed in Rotondo et al. (2011d), the constancy of the generalized Fermi energies proves the impossibility of having a self-consistent configuration fulfilling the condition of local charge neutrality and β -equilibrium (see e.g. Fig. 1 of Rotondo et al. (2011d)). Further, as shown in Rueda et al. (2011), the constancy of the Klein potentials holds in the more general case when the strong interactions between nucleons are taken into account.

Therefore, introducing the new dimensionless variables $\eta_i = \tilde{\mu}_i / (kT)$ and $\beta_i = kT / (m_i c^2)$, the new set of Einstein-Maxwell-Thomas-Fermi equations generalizing the system (C.3.4)–(C.3.9) to the case of finite temperatures is

$$M' = 4\pi r^2 \frac{\mathcal{E}}{c^2} - \frac{4\pi r^3}{c^2} e^{-v/2} \hat{V}' (n_p - n_e), \quad (\text{C.3.65})$$

$$v' = \frac{2G 4\pi r^3 P / c^2 + M - r^3 E^2 / c^2}{c^2 r^2 \left(1 - \frac{2GM}{c^2 r} + \frac{Gr^2 E^2}{c^4} \right)}, \quad (\text{C.3.66})$$

$$\begin{aligned} E_e &= m_e c^2 e^{v/2} (1 + \beta_e \eta_e) - m_e c^2 - eV \\ &= \text{constant}, \end{aligned} \quad (\text{C.3.67})$$

$$\begin{aligned} E_p &= m_p c^2 e^{v/2} (1 + \beta_p \eta_p) - m_p c^2 + eV \\ &= \text{constant}, \end{aligned} \quad (\text{C.3.68})$$

$$E_n = E_e + E_p - (m_n - m_e - m_p) c^2, \quad (\text{C.3.69})$$

$$\begin{aligned} \hat{V}'' + \frac{2}{r} \hat{V}' \left[1 - \frac{r(v' + \lambda')}{4} \right] &= -4\pi \alpha \hbar c e^{v/2} e^\lambda (n_p \\ &- n_e), \end{aligned} \quad (\text{C.3.70})$$

$$e^{v/2} \beta_i = \text{constant}, \quad i = n, p, e, \quad (\text{C.3.71})$$

where Eq. (C.3.69) is the condition of β -equilibrium between neutrons, protons and electrons, and the number density of the i -specie is given by

$$n_i = \frac{2^{1/2} m_i^3 c^3}{\pi^2 \hbar^3} \beta_i^{3/2} (F_{1/2}^i + \beta_i F_{3/2}^i), \quad (\text{C.3.72})$$

where we have introduced the relativistic Fermi-Dirac integrals of order j

$$F_j^i = F_j(\eta_i, \beta_i) = \int_0^\infty \frac{x^j \left(1 + \frac{1}{2} \beta_i x\right)^{1/2}}{1 + e^{x - \eta_i}} dx. \quad (\text{C.3.73})$$

The above formulation generalizes to the case of finite temperatures the Einstein-Maxwell-Thomas-Fermi equations obtained in Rotondo et al. (2011d) and recalled here in Sec. C.3.2. This formulation can be also straightforwardly done in the presence of strong interactions generalizing the formulation of Sec. C.3.4 (see Rueda et al. (2011) for details).

Numerical results

We have integrated numerically the system of equations (C.3.65)–(C.3.71) for given temperatures $T_\infty \neq 0$. As expected, the results are both qualitatively and quantitatively similar to the ones obtained with the degenerate approximation. The largest difference we found is at the surface boundary of the configuration, where, due to the low density of the system, finite temperature effects are more effective. As an example, we compare in Fig. C.6 the electron density for $r > R_p$ in the degenerate and in the non-degenerate case for $T_\infty = 2.3 \times 10^5$ K. For distances $r < R_p$ the results are essentially the same as in the degenerate case. In the region $r \ll R_n$ at large densities $> \rho_{\text{nuc}} = 2.7 \times 10^{14}$ g/cm³, the electro-dynamical properties of the configuration i.e. Coulomb potential and electric field remain unperturbed even for very large temperatures $T_\infty \sim 10^{11}$ K. This is due to the fact that thermal effects are largely compensated by the gravitational potential as given by Eq. (C.3.56); the Coulomb interaction is not involved in this balance and is not affected by the thermal energy.

It is worth to mention that from general computations of the heating and cooling mechanisms it turns out that neutron star interiors are highly isothermal (in the sense of Tolman) due to the high thermal conductivity of degenerate particles (Yakovlev and Pethick, 2004). In real neutron stars, the fluid of neutrons, protons and electrons in β -equilibrium studied in this article does not extend all the way to the neutron star surface but is confined to the neutron star core surrounded by the neutron star crust. In this more general case, the surface structure shown in Fig. C.6 is replaced by the crust composed of nuclei and degenerate electrons. The condition of isothermality breaks down in the surface non-degenerate layers of the star due to existence of high tem-

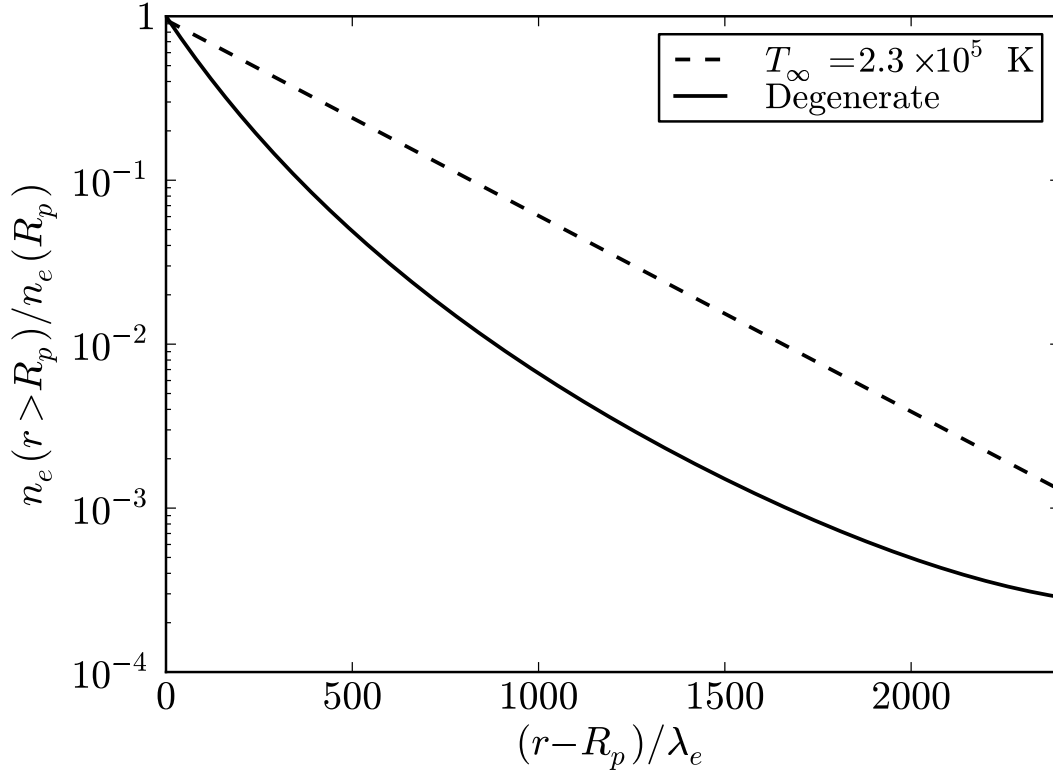


Figure C.6.: Electron number density for $r \geq R_p$ normalized to its value at $r = R_p$ both for $T = 0$ K (degenerate case) and for a finite temperature of $T_\infty = 2.3 \times 10^5$ K.

perature gradients (see e.g. Yakovlev and Pethick (2004), for details).

C.3.6. Concluding Remarks

In this article we have addressed three additional aspects of the description of a self-gravitating system of neutrons, protons and electrons in β -equilibrium:

1) We have first recall the formulation of the constitutive Einstein-Maxwell-Thomas-Fermi equations and their solution in the simple case of self-gravitating neutrons, protons, and electrons in β -equilibrium. The properties of the electromagnetic structure of the configuration shown in Rotondo et al. (2011d) have been also recalled; the Coulomb potential energy inside the configuration is $eV \sim m_\pi c^2$ and the corresponding electric field $E \sim (m_p/m_{\text{Planck}})(m_\pi/m_e)^2 E_c$ and explicitly given in Fig. C.4.

2) We have presented the Newtonian limit of the treatment (Rotondo et al., 2011d) by taking the weak field approximation and the non-relativistic $c \rightarrow \infty$ limit of the general relativistic Thomas-Fermi and Einstein-Maxwell equations (C.3.4)–(C.3.9). The numerical integration of the Newtonian equations shows that the gravito-electrodynamic structure evidenced in Rotondo et al.

(2011d) (see also Sec. C.3.2) is already present in the Newtonian regime. We have also shown how our equations fulfill the Rosseland relation of equilibrium (Rosseland, 1924) for an electron-ion ideal gas in the case of a Newtonian gravitational field, see Eqs. (C.3.17)–(C.3.18), Eqs. (C.3.20)–(C.3.23), and Eqs. (C.3.4)–(C.3.9). The differences in the electromagnetic structure between the Newtonian and the general relativistic treatments are very large (see Fig. C.5).

3) We have recalled in Sec. C.3.4 the extension of the Einstein-Maxwell-Thomas-Fermi equations (C.3.4)–(C.3.9) to the case when strong interactions between nucleons are taken into account by introducing the presence of σ , ω and ρ virtual mesons which mediate nuclear interactions in a Yukawa-like fashion, following our recent work (Rueda et al., 2011), see Eqs. (C.3.25)–(C.3.34).

4) We have then extended all our previous works to the case of finite temperatures enforcing the Tolman “isothermal” condition in general relativity. We have reached a fundamental conclusion: although the thermal energy stored in old neutron stars with surface temperatures $\sim 10^6$ K (Tennant et al., 2001; Weisskopf et al., 2004) is much larger than the internal Coulomb energy (see Sec. C.3.4), still the electromagnetic structure (see Fig. C.5) is unaffected by the presence of the thermal component. Physically this effect is due to the very large Fermi energy of the neutrons ~ 1 GeV, of the protons ~ 10 MeV and of the electrons ~ 0.1 GeV, as can be seen from Eq. (C.3.46). In the general relativistic “isothermal” system there exists a temperature gradient, compensated by the variation of the gravitational potential as dictated by the Tolman condition given by Eq. (C.3.56). The Coulomb interaction is not involved in the balance between the thermal and the gravitational energies and is not affected by the presence of large thermal energies.

We recalled that a surface structure characterized by the presence of three different radii, one for each particle specie, emerges when global Coulomb effects are taken into due account. The radius R_e in the case $T \neq 0$ is larger with respect to the one obtained in the degenerate approximation (see Fig. C.6). However, in realistic neutron stars the surface structure of Fig. C.6 is replaced by the surface layers composed of nuclei and non-degenerate electrons where isothermality breaks down due to existence of high temperature gradients (Yakovlev and Pethick, 2004).

As a by product, we have given the explicit demonstration of the constancy throughout the configuration of the Klein potentials of each species in the more general case of finite temperatures. This generalizes the condition of the constancy of the general relativistic Fermi energies derived in the special case $T = 0$ in Rotondo et al. (2011d).

The above results are relevant to the extension to thermal effects of the relativistic Feynman-Metropolis-Teller treatment of compressed atoms (Rotondo et al., 2011c), recently applied to the construction of general relativistic white dwarf equilibrium configurations (Rotondo et al., 2011b). They are therefore

relevant for the description of the neutron star crust as well as of hot white dwarfs.

The study of the Thomas-Fermi equation within the Einstein-Maxwell system of equations responds to a precise request of consistency of a theoretical treatment. As evidenced in Rotondo et al. (2011d) it overcomes the conceptual difficulties of the Tolman-Oppenheimer-Volkoff treatment. Nevertheless, the two treatments when applied to the case of neutrons, protons, and electrons in β -equilibrium do not give quantitative appreciable differences in the masses and radii of the equilibrium configurations. It becomes therefore natural to ask under which physical conditions the gravito-polarization effects become quantitatively relevant.

When strong interactions are considered (Rueda et al., 2011) a new situation occurs. The neutron star core necessarily presents a sharp boundary surrounded by a crust of nuclei and electrons described by the generalized Feynman-Metropolis-Teller treatment presented in Rotondo et al. (2011c). Under these conditions, the entire theoretical treatment presented in this article and in Rotondo et al. (2011d); Rueda et al. (2011) are not optional and become a necessity.

The presence of a Coulomb potential affects the structure of the phase-transition leading to the occurrence of overcritical electric fields through core-crust boundary interface. Similar electrostatic effects are expected to occur at the interlayer boundaries within the crust of a neutron star where changes of the nucleus charge Z and mass number A of the composing nuclei occur (see e.g. Haensel and Pichon (1994)), as well as at the surface of quark stars (Alcock et al., 1986; Stejner and Madsen, 2005), at the transition from the hadronic phase to the color flavor locked phase in hybrid stars (Alford et al., 2001) and in liquid white dwarfs where it may cause sedimentation of heavy nuclei (Bildsten and Hall, 2001; Althaus et al., 2010; García-Berro et al., 2010b).

In Fig. C.7 we show the expected behavior of the Coulomb potential as modeled in the heuristic simplified approach (Ruffini, 2008c; Popov, 2010; Rotondo et al., 2011e). If the electron Coulomb potential $-eV \sim m_\pi c^2$ suffers a sharp increasing in a scale typical of the electron screening length $\sim \lambda_e = \hbar/(m_e c)$, it will create an electric field of order $\sim (m_\pi/m_e)^2 E_c \sim 10^3 E_c$.

A key result in the present article is that the gravito-polarization effects survive at finite temperatures and we can therefore proceed to the study of neutron star configurations through the theoretical framework formulated in Rueda et al. (2011) and recalled in Sec. C.3.4. It is now possible to confirm if the phase-transition at the boundary of the neutron star core follows the idealization advanced in Ruffini (2008c); Popov (2010); Rotondo et al. (2011e) and shown in Fig. C.7. It is clear that the formation of overcritical fields is of great astrophysical interest. The mass and thickness of the neutron star crust in the two alternative treatments are markedly different. The continuity of the generalized Klein potentials, at the boundary of the core, plays a crucial

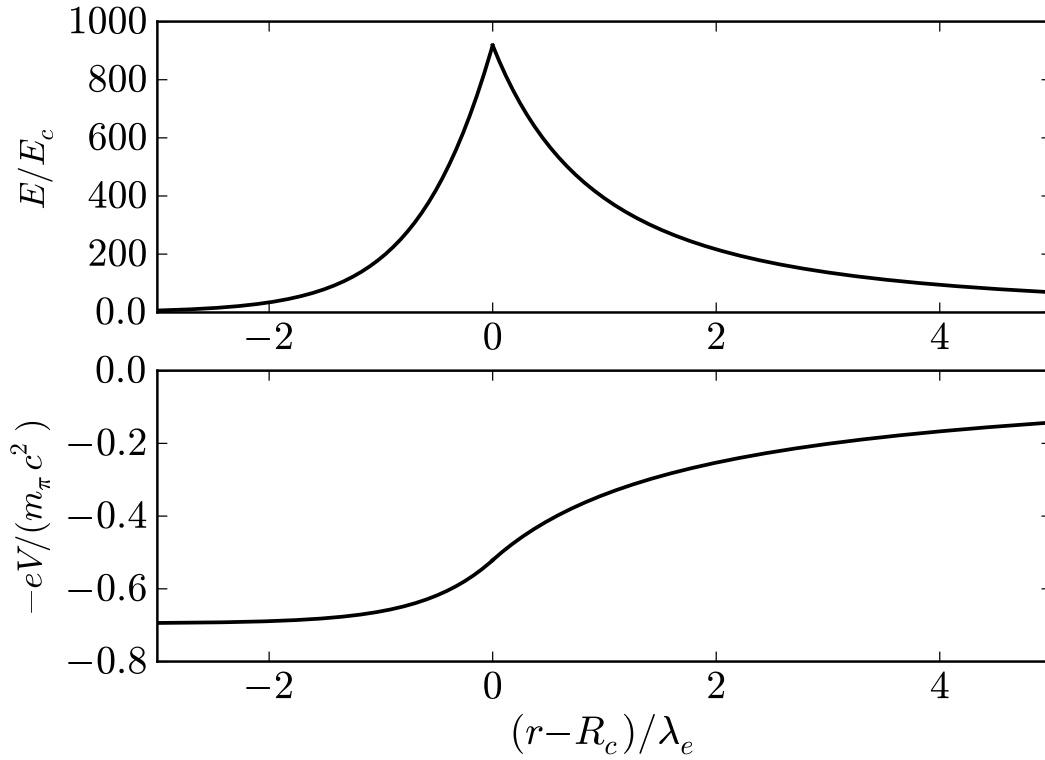


Figure C.7.: Expected enhancement of the electric field at a sharp increasing of the electron Coulomb potential $-eV$ e.g. at a phase transition from the core to the crust in a neutron star as modeled in the simplified approach (Ruffini, 2008c; Popov, 2010; Rotondo et al., 2011e). Here R_c denotes the core radius.

role in the determination of the mass and thickness of the crust (Belvedere et al., 2011). The process of gravitational collapse of a core endowed with electromagnetic structure leads to signatures and energetics markedly different from the ones of a core endowed uniquely of gravitational interactions (Ruffini et al., 2003b,a; Ruffini and Xue, 2008; Ruffini et al., 2010b).

C.4. Neutron star equilibrium configurations within a fully relativistic theory with strong, weak, electromagnetic, and gravitational interactions

C.4.1. Introduction

It is well known that the classic works of Tolman (1939) and of Oppenheimer and Volkoff (1939), for short TOV, addresses the problem of neutron star equilibrium configurations composed only of neutrons. For the more general case when protons and electrons are also considered, in all of the scientific literature on neutron stars it is assumed that the condition of local charge neutrality applies identically to all points of the equilibrium configuration (see e.g. Haensel et al. (2007)). Consequently, the corresponding solutions in this more general case of a non-rotating neutron star, are systematically obtained also on the base of the TOV equations. We have recently shown the the condition of local charge neutrality is

In general, the formulation of the equilibrium of systems composed by different particle species must be established within the framework of statistical physics of multicomponent systems. Thermodynamic equilibrium of these systems is warranted by demanding the constancy throughout the configuration of the generalized chemical potentials, often called “electro-chemical”, of each of the components of the system; see e.g. Klein (1949); Kodama and Yamada (1972); Olson and Baily (1975). Such generalized potentials include not only the contribution due to kinetic energy but also the contribution due to the potential fields, e.g. gravitational and electromagnetic potential energies per particle, and in the case of rotating stars also the centrifugal potential. For such systems in presence of gravitational and Coulomb fields, global electric polarization effects at macroscopic scales occur. The balance of the gravitational and electric forces acting on ions and electrons in ideal electron plasma leading to the occurrence of gravito-polarization was pointed out in the classic work of Rosseland (1924).

If one turns to consider the gravito-polarization effects in neutron stars, the corresponding theoretical treatment acquires remarkable conceptual and theoretical complexity, since it must be necessarily formulated consistently within the Einstein-Maxwell system of equations. Klein (1949) first introduced the constancy of the general relativistic chemical potential of particles, hereafter “Klein potentials”, in the study of the thermodynamic equilibrium of a self-gravitating one-component fluid of neutral particles throughout the configuration within the framework of general relativity. The extension of the Klein’s work to the case of neutral multicomponent degenerate fluids can be found in Kodama and Yamada (1972) and to the case of multi-component

degenerate fluid of charged particles in Olson and Bailyn (1975).

Using the concept of Klein potentials, we have recently proved the impossibility of imposing the condition of local charge neutrality in the simplest case of a self-gravitating system of degenerate neutrons, protons and electrons in β -equilibrium Rotondo et al. (2011d): it has been shown that the consistent treatment of the above system implies the solution of the general relativistic Thomas-Fermi equations, coupled with the Einstein-Maxwell ones, being the TOV equations thus superseded.

We have recently formulated the theory of a system of neutrons, protons and electrons fulfilling strong, electromagnetic, weak and gravitational interactions (Rueda et al., 2011). The role of the Klein first integrals has been again evidenced and their theoretical formulation in the Einstein-Maxwell background and in the most general case of finite temperature has been there presented, generalizing the previous results for the “non-interacting” case (Rotondo et al., 2011d). The strong interactions, modeled by a relativistic nuclear theory, are there described by the introduction of the σ , ω and ρ virtual mesons (Duerr, 1956; Walecka, 1974; Bowers et al., 1973b,a) (see Subsec. C.4.2 for details).

In this article we construct for the first time the equilibrium configurations of non-rotating neutron stars following the new approach (Rotondo et al., 2011d; Rueda et al., 2011). The full set of the Einstein-Maxwell-Thomas-Fermi equations is solved numerically for zero temperatures and for selected parameterizations of the nuclear model.

C.4.2. The Constitutive Relativistic Equations

Core Equations

It has been clearly recognized that, since neutron stars cores may reach density of order $\sim 10^{16}$ – 10^{17} g/cm³, much larger than the nuclear density $\rho_{\text{nuc}} \sim 2.7 \times 10^{14}$ g/cm³, approaches for the nuclear interaction between nucleons based on phenomenological potentials and non-relativistic many-body theories become inapplicable (see Bowers et al. (1973b,a)). A self-consistent relativistic and well-tested model for the nuclear interactions has been formulated in Duerr (1956); Walecka (1974); Bowers et al. (1973b,a). Within this model the nucleons interact with σ , ω and ρ mesons through Yukawa-like couplings and assuming flat spacetime the equation of state of nuclear matter has been determined. However, it has been clearly stated in Rotondo et al. (2011d); Rueda et al. (2011) that, when we turn into a neutron star configuration at nuclear and supranuclear, the global description of the Einstein-Maxwell-Thomas-Fermi equations is mandatory. Associated to this system of equations there is a sophisticated eigenvalue problem, especially the one for the general relativistic Thomas-Fermi equation is necessary in order to fulfill the global charge neutrality of the system and to consistently describe

the confinement of the ultrarelativistic electrons.

The strong interactions between nucleons are described by the exchange of three virtual mesons: σ is an isoscalar meson field providing the attractive long-range part of the nuclear force; ω is a massive vector field that models the repulsive short range and; ρ is the massive isovector field that takes account surface as well as isospin effects of nuclei (see also Boguta and Bodmer (1977); Ring (1996)).

The total Lagrangian density of the system is given by

$$\mathcal{L} = \mathcal{L}_g + \mathcal{L}_f + \mathcal{L}_\sigma + \mathcal{L}_\omega + \mathcal{L}_\rho + \mathcal{L}_\gamma + \mathcal{L}_{\text{int}}, \quad (\text{C.4.1})$$

where the Lagrangian densities for the free-fields are

$$\mathcal{L}_g = -\frac{R}{16\pi G}, \quad (\text{C.4.2})$$

$$\mathcal{L}_\gamma = -\frac{1}{16\pi} F_{\mu\nu} F^{\mu\nu}, \quad (\text{C.4.3})$$

$$\mathcal{L}_\sigma = \frac{1}{2} \nabla_\mu \sigma \nabla^\mu \sigma - U(\sigma), \quad (\text{C.4.4})$$

$$\mathcal{L}_\omega = -\frac{1}{4} \Omega_{\mu\nu} \Omega^{\mu\nu} + \frac{1}{2} m_\omega^2 \omega_\mu \omega^\mu, \quad (\text{C.4.5})$$

$$\mathcal{L}_\rho = -\frac{1}{4} \mathcal{R}_{\mu\nu} \mathcal{R}^{\mu\nu} + \frac{1}{2} m_\rho^2 \rho_\mu \rho^\mu, \quad (\text{C.4.6})$$

where $\Omega_{\mu\nu} \equiv \partial_\mu \omega_\nu - \partial_\nu \omega_\mu$, $\mathcal{R}_{\mu\nu} \equiv \partial_\mu \rho_\nu - \partial_\nu \rho_\mu$, $F_{\mu\nu} \equiv \partial_\mu A_\nu - \partial_\nu A_\mu$ are the field strength tensors for the ω^μ , ρ and A^μ fields respectively, ∇_μ stands for covariant derivative and R is the Ricci scalar. We adopt the Lorenz gauge for the fields A_μ , ω_μ , and ρ_μ . The self-interaction scalar field potential $U(\sigma)$ is a quartic-order polynom for a renormalizable theory (see e.g. Lee and Wick (1974)).

The Lagrangian density for the three fermion species is

$$\mathcal{L}_f = \sum_{i=e,N} \bar{\psi}_i (i\gamma^\mu D_\mu - m_i) \psi_i, \quad (\text{C.4.7})$$

where ψ_N is the nucleon isospin doublet, ψ_e is the electronic singlet, m_i states for the mass of each particle-specie and $D_\mu = \partial_\mu + \Gamma_\mu$, being Γ_μ the Dirac spin connections.

The interacting part of the Lagrangian density is, in the minimal coupling assumption, given by

$$\begin{aligned} \mathcal{L}_{\text{int}} &= -g_\sigma \sigma \bar{\psi}_N \psi_N - g_\omega \omega_\mu J_\omega^\mu - g_\rho \rho_\mu J_\rho^\mu \\ &+ e A_\mu J_{\gamma,e}^\mu - e A_\mu J_{\gamma,N}^\mu, \end{aligned} \quad (\text{C.4.8})$$

where the conserved currents are

$$J_\omega^\mu = \bar{\psi}_N \gamma^\mu \psi_N, \quad (\text{C.4.9})$$

$$J_\rho^\mu = \bar{\psi}_N \tau_3 \gamma^\mu \psi_N, \quad (\text{C.4.10})$$

$$J_{\gamma,e}^\mu = \bar{\psi}_e \gamma^\mu \psi_e, \quad (\text{C.4.11})$$

$$J_{\gamma,N}^\mu = \bar{\psi}_N \left(\frac{1 + \tau_3}{2} \right) \gamma^\mu \psi_N. \quad (\text{C.4.12})$$

The coupling constants of the σ , ω and ρ -fields are g_σ , g_ω and g_ρ , and e is the fundamental electric charge. The Dirac matrices γ^μ and the isospin Pauli matrices satisfy the Dirac algebra in curved spacetime (see e.g. Lee and Pang (1987) for details).

We first introduce the non-rotating spherically symmetric spacetime metric

$$ds^2 = e^{\nu(r)} dt^2 - e^{\lambda(r)} dr^2 - r^2 d\theta^2 - r^2 \sin^2 \theta d\varphi^2, \quad (\text{C.4.13})$$

where the $\nu(r)$ and $\lambda(r)$ are only functions of the radial coordinate r .

For very large number of fermions, we adopt the mean-field approximation in which fermion-field operators are replaced by their expectation values (see Ruffini and Bonazzola (1969) for details). Within this approximation, the full system of general relativistic equations can be written in the form

$$e^{-\lambda(r)} \left(\frac{1}{r^2} - \frac{1}{r} \frac{d\lambda}{dr} \right) - \frac{1}{r^2} = -8\pi G T_0^0, \quad (\text{C.4.14})$$

$$e^{-\lambda(r)} \left(\frac{1}{r^2} + \frac{1}{r} \frac{d\nu}{dr} \right) - \frac{1}{r^2} = -8\pi G T_1^1, \quad (\text{C.4.15})$$

$$V'' + \frac{2}{r} V' \left[1 - \frac{r(\nu' + \lambda')}{4} \right] = -4\pi e e^{\nu/2} e^\lambda (n_p - n_e), \quad (\text{C.4.16})$$

$$\frac{d^2\sigma}{dr^2} + \frac{d\sigma}{dr} \left[\frac{2}{r} - \frac{1}{2} \left(\frac{d\nu}{dr} + \frac{d\lambda}{dr} \right) \right] = e^\lambda [\partial_\sigma U(\sigma) + g_s n_s], \quad (\text{C.4.17})$$

$$\frac{d^2\omega}{dr^2} + \frac{d\omega}{dr} \left[\frac{2}{r} - \frac{1}{2} \left(\frac{d\nu}{dr} + \frac{d\lambda}{dr} \right) \right] = -e^\lambda (g_\omega J_\omega^0 - m_\omega^2 \omega), \quad (\text{C.4.18})$$

$$\frac{d^2\rho}{dr^2} + \frac{d\rho}{dr} \left[\frac{2}{r} - \frac{1}{2} \left(\frac{d\nu}{dr} + \frac{d\lambda}{dr} \right) \right] = -e^\lambda (g_\rho J_\rho^0 - m_\rho^2 \rho), \quad (\text{C.4.19})$$

$$E_e^F = e^{\nu/2} \mu_e - eV = \text{constant}, \quad (\text{C.4.20})$$

$$E_p^F = e^{\nu/2} \mu_p + \mathcal{V}_p = \text{constant}, \quad (\text{C.4.21})$$

$$E_n^F = e^{\nu/2} \mu_n + \mathcal{V}_n = \text{constant}, \quad (\text{C.4.22})$$

where we have introduced the notation $\omega_0 = \omega$, $\rho_0 = \rho$, and $A_0 = V$ for the temporal components of the meson-fields. Here $\mu_i = \partial\mathcal{E}/\partial n_i = \sqrt{(P_i^F)^2 + \tilde{m}_i^2}$

C.4. Neutron star equilibrium configurations within a fully relativistic theory with strong, weak, electromagnetic, and gravitational interactions

and $n_i = (P_i^F)^3 / (3\pi^2)$ are the free-chemical potential and number density of the i -specie with Fermi momentum P_i^F . The particle effective mass is $\tilde{m}_N = m_N + g_s\sigma$ and $\tilde{m}_e = m_e$ and the effective potentials $\mathcal{V}_{p,n}$ are given by

$$\mathcal{V}_p = g_\omega\omega + g_\rho\rho + eV, \quad (\text{C.4.23})$$

$$\mathcal{V}_n = g_\omega\omega - g_\rho\rho. \quad (\text{C.4.24})$$

The constancy of the generalized Fermi energies E_n^F , E_p^F and E_e^F , the Klein potentials, derives from the thermodynamic equilibrium conditions given by the statistical physics of multicomponent systems, applied to a system of degenerate neutrons, protons, and electrons within the framework of general relativity (see Rueda et al. (2011) for details). These constants are linked by the β -equilibrium between the matter constituents

$$E_n^F = E_p^F + E_e^F. \quad (\text{C.4.25})$$

The electron density n_e is, via Eq. (C.4.20), given by

$$n_e = \frac{e^{-3\nu/2}}{3\pi^2} [\hat{V}^2 + 2m_e\hat{V} - m_e^2(e^\nu - 1)]^{3/2}, \quad (\text{C.4.26})$$

where $\hat{V} \equiv eV + E_e^F$. Substituting Eq.(C.4.26) into Eq. (C.4.16) one obtains the general relativistic extension of the relativistic Thomas-Fermi equation recently introduced for the study of compressed atoms (Rotondo et al., 2011c,b). This system of equations has to be solved with the boundary condition of global neutrality; see Rotondo et al. (2011d); Rueda et al. (2011) and below for details.

The scalar density n_s , within the mean-field approximation, is given by the following expectation value

$$n_s = \langle \bar{\psi}_N \psi_N \rangle = \frac{2}{(2\pi)^3} \sum_{i=n,p} \int d^3k \frac{\tilde{m}_N}{\epsilon_i(p)}, \quad (\text{C.4.27})$$

where $\epsilon_i(p) = \sqrt{p^2 + \tilde{m}_i^2}$ is the single particle energy.

In the static case, only the temporal components of the covariant currents survive, i.e. $\langle \bar{\psi}(x)\gamma^i\psi(x) \rangle = 0$. Thus, by taking the expectation values of Eqs. (C.2.10)–(C.2.13), we obtain the non-vanishing components of the currents

$$J_0^{ch} = n_{ch}u_0 = (n_p - n_e)u_0, \quad (\text{C.4.28})$$

$$J_0^\omega = n_b u_0 = (n_n + n_p)u_0, \quad (\text{C.4.29})$$

$$J_0^\rho = n_3 u_0 = (n_p - n_n)u_0, \quad (\text{C.4.30})$$

where $n_b = n_p + n_n$ is the baryon number density and $u_0 = \sqrt{g_{00}} = e^{v/2}$ is the covariant temporal component of the four-velocity of the fluid, which satisfies $u^\mu u_\mu = 1$.

The metric function λ is related to the mass $M(r)$ and the electric field $E(r) = -e^{-(v+\lambda)/2} V'$ through

$$\begin{aligned} e^{-\lambda(r)} &= 1 - \frac{2GM(r)}{r} + Gr^2 E^2(r) \\ &= 1 - \frac{2GM(r)}{r} + \frac{GQ^2(r)}{r^2}, \end{aligned} \quad (\text{C.4.31})$$

being $Q(r)$ the conserved charge, related to the electric field by $Q(r) = r^2 E(r)$.

The energy-momentum tensor of free-fields and free-fermions $T^{\mu\nu}$ of the system is

$$T^{\mu\nu} = T_f^{\mu\nu} + T_\gamma^{\mu\nu} + T_\sigma^{\mu\nu} + T_\omega^{\mu\nu} + T_\rho^{\mu\nu}, \quad (\text{C.4.32})$$

where

$$T_\gamma^{\mu\nu} = -\frac{1}{4\pi} \left(F_\alpha^\mu F^{\alpha\nu} + \frac{1}{4} g^{\mu\nu} F_{\alpha\beta} F^{\alpha\beta} \right), \quad (\text{C.4.33})$$

$$T_\sigma^{\mu\nu} = \nabla^\mu \nabla^\nu \sigma - g^{\mu\nu} \left[\frac{1}{2} \nabla_\sigma \sigma \nabla^\sigma \sigma - U(\sigma) \right], \quad (\text{C.4.34})$$

$$\begin{aligned} T_\omega^{\mu\nu} &= -\Omega_\alpha^\mu \Omega^{\alpha\nu} - \frac{1}{4} g^{\mu\nu} \Omega_{\alpha\beta} \Omega^{\alpha\beta} \\ &+ m_\omega^2 \left(\omega^\mu \omega^\nu - \frac{1}{2} g^{\mu\nu} \omega_\alpha \omega^\alpha \right), \end{aligned} \quad (\text{C.4.35})$$

$$\begin{aligned} T_\rho^{\mu\nu} &= -\mathcal{R}_\alpha^\mu \mathcal{R}^{\alpha\nu} - \frac{1}{4} g^{\mu\nu} \mathcal{R}_{\alpha\beta} \mathcal{R}^{\alpha\beta} \\ &+ m_\rho^2 \left(\mathcal{R}^\mu \mathcal{R}^\nu - \frac{1}{2} g^{\mu\nu} \mathcal{R}_\alpha \omega^\alpha \right), \end{aligned} \quad (\text{C.4.36})$$

$$T_f^{\mu\nu} = (\mathcal{E} + \mathcal{P}) u^\mu u^\nu - \mathcal{P} g^{\mu\nu}, \quad (\text{C.4.37})$$

where the energy-density \mathcal{E} and the pressure \mathcal{P} are given by

$$\mathcal{E} = \sum_{i=n,p,e} \mathcal{E}_i, \quad \mathcal{P} = \sum_{i=n,p,e} \mathcal{P}_i, \quad (\text{C.4.38})$$

being \mathcal{E}_i and \mathcal{P}_i the single fermion fluid contributions

$$\mathcal{E}_i = \frac{2}{(2\pi)^3} \int_0^{P_i^F} \epsilon_i(p) 4\pi p^2 dp, \quad (\text{C.4.39})$$

$$\mathcal{P}_i = \frac{1}{3} \frac{2}{(2\pi)^3} \int_0^{P_i^F} \frac{p^2}{\epsilon_i(p)} 4\pi p^2 dp. \quad (\text{C.4.40})$$

C.4. Neutron star equilibrium configurations within a fully relativistic theory with strong, weak, electromagnetic, and gravitational interactions

It is worth to recall that the equation of state (C.4.38)–(C.4.40) satisfies the thermodynamic law

$$\mathcal{E} + \mathcal{P} = \sum_{i=n,p,e} n_i \mu_i. \quad (\text{C.4.41})$$

The parameters of the nuclear model, namely the coupling constants g_s , g_ω and g_ρ , and the meson masses m_σ , m_ω and m_ρ are usually fixed by fitting experimental properties of nuclei, e.g. saturation density, binding energy per nucleon (or experimental masses), symmetry energy, surface energy, and nuclear incompressibility. In Table C.1 we present selected fits of the nuclear parameters. In particular, we show the following parameter sets: NL3 (Lalazisis et al., 1997), NL-SH (Sharma et al., 1993), TM1 (Sugahara and Toki, 1994), and TM2 (Hirata et al., 1995).

	NL3	NL-SH	TM1	TM2
m_σ (MeV)	508.194	526.059	511.198	526.443
m_ω (MeV)	782.501	783.000	783.000	783.000
m_ρ (MeV)	763.000	763.000	770.000	770.000
g_s	10.2170	10.4440	10.0289	11.4694
g_ω	12.8680	12.9450	12.6139	14.6377
g_ρ	4.4740	4.3830	4.6322	4.6783
g_2 (fm ⁻¹)	-10.4310	-6.9099	-7.2325	-4.4440
g_3	-28.8850	-15.8337	0.6183	4.6076
c_3	0.0000	0.0000	71.3075	84.5318

Table C.1.: Selected parameter sets of the σ - ω - ρ model.

The constants g_2 and g_3 are the third and fourth order constants of the self-scalar interaction as given by the scalar self-interaction potential

$$U(\sigma) = \frac{1}{2}m_\sigma^2\sigma^2 + \frac{1}{3}g_2\sigma^3 + \frac{1}{4}g_3\sigma^4. \quad (\text{C.4.42})$$

The non-zero constant c_3 that appears in the TM1 and TM2 models corresponds to the self-coupling constant of the non-linear vector self-coupling $\frac{1}{4}c_3(\omega_\mu\omega^\mu)^2$. We have not include such a self-coupling vector interaction in the general formulation presented above. However, we show also here the results of the integration when such a self-interaction is taken into account and we refer to Sugahara and Toki (1994); Hirata et al. (1995) for details about the motivations of including that contribution.

The numerical integration of the core equations can be started given a central density and the regularity conditions at the origin; see below Sec. C.4.3 for details. At nuclear density the phase-transition to the “solid” crust takes place. Thus, the radius of the core R_{core} is given by $\mathcal{E}(r = R_{\text{core}})/c^2 = \rho_{\text{nuc}}$. These equations must be solved with the boundary conditions given by the

fulfillment of the condition of global charge neutrality and the continuity of the Klein potentials of particles between the core and the crust.

Core-crust transition layer equations

In the core-crust interface, the mean-field approximation for the meson-fields is not valid any longer and thus a full numerical integration of the meson-field equations of motion, taking into account all gradient terms, must be performed. We expect the core-crust transition boundary-layer to be a region with characteristic length scale of the order of the electron Compton wavelength $\sim \lambda_e = \hbar/(m_e c) \sim 100$ fm corresponding to the electron screening scale. Then, in the core-crust transition layer, the system of equations (C.4.14)–(C.4.22) reduces to

$$V'' + \frac{2}{r}V' = -e^{\lambda_{\text{core}}} e J_{ch}^0, \quad (\text{C.4.43})$$

$$\sigma'' + \frac{2}{r}\sigma' = e^{\lambda_{\text{core}}} [\partial_\sigma U(\sigma) + g_s n_s], \quad (\text{C.4.44})$$

$$\omega'' + \frac{2}{r}\omega' = -e^{\lambda_{\text{core}}} [g_\omega J_\omega^0 - m_\omega^2 \omega], \quad (\text{C.4.45})$$

$$\rho'' + \frac{2}{r}\rho' = -e^{\lambda_{\text{core}}} [g_\rho J_\rho^0 - m_\rho^2 \rho], \quad (\text{C.4.46})$$

$$e^{\nu_{\text{core}}/2} \mu_e - eV = \text{constant}, \quad (\text{C.4.47})$$

$$e^{\nu_{\text{core}}/2} \mu_p + eV + g_\omega \omega + g_\rho \rho = \text{constant}, \quad (\text{C.4.48})$$

$$\mu_n = \mu_p + \mu_e + 2 g_\rho \rho e^{-\nu_{\text{core}}/2}, \quad (\text{C.4.49})$$

due to the fact that the metric functions are essentially constant on the core-crust transition layer and thus we can take their values at the core-radius $e^{\nu_{\text{core}}} \equiv e^{\nu(R_{\text{core}})}$ and $e^{\lambda_{\text{core}}} \equiv e^{\lambda(R_{\text{core}})}$.

The system of equations of the transition layer has a stiff nature due to the existence of two different scale lengths. The first one is associated with the nuclear interactions $\sim \lambda_\pi = \hbar/(m_\pi c) \sim 1.5$ fm and the second one is due to the aforementioned screening length $\sim \lambda_e = \hbar/(m_e c) \sim 100$ fm. Thus, the numerical integration of Eqs. (C.4.43)–(C.4.49) has been performed subdividing the core-crust transition layer in the following three regions: (I) a mean-field-like region where all the fields vary slowly with length scale $\sim \lambda_e$, (II) a strongly interacting region of scale $\sim \lambda_\pi$ where the surface tension due to nuclear interactions dominate producing a sudden decrease of the proton and the neutron densities and, (III) a Thomas-Fermi-like region of scale $\sim \lambda_e$ where only a layer of opposite charge made of electrons is present producing the total screening of the positively charged core. The results of the numerical integration of the equilibrium equations are shown in Fig. C.8-C.9 for the NL3-model.

C.4. Neutron star equilibrium configurations within a fully relativistic theory with strong, weak, electromagnetic, and gravitational interactions

We have integrated numerically Eqs. (C.4.14)–(C.4.22) for the models listed in Table C.1. The boundary conditions for the numerical integration are fixed through the following procedure. We start assuming a value for the central baryon number density $n_b(0) = n_n(0) + n_p(0)$. From the regularity conditions at the origin we have $e^{-\lambda(0)} = 1$ and $n_e(0) = n_p(0)$.

The metric function ν at the origin can be chosen arbitrarily, e.g. $\nu(0) = 0$, due to the fact that the system of equations remain invariant under the shift $\nu \rightarrow \nu + \text{constant}$. The right value of ν is obtained once the end of the integration of the core has been accomplished and duly matched to the crust, by fulfilling the following identity at the surface of the neutron star,

$$e^{\nu(R)} = e^{-\lambda(R)} = 1 - \frac{2GM(R)}{c^2R}, \quad (\text{C.4.50})$$

being $M(R)$ and R the total mass and radius of the star. Then, taking into account the above conditions, we solve the system (C.4.17)–(C.4.22) at the origin for the other unknowns $\sigma(0)$, $\omega(0)$, $\rho(0)$, $n_n(0)$, $n_p(0)$, $n_e(0)$.

The initial conditions for the numerical integration of the core-crust transition layer equations are determined by the final values given by the numerical integration of the core equations, i.e. we take the values of all the variables at the core-radius R_{core} .

In the region I the effect of the Coulomb interaction is clear: on the proton-profile we can see a bump due to Coulomb repulsion while the electron-profile decreases as expected. Such a Coulomb effect is indirectly felt also by the neutrons due to the coupled nature of the system of equations. However, the neutron-bump is much smaller than the one of protons and it is not appreciable in Fig. C.8-C.9 due to the plot-scale. In the region II we see clearly the effect of the surface tension due to nuclear interaction which produces a sharp decrease of the neutron and proton profiles in a characteristic scale $\sim \lambda_\pi$. In addition, it can be seen a neutron skin effect, analogous to the one observed in heavy nuclei, which makes the scale of the neutron density falloff slightly larger with respect to the proton one, in close analogy to the neutron skin effect observed in neutron rich nuclei, see e.g. Tamii et al. (2011). The region III is characterized by a smooth decreasing of the electron density which resembles the behavior of the electrons surrounding a nucleus in the Thomas-Fermi model.

The matching to the crust must be done at the radius $R_{\text{core}} + \delta R$ where full charge neutrality is reached. The thickness of the core-crust transition boundary layer δR as well as the value of the electron density at the edge of the crust, $R_{\text{core}} + \delta R$, depends on the nuclear parameters, especially on the nuclear surface tension.

The equilibrium conditions given by the constancy of the Klein potentials (C.4.20)–(C.4.22) throughout the configuration, impose in the transition layer

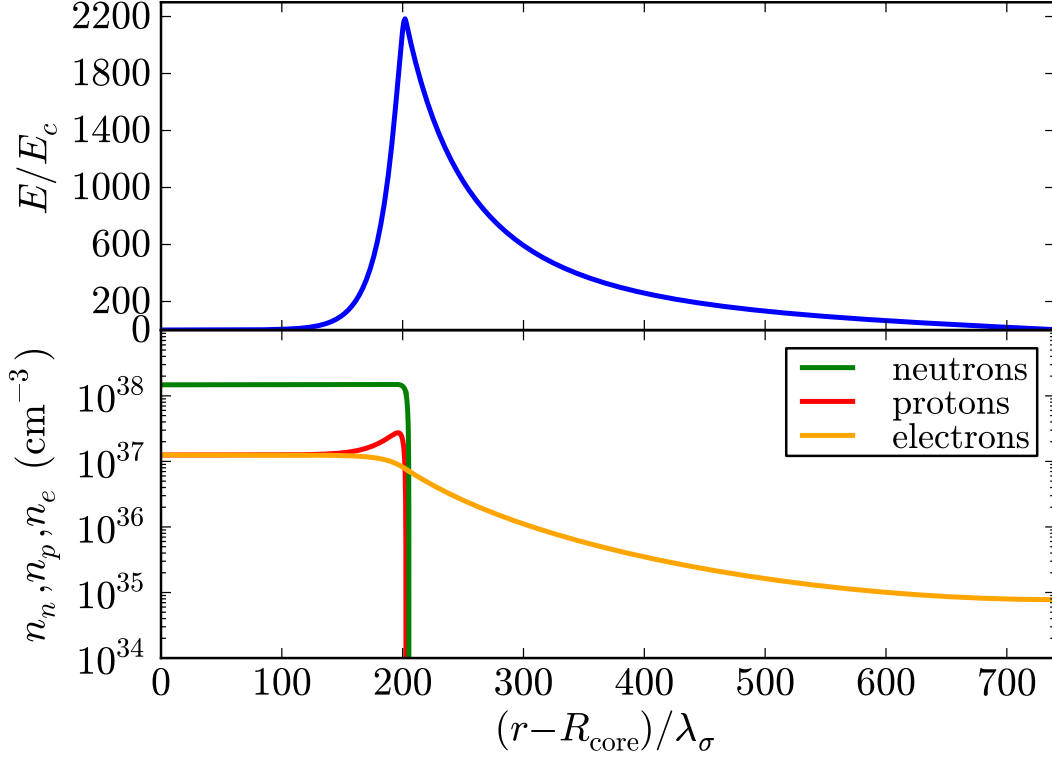


Figure C.8.: Upper panel: electric field in the core-crust transition layer in units of the critical field E_c . Lower panel: particle density profiles in the core-crust boundary interface in units of cm^{-3} . Here we use the NL3-model of Table C.1 and $\lambda_\sigma = \hbar/(m_\sigma c) \sim 0.4$ fm denotes the sigma-meson Compton wavelength. The density at the edge of the crust in this example is $\rho_{\text{crust}} = \rho_{\text{drip}} = 4.3 \times 10^{11}$ g/cm 3 .

the following continuity condition

$$e^{V_{\text{core}}/2} \mu_e^{\text{core}} - eV^{\text{core}} = e^{V_{\text{crust}}/2} \mu_e^{\text{crust}}. \quad (\text{C.4.51})$$

where $\mu_e^{\text{core}} = \mu_e(R_{\text{core}})$, $eV^{\text{core}} = eV(R_{\text{core}})$, and $\mu_e^{\text{crust}} = \mu_e(R_{\text{core}} + \delta R)$, and $e^{V_{\text{crust}}} \simeq e^{V_{\text{core}}}$.

The electron chemical potential and the density decrease, in the boundary interface, until values $\mu_e^{\text{crust}} < \mu_e^{\text{core}}$ and $\rho_{\text{crust}} < \rho_{\text{core}}$. For each central density, an entire family of core-crust interface boundaries and, correspondingly, an entire family of crusts with different mass and thickness, exist. The configuration with $\rho_{\text{crust}} = \rho_{\text{drip}} \sim 4.3 \times 10^{11}$ g/cm 3 separates neutron stars with and without inner crust. In the so-called inner crust, the neutrons dripped from the nuclei in the crust form a fluid that coexist with the nuclei lattice and the degenerate electrons (Baym et al., 1971a). The presence of the neutron fluid in the crust changes the nuclear surface tension at the core radius, in

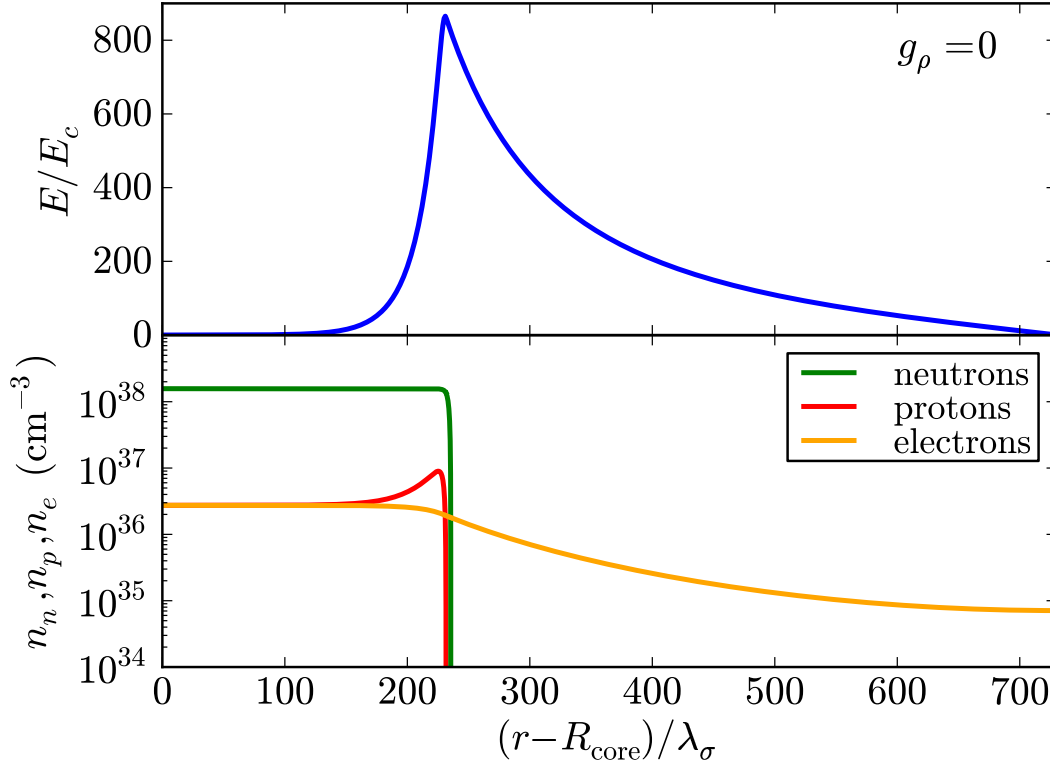


Figure C.9.: The same as Fig. C.8, but setting $g_\rho = 0$ in order to see the effects of the ρ -meson with respect to the case $g_\rho \neq 0$.

close analogy to the reduction of the surface tension of the nuclei in the crust due to the presence of the dripped neutrons, see e.g. Baym et al. (1971a)) for details. This reduction of the nuclear tension is not taken into account in the nuclear parameters which are obtained to fit the properties of bare nuclei, see Table C.1. Thus we present here the results for configurations $\rho_{\text{crust}} \leq \rho_{\text{drip}}$, i.e for neutron stars possessing only outer crust. The construction of configurations with $\rho_{\text{crust}} > \rho_{\text{drip}}$ needs to be studied in more detail and will be the subject of a forthcoming work.

In Figs. C.8 and C.9, we show the core-crust transition layer for the NL3 model of Table C.1 with and without the presence of the ρ -meson respectively. The presence of the ρ -meson is responsible for the nuclear asymmetry within this nuclear model. The relevance of the nuclear symmetry energy on the structure of nuclei and neutron stars is continuously stressed in literature; see e.g. M  ther et al. (1987); Kubis (2007); Sharma and Pal (2009); Hebeler et al. (2010); Loan et al. (2011). The precise value of the nuclear symmetry energy plays here a crucial in determining the precise value of the ρ -meson coupling which, in the present case, is essential in the determination of the intensity of the electric field in the core-crust boundary interface; as can be seen from the comparison of Figs. C.8 and C.9.

Crust equations

Turning now to the crust, it is clear from our recent treatment of white dwarfs (Rotondo et al., 2011b) that also this problem can be solved by the adoption of Wigner-Seitz cells and from the relativistic Feynman-Metropolis-Teller (RFMT) approach (Rotondo et al., 2011c) it follows that the crust is clearly neutral. Thus, the structure equations to be integrated are the TOV equations

$$\frac{d\mathcal{P}}{dr} = -\frac{G(\mathcal{E} + \mathcal{P})(M + 4\pi r^3 \mathcal{P})}{r^2(1 - \frac{2GM}{r})}, \quad (\text{C.4.52})$$

$$\frac{dM}{dr} = 4\pi r^2 \mathcal{E}, \quad (\text{C.4.53})$$

where $M = M(r)$ is the mass enclosed at the radius r .

The effects of the Coulomb interaction in “solid”-like electron-ion systems appears only at the microscopic level e.g. Debye-Hueckel screening in classical systems (Debye and Hueckerl, 1923) and Thomas-Fermi screening in the degenerate case (Mott, 1936). In order to analyze the effects of the microscopic screening on the structure of the configuration we will consider two equations of state for the crust: the locally neutral case or uniform approximation (see e.g. Chandrasekhar (1931b)) and, for simplicity, instead of using the RFMT EoS (Rotondo et al., 2011c), we use as second EoS the one due to Baym, Pethick and Sutherland (BPS) (Baym et al., 1971a), which is by far the most used equation of state in literature for the description of the neutron star crust (see e.g. Haensel et al. (2007)).

In the uniform approximation, both the degenerate electrons and the nucleons distribution are considered constant inside each cell of volume V_{ws} . This kind of configuration can be obtained only imposing microscopically the condition of local charge neutrality

$$n_e = \frac{Z}{V_{ws}}. \quad (\text{C.4.54})$$

The total pressure of the system is assumed to be entirely due to the electrons, i.e.

$$\mathcal{P} = \mathcal{P}_e = \frac{2}{3(2\pi\hbar)^3} \int_0^{p_e^F} \frac{c^2 p^2 4\pi p^2}{\sqrt{c^2 p^2 + m_e^2 c^4}} dp, \quad (\text{C.4.55})$$

while the total energy-density of the system is due to the nuclei, i.e. $\mathcal{E} = (A/Z)m_N n_e$, where m_N is the nucleon mass.

We turn now to the BPS equation of state. The first correction to the uniform model, corresponds to abandon the assumption of the electron-nucleon fluid through the so-called “lattice” model which introduces the concept of Wigner-Seitz cell: each cell of radius R_{ws} contains a point-like nucleus of charge $+Ze$ with A nucleons surrounded by a uniformly distributed cloud

of Z fully-degenerate electrons.

The sequence of the equilibrium nuclides present at each density in the BPS equation of state is obtained by looking for the nuclear composition that minimizes the energy per nucleon for each fixed nuclear composition (Z, A) (see Table C.2 and Baym et al. (1971a) for details). The pressure \mathcal{P} and the energy-density \mathcal{E} of the system are, within this model, given by

$$\mathcal{P} = \mathcal{P}_e + \frac{1}{3}W_L n_N, \quad (\text{C.4.56})$$

$$\frac{\mathcal{E}}{n_b} = \frac{W_N + W_L}{A} + \frac{\mathcal{E}_e(n_b Z/A)}{n_b}, \quad (\text{C.4.57})$$

where the electron energy-density is given by

$$\mathcal{E}_e = \frac{2}{(2\pi)^3} \int_0^{p_e^F} \sqrt{p^2 + m_e^2} 4\pi p^2 dp, \quad (\text{C.4.58})$$

and $W_N(A, Z)$ is the total energy of an isolated nucleus given by the semi-empirical formula

$$W_N = m_n c^2 (A - Z) + m_p c^2 Z - bA, \quad (\text{C.4.59})$$

with b being the Myers and Swiatecki binding energy per nucleon (Myers, 1966). The lattice energy per nucleus W_L is given by

$$W_L = -\frac{1.819620Z^2 e^2}{a}, \quad (\text{C.4.60})$$

where the lattice constant a is related to the nucleon density n_N by $n_N a^3 = 2$.

C.4.3. Neutron star structure

In the traditional TOV treatment the density and the pressure are a priori assumed to be continuous as well as the local charge neutrality of the system. The distinguishing feature of our new solution is that the Klein potentials are constant throughout the three regions; the core, the crust and the transition interface boundary. An overcritical electric field is formed and consequently a discontinuity in density is found with a continuous total pressure including the surface tension of the boundary. In Figs. C.10 and C.11, we compare and contrast the density profiles of configurations obtained from the traditional TOV treatment and with the treatment presented here.

In Figs. C.12–C.18 we show the results of the numerical integration of the system of the general relativistic constitutive equations of the configuration from the center all the way up to the surface with the appropriate boundary conditions between the involved phases. In particular, we have plotted the

mass-radius relation as well as the compactness of the neutron stars obtained with the models listed in Table C.1.

It is worth to note that the inclusion of the Coulomb interaction and in particular the presence of the negative lattice energy W_L results in a decreasing of the pressure of the cells. Such an effect, as shown in Fig. C.15–C.18, leads to a decreasing of the mass and the thickness of the crust with respect to the uniform-approximation case where no Coulomb interactions are taken into account.

Comparing the mass and the thickness of the crust obtained with these two different EoS, we obtain systematically crusts with smaller mass and larger thickness when Coulomb interactions are taken into account. This results are in line with the recent results in Rotondo et al. (2011b), where the mass-radius relation of white-dwarfs has been calculated using an EoS based on the relativistic Feynman-Metropolis-Teller model for compressed atoms (Rotondo et al., 2011c).

In the case of the BPS EoS, the average nuclear composition in the outer crust, namely the average charge to mass ratio of nuclei Z/A , is obtained by calculating the contribution of each nuclear composition present to the mass of the crust. We exemplified the analysis for two different cores: $M_{\text{core}} = 2.56M_{\odot}$, $R_{\text{core}} = 12.79$ km; $M_{\text{core}} = 1.35M_{\odot}$, $R_{\text{core}} = 11.76$ km. The relative abundance of each nuclide within the crust of the star can be obtained as

$$\text{R.A.} = \frac{1}{M_{\text{crust}}^{\text{BPS}}} \int_{\Delta r} 4\pi r^2 \varepsilon dr, \quad (\text{C.4.61})$$

where the integration is carried out in the layer of thickness Δr where the particular nuclide is present; see C.2 and Fig. C.19. Our results are in agreement with the analysis on the neutron star crust composition obtained in Goriely et al. (2011a,b). In both cases we obtain as average nuclear composition $^{105}_{35}\text{Br}$. The corresponding crusts with fixed nuclear composition $^{105}_{35}\text{Br}$ for the two chosen cores are calculated neglecting Coulomb interactions (i.e. using the first EoS). The mass and the thickness of these crusts with fixed $^{105}_{35}\text{Br}$ are different with respect to the ones obtained using the full BPS EoS, leading to such average nuclear composition. For the two selected examples we obtain that the mass and the thickness of the crust with average $^{105}_{35}\text{Br}$ are, respectively, 18% larger and 5% smaller with respect to the ones obtained with the corresponding BPS EoS. This result shows how small microscopic effects due to the Coulomb interaction in the crust of the neutron star leads to quantitative not negligible effects on the macroscopic structure of the configuration.

C.4. Neutron star equilibrium configurations within a fully relativistic theory with strong, weak, electromagnetic, and gravitational interactions

Equilibrium Nuclei Below Neutron Drip						
Nucleus	Z	$\rho_{max}(\text{g cm}^{-3})$	ΔR_1 (km)	R.A.1(%)	ΔR_2 (km)	R.A.2(%)
⁵⁶ Fe	26	8.1×10^6	0.0165	7.56652×10^{-7}	0.0064	6.96927×10^{-7}
⁶² Ni	28	2.7×10^8	0.0310	0.00010	0.0121	0.00009
⁶⁴ Ni	28	1.2×10^9	0.0364	0.00057	0.0141	0.00054
⁸⁴ Se	34	8.2×10^9	0.0046	0.00722	0.0017	0.00683
⁸² Ge	32	2.2×10^{10}	0.0100	0.02071	0.0039	0.01983
⁸⁰ Zn	38	4.8×10^{10}	0.1085	0.04521	0.0416	0.04384
⁷⁸ Ni	28	1.6×10^{11}	0.0531	0.25635	0.0203	0.25305
⁷⁶ Fe	26	1.8×10^{11}	0.0569	0.04193	0.0215	0.04183
¹²⁴ Mo	42	1.9×10^{11}	0.0715	0.02078	0.0268	0.02076
¹²² Zr	40	2.7×10^{11}	0.0341	0.20730	0.0127	0.20811
¹²⁰ Sr	38	3.7×10^{11}	0.0389	0.23898	0.0145	0.24167
¹¹⁸ Kr	36	4.3×10^{11}	0.0101	0.16081	0.0038	0.16344

Table C.2.: ρ_{max} is the maximum density at which the nuclide is present; ΔR_1 , ΔR_2 and R.A.1(%), R.A.2(%) are respectively the thickness of the layer where a given nuclide is present and their relative abundances in the outer crust for two different cases: $M_{\text{core}} = 2.56M_{\odot}$, $R_{\text{core}} = 12.79$ km; $M_{\text{core}} = 1.35M_{\odot}$, $R_{\text{core}} = 11.76$ km.

C.4.4. Observational constraints on the mass-radius relation

It has been recently pointed out that the most up-to-date stringent constraints to the mass-radius relation of neutron stars are provided by the largest mass, the largest radius, the highest rotational frequency, and the maximum surface gravity, observed for pulsars (Trümper, 2011).

So far, the highest neutron star mass measured with a high level of experimental confidence is the mass of the 3.15 millisecond pulsar PSR J1614-2230, $M = 1.97 \pm 0.04M_{\odot}$, obtained from the Shapiro time delay and the Keplerian orbital parameters of the binary system (Demorest et al., 2010). The fitting of the thermonuclear burst oscillation light curves from the accreting millisecond pulsar XTE J1814-338 weakly constrain the mass-radius relation imposing an upper limit to the surface gravity of the neutron star, $GM/(c^2R) < 0.24$ (Bhattacharyya et al., 2005). A lower limit of the radius of RX J1856-3754, as seen by an observer at infinity $R_{\infty} = R[1 - 2GM/(c^2R)]^{-1/2} > 16.8$ km, has been obtained from the fit of the optical and X-ray spectra of the source (Trümper et al., 2004); it gives the constraint $2GM/c^2 > R - R^3/(R_{\infty}^{\text{min}})^2$, being $R_{\infty}^{\text{min}} = 16.8$ km. Assuming a neutron star of $M = 1.4M_{\odot}$ to fit the Chandra data of the low-mass X-ray binary X7, it turns out that the radius of the star satisfies $R = 14.5_{-1.6}^{+1.8}$ km, at 90% confidence level, corresponding to $R_{\infty} = [15.64, 18.86]$ km, respectively (see Heinke et al. (2006) for details). The maximum rotation rate of a neutron star taking into account both the effects of general relativity and deformations has been found to be $\nu_{\text{max}} = 1045(M/M_{\odot})^{1/2}(10 \text{ km}/R)^{3/2}$ Hz, largely independent of the equation of

$M(M_{\odot})$	R_{NL3}	$R_{\text{NL-SH}}$	R_{TM1}	R_{TM2}
1.40	12.31	12.47	12.53	12.93
1.93	12.96	13.14	13.13	13.73
2.01	13.02	13.20	13.17	13.82

Table C.3.: Radii (in km) predicted by the nuclear parametrizations NL3, NL-Sh, TM1 and TM2 of Table C.1, for a canonical neutron star of $M = 1.4M_{\odot}$ and for the millisecond pulsar PSR J1614-2230, $M = 1.97 \pm 0.04M_{\odot}$.

state (Lattimer and Prakash, 2004). The fastest observed pulsar is PSR J1748-2246ad with a rotation frequency of 716 Hz (Hessels et al., 2006), which results in the constraint $M \geq 0.47(R/10 \text{ km})^3 M_{\odot}$. In Fig. C.20 we show all these constraints and the mass-radius relation presented in this article.

As discussed by J. E. Trümper in Trümper (2011), the above constraints strongly favor stiff equations of state which provide high maximum masses for neutron stars. In addition, putting all of them together, the radius of a canonical neutron star of mass $M = 1.4M_{\odot}$ is highly constrained to the range $R \gtrsim 12 \text{ km}$ disfavoring, at the same time, the strange quark hypothesis for these specific objects. It is clear from Fig. C.20 that the mass-radius relation presented here is consistent with all the observation constraints, for all the nuclear parametrizations of Table C.1. We present in Table C.3, the radii predicted by our mass-radius relation for a canonical neutron star of $M = 1.4M_{\odot}$ as well as for the millisecond pulsar PSR J1614-2230, $M = 1.97 \pm 0.04M_{\odot}$.

C.4.5. Comparison with the traditional TOV treatment

In the traditional TOV treatment local charge neutrality as well as the continuity of the pressure and the density in the core-crust transition are assumed. This leads to explicit violation of the constancy of the Klein potentials throughout the configuration (see e.g. Rotonondo et al. (2011d)). In such a case there is a smooth transition from the core to the crust without any density discontinuity and therefore the density at the edge of the crust is $\sim \rho_{\text{nuc}} \sim 2.7 \times 10^{14} \text{ g/cm}^3$. The so-called inner crust in those configurations extends in the range of densities $\rho_{\text{drip}} \lesssim \rho \lesssim \rho_{\text{nuc}}$ while, at densities $\rho \lesssim \rho_{\text{drip}}$, there is the so-called outer crust.

Due to the continuity of the Klein potentials in the transition from the core to the crust, there is a decrease of the Coulomb potential from $\sim m_{\pi}c^2/e$ at the core radius R_{core} down to zero at the edge of the neutral crust. Correspondingly, the electron chemical potential decreases from its value at the core radius until a value approximately given by $\mu_e^{\text{crust}} \sim \mu_e^{\text{drip}} \sim 26 \text{ MeV}$ (see Fig. C.8-C.9). Therefore, no crusts with densities larger than the neutron drip density $\rho_{\text{drip}} \sim 4.3 \times 10^{11} \text{ g/cm}^3$ exist, leading to crusts made only of outer crust.

In Figs. C.21 and C.22 we compare and contrast the mass and the thickness

of the crust as obtained from the traditional TOV treatment with the new configurations presented here.

The markedly differences both in mass and thickness of the crusts (see Figs. C.21 and C.22) obtained from the traditional Tolman-Oppenheimer-Volkoff approach and the new equilibrium configurations presented here, leads to a very different mass-radius relations which we compare and contrast in Fig. C.23.

C.4.6. Concluding Remarks

We have formulated the equations of equilibrium of neutron stars based on our recent works (Rueda et al., 2011; Rotondo et al., 2011c,b,d). The strong, weak, electromagnetic, and gravitational interactions are taken into due account within the framework of general relativity. In particular, the strong interactions between nucleons is described by the exchange of the σ , ω , and ρ mesons. The equilibrium conditions are given by the set of Einstein-Maxwell-Thomas-Fermi equations and by the constancy of the general relativistic Fermi energies of particles, the Klein potentials, throughout the configuration.

We have solved these equilibrium equations numerically, in the case of zero temperatures, for the nuclear parameter sets NL3 (Lalazissis et al., 1997), NL-SH (Sharma et al., 1993), TM1 (Sugahara and Toki, 1994), and TM2 (Hirata et al., 1995); see Table C.1 for details.

A new structure of the star is found: the positively charged core at supranuclear densities is surrounded by an electronic distribution of thickness $\gtrsim \hbar/(m_e c) \sim 10^2 \hbar/(m_\pi c)$ of opposite charge and, at lower densities, a neutral ordinary crust.

In the core interior the Coulomb potential well is $\sim m_\pi c^2/e$ and correspondingly the electric field is $\sim (m_p/m_{\text{Planck}})(m_\pi/m_e)^2 E_c \sim 10^{-14} E_c$. Due to the equilibrium condition given by the constancy of the Klein potentials, there is a discontinuity in the density at the transition from the core to the crust, and correspondingly an overcritical electric field $\sim (m_\pi/m_e)^2 E_c$ develops in the boundary interface; see Fig. C.8–C.9.

The continuity of the Klein potentials at the core-crust boundary interface leads to a decreasing of the electron chemical potential and density, until values $\mu_e^{\text{crust}} < \mu_e^{\text{core}}$ and $\rho_{\text{crust}} < \rho_{\text{core}}$ at the edge of the crust, where global charge neutrality is achieved. For each central density, an entire family of core-crust interface boundaries and, correspondingly, an entire family of crusts with different mass and thickness, exist. The larger ρ_{crust} , the smaller the thickness of the interface, the peak of the electric field, and the larger the mass and the thickness of the crust. The configuration with $\rho_{\text{crust}} = \rho_{\text{drip}} \sim 4.3 \times 10^{11} \text{ g/cm}^3$ separates neutron stars with and without inner crust. The neutron stars with $\rho_{\text{crust}} > \rho_{\text{drip}}$ deserve a further analysis in order to account for the reduction of the nuclear tension at the core-crust transition due to the

presence of dripped neutrons from the nuclei in the crust.

All the above new features lead to crusts with masses and thickness smaller than the ones obtained from the traditional TOV treatment, and we have shown specifically neutron stars with $\rho_{\text{crust}} = \rho_{\text{drip}}$; see Figs. C.21–C.22. The mass-radius relation obtained in this case have been compared and contrasted with the one obtained from the locally neutral TOV approach; see Fig. C.23. We have shown that our mass-radius relation is in line with observations, based on the recent work by J. E. Trümper (Trümper, 2011); see Fig. C.20 for details.

The electromagnetic structure of the neutron star presented here is of clear astrophysical relevance. The process of gravitational collapse of a core endowed with electromagnetic structure leads to signatures and energetics markedly different from the ones of a core endowed uniquely of gravitational interactions; see e.g. Ruffini et al. (2003b,a); Ruffini and Xue (2008); Ruffini et al. (2010b).

It is clear that the release of gravitational energy in the process of gravitational collapse of the core, following the classic work of Gamow and Schoenberg (1941), is carried away by neutrinos. The additional nuclear and electromagnetic energy $\sim 10^{51}$ erg of the collapsing core introduced in this article are expected to be carried away by electron-positron plasma created in the overcritical electromagnetic field in the collapsing core.

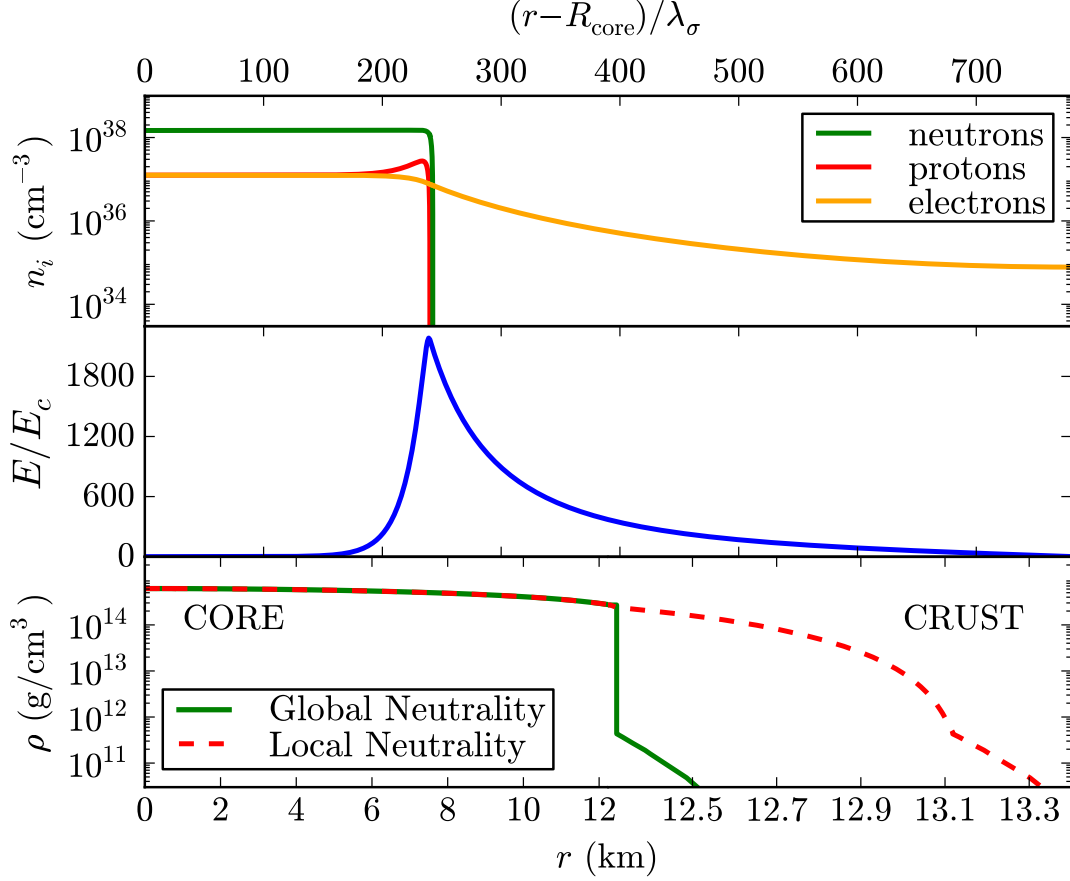


Figure C.10.: Upper panel: electric field in the core-crust transition layer, in units of the critical field E_c . Middle panel: particle density profiles in the core-crust boundary interface, in units of cm^{-3} . Lower panel: density profile inside a neutron star with central density $\rho(0) \sim 5\rho_{\text{nuc}}$. We compare and contrast the structural differences between the solution obtained from the traditional TOV equations (locally neutral case) and the globally neutral solution presented here. We use here the NL3 nuclear parametrization of Table C.1 and $\lambda_\sigma = \hbar/(m_\sigma c) \sim 0.4$ fm, denotes the sigma-meson Compton wavelength. In this example the density at the edge of the crust is $\rho_{\text{crust}} = \rho_{\text{drip}} = 4.3 \times 10^{11} \text{ g/cm}^3$.

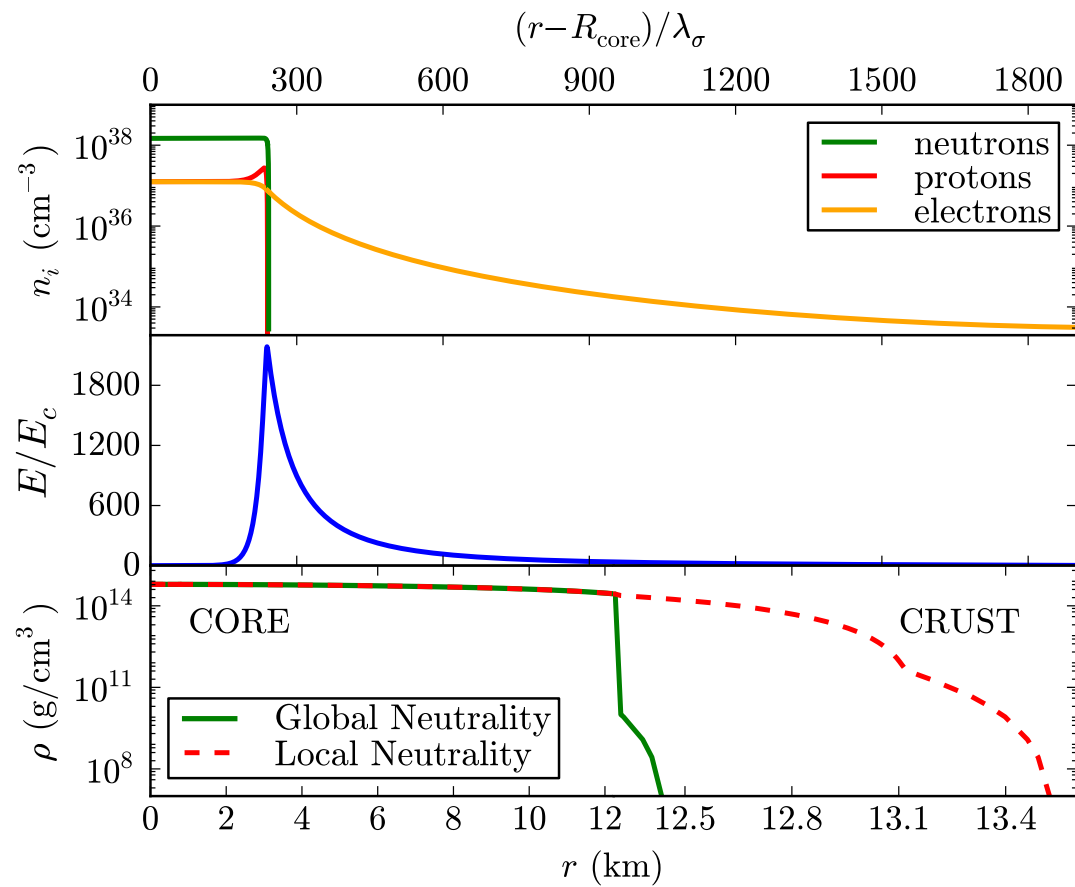


Figure C.11.: Same as Fig. C.10. In this example the density at the edge of the crust is $\rho_{\text{crust}} = 10^{10} \text{ g/cm}^3$.

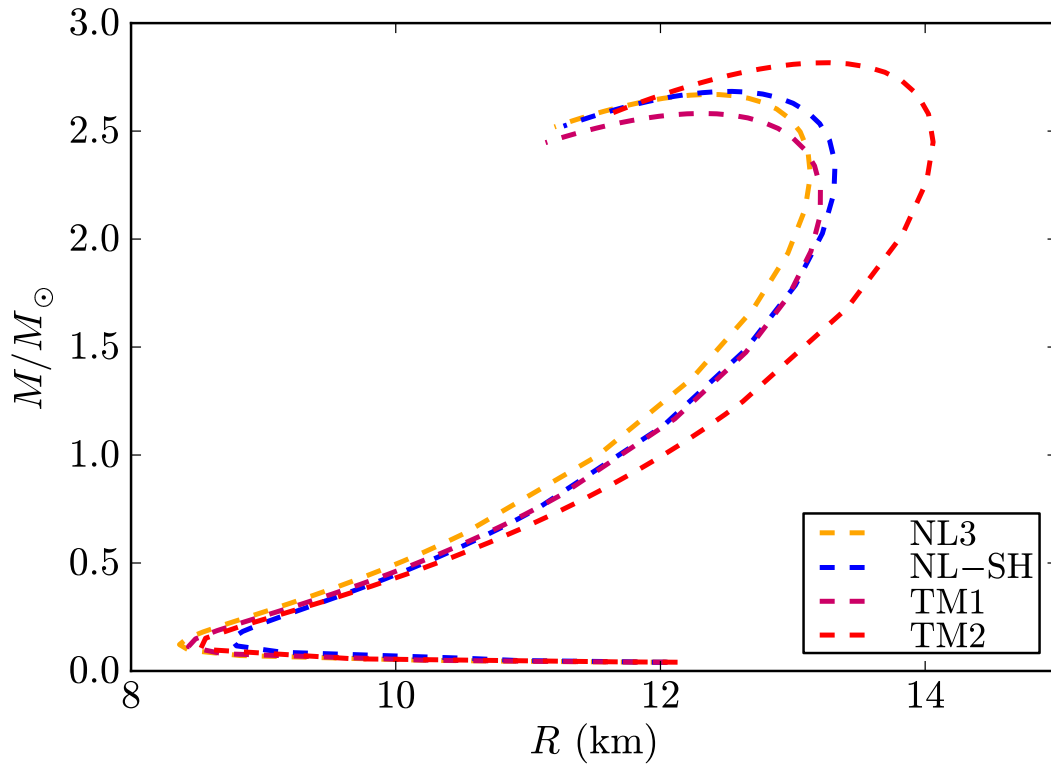


Figure C.12.: Mass-Radius relation for the neutron stars obtained with the nuclear models listed in Table C.1. In the crust we have used the BPS equation of state. The mass is given in solar masses and the radius in km.

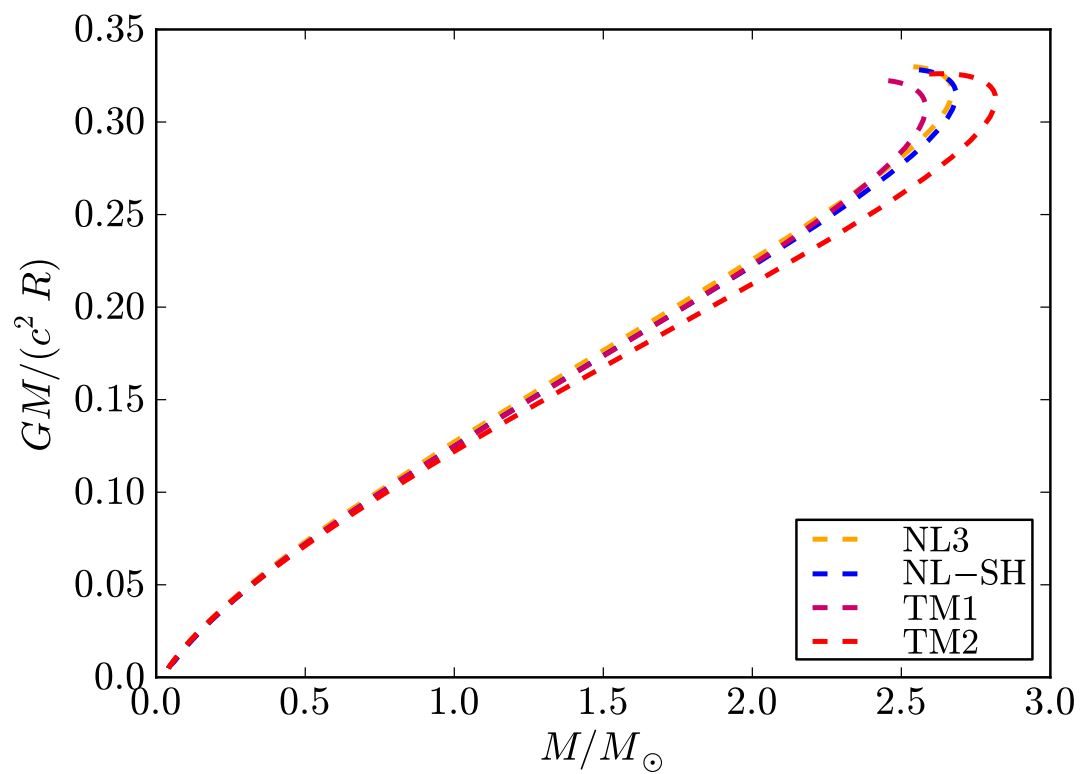


Figure C.13.: Compactness of the star $GM/(c^2 R)$ as a function of the star mass M . In the crust we have used the BPS equation of state and the nuclear models are in Table C.1.

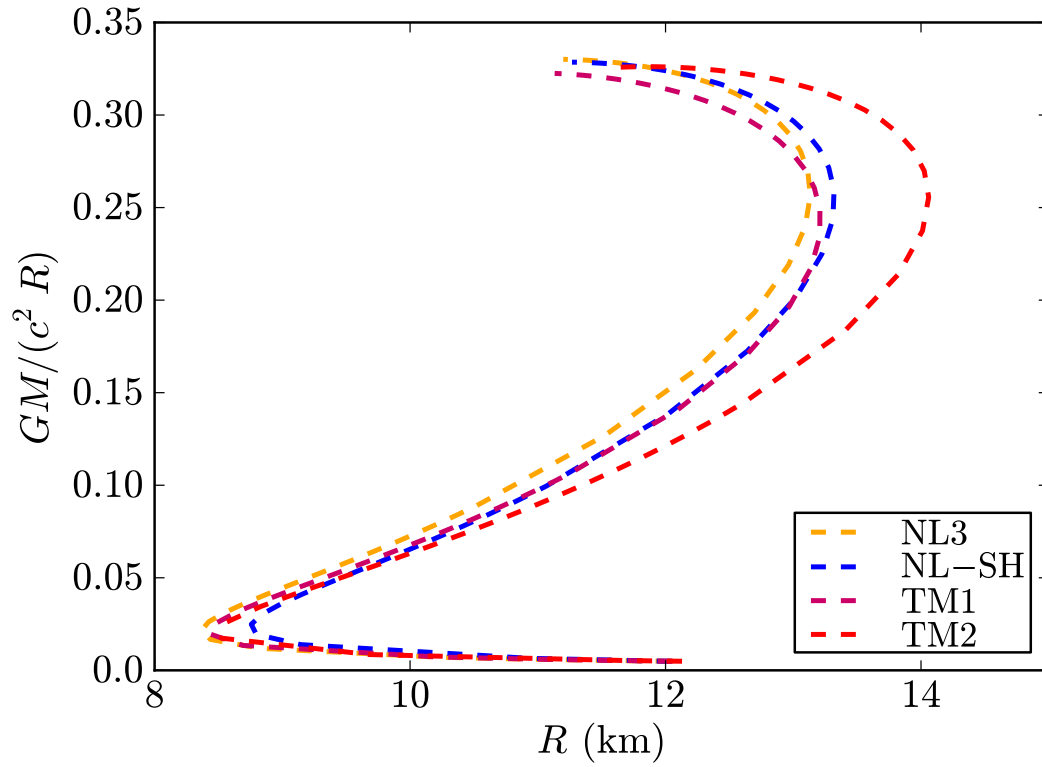


Figure C.14.: Compactness of the star $GM/(c^2 R)$ as a function of the star radius R . In the crust we have used the BPS equation of state and the nuclear models are in Table C.1.

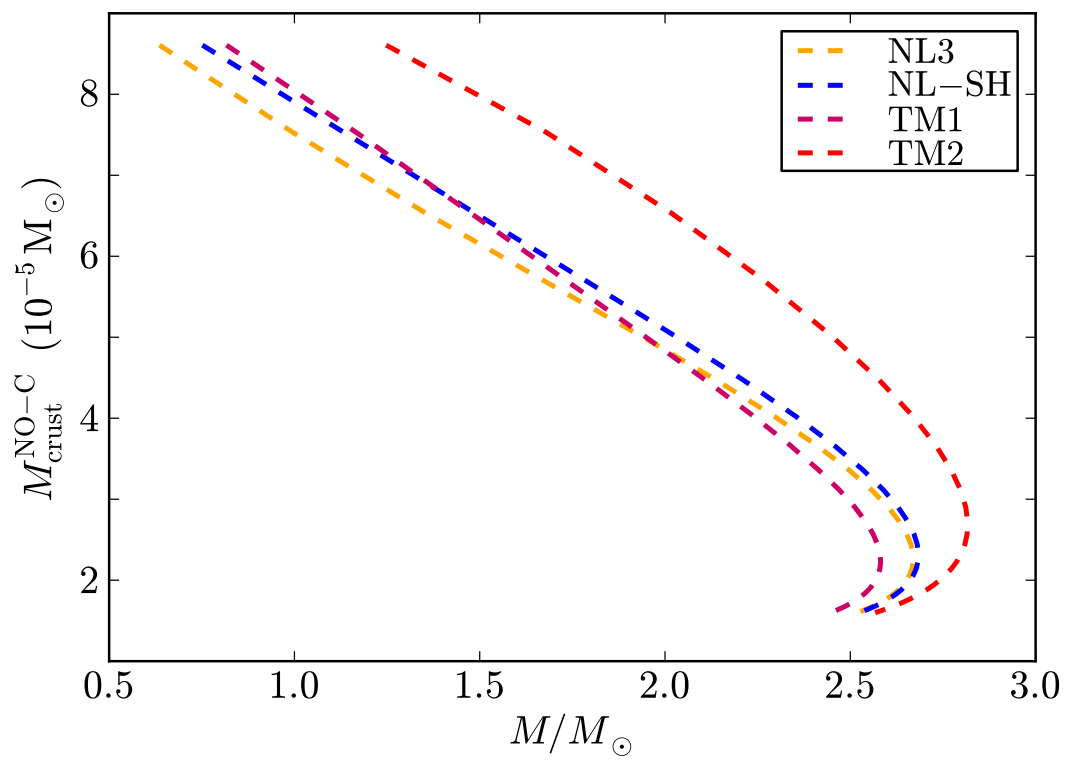


Figure C.15.: Mass of the crust as a function of the compactness for the crust EoS without Coulomb interactions.

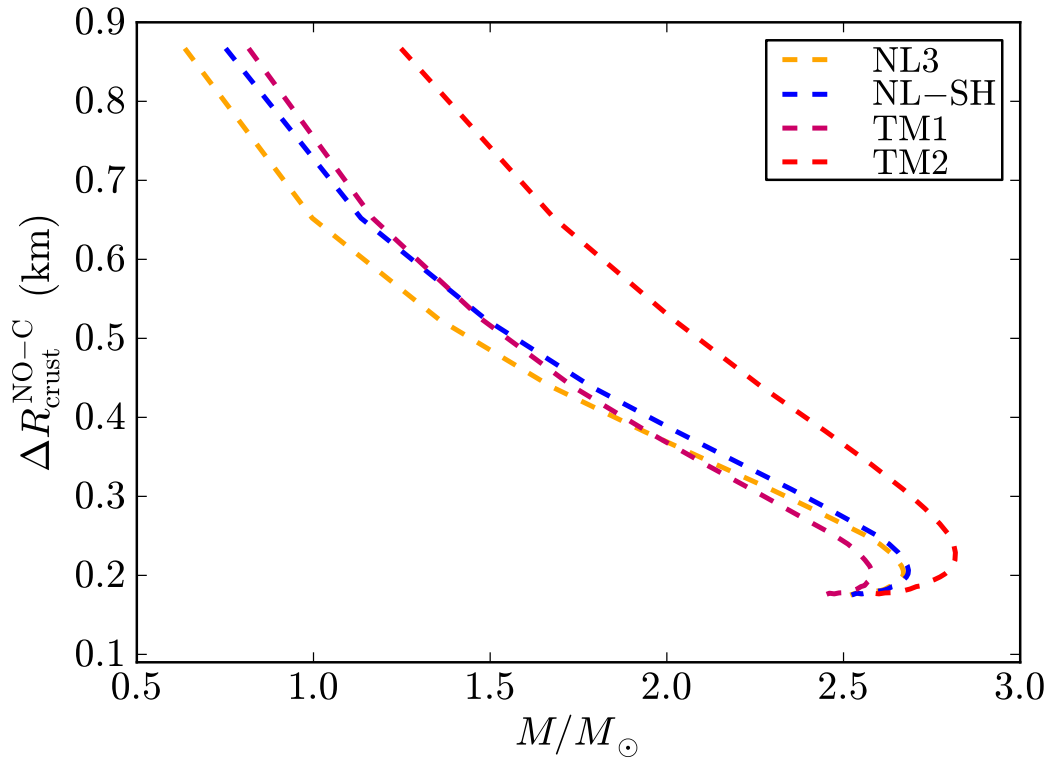


Figure C.16.: Crust-thickness as a function of the compactness for the crust EoS without Coulomb interactions.

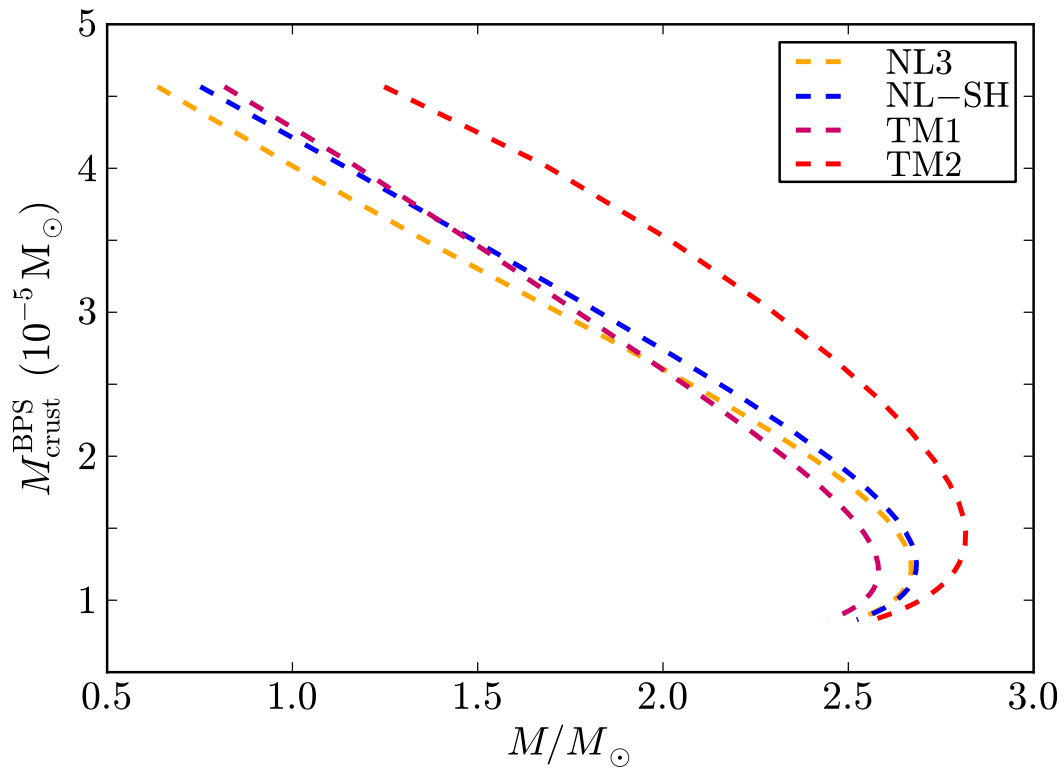


Figure C.17.: Crust mass as a function of the compactness for crust with the BPS EoS.

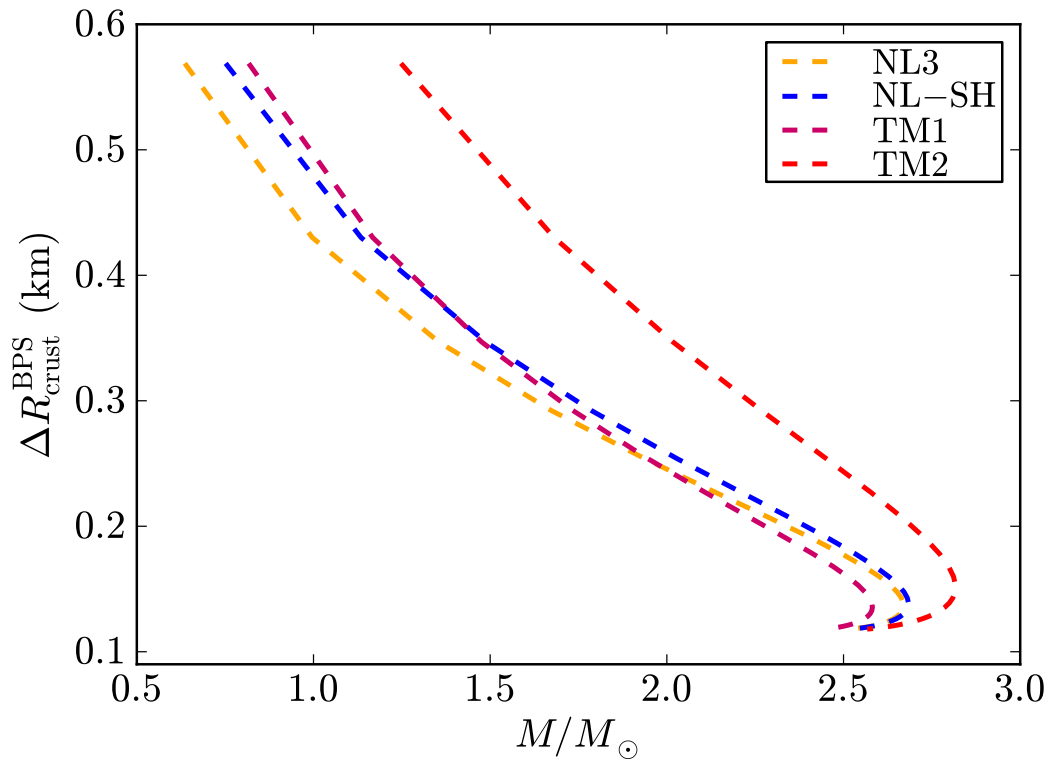


Figure C.18.: Crust thickness as a function of the compactness for crust with the BPS EoS.

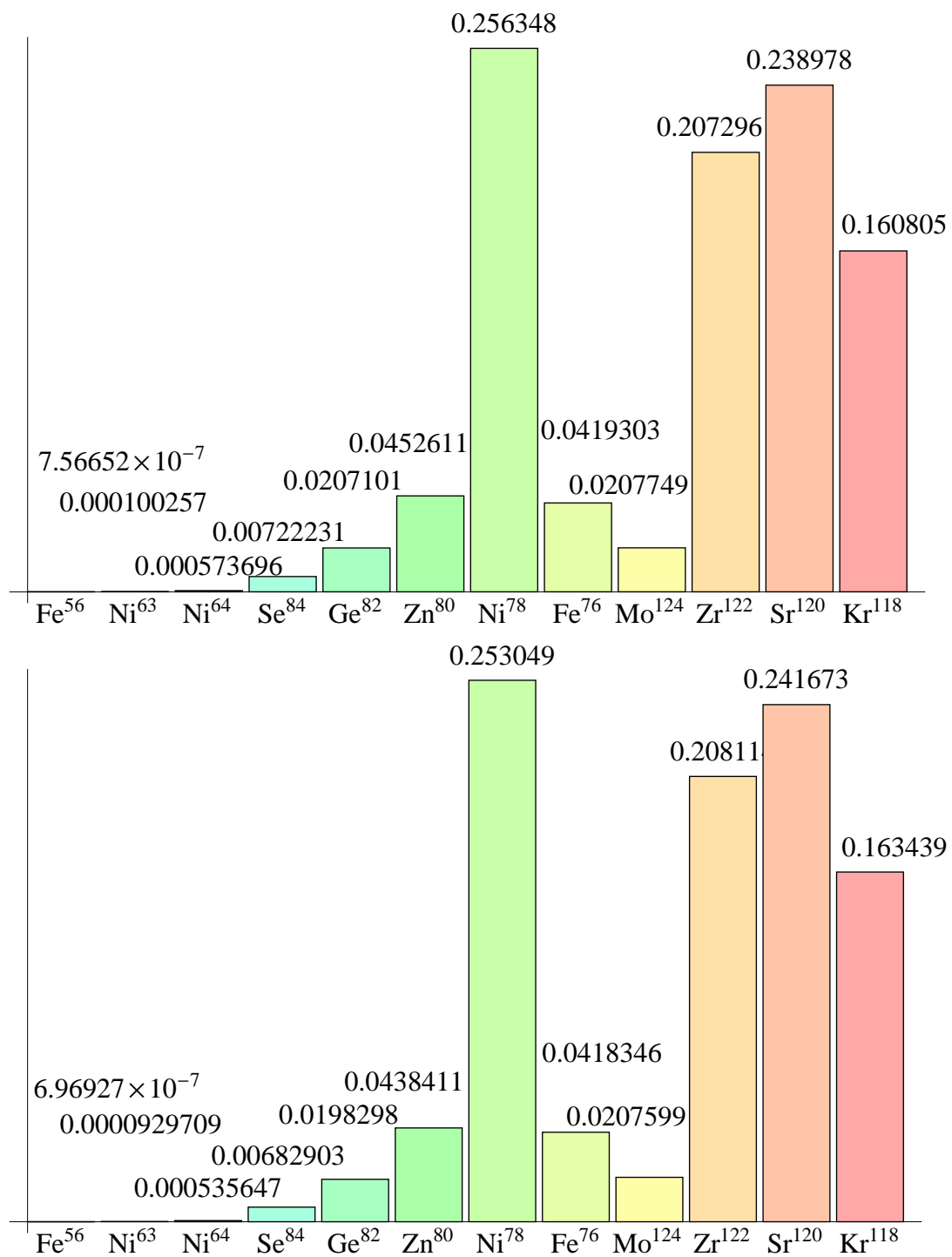


Figure C.19.: Relative abundances of chemical elements in the crust for the two cores analyzed in Table C.2

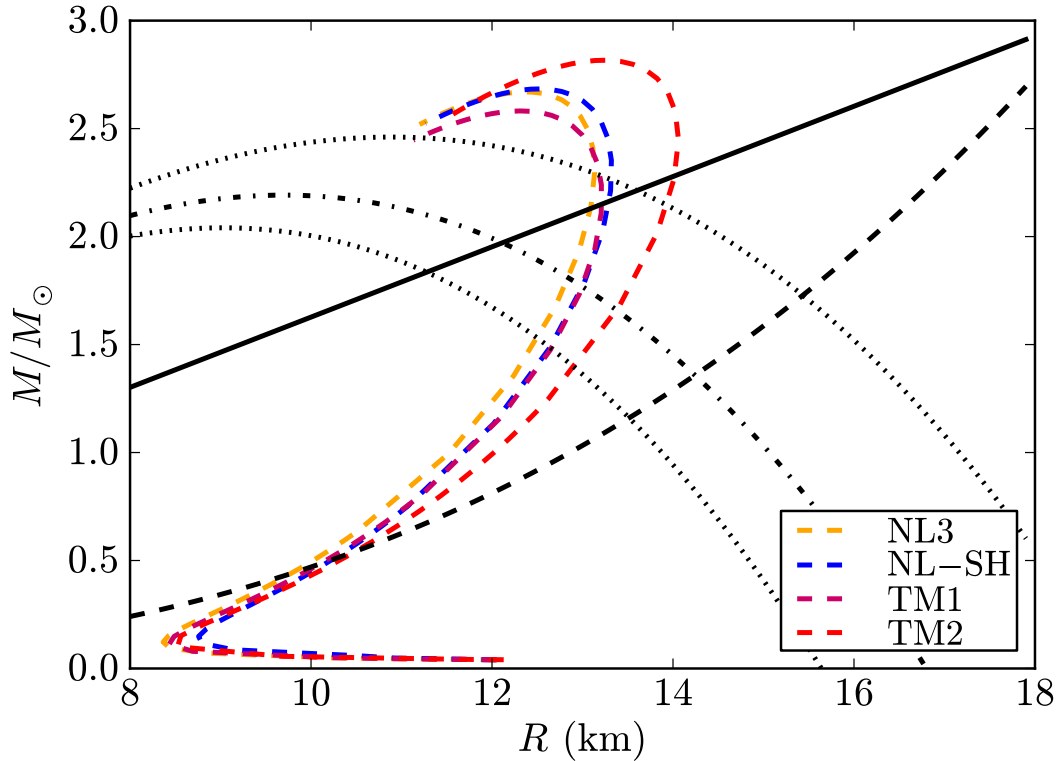


Figure C.20.: Constraints on the mass-radius relation given by J. E. Trümper in Trümper (2011) and the theoretical mass-radius relation presented in this article in Fig. C.12. The solid line is the upper limit of the surface gravity of XTE J1814-338, the dotted-dashed curve corresponds to the lower limit to the radius of RX J1856-3754, the dashed line is the constraint imposed by the fastest spinning pulsar PSR J1748-2246ad, and the dotted curves are the 90% confidence level contours of constant R_∞ of the neutron star in the low-mass X-ray binary X7. Any mass-radius relation should pass through the area delimited by the solid, the dashed and the dotted lines and, in addition, it must have a maximum mass larger than the mass of PSR J1614-2230, $M = 1.97 \pm 0.04M_\odot$.

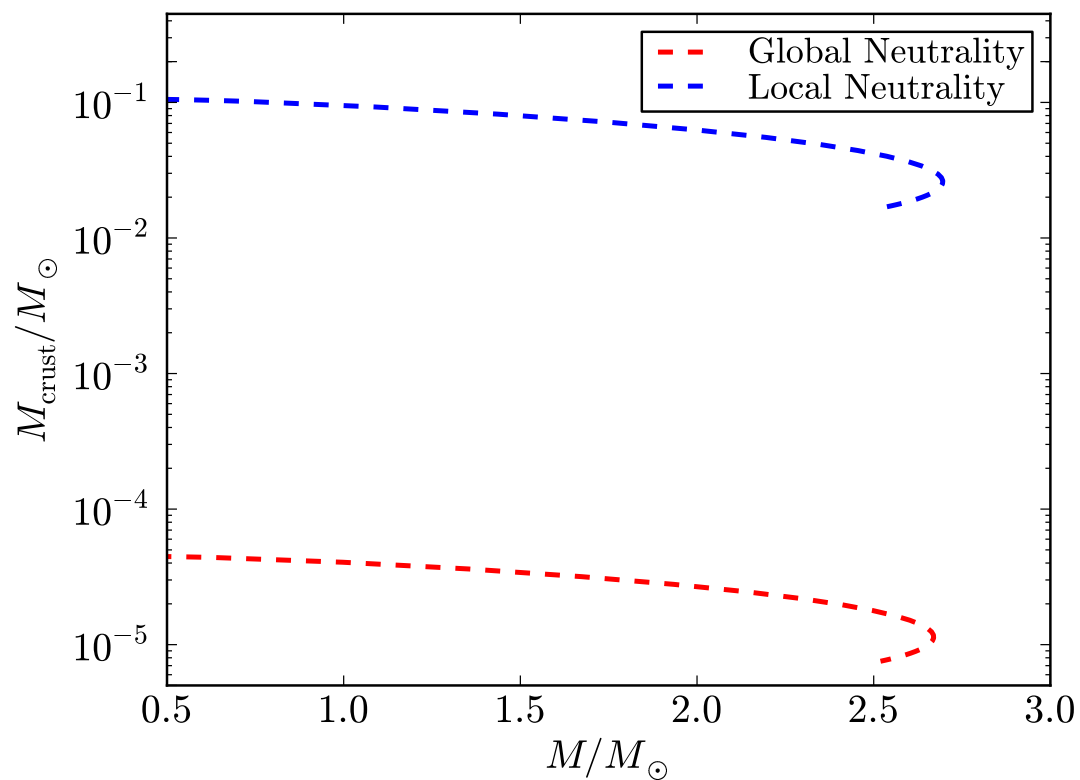


Figure C.21.: Mass of the crust given by the traditional locally neutral Tolman-Oppenheimer-Volkoff treatment and by the new globally neutral equilibrium configurations presented in this article. We use here the NL3 nuclear model, see Table C.1.

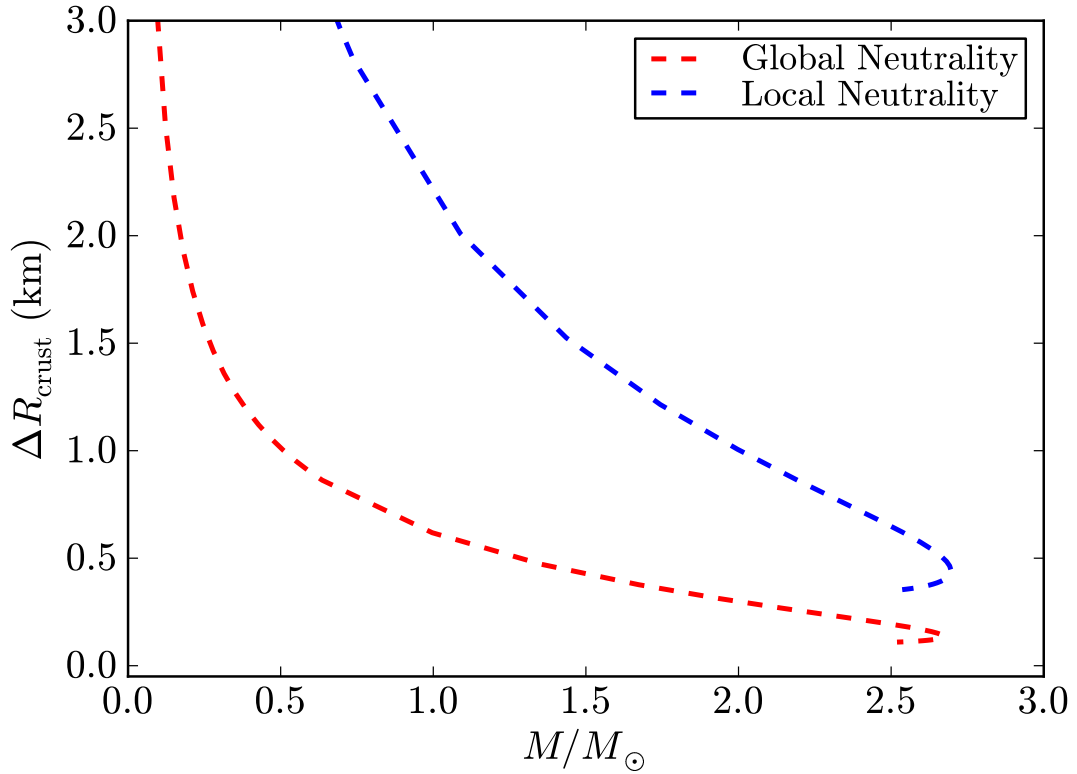


Figure C.22.: Thickness of the crust given by the traditional locally neutral Tolman-Oppenheimer-Volkoff treatment and by the new globally neutral equilibrium configurations presented in this article. We use here the NL3 nuclear model, see Table C.1.

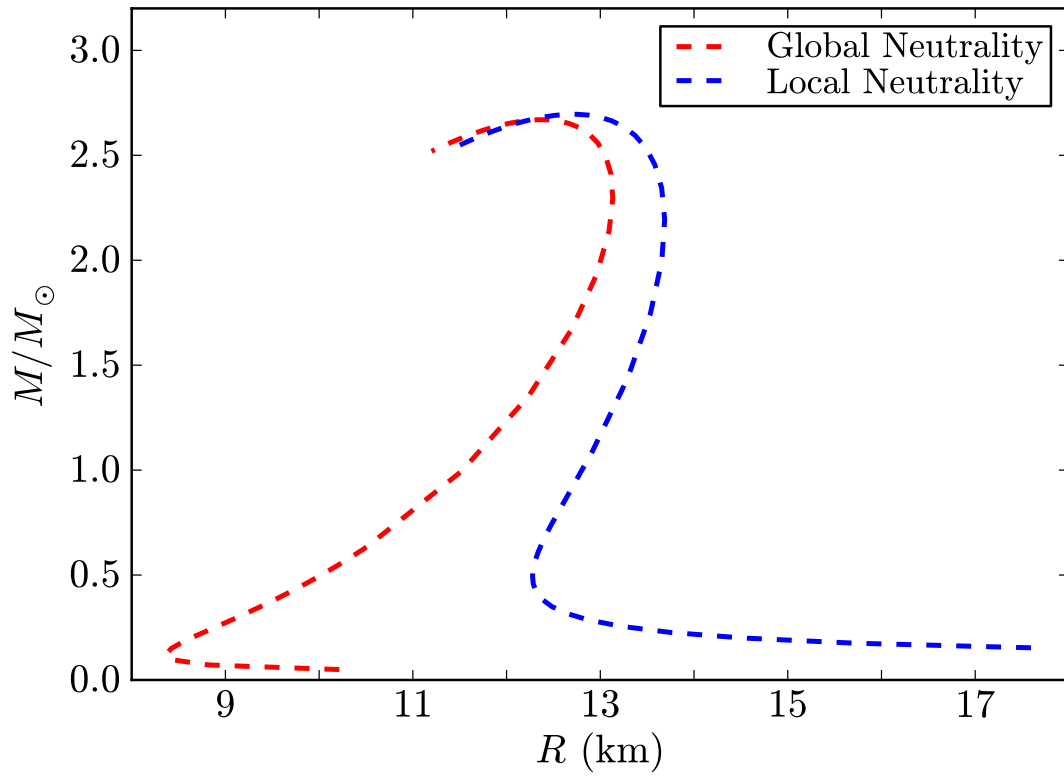


Figure C.23.: Mass-Radius relation obtained with the traditional locally neutral TOV treatment and with the new globally neutral equilibrium configurations presented here. We use here the NL3 nuclear model, see Table C.1.

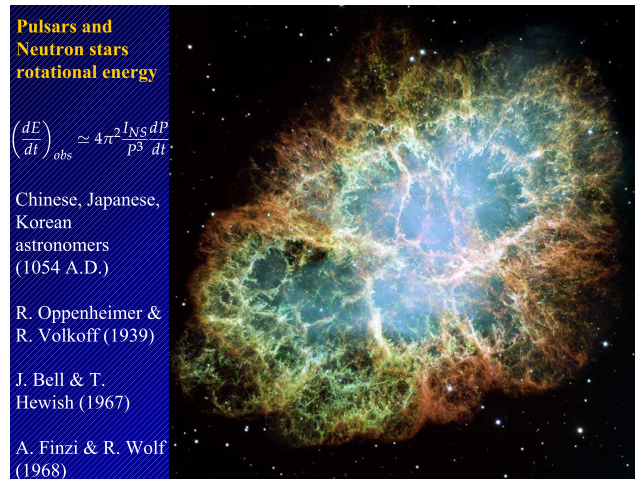
C.5. The Role of Thomas-Fermi approach in Neutron Star Matter

C.5.1. Introduction

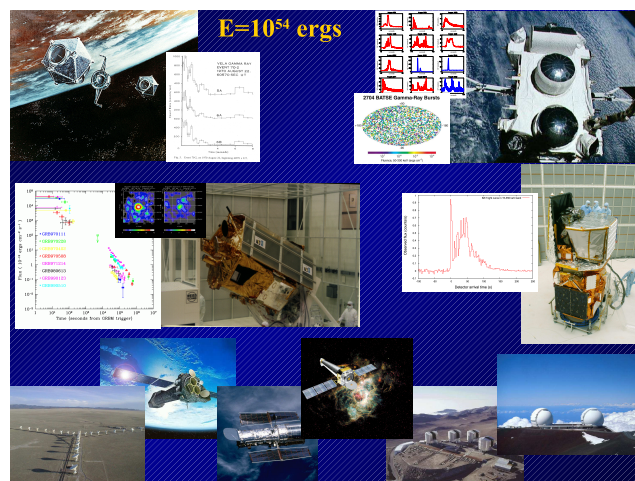
We first recall how certainly one of the greatest success in human understanding of the Universe has been the research activity started in 1054 by Chinese, Korean and Japanese astronomers by the observations of a “Guest Star”(see e.g. Shklovskii (1968)), followed by the discovery of the Pulsar *NPO532* in the Crab Nebula in 1967, (see e.g. Manchester and Taylor (1977)), still presenting challenges in the yet not identified physical process originating the expulsion of the remnant in the Supernova explosion (see e.g. Mezzacappa (2005) and Fig. C.24(a)). We are currently exploring the neutron star equilibrium configuration for a missing process which may lead to the solution of the above mentioned astrophysical puzzle.

We also recall an additional astrophysical observation which is currently capturing the attention of Astrophysicists worldwide: the Gamma ray Bursts or for short GRBs. Their discovery was accidental and triggered by a very unconventional idea proposed by Yacov Borisovich Zel’dovich. It is likely that this idea served as an additional motivation for the United States of America to put a set of four Vela Satellites into orbit, 150,000 miles above the Earth. They were top-secret omnidirectional detectors using atomic clocks to precisely record the arrival times of both X-rays and γ -rays (see Fig. C.24(b)). When they were made operational they immediately produced results (see Fig. C.24(b)). It was thought at first that the signals originated from nuclear bomb explosions on the earth but they were much too frequent, one per day! A systematic analysis showed that they had not originated on the earth, nor even in the solar system. These Vela satellites had discovered GRBs! The first public announcement of this came at the AAAS meeting in San Francisco in a special session on neutron stars, black holes and binary X-ray sources, organized by Herb Gursky and myself (Gursky and Ruffini, 1975).

A few months later, Thibault Damour and myself published a theoretical framework for GRBs based on the vacuum polarization process in the field of a Kerr-Newman black hole (Damour and Ruffini, 1975). We showed how the pair creation predicted by the Heisenberg-Euler-Schwinger theory Heisenberg and Euler (1936); Schwinger (1951, 1954a,b) would lead to a transformation of the black hole, asymptotically close to reversibility. The electron-positron pairs created by this process were generated by what we now call the blackholic energy. In that paper we concluded that this “naturally leads to a very simple model for the explanation of the recently discovered GRBs”. Our theory had two very clear signatures. It could only operate for black holes with mass M_{BH} in the range $3.2-10^6 M_{\odot}$ and the energy released had a characteristic value of



(a)



(b)

Figure C.24.: (a) The expanding shell of the remnant of the Crab Nebulae as observed by the Hubble Space Telescope. Reproduced from Hubble Telescope web site with their kind permission (News Release Number: STScI-2005-37). (b) On the upper left the Vela 5A and 5B satellites and a typical event as recorded by three of the Vela satellites; on the upper right the Compton satellite and the first evidence of the isotropy of distribution of GRB in the sky; on the center left the Beppo Sax satellite and the discovery of the after glow; on the center right a GRB from Integral satellite; in the lower part the Socorro very large array radiotelescope, the Hubble, the Chandra and the XMM telescopes, as well as the VLT of Chile and KECK observatory in Hawaii. All these instruments are operating for the observations of GRBs (Ruffini et al., 2007a).

$$E = 1.8 \times 10^{54} M_{BH}/M_{\odot} \text{ ergs} . \quad (\text{C.5.1})$$

Since nothing was then known about the location and the energetics of these sources we stopped working in the field, waiting for a clarification of the astrophysical scenario.

The situation changed drastically with the discovery of the “afterglow” of GRBs (Costa et al., 1997) by the joint Italian-Dutch satellite BeppoSAX (see Fig. C.24(b)). This X-ray emission lasted for months after the “prompt” emission of a few seconds duration and allowed the GRB sources to be identified much more accurately. This then led to the optical identification of the GRBs by the largest telescopes in the world, including the Hubble Space Telescope, the KECK telescope in Hawaii and the VLT in Chile (see Fig. C.24(b)). Also, the very large array in Socorro made the radio identification of GRBs possible. The optical identification of GRBs made the determination of their distances possible. The first distance measurement for a GRB was made in 1997 for GRB970228 and the truly enormous of isotropical energy of this was determined to be 10^{54} ergs per burst. This proved the existence of a single astrophysical system emitting as much energy during its short lifetime as that emitted in the same time by all other stars of all galaxies in the Universe!^a It is interesting that this “quantum” of astrophysical energy coincided with the one Thibault Damour and I had already predicted, see Eq. (C.5.1). Much more has been learned on GRBs in recent years confirming this basic result (see e.g. Ruffini (2008a)). The critical new important step now is to understand the physical process leading to the critical fields needed for the pair creation process during the gravitational collapse process from a Neutron Stars to a Black Hole.

As third example, we recall the galactic ‘X-ray bursters’ as well as some observed X-ray emission precursor of supernovae events. It is our opinion that the solution of: **a)** the problem of explaining the energetics of the emission of the remnant during the collapse to a Neutron Star, **b)** the problem of formation of the supercritical fields during the collapse to a Black Hole, **c)** the less energetics of galactic ‘X-ray bursters’ and of the precursor of the supernovae explosion event, will find their natural explanation from a yet unexplored field: the electro-dynamical structure of a neutron star. We will outline a few crucial ideas of how a Thomas-Fermi approach to a neutron star can indeed represent an important step in identify this crucial new feature.

C.5.2. Thomas-Fermi model

We first recall the basic Thomas-Fermi non relativistic Equations (see e.g. Landau and Lifshitz (1980)). They describe a degenerate Fermi gas of N_{el}

¹Luminosity of average star = 10^{33} erg/s, Stars per galaxy = 10^{12} , Number of galaxies = 10^9 . Finally, $33 + 12 + 9 = 54!$

electrons in the field of a point-like nucleus of charge Ze . The Coulomb potential $V(r)$ satisfies the Poisson equation

$$\nabla^2 V(r) = 4\pi en, \quad (\text{C.5.2})$$

where the electron number density $n(r)$ is related to the Fermi momentum p_F by $n = p_F^3 / (3\pi^2 \hbar^3)$. The equilibrium condition for an electron, of mass m , inside the atom is expressed by $\frac{p_F^2}{2m} - eV = E_F$. To put Eq. (C.5.2) in dimensionless form, we introduce a function ϕ , related to Coulomb potential by $\phi(r) = V(r) + \frac{E_F}{e} = Ze \frac{\chi(r)}{r}$. Assuming $r = bx$, with $b = \frac{(3\pi)^{3/2}}{2^{7/3}} \frac{1}{Z^{1/3}} \frac{\hbar^2}{me^2}$, we then have the universal equation (Thomas, 1927; Fermi, 1927)

$$\frac{d^2 \chi(x)}{dx^2} = \frac{\chi(x)^{3/2}}{x^{1/2}}. \quad (\text{C.5.3})$$

The first boundary condition for this equation follows from the request that approaching the nucleus one gets the ordinary Coulomb potential therefore $\chi(0) = 1$. The second boundary condition comes from the fact that the number of electrons N_{el} is $1 - \frac{N_{el}}{Z} = \chi(x_0) - x_0 \chi'(x_0)$.

C.5.3. White dwarfs and Neutron Stars as Thomas-Fermi systems

It was at the 1972 Les Houches organized by Bryce and Cecille de Witt summer School (see Fig. C.25(a) and Ruffini (1972)) that, generalizing a splendid paper by Landau (1932), I introduced a Thomas-Fermi description of both White Dwarfs and Neutron Stars within a Newtonian gravitational theory and describing the microphysical quantities by a relativistic treatment. The equilibrium condition for a self-gravitating system of fermions, in relativistic regime is $c\sqrt{p_F^2 + m_n^2 c^2} - m_n c^2 - m_n V = -m_n V_0$, where p_F is the Fermi momentum of a particle of mass m_n , related to the particle density n by $n = \frac{1}{3\pi^2 \hbar^3} p_F^3$. $V(r)$ is the gravitational potential at a point at distance r from the center of the configuration and V_0 is the value of the potential at the boundary R_c of the configuration $V_0 = \frac{GNm_n}{R_c}$. N is the total number of particles. The Poisson equation is $\nabla^2 V = -4\pi Gm_n n$. Assuming $V - V_0 = GNm_n \frac{\chi(r)}{r}$ and $r = bx$, with $b = \frac{(3\pi)^{2/3}}{2^{7/3}} \frac{1}{N^{1/3}} \left(\frac{\hbar}{m_n c}\right) \left(\frac{m_{\text{Planck}}}{m_n}\right)^2$ we obtain the gravitational Thomas-Fermi equation

$$\frac{d^2 \chi}{dx^2} = -\frac{\chi^{3/2}}{\sqrt{x}} \left[1 + \left(\frac{N}{N^*}\right)^{4/3} \frac{\chi}{x} \right]^{3/2}, \quad (\text{C.5.4})$$

where $N^* = \left(\frac{3\pi}{4}\right)^{1/2} \left(\frac{m_{\text{Planck}}}{m_n}\right)^3$. Eq.(C.5.4) has to be integrated with the boundary conditions $\chi(0) = 0$, $-x_b \left(\frac{d\chi}{dx}\right)_{x=x_b} = 1$. Eq. (C.5.4) can be applied as well to the case of white dwarfs.

It is sufficient to assume

$$b = \frac{(3\pi)^{2/3}}{2^{7/3}} \frac{1}{N^{1/3}} \left(\frac{\hbar}{m_e c}\right) \left(\frac{m_{\text{Planck}}}{\mu m_n}\right)^2,$$

$$N^* = \left(\frac{3\pi}{4}\right)^{1/2} \left(\frac{m_{\text{Planck}}}{\mu m_n}\right)^3,$$

$$M = \int_0^{R_c} 4\pi r^2 n_e(r) \mu m_n dr.$$

For the equilibrium condition $c\sqrt{p_F^2 + m^2 c^2} - mc^2 - \mu m_n V = -\mu m_n V_0$, in order to obtain for the critical mass the value $M_{\text{crit}} \approx 5.7 M_{\text{sun}} \mu_e^{-2} \approx 1.5 M_{\text{sun}}$.

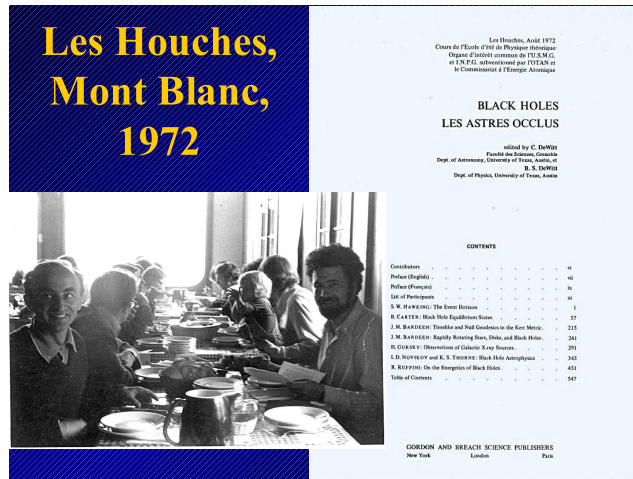
C.5.4. The relativistic Thomas-Fermi equation

In the intervening years my attention was dedicated to an apparently academic problem: the solution of a relativistic Thomas-Fermi Equation and extrapolating the Thomas-Fermi solution to large atomic numbers of $Z \approx 10^4 - 10^6$. Three new features were outlined: **a)** the necessity of introducing a physical size for the nucleus, **b)** the penetration of the electrons in the nucleus, **c)** the definition of an effective nuclear charge (Ferreirinho et al., 1980; Ruffini and Stella, 1981). The electrostatic potential is given by $\nabla^2 V(r) = 4\pi e n$, where the number density of electrons is related to the Fermi momentum p_F by $n = \frac{p_F^3}{3\pi^2 \hbar^3}$. In order to have equilibrium we have $c\sqrt{p_F^2 + m^2 c^2} - mc^2 - eV(r) = E_F$. Assuming $\phi(r) = V(r) + \frac{E_F}{e} = Ze\frac{\chi(r)}{r}$, $Z_c = \left(\frac{3\pi}{4}\right)^{1/2} \left(\frac{\hbar c}{e^2}\right)^{3/2}$, and $r = bx$, with $b = \frac{(3\pi)^{3/2}}{2^{7/3}} \frac{1}{Z^{1/3}} \frac{\hbar^2}{me^2}$, the Eq. (C.5.3) becomes

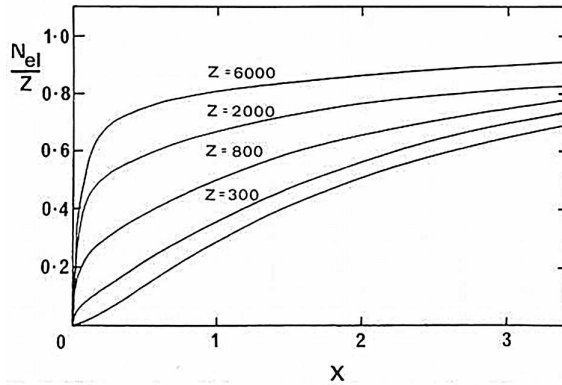
$$\frac{d^2 \chi(x)}{dx^2} = \frac{\chi(x)^{3/2}}{x^{1/2}} \left[1 + \left(\frac{Z}{Z_c}\right)^{4/3} \frac{\chi(x)}{x} \right]^{3/2}. \quad (\text{C.5.5})$$

C.5.5. The essential role of the non point-like nucleus

The point-like assumption for the nucleus leads, in the relativistic case, to a non-integrable expression for the electron density near the origin. We assumed a uniformly charged nucleus with a radius r_{nuc} and a mass number A given by the following semi-empirical formulae



(a)



(b)

Figure C.25.: (a) Lunch at Les Louces summer school on 'Black Holes'. In front, face to face, Igor Novikov and the author; in the right the title of the book in English and in French. It is interesting that in that occasion Cecile de Witt founded the French translation of the word 'Back Hole' in 'Trou Noir' objectionable and she introduced instead the even more objectionable term 'Astres Occlus'. The French nevertheless happily adopted in the following years the literally translated word 'Trou Noir' for the astrophysical concept I introduced in 1971 with J.A. Wheeler (Ruffini and Wheeler, 1971). (b) The number of electrons contained within a distance x of the origin, as a function of the total number Z for a neutral atom. The lowest curve is that given by the solution of the non-relativistic Thomas-Fermi equation.

$$r_{nuc} = r_0 A^{1/3}, \quad r_0 \approx 1.5 \times 10^{-13} \text{cm}, \quad (\text{C.5.6})$$

$$Z \simeq \left[\frac{2}{A} + \frac{3}{200} \frac{1}{A^{1/3}} \right]^{-1}, \quad (\text{C.5.7})$$

Eq.(C.5.5) then becomes

$$\frac{d^2\chi(x)}{dx^2} = \frac{\chi(x)^{3/2}}{x^{1/2}} \left[1 + \left(\frac{Z}{Z_c} \right)^{4/3} \frac{\chi(x)}{x} \right]^{3/2} - \frac{3x}{x_{nuc}^3} \theta(x_{nuc} - x), \quad (\text{C.5.8})$$

where $\theta = 1$ for $r < r_{nuc}$, $\theta = 0$ for $r > r_{nuc}$, $\chi(0) = 0$, $\chi(\infty) = 0$.

Eq.(C.5.8) has been integrated numerically for selected values of Z (see Fig. C.25(b) and Ferreira et al. (1980); Ruffini and Stella (1981)). Similar results had been obtained by Greiner and his school and by Popov and his school with special emphasis on the existence of critical electric field at the surface of heavy nuclei. Their work was mainly interested in the study of the possibility of having process of vacuum polarization at the surface of heavy nuclei to be possibly achieved by heavy nuclei collisions. Paradoxically at the time we were not interested in this very important aspect and we did not compute the strength of the field in our relativistic Thomas-Fermi model which is indeed of the order of the Critical Field $E_c = m^2 c^3 / e \hbar$.

C.5.6. Nuclear matter in bulk: $A \approx 300$ or $A \approx (m_{Planck}/m_n)^3$

The situation clearly changed with the discovery of GRBs and the understanding that the process of vacuum polarization unsuccessfully sought in earthbound experiments could indeed be observed in the process of formation of a Black Hole from the gravitational collapse of a neutron star. The concept of a Dyadosphere, Ruffini (1998); Preparata et al. (1998), was introduced around an already formed Black Hole and it became clear that this concept was of paramount importance in the understanding the energy source for GRBs. It soon became clear that the initial conditions for such a process had to be found in the electro-dynamical properties of neutron stars. Similarly manifest came the crucial factor which had hampered the analysis of the true electro dynamical properties of a neutron star; the unjustified imposition of local charge neutrality as opposed to the global charge neutrality of the system. We have therefore proceeded to make a model of a nuclear matter core of $A \approx (m_{Planck}/m_n)^3$ nucleons (Ruffini et al., 2007c). We generalized to this more general case the concept introduced in their important work by W. Greiner and V. Popov (see Fig. C.26) as follows.

I have assumed that the proton number density is constant inside the core $r \leq R_c$ and vanishes outside the core $r > R_c$:

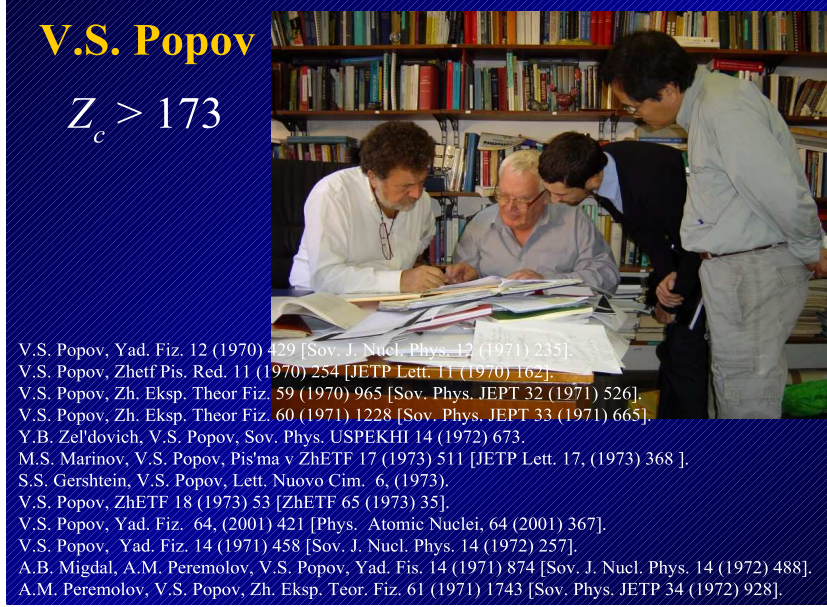


Figure C.26.: Vladimir Popov discussing with the author and Professors She Sheng Xue and Gregory Vereshchagin (Roma 2007). Also quoted the classical contributions of Popov and his school.

$$n_p = \frac{1}{3\pi^2\hbar^3}(P_p^F)^3 = \frac{3N_p}{4\pi R_c^3}\theta(R_c - r), \quad R_c = \Delta \frac{\hbar}{m_\pi c} N_p^{1/3},$$

where P_p^F is the Fermi momentum of protons, $\theta(R_c - r)$ is the step-function and Δ is a parameter. The proton Fermi energy is

$$\mathcal{E}_p(P_p^F) = [(P_p^F c)^2 + m_p^2 c^4]^{1/2} - m_p c^2 + eV, \quad (\text{C.5.9})$$

where e is the proton charge and V is the Coulomb potential. Based on the Gauss law, $V(r)$ obeys the Poisson equation $\nabla^2 V(r) = -4\pi e [n_p(r) - n_e(r)]$ and boundary conditions $V(\infty) = 0$, $V(0) = \text{finite}$, where the electron number density $n_e(r)$ is given by

$$n_e(r) = \frac{1}{3\pi^2\hbar^3}(P_e^F)^3, \quad (\text{C.5.10})$$

being P_e^F the electron Fermi momentum. The electron Fermi energy is

$$\mathcal{E}_e(P_e^F) = [(P_e^F c)^2 + m^2 c^4]^{1/2} - mc^2 - eV. \quad (\text{C.5.11})$$

The energetic equation for an electrodynamic equilibrium of electrons in the Coulomb potential $V(r)$ is $\mathcal{E}_e(P_e^F) = 0$, hence the Fermi momentum and the electron number density can be written as

$$n_e(r) = \frac{1}{3\pi^2\hbar^3c^3} \left[e^2V^2(r) + 2mc^2eV(r) \right]^{3/2}.$$

Introducing the new variable $x = r/(\hbar/m_\pi c)$ (the radial coordinate in unit of pion Compton length $(\hbar/m_\pi c)$, $x_c = x(r = R_c)$), I have obtained the following relativistic Thomas-Fermi Equation (Patricelli et al., 2008):

$$\frac{1}{3x} \frac{d^2\chi(x)}{dx^2} = -\alpha \left\{ \frac{1}{\Delta^3} \theta(x_c - x) - \frac{4}{9\pi} \left[\frac{\chi^2(x)}{x^2} + 2 \frac{m}{m_\pi} \frac{\chi}{x} \right]^{3/2} \right\}, \quad (\text{C.5.12})$$

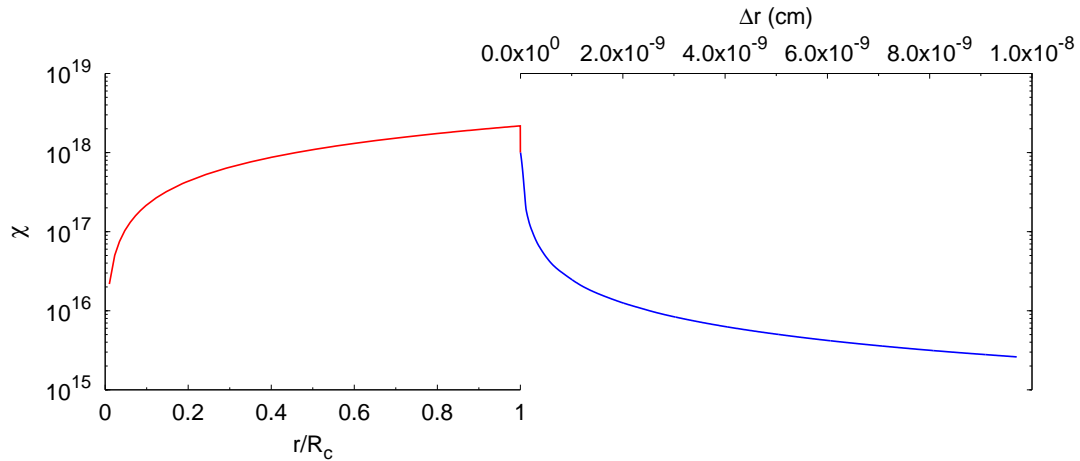
where χ is a dimensionless function defined by $\frac{\chi}{r} = \frac{eV}{\hbar c}$ and α is the fine structure constant $\alpha = e^2/(\hbar c)$. The boundary conditions of the function $\chi(x)$ are $\chi(0) = 0$, $\chi(\infty) = 0$ and $N_e = \int_0^\infty 4\pi r^2 dr n_e(r)$. Instead of using the phenomenological relation between Z and A , given by Eqs. (C.5.6) and (C.5.7), we determine directly the relation between A and Z by requiring the β -equilibrium

$$\mathcal{E}_n = \mathcal{E}_p + \mathcal{E}_e. \quad (\text{C.5.13})$$

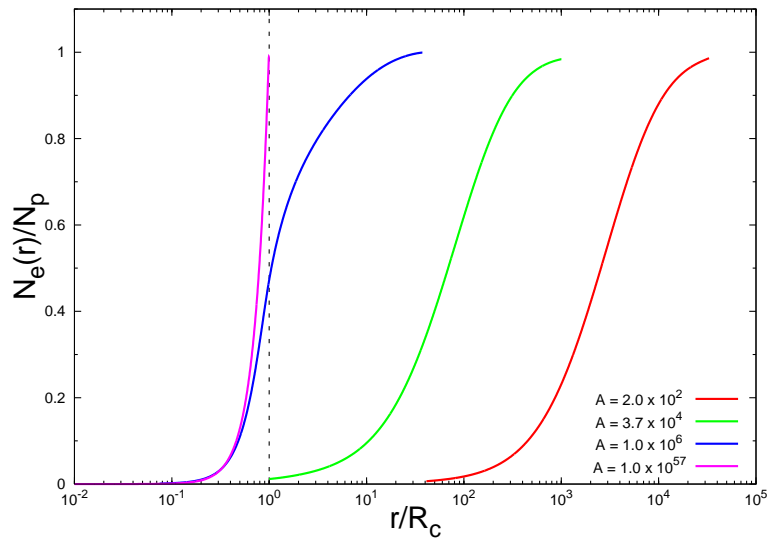
The number-density of degenerate neutrons is given by $n_n(r) = \frac{1}{3\pi^2\hbar^3} (P_n^F)^3$, where P_n^F is the Fermi momentum of neutrons. The Fermi energy of degenerate neutrons is

$$\mathcal{E}_n(P_n^F) = [(P_n^F c)^2 + m_n^2 c^4]^{1/2} - m_n c^2, \quad (\text{C.5.14})$$

where m_n is the neutron mass. Substituting Eqs. (C.5.9, C.5.11, C.5.14) into Eq. (C.5.13), we obtain $[(P_n^F c)^2 + m_n^2 c^4]^{1/2} - m_n c^2 = [(P_p^F c)^2 + m_p^2 c^4]^{1/2} - m_p c^2 + eV$. These equations and boundary conditions form a close set of non-linear boundary value problem for a unique solution for Coulomb potential $V(r)$ and electron distribution (C.5.10), as functions of the parameter Δ , i.e., the proton number-density n_p . The solution is given in Fig. C.27(a). A relevant quantity for exploring the physical significance of the solution is given by the number of electrons within a given radius r , $N_e(r) = \int_0^r 4\pi(r')^2 n_e(r') dr'$. This allows to determine, for selected values of the $A = N_p + N_n$ parameter, the distribution of the electrons within and outside the core and follow the progressive penetration of the electrons in the core at increasing values of A (see Fig. C.27(b)). We can then evaluate, generalizing the results in Ferreira et al. (1980); Ruffini and Stella (1981) , the net charge inside the core $N_{\text{net}} = N_p - N_e(R_c) < N_p$, and consequently determine of the electric field at the core surface, as well as within and outside the core.



(a)



(b)

Figure C.27.: (a) The solution χ of the relativistic Thomas-Fermi Equation for $A = 10^{57}$ and core radius $R_c = 10\text{km}$, is plotted as a function of radial coordinate. The left solid line corresponds to the internal solution and it is plotted as a function of radial coordinate in unit of R_c in logarithmic scale. The right dotted line corresponds to the solution external to the core and it is plotted as function of the distance Δr from the surface in the logarithmic scale in centimeter. (b) The electron number in the unit of the total proton number N_p , for selected values of A , is given as function of radial distance in the unit of the core radius R_c , again in logarithmic scale. It is clear how by increasing the value of A the penetration of electrons inside the core increases.

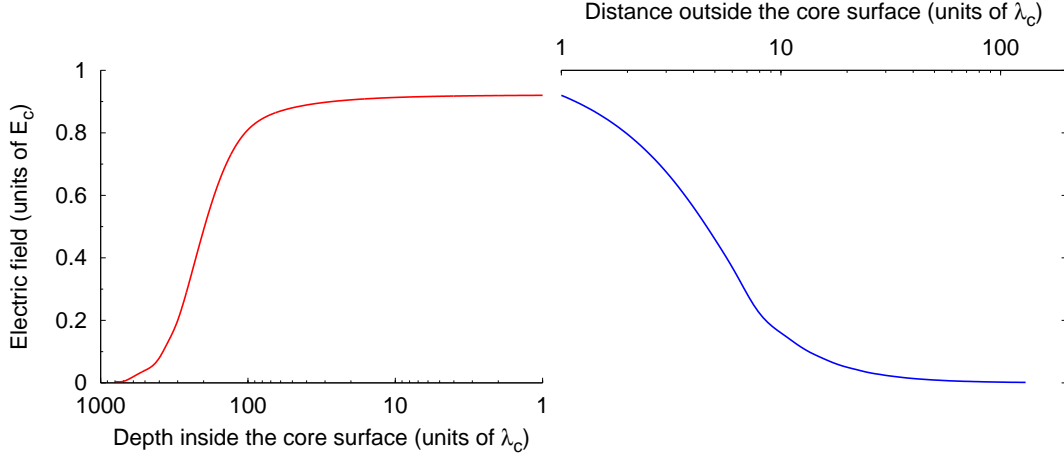


Figure C.28.: The electric field in the unit of the critical field E_c is plotted around the core radius R_c . The left (right) solid (dotted) diagram refers to the region just inside (outside) the core radius plotted logarithmically. By increasing the density of the star the field approaches the critical field.

C.5.7. The energetically favorable configurations

Introducing the new function ϕ defined by $\phi = \Delta \left[\frac{4}{9\pi} \right]^{1/3} \frac{\chi}{x}$, and putting $\hat{x} = \Delta^{-1} \sqrt{\alpha} (12/\pi)^{1/6} x$, $\zeta = \hat{x} - \hat{x}_c$ the ultra-relativistic Thomas-Fermi equation can be written as

$$\frac{d^2 \hat{\phi}(\zeta)}{d\zeta^2} = -\theta(-\zeta) + \hat{\phi}(\zeta)^3, \quad (\text{C.5.15})$$

where $\hat{\phi}(\zeta) = \phi(\zeta + \hat{x}_c)$. The boundary conditions on $\hat{\phi}$ are: $\hat{\phi}(\zeta) \rightarrow 1$ as $\zeta \rightarrow -\hat{x}_c \ll 0$ (at massive core center) and $\hat{\phi}(\zeta) \rightarrow 0$ as $\zeta \rightarrow \infty$. We must also have the continuity of the function $\hat{\phi}$ and the continuity of its first derivative $\hat{\phi}'$ at the surface of massive core $\zeta = 0$.

Eq. (C.5.15) admits an exact solution

$$\hat{\phi}(\zeta) = \begin{cases} 1 - 3 \left[1 + 2^{-1/2} \sinh(a - \sqrt{3}\zeta) \right]^{-1}, & \zeta < 0, \\ \frac{\sqrt{2}}{(\zeta + b)}, & \zeta > 0, \end{cases} \quad (\text{C.5.16})$$

where integration constants a and b are: $\sinh a = 11\sqrt{2}$, $a = 3.439$; $b = (4/3)\sqrt{2}$.

We then have for the Coulomb potential energy, in terms of the variable ζ , $eV(\zeta) = \left(\frac{1}{\Delta^3} \frac{9\pi}{4} \right)^{1/3} m_\pi c^2 \hat{\phi}(\zeta)$, and at the center of massive core $eV(0) = \hbar c (3\pi^2 n_p)^{1/3} = \left(\frac{1}{\Delta^3} \frac{9\pi}{4} \right)^{1/3} m_\pi c^2$, which plays a fundamental role in order to

determine the stability of the configuration.

It is possible to compare energetic properties of different configurations satisfying the different neutrality conditions $n_e = n_p$ and $N_e = N_p$, with the same core radius R_c and total nucleon number A . The total energy in the case $n_e = n_p$ is

$$\begin{aligned}\mathcal{E}_{\text{tot}}^{\text{loc}} &= \sum_{i=e,p,n} \mathcal{E}_{\text{loc}}^i \\ \mathcal{E}_{\text{loc}}^i &= 2 \int \frac{d^3r d^3p}{(2\pi\hbar)^3} \epsilon_{\text{loc}}^i(p) = \\ & \frac{cV_c}{8\pi^2\hbar^3} \left\{ \bar{P}_i^F [2(\bar{P}_i^F)^2 + (m_i c)^2] [(\bar{P}_i^F)^2 + (m_i c)^2]^{1/2} - (m_i c)^4 \text{Arsh} \left(\frac{\bar{P}_i^F}{m_i c} \right) \right\}\end{aligned}$$

The total energy in the case $N_e = N_p$ is

$$\begin{aligned}\mathcal{E}_{\text{tot}}^{\text{glob}} &= \mathcal{E}_{\text{elec}} + \mathcal{E}_{\text{binding}} + \sum_{i=e,p,n} \mathcal{E}_{\text{glob}}^i \\ \mathcal{E}_{\text{elec}} &= \int \frac{E^2}{8\pi} d^3r \approx \frac{3^{3/2}\pi^{1/2}}{4} \frac{N_p^{2/3}}{\sqrt{\alpha}\Delta c} m_\pi \int_{-\kappa R_c}^{+\infty} dx [\phi'(x)]^2 \\ \mathcal{E}_{\text{binding}} &= -2 \int \frac{d^3r d^3p}{(2\pi\hbar)^3} eV(r) \approx -\frac{V_c}{3\pi^2\hbar^3} (P_e^F)^3 eV(0) \\ \mathcal{E}_{\text{glob}}^i &= 2 \int \frac{d^3r d^3p}{(2\pi\hbar)^3} \epsilon_{\text{glob}}^i(p) = \\ & \frac{cV_c}{8\pi^2\hbar^3} \left\{ P_i^F [2(P_i^F)^2 + (m_i c)^2] [(P_i^F)^2 + (m_i c)^2]^{1/2} - (m_i c)^4 \text{Arsh} \left(\frac{P_i^F}{m_i c} \right) \right\}.\end{aligned}$$

We have indicated with \bar{P}_i^F ($i = n, e, p$) the Fermi momentum in the case of local charge neutrality ($V = 0$) and with P_i^F ($i = n, e, p$) the Fermi momentum in the case of global charge neutrality ($V \neq 0$). The energetic difference between local neutrality and global neutrality configurations is positive, $\Delta\mathcal{E} = \mathcal{E}_{\text{tot}}^{\text{loc}} - \mathcal{E}_{\text{tot}}^{\text{glob}} > 0$, so configurations which obey to the condition of global charge neutrality are energetically favorable with respect to one which obey to the condition of local charge neutrality. For a core of 10 Km the difference in binding energy reaches 10^{49} ergs which gives an upper limit to the energy emittable by a neutron star, reaching its electrodynamical ground state.

The current work is three fold: **a)** generalize our results considering the heavy nuclei as special limiting cases of macroscopic nuclear matter cores (Patricelli et al., 2008), **b)** describe a macroscopic nuclear matter core within the realm of General Relativity fulfilling the generalized Tolman, Oppenheimer, Volkoff

equation, c) Generalize the concept of a Dyadosphere to a Kerr-Newman Geometry.

C.5.8. Conclusions

It is clear that any neutron star has two very different components: the core with pressure dominated by a baryonic component and the outer crust with pressure dominated by a leptonic component and density dominated by the nuclear species. The considerations that we have presented above apply to the first component where the baryonic pressure dominates. It is clear that when the density increases and baryons become ultra-relativistic is this baryonic component which undergoes the process of gravitational collapse and its dynamics is completely dominated by the electro-dynamical process which we have presented in this talk.

C.6. A Self-consistent Approach to Neutron Stars

C.6.1. Introduction

Since the seminal work of Oppenheimer and Volkoff (1939) on the general relativistic equilibrium state of a degenerate gas of neutrons, a colossal amount of research has been devoted to neutron star physics. In scientific literature on neutron stars, a “local approach”, where the equation of state of neutron star matter is constructed ignoring global gravitational and Coulombian effects by assuming not only flat space but also local charge neutrality, has been traditionally used. A barotropic relation $P = P(\mathcal{E})$ between the energy-density \mathcal{E} and the pressure P is then obtained (see e.g. Haensel et al. (2007) for a recent compilation of modern neutron star matter equations of state). The gravitational effects are then taken into account by embedding such an equation of state into the so-called Tolman-Oppenheimer-Volkoff equation of hydrostatic equilibrium in spherical symmetry (we use units with $\hbar = c = 1$ hereafter):

$$P' = -\frac{(\mathcal{E} + P)(4\pi Gr^3 P + GM)}{r(r - 2GM)}, \quad (\text{C.6.1})$$

where the mass $M(r)$ is given by

$$M' = 4\pi r^2 \mathcal{E}, \quad (\text{C.6.2})$$

we denote radial derivatives with primes, and $G = 1/m_{\text{Pl}}^2$ with m_{Pl} being the Planck mass. Thus, in the local approach, the problem of the equilibrium state of a self-gravitating system composed of different degenerate fermion-species is reduced to an effective one-component fluid problem by solving the system of equations, given by Eqs. (C.6.1) and (C.6.2), for a barotropic equation of state $P(\mathcal{E})$.

We should consider such an approach as an effective solution of the problem that gives good estimates for the mass and the radius of a neutron star through an oversimplification of the real physical situation. However, recent developments in high-energy astrophysics point to the relevance of overcritical electric fields in neutron stars and black holes (Ruffini et al., 2010b). It has then become apparent that a new approach to neutron stars is necessary and that fundamental gravito-electrodynamical effects are missing in the traditional approach.

We present here the self-consistent equilibrium equations governing a degenerate neutron, proton and electron fluid in beta equilibrium within the framework of relativistic quantum statistics and of the Einstein-Maxwell equations. From this formulation descend the general relativistic Thomas-Fermi equation, which, as in the case of atoms, plays a crucial role by joining Coulombian, gravitational and quantum-statistical effects associated with the equilib-

rium state of a self-gravitating system of degenerate fermions.

C.6.2. The Equilibrium Equations

We consider the equilibrium configurations of a degenerate gas of neutrons, protons and electrons with total matter energy density and pressure

$$\mathcal{E} = \sum_{i=n,p,e} \mathcal{E}_i, \quad P = \sum_{i=n,p,e} P_i, \quad (\text{C.6.3})$$

that satisfy the condition of beta equilibrium

$$\mu_n = \mu_p + \mu_e, \quad (\text{C.6.4})$$

where $\mu_i = \partial\mathcal{E}/\partial n_i$ denotes the free chemical potential of the particle species with number density n_i . In addition, we introduce the extension to general relativity of the Thomas-Fermi equilibrium condition on the generalized Fermi energy E_e^F of the electron component:

$$E_e^F = e^{v/2} \mu_e - m_e - eV = \text{constant}, \quad (\text{C.6.5})$$

where e is the fundamental charge, V is the Coulomb potential of the configuration and we have introduced the metric

$$ds^2 = e^{v(r)} dt^2 - e^{\lambda(r)} dr^2 - r^2 d\theta^2 - r^2 \sin^2 \theta d\varphi^2, \quad (\text{C.6.6})$$

for a spherically-symmetric non-rotating neutron star. The metric function λ is related to the mass $M(r)$ and the electric field $E(r) = -e^{-(v+\lambda)/2} V'$ through

$$e^{-\lambda} = 1 - \frac{2GM(r)}{r} + Gr^2 E^2(r). \quad (\text{C.6.7})$$

Thus, the equations for the neutron star equilibrium configuration consist of the following Einstein-Maxwell equations and general relativistic Thomas-

Fermi equation:

$$M' = 4\pi r^2 \mathcal{E} - 4\pi r^3 e^{-\nu/2} \hat{V}' (n_p - n_e), \quad (\text{C.6.8})$$

$$\frac{\nu'}{r} + \frac{1 - e^\lambda}{r^2} = 8\pi G e^\lambda \left[P - \frac{e^{-(\nu+\lambda)}}{8\pi\alpha} (\hat{V}')^2 \right], \quad (\text{C.6.9})$$

$$P' + \frac{\nu'}{2} (\mathcal{E} + P) = -(P^{\text{em}})' - \frac{4P^{\text{em}}}{r}, \quad (\text{C.6.10})$$

$$\begin{aligned} \hat{V}'' + \hat{V}' \left[\frac{2}{r} - \frac{(\nu' + \lambda')}{2} \right] &= -4\pi\alpha e^{\nu/2} e^\lambda \left\{ n_p \right. \\ &\quad \left. - \frac{e^{-3\nu/2}}{3\pi^2} [(\hat{V} + m_e)^2 - m_e^2 e^\nu]^{3/2} \right\}, \end{aligned} \quad (\text{C.6.11})$$

where α denotes the fine structure constant, $\hat{V} = E_e^F + eV$ and $P^{\text{em}} = -E^2/(8\pi)$.

The assumption of the equilibrium condition in Eq. (C.6.5), together with the beta equilibrium condition in Eq. (C.6.4) and the hydrostatic equilibrium in Eq. (C.6.10), along with the thermodynamic relation $\mathcal{E}_i + P_i = n_i \mu_i$, can be demonstrated to be enough to guarantee the constancy of the generalized Fermi energy

$$E_i^F = e^{\nu/2} \mu_i - m_i + q_i V, \quad i = n, p, e, \quad (\text{C.6.12})$$

for all particle species separately. Here, q_i denotes the particle unit charge of the i -species. Indeed, as shown by Olson and Baily (1975), when the fermion nature of the constituents and their degeneracy are taken into account, in the configuration of minimum energy, the generalized Fermi energies E_i^F defined by Eq. (C.6.12) must be constant over the entire configuration, i.e. r -independent. These minimum energy conditions generalize the equilibrium conditions of Klein (1949) and of Kodama and Yamada (1972) to the case of degenerate multicomponent fluids with particle species with non-zero unit charge. Therefore, the solution to the system of equations composed by Eq. (C.6.4), by Eq. (C.6.5), and by Eqs. (C.6.8)–(C.6.11) represents the ground-state equilibrium configuration.

C.6.3. Some Specific Solutions

The inconsistency of the local charge neutrality condition $n_e(r) = n_p(r)$ with this system of equations was proven in Rotondo et al. (2011d), where, in addition, a globally neutral solution was obtained by solving the above self-consistent equations in the case of non-strongly interacting degenerate neutrons, protons and electrons extending from the center of the star all the way to the border. Although the configuration described in Rotondo et al. (2011d) cannot represent a realistic neutron star, the gravito-electrodynamical effects discovered there deserve further attention.

In a realistic neutron star, the degenerate neutron, proton and electron fluid

is confined to the core and is subjected to the external pressure of the crust formed around by white-dwarf-like material. In this more general case, the constancy of the generalized Fermi energy of the electrons still plays a fundamental role in order to fulfill the matching conditions and in the boundary-value problem (Belvedere et al., 2011). It can be shown that as a consequence of the fulfillment of the core-crust matching conditions and the self-consistent minimum energy equilibrium equations described here, the surface of the core develops a sharp exponential transition surrounded by the neutron star's crust (Belvedere et al., 2011). Furthermore, together with such an exponential density transition, an electric field with an intensity larger than that of the critical field for vacuum polarization,

$$E_c = \frac{m_e^2}{\sqrt{\alpha}}, \quad (\text{C.6.13})$$

extending over all the entire surface of the transition surface, whose thickness is of the order of several electron Compton wavelength $\lambda_e = 1/m_e$, appears.

C.6.4. Conclusions

We have presented the coupled system of equations that must be solved in order to calculate the ground-state equilibrium configuration of a neutron star. In addition, we have shown that the minimum energy configuration exhibits an r -independent generalized particle Fermi energy for all particle species composing the internal fluid. We have also demonstrated that the minimum energy problem of neutron stars can be reformulated as an extension to general relativity of the Thomas-Fermi atom.

The contribution of the hadronic fields to the energy-momentum tensor, to the four-vector current and, consequently, to the Einstein-Maxwell equations are currently under consideration in order to establish a more general formulation of the problem (Rueda et al., 2011). The introduction of strong interactions preserves the r -independence of the generalized Fermi energy of the electrons, requires the fulfillment of the general relativistic Thomas-Fermi equation, and confirms all the gravito-electrodynamical effects here described in the simplest possible example (Rueda et al., 2011).

C.7. On the electrostatic structure of neutron stars

C.7.1. Introduction

From the point of view of Newtonian gravity, an spherically symmetric object composed by a free degenerate gas of neutrons has a maximum mass about $M_{\max} \simeq 5.8M_{\odot}$ (Landau and Lifshitz, 1980). Nevertheless, the strong gravity expected in neutron star interiors imposes the use of general relativity equations as structure equations. For the same free gas of neutrons, Einstein theory strongly reduces the maximum mass limit to $M_{\max} \simeq 0.7M_{\odot}$ as calculated by Oppenheimer & Volkoff (OV) in their seminal paper (Oppenheimer and Volkoff, 1939).

Observations of X-Ray Binary systems ruled out rapidly the OV work finding that usually neutron stars have masses $M_{NS} \gtrsim 1.4M_{\odot}$. Even very recently an extraordinary high value of $M = 2.74 \pm 0.21M_{\odot}$ has been reported for the millisecond pulsar PSR J1748-2021B (Freire et al., 2008). Therefore, researchers directed their attention to the theoretical study of the properties of neutron stars. In particular, the improvement of the Equation of State (EoS) for nuclear matter at densities above the so-called saturation density of ordinary nuclei $\rho_0 \simeq 2.7 \times 10^{14} \text{ g cm}^{-3}$, has been one of the challenges of theoretical physics in the last 40 years.

Despite the effort to understand the nuclear EoS above saturation density ρ_0 , the problem is by far unsolved, due mainly to the lack of a theory for the strong interaction, and to the lack of ground-based experiments able to simulate the extreme conditions expected in neutron star interiors. Consequently, a proliferation of nuclear EoS approaching in different ways the strong interaction is growing day after day. Thus, to avoid any discussion of validity of the EoS we use, we will construct here a simple phenomenological EoS based on the Weizsacker mass formula in nuclear physics, which let us to concentrate the attention to the real scope of the paper, which is devoted to the self-consistent introduction of the electromagnetic interaction inside the equilibrium equations governing neutron stars.

The standard picture of a neutron star assumes at least the existence of three regions: core, inner crust and outer crust. Starting for the more external one, the outer crust is composed by a nuclei lattice (or Coulomb lattice) immersed in sea of free electrons, and extents until a density $\rho_d \simeq 4 \times 10^{11} \text{ g cm}^{-3}$ or neutron drip density. At this density, the dripped neutrons start to form a background of neutrons. This region composed by a nuclei lattice in a background of electrons and neutrons is known as inner crust and exists approximately until the nuclear saturation density $\rho_0 \simeq 2.7 \times 10^{14} \text{ g cm}^{-3}$. At even higher densities, the core of the star is assumed to be a uniform gas composed mainly by neutrons, and a smaller presence of protons and electrons under the constraints of β -equilibrium and local charge neutrality $n_e = n_p$. Here n_e and n_p stand for the electron and proton number densities. There-

fore, in the interior of a neutron star conjugate all the interactions we know in nature, namely, weak, strong, electromagnetic and gravitational. Nevertheless, as we have mentioned, the electromagnetic interaction is not taken into account because the very stringent assumption of local charge neutrality condition $n_e = n_p$ is assumed. In this paper we will relax this condition and impose the more general one $N_e = N_p$ where N_e, N_p are the total number of electrons and protons respectively.

As a natural consequence of global neutrality it appears a transition surface-shell between the core and the crust. The thickness δR of this surface-shell is of order of the electron Compton wavelength $\lambda_e = 1/m_e$ (we use hereafter $\hbar = c = 1$), i.e., of the order of some fermi. Inside the surface-shell a strong electric field develops. It grows until some maximum value and after drops down up to some distance δR from the core radius R_c where it becomes null and the configuration becomes neutral. Therefore, the thickness of the surface-shell δR is given by the global neutrality condition

$$\varphi(R_c + \delta R) = 0, \quad \varphi'(R_c + \delta R) = 0, \quad (\text{C.7.1})$$

where φ is the electrostatic potential.

C.7.2. Structure Equations

The metric for a spherically symmetric spacetime can be written as

$$ds^2 = e^\nu dt^2 - e^\lambda dr^2 - r^2 d\theta^2 - r^2 \sin^2 \theta d\phi^2, \quad (\text{C.7.2})$$

where ν and λ are functions of r only. For this metric the Einstein-Maxwell field equations are

$$M' = 4\pi r^2 (T_0^0 - \mathcal{E}_{\text{em}}) + 4\pi e^{\lambda/2} r^3 e E (n_p - n_e) \quad (\text{C.7.3})$$

$$e^{-\lambda} \left(\frac{\nu'}{r} + \frac{1}{r^2} \right) - \frac{1}{r^2} = -8\pi G T_1^1 \quad (\text{C.7.4})$$

$$e^{-\lambda} \left[\nu'' + (\nu' - \lambda') \left(\frac{\nu'}{2} + \frac{1}{r} \right) \right] = -16\pi G T_2^2 \quad (\text{C.7.5})$$

$$\begin{aligned} (e\varphi)'' + (e\varphi)' \left[\frac{2}{r} - \frac{(\nu' + \lambda')}{2} \right] \\ = -4\pi \alpha e^{\nu/2} e^\lambda (n_p - n_e), \end{aligned} \quad (\text{C.7.6})$$

where T_ν^μ is the energy-momentum tensor of matter and fields, E is the electrostatic field and $\mathcal{E}_{\text{em}} = E^2/2$ is the electromagnetic energy density.

C.7.3. The Equation of State

Core EoS

In phenomenological nuclear physics, the Weizsacker binding energy per nucleon is given by

$$\frac{E_W}{A} = -a_v + a_s \frac{(N - Z)^2}{A^2} + a_C \frac{Z^2}{A^{4/3}} + a_{\text{surf}} A^{-1/3} + \frac{\delta_{\text{even-odd}}}{A}, \quad (\text{C.7.7})$$

where $a_v = 15.8$ MeV, $a_{\text{surf}} = 18.3$ MeV, $a_s = 23.3$ MeV, $a_C = 0.714$ MeV, $\delta_{\text{even-odd}} \simeq 12$ MeV, are the volume, surface, symmetry, Coulomb, and pairing contributions.

If we assume the above formula valid also in the case of neutron rich matter $N \gg Z$ we have

$$\frac{E_W}{A} \simeq -a_v + a_s > 0, \quad (\text{C.7.8})$$

which implies that neutron rich matter is unbounded. However, for a large number of baryons A , the gravitational potential plays an important role. In order to see that, let us to modify the Weizsacker formula by including the gravitational interaction (in the constant density case)

$$\frac{E_W}{A} \simeq -a_v + a_s - \frac{3}{5r_0} \left(\frac{m_n}{m_{\text{Planck}}} \right)^2 A^{2/3}, \quad (\text{C.7.9})$$

where we have assumed

$$M \simeq m_n A, \quad R \simeq r_0 A^{1/3}, \quad m_n \simeq 939 \text{ MeV}. \quad (\text{C.7.10})$$

Then neutron matter is bounded for

$$A > A^* = \left[\frac{5r_0}{3} (-a_v + a_s) \right]^{3/2} \left(\frac{m_{\text{Planck}}}{m_n} \right)^3 \simeq 0.8 \times 10^{56}. \quad (\text{C.7.11})$$

Using this minimum mass number A^* for bounding we calculate the minimum mass as given by the modified Weizsacker formula (C.7.9)

$$M_W \gtrsim m_n A^* \simeq 0.07 M_\odot, \quad (\text{C.7.12})$$

which is very close to the value given by most accepted nuclear EoS.

Therefore the nuclear potential energy should properly be included into the mass–energy of neutron star cores. Applying the Weizsacker formula (C.7.7) to a local thin–shell of neutron star cores, we write the energy density for the core in the form

$$\mathcal{E} = \mathcal{E}_k + \mathcal{E}_W + \mathcal{E}_{\text{em}} \quad (\text{C.7.13})$$

where

$$\mathcal{E}_k = \frac{2}{(2\pi)^3} \sum_{i=e,p,n} \int_0^{k_i^F} 4\pi k^2 \sqrt{k^2 + m_i^2} dk, \quad (\text{C.7.14})$$

$$\mathcal{E}_W = -a_v^* n + a_s^* n T^2 + a_{\text{surf}} n^{2/3} \delta(r - R_c), \quad (\text{C.7.15})$$

where

$$T \equiv \frac{n_n - n_p}{n}, \quad n \equiv n_p + n_n, \quad (\text{C.7.16})$$

are the asymmetry parameter and the baryon number density. The parameters a_v^* and a_s^* must be calculated avoiding double counting of the kinetic contribution to the volume and symmetry energy. For the surface contribution we have introduced a δ -distribution about the core radius R_c to recall that it acts just on the surface of the core. The radius of the core is defined as the radius at which the rest-mass density of the core reach nuclear density, namely, $\rho(R_c) = \rho_0 \simeq 2.7 \times 10^{14} \text{ g cm}^{-3}$. The delta distribution has dimension L^{-1} , and it is given by the characteristic range of the strong interaction, so it should be of the order of some fermi.

To obtain the parameters a_v^* and a_s^* , we expand the kinetic energy (C.7.13) about $n_n = n_p$ ($T = 0$), i.e. for symmetric nuclear matter

$$\frac{\mathcal{E}_k}{n} - m = \tilde{a}_v + \tilde{a}_s T^2 + \dots, \quad (\text{C.7.17})$$

$$\tilde{a}_v \simeq 21.84 \text{ MeV}, \quad \tilde{a}_s = \frac{k_0^F}{6\sqrt{(k_0^F)^2 + m^2}} \simeq 11.84 \text{ MeV}, \quad (\text{C.7.18})$$

where we have assumed $m_p \simeq m_n \simeq m = 939 \text{ MeV}$, and

$$k_p^F = k_n^F = k_0^F = \left(\frac{3\pi^2 n_0}{2} \right)^{1/3} \simeq 263.26 \text{ MeV}, \quad (\text{C.7.19})$$

where $n_0 \simeq 0.16 \text{ fm}^{-3}$. Then we obtain

$$a_v^* = a_v - \tilde{a}_v \simeq 37.64 \text{ MeV}, \quad (\text{C.7.20})$$

$$a_{\text{as}}^* = a_s - \tilde{a}_s \simeq 11.45 \text{ MeV}. \quad (\text{C.7.21})$$

Therefore, the relevant components of the energy-momentum tensor in the core are

$$T_0^0 = \mathcal{E}_k + \mathcal{E}_{\text{em}} + \mathcal{E}_W, \quad (\text{C.7.22})$$

$$T_1^1 = -P_k + \mathcal{E}_{\text{em}} - P_W, \quad (\text{C.7.23})$$

$$T_2^2 = -P_k - \mathcal{E}_{\text{em}} - P_W. \quad (\text{C.7.24})$$

The pressure terms are calculated by thermodynamical self-consistency as

$$P_i = n^2 \frac{\partial \mathcal{E}_i / n}{\partial n}. \quad (\text{C.7.25})$$

where $i = k, \text{em}, W$ respectively indicates kinetic, electromagnetic and nuclear components. In addition, we calculate chemical potentials of neutrons, protons and electrons by using usual definition

$$\mu_{n,p,e} = \frac{\partial \mathcal{E}}{\partial n_{n,p,e}}. \quad (\text{C.7.26})$$

The system must satisfy some additional constraints. The first one is related with the equilibrium of the electron gas which can be written as

$$E_e^F = e^{\nu/2} \mu_e - e\varphi = \text{constant} > 0, \quad (\text{C.7.27})$$

while the second one is the β -equilibrium of the system given by

$$E_n^F = E_e^F + E_p^F, \quad (\text{C.7.28})$$

where

$$E_p^F = e^{\nu/2} \mu_p + e\varphi. \quad (\text{C.7.29})$$

Using the above constraints, we can write the electron and neutron number densities as

$$n_e = \frac{[e^{-\nu/2} (E_e^F + e\varphi)]^3}{3\pi^2} \quad (\text{C.7.30})$$

$$n_n = \frac{(e^{-\nu/2})^3}{3\pi^2} \{ (E_e^F + E_p^F + m_n)^2 - m_n^2 e^\nu \}^{3/2}, \quad (\text{C.7.31})$$

where we have used the ultra-relativistic approximation for the electrons $\mu_e \simeq P_e^F$, with P_e^F the electron Fermi momentum.

Crust EoS

For the inner crust we adopt the well-known EoS by Baym, Bethe and Pethick (BBP) (Baym et al., 1971a), which is well fitted by the following polytropic-like form

$$P = K \mathcal{E}^\Gamma, \quad K = 0.000287961, \quad \Gamma = 1.68051, \quad (\text{C.7.32})$$

where P and \mathcal{E} are the total pressure and energy density. Of course for each value of pressure (and density) we need the self-consistent values of the chemical potential of neutrons and electrons, which can be obtained from the entries on the tables in Baym et al. (1971a).

In the outer crust we have white-dwarf-like material, so we can obtain most

of its properties from the equilibrium condition (Landau and Lifshitz, 1980)

$$e^{\nu/2}(\mu_e + 2m_n) = \text{constant} = e^{\nu(R)/2}(m_e + 2m_n), \quad (\text{C.7.33})$$

where R is the radius of the configuration, which is calculated as the point where $P(R) = 0$. From the matching conditions with the exterior spacetime, which must be the Schwarzschild solution we obtain

$$e^{\nu(R)/2} = \sqrt{1 - \frac{2M(R)}{R}}. \quad (\text{C.7.34})$$

C.7.4. Numerical Integration

We describe now the main steps to construct the solutions:

1. Select a value for the central rest-mass density

$$\rho(0) = \sum_{i=e,p,n} m_i n_i(0). \quad (\text{C.7.35})$$

2. Select a positive value for E_e^F . It determines the electron chemical potential at the edge of the crust

$$\mu_e^{crust} = \mu_e(R_c + \delta R) = e^{-\nu(R_c)/2} E_e^F, \quad (\text{C.7.36})$$

where we have used the global neutrality condition and the fact that at very small scales the gravitational potential is constant, which is exactly the case for the region $R_c \leq r \leq R_c + \delta R$, for $\delta R \ll R_c$.

3. From the regular behavior at the center $r = 0$ we have $n_e(0) = n_p(0)$.
4. From 1–3 and the β -equilibrium condition (C.7.28) we obtain the central particle chemical potential $\mu_e(0)$, $\mu_p(0)$, and $\mu_n(0)$.
5. Select a value for the central electrostatic potential $\varphi(0)$.
6. Now we can calculate the central gravitational potential using (C.7.27) by

$$e^{\nu(0)/2} = \frac{E_e^F + e\varphi(0)}{\mu_e(0)}. \quad (\text{C.7.37})$$

7. Having all the initial conditions determined, it is possible to integrate the equations in the core up to the a radius R_c defined by $\rho(R_c) = \rho_0$, i.e., until the surface of the core.
8. The next step is to calculate the properties of the transition surface-shell between the core and the crust. Due to the surface tension neutron and

proton profiles will drop down. In this work the value of the surface tension is taken to be the one given by the Weizsacker formula (C.7.15). We calculate properly the electric field coming out from the surface charge separation between electrons and protons. The transition surface finishes when we reach global charge neutrality.

9. Finally we integrate the crust equations until reach at the radius of the configuration $P(R) = 0$. At the end of the integration we verify the matching condition with the Schwarzschild solution given by (C.7.34). If it is not satisfied we change the central gravitational potential value by changing the central potential as dictated by (C.7.37). In other words, the correct value of the central electrostatic potential is the one for which we satisfy correctly all the boundary conditions of the system.

Below we show an example of the integration for the initial conditions $\rho(0) \simeq 5.7\rho_0$ and $P(0) \simeq 40.63 \text{ MeV/fm}^3$. In Fig. C.29 we have plotted the mass function in the core of the star in solar masses, while in Fig. C.30 we show the electrostatic field in the core in unit of the critical electric field for vacuum polarization $E_c = m_e^2 c^3 / e\hbar \sim 10^{16} \text{ V/cm}$. Fig. C.31 shows the electrostatic potential energy of protons in the core in units of the pion mass and in Fig. C.32 we show the number density of neutrons, protons, and electrons normalized to the nuclear number density n_0 in the core. In Fig. C.33 it is shown the internal pressure in the core. In Figs. C.34 and C.35 we show the electrostatic field and proton Coulomb energy in the transition surface-shell between the core and the crust, while in Figs. C.36 and C.37 we have plotted the number density of particles and internal pressure in the surface-shell.

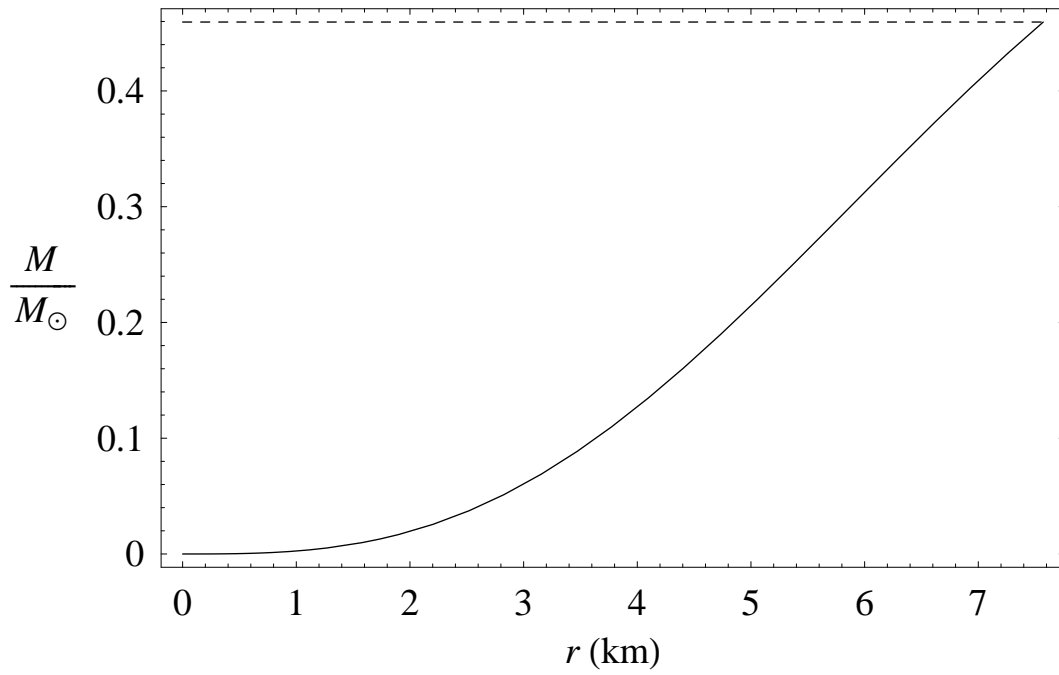


Figure C.29.: Mass of the core in solar masses.

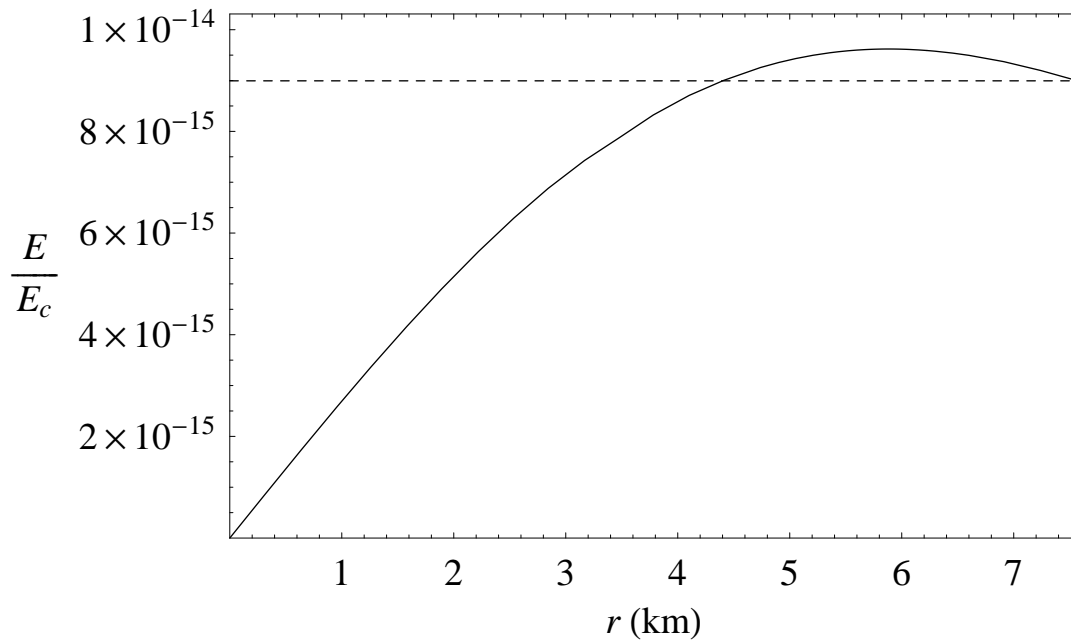


Figure C.30.: Electric field of the core in units of the critical field

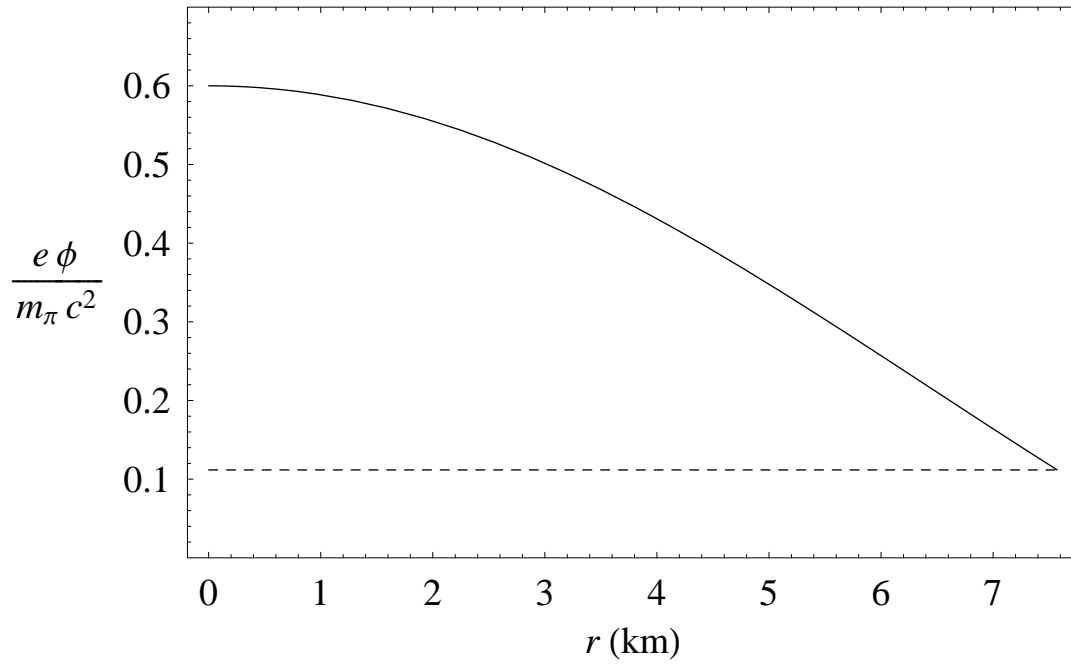


Figure C.31.: Electrostatic potential of the core in units of the pion mass.

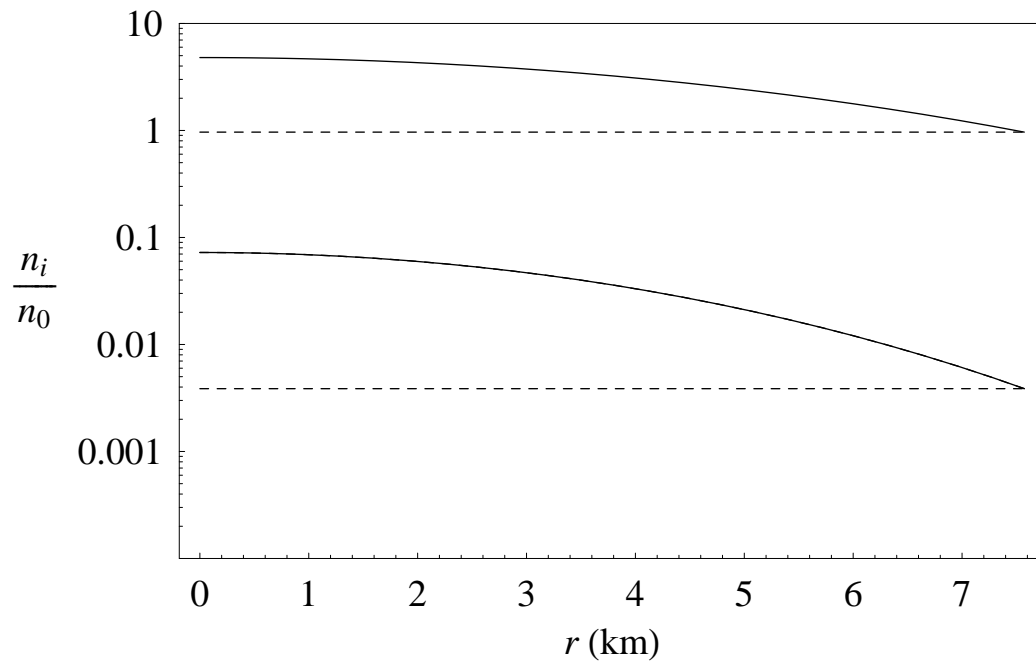


Figure C.32.: Number densities inside the core in units of the nuclear density n_0 .

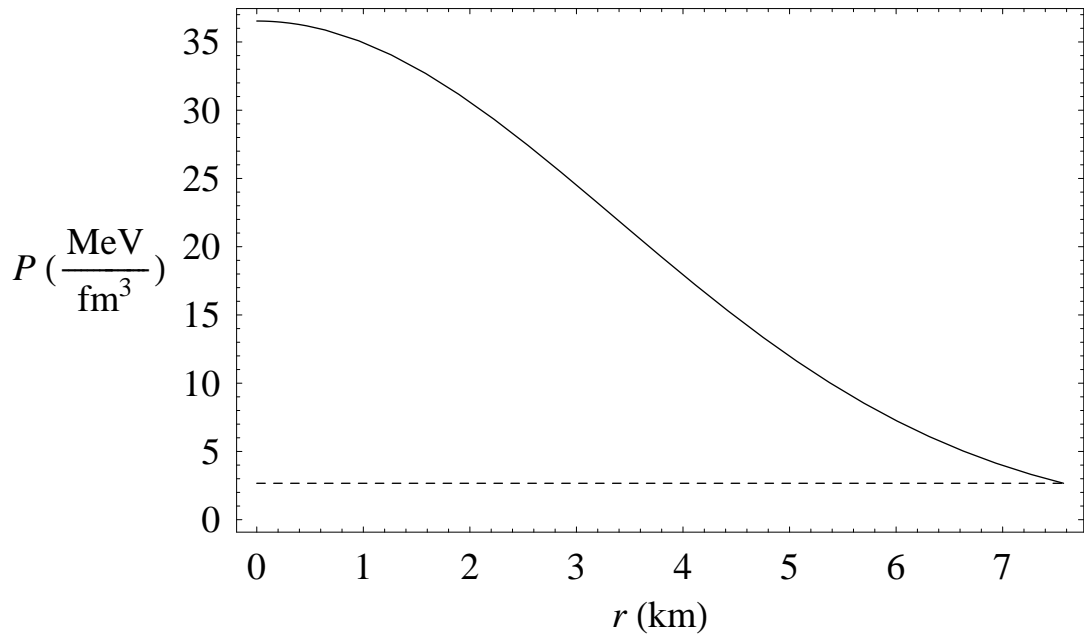


Figure C.33.: Pressure inside the core.

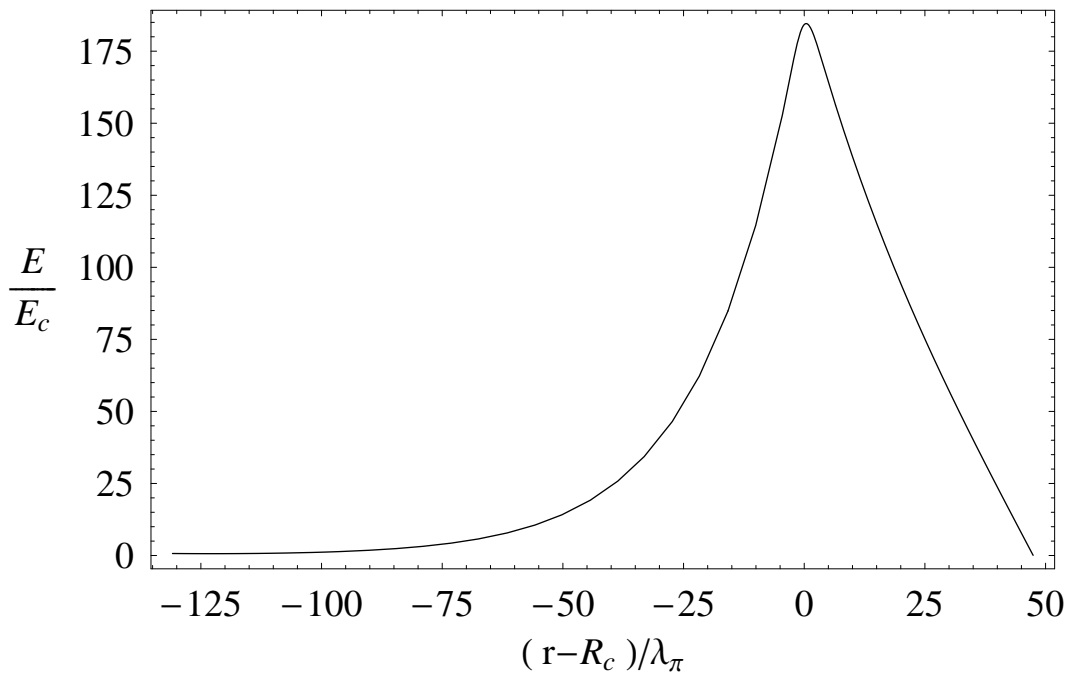


Figure C.34.: Surface electric field in units of the critical field.

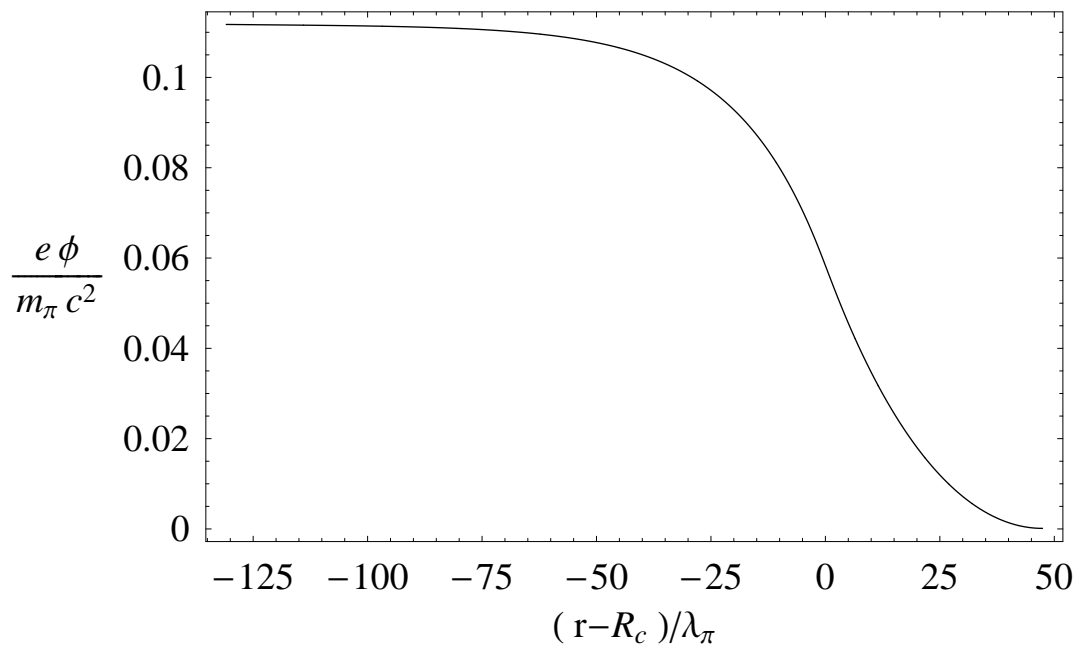


Figure C.35.: Surface electrostatic potential of the core in units of the pion mass.

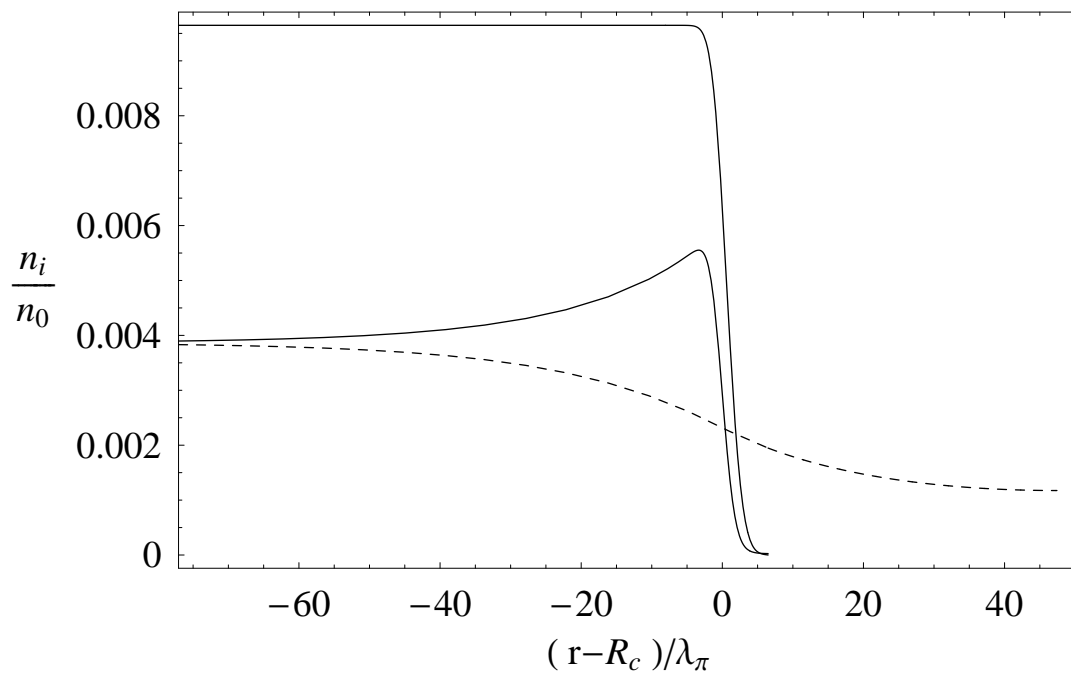


Figure C.36.: Surface number densities in units of the nuclear density n_0 .

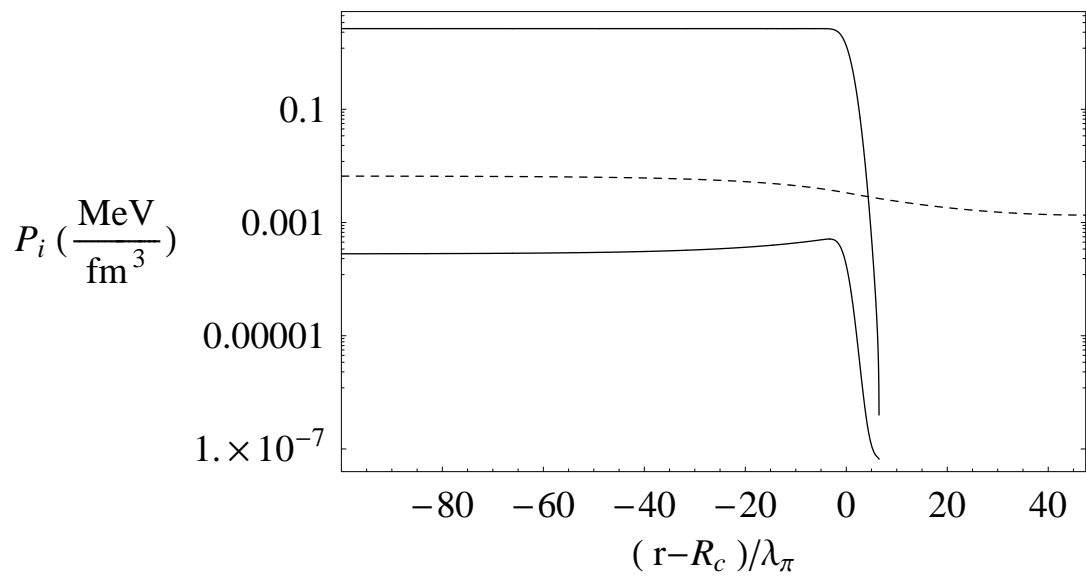


Figure C.37.: Surface pressure

C.8. A New Family of Neutron Star Models: Global Neutrality vs. Local Neutrality

C.8.1. Introduction

Traditionally, neutron star equilibrium configurations have been constructed following a “local approach”. In such an approach, the equation of state of neutron star matter is constructed ignoring global gravitational and Coulomb effects by assuming flat spacetime as well as local charge neutrality. Then, it is obtained a relation $P = P(\mathcal{E})$ between the energy-density \mathcal{E} and the pressure P (see Haensel et al. (2007) for a recent compilation of modern neutron star matter equations of state). The gravitational effects are then taken into account by embedding such an equation of state into the so-called Tolman-Oppenheimer-Volkoff equation of hydrostatic equilibrium in spherical symmetry

$$\frac{dP(r)}{dr} = -\frac{G[\mathcal{E}(r) + P(r)][4\pi r^3 P(r)/c^2 + M(r)]}{c^2 r(r - 2GM(r)/c^2)}, \quad (\text{C.8.1})$$

where the mass $M(r)$ is obtained from $dM(r)/dr = 4\pi r^2 \mathcal{E}(r)/c^2$. Thus, in the local approach, the problem of the equilibrium state of a self-gravitating system composed of different particle-species is reduced to an effective one-component fluid problem by solving the above equations for a certain equation of state $P(\mathcal{E})$.

This approach, although gives good estimates for the mass and the radius of a neutron star, should be consider as an effective solution of the problem that oversimplifies the real physical situation, where fundamental gravito-electrodynamical effects exist. We present here the self-consistent equilibrium equations governing a degenerate neutron, proton and electron fluid in beta equilibrium within the framework of relativistic quantum statistics and of the Einstein-Maxwell equations. From this formulation descend the general relativistic Thomas-Fermi equation, which, as in the case of atoms, plays a crucial role by joining Coulombian, gravitational and quantum-statistical effects associated with the equilibrium state of a self-gravitating system of degenerate fermions.

C.8.2. The equilibrium equations

We consider equilibrium configurations of a degenerate gas of neutrons, protons and electrons with total matter energy density $\mathcal{E} = \sum_{i=n,p,e} \mathcal{E}_i$ and pressure $P = \sum_{i=n,p,e} P_i$ where \mathcal{E}_i and P_i are the energy density and pressure of a degenerate fluid of 1/2-spin fermions of mass m_i , Fermi momentum P_i^F and number density $n_i = (P_i^F)^3 / (3\pi^2 \hbar^3)$.

We define at first, the generalized Fermi energy $E_i^F = e^{\nu/2} \mu_i - m_i c^2 + q_i V$

for the i -particle specie, where q_i is the particle unit charge, $\mu_i = \partial\mathcal{E}/\partial n_i$ is the free-chemical potential, and V denotes the Coulomb potential of the configuration. Thus, the equations for the neutron star equilibrium configuration are given by the beta equilibrium condition, the general relativistic Thomas-Fermi equilibrium condition for electrons and the Einstein-Maxwell equations

$$E_n^F + m_n c^2 = E_p^F + m_p c^2 + E_e^F + m_e c^2, \quad (\text{C.8.2})$$

$$E_e^F = e^{v/2} \mu_e - m_e c^2 - eV = \text{constant}, \quad (\text{C.8.3})$$

$$\frac{dM}{dr} = 4\pi r^2 \frac{\mathcal{E}}{c^2} - 4\pi r^3 e^{-v/2} \frac{d\hat{V}/c^2}{dr} (n_p - n_e), \quad (\text{C.8.4})$$

$$\frac{1}{r} \frac{dv}{dr} + \frac{1 - e^\lambda}{r^2} = \frac{8\pi G}{c^4} e^\lambda \left[P - \frac{e^{-(v+\lambda)}}{8\pi\alpha \hbar c} \left(\frac{d\hat{V}}{dr} \right)^2 \right], \quad (\text{C.8.5})$$

$$\frac{dP}{dr} + \frac{1}{2} \frac{dv}{dr} (\mathcal{E} + P) = -\frac{dP^{\text{em}}}{dr} - \frac{4P^{\text{em}}}{r}, \quad (\text{C.8.6})$$

$$\begin{aligned} & \frac{d^2\hat{V}}{dr^2} + \frac{d\hat{V}}{dr} \left[\frac{2}{r} - \frac{1}{2} \left(\frac{dv}{dr} + \frac{d\lambda}{dr} \right) \right] = -4\pi\alpha \hbar c e^{v/2} e^\lambda \left\{ n_p \right. \\ & \left. - \frac{e^{-3v/2}}{3\pi^2 \hbar^3 c^3} [(\hat{V} + m_e c^2)^2 - m_e^2 c^4 e^v]^{3/2} \right\}, \end{aligned} \quad (\text{C.8.7})$$

where α denotes the fine structure constant, $\hat{V} = E_e^F + eV$ and $P^{\text{em}} = -E^2/(8\pi)$ and we have introduced the metric $g_{\alpha\beta} = \text{diag}(e^{v(r)}, -e^{\lambda(r)}, -r^2, -r^2 \sin^2 \theta)$ for a spherically-symmetric non-rotating neutron star. The metric function λ is related to the mass $M(r)$ and the electric field $E(r) = -e^{-(v+\lambda)/2} dV/dr$ through

$$e^{-\lambda} = 1 - \frac{2GM(r)}{c^2 r} + \frac{Gr^2 E^2(r)}{c^4}. \quad (\text{C.8.8})$$

It has been demonstrated in Rotondo et al. (2011d) that, from the above system of equations follows that indeed all the generalized particle Fermi energies E_i^F are constant through the entire configuration, for all particle-species separately. This is in line with the results of Klein (1949), of Kodama and Yamada (1972), and of Olson and Baily (1975).

C.8.3. Discussion

The inconsistency of locally neutral neutron stars was proven in Rotondo et al. (2011d), where violation of the thermodynamic equilibrium condition of constancy of the generalized particle Fermi energies was explicitly shown for such configurations. Instead, globally neutral systems can be obtained from the above self-consistent equations. The specific solution for non-strongly interacting degenerate neutrons, protons and electrons extending from the

center of the star all the way to the border was obtained in Rotondo et al. (2011d). Although such a system cannot represent a realistic neutron star, essential gravito-electrodynamical effects were shown and the typical depth of the Coulomb potential was obtained.

In realistic neutron stars, the degenerate neutrons, protons and electrons are confined to the core and are subjected to the external pressure of the crust. In this more general case, the constancy of the generalized Fermi energy of the electrons still plays a fundamental role in the matching and boundary conditions. All the new gravito-electrodynamical effects discussed here deserve further analysis in view of the recent developments in high-energy astrophysics pointing to the relevance of overcritical electric fields in neutron stars and black holes (Ruffini et al., 2010b). The introduction of strong interactions to the energy-momentum tensor, to the four-vector current and, consequently, to the Einstein-Maxwell equations establishes a more general formulation of the problem (Rueda et al., 2011).

C.9. The Outer Crust of Neutron Stars

C.9.1. The General Relativistic Model

The Outer Crust of Neutron Stars is the region of Neutron Stars characterized by a mass density less than the “neutron drip” density $\rho_{drip} = 4.3 \cdot 10^{11} \text{ g cm}^{-3}$ (Baym et al., 1971b) and composed by White Dwarf - like material (fully ionized nuclei and free electrons). Its internal structure can be described by the Tolman-Oppenheimer-Volkoff (TOV) equation

$$\frac{dP}{dr} = -\frac{G \left(\rho + \frac{P}{c^2} \right) \left(m + \frac{4\pi r^3 P}{c^2} \right)}{r^2 \left(1 - \frac{2Gm}{rc^2} \right)}, \quad (\text{C.9.1})$$

together with the equation

$$\frac{dm}{dr} = 4\pi r^2 \rho, \quad (\text{C.9.2})$$

where m , ρ and P are the mass, the density and the pressure of the system. We have determined M_{crust} and ΔR_{crust} by integrating eq. (C.9.1) and (C.9.2) from $r_{in} = R_{is}$, where R_{is} is the radius of the inner part of the star (the base of the Outer Crust).

The pressure and the mass density of the system are

$$P \approx P_e, \quad (\text{C.9.3})$$

$$\rho \approx \mu_e m_n n_e. \quad (\text{C.9.4})$$

P_e is the pressure of electrons, given by Shapiro and Teukolsky (1983)

$$P_e = k_e \phi_e, \quad (\text{C.9.5})$$

where

$$k_e = \frac{m_e c^2}{8\pi^2 \lambda_e^3}, \quad (\text{C.9.6})$$

$$\phi_e = \quad (\text{C.9.7})$$

$$\xi_e \left(\frac{2}{3} \xi_e^2 - 1 \right) \sqrt{\xi_e^2 - 1} + \log \left(\xi_e + \sqrt{\xi_e^2 - 1} \right), \quad (\text{C.9.8})$$

with λ_e the Compton wavelenght of electrons, $\xi_e = \sqrt{1 + x_e^2}$ and x_e the Fermi momentum of electrons normalized to $(m_e c)$. μ_e is the mean molecular weight per electron that, for a completely ionized element of atomic weight A and number Z , is equal to A/Z (for simplicity, we assume $\mu_e = 2$), m_n is

the mass of neutrons and n_e is the number density of electrons

$$n_e = \frac{x_e^3}{3\pi^2\lambda_e^3}. \quad (\text{C.9.9})$$

In eq. (C.9.4) we have assumed the local charge neutrality of the system.

C.9.2. The mass and the thickness of the crust

We have integrated eq. (C.9.1) and (C.9.2) for different sets of initial conditions; in fig. C.38 are shown the results obtained assuming

$$\begin{aligned} 10 \text{ km} &\leq R_{is} \leq 20 \text{ km}, \\ 1M_\odot &\leq M_{is} \leq 3M_\odot \end{aligned}$$

and an initial pressure equal to $1.6 \cdot 10^{30} \text{ dyne cm}^{-2}$, that corresponds to a mass density equal to ρ_{drip} .

It can be seen that M_{crust} has values ranging from $10^{-6}M_\odot$ to $10^{-3}M_\odot$; both M_{crust} and ΔR_{crust} increase by increasing R_{is} and decreasing M_{is} (see fig. C.38, C.39).

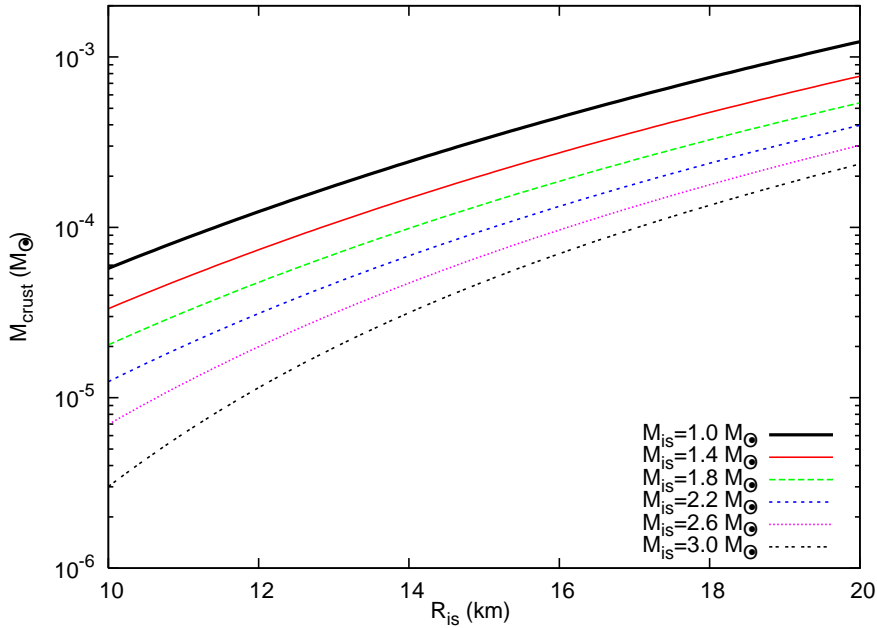


Figure C.38.: Values of M_{crust} in units of solar masses, as function of R_{is} , for different values of M_{is} (see legend).

It's important to note that the values estimated for M_{crust} strongly depend on the values of M_{is} and R_{is} used; in particular, the values of M_{is} considered are greater than the maximum mass calculated for neutrons stars with a core

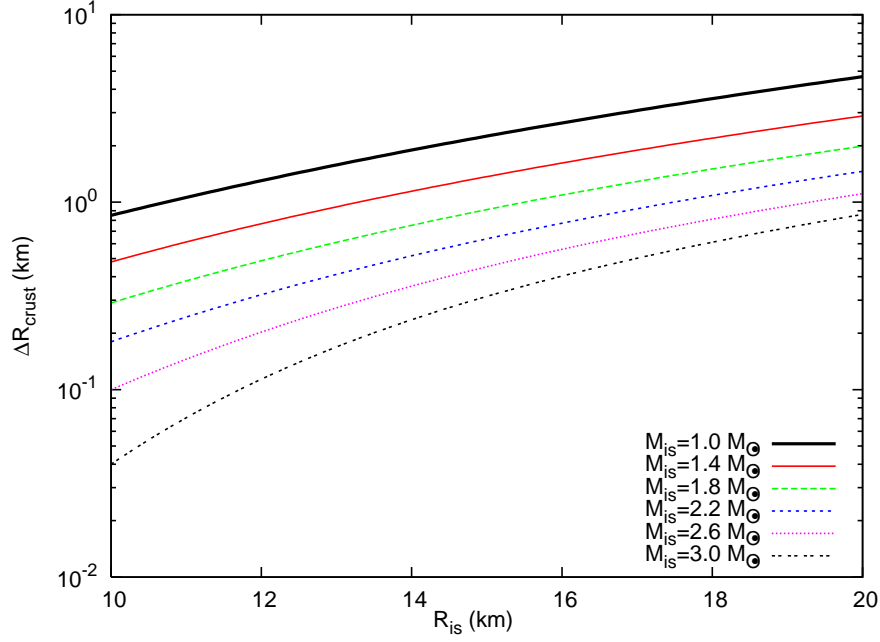


Figure C.39.: Values of thickness of the Outer Crust ΔR_{crust} in km, as function of R_{is} , for different values of M_{is} (see legend).

of degenerate relativistic electrons, protons and neutrons in local charge neutrality ($M_{max} = 0.7M_{\odot}$ (Oppenheimer and Volkoff, 1939)). The outstanding theoretical problem to address is to identify the physical forces influencing such a strong departure; the two obvious candidate are the electromagnetic structure in the core and/or the strong interactions.

C.9.3. The Fireshell Model of GRBs

In the Fireshell Model (Ruffini, 2008a) GRBs are generated by the gravitational collapse of the star progenitor to a charged black hole. The electron-positron plasma created in the process of black hole (BH) formation expands as a spherically symmetric “fireshell”. It evolves and encounters the *baryonic remnant* of the star progenitor of the newly formed BH, then is loaded with baryons and expands until the transparency condition is reached and the Proper - GRB is emitted. The afterglow emission starts due to the collision between the remaining optically thin fireshell and the CircumBurst Medium. A schematization of the model is shown in fig. C.40.

The baryon loading is measured by the dimensionless quantity

$$B = \frac{M_B c^2}{E_{dya}}, \quad (\text{C.9.10})$$

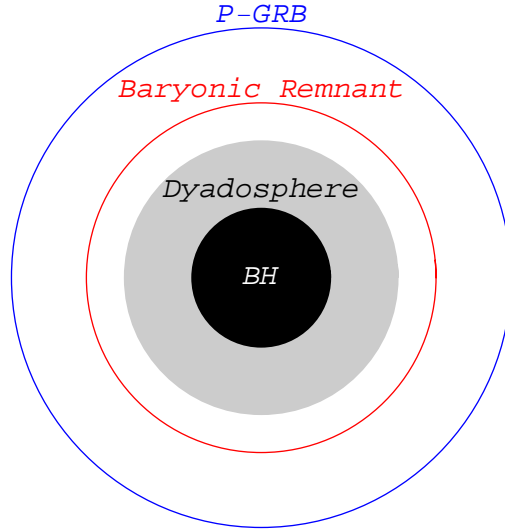


Figure C.40.: Schematization of the Fireshell Model of GRBs.

GRB	M_B/M_\odot
970228	5.0×10^{-3}
050315	4.3×10^{-3}
061007	1.3×10^{-3}
991216	7.3×10^{-4}
011121	9.4×10^{-5}
030329	5.7×10^{-5}
060614	4.6×10^{-6}
060218	1.3×10^{-6}

Table C.4.: GRBs and correspondent values of M_B used to reproduce the observed data within the Fireshell Model, in units of solar masses.

where M_B is the mass of the baryonic remnant and E_{dya} is the energy of the dyadosphere, the region outside the horizon of a BH where the electric field is of the order of the critical value for electron positron pair creation (Heisenberg and Euler, 1936; Sauter, 1931; Schwinger, 1951, 1954a,b)

$$E_c = \frac{m_e^2 c^3}{e \hbar} \approx 10^{16} \text{ V cm}^{-1}. \quad (\text{C.9.11})$$

B and E_{dya} are the two free parameters of the model.

C.9.4. The mass of the crust and M_B

Using the values of B and E_{dya} constrained by the observational data of several GRBs and eq. (C.9.10), we have obtained the correspondent values of M_B (see table C.4).

It can be seen that these values are compatible with the ones of M_{crust} .

C.10. Cooling of young neutron stars in GRB associated to Supernova

C.10.1. Introduction

The investigation of the thermal evolution of neutron stars is a powerful tool to probe the inner composition of these objects. The cooling of neutron stars has been investigated by many authors, where many different microscopic models were assumed (see Schaab et al., 1996; Page et al., 2004, 2006, 2009; Blaschke et al., 2000; Grigorian et al., 2005; Blaschke et al., 2006; Negreiros et al., 2010). Most of the research on the thermal evolution of compact stars focus on objects with ages greater than 10-100 years, which is comprehensible if one consider that the thermal data, currently available to us, is for pulsars with estimated ages of or greater than 330 years (Page et al., 2004, 2009). In this letter we discuss the thermal evolution of young neutron stars, in the little explored time window that spans from ages greater than 1 minute (just after the proto-neutron star regime (Prakash et al., 2001)) to ages $\leq 10-100$ years, when the neutron star becomes isothermal (see Gnedin et al., 2001, for details).

We discuss the possibility that the late X-ray emission (URCA hereafter¹) following a few GRBs associated with SNe; e.g. URCA-1 in GRB980425-SN1998bw (Ruffini et al., 2004; Frascchetti et al., 2005; Bernardini et al., 2008), URCA-2 in GRB030329-SN2003dh (Bernardini et al., 2004, 2005b), and URCA-3 in GRB031203-SN2003lw (Bernardini et al., 2005a; Ruffini et al., 2007b, 2008) (see Fig. C.43 for details), might actually be originated by young ($t \sim 1$ minute–(10–100) years), hot ($T \sim 10^7-10^8$ K) neutron stars, that are remnants of the SN (Ruffini et al., 2007b) and which we have here called neo-neutron stars. Relevant also are the observations of the isolated Type Ic Supernova SN 1994I (Immler et al., 2002) and SN 2002ap (Soria et al., 2004) which present late emissions similar to the ones observed in URCA-1, URCA-2, and URCA-3.

In this letter we propose a revision of the boundary conditions usually employed in the thermal cooling theory of neutron stars, in order to match the proper conditions of the atmosphere at young ages. We also discuss the importance of the thermal processes taking place in the crust, which also have important effects on the initial stages of thermal evolution. We stress that we are not calling into question the validity of the current treatment of the atmosphere of compact stars but, instead, we point out the need of extending

¹The name URCA-1 and URCA-2 mentioned here were given to these sources when presented for the first time at the MG10 meeting held in Rio de Janeiro in the town of URCA. The location of the MG10 meeting was very close to the “Cassino da URCA” where George Gamow and Mario Schoenberg conceived the process of neutrino emission for the cooling process of neutron stars which also took the name from the town of URCA, the URCA process (see e.g detailed history in Ruffini et al., 2005; Gamow, 1970)

them to appropriately describe the conditions of neo-neutron stars.

C.10.2. Cooling of Young, Hot Neutron Stars

There are three important ingredients that govern the thermal evolution of a compact star, these are: 1) the microscopic input, that accounts for the neutrino emissivities, specific heat and thermal conductivity; 2) the macroscopic structure of the star, namely its mass, radius, pressure profile, crust size, etc.; and 3) the boundary condition at the surface of the star, that provides a relationship between the mantle temperature and that of the atmosphere, the latter being what we ultimately observe. These ingredients have been extensively studied, and a comprehensive review can be found in Page et al. (2006). As discussed in Gnedin et al. (2001), during the initial stages of thermal evolution (ages $\leq 10 - 100$ years), the core and the crust of the neutron star are thermally decoupled. This is due to the fact that the high density core is emitting neutrinos at a much higher rate than the crust, which causes it to cool down more quickly. This effectively means, that initially the neutron star is cooling “inside out”, with the core colder than the outer layers. This scenario is schematically depicted in Figure C.41.

The dominant neutrino emission processes in the crust are given by the Bremsstrahlung, plasmon decay, and electron-positron annihilation processes. Following the footsteps of Gnedin et al. (2001), we calculate the thermal evolution of neutron stars, by adding artificially a phenomenological source of heat (see details in Sec. C.10.4). This allow us to estimate how much heat is needed, so that the thermal evolution of a neo-neutron star matches the X-ray light curve of late emission of GRB-SN.

After this initial core-crust decoupled state, the “cooling wave” originated in the core reaches the crust, and the object becomes isothermal. The time scale of this process is between 10–100 years, depending on the properties of the crust (Gnedin et al., 2001). This means that during the initial stages of thermal evolution the crust shields the core, and all the information we might obtain at this stage, refers only to the crust and to the atmosphere of the star. This raises another issue, that concerns the atmosphere of the star. The thermal connection between the mantle and the atmosphere is what defines the photon luminosity, which is what we observe. Therefore, the appropriate description of the atmosphere is key to the correct understanding of the thermal evolution of neutron stars. In the usual approach, the thermal relaxation-time of the atmosphere is assumed to be much smaller than that of the neutron star, furthermore neutrino emissions from the atmosphere are also considered negligible (see Gudmundsson et al., 1983). Under these assumptions, and assuming a plane-parallel approximation (which is reasonable since the atmosphere is ~ 100 m thick), one can get a relationship between the temperature of the mantle T_b and the temperature of atmosphere T_e , or equivalently

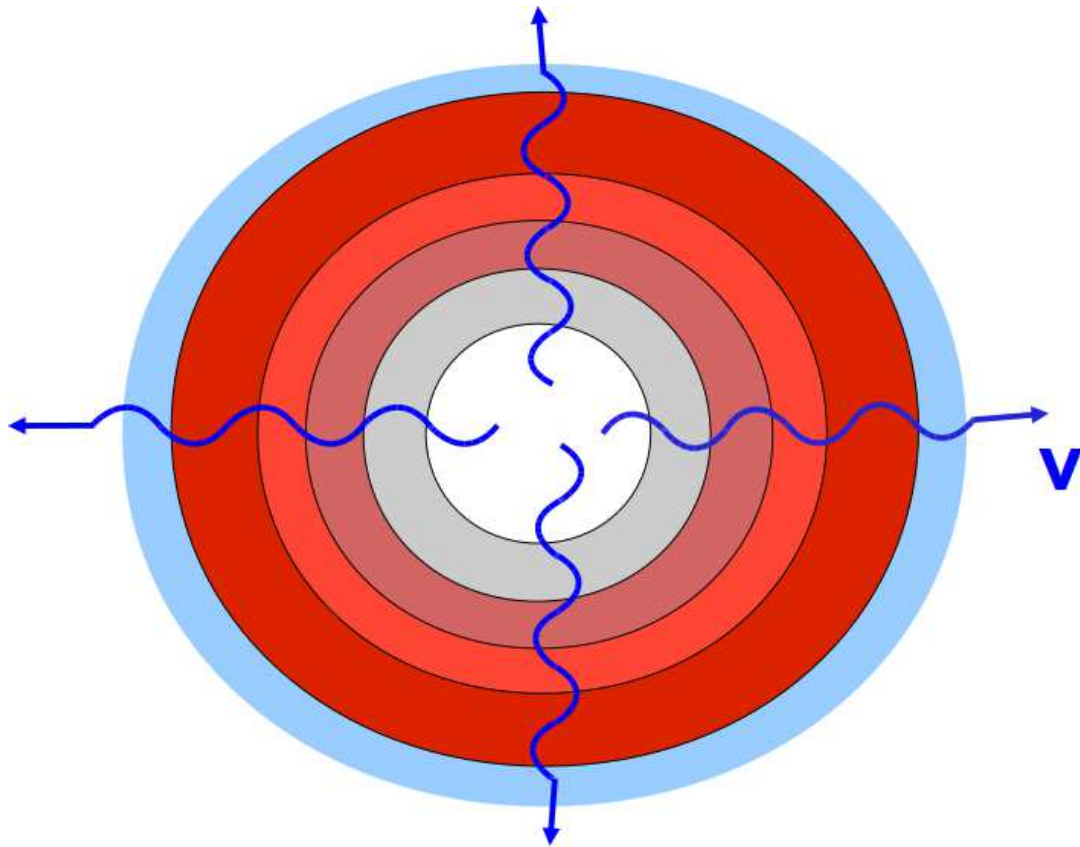


Figure C.41.: Schematic representation of the cooling of a young neutron star. Due to stronger neutrino emissivities, the core of the star cools down more quickly than the crust, causing the star to cool inside out. Darker and lighter areas represent higher and lower temperatures respectively.

the luminosity L_e . Gudmundsson et al. (1983) have originally found a T_b - T_e relationship that depends on the surface gravity of the neutron star. This relationship was further developed by Potekhin et al. (1997), to account for the possibility of mass accreted in the initial stages, and of magnetic fields effects. As pointed out by Gudmundsson et al. (1983), such assumptions for the atmosphere of the star are only valid for objects older than a few 10 years, when the temperature, for densities below 10^{10} g/cm³, has dropped below 10^9 K. In fact, we see that the current boundary conditions yields temperatures $\sim 10^7$ K ($L \sim 10^{37}$ erg/s, equivalently) for young neutron stars (age < 1 –10 years). This should raise some suspicion since proto-neutron stars studies (see Prakash et al., 2001, and references therein), indicate that neutron stars just after this regime have temperatures $\sim 10^{10}$ – 10^{11} K.

The properties of the atmosphere of a sufficiently hot, nascent neutron star should differ significantly from those considered in Gudmundsson et al. (1983) and Potekhin et al. (1997). Especially since at hot temperatures ($T \gtrsim 10^9$ K) the atmosphere might not be transparent to neutrinos, and thus the neutrino transport equations have to be considered. The coupled equations of neutrino and photon transport, in the atmosphere of a neutron star, were solved by Salpeter and Shapiro (1981), and Duncan et al. (1986). In these works the authors have performed detailed calculations of the atmosphere properties of hot neutron stars. They have found the following photon luminosity, as observed at infinity,

$$L_\infty = 50 \times t^{-7/12} \times (T_{10})^{7/4} \times (R_{10})^{17/9} \times \left(\frac{M}{M_\odot}\right)^{-1} \times L_E, \quad (\text{C.10.1})$$

where t is time in seconds, T_{10} is the initial temperature in units of 10 MeV, R_{10} is the neutron star radius in units of 10 km, M is the neutron star mass, and $L_E \sim 2.0 \times 10^{38}$ erg/s is the Eddington luminosity. Duncan et al. (1986) found that the above expression should be valid for at least the initial 100 s. In Fig. C.42 we can see how the luminosity of the star changes for the first 100 s, for stars with different initial temperatures.

According to these results, during the initial 100 s, the photon luminosity emerging from the atmosphere will be higher than the Eddington luminosity. This implies that there will be mass loss, due to neutrino-driven winds from the young atmosphere. As shown by Duncan et al. (1986), the total mass loss only becomes appreciable for neutron stars with large radii and high initial temperatures. For a typical neutron star with the canonical mass of $1.4M_\odot$, a radius of 13 km and initial temperature of $\sim 10^{11}$ K, the total mass loss was estimated to be $\sim 6.2 \times 10^{-6}M_\odot$.

In addition to the high luminosities associated to the atmosphere of young neutron stars, one need also to consider fallback onto the surface of the neutron star. Potekhin et al. (1997) discussed how fallback, at earlier stages of evolution, would modify the properties of the atmosphere, and hence of the

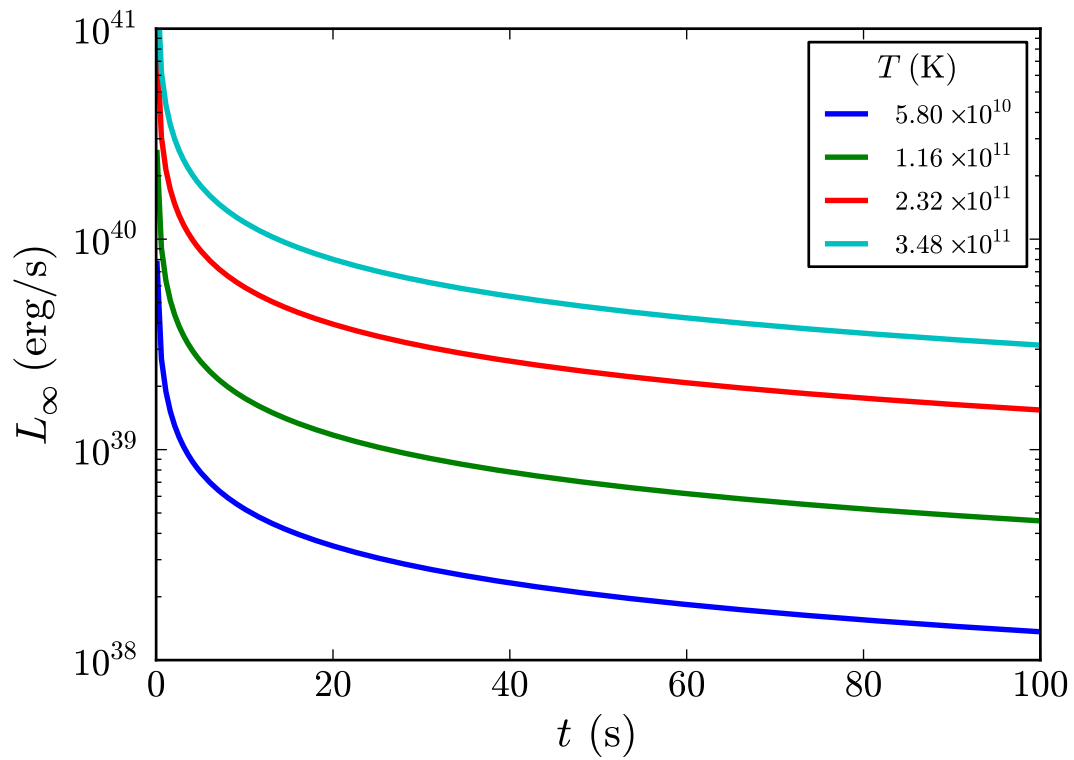


Figure C.42.: Luminosity of a hot nascent neutron star as observed at infinity given by Eq. (C.10.1) during the initial 100 s (Duncan et al., 1986), with the initial temperatures indicated. The neutron star is assumed to have a mass of $1.4M_\odot$, and a radius of 13 km.

boundary conditions. Once more however, in this investigation, such a fallback is assumed to have happened at early times and the modified boundary conditions are only valid if the fallback has already ceased. Chevalier (1989) has studied the fallback onto young neutron stars, and found that while there is an envelope, a luminosity near the Eddington limit should be present. Furthermore, the authors have found that in this case the energy from the envelope can be radiated away in a time of ~ 1 year. This timescale however, might be lengthened if effects of rotation are accounted during the fallback. In addition to that, Turolla et al. (1994) have discussed the possibility of “hot solutions” for the atmosphere of neutron stars undergoing spherical accretion. It was shown that for $L \geq 10^{-2}L_E$ the temperature at the atmosphere of a neutron star might be $\sim 10^9$ – 10^{11} K.

C.10.3. Late X-Ray Emission in GRBs associated to Supernovae: URCA

It seems clear to us that, after the analysis of the scenario described above, we must extend the current model for the boundary conditions used in cooling calculations, to include the effects of a high temperature atmosphere, with possibly super-Eddington luminosity. Up until this point however, little attention has been given to the thermal evolution of young neutron stars, mainly due to the absence of observational data of neutron stars with ages < 330 years. It has been recently proposed (see Ruffini et al., 2007b, for details) that the long lasting X-ray emission called there URCA (see Fig. C.43) of a few GRBs associated to SNe; URCA-1 in GRB980425-SN1998bw (Ruffini et al., 2004; Frascetti et al., 2005; Bernardini et al., 2008), URCA-2 in GRB030329-SN2003dh (Bernardini et al., 2004, 2005b), and URCA-3 in GRB031203-SN2003lw (Bernardini et al., 2005a; Ruffini et al., 2007b, 2008), might actually be originated in the compact star remnant of the SN: a neo-neutron star. In this scenario the GRB is described as the core collapse of a massive star, whose remnant is a black hole. This massive star is supposed to be in a binary system, whose companion is on the verge of going supernova. The GRB triggers the supernova explosion in the companion star, which in turns leaves behind a neutron star (Ruffini et al., 2001). An alternative scenario has been recently suggested in which the so-called GRB is actually not a GRB but the observed X-ray emission originates from a collapsing core: a proto-neutron star leading directly to a SN explosion. This concept is very similar to the one of a proto-black hole introduced in Ruffini et al. (2011, 2010a); Izzo et al. (2011), where the emission from the collapsing core is clearly well distinguished from the GRB. In that case the collapsing core leads to the formation of the black hole while in the present case it leads to the formation of a neutron star.

Both scenarios lead to the formation of a neo-neutron star and they are supported by the observation of Supernova 1979C (Patnaude et al., 2011),

Table C.5.: a) see Kaneko et al. (2007); b) Mazzali, P., private communication at MG11 meeting in Berlin, July 2006, Iwamoto et al. (1998); c) evaluated fitting the URCA with a power law followed by an exponentially decaying part; d) evaluated assuming a mass of the neutron star $M = 1.5M_{\odot}$ and $T \sim 5\text{--}7$ keV in the source rest frame; e) see Galama et al. (1998); Greiner et al. (2003); Prochaska et al. (2004); Mirabal et al. (2006). Here $E_{e^{\pm}}^{\text{tot}}$ is the total energy of GRB, $E_{\text{SN}}^{\text{bolom}}$ and $E_{\text{SN}}^{\text{kin}}$ are the bolometric and the kinetic energy of the SN, E_{URCA} is the energy of the late X-ray emission URCA (see Fig. C.43), R_{NS} is the radius of the neutron star and z is the redshift of the event.

GRB	$E_{e^{\pm}}^{\text{tot}}$ (erg)	$E_{\text{SN}}^{\text{bolom}}$ (erg) ^a	$E_{\text{SN}}^{\text{kin}}$ (erg) ^b	E_{URCA} (erg) ^c	$\frac{E_{e^{\pm}}^{\text{tot}}}{E_{\text{URCA}}}$	$\frac{E_{\text{SN}}^{\text{kin}}}{E_{\text{URCA}}}$	R_{NS} (km) ^d	z^e
980425	1.2×10^{48}	2.3×10^{49}	1.0×10^{52}	3×10^{48}	0.4	1.7×10^4	8	0.0085
030329	2.1×10^{52}	1.8×10^{49}	8.0×10^{51}	3×10^{49}	6×10^2	1.2×10^3	14	0.1685
031203	1.8×10^{50}	3.1×10^{49}	1.5×10^{52}	2×10^{49}	8.2	3.0×10^3	20	0.105
060218	1.8×10^{50}	9.2×10^{48}	2.0×10^{51}	?	?	?	?	0.033

where a similar X-ray light curve also followed the supernova. In Fig. C.43 we show the X-ray light curve associated with the URCA.

From Fig. C.43 we can see that the X-ray luminosities of these sources are of the same magnitude as that expected for neo-neutron stars, as discussed above. In Table C.5 we summarize the representative parameters of the four GRB-SN systems, including the very large kinetic energy observed in all SNe (Mazzali, 2006). We have also included the association GRB060218-SN2006aj (see Dainotti et al., 2007, 2010, for details). It must be noted that similar prolonged X-ray emission has been observed also in connection with other Type Ic SN not associated with GRBs, like e.g. SN1994I (Immler et al., 2002) and SN2002ap (Soria et al., 2004) (see Fig. C.44 for details).

C.10.4. Neo-Neutron Star Luminosity and the URCA

Another important ingredient for the cooling of young neutron stars are the crust properties. As illustrated in Fig. C.41, due to the stronger neutrino emission from the core, during the initial stages the core and crust are thermally decoupled. For that reason, the initial stages of the thermal evolution reflects the properties of the crust, while the core remains invisible. Thus the proper description of the crust structure and composition, is also fundamental for understanding the initial thermal evolution stages of a neutron star. We now briefly discuss the current understanding of the crustal processes and how such might be related with the data available from the URCA.

There are several active emission mechanisms in the neutron star crust, e.g. e -Ion Bremsstrahlung, plasmon decay, e^+e^- annihilation, e - e and n - n Bremsstrahlung, synchrotron emission, as well as Cooper pair processes for temperatures smaller than the critical temperature for superfluidity T_{crit} . However, as shown by Yakovlev et al. (2001), for temperatures above 10^8 K, which is the regime we are interested, the first three processes are the dominant

ones. For instance, synchrotron emission channels might become slightly relevant, but only for $T < 10^8$ K and for very high magnetic fields $> 10^{14}$ G. The Cooper pair mechanism, possibly important for objects of a few hundred years old like Cas A (see e.g. Page et al., 2011; Shternin et al., 2011, for details), is irrelevant in the present case since we are dealing with neutron star ages < 10 years and thus temperatures well above T_{crit} .

At temperatures $T \sim 3 \times 10^9$ K, we can write for the most important emission processes in the crust

$$\epsilon_B \sim 10^{21} \text{erg s}^{-1} \text{cm}^{-3}, \quad (\text{C.10.2})$$

$$\epsilon_P \sim 10^{22} \text{erg s}^{-1} \text{cm}^{-3}, \quad (\text{C.10.3})$$

$$\epsilon_{ep} \sim 10^{19} \text{erg s}^{-1} \text{cm}^{-3}, \quad (\text{C.10.4})$$

where ϵ_i denotes the emissivity and the indexes B, P, ep denote the Bremsstrahlung, plasmon decay, and pair annihilation processes, respectively.

In order to estimate the amount of heat needed to match the theoretical thermal evolution of a neo-neutron star to the light curve of the URCA's we have added a phenomenological source of heat parametrized by

$$H = H_0 e^{-t/\tau_S}, \quad (\text{C.10.5})$$

with H_0 being the magnitude of the heat source, and τ_S being the time scale in which it is active. For our calculations we set $\tau_S = 1$ year.

In addition, we have introduced a phenomenological boundary condition for the early stages of evolution of the surface temperature T_s that follows the form $T_s = T_x g_{s14}^{1/4} T_8^{0.55}$ K, where $T_x = 0.87 \times 10^6 + (T_0 - 0.87 \times 10^6) e^{-t/\tau_S}$ K, T_8 is the mantle temperature T_b in units of 10^8 K, T_0 is the initial temperature of the atmosphere, and g_{s14} is the surface acceleration of gravity in units of 10^{14} cm/s². With this new boundary condition we can mimic the high temperature of the atmosphere for young neutron stars by setting the temperature at early times to a higher value and, for times greater than τ_S , it asymptotically goes to its traditional value $\sim 0.87 \times 10^6$ K.

In Fig. C.45 we show the cooling curves of neo-neutron stars resulting from the presence of the heating source given by Eq. (C.10.5), in addition to the traditional cooling processes of neutron stars. The cooling curves are obtained self-consistently by solving the full, general relativistic, energy transport and balance equations with no approximations as described in Schaab et al. (1996); Page et al. (2006); Negreiros et al. (2010). We show also the observed data for the X-ray light curve associated with the URCA's. This allow us to identify the key factor leading to the matching of the neo-neutron star luminosity with the X-ray emission of the URCA's.

C.10.5. Discussion and Conclusions

The major role played by the neutrino emissions from the crust of a neo-neutron star at the initial stages of the object is illustrated by Fig. C.45. In addition, by calibrating our additional heating source at early times to $H_0 \sim 10^{12}-10^{15}$ erg/g/s, we find a striking agreement of the luminosity obtained from the cooling of a neo-neutron stars with the prolonged ($t = 10^8-10^9$ s) X-ray emission observed in GRB associated with Supernova (see Fig. C.45 for details). This could indicate that something might be missing in our current understanding of the crust of neutron stars. It might be that, as is the case for the atmosphere, we need to further develop our current models for the crust, as to describe properly the properties of neo-neutron stars. The traditional thermal processes taking place in the crust might be enhanced by the extreme high temperature conditions of neo-neutron star and, additional heating processes not yet studied within this context could also take place under such conditions and deserve further analysis.

Particularly interesting in this respect are the processes of e^+e^- pair creation expected to occur in the interphase between the core and the crust during the neutron star formation leading to the appearance of critical fields (see Ruffini et al., 2007d; Ruffini, 2008b; Rueda et al., 2010a,b; Popov, 2010; Ruffini et al., 2010b; Rotondo et al., 2011c,d,e,a; Rueda et al., 2011, for details)

It is also worth to mention that the additional heating source needed at early times, $H_0 \sim 10^{12}-10^{15}$ erg/g/s (or $H_0 \sim 10^{-6}-10^{-3}$ MeV/Nucleon/s), is in striking agreement with the heat released from nuclear fusion reactions, radiative neutron captures and photodisintegrations in the early stages of neutron star mergers found by Goriely et al. (2011a,b). Fission as well as β -decays have been also there included; i.e neutron-induced fission, spontaneous fission, β -delayed fission, photofission, as well as β -delayed neutron emission.

All this suggests the exciting possibility that we are, for the first time, observing a nascent hot neutron star. This possibility alone warrants further studies on this subject, so we might obtain a more concrete picture of the thermal evolution of neo-neutron stars. A proposal has been recently submitted by E. Pian et al. to the Chandra satellite to observe if a similar prolonged X-ray emission exists also in GRB100316D associated with SN2010bh (Pian et al., 2011). We encourage also dedicated observations of isolated SN in view of the similarities between URCA-1-URCA-3 and the Type Ic Supernova SN 1994I (Immler et al., 2002) and SN 2002ap (Soria et al., 2004).

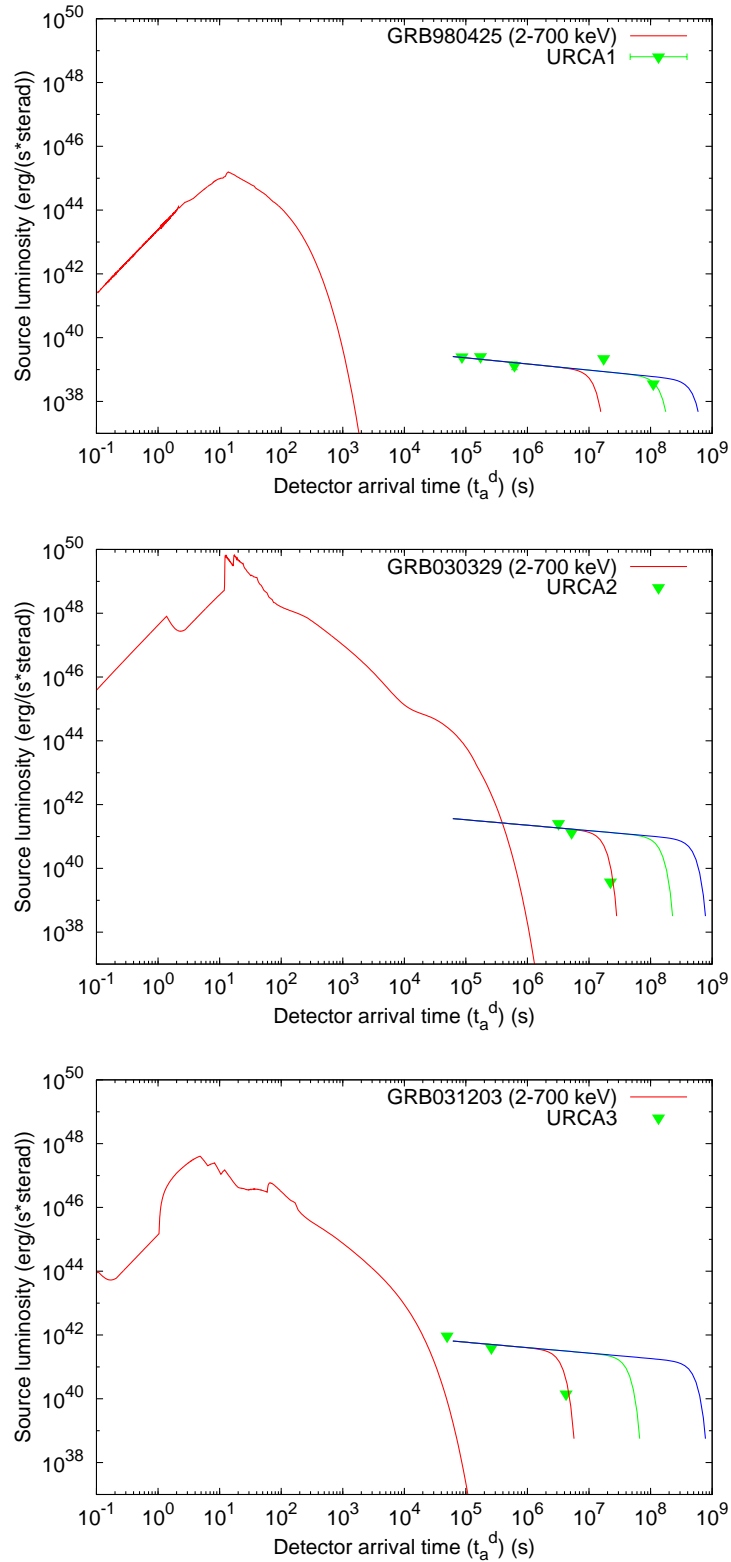


Figure C.43.: Synthetic light curves of GRB980425 (A) (Ruffini et al., 2004; Frascchetti et al., 2005; Bernardini et al., 2008) , GRB030329 (B) (Bernardini et al., 2004, 2005b) and GRB031203 (C) (Bernardini et al., 2005a; Ruffini et al., 2007b, 2008) . The solid curves represent the hard X-ray emission (10-200 keV range) and the triangles are 2-10 keV flux points. The optical luminosities of the SNe accompanying these GRBs are also reported with crosses (see Ruffini et al., 2007b, for details). The curves fitting the late X-ray luminosity (URCAs) are qualitative cooling curves based on Canuto (1978); see also Ruffini et al. (2004, 2007b, 2008); Bernardini et al. (2004, 2005a,b, 2008); Frascchetti et al. (2005), for details.

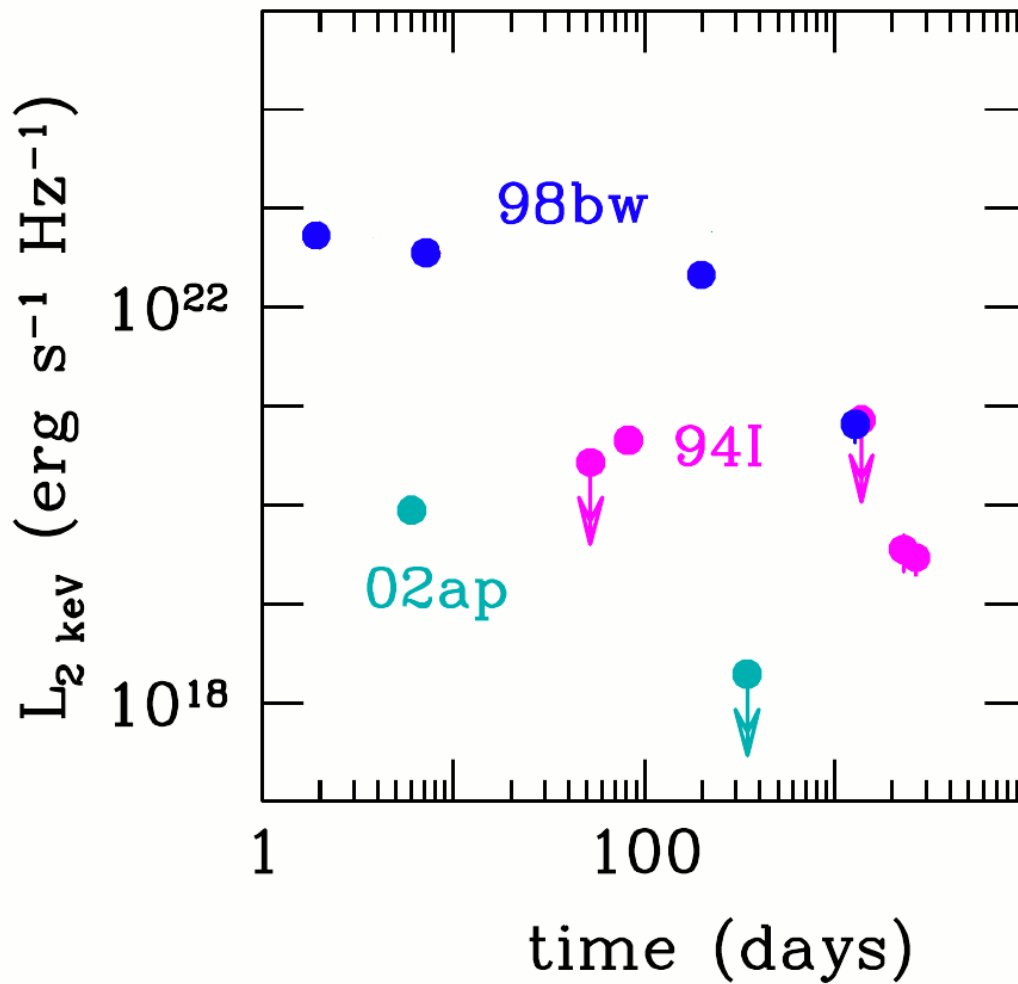


Figure C.44.: X-ray light curves of the counterparts of GRB980425-SN1998bw and of two Type Ic SNe not accompanied by GRBs: SN1994I (“normal”) and SN2002ap (broad-lined). The data are from Pian et al. (2000); Immler et al. (2002); Kouveliotou et al. (2004); Soria et al. (2004).

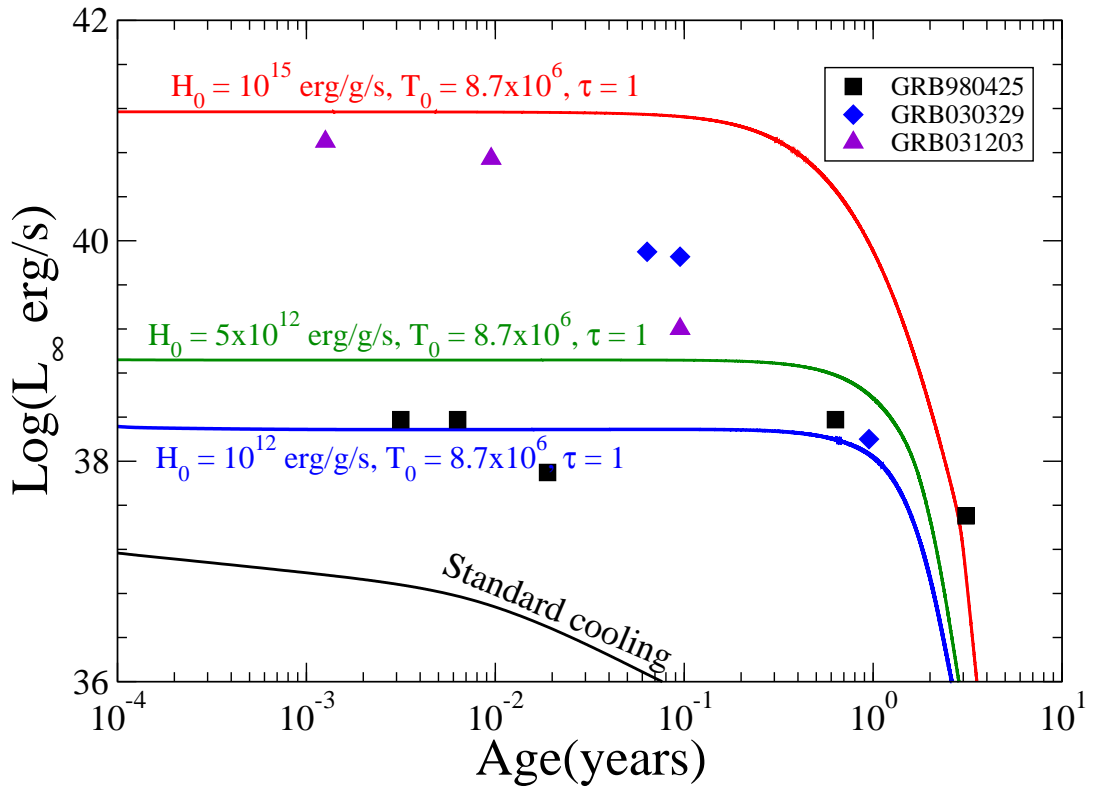


Figure C.45.: Thermal evolution of neo-neutron stars for selected values of the heating source $H_0 = [10^{12}, 5 \times 10^{12}, 10^{15}] \text{ erg/g/s}$ and for an initial temperature of the atmosphere $T_0 = 8.7 \times 10^6 \text{ K}$. The observed data represents the X-ray light curve associated with the URCA's.

Bibliography

«On the critical mass: the case of white dwarfs».

In H. Gursky, R. Ruffini, & L. Stella (ed.), *Exploring the universe: a Festschrift in honor of Riccardo Giacconi "Dedicated to Riccardo Giacconi for his sixty-fifth birthday, on the occasion of his being awarded a "Laurea Honoris Causa" in physics at the University of Rome "La Sapienza". Rome, Italy, October 1997* Singapore: World Scientific, 2000, xii, 383 p., *Advanced series in astrophysics and cosmology*, v.13. Edited by H. Gursky, R. Ruffini, and L. Stella. ISBN 9810244231 (2000).

AKSENOV, A.G., RUFFINI, R. AND VERESHCHAGIN, G.V.

«Thermalization of Nonequilibrium Electron-Positron-Photon Plasmas».
Physical Review Letters, **99(12)**, pp. 125003–+ (2007).

ALCOCK, C., FARHI, E. AND OLINTO, A.

«Strange stars».
Astrophysical Journal, **310**, pp. 261–272 (1986).

ALFORD, M., RAJAGOPAL, K., REDDY, S. AND WILCZEK, F.

«Minimal color-flavor-locked-nuclear interface».
Physical Review D, **64(7)**, pp. 074017–+ (2001).

ALLEN, M.P. AND HORVATH, J.E.

«Influence of an Internal Magnetar on Supernova Remnant Expansion».
Astrophysical Journal, **616**, pp. 346–356 (2004).

ALTHAUS, L.G., GARCÍA-BERRO, E., ISERN, J. AND CÓRSICO, A.H.

«Mass-radius relations for massive white dwarf stars».
Astronomy & Astrophysics, **441**, pp. 689–694 (2005).

ALTHAUS, L.G., GARCÍA-BERRO, E., ISERN, J., CÓRSICO, A.H. AND ROHRMANN, R.D.

«The age and colors of massive white dwarf stars».
Astronomy & Astrophysics, **465**, pp. 249–255 (2007).

ALTHAUS, L.G., GARCÍA-BERRO, E., RENEDO, I., ISERN, J., CÓRSICO, A.H. AND ROHRMANN, R.D.

«Evolution of White Dwarf Stars with High-metallicity Progenitors: The Role of ^{22}Ne Diffusion».
Astrophysical Journal, **719**, pp. 612–621 (2010).

- ANGEL, J.R.P., BORRA, E.F. AND LANDSTREET, J.D.
«The magnetic fields of white dwarfs».
Astrophysical Journal Supplement Series, **45**, pp. 457–474 (1981).
- AUDI, G., WAPSTRA, A.H. AND THIBAUT, C.
«The Ame2003 atomic mass evaluation (II). Tables, graphs and references».
Nuclear Physics A, **729**, pp. 337–676 (2003).
- BARSTOW, M.A., JORDAN, S., O'DONOGHUE, D., BURLEIGH, M.R., NAPIWOTZKI, R. AND HARROP-ALLIN, M.K.
«RE J0317-853: the hottest known highly magnetic DA white dwarf».
Monthly Notices of the Royal Astronomical Society, **277**, pp. 971–985 (1995).
- BAYM, G., BETHE, H.A. AND PETHICK, C.J.
«Neutron star matter».
Nuclear Physics A, **175**, pp. 225–271 (1971a).
- BAYM, G., PETHICK, C. AND SUTHERLAND, P.
«The Ground State of Matter at High Densities: Equation of State and Stellar Models».
Astrophysical Journal, **170**, pp. 299–+ (1971b).
- BAYM, G. AND PINES, D.
«Neutron starquakes and pulsar speedup.»
Annals of Physics, **66**, pp. 816–835 (1971).
- BELL, S.J. AND HEWISH, A.
«Angular Size and Flux Density of the Small Source in the Crab Nebula at 81.5 Mc/s».
Nature, **213**, pp. 1214–1216 (1967).
- BELVEDERE, R., PUGLIESE, D., RUEDA, J.A., RUFFINI, R. AND XUE, S.S.
submitted to Nuclear Physics A (2011).
- BERNARDINI, F., ISRAEL, G.L., DALL'OSSO, S., STELLA, L., REA, N., ZANE, S., TUROLLA, R., PERNA, R., FALANGA, M., CAMPANA, S. ET AL.
«From outburst to quiescence: the decay of the transient AXP XTE J1810-197».
Astronomy & Astrophysics, **498**, pp. 195–207 (2009).
- BERNARDINI, M.G., BIANCO, C.L., CAITO, L., DAINOTTI, M.G., GUIDA, R. AND RUFFINI, R.
«Grb980425 and the puzzling urca1 emission».
In R.T. Jantzen, H. Kleinert and R. Ruffini (eds.), *The Eleventh Marcel Grossmann Meeting* (Singapore: World Scientific, 2008).

- BERNARDINI, M.G., BIANCO, C.L., CHARDONNET, P., FRASCHETTI, F., RUFFINI, R. AND XUE, S.S.
«A new astrophysical "triptych": Grb030329/sn2003dh/urca-2».
In E. Fenimore and M. Galassi (eds.), *Gamma-Ray Bursts: 30 Years of Discovery*, volume 727 of *American Institute of Physics Conference Series*, pp. 312–315 (2004).
- BERNARDINI, M.G., BIANCO, C.L., CHARDONNET, P., FRASCHETTI, F., RUFFINI, R. AND XUE, S.S.
«Theoretical interpretation of the luminosity and spectral properties of grb 031203».
ApJ, **634**, pp. L29–L32 (2005a).
- BERNARDINI, M.G., BIANCO, C.L., RUFFINI, R., XUE, S.S., CHARDONNET, P. AND FRASCHETTI, F.
«General features of grb 030329 in the embh model».
In M. Novello, S. Perez Bergliaffa and R. Ruffini (eds.), *The Tenth Marcel Grossmann Meeting. On recent developments in theoretical and experimental general relativity, gravitation and relativistic field theories*, p. 2459 (Singapore: World Scientific, 2005b).
- BERTONE, G. AND RUFFINI, R.
«Equilibrium configurations of relativistic white dwarfs».
Nuovo Cimento B Serie, **115**, pp. 935–+ (2000).
- BETHE, H.A.
Energy production in stars. Nobel lecture. (1968).
- BETHE, H.A., BORNER, G. AND SATO, K.
«Nuclei in Neutron Matter».
Astronomy & Astrophysics, **7**, pp. 279–+ (1970).
- BHATTACHARYYA, S., STROHMAYER, T.E., MILLER, M.C. AND MARKWARDT, C.B.
«Constraints on Neutron Star Parameters from Burst Oscillation Light Curves of the Accreting Millisecond Pulsar XTE J1814-338».
Astrophysical Journal, **619**, pp. 483–491 (2005).
- BILDSTEN, L. AND HALL, D.M.
«Gravitational Settling of ^{22}Ne in Liquid White Dwarf Interiors».
Astrophysical Journal, **549**, pp. L219–L223 (2001).
- BINI, D., BOSHKAYEV, K., RUFFINI, R. AND SIUTSOU, I.
«».
in preparation (2011).

- BLASCHKE, D., KLAHN, T. AND VOSKRESENSKY, D.
«Diquark condensates and compact star cooling».
ApJ, **533**, p. 406412 (2000).
- BLASCHKE, D., VOSKRESENSKY, D. AND GRIGORIAN, H.
«Cooling of Neutron Stars with Color Superconducting Quark Cores».
Nuclear Physics A, **774**, pp. 815–818 (2006).
ISSN 03759474.
- BOCCALETTI, D. AND RUFFINI, R.
Fermi and Astrophysics (World Scientific, Singapore, 2010).
- BOGUTA, J. AND BODMER, A.R.
«Relativistic calculation of nuclear matter and the nuclear surface».
Nuclear Physics A, **292**, pp. 413–428 (1977).
- BORKOWSKI, J., GOTZ, D., MEREGHETTI, S., MOWLAVI, N., SHAW, S. AND
TURLER, M.
«Giant flare from Sgr 1806-20 detected by INTEGRAL.»
GRB Coordinates Network, **2920**, pp. 1–+ (2004).
- BOSHKAYEV, K., RUEDA, J.A. AND RUFFINI, R.
«On the minimum rotational period of white dwarfs».
In A. Mezzacappa (ed.), *From Nuclei to White Dwarfs to Neutron Stars* (2011).
- BOWERS, R.L., CAMPBELL, J.A. AND ZIMMERMAN, R.L.
«Relativistic Baryon Effective Masses and Thresholds for Strongly Interact-
ing Superdense Matter».
Physical Review D, **8**, pp. 1077–1087 (1973a).
- BOWERS, R.L., CAMPBELL, J.A. AND ZIMMERMAN, R.L.
«Relativistic Many-Body Theory for Strongly Interacting Matter».
Physical Review D, **7**, pp. 2278–2288 (1973b).
- BÜRVENICH, T.J., MISHUSTIN, I.N. AND GREINER, W.
«Nuclei embedded in an electron gas».
Physical Review C, **76(3)**, pp. 034310–+ (2007).
- CAMERON, A.G.W.
«Neutron Stars».
Annual Review of Astronomy and Astrophysics, **8**, pp. 179–+ (1970).
- CANUTO, V.
«Neutron stars».
In R. Giacconi and R. Ruffini (eds.), *Physics and Astrophysics of Neutron Stars
and Black Holes*, pp. 448–527 (1978).

- CASE, K.M.
«Singular Potentials».
Physical Review, **80**, pp. 797–806 (1950).
- CASTRO-TIRADO, A.J., DE UGARTE POSTIGO, A., GOROSABEL, J., JELÍNEK, M., FATKHULLIN, T.A., SOKOLOV, V.V., FERRERO, P., KANN, D.A., KLOSE, S., SLUSE, D. ET AL.
«Flares from a candidate Galactic magnetar suggest a missing link to dim isolated neutron stars».
Nature, **455**, pp. 506–509 (2008).
- CHABRIER, G. AND POTEKHIN, A.Y.
«Equation of state of fully ionized electron-ion plasmas».
Physical Review E, **58**, pp. 4941–4949 (1998).
- CHANDRASEKHAR, S.
«The highly collapsed configurations of a stellar mass».
Monthly Notices of the Royal Astronomical Society, **91**, pp. 456–466 (1931a).
- CHANDRASEKHAR, S.
«The Maximum Mass of Ideal White Dwarfs».
Astrophysical Journal, **74**, pp. 81–+ (1931b).
- CHANDRASEKHAR, S.
«The highly collapsed configurations of a stellar mass (Second paper)».
Monthly Notices of the Royal Astronomical Society, **95**, pp. 207–225 (1935).
- CHANDRASEKHAR, S.
An introduction to the study of stellar structure (1939).
- CHANDRASEKHAR, S.
Ellipsoidal figures of equilibrium (1969).
- CHANDRASEKHAR, S.
The mathematical theory of black holes (1992).
- CHERUBINI, C., GERALICO, A., J. A. RUEDA, H. AND RUFFINI, R.
« $e^- - e^+$ pair creation by vacuum polarization around electromagnetic black holes».
Physical Review D, **79(12)**, pp. 124002–+ (2009).
- CHEVALIER, R.A.
«Neutron star accretion in a supernova».
ApJ, **346**, p. 847 (1989).
ISSN 0004-637X.

- CHOI, C.S. AND DOTANI, T.
«A Flare of AE Aquarii Observed with XMM-Newton».
Astrophysical Journal, **646**, pp. 1149–1159 (2006).
- CHRISTIANSEN, M.B. AND GLENDENNING, N.K.
«Finite size effects and the mixed quark-hadron phase in neutron stars».
Physical Review C, **56**, pp. 2858–2864 (1997).
- CHRISTIANSEN, M.B., GLENDENNING, N.K. AND SCHAFFNER-BIELICH, J.
«Surface tension between a kaon condensate and the normal nuclear matter phase».
Physical Review C, **62(2)**, pp. 025804+ (2000).
- CIUFOLINI, I. AND RUFFINI, R.
«Equilibrium configurations of neutron stars and the parametrized post-Newtonian metric theories of gravitation».
Astrophysical Journal, **275**, pp. 867–877 (1983).
- COHEN, R.H., COPPI, B. AND TREVES, A.
«Magnetic Configuration in the Neighborhood of a Collapsed Star».
Astrophysical Journal, **179**, pp. 269–276 (1973).
- COPPI, B., PELLAT, R., ROSENBLUTH, M., RUTHERFORD, P. AND GALVAO, R.
«Resistive internal kink modes».
Soviet Journal of Plasma Physics, **2**, pp. 961–966 (1976).
- COSTA, E., FRONTERA, F., HEISE, J., FEROCI, M., IN'T ZAND, J., FIORE, F., CINTI, M.N., DAL FIUME, D., NICASTRO, L., ORLANDINI, M. ET AL.
«Discovery of an X-ray afterglow associated with the γ -ray burst of 28 February 1997».
Nature, **387**, pp. 783–785 (1997).
- DAINOTTI, M.G., BERNARDINI, M.G., BIANCO, C.L., CAITO, L., GUIDA, R. AND RUFFINI, R.
«Grb 060218 and grbs associated with supernovae ib/c».
A&A, **471**, pp. L29–L32 (2007).
- DAINOTTI, M., BERNARDINI, M.G., BIANCO, C.L., CAITO, L., GUIDA, R. AND RUFFINI, R.
«The astrophysical tryptic: Grb, sn and urca can be extended to grb060218?»
J. Kor. Phys. Soc., **56**, p. 1588 (2010).
- DAMOUR, T. AND RUFFINI, R.
«Quantum Electrodynamical Effects in Kerr-Newmann Geometries».
Physical Review Letters, **35**, pp. 463–466 (1975).

- DARWIN, C.G.
«The Wave Equations of the Electron».
Royal Society of London Proceedings Series A, **118**, pp. 654–680 (1928).
- DAVIES, S.R., COE, M.J. AND WOOD, K.S.
«HEAO-1 observations of the X-ray pulsar 1E2259 + 586».
Monthly Notices of the Royal Astronomical Society, **245**, pp. 268–274 (1990).
- DE JAGER, O.C., MEINTJES, P.J., O'DONOGHUE, D. AND ROBINSON, E.L.
«The Discovery of a Brake on the White Dwarf in Ae-Aquarii».
Monthly Notices of the Royal Astronomical Society, **267**, pp. 577–+ (1994).
- DEBYE, P. AND HUECKERL, E.
Phys. Zeitschr., **24**, p. 185 (1923).
- DEMOREST, P.B., PENNUCCI, T., RANSOM, S.M., ROBERTS, M.S.E. AND HESSELS, J.W.T.
«A two-solar-mass neutron star measured using Shapiro delay».
Nature, **467**, pp. 1081–1083 (2010).
- DIB, R., KASPI, V.M. AND GAVRIIL, F.P.
«Rossi X-Ray Timing Explorer Monitoring of the Anomalous X-ray Pulsar 1E 1048.1 - 5937: Long-term Variability and the 2007 March Event».
Astrophysical Journal, **702**, pp. 614–630 (2009).
- DIRAC, P.A.M.
«The Quantum Theory of the Electron».
Royal Society of London Proceedings Series A, **117**, pp. 610–624 (1928a).
- DIRAC, P.A.M.
«The Quantum Theory of the Electron. Part II».
Royal Society of London Proceedings Series A, **118**, pp. 351–361 (1928b).
- DIRAC, P.A.M.
Proc. Cambridge Phil. Soc., **26**, pp. 376–+ (1930).
- DIRAC, P.A.M.
Principles of Quantum Mechanics (1958).
- DOUCHIN, F. AND HAENSEL, P.
«A unified equation of state of dense matter and neutron star structure».
Astronomy & Astrophysics, **380**, pp. 151–167 (2001).
- DUERR, H.
«Relativistic Effects in Nuclear Forces».
Physical Review, **103**, pp. 469–480 (1956).

- DUNCAN, R.C. AND THOMPSON, C.
«Formation of very strongly magnetized neutron stars - Implications for gamma-ray bursts».
Astrophysical Journal, **392**, pp. L9–L13 (1992).
- DUNCAN, R.C., SHAPIRO, S.L. AND WASSERMAN, I.
«Neutrino-driven winds from young, hot neutron stars».
ApJ, **309**, p. 141 (1986).
ISSN 0004-637X.
- DURANT, M., KARGALTSEV, O. AND PAVLOV, G.G.
Astrophysical Journal, in press; *arXiv:1108.3340* (2011).
- DURISEN, R.H.
«Upper mass limits for stable rotating white dwarfs».
Astrophysical Journal, **199**, pp. 179–183 (1975).
- EDDINGTON, SIR, A.S.
«On "relativistic degeneracy,"».
Monthly Notices of the Royal Astronomical Society, **95**, pp. 194–206 (1935).
- EMDEN, R.
Gaskugeln Anwendungen der Mechanischen Wärmetheorie auf Kosmologische und Meteorologische Probleme (Leipzig, Teubner, Berlin, 1907).
- ERACLEOUS, M., PATTERSON, J. AND HALPERN, J.
«A search for periodicities in the X-ray emission from cataclysmic variables».
Astrophysical Journal, **370**, pp. 330–340 (1991).
- ESPOSITO, P., ISRAEL, G.L., TUROLLA, R., TIENGO, A., GÖTZ, D., DE LUCA, A., MIGNANI, R.P., ZANE, S., REA, N., TESTA, V. ET AL.
«Early X-ray and optical observations of the soft gamma-ray repeater SGR0418+5729».
Monthly Notices of the Royal Astronomical Society, **405**, pp. 1787–1795 (2010).
- FAHLMAN, G.G. AND GREGORY, P.C.
«An X-ray pulsar in SNR G109.1-1.0».
Nature, **293**, pp. 202–204 (1981).
- FERMI, E.
«Un Metodo Statistico per la Determinazione di alcune Priopriet dell'Atomo».
Rend. Accad. Naz. Lincei, **6**, pp. 602–+ (1927).
- FERMI, E. (ed.).
Nuclear physics (1950).

- FERMI-LAT COLLABORATION.
«Gamma-ray flares from the Crab Nebula».
arXiv:1011.3855 (2010).
- FERRARI, A. AND RUFFINI, R.
«Theoretical Implications of the Second Time Derivative of the Period of the Pulsar NP 0532».
Astrophysical Journal, **158**, pp. L71+ (1969).
- FERRARIO, L., VENNES, S., WICKRAMASINGHE, D.T., BAILEY, J.A. AND CHRISTIAN, D.J.
«EUVE J0317-855 A rapidly rotating, high-field magnetic white dwarf».
Monthly Notices of the Royal Astronomical Society, **292**, pp. 205+ (1997).
- FERRARIO, L. AND WICKRAMASINGHE, D.
«Modelling of isolated radio pulsars and magnetars on the fossil field hypothesis».
Monthly Notices of the Royal Astronomical Society, **367**, pp. 1323–1328 (2006).
- FERRARIO, L., WICKRAMASINGHE, D., LIEBERT, J. AND WILLIAMS, K.A.
«The open-cluster initial-final mass relationship and the high-mass tail of the white dwarf distribution».
Monthly Notices of the Royal Astronomical Society, **361**, pp. 1131–1135 (2005).
- FERRARIO, L. AND WICKRAMASINGHE, D.T.
«Magnetic fields and rotation in white dwarfs and neutron stars».
Monthly Notices of the Royal Astronomical Society, **356**, pp. 615–620 (2005).
- FERREIRINHO, J., RUFFINI, R. AND STELLA, L.
«On the relativistic Thomas-Fermi model».
Physics Letters B, **91**, pp. 314–316 (1980).
- FEYNMAN, R.P., METROPOLIS, N. AND TELLER, E.
«Equations of State of Elements Based on the Generalized Fermi-Thomas Theory».
Physical Review, **75**, pp. 1561–1573 (1949).
- FOWLER, R.H.
«On dense matter».
Monthly Notices of the Royal Astronomical Society, **87**, pp. 114–122 (1926).
- FRASCHETTI, F., BERNARDINI, M.G., BIANCO, C.L., RUFFINI, R., XUE, S.S. AND CHARDONNET, P.
«Inferences on the ism structure around grb 980425 and grb 980425-sn1998bw association in the embh model».
In M. Novello, S. Perez Bergliaffa and R. Ruffini (eds.), *The Tenth Marcel Grossmann Meeting. On recent developments in theoretical and experimental*

- general relativity, gravitation and relativistic field theories*, p. 2451 (Singapore: World Scientific, 2005).
- FREIRE, P.C.C., RANSOM, S.M., BÉGIN, S., STAIRS, I.H., HESSELS, J.W.T., FREY, L.H. AND CAMILO, F.
«Eight New Millisecond Pulsars in NGC 6440 and NGC 6441».
Astrophysical Journal, **675**, pp. 670–682 (2008).
- FRENKEL, Y.I.
Zeit. fur Phys., **50**, p. 234 (1928).
- FRIEDMAN, J.L., IPSER, J.R. AND SORKIN, R.D.
«Turning-point method for axisymmetric stability of rotating relativistic stars».
Astrophysical Journal, **325**, pp. 722–724 (1988).
- FRIEDMAN, J.L., PARKER, L. AND IPSER, J.R.
«Rapidly rotating neutron star models».
Astrophysical Journal, **304**, pp. 115–139 (1986).
- GAENSLER, B.M., SLANE, P.O., GOTTHELF, E.V. AND VASISHT, G.
«Anomalous X-Ray Pulsars and Soft Gamma-Ray Repeaters in Supernova Remnants».
Astrophysical Journal, **559**, pp. 963–972 (2001).
- GALAMA, T.J., VREESWIJK, P.M., VAN PARADIJS, J., KOUVELIOTOU, C., AUGUSTEIJN, T., BÖHNHARDT, H., BREWER, J.P., DOUBLIER, V., GONZALEZ, J.F., LEIBUNDGUT, B. ET AL.
«An unusual supernova in the error box of the γ -ray burst of 25 april 1998».
Nature, **395**, pp. 670–672 (1998).
- GAMOW, G.
Constitution of Atomic Nuclei and Radioactivity (1931).
- GAMOW, G.
My world line: An informal autobiography. (1970).
- GAMOW, G. AND SCHOENBERG, M.
«Neutrino Theory of Stellar Collapse».
Physical Review, **59**, pp. 539–547 (1941).
- GARCIA-BERRO, E., HERNANZ, M., ISERN, J. AND MOCHKOVITCH, R.
«Properties of high-density binary mixtures and the age of the universe from white dwarf stars».
Nature, **333**, pp. 642–644 (1988).

- GARCIA-BERRO, E., ISERN, J., LOREN-AGUILAR, P., RUEDA, J.A. AND RUFFINI, R.
in preparation (2011).
- GARCÍA-BERRO, E., TORRES, S., ALTHAUS, L.G., RENEDO, I., LORÉN-AGUILAR, P., CÓRSICO, A.H., ROHRMANN, R.D., SALARIS, M. AND ISERN, J.
«A white dwarf cooling age of 8Gyr for NGC 6791 from physical separation processes».
Nature, **465**, pp. 194–196 (2010a).
- GARCÍA-BERRO, E., TORRES, S., ALTHAUS, L.G., RENEDO, I., LORÉN-AGUILAR, P., CÓRSICO, A.H., ROHRMANN, R.D., SALARIS, M. AND ISERN, J.
«A white dwarf cooling age of 8Gyr for NGC 6791 from physical separation processes».
Nature, **465**, pp. 194–196 (2010b).
- GELFAND, J.D. AND GAENSLER, B.M.
«The Compact X-Ray Source 1E 1547.0-5408 and the Radio Shell G327.24-0.13: A New Proposed Association between a Candidate Magnetar and a Candidate Supernova Remnant».
Astrophysical Journal, **667**, pp. 1111–1118 (2007).
- GIACCONI, R.
The dawn of x-ray astronomy. Nobel lecture. (2002).
- GIACCONI, R. AND RUFFINI, R. (eds.).
Physics and astrophysics of neutron stars and black holes (1978 Reprinted 2010).
- GINZBURG, V.L.
«The Magnetic Fields of Collapsing Masses and the Nature of Superstars».
Soviet Physics Doklady, **9**, pp. 329–+ (1964).
- GLENDENNING, N.K.
«First-order phase transitions with more than one conserved charge: Consequences for neutron stars».
Physical Review D, **46**, pp. 1274–1287 (1992).
- GLENDENNING, N.K.
«Phase transitions and crystalline structures in neutron star cores».
Physics Reports, **342**, pp. 393–447 (2001).
- GLENDENNING, N.K. AND PEI, S.
«Crystalline structure of the mixed confined-deconfined phase in neutron stars».
Physical Review C, **52**, pp. 2250–2253 (1995).

- GLENDENNING, N.K. AND SCHAFFNER-BIELICH, J.
«First order kaon condensate».
Physical Review C, **60(2)**, pp. 025803–+ (1999).
- GNEDIN, O.Y., YAKOVLEV, D.G. AND POTEKHIN, A.Y.
«Thermal relaxation in young neutron stars».
MNRAS, **324(3)**, pp. 725–736 (2001).
ISSN 0035-8711.
- GOLDSTEIN, A., PREECE, R.D., BRIGGS, M.S., VAN DER HORST, A.J.,
MCBREEN, S., KOUVELIOTOU, C., CONNAUGHTON, V., PACIASAS, W.S.,
MEEGAN, C.A., BHAT, P.N. ET AL.
«A New Derivation of GRB Jet Opening Angles from the Prompt Gamma-
Ray Emission».
arXiv:1101.2458 (2011).
- GOMBÁS, P.
Die Statistische Theorie des Atoms und Ihre Anwendungen (1949).
- GORDON, W.
«Über den Stoß zweier Punktladungen nach der Wellenmechanik».
Zeitschrift für Physik, **48**, pp. 180–191 (1928).
- GORIELY, S., BAUSWEIN, A. AND JANKA, H.T.
«r-process Nucleosynthesis in Dynamically Ejected Matter of Neutron Star
Mergers».
Astrophysical Journal, **738**, pp. L32+ (2011a).
- GORIELY, S., CHAMEL, N., JANKA, H.T. AND PEARSON, J.M.
«The decompression of the outer neutron star crust and r-process nucle-
osynthesis».
Astronomy & Astrophysics, **531**, pp. A78+ (2011b).
- GREENBERG, J.S. AND GREINER, W.
«Search for the sparking of the vacuum».
Physics Today, **35**, pp. 24–35 (1982).
- GREGORY, P.C. AND FAHLMAN, G.G.
«An extraordinary new celestial X-ray source».
Nature, **287**, pp. 805–+ (1980).
- GREINER, J., PEIMBERT, M., ESTABAN, C., KAUFER, A., JAUNSEN, A.,
SMOKE, J., KLOSE, S. AND REIMER, O.
«Redshift of GRB 030329.»
GCN Circ., **2020** (2003).

- GRIGORIAN, H., BLASCHKE, D. AND VOSKRESENSKY, D.
«Cooling of neutron stars with color superconducting quark cores».
Phys. Rev. C, **71(4)**, pp. 1–8 (2005).
ISSN 0556-2813.
- GUDMUNDSSON, E.H., PETHICK, C.J. AND EPSTEIN, R.I.
«Structure of neutron star envelopes».
ApJ, **272**, p. 286 (1983).
ISSN 0004-637X.
- GURSKY, H. AND RUFFINI, R. (eds.).
Neutron stars, black holes and binary X-ray sources; Proceedings of the Annual Meeting, San Francisco, Calif., February 28, 1974, volume 48 of *Astrophysics and Space Science Library* (1975).
- HAENSEL, P. AND PICHON, B.
«Experimental nuclear masses and the ground state of cold dense matter».
Astronomy & Astrophysics, **283**, pp. 313–318 (1994).
- HAENSEL, P., POTEKHIN, A.Y. AND YAKOVLEV, D.G. (eds.).
Neutron Stars 1 : Equation of State and Structure, volume 326 of *Astrophysics and Space Science Library* (2007).
- HAENSEL, P. AND ZDUNIK, J.L.
«Equation of state and structure of the crust of an accreting neutron star».
Astronomy & Astrophysics, **229**, pp. 117–122 (1990a).
- HAENSEL, P. AND ZDUNIK, J.L.
«Non-equilibrium processes in the crust of an accreting neutron star».
Astronomy & Astrophysics, **227**, pp. 431–436 (1990b).
- HAMADA, T. AND SALPETER, E.E.
«Models for Zero-Temperature Stars.»
Astrophysical Journal, **134**, pp. 683–+ (1961).
- HANSEN, B.M.S.
«Stellar Collisions and Pulsar Planets».
In M. M. Shara (ed.), *Stellar Collisions, Mergers and their Consequences*, volume 263 of *Astronomical Society of the Pacific Conference Series*, p. 221 (2002).
- HARRISON, B.K., THORNE, K.S., WAKANO, M. AND WHEELER, J.A.
Gravitation Theory and Gravitational Collapse (1965).
- HARRISON, B.K., WAKANO, M. AND WHEELER, J.A.
Onzieme Conseil de Physique de Solvay (1958).

HARTLE, J.B.

«Slowly Rotating Relativistic Stars. I. Equations of Structure».
Astrophysical Journal, **150**, pp. 1005–+ (1967a).

HARTLE, J.B.

«Slowly Rotating Relativistic Stars. I. Equations of Structure».
Astrophysical Journal, **150**, pp. 1005–+ (1967b).

HARTLE, J.B. AND THORNE, K.S.

«Slowly Rotating Relativistic Stars. II. Models for Neutron Stars and Supermassive Stars».
Astrophysical Journal, **153**, pp. 807–+ (1968a).

HARTLE, J.B. AND THORNE, K.S.

«Slowly Rotating Relativistic Stars. II. Models for Neutron Stars and Supermassive Stars».
Astrophysical Journal, **153**, pp. 807–+ (1968b).

HEBELER, K., LATTIMER, J.M., PETHICK, C.J. AND SCHWENK, A.

«Constraints on Neutron Star Radii Based on Chiral Effective Field Theory Interactions».
Physical Review Letters, **105(16)**, 161102 (2010).

HEINKE, C.O., RYBICKI, G.B., NARAYAN, R. AND GRINDLAY, J.E.

«A Hydrogen Atmosphere Spectral Model Applied to the Neutron Star X7 in the Globular Cluster 47 Tucanae».
Astrophysical Journal, **644**, pp. 1090–1103 (2006).

HEISENBERG, W. AND EULER, H.

«Folgerungen aus der Diracschen Theorie des Positrons».
Zeitschrift für Physik, **98**, pp. 714–732 (1936).

HESELS, J.W.T., RANSOM, S.M., STAIRS, I.H., FREIRE, P.C.C., KASPI, V.M. AND CAMILO, F.

«A Radio Pulsar Spinning at 716 Hz».
Science, **311**, pp. 1901–1904 (2006).

HEWISH, A.

Pulsars and High Density Physics. Nobel lecture. (1974).

HIRATA, D., TOKI, H. AND TANIHATA, I.

«Relativistic mean-field theory on the xenon, cesium and barium isotopes».
Nuclear Physics A, **589**, pp. 239–248 (1995).

HOYLE, F. AND FOWLER, W.A.

«Nucleosynthesis in Supernovae.»
Astrophysical Journal, **132**, pp. 565–+ (1960).

- HUGHES, V.A., HARTEN, R.H. AND VAN DEN BERGH, S.
«A new supernova remnant G109.2-1.0».
Astrophysical Journal, **246**, pp. L127–L131 (1981).
- HULLEMAN, F., VAN KERKWIJK, M.H. AND KULKARNI, S.R.
«An optical counterpart to the anomalous X-ray pulsar 4U0142+61».
Nature, **408**, pp. 689–692 (2000).
- HUND, F.
Erg. d. exacten Natwis., **15**, p. 189 (1936).
- HURLEY, K., BOGGS, S.E., SMITH, D.M., DUNCAN, R.C., LIN, R.,
ZOGLAUER, A., KRUCKER, S., HURFORD, G., HUDSON, H., WIGGER, C.
ET AL.
«An exceptionally bright flare from SGR 1806-20 and the origins of short-
duration γ -ray bursts».
Nature, **434**, pp. 1098–1103 (2005).
- IBEN, JR., I. AND TUTUKOV, A.V.
«Supernovae of type I as end products of the evolution of binaries with
components of moderate initial mass (M not greater than about 9 solar
masses)».
Astrophysical Journal Supplement Series, **54**, pp. 335–372 (1984).
- IKHSANOV, N.R. AND BESKROVNAYA, N.G.
«AE Aquarii: The first white dwarf in the family of spin-powered pulsars».
arXiv:0809.1169 (2008).
- IKHSANOV, N.R. AND BIERMANN, P.L.
«High-energy emission of fast rotating white dwarfs».
Astronomy & Astrophysics, **445**, pp. 305–312 (2006).
- IMMLER, S., WILSON, A.S. AND TERASHIMA, Y.
«X-Ray Emission from the Type Ic Supernova 1994I Observed with Chan-
dra».
ApJ, **573**, pp. L27–L30 (2002).
- IOSILEVSKIY, I.L.
«Plasma polarization in massive astrophysical objects».
Journal of Physics A Mathematical General, **42(21)**, p. 214008 (2009).
- ISRAEL, G.L., CAMPANA, S., DALL’OSSO, S., MUNO, M.P., CUMMINGS, J.,
PERNA, R. AND STELLA, L.
«The Post-Burst Awakening of the Anomalous X-Ray Pulsar in Westerlund
1».
Astrophysical Journal, **664**, pp. 448–457 (2007).

- ISRAEL, G.L., STELLA, L., ANGELINI, L., WHITE, N.E., KALLMAN, T.R., GIOMMI, P. AND TREVES, A.
«The Discovery of 13 Second X-Ray Pulsations from the Hydrogen-depleted Subdwarf O6 Star Binary HD 49798».
Astrophysical Journal, **474**, pp. L53+ (1997).
- ITOH, K., OKADA, S., ISHIDA, M. AND KUNIEDA, H.
«Density Diagnostics of the Hot Plasma in AE Aquarii with XMM-Newton».
Astrophysical Journal, **639**, pp. 397–404 (2006).
- ITOH, N.
«Hydrostatic Equilibrium of Hypothetical Quark Stars».
Progress of Theoretical Physics, **44**, pp. 291–292 (1970).
- IWAMOTO, K., MAZZALI, P.A., NOMOTO, K., UMEDA, H., NAKAMURA, T., PATAT, F., DANZIGER, I.J., YOUNG, T.R., SUZUKI, T., SHIGEYAMA, T. ET AL.
«A hypernova model for the supernova associated with the γ -ray burst of 25 april 1998».
Nature, **395**, pp. 672–674 (1998).
- IZZO, L., RUFFINI, R., PENACCHIONI, A.V., BIANCO, C.L., CAITO, L., CHAKRABARTI, S.K., RUEDA, J.A., NANDI, A. AND PATRICELLI, B.
Astronomy & Astrophysics, submitted (2011).
- JUDGE, P.G., SOLOMON, S.C. AND AYRES, T.R.
«An Estimate of the Sun's ROSAT-PSPC X-Ray Luminosities Using SNOE-SXP Measurements».
Astrophysical Journal, **593**, pp. 534–548 (2003).
- KANEKO, Y., RAMIREZ-RUIZ, E., GRANOT, J., KOUVELIOTOU, C., WOOSLEY, S.E., PATEL, S.K., ROL, E., ZAND, J.J.M.I., VAN DER HORST, A.J., WIJERS, R.A.M.J. ET AL.
«Prompt and afterglow emission properties of gamma-ray bursts with spectroscopically identified supernovae».
ApJ, **654**, pp. 385–402 (2007).
- KASEN, D. AND BILDSTEN, L.
«Supernova Light Curves Powered by Young Magnetars».
Astrophysical Journal, **717**, pp. 245–249 (2010).
- KASHIYAMA, K., IOKA, K. AND KAWANAKA, N.
«White dwarf pulsars as possible cosmic ray electron-positron factories».
Physical Review D, **83(2)**, pp. 023002+ (2011).

- KASPI, V.M., GAVRIIL, F.P., WOODS, P.M., JENSEN, J.B., ROBERTS, M.S.E. AND CHAKRABARTY, D.
«A Major Soft Gamma Repeater-like Outburst and Rotation Glitch in the No-longer-so-anomalous X-Ray Pulsar 1E 2259+586».
Astrophysical Journal, **588**, pp. L93–L96 (2003).
- KATZ, J.I.
«The Eddington Limit and Soft Gamma Repeaters».
Astrophysical Journal, **463**, p. 305 (1996).
- KEPLER, S.O., KLEINMAN, S.J., PELISOLI, I., PEÇANHA, V., DIAZ, M., KOESTER, D., CASTANHEIRA, B.G. AND NITTA, A.
«Magnetic White Dwarfs in the SDSS and Estimating the Mean Mass of Normal DA and DB WDs».
In K. Werner & T. Rauch (ed.), *American Institute of Physics Conference Series*, volume 1273 of *American Institute of Physics Conference Series*, pp. 19–24 (2010).
- KETTNER, C., WEBER, F., WEIGEL, M.K. AND GLENDENNING, N.K.
«Structure and stability of strange and charm stars at finite temperatures».
Physical Review D, **51**, pp. 1440–1457 (1995).
- KLEIN, O.
«On the Thermodynamical Equilibrium of Fluids in Gravitational Fields».
Reviews of Modern Physics, **21**, pp. 531–533 (1949).
- KLEINERT, H., RUFFINI, R. AND XUE, S.
«Electron-positron pair production in space- or time-dependent electric fields».
Physical Review D, **78(2)**, pp. 025011–+ (2008).
- KODAMA, T. AND YAMADA, M.
«Theory of Superdense Stars».
Progress of Theoretical Physics, **47**, pp. 444–459 (1972).
- KONACKI, M., LEWANDOWSKI, W., WOLSZCZAN, A., DOROSHENKO, O. AND KRAMER, M.
«Are There Planets around the Pulsar PSR B0329+54?»
Astrophysical Journal, **519**, pp. L81–L84 (1999).
- KONACKI, M. AND WOLSZCZAN, A.
«Masses and Orbital Inclinations of Planets in the PSR B1257+12 System».
Astrophysical Journal, **591**, pp. L147–L150 (2003).
- KOUVELIOTOU, C., WOOSLEY, S.E., PATEL, S.K., LEVAN, A., BLANDFORD, R., RAMIREZ-RUIZ, E., WIJERS, R.A.M.J., WEISSKOPF, M.C., TENNANT, A., PIAN, E. ET AL.

- «Chandra observations of the x-ray environs of sn 1998bw/grb 980425». *ApJ*, **608**, pp. 872–882 (2004).
- KRAMER, M.
private communication (2010).
- KUBIS, S.
«Nuclear symmetry energy and stability of matter in neutron stars». *Physical Review C*, **76(2)**, 025801 (2007).
- KUIPER, L. AND HERMSEN, W.
«High-energy characteristics of the schizophrenic pulsar PSR J1846-0258 in Kes 75. Multi-year RXTE and INTEGRAL observations crossing the magnetar-like outburst». *Astronomy & Astrophysics*, **501**, pp. 1031–1046 (2009).
- KÜLEBI, B., JORDAN, S., EUCHNER, F., GAENSICKE, B.T. AND HIRSCH, H.
«Magnetic fields in white dwarfs (Kuelebi+, 2009)». *VizieR Online Data Catalog*, **350**, pp. 61341–+ (2010a).
- KÜLEBI, B., JORDAN, S., EUCHNER, F., GÄNSICKE, B.T. AND HIRSCH, H.
«Analysis of hydrogen-rich magnetic white dwarfs detected in the Sloan Digital Sky Survey». *Astronomy & Astrophysics*, **506**, pp. 1341–1350 (2009).
- KÜLEBI, B., JORDAN, S., NELAN, E., BASTIAN, U. AND ALTMANN, M.
«Constraints on the origin of the massive, hot, and rapidly rotating magnetic white dwarf RE J 0317-853 from an HST parallax measurement». *Astronomy & Astrophysics*, **524**, pp. A36+ (2010b).
- KUMAR, H.S. AND SAFI-HARB, S.
«Variability of the High Magnetic Field X-Ray Pulsar PSR J1846-0258 Associated with the Supernova Remnant Kes 75 as Revealed by the Chandra X-Ray Observatory». *Astrophysical Journal*, **678**, pp. L43–L46 (2008).
- LALAZISSIS, G.A., KÖNIG, J. AND RING, P.
«New parametrization for the Lagrangian density of relativistic mean field theory». *Physical Review C*, **55**, pp. 540–543 (1997).
- LANDAU, L.D.
«On the theory of stars». *Phys. Z. Sowjetunion*, **1**, pp. 285–288 (1932).
- LANDAU, L.D.
Nature, **19**, p. 333 (1938).

- LANDAU, L.D. AND LIFSHITZ, E.M.
Statistical physics. Part1 (Pergamon Press, Oxford, 1980).
- LATTIMER, J.M. AND PRAKASH, M.
«The Physics of Neutron Stars».
Science, **304**, pp. 536–542 (2004).
- LEE, T.D. AND PANG, Y.
«Fermion soliton stars and black holes».
Physical Review D, **35**, pp. 3678–3694 (1987).
- LEE, T.D. AND WICK, G.C.
«Vacuum stability and vacuum excitation in a spin-0 field theory».
Physical Review D, **9**, pp. 2291–2316 (1974).
- LEVAN, A.J., WYNN, G.A., CHAPMAN, R., DAVIES, M.B., KING, A.R.,
PRIDDEY, R.S. AND TANVIR, N.R.
«Short gamma-ray bursts in old populations: magnetars from white
dwarf-white dwarf mergers».
Monthly Notices of the Royal Astronomical Society, **368**, pp. L1–L5 (2006).
- LIEB, E.H.
«Thomas-fermi and related theories of atoms and molecules».
Reviews of Modern Physics, **53**, pp. 603–641 (1981).
- LIEB, E.H. AND SIMON, B.
«Thomas-Fermi Theory Revisited».
Physical Review Letters, **31**, pp. 681–683 (1973).
- LIEBERT, J., SCHMIDT, G.D., GREEN, R.F., STOCKMAN, H.S. AND MCGRAW,
J.T.
«Two hot, low-field magnetic DA white dwarfs».
Astrophysical Journal, **264**, pp. 262–272 (1983).
- LOAN, D.T., TAN, N.H., KHOA, D.T. AND MARGUERON, J.
«Equation of state of neutron star matter, and the nuclear symmetry en-
ergy».
Physical Review C, **83(6)**, 065809 (2011).
- LUNDQVIST, S. AND MARCH, N.H.
Theory of the Inhomogeneous Electro Gas (1983).
- LYUTIKOV, M. AND GAVRIIL, F.P.
«Resonant cyclotron scattering and Comptonization in neutron star mag-
netospheres».
Monthly Notices of the Royal Astronomical Society, **368**, pp. 690–706 (2006).

- MANCHESTER, R.N. AND TAYLOR, J.H.
Pulsars (1977).
- MARCH, N.H.
«The Thomas-Fermi approximation in quantum mechanics».
Advances in Physics, **6**, pp. 1–101 (1957).
- MARSH, J.S.
«Magnetic and electric fields of rotating charge distributions».
American Journal of Physics, **50**, pp. 51–53 (1982).
- MAZETS, E.P., GOLENTSKII, S.V., ILINSKII, V.N., APTEKAR, R.L. AND GURYAN, I.A.
«Observations of a flaring X-ray pulsar in Dorado».
Nature, **282**, pp. 587–589 (1979).
- MAZZALI, P.
talk presented at the congress “Swift and GRBs: unveiling the relativistic universe”, Venice, Italy, June 5-9 (2006).
- MEINTJES, P.J., DE JAGER, C.O. AND ET AL.
«Persistent Optical-like Pulsed TeV γ -Ray Emission from AE Aquarii».
In *International Cosmic Ray Conference*, volume 1 of *International Cosmic Ray Conference*, pp. 338–+ (1993).
- MEINTJES, P.J., RAUBENHEIMER, B.C., DE JAGER, O.C., BRINK, C., NEL, H.I., NORTH, A.R., VAN URK, G. AND VISSER, B.
«AE Aquarii - an emitter of pulsed TeV gamma rays resembling optical emission during flares».
Astrophysical Journal, **401**, pp. 325–336 (1992).
- MEREGHETTI, S.
«The strongest cosmic magnets: soft gamma-ray repeaters and anomalous X-ray pulsars».
Astronomy & Astrophysics Review, **15**, pp. 225–287 (2008).
- MEREGHETTI, S., LA PALOMBARA, N., TIENGO, A., PIZZOLATO, F., ESPOSITO, P., WOUTD, P.A., ISRAEL, G.L. AND STELLA, L.
«X-Ray and Optical Observations of the Unique Binary System HD 49798/RX J0648.0-4418».
Astrophysical Journal, **737**, 51 (2011).
- MEREGHETTI, S., TIENGO, A., ESPOSITO, P., GÖTZ, D., STELLA, L., ISRAEL, G.L., REA, N., FEROCI, M., TUROLLO, R. AND ZANE, S.
«An XMM-Newton View of the Soft Gamma Repeater SGR 1806-20: Long-Term Variability in the Pre-Giant Flare Epoch».
Astrophysical Journal, **628**, pp. 938–945 (2005).

- MEREGHETTI, S., TIENGO, A., ESPOSITO, P., LA PALOMBARA, N., ISRAEL, G.L. AND STELLA, L.
«An Ultramassive, Fast-Spinning White Dwarf in a Peculiar Binary System».
Science, **325**, pp. 1222– (2009).
- MEZZACAPPA, A.
«Open Issues in Core Collapse Supernova Theory: An Overview».
In A. Mezzacappa & G. M. Fuller (ed.), *Open Issues in Core Collapse Supernova Theory*, pp. 3–+ (2005).
- MICHEL, F.C.
«Radio pulsar disk electrodynamics».
Astrophysical Journal, **266**, pp. 188–200 (1983).
- MICHEL, F.C. AND DESSLER, A.J.
«Pulsar disk systems».
Astrophysical Journal, **251**, pp. 654–664 (1981).
- MIGDAL, A.B., POPOV, V.S. AND VOSKRESENSKIĬ, D.N.
«The vacuum charge distribution near super-charged nuclei».
Soviet Journal of Experimental and Theoretical Physics, **45**, pp. 436–+ (1977).
- MIGDAL, A.B., VOSKRESENSKIĬ, D.N. AND POPOV, V.S.
«Distribution of vacuum charge near supercharged nuclei».
Soviet Journal of Experimental and Theoretical Physics Letters, **24**, pp. 163–+ (1976).
- MILNE, E.A.
«The analysis of stellar structure».
Monthly Notices of the Royal Astronomical Society, **91**, pp. 4–55 (1930).
- MIRABAL, N., HALPERN, J.P., AN, D., THORSTENSEN, J.R. AND TERNDRUP, D.M.
«Grb 060218/sn 2006aj: A gamma-ray burst and prompt supernova at $z = 0.0335$ ».
ApJ, **643**, pp. L99–L102 (2006).
- MORINI, M., ROBBA, N.R., SMITH, A. AND VAN DER KLIS, M.
«EXOSAT observations of the supernova remnant G109.1-1.0 and the X-ray pulsar 1E 2259+586».
Astrophysical Journal, **333**, pp. 777–787 (1988).
- MOTT, N.F.
«The Electrical Resistance of Dilute Solid Solutions».
Proceedings of the Cambridge Philosophical Society, **32**, p. 281 (1936).

- MÜLLER, B., PEITZ, H., RAFELSKI, J. AND GREINER, W.
«Solution of the Dirac Equation for Strong External Fields».
Physical Review Letters, **28**, pp. 1235–1238 (1972).
- MÜLLER, B. AND RAFELSKI, J.
«Stabilization of the Charged Vacuum Created by Very Strong Electrical Fields in Nuclear Matter».
Physical Review Letters, **34**, pp. 349–352 (1975).
- MÜTHER, H., PRAKASH, M. AND AINSWORTH, T.L.
«The nuclear symmetry energy in relativistic Brueckner-Hartree-Fock calculations».
Physics Letters B, **199**, pp. 469–474 (1987).
- MYERS, W.
«Nuclear masses and deformations».
Nuclear Physics A, **81**, pp. 1–60 (1966).
- NALEŻYTY, M. AND MADEJ, J.
«A catalogue of isolated massive white dwarfs. Mass distribution of massive star».
Astronomy & Astrophysics, **420**, pp. 507–513 (2004).
- NEGREIROS, R., DEXHEIMER, V. AND SCHRAMM, S.
«Modeling hybrid stars with an SU(3) nonlinear σ model».
Phys. Rev. C, **82(3)**, pp. 1–9 (2010).
ISSN 0556-2813.
- NG, C., KASPI, V.M., DIB, R., OLAUSEN, S.A., SCHOLZ, P., GEVER, T., OZEL, F., GAVRIIL, F.P. AND WOODS, P.M.
«Chandra and RXTE Observations of 1E 1547.0-5408: Comparing the 2008 and 2009 Outbursts».
arXiv:1008.1165 (2010).
- OLSON, E. AND BAILYN, M.
«Internal structure of multicomponent static spherical gravitating fluids».
Physical Review D, **12**, pp. 3030–3036 (1975).
- OLSON, E. AND BAILYN, M.
«Charge effects in a static, spherically symmetric, gravitating fluid».
Physical Review D, **13**, pp. 2204–2211 (1976).
- OLSON, E. AND BAILYN, M.
«Internal structure of multicomponent fluids».
Physical Review D, **18**, pp. 2175–2179 (1978).

- OPPENHEIMER, J.R. AND VOLKOFF, G.M.
«On Massive Neutron Cores».
Physical Review, **55**, pp. 374–381 (1939).
- OSTRIKER, J.P. AND BODENHEIMER, P.
«Rapidly Rotating Stars. II. Massive White Dwarfs».
Astrophysical Journal, **151**, pp. 1089–+ (1968).
- PACZYNSKI, B.
«Evolution of cataclysmic binaries».
In D. Q. Lamb & J. Patterson (ed.), *Cataclysmic Variables and Low-Mass X-ray Binaries*, volume 113 of *Astrophysics and Space Science Library*, pp. 1–12 (1985).
- PACZYNSKI, B.
«X-ray pulsar 1E 2259 + 586 - A merged white dwarf with a 7 second rotation period?»
Astrophysical Journal, **365**, pp. L9–L12 (1990).
- PACZYNSKI, B.
«GB 790305 as a very strongly magnetized neutron star».
Acta Astronomica, **42**, pp. 145–153 (1992).
- PAGE, D., GEPPERT, U. AND WEBER, F.
«The cooling of compact stars».
Nuclear Physics A, **777**, pp. 497–530 (2006).
ISSN 03759474.
- PAGE, D., LATTIMER, J., PRAKASH, M. AND STEINER, A.W.
«Minimal Cooling of Neutron Stars: A New Paradigm».
ApJSS, **155(2)**, pp. 623–650 (2004).
ISSN 0067-0049.
- PAGE, D., LATTIMER, J., PRAKASH, M. AND STEINER, A.W.
«Neutrino Emission From Cooper Pairs and Minimal Cooling of Neutron Stars».
ApJ, **707(2)**, pp. 1131–1140 (2009).
ISSN 0004-637X.
- PAGE, D., PRAKASH, M., LATTIMER, J.M. AND STEINER, A.W.
«Rapid Cooling of the Neutron Star in Cassiopeia A Triggered by Neutron Superfluidity in Dense Matter».
Physical Review Letters, **106(8)**, pp. 081101–+ (2011).
- PAKMOR, R., KROMER, M., RÖPKE, F.K., SIM, S.A., RUITER, A.J. AND HILLEBRANDT, W.

- «Sub-luminous type Ia supernovae from the mergers of equal-mass white dwarfs with mass $0.9M_{\odot}$ ».
Nature, **463**, pp. 61–64 (2010).
- PARKER, E.N.
«Acceleration of Cosmic Rays in Solar Flares».
Physical Review, **107**, pp. 830–836 (1957).
- PATNAUDE, D.J., LOEB, A. AND JONES, C.
«Evidence for a Black Hole Remnant in the Type III Supernova 1979C».
arXiv:0912.1571 (2009).
- PATNAUDE, D., LOEB, A. AND JONES, C.
«Evidence for a possible black hole remnant in the Type III Supernova 1979C».
New Astronomy, **16(3)**, pp. 187–190 (2011).
ISSN 13841076.
- PATRICELLI, B., ROTONDO, M. AND RUFFINI, R.
«On the Charge to Mass Ratio of Neutron Cores and Heavy Nuclei».
In C. L. Bianco & S.-S. Xue (ed.), *Relativistic Astrophysics*, volume 966 of *American Institute of Physics Conference Series*, pp. 143–146 (2008).
- PERES, G., ORLANDO, S., REALE, F., ROSNER, R. AND HUDSON, H.
«The Sun as an X-Ray Star. II. Using the Yohkoh/Soft X-Ray Telescope-derived Solar Emission Measure versus Temperature to Interpret Stellar X-Ray Observations».
Astrophysical Journal, **528**, pp. 537–551 (2000).
- PERLMUTTER, S., ALDERING, G., GOLDHABER, G., KNOP, R.A., NUGENT, P., CASTRO, P.G., DEUSTUA, S., FABBRO, S., GOOBAR, A., GROOM, D.E. ET AL.
«Measurements of Omega and Lambda from 42 High-Redshift Supernovae».
Astrophysical Journal, **517**, pp. 565–586 (1999).
- PHILLIPS, M.M.
«The absolute magnitudes of Type IA supernovae».
Astrophys. J. Lett., **413**, pp. L105–L108 (1993).
- PIAN, E., AMATI, L., ANTONELLI, L.A., BUTLER, R.C., COSTA, E., CUSUMANO, G., DANZIGER, J., FEROCI, M., FIORE, F., FRONTERA, F. ET AL.
«BeppoSAX observations of grb 980425: Detection of the prompt event and monitoring of the error box».
ApJ, **536**, pp. 778–787 (2000).

- PIAN, E. ET AL.
Proposal for Chandra Observations: The X-Ray Remnant of XRF100316D/SN2010BH (2011).
- PIEPER, W. AND GREINER, W.
«Interior electron shells in superheavy nuclei».
Zeitschrift fur Physik, **218**, pp. 327–340 (1969).
- POPOV, V.
«From super-charged nuclei to massive nuclear density cores».
In R. Ruffini & G. Vereshchagin (ed.), *American Institute of Physics Conference Series*, volume 1205 of *American Institute of Physics Conference Series*, pp. 127–131 (2010).
- POPOV, V.S.
«Electron Energy Levels at $Z \approx 137$ ».
Soviet Journal of Experimental and Theoretical Physics Letters, **11**, pp. 162–+ (1970).
- POPOV, V.S.
«On the Properties of the Discrete Spectrum for Z Close to 137».
Soviet Journal of Experimental and Theoretical Physics, **33**, pp. 665–+ (1971a).
- POPOV, V.S.
«Position Production in a Coulomb Field with $Z \approx 137$ ».
Soviet Journal of Experimental and Theoretical Physics, **32**, pp. 526–+ (1971b).
- POTEKHIN, A.Y., CHABRIER, G. AND ROGERS, F.J.
«Equation of state of classical Coulomb plasma mixtures».
Physical Review E, **79(1)**, pp. 016411–+ (2009).
- POTEKHIN, A.Y., CHABRIER, G. AND YAKOVLEV, D.G.
«Internal temperatures and cooling of neutron stars with accreted envelopes».
A&A, **323**, pp. 415–428 (1997).
- PRAKASH, M., LATTIMER, J., PONS, J., STEINER, A. AND REDDY, S.
«Evolution of a neutron star from its birth to old age».
Physics of Neutron Star Interiors, pp. 364–423 (2001).
- PREPARATA, G., RUFFINI, R. AND XUE, S.
«The dyadosphere of black holes and gamma-ray bursts».
Astronomy & Astrophysics, **338**, pp. L87–L90 (1998).
- PROCHASKA, J.X., BLOOM, J.S., CHEN, H.W., HURLEY, K.C., MELBOURNE, J., DRESSLER, A., GRAHAM, J.R., OSIP, D.J. AND VACCA, W.D.

- «The host galaxy of grb 031203: Implications of its low metallicity, low redshift, and starburst nature».
ApJ, **611**, pp. 200–207 (2004).
- RAFELSKI, J., FULCHER, L.P. AND KLEIN, A.
«Fermions and bosons interacting with arbitrarily strong external fields».
Physics Reports, **38**, pp. 227–361 (1978).
- REA, N., ESPOSITO, P., TUROLLA, R., ISRAEL, G.L., ZANE, S., STELLA, L., MEREGHETTI, S., TIENGO, A., GÖTZ, D., GÖĞÜŞ, E. ET AL.
«A Low-Magnetic-Field Soft Gamma Repeater».
Science, **330**, pp. 944– (2010).
- REA, N., JONKER, P.G., NELEMANS, G., PONS, J.A., KASLIWAL, M.M., KULKARNI, S.R. AND WIJNANDS, R.
«The X-ray quiescence of Swift J195509.6+261406 (GRB 070610): an optical bursting X-ray binary?»
arXiv:1101.3483 (2011).
- REA, N., ZANE, S., TUROLLA, R., LYUTIKOV, M. AND GÖTZ, D.
«Resonant Cyclotron Scattering in Magnetars' Emission».
Astrophysical Journal, **686**, pp. 1245–1260 (2008).
- REISENEGGER, A.
«Chemical Equilibrium and Stable Stratification of a Multicomponent Fluid: Thermodynamics and Application to Neutron Stars».
Astrophysical Journal, **550**, pp. 860–862 (2001).
- REISENEGGER, A.
«Magnetic field evolution in neutron stars».
Astronomische Nachrichten, **328**, pp. 1173–+ (2007).
- REISENEGGER, A., BENGURIA, R., PRIETO, J.P., ARAYA, P.A. AND LAI, D.
«Hall drift of axisymmetric magnetic fields in solid neutron-star matter».
Astronomy & Astrophysics, **472**, pp. 233–240 (2007).
- RIESS, A.G., FILIPPENKO, A.V., CHALLIS, P., CLOCCHIATTI, A., DIERCKS, A., GARNAVICH, P.M., GILLILAND, R.L., HOGAN, C.J., JHA, S., KIRSHNER, R.P. ET AL.
«Observational Evidence from Supernovae for an Accelerating Universe and a Cosmological Constant».
Astronomical Journal, **116**, pp. 1009–1038 (1998).
- RIESS, A.G., STROLGER, L., TONRY, J., CASERTANO, S., FERGUSON, H.C., MOBASHER, B., CHALLIS, P., FILIPPENKO, A.V., JHA, S., LI, W. ET AL.

- «Type Ia Supernova Discoveries at $z \lesssim 1$ from the Hubble Space Telescope: Evidence for Past Deceleration and Constraints on Dark Energy Evolution».
Astrophysical Journal, **607**, pp. 665–687 (2004).
- RING, P.
«Relativistic mean field theory in finite nuclei».
Progress in Particle and Nuclear Physics, **37**, pp. 193–263 (1996).
- ROMANI, R.W. AND WATTERS, K.P.
«Constraining Pulsar Magnetosphere Geometry with γ -ray Light Curves».
Astrophysical Journal, **714**, pp. 810–824 (2010).
- ROSSELAND, S.
«Electrical state of a star».
Monthly Notices of the Royal Astronomical Society, **84**, pp. 720–728 (1924).
- ROTONDO, M., RUEDA, J.A., RUFFINI, R. AND XUE, S.S.
«On the equilibrium of self-gravitating neutrons, protons and electrons in β -equilibrium».
ArXiv: 1107.2777 (2011a).
- ROTONDO, M., RUEDA, J.A., RUFFINI, R. AND XUE, S.S.
«Relativistic Feynman-Metropolis-Teller theory for white dwarfs in general relativity».
Physical Review D, **84(8)**, 084007 (2011b).
- ROTONDO, M., RUEDA, J.A., RUFFINI, R. AND XUE, S.S.
«Relativistic Thomas-Fermi treatment of compressed atoms and compressed nuclear matter cores of stellar dimensions».
Physical Review C, **83(4)**, 045805 (2011c).
- ROTONDO, M., RUEDA, J.A., RUFFINI, R. AND XUE, S.S.
«The self-consistent general relativistic solution for a system of degenerate neutrons, protons and electrons in β -equilibrium».
Physics Letters B, **701**, pp. 667–671 (2011d).
- ROTONDO, M., RUFFINI, R., XUE, S.S. AND POPOV, V.
«On Gravitationally and Electrodynamically Bound Nuclear Matter Cores of Stellar Dimensions».
International Journal of Modern Physics D, **20**, pp. 1995–2002 (2011e).
- ROXBURGH, I.W. AND DURNEY, B.R.
«Structure, Oscillations and Stability of Rotating White Dwarfs».
Zeitschrift für Astrophysik, **64**, pp. 504–+ (1966).

RUDERMAN, M.

«Pulsars: Structure and Dynamics».

Annual Review of Astronomy and Astrophysics, **10**, pp. 427–+ (1972).

RUDERMAN, M.

«Spin-Driven Changes in Neutron Star Magnetic Fields».

Journal of Astrophysics and Astronomy, **16**, pp. 207–+ (1995).

RUEDA, J.A., ROTONDO, M., RUFFINI, R. AND XUE, S.S.

«A self-consistent approach to neutron stars».

Journal of Korean Physical Society, **57**, pp. 560–+ (2010a).

RUEDA, J.A., RUFFINI, R. AND XUE, S..

«The Klein first integrals in an equilibrium system with electromagnetic, weak, strong and gravitational interactions».

Nuclear Physics A, in press; *arXiv:1104.4062* (2011).

RUEDA, J.A., RUFFINI, R. AND XUE, S.S.

«On the electrostatic structure of neutron stars».

In R. Ruffini & G. Vereshchagin (ed.), *American Institute of Physics Conference Series*, volume 1205 of *American Institute of Physics Conference Series*, pp. 143–147 (2010b).

RUFFINI, R.

«On the energetics of Black Holes».

In C. De Witt, B. S. De Witt (ed.), *Black Holes - Les astres occlus* (1972).

RUFFINI, R.

«On the energetics of black holes.»

In A. Giannaras (ed.), *Black Holes (Les Astres Occlus)*, pp. 451–546 (1973).

RUFFINI, R.

«Beyond the Critical Mass: The Dyadosphere of Black Holes».

In H. Sato & N. Sugiyama (ed.), *Frontiers Science Series 23: Black Holes and High Energy Astrophysics*, pp. 167–+ (1998).

RUFFINI, R.

«On Gamma-Ray Bursts».

In H. Kleinert, R. T. Jantzen, R. Ruffini (ed.), *Proceedings of the Eleventh Marcel Grossmann Meeting on General Relativity, Singapore, World Scientific, 2008* (2008a).

RUFFINI, R.

«The Role of Thomas-Fermi Approach in Neutron Star Matter».

In *Path Integrals - New Trends and Perspectives*, pp. 207–218 (2008b).

- RUFFINI, R.
«The Role of Thomas-Fermi Approach in Neutron Star Matter».
In *Path Integrals - New Trends and Perspectives*, pp. 207–218 (2008c).
- RUFFINI, R.
«Title of the Talk».
In T. Damour and R. Ruffini (ed.), *Proceedings of the 12th Marcel Grossmann Meeting on General Relativity*, World Scientific, Singapore (2009).
- RUFFINI, R., BERNARDINI, M.G., BIANCO, C.L., CAITO, L., CHARDONNET, P., DAINOTTI, M.G., FRASCHETTI, F., GUIDA, R., ROTONDO, M., VERESHCHAGIN, G. ET AL.
«The Blackholic energy and the canonical Gamma-Ray Burst».
In M. Novello & S. E. Perez Bergliaffa (ed.), *XIIIth Brazilian School of Cosmology and Gravitation*, volume 910 of *American Institute of Physics Conference Series*, pp. 55–217 (2007a).
- RUFFINI, R., BERNARDINI, M.G., BIANCO, C.L., CAITO, L., CHARDONNET, P., DAINOTTI, M.G., FRASCHETTI, F., GUIDA, R., VERESHCHAGIN, G. AND XUE, S.S.
«The role of grb 031203 in clarifying the astrophysical grb scenario».
In S. Grebenev, R. Sunyaev, C. Winkler, A. Parmar and L. Ouwehand (eds.), *The 6th Integral Workshop - The Obscured Universe*, volume SP-622 of *ESA Special Publication*, p. 561 (2007b).
- RUFFINI, R., BERNARDINI, M.G., BIANCO, C.L., CHARDONNET, P., FRASCHETTI, F. AND XUE, S.S.
«Grb 980425, sn1998bw and the embh model».
Advances in Space Research, **34**, pp. 2715–2722 (2004).
- RUFFINI, R., BERNARDINI, M.G., BIANCO, C.L., CHARDONNET, P., FRASCHETTI, F. AND XUE, S.
«Theoretical Interpretation of GRB 031203 and URCA-3».
In B. Aschenbach, V. Burwitz, G. Hasinger and B. Leibundgut (eds.), *Relativistic Astrophysics Legacy and Cosmology - Einstein's Legacy*, p. 399 (2008).
- RUFFINI, R., BERNARDINI, M.G., BIANCO, C.L., VITAGLIANO, L., XUE, S.S., CHARDONNET, P., FRASCHETTI, F. AND GURZADYAN, V.
«Black hole physics and astrophysics: The grb-supernova connection and urca-1 - urca-2».
In M. Novello, S. Perez Bergliaffa and R. Ruffini (eds.), *The Tenth Marcel Grossmann Meeting. On recent developments in theoretical and experimental general relativity, gravitation and relativistic field theories*, p. 369 (Singapore: World Scientific, 2005).

- RUFFINI, R., BIANCO, C.L., CHARDONNET, P., FRASCHETTI, F. AND XUE, S.S.
«On a possible gamma-ray burst-supernova time sequence».
ApJ, **555**, pp. L117–L120 (2001).
- RUFFINI, R. AND BONAZZOLA, S.
«Systems of Self-Gravitating Particles in General Relativity and the Concept of an Equation of State».
Physical Review, **187**, pp. 1767–1783 (1969).
- RUFFINI, R., CHAKRABARTI, S.K. AND IZZO, L.
«Possible multiple components in a GRB: the case of GRB 090618».
Submitted to Adv. Sp. Res. (2010a).
- RUFFINI, R., IZZO, L., PENACCHIONI, A.V., BIANCO, C.L., CAITO, L., CHAKRABARTI, S.K. AND NANDI, A.
«GRB 090618: a possible case of multiple GRB?»
PoS(Texas2010), p. 101 (2011).
- RUFFINI, R., ROTONDO, M. AND XUE, S.
«Electrodynamics for Nuclear Matter in Bulk».
International Journal of Modern Physics D, **16**, pp. 1–9 (2007c).
- RUFFINI, R., ROTONDO, M. AND XUE, S.S.
«Electrodynamics for nuclear matter in bulk».
IJMPD, **16**, pp. 1–9 (2007d).
- RUFFINI, R. AND STELLA, L.
«Some comments on the relativistic Thomas-Fermi model and the Vallarta-Rosen equation».
Physics Letters B, **102**, pp. 442–444 (1981).
- RUFFINI, R., VERESHCHAGIN, G. AND XUE, S.
«Electron-positron pairs in physics and astrophysics: From heavy nuclei to black holes».
Physics Reports, **487**, pp. 1–140 (2010b).
- RUFFINI, R., VITAGLIANO, L. AND XUE, S.S.
«On a separatrix in the gravitational collapse to an overcritical electromagnetic black hole».
Physics Letters B, **573**, pp. 33–38 (2003a).
- RUFFINI, R., VITAGLIANO, L. AND XUE, S.S.
«On plasma oscillations in strong electric fields».
Physics Letters B, **559**, pp. 12–19 (2003b).

- RUFFINI, R. AND WHEELER, J.A.
«Introducing the black hole.»
Physics Today, **24**, pp. 30–36 (1971).
- RUFFINI, R. AND XUE, S.S.
«Effective Dyadosphere».
In Y.-F. Huang, Z.-G. Dai, & B. Zhang (ed.), *American Institute of Physics Conference Series*, volume 1065 of *American Institute of Physics Conference Series*, pp. 289–293 (2008).
- SALPETER, E.E.
«Energy and Pressure of a Zero-Temperature Plasma.»
Astrophysical Journal, **134**, pp. 669–+ (1961).
- SALPETER, E.E. AND SHAPIRO, S.L.
«Neutrino and photon emission from a dense, high temperature atmosphere».
ApJ, **251**, p. 311 (1981).
ISSN 0004-637X.
- SASAKI, M., PLUCINSKY, P.P., GAETZ, T.J., SMITH, R.K., EDGAR, R.J. AND SLANE, P.O.
«XMM-Newton Observations of the Galactic Supernova Remnant CTB 109 (G109.1-1.0)».
Astrophysical Journal, **617**, pp. 322–338 (2004).
- SAUTER, F.
«Über das Verhalten eines Elektrons im homogenen elektrischen Feld nach der relativistischen Theorie Diracs».
Zeitschrift für Physik, **69**, pp. 742–764 (1931).
- SCHAAB, C., WEBER, F., WEIGEL, M. AND GLENDENNING, N.K.
«Thermal evolution of compact stars».
Nuclear Phys A, **605**, p. 531 (1996).
- SCHMIDT, G.D., BERGERON, P., LIEBERT, J. AND SAFFER, R.A.
«Two ultramassive white dwarfs found among candidates for magnetic fields».
Astrophysical Journal, **394**, pp. 603–608 (1992).
- SCHMIDT, G.D., WEST, S.C., LIEBERT, J., GREEN, R.F. AND STOCKMAN, H.S.
«The new magnetic white dwarf PG 1031 + 234 - Polarization and field structure at more than 500 million Gauss».
Astrophysical Journal, **309**, pp. 218–229 (1986).

SCHWINGER, J.

«On Gauge Invariance and Vacuum Polarization».
Physical Review, **82**, pp. 664–679 (1951).

SCHWINGER, J.

«The Theory of Quantized Fields. V».
Physical Review, **93**, pp. 615–628 (1954a).

SCHWINGER, J.

«The Theory of Quantized Fields. VI».
Physical Review, **94**, pp. 1362–1384 (1954b).

SEGRÉ, E.

Nuclei and Particles (1977).

SHAPIRO, S.L. AND TEUKOLSKY, S.A.

Black holes, white dwarfs, and neutron stars: The physics of compact objects (1983).

SHARMA, B.K. AND PAL, S.

«Nuclear symmetry energy effects in finite nuclei and neutron star».
Physics Letters B, **682**, pp. 23–26 (2009).

SHARMA, M.M., NAGARAJAN, M.A. AND RING, P.

«Rho meson coupling in the relativistic mean field theory and description of exotic nuclei».
Physics Letters B, **312**, pp. 377–381 (1993).

SHKLOVSKII, I.S.

Supernovae (1968).

SHTERNIN, P.S., YAKOVLEV, D.G., HEINKE, C.O., HO, W.C.G. AND PATNAUDE, D.J.

«Cooling neutron star in the Cassiopeia A supernova remnant: evidence for superfluidity in the core».
Monthly Notices of the Royal Astronomical Society, **412**, pp. L108–L112 (2011).

SLATER, J.C. AND KRUTTER, H.M.

«The Thomas-Fermi Method for Metals».
Phys. Rev., **47**, pp. 559–+ (1935).

SOMMERFELD, A.

«Asymptotische Integration der Differentialgleichung des Thomas-Fermischen Atoms».
Zeitschrift für Physik, **78**, pp. 283–308 (1932).

- SORIA, R., PIAN, E. AND MAZZALI, P.A.
«A second glance at SN 2002ap and the M 74 field with XMM-Newton». *A&A*, **413**, pp. 107–119 (2004).
- SPRUCH, L.
«Pedagogic notes on Thomas-Fermi theory (and on some improvements): atoms, stars, and the stability of bulk matter». *Reviews of Modern Physics*, **63**, pp. 151–210 (1991).
- SPRUIT, H.C.
«Dynamo action by differential rotation in a stably stratified stellar interior». *Astronomy & Astrophysics*, **381**, pp. 923–932 (2002).
- STAIRS, I.H.
«Pulsars in Binary Systems: Probing Binary Stellar Evolution and General Relativity». *Science*, **304**, pp. 547–552 (2004).
- STEFANESCU, A., KANBACH, G., SŁOWIKOWSKA, A., GREINER, J., MCBREEN, S. AND SALA, G.
«Very fast optical flaring from a possible new Galactic magnetar». *Nature*, **455**, pp. 503–505 (2008).
- STEJNER, M. AND MADSEN, J.
«Gaps below strange star crusts». *Physical Review D*, **72(12)**, 123005 (2005).
- STERGIOULAS, N.
«Rotating Stars in Relativity». *Living Reviews in Relativity*, **6**, pp. 3–+ (2003).
- STONER, E.C.
«The limiting density of White Dwarfs». *Philosophical Magazine (Series 7)*, **7**, pp. 63–70 (1929).
- SUGAHARA, Y. AND TOKI, H.
«Relativistic mean-field theory for unstable nuclei with non-linear σ and ω terms». *Nuclear Physics A*, **579**, pp. 557–572 (1994).
- SWEET, P.A.
«The Neutral Point Theory of Solar Flares». In B. Lehnert (ed.), *Electromagnetic Phenomena in Cosmical Physics*, volume 6 of *IAU Symposium*, pp. 123–+ (1958).

- TAMII, A., POLTORATSKA, I., VON NEUMANN-COSEL, P., FUJITA, Y., ADACHI, T., BERTULANI, C.A., CARTER, J., DOZONO, M., FUJITA, H., FUJITA, K. ET AL.
«Complete Electric Dipole Response and the Neutron Skin in Pb208».
Physical Review Letters, **107**(6), 062502 (2011).
- TAURIS, T.M. AND BAILES, M.
«The origin of millisecond pulsar velocities.»
Astronomy & Astrophysics, **315**, pp. 432–444 (1996).
- TAURIS, T.M. AND TAKENS, R.J.
«Runaway velocities of stellar components originating from disrupted binaries via asymmetric supernova explosions».
Astronomy & Astrophysics, **330**, pp. 1047–1059 (1998).
- TAVANI, M.
«AGILE Discovery of Gamma-ray Flares from the Crab Nebula».
In *American Astronomical Society Meeting Abstracts*, volume 217 of *American Astronomical Society Meeting Abstracts*, pp. 434.06–+ (2011).
- TAYLER, R.J.
«The adiabatic stability of stars containing magnetic fields-I.Toroidal fields».
Monthly Notices of the Royal Astronomical Society, **161**, pp. 365–+ (1973).
- TENNANT, A.F., BECKER, W., JUDA, M., ELSNER, R.F., KOLODZIEJCZAK, J.J., MURRAY, S.S., O'DELL, S.L., PAERELS, F., SWARTZ, D.A., SHIBAZAKI, N. ET AL.
«Discovery of X-Ray Emission from the Crab Pulsar at Pulse Minimum».
Astrophysical Journal, **554**, pp. L173–L176 (2001).
- TERADA, Y.
«White Dwarf Equivalent of Pulsars, Discovered with Suzaku».
Astronomical Herald, **101**, pp. 526–534 (2008).
- TERADA, Y., HAYASHI, T., ISHIDA, M., MAKISHIMA, K., MUKAI, K., DOTANI, T., OKADA, S., NAKAMURA, R., NAIK, S., BAMBA, A. ET AL.
«Suzaku Discovery of Hard X-ray Pulsations from the Rotating Magnetized White Dwarf, AE Aquarii».
In *AAS/High Energy Astrophysics Division #10*, volume 10 of *AAS/High Energy Astrophysics Division*, pp. 10.03–+ (2008a).
- TERADA, Y., HAYASHI, T., ISHIDA, M., MUKAI, K., DOTANI, T., BAMBA, A., OKADA, S., NAKAMURA, R., MAKISHIMA, K., MORIGAMI, K. ET AL.
«Suzaku Observation of a White Dwarf as a new Candidate of Cosmic-ray Origin».

- In F. A. Aharonian, W. Hofmann, & F. Rieger (ed.), *American Institute of Physics Conference Series*, volume 1085 of *American Institute of Physics Conference Series*, pp. 689–692 (2008b).
- TERADA, Y., HAYASHI, T., ISHIDA, M., MUKAI, K., DOTANI, T., OKADA, S., NAKAMURA, R., NAIK, S., BAMBIA, A. AND MAKISHIMA, K.
«Suzaku Discovery of Hard X-Ray Pulsations from a Rotating Magnetized White Dwarf, AEAquarii».
Publ. Astron. Soc. Japan, **60**, pp. 387– (2008c).
- TERADA, Y., ISHIDA, M., MUKAI, K., DOTANI, T., MAKISHIMA, K., NAIK, S., HAYASHI, T., OKADA, S., NAKAMURA, R. AND ENOTO, T.
«Possible Suzaku detection of non-thermal X-ray signals from a rotating magnetized white dwarf».
Advances in Space Research, **41**, pp. 512–517 (2008d).
- THOMAS, L.H.
«The calculation of atomic fields».
Proc. Cambridge Phil. Soc., **23**, pp. 542–+ (1927).
- THOMPSON, C. AND DUNCAN, R.C.
«Neutron star dynamos and the origins of pulsar magnetism».
Astrophysical Journal, **408**, pp. 194–217 (1993).
- THOMPSON, C. AND DUNCAN, R.C.
«The soft gamma repeaters as very strongly magnetized neutron stars - I. Radiative mechanism for outbursts».
Monthly Notices of the Royal Astronomical Society, **275**, pp. 255–300 (1995).
- THOMPSON, C. AND DUNCAN, R.C.
«The Soft Gamma Repeater as Very Strongly Magnetized Neutron Stars. II. Quiescent Neutrino, X-Ray, and Alfvén Wave Emission».
Astrophysical Journal, **473**, pp. 322–+ (1996).
- THOMPSON, C., LYUTIKOV, M. AND KULKARNI, S.R.
«Electrodynamics of Magnetars: Implications for the Persistent X-Ray Emission and Spin-down of the Soft Gamma Repeater and Anomalous X-Ray Pulsars».
Astrophysical Journal, **574**, pp. 332–355 (2002).
- TIENGO, A., ESPOSITO, P., MEREGHETTI, S., REA, N., STELLA, L., ISRAEL, G.L., TUROLLA, R. AND ZANE, S.
«The calm after the storm: XMM-Newton observation of SGR 1806-20 two months after the Giant Flare of 2004 December 27».
Astronomy & Astrophysics, **440**, pp. L63–L66 (2005).

- TOLMAN, R.C.
«On the Weight of Heat and Thermal Equilibrium in General Relativity».
Physical Review, **35**, pp. 904–924 (1930).
- TOLMAN, R.C.
«Static Solutions of Einstein’s Field Equations for Spheres of Fluid».
Physical Review, **55**, pp. 364–373 (1939).
- TOLMAN, R.C. AND EHRENFEST, P.
«Temperature Equilibrium in a Static Gravitational Field».
Physical Review, **36**, pp. 1791–1798 (1930).
- TONG, H., SONG, L.M. AND XU, R.X.
«Non-detection in a Fermi/LAT Observation of AXP 4U 0142+61: Magnets?»
Astrophysical Journal, **725**, pp. L196–L199 (2010).
- TONG, H., SONG, L.M. AND XU, R.X.
«AXPs and SGRs in the outer gap model: confronting Fermi observations».
arXiv:1101.2289 (2011).
- TOROK, G., BAKALA, P., STUCHLIK, Z. AND CECH, P.
«Modeling the Twin Peak QPO Distribution in the Atoll Source 4U 1636-53».
Acta Astronomica, **58**, pp. 1–14 (2008).
- TRÜMPER, J.E.
«Observations of neutron stars and the equation of state of matter at high densities».
Progress in Particle and Nuclear Physics, **66**, pp. 674–680 (2011).
- TRÜMPER, J.E., BURWITZ, V., HABERL, F. AND ZAVLIN, V.E.
«The puzzles of RX J1856.5-3754: neutron star or quark star?»
Nuclear Physics B Proceedings Supplements, **132**, pp. 560–565 (2004).
- TUROLLA, R., ZAMPIERI, L., COLPI, M. AND TREVES, A.
«Spherical accretion onto neutron stars revisited: Are hot solutions possible?»
ApJ, **426**, p. L35 (1994).
ISSN 0004-637X.
- USOV, V.V.
«Glitches in the X-ray pulsar 1E 2259+586».
Astrophysical Journal, **427**, pp. 984–986 (1994).
- USOV, V.V.
«Bare Quark Matter Surfaces of Strange Stars and e^+e^- Emission».
Physical Review Letters, **80**, pp. 230–233 (1998).

- VINK, J.
«Supernova remnants with magnetars: Clues to magnetar formation».
Advances in Space Research, **41**, pp. 503–511 (2008).
- VINK, J. AND KUIPER, L.
«Supernova remnant energetics and magnetars: no evidence in favour of millisecond proto-neutron stars».
Monthly Notices of the Royal Astronomical Society, **370**, pp. L14–L18 (2006).
- WALECKA, J.D.
«A theory of highly condensed matter.»
Annals of Physics, **83**, pp. 491–529 (1974).
- WEISSKOPF, M.C., O'DELL, S.L., PAERELS, F., ELSNER, R.F., BECKER, W.,
TENNANT, A.F. AND SWARTZ, D.A.
«Chandra Phase-Resolved X-Ray Spectroscopy of the Crab Pulsar».
Astrophysical Journal, **601**, pp. 1050–1057 (2004).
- WERNER, F.G. AND WHEELER, J.A.
«Superheavy Nuclei».
Physical Review, **109**, pp. 126–144 (1958).
- WITTEN, E.
«Cosmic separation of phases».
Physical Review D, **30**, pp. 272–285 (1984).
- WOLTJER, L.
«X-Rays and Type i Supernova Remnants.»
Astrophysical Journal, **140**, pp. 1309–1313 (1964).
- WOODS, P.M., KASPI, V.M., THOMPSON, C., GAVRIIL, F.P., MARSHALL,
H.L., CHAKRABARTY, D., FLANAGAN, K., HEYL, J. AND HERNQUIST, L.
«Changes in the X-Ray Emission from the Magnetar Candidate 1E
2259+586 during Its 2002 Outburst».
Astrophysical Journal, **605**, pp. 378–399 (2004).
- WOOSLEY, S.E.
«Bright Supernovae from Magnetar Birth».
Astrophysical Journal, **719**, pp. L204–L207 (2010).
- YAKOVLEV, D.G., KAMINKER, A.D., GNEDIN, O.Y. AND HAENSEL, P.
«Neutrino emission from neutron stars».
Physics Reports, **354(1-2)**, pp. 1–155 (2001).
ISSN 03701573.
- YAKOVLEV, D.G. AND PETHICK, C.J.
«Neutron Star Cooling».
Annual Review of Astronomy & Astrophysics, **42**, pp. 169–210 (2004).

ZANE, S., REA, N., TUROLLA, R. AND NOBILI, L.

«X-ray spectra from magnetar candidates - III. Fitting SGR/AXP soft X-ray emission with non-relativistic Monte Carlo models».

Monthly Notices of the Royal Astronomical Society, **398**, pp. 1403–1413 (2009).

ZEL'DOVICH, I.B.

«Nuclear Reactions in Super-Dense Cold Hydrogen».

Soviet Journal of Experimental and Theoretical Physics, **6**, pp. 760–+ (1958).

ZELDOVICH, Y.B. AND POPOV, V.S.

«Reviews of Topical Problems: Electronic Structure of Superheavy Atoms».

Soviet Physics Uspekhi, **14**, pp. 673–694 (1972).

ZHANG, B. AND GIL, J.

«GCRT J1745-3009 as a Transient White Dwarf Pulsar».

Astrophysical Journal, **631**, pp. L143–L146 (2005).